

This work is protected by copyright and other intellectual property rights and duplication or sale of all or part is not permitted, except that material may be duplicated by you for research, private study, criticism/review or educational purposes. Electronic or print copies are for your own personal, non-commercial use and shall not be passed to any other individual. No quotation may be published without proper acknowledgement. For any other use, or to quote extensively from the work, permission must be obtained from the copyright holder/s.



The sedimentary architecture and spatial variations of dryland ephemeral fluvial systems

Charlotte Louise Priddy

This thesis is submitted in accordance with the requirements of the University of Keele for the degree of Doctor of Philosophy.

October 2021

BASIN DYNAMICS RESEARCH GROUP



Acknowledgements

I would firstly like to thank my supervisors Dr Stuart Clarke and Dr Jamie Pringle at Keele University and Dr Tom Randles at the British Geological Survey for their continued support, wisdom and effort throughout the entire process of my PhD. This research was undertaken as part of the Natural Environment Research Council (NERC) Centre for Doctoral Training (CDT) in Oil & Gas under its Extending the Life of Mature Basins theme [grant number: NEM00578X/1]. It is sponsored by NERC and the British Geological Survey (BGS) via the British University Funding Initiative (BUFI) whose support is gratefully acknowledged.

I would also like to thank all of the support staff within the department, especially Rich Burgess for all his IT support, Peter Greatbatch and David Wilde within the Thin Section Lab, Andy Lawrence for printing our ridiculously large posters for AAPG. Thank you also to Scott Renshaw and the rest of the Core Store staff at the BGS for laying out over 2000 metres of core and allowing me to conduct research during a difficult time between COVID-19 lockdowns.

The fieldwork component of my PhD would have not been possible without the United States National Park Service for permitting this research and granting scientific research permits for Arches, Canyonlands, Capitol Reef and Zion National Parks, and to the Navajo Nation for granting access to conduct research within their land, to whom I am incredibly grateful. Thank you to the best field team a girl could ask for, Ross Pettigrew, Andy Mitten and Dave Cousins, you really made the summer months camping in Utah, Arizona and Colorado an unforgettable experience.

I must also thank all my fellow PhD students on the NERC CDT in Oil and Gas, and members of the Basin Dynamics Research Group (BDRG) for their unwavering support and friendship, in particular James Foey who has acted like a big brother to me throughout this process. Thank you all for the great nights and sometimes days spent in the KPA. To the best housemates and friends, Felicity Duty and Amy Regis, thank you for all your friendship and support, especially during COVID-19. And Ross, thank you for your love and support through everything.

Finally, I am eternally grateful and completely indebted to my entire family for their continued support and encouragement, in particular my parents without whom I would not be where I am today and I cannot thank them enough.

Preface

The work within this thesis is based upon several manuscripts published during the course of this study. Chapters Three, Four, Five, Six, Seven and Nine are compiled based upon these manuscripts, as such, no one chapter is solely based upon a singular manuscript.

Publications (at the time of submission):

Priddy, C. L., Pringle, J. K., Clarke, S. M., & Pettigrew, R. P. (2019). Application of photogrammetry to generate quantitative geobody data in ephemeral fluvial systems. *The Photogrammetric Record*, **34(168)**, 428-444.

Priddy, C. L., & Clarke, S. M. (2020). The sedimentology of an ephemeral fluvial–aeolian succession. *Sedimentology*, **67(5)**, 2392-2425.

Priddy, C. L., & Clarke, S. M. (2021). Spatial variation in the sedimentary architecture of a dryland fluvial system. *Sedimentology*. Article first published online: 02 APRIL 2021. DOI: 10.1111/sed.12876.

Abstract

Ancient dryland continental basins commonly comprise sedimentary fill that records the activity of both fluvial and aeolian environments. Despite extensive studies of dryland ephemeral fluvial systems, detailed three-dimensional facies models for these systems are appreciably fewer in number and are less developed compared to those of their meandering and braided fluvial counterparts. This is despite the fact that depositional models illustrate the arrangement and interactions between depositional elements, along with the vertical and lateral connectivity of those elements, which are particularly useful and important for reservoir characterisation.

This work focusses on an extensive outcrop analogue study of the dryland fluvial Kayenta Formation of the Colorado Plateau, USA, and applies the findings to a detailed core study of the Leman Sandstone, a similar depositional setting within the subsurface of the Southern North Sea, UK. The work utilises extensive regional fieldwork to examine the sedimentology, geometries, and interactions of ephemeral fluvial and aeolian environments, along with analysis of the spatial and temporal variations across the depositional system.

Results show that the Kayenta ephemeral fluvial system is dominated by sandy laterally and vertically amalgamated, poorly channelised to sheet-like elements, with abundant upper flow regime structures. Spatial analysis of the system indicates many trends that are similar to those of a dryland terminal fluvial system, whereas temporal analysis indicates an overall regression of the fluvial system through time.

This study provides valuable sedimentological data for characterising dryland fluvial systems, particularly when analysing the spatial and temporal variations of the system and demonstrates the inherent complexity in dryland fluvial systems and the downstream architectural and compositional relationships that they depict. These results are used to reconstruct the Leman Sandstone, providing valuable three-dimensional data, in order to better characterise basin-scale migration and reservoir quality.

Table of Contents

Acknowledgements	i
Preface	ii
Publications (at the time of submission):	ii
Abstract	iii
List of Figures	ix
List of Tables	xvii
Chapter 1: Introduction	1
1.1. Research aims and objectives.....	4
1.1.1. Aim 1: Outcrop sedimentology.....	4
1.1.2. Aim 2: Spatial and temporal variations	5
1.1.3. Aim 3: Application	6
1.2. Thesis overview	7
Chapter 2: Literature review	10
2.1. Introduction.....	10
2.2. Fluvial transport, processes and products.....	10
2.2.1. Transport and depositional processes.....	10
2.2.2. Fluvial bedforms and facies	11
2.2.3. Fluvial architectural elements	16
2.2.4. Bounding surfaces	20
2.3. Fluvial styles.....	22
2.3.1. Ephemeral fluvial systems	22
2.4. Aeolian transport, processes and products.....	25
2.4.1. Transport and depositional processes.....	25
2.4.2. Aeolian bedforms	26
2.4.3. Bedform morphology	28
2.4.4. Sedimentary structures	30
2.4.5. Aeolian architectural elements	31
2.4.6. Aeolian bounding surfaces	33
2.5. Geological evolution of the Colorado Plateau.....	34
2.5.1. Geological History.....	35
2.5.2. Glen Canyon Group.....	41
2.6. Summary.....	44

Chapter 3: Methods	46
3.1. Sedimentological methods.....	46
3.1.1. Graphical vertical sections: Sedimentary logs	46
3.1.2. Spatial analysis	47
3.1.3. Palaeocurrent Analysis.....	48
3.1.4. Core analysis	50
3.2. Photogrammetric methods.....	52
3.2.1. Data Acquisition	54
3.2.2. Data Processing.....	57
3.2.3. Post-processing	62
3.3. Summary	63
Chapter 4 – The Sedimentology of an Ephemeral Fluvial Outcrop Analogue: The Kayenta Formation	65
4.1. Literature review summary.....	65
4.1.1. Kayenta Formation.....	65
4.1.2. Springdale Member.....	66
4.1.3. Kayenta main body.....	67
4.1.4. Tenny Canyon Tongue.....	67
4.1.5. Sedimentology of the Kayenta Formation	68
4.1.6. Kayenta-Navajo Transition	70
4.1.7. Dating the Kayenta Formation	70
4.2. Methods.....	71
4.3. Lithofacies of the Kayenta Formation.....	72
4.4. Summary	84
Chapter 5: Interpretation of the Sedimentology of an Ephemeral Fluvial Outcrop Analogue: The Kayenta Formation.....	85
5.1. Architectural Elements.....	85
5.1.1. Fluvial channel elements.....	86
5.1.2. Fluvial sheet-like elements.....	92
5.1.3. Lateral accretion element	95
5.1.4. Downstream accretion element	96
5.1.5. Bank collapse element	98
5.1.6. Overbank/floodplain elements	98
5.1.7. Compound aeolian dune element	99
5.1.8. Aeolian sandsheet element.....	104

5.1.9. Interdune elements	104
5.2. Depositional Elements	105
5.2.1. Amalgamated Sandstone-Dominated Channel-Fill	108
5.2.2. Isolated Sandstone-Dominated Channel-Fill	111
5.2.3. Isolated Gravel-Dominated Channel-Fill.....	112
5.2.4. Compound Sandstone-Dominated Fluvial Sheets	113
5.2.5. Overbank	113
5.3. System-scale Associations	115
5.3.1. Dominantly aeolian deposition.....	115
5.3.2. Dominantly braided fluvial deposition	115
5.3.3. Dominantly ephemeral fluvial deposition	116
5.4. Summary.....	117

Chapter 6: Spatial and Temporal Variations of the Ephemeral Fluvial Kayenta Formation and their Interactions with a Competing Aeolian Environment	118
6.1. Methods.....	118
6.2. General Spatial Variations of the Kayenta Formation	121
6.2.1. Architecture of the Kayenta Formation.....	121
6.2.2. Thickness variations within the Kayenta Formation	122
6.2.3. Composition of the Kayenta Formation	122
6.2.4. Overall Grainsize of the Kayenta Formation.....	123
6.3. Interpretation of the Spatial Variations in the Sedimentology of the Kayenta Formation	123
6.4. Analysis of the Depositional Elements	127
6.4.1. Distribution of the Depositional Elements	127
6.4.2. Thickness of the Depositional Elements.....	128
6.4.3. Grainsize Distribution of the Depositional Elements.....	130
6.5. Interpretation of the Spatial Variations in the Depositional Elements	133
6.6. Temporal Variations	137
6.7. Interpretation of the Temporal Variations.....	137
6.8. Interactions.....	141
6.8.1. Facies-scale interactions.....	141
6.8.2. Element-scale interactions	142
6.8.3. System-scale interactions	145
6.9. Summary.....	146

Chapter 7: Digital Outcrop Models, Geobody Analysis and Reconstruction of Depositional Environments	148
7.1. Introduction	148
7.2. Outcrop Photo Panels	149
7.3. Digital Outcrop Models	154
7.4. Depositional Models	155
7.5. Summary	161
Chapter 8: Application of the Kayenta Formation to the Lemna Sandstone of the Southern North Sea	163
8.1. Introduction	163
8.2. Geological Setting	163
8.2.1. Silverpit Formation.....	164
8.2.2. Lemna Sandstone.....	165
8.3. Methods	167
8.4. Lithofacies of the Lemna Sandstone and Silverpit Formations.....	168
8.5. Facies Associations.....	177
8.5.1. Aeolian Dune	177
8.5.2. Aeolian Dune Plinth.....	178
8.5.3. Aeolian Sandsheet.....	178
8.5.4. Dry Interdune	181
8.5.5. Damp to wet Interdune.....	182
8.5.6. Fluvial Channel	186
8.5.7. Fluvial Sheet	187
8.5.8. Overbank.....	188
8.5.9. Lake Margin.....	192
8.5.10. Lake Centre	194
8.5.11. Ephemeral Saline Lake/Mudflat.....	194
8.6. Comparison to the Kayenta Formation.....	197
8.7. Depositional Model.....	198
8.8. Summary	203
Chapter 9: Discussion.....	204
9.1. Sedimentology of the Kayenta Formation	204
9.2. Spatial variations of the Kayenta Formation.....	206
9.2.1. Spatial variations in architectural elements.....	207

9.2.2. Spatial variations in depositional elements.....	209
9.2.3. Comparison of spatial trends to previously published models	211
9.3. Temporal variations of the Kayenta Formation	213
9.4. Digital outcrop models	215
9.5. Application to the Leman Sandstone	217
9.5.1. Fluid flow predictions	218
9.6. Summary.....	219
Chapter 10: Conclusions and Further Work	222
10.1. Introduction.....	222
10.2. Research aims.....	223
10.2.1. Aim 1: Identify and fully describe the sedimentology of a dryland ephemeral braided fluvial system and its competing coeval aeolian environment	223
10.2.2. Aim 2: Identify and quantify the regional spatial and temporal variations of the depositional system along with the interactions between the fluvial and aeolian environments	224
10.2.3. Aim 3: Apply findings to subsurface data of a similar depositional setting to better characterise architectural and geometrical relationships within potential reservoir units.....	226
10.3. Further Work	227
10.3.1. Analysis of modern-day systems	228
10.3.2. Provenance studies.....	228
10.3.3. Numerical modelling.....	229
10.4. Summary.....	230
References	232
Appendices	256
Appendix 1 - Kayenta logs	257
Appendix 2 - Kayenta statistics.....	276
Appendix 3 - Leman logs.....	283

List of Figures

- Figure 2.1. Two dominant transport mechanisms in fluvial systems; bedload transport - a combination of saltation and reptation of grains, and transport by suspension where the sediment is carried within in the flow without coming into contact with the bed. Modified after Collinson et al. (2006).....12
- Figure 2.2. Phase diagram for bedforms produced by various grain sizes (mm) and mean flow velocities (cm s^{-1}) within a confined flow 20cm deep and at 10°C. Modified after Southard (1971), Ashley (1990), Leeder (1982; 2011), Hsu and Hanes (2004), Hsu et al., (2004) and Collinson et al. (2006).13
- Figure 2.3. Schematic representation of ripple and dune-scale bedforms and the downstream migration of the bedforms. (A) Ripple-scale bedforms – where the upper flow is undisturbed, (B) Dune-scale bedforms – where the upper and lower flow is disturbed, creating boils in the upper flow, (C) Initial phase of bedform migration – where eddy currents form within the troughs of the bedforms and grains are transported up the stoss slope, (D) Second phase of bedform migration – where grains avalanche down the lee slope of the bedforms resulting in subsequent downstream accretion. Modified after Collinson et al. (2006) and Nichols (2009).13
- Figure 2.4. (A) Schematic representation of antidune migration formed when standing waves break in the upstream direction depositing sediment on the stoss slope, (B) Line drawings of the internal sedimentary structures of antidune from humpback dunes formed in the lower to upper flow regime transition to chutes and pools. Modified after Collinson et al. (2006) and Fielding (2006).14
- Figure 2.5. Bounding surface hierarchy within a fluvial system, numbers correlate to the bounding surfaces shown in Table 2.3. Modified after Miall (2010).21
- Figure 2.6. Depositional models of typical ephemeral fluvial systems. The distal braidplain model is dominated by sandy bedforms and deposits from ephemeral discharge. The sheetflood fluvial plain model is dominated by laminated sheets and deposits from highly flashy discharge. Modified after Miall (1985).23
- Figure 2.7. Various modes of aeolian transport, governed primarily by grain size. Particles approximately $<20\text{-}70\ \mu\text{m}$ are transported in suspension, larger particles between $70\text{-}500\ \mu\text{m}$ move downwind by saltation and particles greater than $500\ \mu\text{m}$ are transported by reptation. Modified after Nickling and McKenna Neuman (2009).26
- Figure 2.8. Formation of aeolian ripples by saltating sand grains. Note the finer grained core of the ripples. Modified after Durán et al. (2011).27
- Figure 2.9. The transport mechanisms for dune and draa formation. Modified after Miall (1978).....28
- Figure 2.10. Three dimensional forms of common aeolian dune/draa morphologies. The arrows mark the dominant wind direction. Modified after Collinson et al. (2006).29
- Figure 2.11. Schematic diagram of the common small-scale stratification types present in aeolian dunes and draa. Modified after Hunter (1977) and Cain (2009).31
- Figure 2.12. The Colorado Plateau located across the Four Corners states, divided into six modern-day physi-geographical sections and showing the modern day San Juan, Green and Colorado rivers. The Kayenta fluvial systems deposited sediment across the Colorado Plateau sourced from the Ancestral

Rocky Mountains to the Northeast and the Mongollon Highlands to the southwest. Modified after Foos (1999).....	34
Figure 2.13. The structure of the Colorado Plateau outlined in black, with locations of uplifts in orange, basins in blue and monoclines in green. Modified after Baars (2000); Barbeau (2003) & Baars and Stevenson (1981).	36
Figure 2.14. Map of the extent of the Lower Jurassic deposits, showing the location of the Utah-Idaho trough, Zuni Sag (Locus for Lower Jurassic rivers) and several uplifts. Modified after Bjerrum & Dorsey (1995).....	38
Figure 2.15. The Colorado Plateau with locations of volcanic and igneous centres (red). Modified after Foos (1999)	40
Figure 2.16. The stratigraphy of the Glen Canyon Group including members, facies and spatial distribution of facies across the Colorado Plateau. The focus of this study is the Kayenta Formation that, along with the underlying Wingate and overlying Navajo formations, form the Glen Canyon Group. Modified after North & Taylor (1996); Tanner & Lucas (2007). TCT = Tenny Canyon Tongue.	41
Figure 2.17. Cross section through the Lower and Middle Jurassic Stratigraphy, highlighting the unconformities that bound the Glen Canyon Group. Modified after Blakey (1994).	42
Figure 3.1. The study area in the western USA highlighting the extent of exposure of Triassic-Jurassic sediments (yellow) across the Colorado Plateau, along with the positions and names of the sedimentary logs collected (grey squares) and locations and names of the sedimentary logs where photogrammetry was also conducted (purple squares) for this study. The base map and outcrop limits are modified after Dickinson, 2018.	49
Figure 3.2. Palaeogeographical map of the Lemn Sandstone of the Southern North Sea. Modified after George & Berry (1993;1997)	51
Figure 3.3. Simplified schematic representation of image acquisition for 3D photogrammetric modelling used in this study. The blue triangles represent the field of view of the camera from the positions shown, with the darkness of the triangles increasing with the amount of overlap. (A) Photo acquisition for ground-based photogrammetry in plan view, (B) Photo acquisition used for UAV-based photogrammetry in profile view, highlighting the angled camera locations to fully capture the 3D nature of the outcrop, looking obliquely to the outcrop face (modified after Bemis et al., 2014).	56
Figure 3.4. General workflow of the 3D photogrammetric model reconstruction process, data collection (blue), desktop processing (orange), the generation of 3D models using Agisoft PhotoScan™ (purple), including the points in which structure-from-motion (SfM) and multi-view stereo (MVS) were used, and post processing architectural element analysis within Virtual Reality Geological Studio (VRGS) software (green). Rectangle icons represent 3D photogrammetric model reconstruction steps, diamond icons represent outputs from each process (modified after Bemis et al. 2014; Schmitz et al. 2014; Kehl et al. 2017).....	58
Figure 3.5. Construction of Model 1 (proximal – Lions Park) using Agisoft PhotoScan. (A) Sparse point cloud generated using SfM – 26,703 points. (B) Dense point cloud generated using MVS with pixel grid-based matching – 289,130,233 points. (C) Photo-realistic textured model.....	59

Figure 3.6. Construction of Model 2 (medial – Comb Ridge) using Agisoft PhotoScan. (A) Sparse point cloud generated using SfM – 141,313 points. (B) Dense point cloud generated using MVS with pixel grid-based matching – 49,167,525 points. (C) Photo-realistic textured model.....60

Figure 3.7. Construction of Model 3 (distal – Squaw Trail) using Agisoft PhotoScan. (A) Sparse point cloud generated using SfM – 275,486 points. (B) Dense point cloud generated using MVS with pixel grid-based matching – 121,506,632 points. (C) Photo-realistic textured model.....61

Figure 3.8. Categories of geobody lengths exposed at outcrop (modified after Geehan & Underwood, 1993; Visser & Chessa, 2000a).63

Figure 4.1. Generalised distribution of the ‘sandy’ and ‘silty’ facies of the Kayenta Formation across the Four Corners states and Nevada, with generalised fluvial palaeoflow direction and possible sources. (after Harshbarger et al., 1957; Middleton & Blakey, 1983; Luttrell, 1993).66

Figure 4.2. The Colorado Plateau, situated in the Four Corner states, USA, showing the extent of the Kayenta Formation deposition. The Kayenta fluvial systems deposited sediment across the Colorado Plateau sourced from the Ancestral Rocky Mountains (Uncompahgre Uplift) to the northeast and the Cordilleran Magmatic Arc to the southwest, locations of logged sections are indicated in white ellipses (see key) (modified after Harshbarger et al., 1957; Middleton & Blakey, 1983; Blakey 1994). The rose diagram depicts palaeocurrent measurements from the ‘silty’ (brown) and ‘sandy’ (light yellow) fluvial system and the aeolian system (yellow), along with their arithmetic averages (arrows); ‘n’ gives the number of measurements in each set.72

Figure 4.3. Representative sedimentary logs showing the downstream lithofacies and palaeocurrent variations observed in the Kayenta Formation. Sedimentary logs are coloured by lithofacies (see key) with architectural element codes and broad facies associations listed down the side. Examples of bounding surfaces are highlighted by hierarchical numbers. See Fig. 4.2 for locations.74

Figure 4.4. Photopanel of unique facies within the Kayenta Formation. A) Planar-bedded sandstone formed under upper flow regime conditions, each bed is approximately 5-10 cm thick; B) Parallel-laminated sandstone formed under upper flow regime conditions, 30 cm hammer for scale; C) Supercritical climbing ripples with preservation of both the stoss slope and less slope of the bedform and an angle of climb of 16° formed under lower flow regime conditions with significant sediment supply, yellow measuring tape for scale (6 cm); D) Sigmoidal bedded sandstone - humpback cross-bedding of antidunes with a symmetrical geometry and preservation of the stoss and lee slope of the bedform, formed between conditions of lower flow regime dune formation to upper flow regime plane bed formation, gallon water jug for scale (30 cm); E) Recumbent cross-bedded sandstone with ‘ripped back’ topsets of the foresets, formed under lower flow regime conditions with fluctuations within flow conditions and sediment load, yellow measuring tape for scale (6 cm); F) Soft sediment deformed sandstone (bank collapse) containing contorted intra-formational clasts with mud-draping along the folded foresets, interpreted as a mass-transport debris-flow deposit, clasts are approximately 20-30 cm wide.81

Figure 5.1. Summary table of architectural elements with brief description and geometry, their contained facies (see chapter 4, Table 4.3 for detailed facies descriptions), and bounding surface analysis. Two-dimensional illustrations of commonly occurring relationships with overlying and underlying elements are indicated along with their respective palaeocurrent measurements, n = number of measurements, m = mean palaeocurrent direction.87

Figure 5.2. Architectural element outcrop panel for the proximal Kayenta Formation with hierarchical bounding surface analysis and palaeocurrent measurements. The proximal region is dominated by vertically and laterally amalgamated fluvial channel, sheets and accretionary elements with sporadic small isolated pockets of overbank. 88

Figure 5.3. Architectural element outcrop panel for the medial Kayenta Formation with hierarchical bounding surface analysis and palaeocurrent measurements. The medial region is dominated by vertically and laterally amalgamated fluvial channel, sheets and accretionary elements, however, channels are more isolated and overbank elements are thicker and more laterally extensive. 89

Figure 5.4. Architectural element outcrop panel for the distal Kayenta Formation with hierarchical bounding surface analysis and palaeocurrent measurements. In the distal region the degree of stacking between channel, sheets and accretionary elements is significantly reduced, with several channel and sheet-like elements being isolated within laterally extensive overbank deposits. 90

Figure 5.5. Summary panel of fluvial channel architectural element with palaeocurrent, idealised log, photographs and facies model. 91

Figure 5.6. Summary panel of sheetflood architectural element with palaeocurrent, idealised log, photographs and facies model. 94

Figure 5.7. Summary panel of lateral and downstream accretion architectural elements with palaeocurrent, idealised log, photograph and facies model. 97

Figure 5.8. Summary panel of bank collapse architectural element with locations map, idealised log, photographs and facies model. 100

Figure 5.9. Summary panel of overbank architectural element with idealised logs, photographs and facies model. 101

Figure 5.10. Summary panel of aeolian dune architectural element with palaeocurrent, idealised logs, photographs and facies model. 103

Figure 5.11. Summary panel of aeolian sandsheet architectural element with idealised logs, photographs and facies model. 106

Figure 5.12. Summary panel of aeolian interdune architectural elements with idealised logs, photographs and facies model. 107

Figure 5.13. Representation of the internal composition, architecture, and geometries of the large-scale depositional elements. Architectural elements: FC = fluvial channel, LA = lateral accretion, GC = gravel-dominated channel, SF = fluvial sheet, OB = overbank. Depositional elements: AC = amalgamated sandstone-dominated channel-fill, IC = isolated sandstone-dominated channel-fill, GC = isolated gravel-dominated channel-fill, CS = compound sandstone-dominated fluvial sheet, OB = overbank. 108

Figure 5.14. Summary table of fluvial depositional elements within the Kayenta Formation. 110

Figure 6.1. Architecture outcrop panels from three locations across the extent of the Kayenta Formation deposition depicting the change in architecture downstream, from highly amalgamated

channels and sheets within the proximal to isolated channels and sheets within the distal. (A) Proximal architecture panel of Uravan, Colorado. (B) Medial architecture panel of Comb Ridge, southeast Utah. (C) Distal architecture panel of Kanab, southwest Utah. (D) Locations map illustrating the positions of panels A-C.124

Figure 6.2.(A) Contour map of fluvial sediment thickness at each locality. (B) Graph of total fluvial sediment thickness against distance downstream. (C) Contour map of aeolian sediment thickness at each locality. (D) Graph of total aeolian sediment thickness against distance downstream. (E) Contour map of sand percentage at each locality. (F) Graph of sand percentage against distance downstream. (G) Contour map of conglomerate percentage at each locality. (H) Graph of conglomerate percentage against distance downstream. (I) Contour map of the average grainsize (Φ) at each locality. (J) Graph of average grainsize (Φ) against distance downstream. Average measurements of proximal, medial and distal portions are denoted as P (av), M (av), and D (av) on each graph. Dashed line in each case is a linear best fit to the total dataset and the dotted line is a linear best fit line excluding the data influenced by the secondary fluvial source.125

Figure 6.3. Contour maps and graphs illustrating the percentage that each depositional element constitutes of the whole fluvial succession at each locality. (A) Amalgamated channels contour map. (B) Graph of amalgamated channel percentage against distance downstream. (C) Isolated channels contour map. (D) Graph of isolated channel percentage against distance downstream. (E) Gravel-dominated channel contour map. (F) Graph of gravel-dominated channel percentage against distance downstream. (G) Compound fluvial sheet contour map. (H) Graph of compound fluvial sheet percentage against distance downstream. (I) Overbank contour map. (J) Graph of overbank percentage against distance downstream. Average measurements of proximal, medial and distal portions are denoted as P (av), M (av), and D (av) on each graph. Dashed line in each case is a linear best fit to the total dataset and the dotted line in each case is a linear best fit line excluding the data influenced by the secondary fluvial source.129

Figure 6.4. Graphs illustrating the average and range of sediment thickness at each locality for each depositional element plotted against distance downstream and box and whisker plots illustrating the median, interquartile range and outliers for each locality for each depositional element plotted against distance downstream. Average measurements of proximal, medial and distal portions are denoted as P (av), M (av), and D (av) on each graph. Dashed line in each case is a linear best fit to the total dataset and the dotted line in each case is a linear best fit line excluding the data influenced by the secondary fluvial source.131

Figure 6.5. Contour maps and graphs illustrating the average grainsize (Φ) that each depositional element constitutes of the fluvial succession at each locality. (A) Amalgamated channel contour map. (B) Graph of amalgamated channel average grainsize against distance downstream. (C) Isolated channel contour map. (D) Graph of isolated channel average grainsize against distance downstream. (E) Gravel-dominated channel contour map. (F) Graph of gravel-dominated channel average grainsize against distance downstream. (G) Compound fluvial sheet contour map. (H) Graph of compound fluvial sheet average grainsize against distance downstream. (I) Overbank contour map. (J) Graph of overbank average grainsize against distance downstream. Average measurements of proximal, medial and distal portions are denoted as P (av), M (av), and D (av) on each graph. Dashed line in each case is a linear best fit to the total dataset and the dotted line in each case is a linear best fit line excluding the data influenced by the secondary fluvial source.134

Figure 6.6. Log height of channel body against channel body thickness for each proximal succession studied. Coloured dots represent the interpreted channel depositional element present. The dashed line represents moving averages, and the pie chart breakdown shows the percentage of channel depositional element types for each locality. 138

Figure 6.7. Log height of channel body against channel body thickness for each medial succession studied. Coloured dots represent the interpreted channel depositional element present. The dashed line represents moving averages, and the pie chart breakdown shows the percentage of channel depositional element types for each locality. See Fig. 6.6 for key to colours. 139

Figure 6.8. Log height of channel body against channel body thickness for each distal succession studied. Coloured dots represent the interpreted channel depositional element present. The dashed line represents moving averages, and the pie chart breakdown shows the percentage of channel depositional element types for each locality. See Fig. 6.6 for key to colours. 140

Figure 6.9. Thin sections in XPL of: (A) Aeolian sediments from Sevenmile Canyon, UT, and (B) Fluvial sediments from Comb Wash, UT, showing extensive recycling and reworking of sediments from both environments..... 142

Figure 6.10. Element-scale interactions during differing dominant environments with rose diagrams depicting the variability in palaeocurrents dependant on the dominant depositional system. 144

Figure 6.11. Element-scale transitions depicted on idealised log succession from dominantly aeolian to fluvial and dominantly fluvial to aeolian. 145

Figure 6.12. Palaeocurrent analysis across the fluvial-aeolian transition showing a dominant fluvial palaeoflow towards the souhtwest, a dominant aeolian palaeowind direction to the southeast and a transitional period with both fluvial and aeolian palaeoflow directions to the southwest. Arithmetic averages are given in bold, along with the number of measurements..... 146

Figure 7.1. Architectural element outcrop panel for the proximal Kayenta Formation with hierarchical bounding surface analysis and palaeocurrent measurements. The proximal region is dominated by vertically and laterally amalgamated fluvial channel, sheets and accretionary elements with sporadic small isolated pockets of overbank. 150

Figure 7.2. Architectural element outcrop panel for the medial Kayenta Formation with hierarchical bounding surface analysis and palaeocurrent measurements. The medial region is dominated by vertically and laterally amalgamated fluvial channel, sheets and accretionary elements, however, channels are more isolated and overbank elements are thicker and more laterally extensive. 151

Figure 7.3. Architectural element outcrop panel for the distal Kayenta Formation with hierarchical bounding surface analysis and palaeocurrent measurements. In the distal region the degree of stacking between channel, sheets and accretionary elements is significantly reduced, with several channel and sheet-like elements being isolated within laterally extensive overbank deposits..... 152

Figure 7.4. Summary sedimentary fluvial architectural element width to depth box and whisker plots of channels (green) and sheets (purple) extracted from models 1 (proximal, 2 (medial) and 3 (distal). Minimum, average and maximum width measurements are shown, along with 1 SD error bars. 155

Figure 7.5. Mapped geobodies on (A) Model 1 - Lions Park, (B) Model 2 - Comb Ridge, and (C) Model 3 - Squaw Trail. Channel geobodies are depicted in green and sheet geobodies in purple.....156

Figure 7.6. Depositional model of an ephemeral fluvial system based upon field data from the Kayenta Formation. The model highlights the interaction between the aeolian and fluvial environments, and the dominance of upper flow regime and high sediment load structures within the fluvial environment.158

Figure 7.7. Depositional models of an arid ephemeral fluvial system from (A) proximal to (B) medial to (C) distal, based upon field data from the Kayenta Formation. The models show the detailed sedimentology and key characteristics observed, as along with the interaction between the aeolian and fluvial environment.159

Figure 7.8. System-scale depositional model of the Kayenta Formation sub-divided into proximal, medial, and distal sections with a cross-section of the internal architecture and stacking patterns for each section. Depositional element proportions (%) are displayed along the side of each section of the system-scale model, along with their key characteristics. Architectural element-scale facies models (from Figure 7.7) of the proximal, medial, and distal settings highlight the detailed sedimentology observed within the depositional elements on the system-scale model.160

Figure 8.1. Distribution of the Lemna Sandstone and Silverpit Formation within the Southern North Sea, with detailed facies distribution within the Lemna Sandstone (modified after Cameron et al., 1992).164

Figure 8.2. Lithostratigraphy of the Upper Rotliegend Group and relationships between the diachronous Lemna and Silverpit formations (modified after Glennie, 1986 and Howell & Mountney, 1997).166

Figure 8.3. Palaeogeographical map of the Lemna Sandstone of the Southern North Sea with locations of studied wells within quadrants 43, 44, 48 and 49 (modified after George & Berry, 1997).168

Figure 8.4. Selected logged sections depicting the varied sedimentology of the Lemna Sandstone/Silverpit transition.169

Figure 8.5. Summary panel of the aeolian dune association of the Lemna Sandstone with an idealised log and photographs of the internal facies.179

Figure 8.6. Summary panel of the aeolian dune plinth association of the Lemna Sandstone with an idealised log and photographs of the internal facies.180

Figure 8.7. Summary panel of the aeolian sandsheet association of the Lemna Sandstone with an idealised log and photographs of the internal facies.183

Figure 8.8. Summary panel of the aeolian dry interdune association of the Lemna Sandstone with an idealised log and photographs of the internal facies.184

Figure 8.9. Summary panel of the aeolian damp/wet interdune association of the Lemna Sandstone with an idealised log and photographs of the internal facies.185

Figure 8.10. Summary panel of the fluvial channel association of the Lemman Sandstone with an idealised log and photographs of the internal facies.	189
Figure 8.11. Summary panel of the fluvial sheet association of the Lemman Sandstone with an idealised log and photographs of the internal facies.	190
Figure 8.12. Summary panel of the overbank association of the Lemman Sandstone with an idealised log and photographs of the internal facies.	191
Figure 8.13. Summary panel of the lake margin association of the Lemman Sandstone with an idealised log and photographs of the internal facies.	193
Figure 8.14. Summary panel of the lake centre association of the Lemman Sandstone with an idealised log and photographs of the internal facies.	195
Figure 8.15. Summary panel of the ephemeral saline lake/mudflat association of the Lemman Sandstone with an idealised log and photographs of the internal facies.	196
Figure 8.16. Comparison of channel, fluvial sheet and aeolian set thicknesses from the Kayenta Formation and Lemman Sandstone including (A-F) Histogram plots of thicknesses and (G) Box and whisker plots illustrating the median, average, interquartile range and outliers.....	199
Figure 8.17. Comparison of sedimentary logs from the Kayenta Formation and Lemman Sandstone including photographs of key sedimentary structures.....	200
Figure 8.18. Large-scale depositional model of the Lemman Sandstone with two smaller-scale facies models depicting key sedimentary interactions. (A) Facies model depicting the sedimentary interactions between aeolian and lacustrine systems as the lake and saline mudflat expand into the dune field. (B) Facies model depicting the sedimentary interactions between aeolian and fluvial system as the rivers are confined down interdune corridors.....	201
Figure 9.1. Spatial distribution of architectural elements across proximal, medial and distal settings within Kayenta Formation, with three transects through logged localities. Fluvial channel and sheet-like elements remain fairly constant across the system, accretionary elements are most prevalent within the proximal and medial regions, whereas overbank elements are most prevalent within the distal region.	208
Figure 9.2. Palaeocurrent measurements of the fluvial sediment at each locality depicted by rose diagrams coloured by sediment source. The black arrows indicate the average palaeocurrent direction per locality along with the number of measurements and degree of dispersion per locality.....	212
Figure 9.3. Comparison of key characteristics of a distributive fluvial system. Triangles represent whether a key characteristic increases or decreases downstream and are coloured by similarities and differences in findings from previously published literature.	214
Figure 9.4. Block diagrams showing the most and least likely pathways through architectural elements and multiple scales, from facies-scale (top left) to element-scale (top right) and system-scale (bottom). Modified after Chandler et al., 1989.	219

List of Tables

Table 2.1. Facies scheme for fluvial systems from Miall (1978; 1996; 2010).	15
Table 2.2. Architectural element scheme developed by Miall (1978; 1985; 2010)	17
Table 2.3. Bounding surface hierarchical scheme (adapted from Brookfield; 1977; Allen, 1983; Miall, 1988; 1991; 2010).	20
Table 2.4. Common aeolian sedimentary structures, their process of formation and the architectural elements commonly associated with the sedimentary structure.	30
Table 2.5. Common aeolian architectural elements and their process of formation.....	32
Table 3.1. Sedimentary log metadata for the logs collected in this study. All coordinates from grid system UTM 12S. *location of photogrammetric models	50
Table 3.2. Sedimentary log metadata for the Leman Sandstone wells studied. *Log was excluded from data analysis due to poor recovery.....	52
Table 3.3. Summary of number of photographs and methods used for each outcrop, including the length and height, the number of points within the dense point cloud and the reconstruction error of each model. See Fig. 3.1 and Table 3.1 for locations.....	54
Table 4.1. Main facies identified in the Kayenta Formation in the eastern part of the Colorado Plateau (Modified after Miall, 1977; Miall, 1978; Bromley, 1991; Luttrell, 1993; North & Taylor, 1996).....	68
Table 4.2. Summary of the four main fluvial facies associations of the Kayenta Formation (Modified after Luttrell, 1993; Sanabria, 2001).	69
Table 4.3. Summary of lithofacies observed in the Kayenta Formation. Smbx : Sub-aerial planar cross-bedded sandstone, Smtxb : Sub-aerial trough cross-bedded sandstone, Smpb : Sub-aerial planar bedded sandstone, Smbw : Sub-aerial undulose laminated sandstone, Sm : Sub-aerial structureless sandstone, Sxb : Sub-aqueous planar cross-bedded sandstone, Stxb : Sub-aqueous trough cross-bedded sandstone, Slxb : Sub-aqueous low-angle cross-bedded sandstone, Spb : Sub-aqueous planar bedded sandstone, Spl : Sub-aqueous parallel laminated sandstone, Sfrl : Sub-aqueous cross-laminated sandstone, Smf : Sub-aqueous structureless sandstone, Sma : Sub-aqueous sigmoidal bedded sandstone, Srb : Sub-aqueous recumbent cross-bedded sandstone, Sfl : Sub-aqueous flaser laminated sandstone, Sssd : Sub-aqueous soft sediment deformed sandstone, Stpl : Sub-aqueous parallel laminated siltstone, Cms : Sub-aqueous matrix-supported conglomerate, Ccs : Sub-aqueous clast-supported conglomerate, Cru : Sub-aqueous rip-up clast conglomerate, Lm : Sub-aqueous siliciclastic-rich limestone.....	80
Table 7.1. Summary of average channel and sheetflood fluvial architectural element data including: 1D sedimentary log relative proportion and thickness data, 2D schematic panel thickness and width:depth data and 3D photogrammetric model relative proportion, width:depth ratios and thickness data. All based on 20 measurements each.	153
Table 8.1. Summary of lithofacies observed in the Leman and Silverpit Formations. Smbx : Sub-aerial planar cross-bedded sandstone, Smbxc : Sub-aerial planar cross-bedded sandstone couplets, Smtxb :	

Sub-aerial trough cross-bedded sandstone, **Smpb**: Sub-aerial planar bedded sandstone, **Smpl**: Sub-aerial planar laminated sandstone, **Smwr**: Sub-aerial ripple-cross-laminated sandstone, **Smbw**: Sub-aerial undulose laminated sandstone, **Sm**: Sub-aerial structureless sandstone, **Sxb**: Sub-aqueous planar cross-bedded sandstone, **Stxb**: Sub-aqueous trough cross-bedded sandstone, **Slix**: Sub-aqueous low-angle cross-bedded sandstone, **Spb**: Sub-aqueous planar bedded sandstone, **Spl**: Sub-aqueous parallel laminated sandstone, **Sfrl**: Sub-aqueous cross-laminated sandstone, **Smf**: Sub-aqueous structureless sandstone, **Stpl**: Sub-aqueous planar laminated mudstone/siltstone, **Cms**: Sub-aqueous matrix-supported conglomerate, **Ccs**: Sub-aqueous clast-supported conglomerate, **Ms**: Sub-aqueous structureless mudstone, **Sul**: Sub-aqueous undulose bedded sandstone, **Seb**: Sub-aqueous evaporitic bedded sandstone, **Steul**: Sub-aqueous evaporitic siltstone, **Sml**: Sub-aqueous structureless sandstone, **Spbl**: Sub-aqueous planar bedded sandstone, **Spil**: Sub-aqueous planar laminated siltstone, **Sxl**: Sub-aqueous cross-laminated sandstone. 176

Chapter 1: Introduction

Ancient dryland continental basins commonly comprise sedimentary fill that records the activity of both fluvial and aeolian environments. The preserved deposits from each individual environment have been studied in great depth and are relatively well constrained (*Fluvial*: Allen, 1965; Miall, 1978; 1985; 1988; 1996; 2010; Bromley, 1991; Luttrell, 1993; Stephens, 1994; Sanabria, 2001; Colombera *et al.*, 2013; *Aeolian*: Hunter, 1977; 1981; Kocurek, 1981; Kocurek & Neilson, 1986; Neilson & Kocurek, 1986; Fryberger *et al.*, 1988; Mountney, 2006), along with the sedimentary interactions between the deposits of coeval depositional systems, (e.g. Langford, 1989; Langford & Chan, 1989; Herries, 1993; Veiga *et al.*, 2002; Al-Masrahy & Mountney, 2015; Reis *et al.*, 2019; Formolo Ferronato *et al.*, 2019). In many cases, these relationships can be related to a cyclo-stratigraphical framework based upon a climatic control (Howell & Mountney, 1997; Mountney & Jagger, 2004; Hassan *et al.*, 2018; Soares *et al.*, 2018; Xu *et al.*, 2019).

Fluvial systems are typically classified by hydrological regime (e.g. ephemeral versus perennial), by planform morphology (e.g. braided or meandering) and by prevailing climatic regime (e.g. arid, semi-arid, sub-humid, per-humid) (Colombera *et al.*, 2013; Colombera & Mountney, 2019). The fluvial deposits within dryland settings are often ephemeral or perennial in nature, and can be influenced strongly by climate (Mather, 2007; Hooke, 2016) amongst a number of other factors.

Depositional facies models have long been used to aid our understanding of these sedimentary systems and processes by combining data from both ancient and modern systems (Reading, 1978, Walker, 1979; 1984). Recent advancements have focused on quantifying such models in terms of statistics pertaining to the physical dimensions and distributions of elements they contain, and therefore the distribution of sediments and sediment properties, at multiple scales (Colombera *et al.*, 2013; Colombera & Mountney, 2019), to provide valuable data for subsurface prediction (Walker, 1984; 2006).

However, despite detailed studies of ephemeral fluvial systems from within the rock record (e.g. Bromley, 1991; North & Taylor, 1996; Gulliford *et al.*, 2014; Bachmann & Wang, 2014; Lowe & Arnott, 2016; Bartz *et al.*, 2017; Horn *et al.*, 2018) and from present-day settings (e.g. Thomas *et al.*, 1997; Tooth, 2005; 2013; Sutfin *et al.*, 2014; Goudie & Viles, 2015; Jaeger *et al.*, 2017; Billi *et al.*, 2018; Carling & Leclair, 2019; Lima & Lupinacci, 2019; Colombera & Mountney, 2019), detailed three-dimensional facies models for ephemeral fluvial systems are appreciably fewer in number and are less developed compared to those of their meandering and braided fluvial counterparts. In particular, comparatively fewer models depict detailed lateral and vertical variations in architectural elements and the nature of interactions with sediments of competing and coeval dispositional systems compared to models for other fluvial settings. This is despite the fact that three-dimensional depositional models capable of illustrating the arrangement and interactions between depositional elements, along with the vertical and lateral connectivity of those elements, are particularly useful and important when searching for economic resources such as oil, gas, water and minerals.

Fluvial-aeolian environments constitute the main reservoirs in many oil and gas fields (North & Taylor, 1996), including the Leman Sandstone Formation of the Southern North Sea. Typically, the more geologically simple reservoir targets have already been exploited; however the inherent complexity within the zones of interactions between depositional systems, still have the potential for exploration. Thus, the need for a comprehensive knowledge of the interactions between coeval depositional environments is vital for the improved understanding and prediction of basin-scale fluid migration and reservoir characterisation.

Since direct observation of detailed three-dimensional facies architectures is not possible for subsurface hydrocarbon reservoirs, geological studies of outcrops in both modern and ancient environments, that are analogous to subsurface reservoir, are often used as a valued guide for the prediction of subsurface sedimentary architecture, connectivity and heterogeneity.

The analogue for this study focuses upon the Lower Jurassic Kayenta Formation that is exposed across the Colorado Plateau of southwestern USA. The Kayenta Formation comprises the middle lithostratigraphical unit of the Upper Triassic to Lower Jurassic Glen Canyon Group. The strata comprise a continental redbed assemblage of fine to coarse-grained sandstones, siltstones and occasional intraformational conglomerates (Harshbarger *et al.*, 1957; Peterson & Pippingos, 1979; Luttrell, 1993), deposited in a dominantly ephemeral-fluvial system, with minor perennial influxes and aeolian interactions. Deposition occurred upon a broad alluvial plain by a dominantly south-westward to westward flowing ephemeral fluvial system sourced from the Uncompahgre Uplift in the Ancestral Rocky Mountains (North & Taylor, 1996), supplemented by a north-westward flowing system sourced from the Mogollon Highlands in the Cordilleran Magmatic Arc (Luttrell, 1993; Hassan *et al.*, 2018). The sediments were deposited dominantly in channel-forms and sheets (Harshbarger *et al.*, 1957; Peterson & Pippingos, 1979; Bromley, 1991, Luttrell, 1993), and are typically described as a 'sandy' facies in south-eastern Utah and western Colorado and a 'silty' facies in north-western Arizona (Harshbarger *et al.*, 1957).

The resultant architectural element geometries and spatial variations within the sediments of the Kayenta Formation have been applied to a subsurface study of the Leman Sandstone of the Rotliegend Group of the Southern North Sea. The early Permian Leman Sandstone is composed almost entirely of strata of aeolian and fluvial origin. The fluvial sediments were deposited upon alluvial plains and floodplains by rivers flowing northwards from the Variscan highland, through an extensive aeolian dune field and towards the Silverpit desert palaeolake (Marie, 1975). The depositional models and architectural element geometries of the Kayenta Formation guide the interpretation and resultant depositional models of the Leman Sandstone, by adding the three-dimensional relationships that are often difficult to determine within subsurface studies.

1.1. Research aims and objectives

The overarching aim of this study is to develop a series of both small-scale and regional-scale models to better understand the processes that result in the sedimentary architecture and spatial variations of dryland fluvial systems and their competing coeval depositional environments. The models will be used to better understand the facies distributions, and geometry and interactions of associations within potential subsurface reservoir units. This body of work sets out to address the following three key aims:

- Aim 1: Identify and fully describe the sedimentology of a dryland ephemeral braided fluvial system and its competing coeval aeolian environment.
- Aim 2: Identify and quantify the regional spatial and temporal variations of the depositional system along with the interactions between the fluvial and aeolian environments.
- Aim 3: Apply findings to subsurface data of a similar depositional setting to better characterise architectural and geometrical relationships within potential reservoir units.

1.1.1. Aim 1: Outcrop sedimentology

This work will describe the sedimentology and depositional environmental interactions of dryland fluvial-aeolian systems using the Lower Jurassic Kayenta Formation of the Colorado Plateau, USA. It will critically evaluate the applicability of current sedimentary models for ephemeral fluvial systems to an ancient dryland fluvial example and demonstrate the impact of aeolian interactions upon sedimentary architecture of the preserved deposits.

Detailed sedimentary logging across the regional extent of the Kayenta Formation, utilising thorough sedimentological investigation of grain size, shape, sorting and mineralogy, is used to characterise the sedimentology of the deposits and is augmented by palaeocurrent measurements from both fluvial and aeolian structures. Facies analysis is applied to the data to identify depositional processes and

small-scale interactions between the competing environments. Facies are then grouped into architectural elements and depositional elements, allowing for identification of larger scale environmental interactions and reconstruction of past depositional settings.

Sedimentary logs are combined with digital outcrop models to examine and record in detail the spatial interactions, geometry and dimensions of architectural elements and facies distributions of the aeolian and ephemeral fluvial environments.

In order to achieve this first research aim, the specific research objectives are:

- Facies analysis of the Kayenta Formation from detailed sedimentological logging at 25 selected locations, spaced approximately 25 km apart over the expanse of the outcrop exposure.
- Interpretation of palaeocurrent trends on a regional scale from statistically significant quantities of palaeocurrent measurements of both the fluvial and aeolian strata.
- Interpretation and analysis of architectural element geobodies from digital outcrop models at key locations within the proximal, medial and distal regions of the fluvial depositional area.
- Development of three-dimensional depositional facies models using the detailed sedimentology from the sedimentary logs and mapped geobodies from the digital outcrop models.

1.1.2. Aim 2: Spatial and temporal variations

Analysis of the data derived from sedimentary logging and digital outcrop models across the Colorado Plateau is used to identify the spatial and temporal variations across the expanse of the Kayenta Formation to unravel the complex controls upon the sedimentology and provide insight into the trends in downstream spatial sedimentary architecture that may be attributable to dryland ephemeral fluvial systems.

Spatial variations in compositional characteristics including the thicknesses of fluvial and aeolian strata, the percentage of sand, the percentage of conglomerate, and the grain-size distribution of the fluvial sediments, are quantified. Analysis of spatial variations within the identified depositional elements, including the percentage of each depositional element per locality, and the average thickness and average grain size of each type of depositional element per locality, are also quantified.

Temporal variations within the system along with the interactions between the fluvial and aeolian settings are also examined using sedimentary logs and digital outcrop models.

In order to achieve this second research aim, the specific research objectives are:

- Interpretation of spatial variations of the fluvial system and fluvial depositional elements from downstream stream trends identified within the sedimentary logs and digital outcrop models.
- Interpretation of temporal variations within the depositional expanse of the Kayenta from channel body thicknesses identified within the sedimentary logs.
- Interpretation of the interactions between the fluvial and aeolian sediments at multiple scales.
- Development of three-dimensional depositional facies models using the detailed sedimentology from the sedimentary logs and mapped geobodies from the digital outcrop models along with the analysis of the spatial and temporal variations of the system.

1.1.3. Aim 3: Application

Outcrop data will be complemented with study of core from the Leman Sandstone of the Southern North Sea: a similar basinal setting. As before, facies and facies associations will be derived from core data allowing for comparison between the two different formations. From this, three-dimensional depositional models will be derived from the sedimentary logs and statistical analysis of the

photogrammetric models of the outcrop analogue is used to predict the likely size and frequency of the depositional elements.

In order to achieve this third research aim, the specific research objectives are:

- Facies analysis of the Leman Sandstone using detailed core logging of 20 carefully selected cores arranged within a grid pattern.
- Comparison of sedimentological analysis from the Kayenta Formation and Leman Sandstone to assess the suitability as an outcrop analogue for subsurface reservoir characterisation.
- Development of three-dimensional depositional facies models for the Leman Sandstone using the detailed sedimentological analysis of the core logs combined with the likely geometries, interactions and scales based upon analogue models.

1.2. Thesis overview

This section outlines the contents of each of the following chapters within this thesis. A summary of the current literature regarding fluvial and aeolian depositional processes and products along with the geological evolution of the outcrop analogue study area of the Colorado Plateau is provided in Chapter Two. The methods used within this study are detailed in Chapter Three. The deposits of the outcrop analogue of the Kayenta Formation are described and interpreted within Chapters Four and Five, and their spatial and temporal variations, along with their interactions with coeval aeolian deposits are described in Chapter Six. Chapter Seven brings together the work outlined in the previous chapters and combines digital outcrop models and modern analogues to build semi-quantified depositional models. The sedimentology of the subsurface study of the Leman Sandstone is described within Chapter Eight along with combining the geometrical measurements of the Kayenta Formation from Chapter Seven. Finally, the implications of this research are outlined in Chapter Nine and the conclusions and further work are summarised in Chapter Ten.

Chapter	Title	Description
2	Literature Review	<i>This chapter summarises the current literature on the depositional processes and products of fluvial systems and aeolian systems, with a specific focus on ephemeral fluvial deposits, as well as summarising the geological evolution and deposits of the outcrop analogue study area of the Colorado Plateau.</i>
3	Methods	<i>This chapter details the methods used for data collection and analysis. Sedimentological fieldwork combined with three-dimensional photogrammetry techniques were used to examine the detailed sedimentology, geometrical relationships of architectural elements and spatial variations of the Kayenta Formation. Core analysis was also conducted to examine the sedimentology of the Lemn Sandstone of the Southern North Sea.</i>
4	The Sedimentology of an Ephemeral Fluvial Outcrop Analogue: The Kayenta Formation	<i>This chapter describes the sedimentology of a dryland ephemeral fluvial system using the Lower Jurassic Kayenta Formation as an example. The chapter contains a summary literature review of the Kayenta Formation and its deposits before detailing the twenty-one facies observed. The facies are based principally on the lithological, sedimentary textures and structures present within them, and are grouped according to their depositional process, either: sub-aqueous or sub-aerial processes.</i>
5	Interpretation of the Sedimentology of an Ephemeral Fluvial Outcrop Analogue: The Kayenta Formation	<i>This chapter interprets the sedimentology of a dryland ephemeral fluvial system using the Lower Jurassic Kayenta Formation as an example. The chapter draws upon the observed facies described in Chapter Four and details nine architectural elements, five depositional elements and three depositional environments. The architectural elements contain multiple facies and are grouped by depositional environment, either: fluvial or aeolian. The depositional elements are grouped based upon the internal stacking patterns and composition of the architectural elements within them.</i>
6	Spatial and Temporal Variations of the Ephemeral	<i>This chapter analyses the spatial and temporal variations of the ephemeral fluvial system and in so doing, the work explores the controlling factors upon the sedimentology of such a system. The</i>

	Fluvial Kayenta Formation and their Interactions with a Competing Aeolian Environment	<i>sedimentary interactions between the dryland ephemeral fluvial system and the competing coeval aeolian depositional system are also analysed from the facies-scale reworking of aeolian sediment into the fluvial system, to the system-scale inter-tonguing of the aeolian Navajo Sandstone within the top third of the Kayenta.</i>
7	Digital Outcrop Models, Geobody Analysis and Reconstruction of Depositional Environments	<i>This chapter builds upon the sedimentology, and spatial and temporal variations of the Kayenta Formation in the previous chapters and combines them with quantified geobody data from three-dimensional digital outcrop models to build semi-quantitative facies and depositional models at multiple scales.</i>
8	Application of the Kayenta Formation to the Lemman Sandstone of the Southern North Sea	<i>This chapter details the sedimentology of the Lemman Sandstone and Silverpit Formations of the UK sector of the Southern North Sea and applies the geometrical measurements of architectural elements identified within the Kayenta Formation; a similar depositional setting, to aid in reservoir characterisation and build semi-quantified depositional models.</i>
9	Discussion	<i>This chapter discusses the inherent complexities when analysing dryland environments along with the limitations of qualitative to semi-quantitative models. This chapter also discusses the applicability of depositional models to subsurface datasets and the ability use outcrop datasets to help predict fluid-migration in the subsurface at multiple scales.</i>
10	Conclusions and Further Work	<i>The final chapter of the thesis presents the conclusions of the work and outlines further direction for not only the understanding of the Kayenta Formation and Lemman Sandstone but for dryland sedimentology, from a facies-scale to depositional system-scale.</i>

Chapter 2: Literature review

This chapter summarises the current literature on the depositional processes and products of fluvial systems and aeolian systems, with a specific focus on dryland ephemeral fluvial deposits, as well as summarising the geological evolution and deposits of the outcrop analogue study area of the Colorado Plateau.

2.1. Introduction

Many arid continental basins comprise a sedimentary fill that records the activity of both fluvial and aeolian environments. The preserved deposits from each individual environment have been studied in great depth, along with the sedimentary interactions between the deposits of coeval depositional systems (e.g. Langford, 1989; Langford & Chan, 1989; Herries, 1993; Veiga *et al.*, 2002; Al-Masrahy & Mountney, 2015; Reis *et al.*, 2019; Formolo Ferronato *et al.*, 2019), and in many cases, these relationships have been related to a cyclo-stratigraphical framework based upon a climatic control (Howell & Mountney, 1997; Mountney & Jagger, 2004; Hassan *et al.*, 2018; Soares *et al.*, 2018; Xu *et al.*, 2019). The interactions and relationships between these two systems can occur on a variety of scales; from grain to bed-scale interactions, and architectural element to system-scale intertonguing.

2.2. Fluvial transport, processes and products

2.2.1. Transport and depositional processes

In fluvial environments, there are two main mechanisms of sediment transportation: suspension and bedload (Fig. 2.1) (Martin, 2000; Collinson & Mountney, 2019). Suspension is the transport of sediment carried within the flow without coming into contact with the bed, where the sediment is supported by fluid turbulence (Diskin & Lane, 1972; Collinson *et al.*, 2006; Leeder, 2011; Collinson & Mountney, 2019). By contrast, bedload transportation occurs when the energy required to lift the sediment is

greater than the velocity of the flow, resulting in sediment being transported along the sediment-water interface (bed). Grains are transported along the interface by saltation, reptation, rolling or creep (Leeder, 1982; 2011; Collinson & Mountney, 2019). Saltation results from bouncing and collision of grains – ultimately transferring kinetic energy from particle to particle as they knock into each other (Perry & Taylor, 2007) – close to the bed surface during vigorous bedload movement (Collinson & Mountney, 2019). Reptation occurs when grains are too large/dense to be transported by saltation and are temporarily lifted off the bed, often as a result from impact of other grains, and hop short distances downstream (Collinson & Mountney, 2019). Creep occurs when the impact of other grains is not sufficient enough to cause reptation and results in grains being pushed short distances downstream along the bed (Collinson & Mountney, 2019).

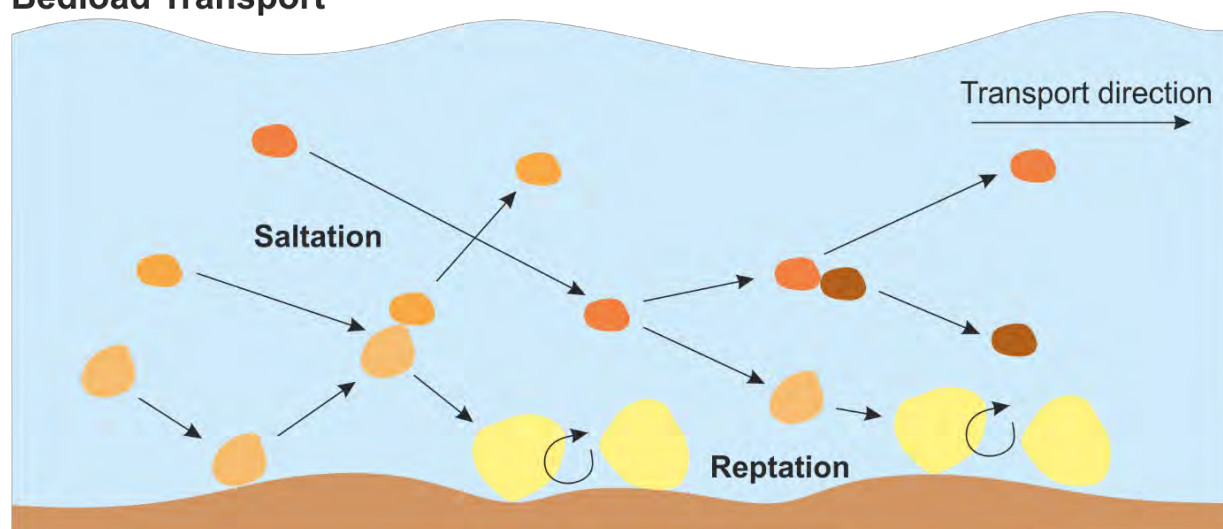
2.2.2. Fluvial bedforms and facies

Bedforms are produced as a result of sediment deposition and transportation, where the bedform type is dictated by the characteristics of the flow and the transportation of the sediment. The bedform phase diagram illustrates the type of bedforms generated from variations in flow velocity and grain size at a given depth and temperature (Fig. 2.2) (Guy *et al.*, 1966; Williams, 1970; Costello, 1974; Leeder, 1980; 1982; 1983; 2011; Mantz, 1980; Allen, 1982; Southard & Boguchwal, 1990; Ashley, 1990). Two general flow regimes are defined, the lower flow regime and upper flow regime conditions (Fig. 2.2) (Simons *et al.*, 1965).

Lower flow regime conditions are generated within a confined flow, with a Froude number less than 0.84 (Meyers, 2010). The resultant bedforms formed under these conditions are plane beds, ripples and dunes (Paola & Borgman, 1991). Ripples and dunes both form within a turbulent flow stimulated by an irregular bed surface (Tucker, 2001). Ripple-scale bedforms develop when eddy currents close to the bed surface are sufficient enough to entrain sediment into the flow but insufficient enough to disturb the rest of the water column or break through the surface of the confined flow (Fig. 2.3A) (Baas *et al.*, 1993; Baas, 1994; 1999; Leeder, 2011). Dune-scale bedforms develop when eddy currents close

to the bed surface are sufficient enough to disturb upper layers of the water column and cause turbulent 'boils' on the surface (Fig. 2.3B) (Simons *et al.*, 1961; Tjerry & Fredsøe, 2005; Best, 2005; Leeder, 2011). Both bedforms types form and migrate by bedload transport (dominantly saltation) of sediment up the stoss slope of the bedform before being deposited down the lee slope, creating a bedform foreset (Fig. 2.3C & D) (Simons *et al.*, 1961; Collinson *et al.*, 2006; Leeder, 2011). The transition from ripple-scale to dune-scale bedforms is marked by: (i) the wavelength and height of the bedform relative to flow depth; (ii) a grainsize increase, and; (iii) an increase in bedform migration and sediment transport rate (Simons *et al.* 1961; Mazumder, 2003; Lin & Venditti, 2013).

Bedload Transport



Suspension

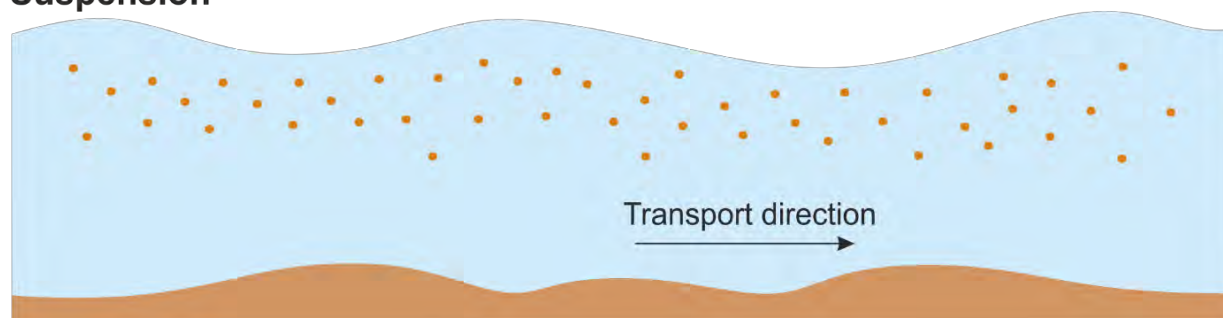


Figure 2.1. Two dominant transport mechanisms in fluvial systems; bedload transport - a combination of saltation and reptation of grains, and transport by suspension where the sediment is carried within in the flow without coming into contact with the bed. Modified after Collinson *et al.* (2006).

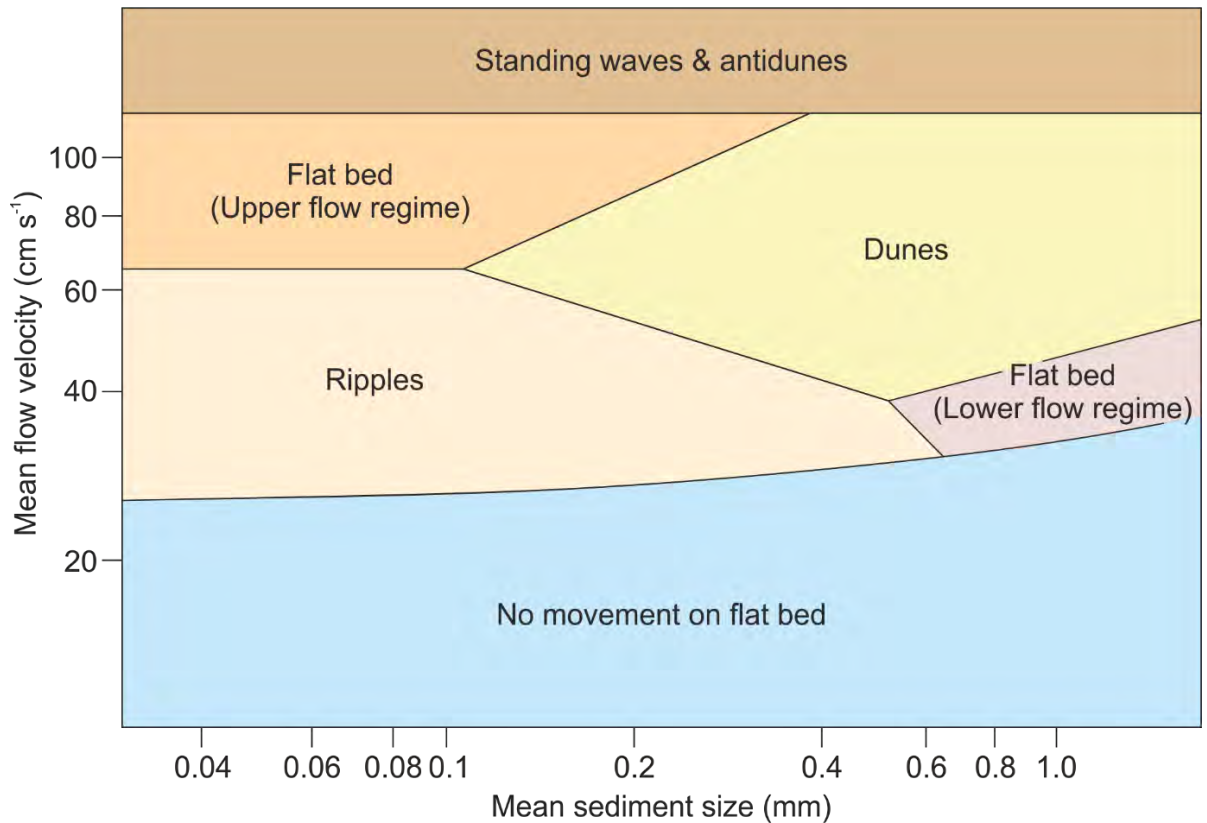


Figure 2.2. Phase diagram for bedforms produced by various grain sizes (mm) and mean flow velocities (cm s^{-1}) within a confined flow 20cm deep and at 10°C . Modified after Southard (1971), Ashley (1990), Leeder (1982; 2011), Hsu and Hanes (2004), Hsu et al., (2004) and Collinson et al. (2006).

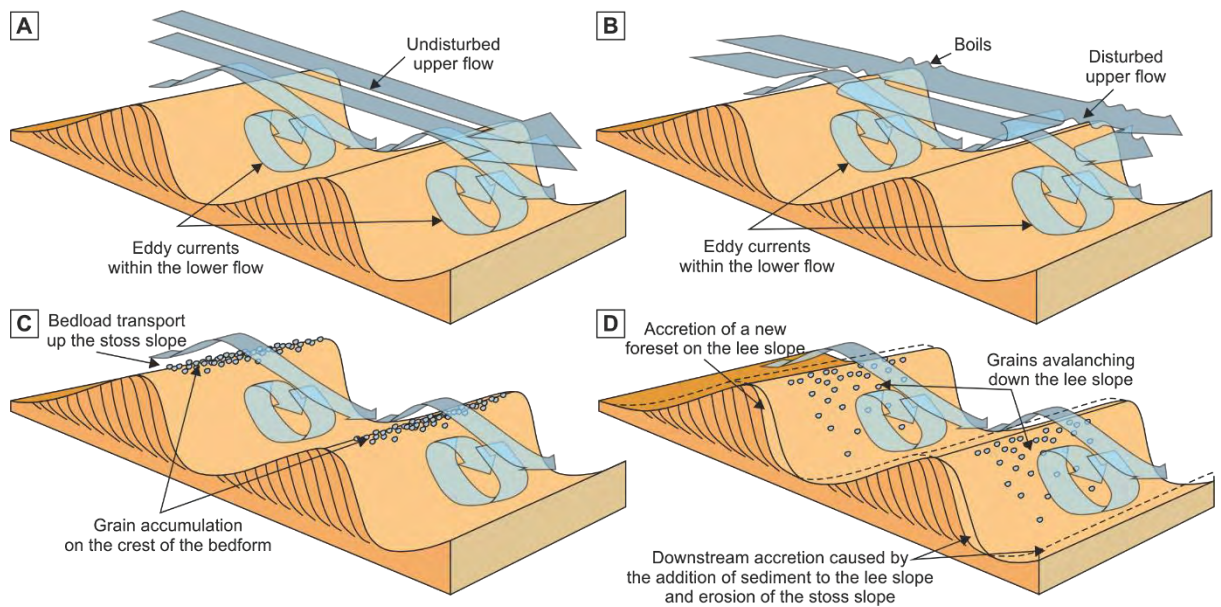


Figure 2.3. Schematic representation of ripple and dune-scale bedforms and the downstream migration of the bedforms. (A) Ripple-scale bedforms – where the upper flow is undisturbed, (B) Dune-scale bedforms – where the upper and lower flow is disturbed, creating boils in the upper flow, (C) Initial phase of bedform migration – where eddy currents form within the troughs of the bedforms and grains are transported up the stoss slope, (D) Second phase of bedform migration – where grains avalanche down the lee slope of the bedforms resulting in subsequent downstream accretion. Modified after Collinson et al. (2006) and Nichols (2009).

Upper flow regime plane beds are produced by high flow velocities and shallow water depths. High flow velocities along the lee slope of the bedform and a deceleration of flow within the trough, creates low amplitude and long wavelength bedforms (Leeder, 2011). Primary current lineations are common features of upper flow regime plane beds and can help distinguish between the plane beds of the lower flow regime. With increased flow velocities and Froude numbers greater than 1, antidunes are formed within supercritical flows. Antidunes were initially thought to form when standing waves break in the upstream direction depositing sediment on the stoss side of a developed dune-form to create bedforms that migrate upstream (Fig. 2.4A). The sediment deposited when a standing wave breaks is generally picked-up again within the turbulent flow (Kennedy, 1969). However, further study shows antidunes can also migrate downstream and remain stationary and aggrade (Fig. 2.4B) (Fielding, 2006).

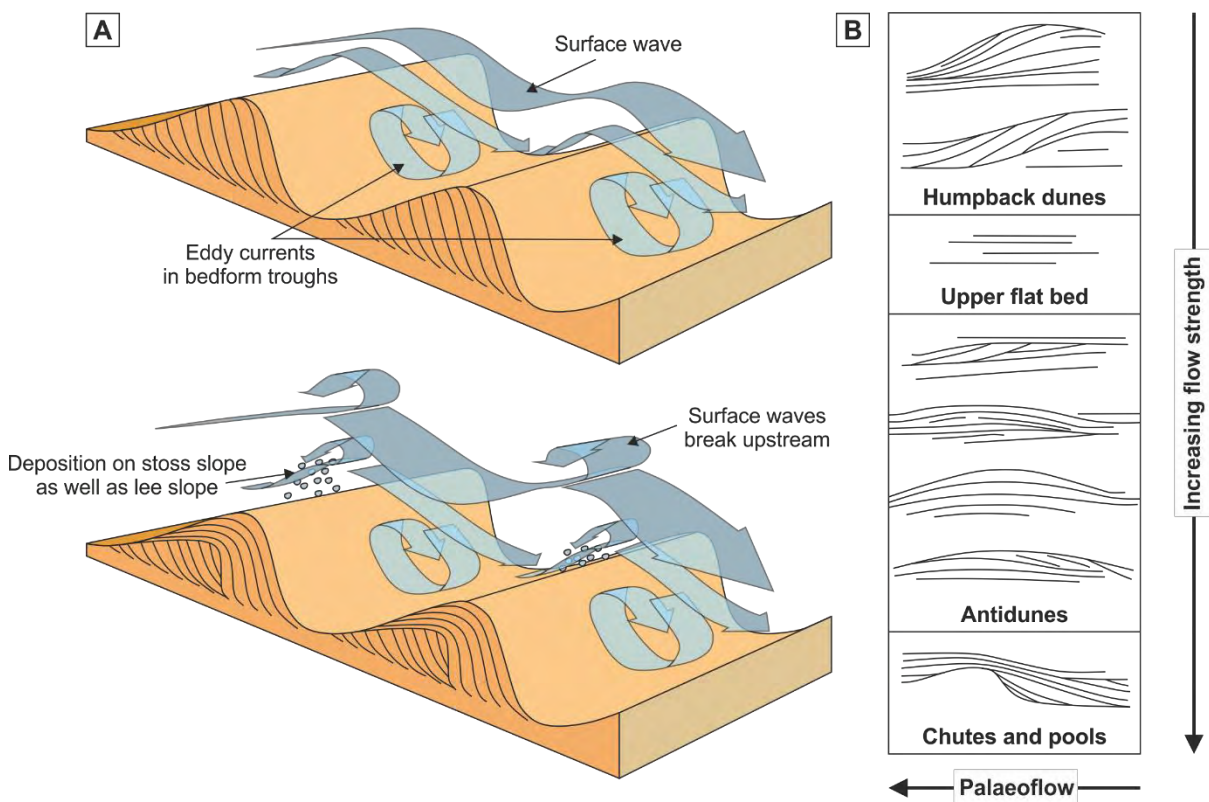


Figure 2.4. (A) Schematic representation of antidune migration formed when standing waves break in the upstream direction depositing sediment on the stoss slope, (B) Line drawings of the internal sedimentary structures of antidune from humpback dunes formed in the lower to upper flow regime transition to chutes and pools. Modified after Collison et al. (2006) and Fielding (2006).

For the lower and upper flow regime bedforms to be preserved, the bedforms must migrate and climb over the preceding bedform train. The angle of bedform climb is governed by the ratio of the rate of downstream bedform migration and the rate of aggradation of the bed of the flow. Consequently, bedforms climb at increasing angles with increasing sediment load. This process subsequently preserves the bedforms as sedimentary structures, which are used to develop lithofacies schemes to analyse the depositional environment. Lithofacies typically consist of the size, sorting, rounding and sphericity of individual grains within the sediment, coupled with larger scale observations of colour, sedimentary structures, and other post-depositional features. The lithofacies of fluvial systems have been studied in great depth, and as a result Miall (1996) developed a standardised facies scheme (Table 2.1).

Table 2.1. Facies scheme for fluvial systems from Miall (1978; 1996; 2010).

Code	Facies	Sedimentary Structures	Interpretation
Gmm	Matrix supported, gravel	Weak grading	Plastic debris flow
Gmg	Matrix supported gravel	Inverse to normal grading	Pseudoplastic debris flow
Gci	Clast supported gravel	Inverse grading	Clast rich debris flow or pseudoplastic debris flow
Gcm	Clast supported gravel	Structureless	Pseudoplastic debris flow
Gh	Clast supported, crudely bedded gravel	Horizontal bedding, imbrication	Longitudinal bedforms, lag deposits, sieve deposits
Gt	Gravel stratified	Trough cross-bedding	Minor channel fills
Gp	Gravel stratified	Planar cross-bedding	Transverse barforms, deltaic growths from older remnant bars
St	Sand, fine to very coarse, may be pebbly	Solitary or grouped trough cross-bedding	Sinuuous crested and lingoid dunes
Sp	Sand, fine to very coarse, may be pebbly	Solitary or grouped planar cross-bedding	Transverse and lingoid bedforms

Sr	Sand, very fine to coarse	Ripple-cross-lamination	Ripples
Sh	Sand, fine to very coarse, may be pebbly	Horizontal-lamination parting or streaming lamination	Plane bed flow
Sl	Sand, fine to very coarse, may be pebbly	Low angle (>15°) cross-bedding	Scour fills, humpback or wash-out dunes, antidunes
Ss	Sand, fine to very coarse, may be pebbly	Broad shallow scours	Scour fill
Sm	Sand, fine to coarse	Structureless to faint lamination	Sediment gravity flow deposits
Fl	Sand, silt, mud	Fine lamination, very fine ripples	Overbank, abandoned channel, waning flood deposits
Fsm	Silt, mud	Structureless	Backswamp, or abandoned channel
Fm	Mud, silt	Structureless, desiccation cracks	Overbank, abandoned channel, or drape deposits
Fr	Mud, silt	Massive, roots, bioturbation	Root bed, incipient soil
C	Coal, carbonaceous mud	Plant, mud films	Vegetated swamp deposits
P	Palaeosol carbonate	Pedogenic features: nodules, filaments	Soil with chemical precipitation

2.2.3. Fluvial architectural elements

Facies are most commonly grouped into architectural elements, such as, channels, barforms, sheets and floodplain. Architectural elements are defined as a component of a depositional system that is characterised by a distinctive facies assemblage, internal geometry and external form (Miall, 2010). Eight standardised architectural elements have been recognised within fluvial systems and are summarised in Table 2.2 (Miall, 1996). These elements represent the major geomorphological building blocks of any modern or ancient fluvial system, and the abundance, distribution and size of the

individual elements varies dependant on fluvial system, discharge regime and localised climate and tectonics.

Table 2.2. Architectural element scheme developed by Miall (1978; 1985; 2010)

Element	Symbol	Principle facies assemblage	Geometry and relationships
Channels	CH	Any combination	Finger, lens or sheet; concave-up erosional base; scale and shape highly variable; internal concave 3rd order erosion surfaces common
Gravel bars and bedforms	GB	Gm, Gp, Gt	Lens, blanket; usually tabular bodies; commonly interbedded with SB
Sandy bedforms	SB	St, Sp, Sh, Sl, Sr, Se, Ss	Lens, sheet, blanket, wedge, occurs as channel fills, crevasse splays, minor bars
Downstream-accretion macroforms	DA	St, Sp, Sh, Sl, Sr, Se, Ss	Lens resting on flat or channelised base, with convex up 3rd order internal erosion surfaces and upper 4th order bounding surfaces
Lateral-accretion macroforms	LA	St, Sp, Sh, Sl, Sr, Se, Ss, less commonly Gm, Gt, Gp	Wedge shaped, sheet, lobe; characterised by internal lateral accretion 3rd order surfaces
Scour hollows	HO	Gh, Gt, St, Sl	Scoop shaped hollow with asymmetric fill
Sediment gravity flows	SG	Gmm, Gmg, Gci, Gcm	Lobe, sheet, typically interbedded with GB
Laminated sand sheets	LS	Sh, Sl, minor Sp, Sr	Sheet, blanket
Overbank fines	FF	Fm, Fl	Thin to thick blankets commonly interbedded with SB; may fill abandoned channels

Channel-fill elements

Channel-fill elements can range in size from small-scale scour-and-fill events, with no macroform growth, to autocyclic-scale scours containing an intricate fill of bar complexes and small-scale channels (Miall, 1985). The channel-fill elements described within this thesis are representative of smaller scale scour-and-fill events, where a channel flow erodes down into the underlying sediment creating a concave-up erosional base, filled with a fining upwards facies succession as the flow wanes (Miall, 1985; Hornung & Aigner, 1999). Channels are bound by erosional basal fifth-order bounding surfaces commonly overlain by channel lag facies in the topographically lowest portion of the channel (Miall, 1993; Li *et al.*, 2015). The upper bounding surface is either gradational, grading from waning flow deposits of the channel into floodplain sedimentation, or erosional, due to subsequent channel scour events (Miall, 1985; 1993; McLaurin & Steel, 2007). The geometry and size of a channel fill is defined by its width-to-depth ratio (Miall, 1985; Gibling, 2006). The internal structure of the channels typically contains the deposits of isolated dunes or dune trains that stack and aggrade, filling the channel as the flow wanes (Miall, 1985; Ghazi & Mountney, 2009).

Sheet elements

Sheet-like elements are most commonly associated with ephemeral fluvial systems (Miall, 1985; North & Taylor, 1996). The elements are often dominated by parallel laminations deposited under upper flow regime plane bed conditions during flash floods (Miall, 1977, 1984; Rust, 1978; Tunbridge, 1981; 1984; Sneh, 1983). Sheets are bound by a flat to slightly scoured erosional basal bounding surfaces and gradational or erosional upper bounding surfaces dependent upon the presence of subsequent channel scour into the waning sheet fill (Tunbridge, 1981; 1984; Sneh, 1983; Miall, 1985).

Lateral accretion elements

Lateral accretion elements are most common at channel and barform margins and represent the sinuous migration of a fluvial system or the mature lateral growth of a compound barform (Bristow, 1995; Miall, 1996; Best *et al.*, 2003). The deposits form where the main flow in a channel is directed

away from the bank, i.e. the inside of the meander bend. Centrifugal forces lead to the development of a helical flow and a secondary current passing obliquely up the bed of the inner meander bend bank. The reduced shear stress associated with this current results in significant sedimentation on the inner bank causing the bank to accrete laterally at a high angle to the principal flow direction (Miall, 1985). Lateral accretion elements have an erosional basal bounding surface and either a gradational upper bounding surface, from waning flow, or erosional upper bounding surface from subsequent channel scour. The facies composition of these elements can be highly variable, and is dependant upon sediment load, discharge variability channel geometry (Miall, 1985; 1996), however, the element is usually dominated by sets and cosets of cross-bedded strata and gently dipping second-order bounding surfaces (Miall, 1985).

Downstream accretion elements

Downstream accretion elements are situated in the middle of channel reaches, where sediment supply and topographic variation is large enough to encourage bar development (Bristow, 1993; Miall, 1996). Downstream accretion elements represent the downstream growth of barforms, where the bar flanks undergo erosion (Krigstrom, 1962; Best *et al.*, 2003) and the growth of the barform is produced by the sporadic variations in discharge (Cant & Walker, 1978; Miall, 1996; Sambrook Smith *et al.*, 2006). These elements are dominated by the downstream migration and climb of dune forms over one another resulting in deposits dominantly composed of sets and cosets of cross-bedded strata. The barforms have internal second and third-order internal bounding surfaces that dip in the general downstream flow direction (Miall, 1993; 1994; Li *et al.*, 2015).

Floodplain elements

The floodplain represents an area of relatively flat land adjacent to a channel system. These elements typically have a tabular or sheet-like geometry, reflecting the aggradational nature of deposition (Miall, 1985). The geometry and thickness of floodplain elements and their relative importance in a fluvial succession are dependent upon multiple factors, including, sediment supply, channel pattern,

subsidence rate and channel migration/avulsion behaviour (Miall, 1985). Elements of this type are dominantly composed of laminated mudstones to fine-grained sandstones with minor cross-lamination (Miall, 1985). Several sub-environments are also recognised within these elements, such as, crevasse splays and chute channels (Miall, 1985).

2.2.4. Bounding surfaces

Bounding surfaces divide up sedimentary successions at multiple scales, ranging from foreset bounding surfaces to sequence boundary surfaces, and have specific genetic definitions dependent upon their rank (Table 2.3). The hierarchical order is dictated by the concordance and discordance of bounding surfaces relative to one another, the time scale they represent, and the lithofacies they bound (Fig. 2.5). A summary of fluvial bounding surfaces is provided in Table 2.3.

Table 2.3. Bounding surface hierarchical scheme (adapted from Brookfield; 1977; Allen, 1983; Miall, 1988; 1991; 2010).

Rank	Description	Time scale (yrs)
0 th order	Foreset bounding surface	10 ⁻⁶
1 st order	Cross-bed set bounding surface: little to no internal erosion, represents continuous sedimentation	10 ⁻⁵ -10 ⁻³
2 nd order	Coset bounding surface: change in flow conditions or direction with no significant break in time	10 ⁻² -10 ⁻¹
3 rd order	Cross-cutting erosional surfaces: low angle reactivation surfaces within macroforms	10 ⁻¹ -10 ¹
4 th order	Upper bounding surface of macroforms or basal scour surface of minor channels	10 ¹ -10 ³
5 th order	Bounding surfaces of major sand bodies such as channel-fill complexes	10 ³ -10 ⁴
6 th order	Mappable stratigraphic units, lithostratigraphic members or sub-members	10 ⁴ -10 ⁵
7 th order	Bounding surfaces of major lithosomes produced by allogenic processes, e.g. 4 th order Milankovitch cycle	10 ⁵ -10 ⁶
8 th order	Regional disconformities produced by continental or global scale allogenic events, e.g. 3 rd order Milankovitch cycle	10 ⁶ -10 ⁷

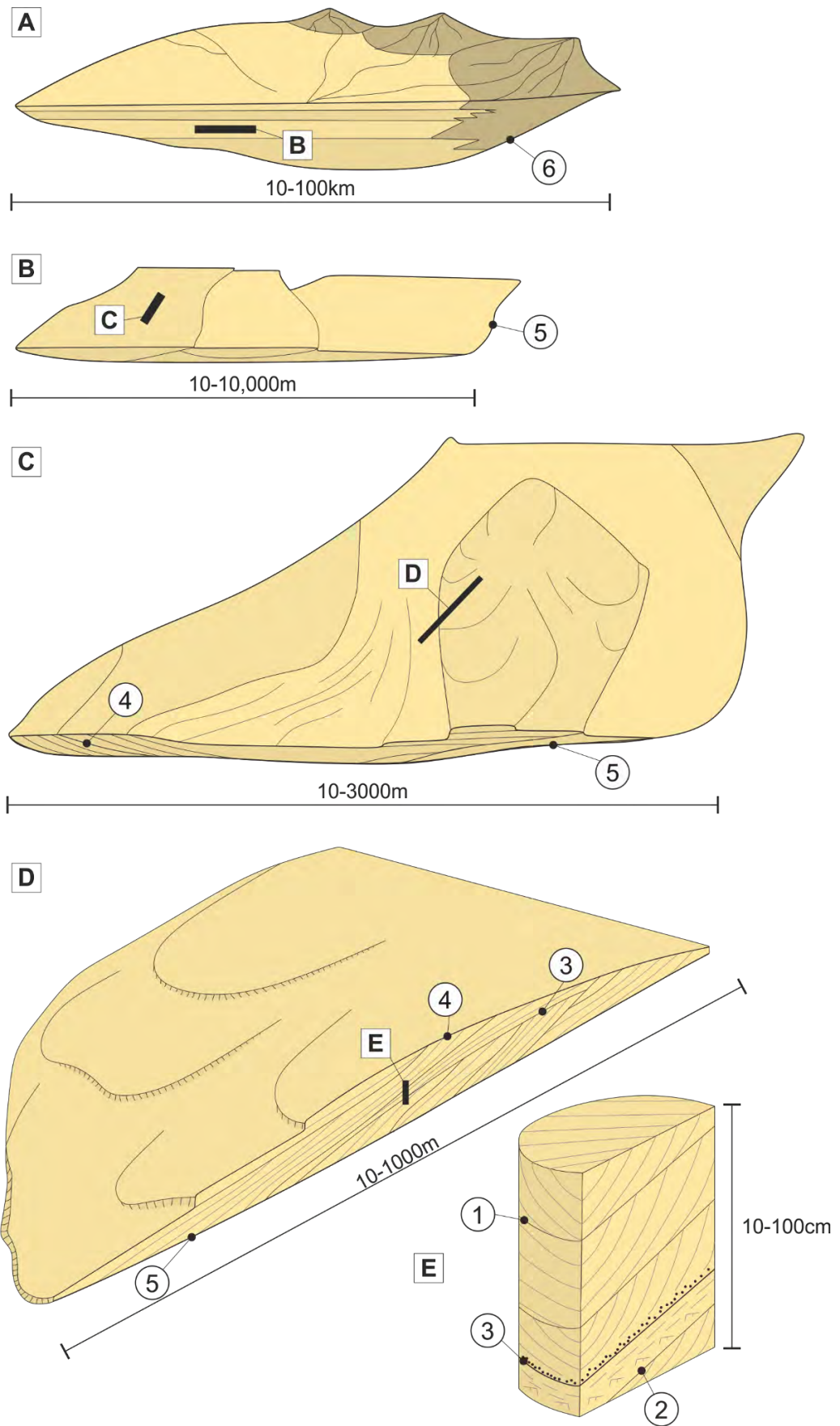


Figure 2.5. Bounding surface hierarchy within a fluvial system, numbers correlate to the bounding surfaces shown in Table 2.3. Modified after Miall (2010).

2.3. Fluvial styles

Fluvial style is governed by a multitude of autogenic and allogenic controls, these controls dictate the formation of architectural elements and the mode of transportation. Architectural element analysis is used to understand the nature and style of a fluvial system in three-dimensions. This review will now focus on the deposits of ephemeral fluvial systems and elaborate upon the two ephemeral fluvial models proposed by Miall (1985); the “distal braidplain”, dominated by sandy bedform (SB) elements and the “sheetflood fluvial plain”, dominated by laminated sand sheet (LS) elements (Fig. 2.6).

2.3.1. Ephemeral fluvial systems

Fluvial systems in dryland settings are commonly ephemeral in nature and are typically characterised by seasonal to strongly intermittent discharge (Mabutt, 1977; Tunbridge, 1984; Horn *et al.*, 2018; Billi *et al.*, 2018) as a result of seasonal and longer-term climatic variations in rainfall (Mather, 2007; Hooke, 2016; Billi *et al.*, 2018).

Transport and depositional processes

The nature of flow in ephemeral systems is largely non-Newtonian, where the shear stress and shear rate are not linear. This is largely a result of high sediment load. Periodically high concentrations of sediment result in non-Newtonian to pseudo-plastic flows, both channel-confined and unconfined in nature, that deposit dominantly structureless debris flows (Reid & Laronne, 1995; Tooth, 2000; Billi, 2011; Miall, 2013). The sediment deposited has a bimodal grain-size distribution, with a dominance of fine-grained mud/silt and coarser sediment that ranges from very coarse-grained sand to large pebbles (Dreyer, 1993; Reid *et al.*, 1995; Billi, 2007). The conglomeratic sediment is typically poorly sorted, sub-angular to sub-rounded, contains both intra-formational and extra-formational clasts, and ranges from matrix to clast supported (Dreyer, 1993; Batezelli *et al.*, 2019).

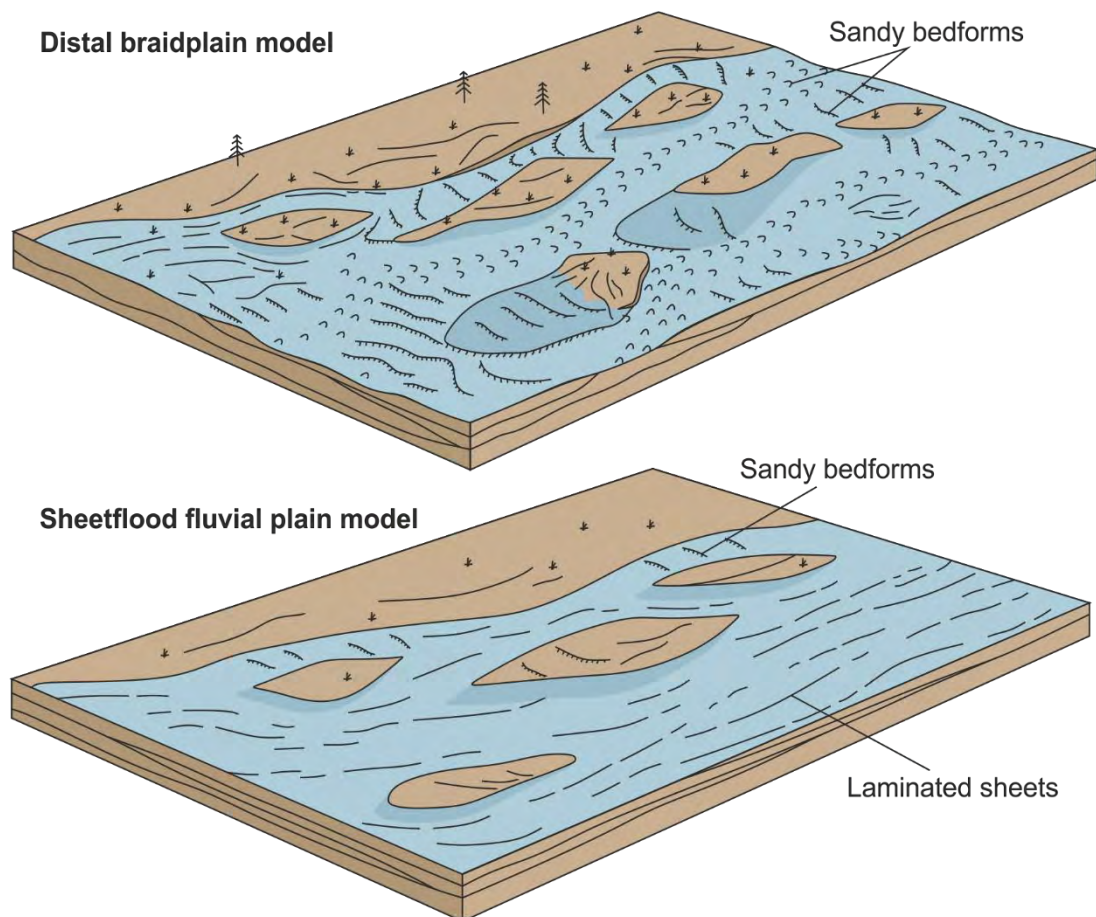


Figure 2.6. Depositional models of typical ephemeral fluvial systems. The distal braidplain model is dominated by sandy bedforms and deposits from ephemeral discharge. The sheetflood fluvial plain model is dominated by laminated sheets and deposits from highly flashy discharge. Modified after Miall (1985).

The nature of flow within ephemeral systems is highly variable. With normal sediment concentrations, bedload is the dominant method of transportation in ephemeral rivers due to the high energy nature of the system (Reid & Laronne, 1995). In addition to cross-strata produced by Newtonian subcritical flows that are typical of many fluvial systems, non-Newtonian flows tend to generate unconfined sheet-like deposits that display sedimentary textures and structures typical of a high sediment load (Picard & High, 1973; Jaeger *et al.*, 2017), such as structureless sandstones (Horn *et al.*, 2018). Periods of supercritical Newtonian flow result in antidune cross strata and upper flow regime plane beds (Long, 2006; 2011; Fielding, 2006), along with some rarer features such as recumbent cross-bedding (Allen & Banks, 1972) and mudballs (Karcz, 1972; Foley, 1978; Bachmann & Wang, 2014). These features are typically described as the product of intermediate to high discharge variance (Fielding *et al.*, 2018).

Rapid variations in both discharge and sediment load promote preservation of these features by comparison to non-ephemeral systems where they are typically reworked into lower flow regime structures as the flow wanes.

Architecture

The fluvial architecture typically comprises sand-bodies representative of sheet-like and channelised elements with high width-to-depth ratios (Williams, 1971; Tunbridge, 1984; Sutfin *et al.*, 2014; Al-Masrahy & Mountney, 2015), which decrease in size downstream and preserve the sedimentary evidence to indicate a progressive downstream decrease in discharge (Babcock & Cushing, 1941; Cornish, 1961; Lane *et al.*, 1971; Mabutt, 1977; Tunbridge, 1984, Sutfin *et al.*, 2014). This is a result of substantial transmission losses due to high rates of evapotranspiration and infiltration into the surrounding dry substrate (Tooth, 2000; Sutfin *et al.*, 2014). The fluvial architecture of these systems varies significantly downstream, with proximal regions characterised by highly amalgamated channels and sheets, and distal regions dominantly characterised by laterally extensive sheet and overbank deposits (Cain & Mountney, 2009; 2011; Hartley *et al.*, 2010; Weissmann *et al.*, 2010; 2013; Owen *et al.*, 2015; Coronel *et al.*, 2020). The expected geometries associated with ephemeral systems are very reliant on the relationship between high magnitude: low frequency events. Channels are usually wide in geometry, as a result large multiple terraces can be seen in outcrop. More frequent, lower magnitude events incise into these terraces, resulting in smaller terraces cutting into the more laterally extensive terraces related to higher magnitude events (Wolman & Gerson, 1978; Mather *et al.*, 2008).

Depositional systems

Many sandy ephemeral fluvial systems are endorheic and terminate within muddy flood plains or ephemeral lakes (Tunbridge, 1981; 1984; Coronel *et al.*, 2020), similar to that of terminal fluvial fans (Nichols, 1987; 1989; Hampton & Horton, 2007; Nichols & Fisher, 2007; Fisher *et al.*, 2007; 2008; Cain & Mountney, 2009; Gulliford *et al.*, 2014; Coronel *et al.*, 2020) and in some distributive fluvial systems more generally (Hartley *et al.*, 2010; Weissmann *et al.*, 2010; 2013; Owen *et al.*, 2015).

The preserved deposits of these systems tend to exhibit the following downstream trends: (i) increased dispersal of palaeocurrent directions due to radiating channel patterns from an apex (Owen *et al.*, 2015), (ii) a decrease in modal grain size due to reduced fluvial discharge with an increase in the proportion of floodplain deposits (Weissmann *et al.*, 2010; 2013; Owen *et al.*, 2015), (iii) a decrease in channel element width-to-depth ratios due to channel bifurcation and high rates of infiltration and evapotranspiration into the dry substrate (Horton & DeCelles, 2001; Nichols & Fisher, 2007; Weissmann *et al.*, 2010; 2013; Davidson *et al.*, 2013; Ventra & Clarke, 2018), and (iv) a decrease in channel element confinement due to a lack of lateral constraints on channel mobility (Weissmann *et al.*, 2013; Terwisscha van Scheltinga *et al.*, 2020). Whilst the individual characteristics of this model, when taken in isolation, are true for many types of fluvial system (Sambrook Smith *et al.*, 2010), a combination of all these characteristics forms a strong basis for an interpretation of the system as an ancient dryland DFS (Terwisscha van Scheltinga *et al.*, 2020).

2.4. Aeolian transport, processes and products

2.4.1. Transport and depositional processes

Aeolian processes occur when there is a supply of granular material and winds with sufficient strength to move them. The volume of sediment transported in aeolian environments depends on several factors: the availability of suitably sized sediment, the source rock geology and geography, and the transport capacity of wind (Bagnold, 1941). The transportation of granules by wind is a strong erosional force; and can be quantified by the shear velocity, which is directly proportional to the rate of increase of velocity (Yaalon, 1990). The ability to erode the shear surface is related to threshold shear velocity, which largely depends on the vegetation and soil of the surface (Ravi *et al.*, 2004).

There are three different modes of aeolian transport: saltation, reptation and suspension, which primarily depend on the grain size of the available sediment (Fig. 2.7) (Bagnold, 1941). Particles approximately <20-70 μm are transported in suspension and can be kept suspended for relatively long distances by turbulent eddies in the wind. Suspension occurs where Stoke's settling velocity is less than

the vertical component of the wind velocity during turbulent flow. Larger particles between 70-500 μm are transported downwind by saltation, which involves the collision of particles with each other within the air. For saltation to occur Stoke's settling velocity needs to be more than the vertical component of the wind velocity. Reptation occurs when the impact of saltating particles with the surface causes short-distance movement of adjacent grains. Large particles ($>500 \mu\text{m}$) may also be pushed or rolled along the surface by the impact of saltating grains (Ungar & Haff, 1987; Lancaster & Nickling, 1994). Deposition occurs when wind velocity drops below the threshold required for keeping particles suspended, or when there is not enough energy to move particles by saltation or reptation.

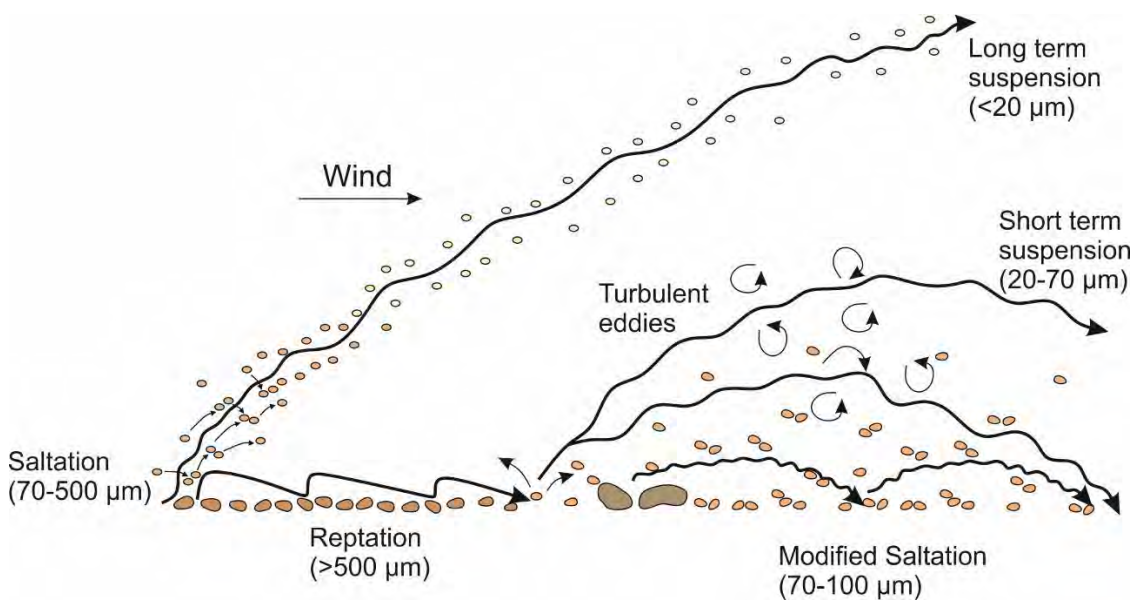


Figure 2.7. Various modes of aeolian transport, governed primarily by grain size. Particles approximately $<20-70 \mu\text{m}$ are transported in suspension, larger particles between $70-500 \mu\text{m}$ move downwind by saltation and particles greater than $500 \mu\text{m}$ are transported by reptation. Modified after Nickling and McKenna Neuman (2009).

2.4.2. Aeolian bedforms

Aeolian bedforms range in size from grain-scale ripples ($< 1\text{mm}$ in height) to large-scale draa (> 100 metres in height), primarily dependent on sediment supply (Wilson, 1972).

Aeolian ripples form under different conditions compared to subaqueous ripples and can be distinguished by their characteristic inverse grading. Aeolian ripples form when saltating grains collide obliquely onto a sand bed, generating a small depression on the surface, which then develop a chain

of rough, small-scale undulations, with a gently dipping stoss slope and a more steeply dipping lee slope, known as the “shadow zone” (Fig. 2.8) (Kok *et al.*, 2012; Leeder, 2012). Grain collisions, as a result of saltation, dominantly occur on the stoss slope, due to the grains within the shadow zones being shielded. The collisions on the stoss slope from saltating grains cause the reptation of larger grains over the finer grained sediment (Leeder, 2012). Due to saltation impacts on the stoss side and minimal lee side grain avalanches, there is no clear internal structure of cross-lamination in aeolian ripples (Leeder, 2012).

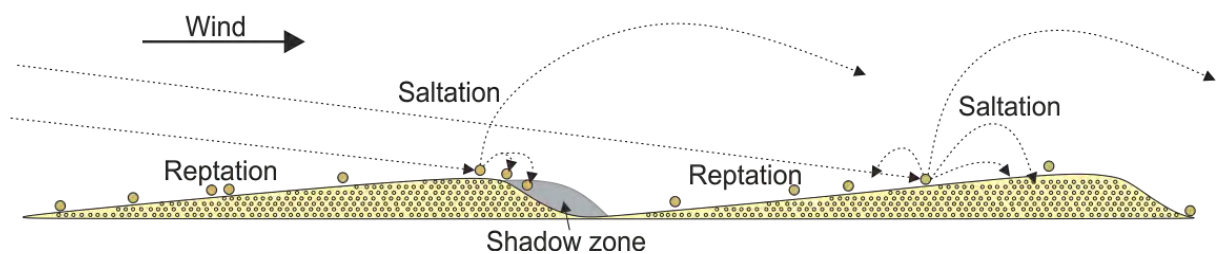


Figure 2.8. Formation of aeolian ripples by saltating sand grains. Note the finer grained core of the ripples. Modified after Durán *et al.* (2011).

Dunes and draa are created by interactions between granular material (sand) and shearing flow (the atmospheric boundary layer) (Lancaster, 2005). Dunes and draa cause a disruption to the wind/flow velocity, as sand particles are transported up the stoss slope by saltation and reptation (Fig. 2.9), the flow becomes compressed and accelerates, thus increasing the transportation rate up the stoss slope. Once the flow reaches the crest of the dune, it expands into the open space on the lee slope, which decreases the velocity, allowing particles to fall out of suspension, by a process known as grainfall (Fig. 2.9). As a dune grows, the sand accumulates at its crest, and when the angle of repose (32-34°) is surpassed, the dune crestline becomes unstable, resulting in sediment avalanching down the lee slope, by a process known as grainflow (Fig. 2.9). This results in the formation of a slip face and internal reverse grading of a foreset (Kok *et al.*, 2012).

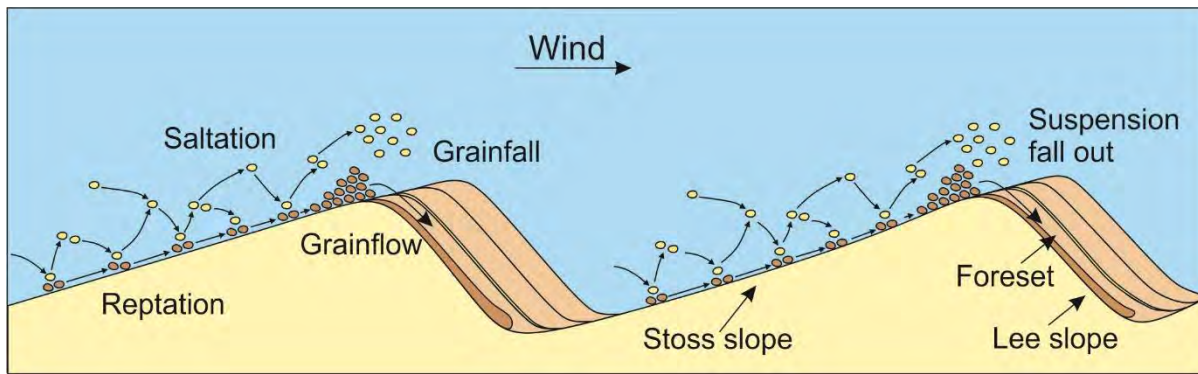


Figure 2.9. The transport mechanisms for dune and draa formation. Modified after Miall (1978).

Draa-scale bedforms can be divided into three categories (Mckee, 1979):

- **Simple dunes/draa:** individual dune forms which are spatially separate from nearby dunes and lack superimposition of bedforms.
- **Compound dunes/draa:** two or more dunes of the same type which have coalesced or are superimposed.
- **Complex dunes/draa:** two or more different types of simple dunes which have coalesced or are superimposed.

2.4.3. Bedform morphology

Dune and draa-scale bedforms can be classified further depending on their morphology, which is based upon the number of lee faces and the orientation of the crestlines relative to the dominant wind direction (Fig. 2.10) (Collinson *et al.*, 2006).

Wind direction and volume of sediment available for transport are the dominant controlling factors of aeolian bedform shape (Wasson & Hyde, 1983). Barchan and parabolic dunes are examples of isolated three-dimensional bedforms formed by unidirectional flow and fairly low sediment supply, and are most likely situated in an erg margin setting (Kok *et al.*, 2012). Two-dimensional bedforms also form in unidirectional flow but higher sediment supply conditions. The bedforms have straight crestlines and are usually classified into 3 types: transverse, which have a crestline perpendicular to the predominant wind direction; longitudinal, which have a crestline parallel to the wind direction; and oblique, where the crestline is neither parallel or perpendicular, but it is a mixture of the two (Fig. 2.10) (Collinson *et*

al., 2006). Three-dimensional bedforms have sinuous crestlines and generally represent a higher sediment supply, for example, barchanoid bedforms, which have a crestline perpendicular to the predominant wind direction, with the sinuosity of the successive bedform either being in phase or out of phase (Fig. 2.10). Seif bedforms are examples of longitudinal three-dimensional bedforms which form parallel to the dominant transport direction (Fig. 2.10) (Collinson *et al.*, 2006). Star and dome bedforms have multiple slip faces radiating from a central peak as a result of several wind directions (Fig. 2.10) (Lancaster, 1989).

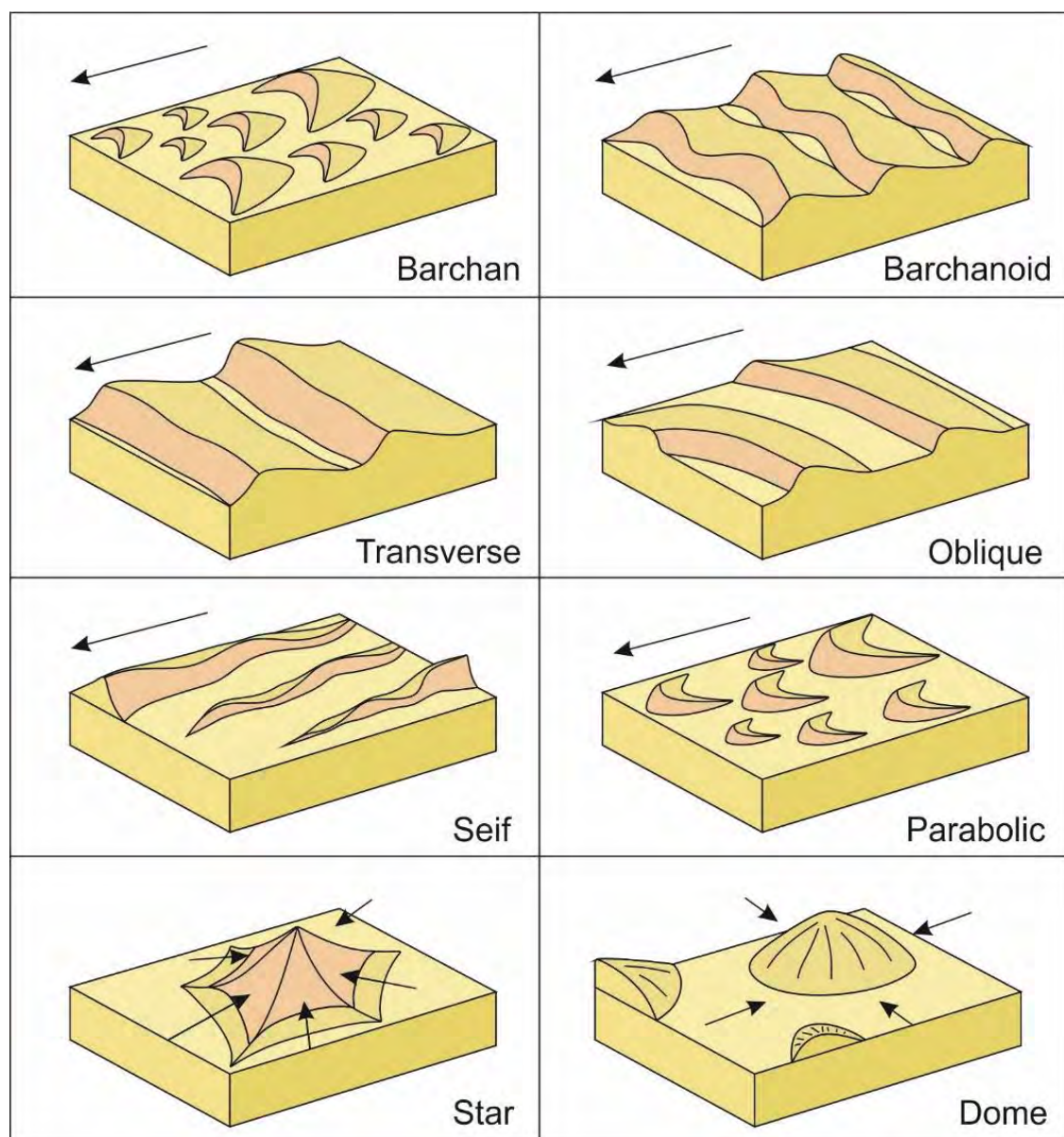


Figure 2.10. Three dimensional forms of common aeolian dune/draa morphologies. The arrows mark the dominant wind direction. Modified after Collinson *et al.* (2006).

2.4.4. Sedimentary structures

Similar to fluvial systems, bedforms must climb to preserve any sedimentary structures. A summary of common aeolian sedimentary structures and the process in which they are formed is provided in Table 2.4 and Figure 2.11.

Table 2.4. Common aeolian sedimentary structures, their process of formation and the architectural elements commonly associated with the sedimentary structure.

Sedimentary structure	Process	Architectural element	References
Wind ripples	Saltation of fine-grained sand, then reptation of coarser grains over the accumulated grains, leading to inverse grading and no cross-lamination. Preserved as pinstripe laminae	Sandsheets, dry interdunes, low relief dunes/draa	Sharp, 1963; Fryberger <i>et al.</i> , 1988; Collinson <i>et al.</i> , 2006
Grainfall	Particles fall out of suspension onto the upper lee slope due to the reduction in wind transport capacity as the wind carries saltating grains over the lee side of a dune.	Dunes/draa	Walker & Nickling, 2002; Mountney, 2006
Grainflow	Avalanche of particles down the lee slope when angles of 34° (angle of repose) are exceeded. Resulting in reverse grading.	Dunes/draa	Howell & Mountney, 2001; Mountney, 2006
Cross-bedding	Continual and repetitive sedimentation on the lee slope of aeolian dunes due to grainfall and grainflow processes.	Dunes/draa	Mountney, 2006
Plane bed stratification	Saltation and reptation of wind-blown sand, where the angle of repose is never reached.	Low angle dunes/draa, sandsheets	Collinson <i>et al.</i> , 2006
Soft sediment deformation	Small-scale: Intradunal folding caused by near surface liquefaction or slumping of moist lee slope. Large-scale: liquefaction below the water table due to loading of saturated sand by an advancing dune.	Dunes/draa, interdunes	Doe and Dott, 1980; Mckee <i>et al.</i> , 1971, Collinson, 1994, Horowitz, 1982, Mountney, 2006

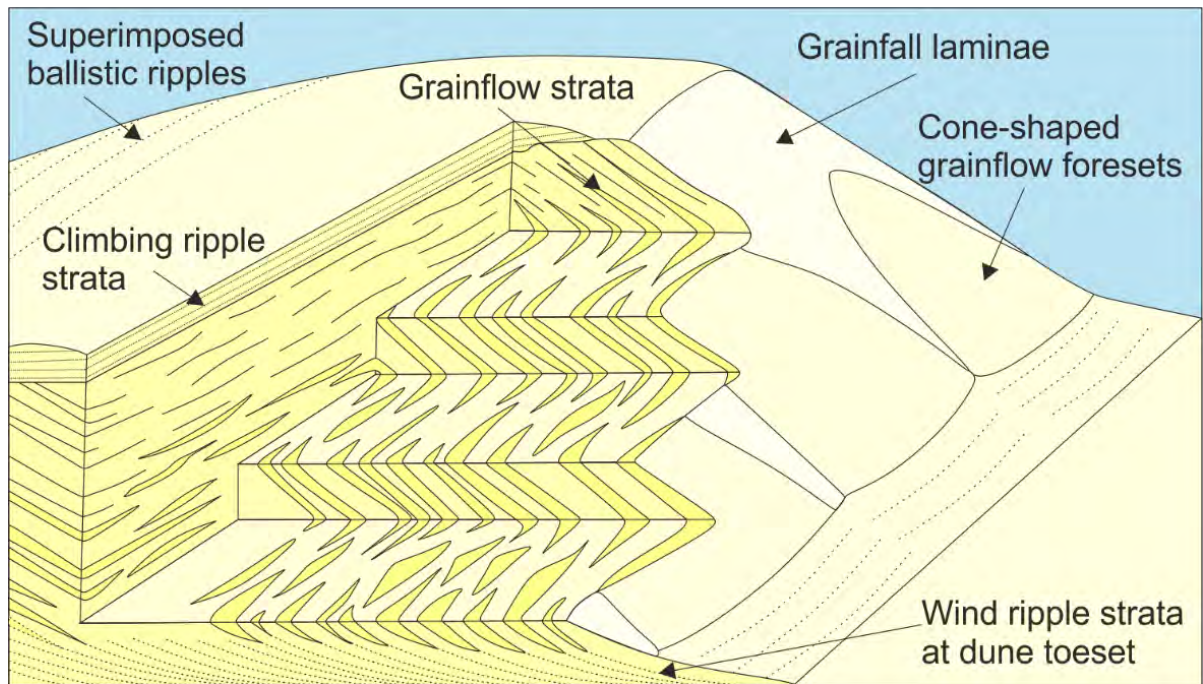


Figure 2.11. Schematic diagram of the common small-scale stratification types present in aeolian dunes and draa. Modified after Hunter (1977) and Cain (2009).

Non-aeolian features are also common in aeolian systems and result from physical, chemical and biological processes. Physical features include desiccation cracks, raindrop imprints, current ripples, cross-strata and wavy laminations formed from interactions with water, either from fluvial systems or elevated groundwater levels (Ahlbrandt *et al.*, 1978; Langford, 1989; Langford & Chan, 1989). Chemical features include evaporitic crusts, tepee structures, pseudomorphs and fenestral porosity (Kocurek, 1981; Mountney, 2006). Biogenic features include trackways, burrows, root structures and rhizoliths and algae growths (Ahlbrandt *et al.*, 1978; Loope, 1988; Hasiotis, 2007). Palaeosols are also common deposits within desert systems, formed from the modification of previous deposits (Kocurek *et al.*, 1991; Mountney, 2006).

2.4.5. Aeolian architectural elements

Three main architectural elements are identified within aeolian systems; dunes, interdunes and sandsheets. Interdunes can be further subdivided into dry, damp and wet interdunes dependent on

the sedimentary structures present. The aeolian architectural elements and their process of formation are summarised in Table 2.5.

Table 2.5. Common aeolian architectural elements and their process of formation.

Architectural element	Process	Structures	References
Dune	Migration of sediment up the stoss slope by reptation and saltation, deposition on the lee slope by grainfall or grain flow.	Grainfall, grainflow, wind ripples	Collinson <i>et al.</i> , 2006
Dry Interdune	No influence from the water table.	Grainfall deposits, wind ripples	Hunter, 1977; Mountney, 2006
Damp Interdune	Depositional surface in contact of the capillary fringe of the water table, restriction of sediment for aeolian transport.	Adhesion warts and ripples, possible roots, burrows & traces	Ahlbrandt & Fryberger, 1981; Kocurek, 1981; Ahlbrandt <i>et al.</i> , 1978; Loope, 1988; Hasiotis, 2002
Wet Interdune	Water table at or above the depositional surface resulting in flooding of the interdune	Wave ripple laminations, desiccation cracks, mud curls, roots, limestones	Driese, 1985; Kocurek, 1981; Doe & Dott, 1980; Fryberger, 1990
Sandsheet	Inhibited dune development due to: lack of sediment supply due to high water table, lack of time available due to periodic flooding, coarse sediment or presence of vegetation	Low angle stratification, wind ripples	Nielson & Kocurek, 1986; Kocurek & Nielson, 1986; Kocurek, 1996

2.4.6. Aeolian bounding surfaces

Bounding surfaces are erosional surfaces that truncate aeolian cross strata and depict cross-cutting relationships between different scale bedforms (Brookfield, 1977). There are multiple types of bounding surfaces, distinguishable by their shape, orientation relative to the cross-strata they truncate, lateral extent and relationships to each other. Similar to fluvial systems, a numbered hierarchical system is applied (Kocurek, 1996). The four most common bounding surfaces, ranked in descending order are; supersurfaces, interdune migration surfaces (1st order), superimposition surfaces (2nd order) and reactivation surfaces (3rd order).

Supersurfaces are major stratigraphic surfaces that extend over tens of kilometres through an erg (Miall, 2016). The supersurface delineates a bounding discontinuity which can be used to place aeolian deposits within the context of allostratigraphy and sequence stratigraphy (Brookfield, 1992), however, these surfaces may only consist of a very thin, coarser grained lag which can be difficult to detect (Brookfield, 1992).

Interdune migration surfaces are near horizontal bedding planes cutting across all underlying aeolian structures and are attributed to the migration of the dunes.

Superimposition surfaces are planar to highly scallop-shaped and have a large range of dip orientations. These surfaces are attributed to the migration of one dune over another dune, often occurring without erosion into the underlying dune. (Collinson *et al.*, 2006).

Reactivation surfaces are planar to scallop-shaped and are formed by slight changes in the dominant wind direction or sediment supply. They predominantly dip down wind, with inclinations less than that of the cross-strata they truncate and can be traced over short distances (metres) (Collinson *et al.*, 2006).

2.5. Geological setting of outcrop study area

The following section summarises the literature regarding the geological history of the outcrop analogue study area of the Colorado Plateau, south-western USA, with particular focus on the Upper Triassic to Lower Jurassic age Glen Canyon Group. A further, more detailed literature review summarising the outcrop analogue formation is provided in Chapter Four.

The Colorado Plateau is a large high-standing block, approximately two-thousand metres above sea level, which spans approximately three-hundred and eighty-thousand square kilometres across south-eastern Utah, north-eastern Arizona, south-western Colorado and north-western New Mexico (Gilfillan *et al.*, 2008). The Uinta and Rocky Mountains define the northern and north-eastern boundaries, the Rio Grande Rift Valley defines the eastern boundary, and the Mogollon Rim marks the southern boundary (Fig. 2.12). The western boundary is less well defined by a transition between the geological features of the Colorado Plateau and the Basin and Range Province (Foos, 1999).

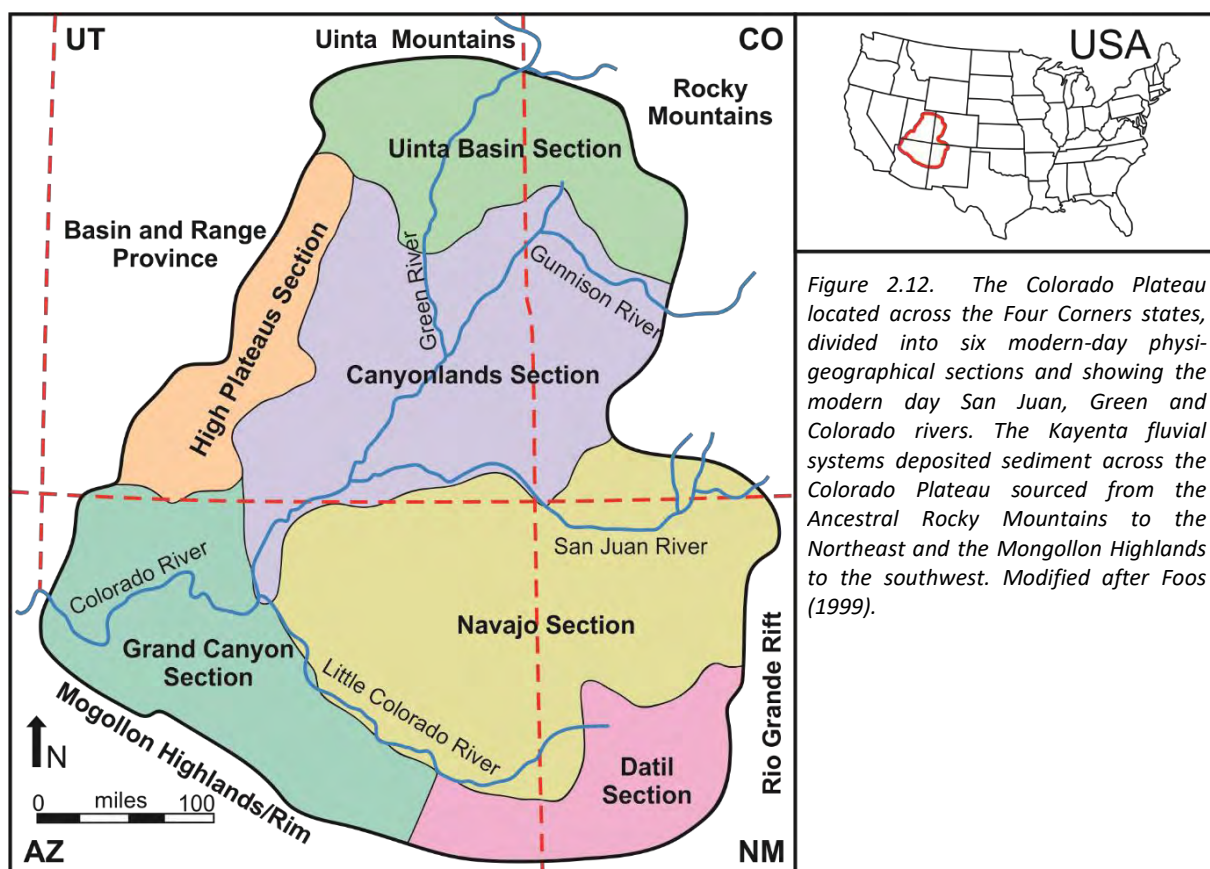


Figure 2.12. The Colorado Plateau located across the Four Corners states, divided into six modern-day physiogeographical sections and showing the modern day San Juan, Green and Colorado rivers. The Kayenta fluvial systems deposited sediment across the Colorado Plateau sourced from the Ancestral Rocky Mountains to the Northeast and the Mogollon Highlands to the southwest. Modified after Foos (1999).

There are several major structures across the Colorado Plateau, including north - south trending monoclines and normal faults, and salt anticlines and domes. These north - south monoclines including; Comb Ridge, the San Rafael Swell and Waterpocket Fold (Fig. 2.13), and long normal faults divide the Plateau into a series of smaller basins (Fig. 2.13), which were formed due to the movement of the crustal blocks within the Precambrian basement during the Pennsylvanian Period. The monoclines resulted from the inversion of normal faults, which are more common in the east of the Plateau, whereas the normal faults to the west have not experienced inversion (Foos, 1999).

2.5.1. Geological History

The Colorado Plateau consists of several smaller basins (Fig. 2.13), filled with relatively flat-lying sediments, ranging in age from the Cambrian Period to present, which were deposited on top of horizontal or tilted Neoproterozoic sediments and a Paleoproterozoic basement (Precambrian crystalline rocks) (Morgan, 2003). The Precambrian basement rocks were thought to have intruded approximately 1.75 Ga from granitoids during the collision of North America with a chain of volcanic islands (Morgan, 2003; Blakey & Ranney, 2008), and signify the growth of the Laurentian supercontinent (Ilg *et al.*, 1996). The consequent north - south compression resulted in continental-scale wrench fault zones trending north-west and north-east (Foos, 1999).

The Palaeoproterozoic basement was uplifted and eroded during the Late Palaeoproterozoic before Mesoproterozoic to Neoproterozoic sediments, known as the Grand Canyon Supergroup, were deposited, creating an angular unconformity (Ilg *et al.*, 1996; Timmons *et al.*, 2001), known as 'the Great Unconformity' (Morgan, 2003). The Grand Canyon Supergroup was deposited in shallow marine to coastal environments and is broken up by several disconformities, suggesting that the Plateau must have been eroded to sea level, and then slowly subsided after the intrusion of the Paleoproterozoic basement (Morgan, 2003). A break in deposition of the Proterozoic sediments occurred approximately 800 Ma, and is thought to be associated with the breakup of Rodinia (Dalziel, 1997; Morgan, 2003). As

a result of the Rodinian breakup, sediments of the Grand Canyon supergroup are preserved only within rotated fault blocks from active margin extension.

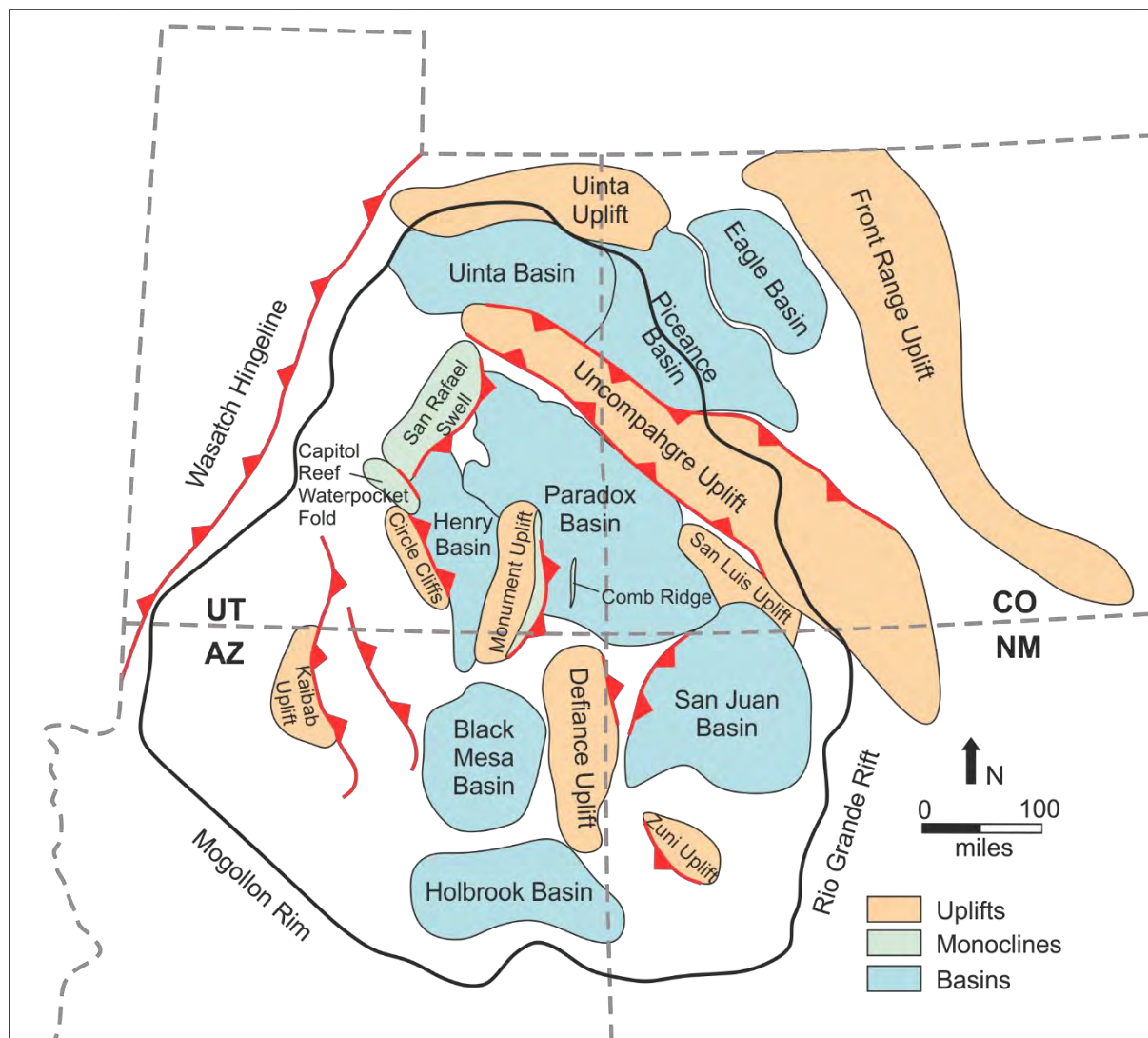


Figure 2.13. The structure of the Colorado Plateau outlined in black, with locations of uplifts in orange, basins in blue and monoclines in green. Modified after Baars and Stevenson (1981); Baars (2000) & Barbeau (2003).

By the latest Proterozoic Period, the area that was to become the Colorado Plateau and the Southern Rocky Mountains, was eroded to a broad, gently sloping ridge, known as the Transcontinental Arch (Morgan, 2003). Deposition and erosion from the Cambrian through to Mississippian periods was strongly controlled by the Transcontinental arch, during cycles of transgression and regression in response to eustatic sea level change (Morgan, 2003). Cambrian shallow marine shelf deposits thicken westward, reaching up to five-thousand metres thick in eastern Nevada and western Utah. This is due

to the structural change of the Wasatch line (Fig. 2.13) or Cordilleran hingeline (Blakey, 2008), which following the breakup of Rodinia, became passive, and a period of post-rift passive subsidence proceeded, allowing for the increase in accumulation near the rapidly subsiding Wasatch line, which developed during the Late Precambrian Eon.

Ordovician and Silurian deposits are not present across the Colorado Plateau as transgression lead to a major unconformity (approximately 135-million-year hiatus), but the deposits are thought to have reflected the Cambrian strata (Blakey, 2008).

Devonian strata reflect a transgressive event onto the Transcontinental arch. The mixed carbonates and clastics cover most of the Plateau, thinning over topographic highs and thickening west of the Wasatch Line (Blakey, 2008). The Late Devonian Period symbolises a change in tectonic setting, which resulted in thrusting and thickening of the crust, and development of a rapidly subsiding foreland basin, filled with Late Devonian and Lower Mississippian siliciclastics (Miller, 1992; Blakey, 2008).

Disruption of sedimentation occurred during the Pennsylvanian Period, as several Precambrian basement faults we reactivated during the final stages of the formation of Pangaea. This created enclosed basins including the Paradox Basin, elevations including the Ancestral Rocky Mountains, the Uncompahgre Uplift and the Kaibab Uplift, and new sources of clastic sediments, as upstanding areas were eroded (Fig. 2.13) (Morgan, 2003; Blakey & Ranney, 2008). Pennsylvanian and Permian deposits have a strong cyclic nature due to global sea level changes during the Late Paleozoic (Soreghan, 1994; Blakey, 2008). During periods of regression, much of the Colorado Plateau was covered by aeolian dune deposits, whereas during periods of transgression carbonates were deposited on shallow marine shelves. Locally extensive evaporites were also deposited, however there is some debate whether their origin is from marine or continental influence. By the Late Permian Period, regression caused a halt in deposition across most of the Plateau, resulting in the Permian-Triassic unconformity (Blakey, 2008).

The initial stages of fragmentation of Pangaea began during the Triassic Period, resulting in global transgressions through to the Cretaceous Period. To the east of the Wasatch Line, Triassic sediments

mainly comprise continental deposits, whereas to the west they mainly comprise marine carbonates which thicken westward. During the Triassic, the Sonoman Orogeny marked a change in tectonic patterns, due to arc collapse and collision with North America, this led to the development of a back-arc basin (Lawton, 1994; Blakey, 2008). The continental sediments mainly consist of fluvial deposits, from Triassic rivers that dominantly flowed towards the north-west. During uplift of the back-arc basin, the Upper Triassic rocks were eroded to the west of the Wasatch Line (Blakey 2008).

The Utah-Idaho trough developed during the Early Jurassic Period, and has been described as either a back-arc or foreland basin, which developed rapidly along the Wasatch line (Blakey, 2008). Continental environments, predominately aeolian, dominated into the Early Jurassic Period, infilling the slowly subsiding Utah-Idaho trough (Fig. 2.14) (Blakey, 2008).

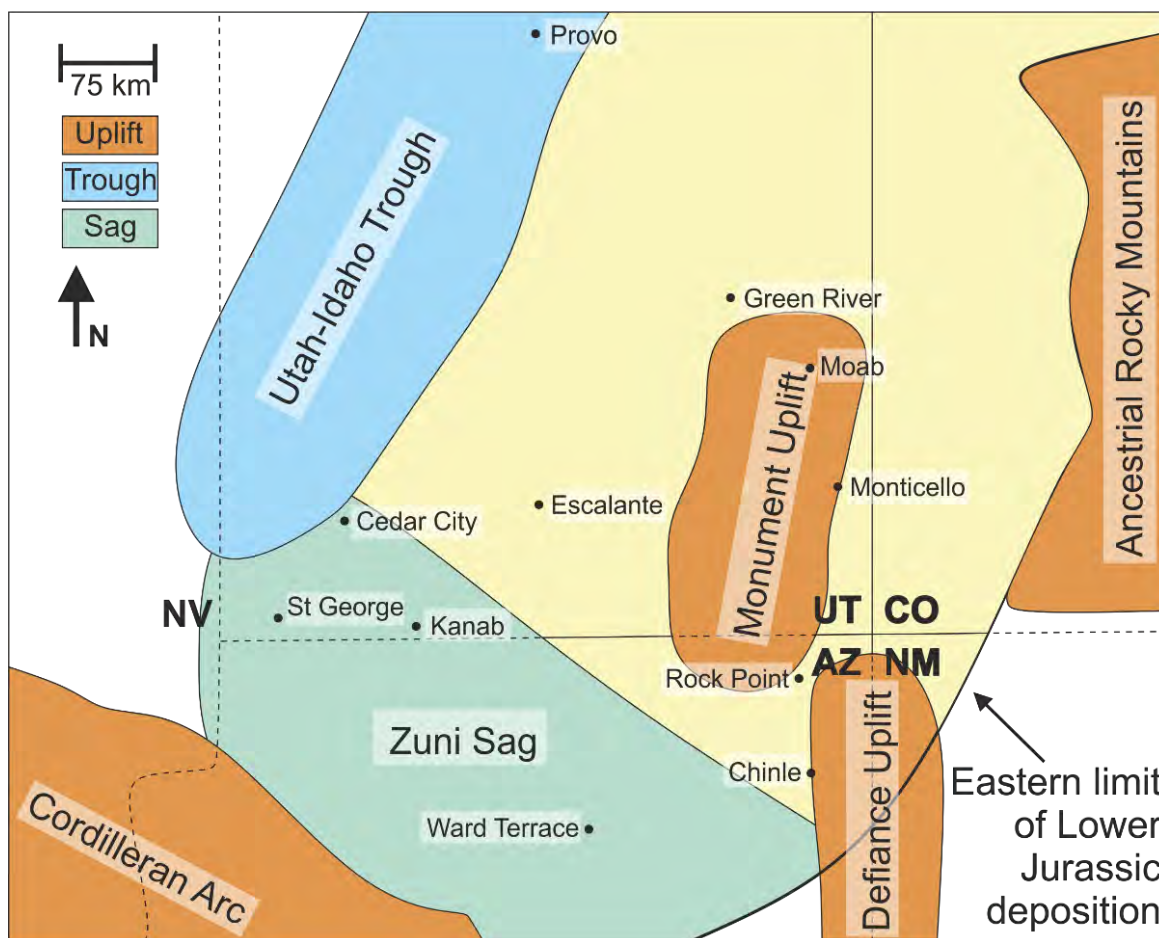


Figure 2.14. Map of the extent of the Lower Jurassic deposits, showing the location of the Utah-Idaho trough, Zuni Sag (Locus for Lower Jurassic rivers) and several uplifts. Modified after Bjerrum & Dorsey (1995).

The Lower Jurassic sediments are known as the Glen Canyon Group (Section 2.5.3) and are the main focus of the study and are described further in the following section.

By the Middle Jurassic, marine conditions returned and dominated the basin centre of the rapidly subsiding Utah-Idaho trough (Morgan, 2003; Blakey 2008). A change in drainage direction of the fluvial system also occurred during the Middle Jurassic Period, from north-west to north-east. The Nevadan orogeny started in the Late Jurassic and results from the westward movement of the North American plate, causing the thrusting of oceanic crust under the North American continent along a subduction trench, and was the first significant phase of Cordilleran mountain building (Blakey, 2008). The final stages of the Nevadan Orogeny resulted in the formation of a foreland basin and forebulge-backbulge complex to the west of the Colorado Plateau, which also altered the fluvial systems direction to eastward across the Plateau (Blakey, 2008).

Cretaceous sedimentation consists of a series of transgressive-regressive cycles depositing a range of sediment, from mudstones to conglomerates, within the Sevier foreland basin to the east of the Wasatch Line. The Sevier Orogeny caused uplift of the Sevier Highlands in Nevada which supplied an abundance of sediment to the Plateau, while the Cretaceous Interior Seaway flooded the Plateau from the east and deposited marine mudstones across the landscape. Towards the end of Cretaceous Period, the Colorado Plateau would have been near sea level, however the Laramide Orogeny caused widespread uplift during the Paleogene Period, and the Pennsylvanian to Jurassic aged strata were eroded from the tops of the uplifts (Blakey, 2008).

In the Cenozoic Era, the Laramide Orogeny resulted in the formation of the Rocky Mountains and deformation of the Colorado Plateau, resulting in the formation of monoclines (uplifts) which were separated by basins. The Laramide structures were then buried during the Eocene Period (Foos, 1999).

The margins of the Plateau are marked by volcanic accumulations; intrusive laccoliths and extrusive volcanics, the majority of which occur along the Rio Grande Rift and the south-western transitional

boundary (Fig. 2.15) (Gilfillan *et al.*, 2008). The magmas intruded through basement faults in the Oligocene Series, resulting in basaltic volcanism and intermediate laccoliths (Foos, 1999).

Approximately five million years ago, the Rocky Mountains and Colorado Plateau experienced an epeirogenic uplift of approximately 1200 m to 1800 m. The movement on the Colorado Plateau was facilitated by reactivation along pre-existing faults and resulted in the Plateau being tilted towards the north (Foos, 1999).

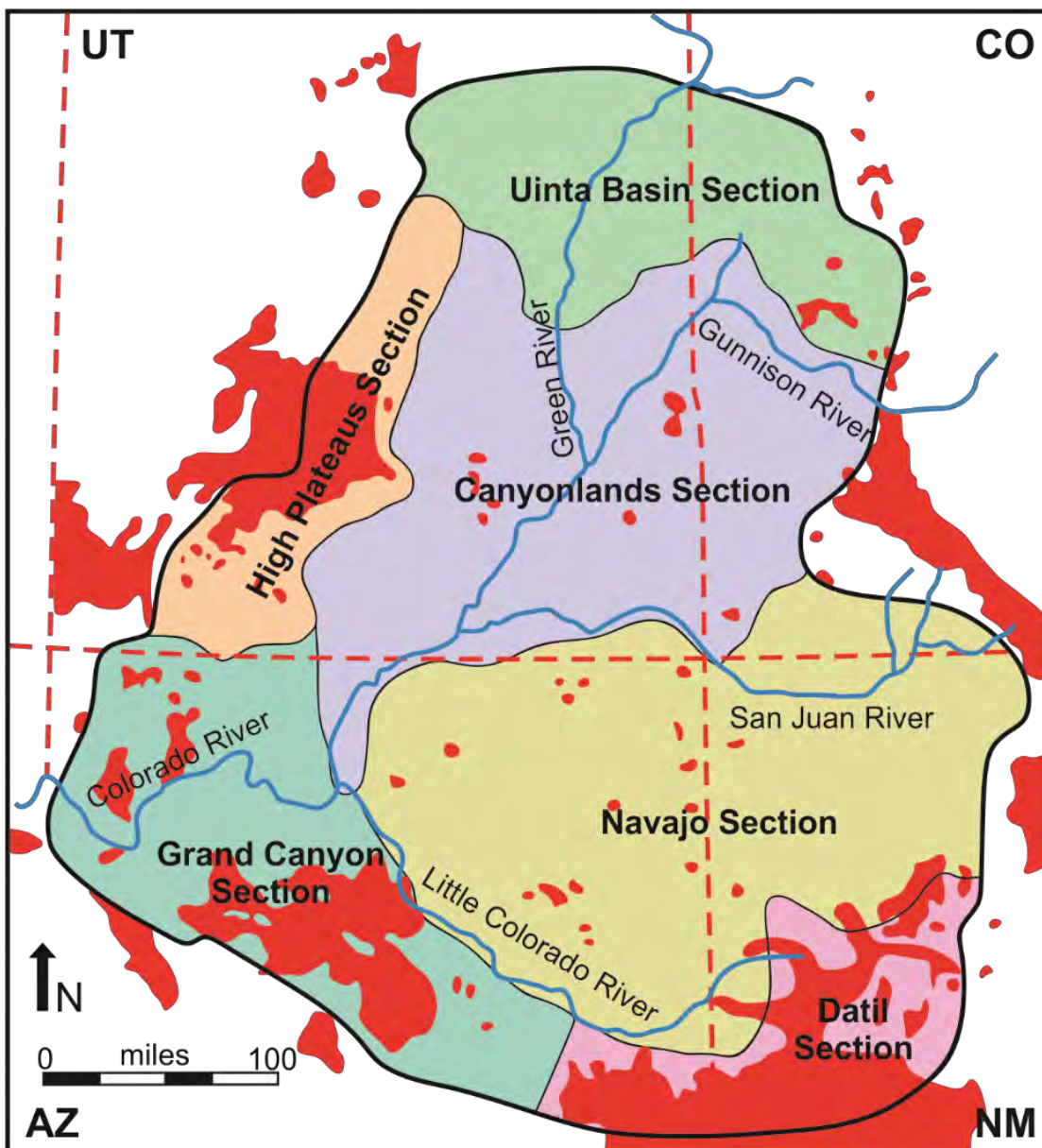


Figure 2.15. The Colorado Plateau with locations of volcanic and igneous centres (red). Modified after Foos (1999)

2.5.2. Glen Canyon Group

During the time of deposition of the Glen Canyon Group, two basins developed: the Zuni sag and the Utah-Idaho trough (Fig. 2.14), which marked a transition from older tectonic trends to deposition in a foreland basin. Due to this change, the rocks of the Glen Canyon Group thicken abruptly westward into the Utah-Idaho trough, where they are truncated by sub-Cretaceous or sub-Tertiary unconformities (Blakey, 2008). The Zuni sag is a subtle trough trending north-west along the south-west of the Colorado Plateau, and was the locus of the Glen Canyon Group rivers which ultimately flowed into the Utah-Idaho trough (Blakey, 1994).

The Glen Canyon Group comprises four formations of Upper Triassic to Lower Jurassic age: the Moenave, Wingate, Kayenta and Navajo formations, with a range of depositional environments from aeolian to fluvial, which intertongue frequently throughout the Group, indicating near continuous deposition (Fig. 2.16) (Middleton & Blakey, 1983). The Group is bound by a series of unconformities: J-0, J-1 and J-2, which truncate each other at low angles (Fig. 2.17) (Pipiringos & O'Sullivan; 1978).

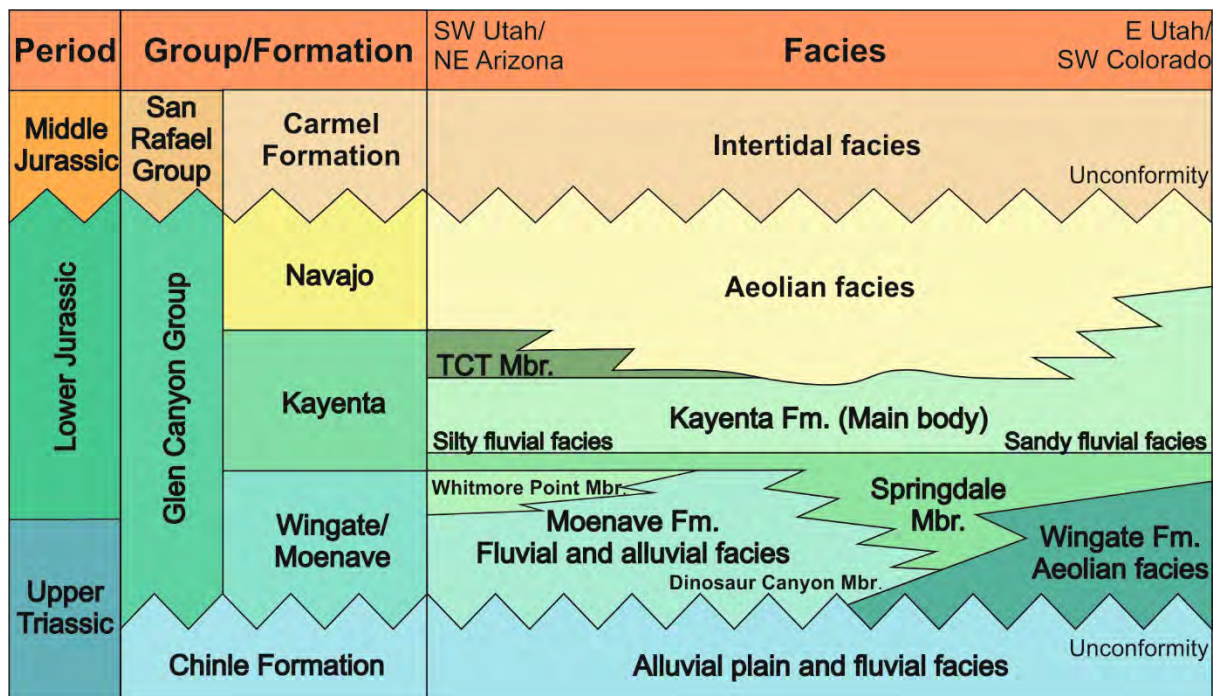


Figure 2.16. The stratigraphy of the Glen Canyon Group including members, facies and spatial distribution of facies across the Colorado Plateau. The focus of this study is the Kayenta Formation that, along with the underlying Wingate and overlying Navajo formations, form the Glen Canyon Group. Modified after North & Taylor (1996); Tanner & Lucas (2007). TCT = Tenny Canyon Tongue.

The oldest formation within the Glen Canyon Group consists of the Moenave Formation and the lateral equivalent Wingate Sandstone, which were deposited during the latest Triassic to earliest Jurassic periods (Blakey, 1994; Tanner & Lucas, 2007). There is some debate on the position of the Triassic-Jurassic boundary, as many believe the boundary follows the J-0 unconformity between the Chinle and Wingate Formations (Harshbarger *et al.*, 1957; Blakey *et al.*, 1988; Clemmensen & Blakey, 1989). However, recent biostratigraphy and magnetostratigraphy have helped more accurately position the boundary. In the lower strata of the Wingate Sandstone, trackways of *Brachychirotherium* and *Eosauropus* have been identified, which are found only in Triassic strata (Lockley *et al.*, 2004; 2011; Lucas *et al.*, 2006; 2011), and *Otozoum* footprints have been identified from stratigraphically higher in the Wingate Sandstone, which are found only in Jurassic strata (Lockley *et al.*, 2004). Magnetostratigraphy also supports the position of the boundary within the upper Wingate/Moenave (Donohoo-Hurley *et al.*, 2010).

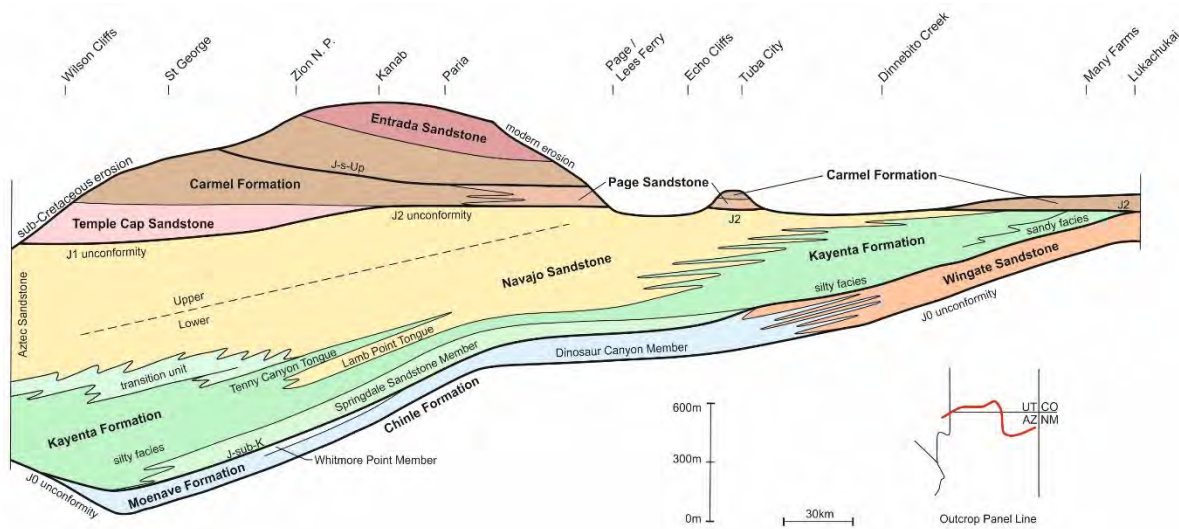


Figure 2.17. Cross section through the Lower and Middle Jurassic Stratigraphy, highlighting the unconformities that bound the Glen Canyon Group. Modified after Blakey (1994).

The Wingate Formation outcrops across most of the Colorado Plateau, and is exposed predominately as steep cliff faces due to weathering. Mainly composed of fine to medium-grained, well sorted and well-rounded sandstones with impressive small to large scale cross-bedding. This aeolian erg system

dominated a large proportion of the Colorado Plateau during the Upper Triassic to Lower Jurassic periods, with a primary wind direction to the south-east (Fillmore, 2011).

In northern Arizona, the Wingate Formation grades into its lateral equivalent, the Moenave Formation, which comprises approximately one hundred metres of continental successions of sandstones, siltstones and mudstones deposited in a range of environments: fluvial, lacustrine and aeolian (Harshbarger *et al.*, 1957; Clemmensen *et al.*, 1989; Tanner & Lucas, 2007). The Moenave Formation is divided into two Members, the Dinosaur Canyon and Whitmore Point Members (Fig. 2.16 & 2.17). The Dinosaur Canyon Member comprises siltstones and sandstones from fluvial and aeolian origin, whereas the Whitmore Point Member comprises lacustrine shales, mudstones, siltstones and limestones (Harshbarger *et al.*, 1957; Tanner & Lucas, 2007). The boundary between the Wingate/Moenave and overlying Kayenta Formation is thought to be conformable and in some places gradational (Baker *et al.*, 1936; Clemmensen & Blakey, 1989; Bromley, 1991), however recent evidence suggests a possible unconformity between these two formations as the Kayenta can be seen downcutting into the Wingate, and has been termed the J-sub-k unconformity (Harshbarger *et al.*, 1957; Blakey, 1994; Lucas & Tanner, 2006; Lucas & Tanner, 2014).

The Kayenta Formation is the middle third of the Glen Canyon Group and comprises a continental redbed assemblage of fine to coarse-grained sandstones, siltstones and sporadic intraformational conglomerates (Harshbarger *et al.*, 1957; Peterson & Pippingos, 1979; Luttrell, 1993), deposited in a dominantly ephemeral fluvial system, with minor perennial influxes and aeolian interactions. The Kayenta is the main focus of this thesis and is described further in Chapter Four.

The upper third, and youngest formation within the Glen Canyon Group is the Navajo Sandstone, which has been interpreted as one of the largest aeolian erg systems preserved in the stratigraphic record, exhibiting large-scale high-angle cross-bedding, weathering into cliffs, rounded mounds and occasionally arches (Harshbarger *et al.*, 1957; Baars & Doelling, 1987; Blakey *et al.*, 1988; Beitler *et al.*, 2003; Fillmore, 2011). Texturally mature, the Navajo mainly consists of fine to medium-grained, well

sorted, well to sub-rounded, quartz-rich sandstones, with occasional, localised freshwater limestones (Middleton & Blakey, 1983).

In south-eastern Nevada and California, the Navajo has been correlated to the Aztec Sandstone (Fig. 2.17) and the Nugget Sandstone in the Wasatch Mountains, north-eastern Utah, north-western Colorado and south-western Wyoming (Baker *et al.*, 1936; Harshbarger *et al.*, 1957). The base of the Navajo Sandstone and its equivalents have a gradational contact with the underlying Kayenta Formation, whereas the top of the formation is marked by the J-1 unconformity in south-western Utah and Nevada, and the J-2 unconformity across most of the Four Corners states, separating the Glen Canyon and San Rafael Groups (Fig. 2.17).

2.6. Summary

This chapter provides a detailed literature review on the processes and products of fluvial and aeolian depositional environments, with a focus on dryland ephemeral fluvial systems. Fluvial systems transport sediment via suspension and/or bedload. Bedforms are then produced as a result of sediment transportation and deposition. Facies analysis can then be applied to resultant preserved deposits, along with the analysis of facies associations, architectural elements, and bounding surfaces. These analyses allow for the interpretation and reconstruction of ancient depositional environments.

In dryland ephemeral fluvial systems, the nature of flow is highly variable, and rapid variations in discharge and sediment load promote the preservation of non-Newtonian flows and Newtonian upper flow regime bedforms. The fluvial architecture typically comprises sand-bodies representative of sheet-like and channelised elements with high width-to-depth, which decrease in size downstream.

Aeolian systems transport sediment via saltation, reptation and suspension, each of which primarily depend on the grain size of the sediment available. Like fluvial systems, facies, facies associations, architectural elements and bounding surface analysis can be applied to reconstruct the depositional system and build three-dimensional facies/depositional models.

A summary of the geological evolution and deposits of the outcrop analogue study area of the Colorado Plateau, south-western USA is also provided, with a focus on the late Triassic to early Jurassic Glen Canyon Group. The Colorado Plateau is a large high-standing block spanning parts of Utah, Arizona, Colorado and New Mexico, which consists of several smaller basins filled with sediments ranging in age from the Cambrian Period to present day. The sediments were deposited in a range of environments, from deep marine to aeolian, and preserve the expression of several orogenic events.

The Glen Canyon Group comprises four formations: the Moenave, Wingate, Kayenta and Navajo, each record the deposition of continental environments: lacustrine, fluvial and aeolian. The Group is also bound by a series of unconformities: J-0, J-1 and J-2, which truncate each other at low angles.

The following chapters will relate primary data back to the published literature to contextualise depositional interpretations of the sediments encountered, focusing on the dryland ephemeral fluvial system of the Lower Jurassic Kayenta Formation. A detailed summary of the Kayenta Formation is provided at the start of Chapter Four.

Chapter 3: Methods

This chapter details the methods used for data collection and analysis. Sedimentological fieldwork combined with three-dimensional photogrammetry techniques were used to examine the detailed sedimentology, geometrical relationships of architectural elements and spatial variations of the Kayenta Formation. Core analysis was also conducted to examine the sedimentology of the Lemman Sandstone of the Southern North Sea. Chapters Four, Five, Six and Eight will draw upon the sedimentological methods (Section 3.1) outlined within this chapter, whereas Chapter Seven will draw upon the photogrammetric methods (Section 3.2).

3.1. Sedimentological methods

This study used extensive regional sedimentological fieldwork in conjunction with three-dimensional photogrammetry techniques to examine the sedimentary detail and interactions of fluvial and aeolian deposits of the Kayenta Formation across the Colorado Plateau, from proximal to distal settings (Fig. 3.1). The data for this study was collected during three separate field seasons between the summers of 2016 and 2018, totalling approximately seven months of fieldwork. This work was combined with detailed sedimentary analysis of core data from a subsurface analogue to aid in the understanding of fluvial-aeolian interactions of the Lemman Sandstone of the Southern North Sea.

3.1.1. Graphical vertical sections: Sedimentary logs

To investigate the sedimentology and sedimentary interactions, twenty-five detailed vertical sections were logged, with a cumulative length over 1700 m, each spaced laterally approximately 25 km apart over an area of approximately 200 km², constrained to as close to a grid pattern as exposure allows (Fig. 3.1). The measured vertical sections record continuous profiles through the entire succession of the Kayenta Formation, from its basal contact with the underlying Wingate Formation, or laterally equivalent Moenave Formation, to the last main fluvial occurrence within the gradational,

interfingering contact with the overlying Navajo Sandstone. In southern Utah and northern Arizona, this succession includes the basal Springdale Sandstone member of the Kayenta Formation. The preserved thickness of the Kayenta Formation varies from 9.0 m to 255.4 m (Table 3.1).

From the twenty-five sedimentary logs, twenty-one facies were identified based principally on the lithological, sedimentary textures and structures present. The facies were grouped based upon depositional processes to form nine architectural elements, five fluvial depositional elements and three broad-scale depositional environments.

Facies proportions within each architectural element have been calculated from the thickness of units present in the measured vertical sections.

3.1.2. Spatial analysis

Spatial analysis of the fluvial system was conducted using the five fluvial depositional elements identified from the twenty-five vertical sections to quantify the spatial variations in the fluvial system downstream.

Spatial variations in compositional characteristics; including the thicknesses of fluvial and aeolian strata, along with the percentage of sand, the percentage of conglomerates, and the grainsize distribution of the fluvial sediments, have been calculated and are illustrated as contour maps across the study area. Fluvial and aeolian sediment thicknesses are the total thicknesses of strata of each type observed within the Kayenta Formation at each locality. The percentages of fluvial sand and fluvial conglomerates at each locality were calculated by summing the thicknesses of individual beds of fluvial sediment with average grain sizes of each and comparing these values to the total thicknesses of fluvial sediment at each locality. The average grain size for each locality was calculated from the observed average grain size of each individual bed, with measurements determined per unit thickness in order to normalise by bed thickness.

Analysis of spatial variations in the five identified depositional elements has also been conducted. This includes the percentage of each depositional element per locality, calculated from the total thicknesses of elements of each type displayed in the sedimentary logs, and the average thickness and average grain size of each type of depositional element per locality.

Each contour plot of data is supplemented with a line graph depicting the spatial variations downstream from the Uncompahgre Uplift (following the dominant direction of flow indicated by palaeocurrent data), a line of best fit, and arithmetic averages for the proximal, medial, and distal regions. The localities affected by the secondary fluvial source from the Mogollon Highlands have been highlighted on each contour plot and each graph, and secondary lines of best fit demonstrate trends excluding these data. For the sake of ease, all four data points within the distal region have been excluded when calculating the best fit trend as it is difficult to determine the source of some depositional elements, particularly when no palaeocurrent data was available.

3.1.3. Palaeocurrent Analysis

A total of 362 palaeocurrent measurements were collected across the study area, of which 235 are measured from planar and trough cross-bedded foresets, ripple-cross-laminated foresets and primary current lineations within fluvial sediments. The remainder are measured from planar and trough cross-bedded foresets within aeolian sediments.

Palaeocurrent measurements provided a means of determining the local direction of palaeoflow from the mean azimuth of cross-bedded foresets within channel-fill elements, and for assessing the accretionary nature of adjacent elements. The nature of element accretion was inferred from the angle between the dip-azimuth of accretionary surfaces within the element and the direction of local palaeoflow. Angles of less than 60° indicate downstream accretion; angles between 60° and 120° indicate mixed downstream/lateral accretion; and angles of 120 to 180° indicate up-flow element accretion (*cf.* Miall, 1994; Long, 2006, 2011; Ielpi & Rainbird, 2015; Lebeau & Ielpi, 2017).

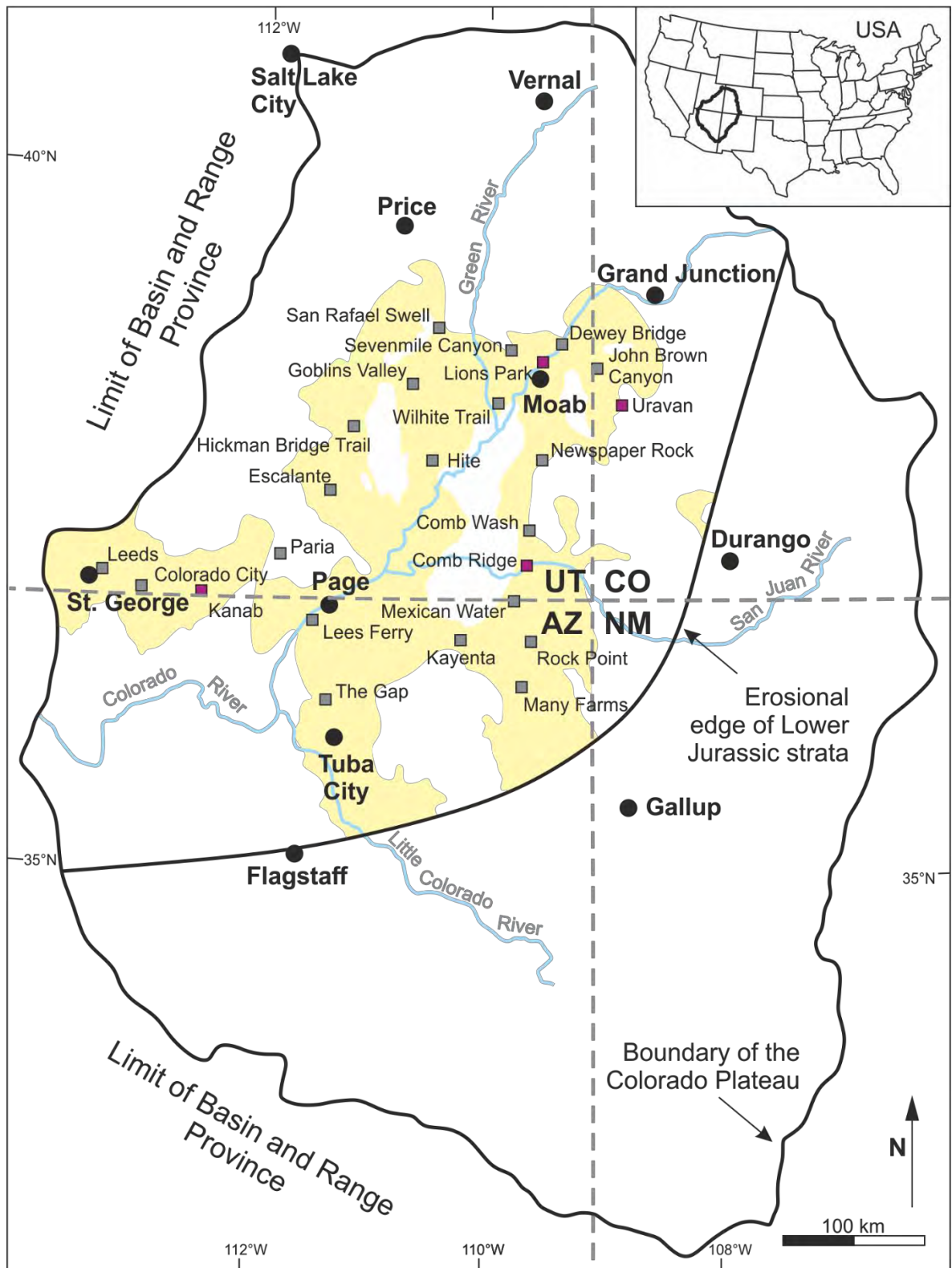


Figure 3.1. The study area in the western USA highlighting the extent of exposure of Triassic-Jurassic sediments (yellow) across the Colorado Plateau, along with the positions and names of the sedimentary logs collected (grey squares) and locations and names of the sedimentary logs where photogrammetry was also conducted (purple squares) for this study. The base map and outcrop limits are modified after Dickinson, 2018.

Table 3.1. Sedimentary log metadata for the logs collected in this study. All coordinates from grid system UTM 12S.
*location of photogrammetric models

Region	Log Code	Log Name	Easting	Northing	Thickness (m)	
Proximal	JB	John Brown Canyon	0673540	4277594	47.6	
	U	Uravan – Y11 Road*	0694091	4250686	29.0	
	DB	Dewey Bridge	0646525	4296336	40.5	
	LP	Lions Park*	0625071	4273518	51.2	
	PS	Poison Spider Trail	0620643	4265414	71.1	
	7MC	Sevenmile Canyon	0610590	4278269	70.0	
	NR	Newspaper Rock	0630836	4205281	41.6	
	WT	Wilhite Trail	0594947	4250733	39.4	
	SR	San Rafael Swell	0549489	4310625	70.0	
	GV	Goblins Valley	0528361	4279192	54.4	
Medial	CW	Comb Wash	0619737	4150468	37.0	
	CR	Comb Ridge*	0617640	4124297	37.6	
	H	Hite	0543155	4204980	47.8	
	MW	Mexican Water	0608319	4097217	14.8	
	HB	Hickman Bridge Trail	0480051	4237697	54.5	
	RP	Rock Point	0626384	4066472	15.5	
	E	Escalante	0463420	4182686	25.3	
	MF	Many Farms	0615227	4027258	9.0	
KT	Kayenta	0580980	4072039	64.0		
Distal	LF	Lee’s Ferry	0448500	4080022	72.0	
	G	The Gap	0459101	4017758	94.0	
	K	Kanab	Squaw Trail*	0364212	4102576	90.0
			White Rim	0363493	4105216	55.7
			Moqui Cave	0361155	4109404	33.6
	CC	Colorado City	0323779	4097105	87.8	
	L	Leeds	0287962	4122235	255.4	
	SC	Snow Canyon	0264804	4117811	107.6	

3.1.4. Core analysis

The core data for this study was collected over three visits to the British Geological Survey’s National Geological Repository. Nineteen detailed vertical sections were logged, with a cumulative length of over 2000 m, each spaced laterally approximately 20 km apart over an area of approximately 50 km² and constrained to as close to a grid pattern as well localities allowed (Fig. 3.2). The log localities were

chosen based upon the current spatial understanding of the depositional environments for the Lemn Sandstone (Fig. 3.2). Where possible, the core logs record full successions of the Lemn Sandstone, from the unconformity with the underlying Carboniferous Coal Measures, through the Lower Lemn, Silverpit Formation and Upper Lemn intervals, to the overlying claystone of the Kupferschiefer Unit. The logged thickness of the Lemn Sandstone varies from 13.6 m to 271.6 m (Table 3.2).

From the nineteen sedimentary logs, twenty-six facies were identified based principally on the lithological, sedimentary textures and structures present. The facies were grouped based upon depositional processes to form eleven facies associations.

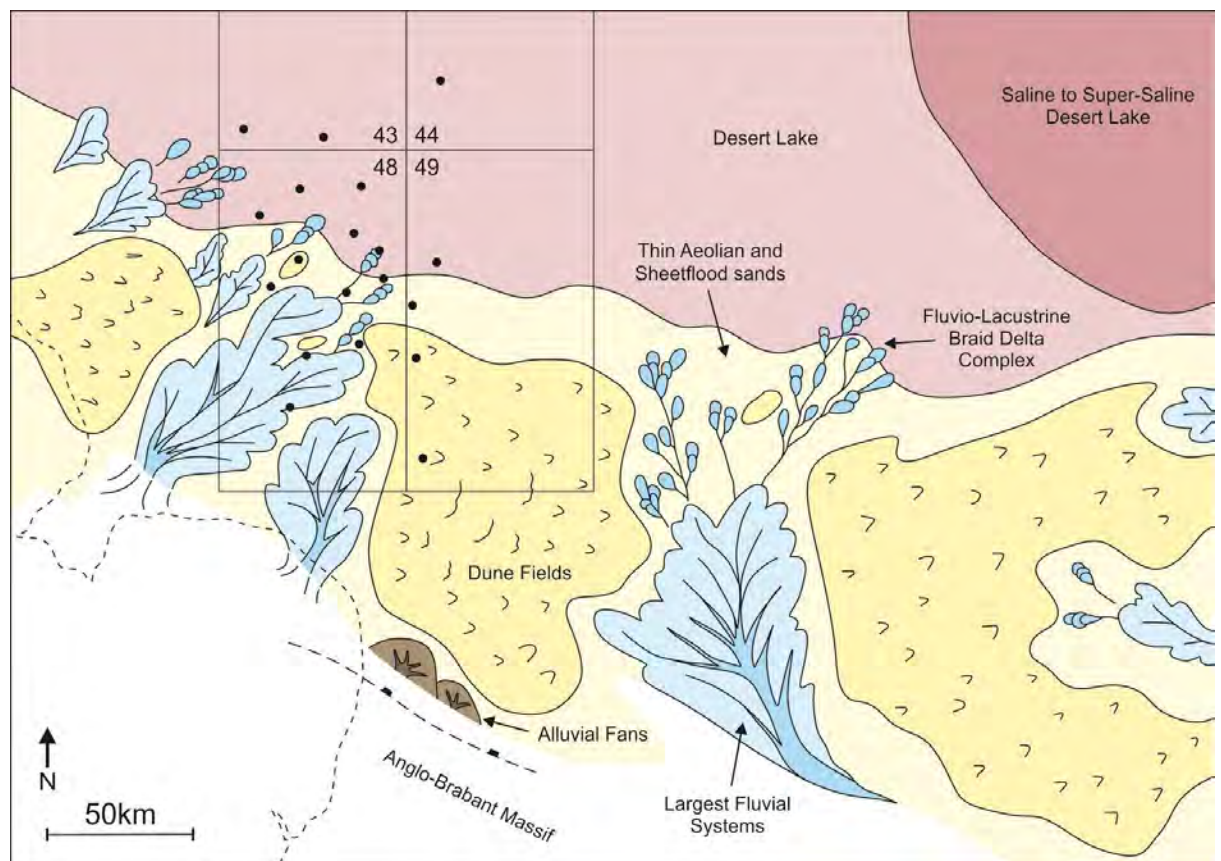


Figure 3.2. Palaeogeographical map of the Lemn Sandstone of the Southern North Sea. Modified after George & Berry (1993; 1997)

Table 3.2. Sedimentary log metadata for the Leman Sandstone wells studied. *Log was excluded from data analysis due to poor recovery.

Well	Thickness (m)	Top depth (ft)	Bottom depth (ft)	Deviation type	Core recovery (%)
43/26a-8	39.85	10653	10801	Vertical	88.4
43/28-2	88.35	11879.9	12171.9	Vertical	99.2
44/21-1*	28.75	12671	13876	Vertical	7.8
48/03-1	65.8	11212	11543	Vertical	64.3
48/04-1	120.85	12373	12770	Deviated	99.9
48/07b-8	187.0	10180.2	10793.7	Vertical	93.4
48/08a-1	99.0	9266	9594	Deviated	94.8
48/09-2	137.35	11009	11437	Vertical	99.1
48/10b-4	102.1	12259	12598.4	Deviated	96.1
48/12b-5	115.85	9938	10294.8	Vertical	99.9
48/13-1	192.8	8601	9327.4	Vertical	82.9
48/15b-8	30.25	9850	9951	Vertical	98.2
48/18a-4	70.15	8442	8676	Vertical	89.6
48/19-1	142.4	8123	8775	Vertical	71.5
48/22-2	13.15	7374.9	7424.1	Vertical	87.7
49/06-2	169.7	11416.8	11989.8	Vertical	97.2
49/11a-4	162.6	9581	10121	Vertical	98.8
49/16-10	152.4	8089	8591	Deviated	98.6
49/26-A6	271.6	6594	7640	Deviated?	85.1

3.2. Photogrammetric methods

Within the geosciences, photogrammetry has been used throughout most of the 20th Century, primarily for plan-view landform studies such as topographical and digital elevation models (Chandler, 1999; Fonstad *et al.*, 2013). Early approaches used stereoscopic instruments to produce 3D images (Birdseye, 1940), but later methods employed computer technology to generate virtual 3D surfaces. More recent advancements have focussed on structure-from-motion (SfM) modelling of dynamic processes, such as rockfalls (Sturzenegger & Stead, 2012), landslides (Niethammer *et al.*, 2012) and volcanic eruptions (Baldi *et al.*, 2005). SfM detects common points within the outcrop from multiple photographs, to reconstruct the 3D virtual outcrop (Westoby *et al.*, 2012; Bemis *et al.*, 2014; Carrivick *et al.*, 2016). Further improvements in data acquisition and processing have enhanced 3D triangulated point clouds, orthomosaics and textured models (Pringle *et al.*, 2006; 2010; Schmitz *et al.*, 2014). With

increased spatial accuracy of triangulated 3D point clouds, structural and geological features can now be mapped in 3D models (Carrivick *et al.*, 2016). With the addition of sedimentological measurements, such as palaeocurrent flow directions, measured widths and thicknesses for architectural elements can be corrected for the attitude of the outcrop to give flow-perpendicular measurements (Hodgetts, 2013).

Terrestrial and unmanned aerial vehicle (UAV) photogrammetry surveys were used to study the geometry and geometrical relationships of preserved architectural elements within the mixed ephemeral fluvial and aeolian deposits of the Lower Jurassic Kayenta Formation across the expanse of the Colorado Plateau, south-western USA.

Three photogrammetric models, totalling a combined outcrop length of 5 km, were generated. Model 1, from the proximal sediments of the Kayenta, was collected from beside the Colorado River in Moab, Utah (Fig. 3.1). Model 2, from the medial sediments of the Kayenta, was collected from along the Comb Ridge monocline near Bluff, Utah (Fig. 3.1). Model 3, from the distal sediments of the Kayenta, was collected from along Squaw Trail, Kanab, Utah (Fig. 3.1). The digital outcrop models depict: 1) the lateral and vertical relationships between fluvial and aeolian architectural elements; 2) the geometry and dimensions of the elements; 3) the nature of the interactions between the elements; 4) the changes in architecture and sedimentology from proximal to distal settings; and 5) the vertical changes within the formation that represent the temporal evolution of the system. Table 3.3 summarises key parameters of the three outcrops and pertinent statistical details. Sedimentary logging was conducted at each location where the DOMs were acquired and has been used to constrain the sedimentary architecture, geometry and width-to-depth ratios.

Table 3.3. Summary of number of photographs and methods used for each outcrop, including the length and height, the number of points within the dense point cloud and the reconstruction error of each model. See Fig. 3.1 and Table 3.1 for locations.

Outcrop	Method	No. Photos	Outcrop Length (m)	Outcrop Height (m)	No. Data Cloud Points	Reconstruction Error (%)
Model 1: Lions Park	Ground	411	1,261	304	289,130,233	0.13
Model 2: Comb Ridge	UAV	564	516	136	49,167,525	0.50
Model 3: Squaw Trail	UAV	443	323	355	121,506,632	0.66

3.2.1. Data Acquisition

For data acquisition, lightweight equipment was vital as many of the remote outcrops can only be accessed by foot. For this reason, ground-based and UAV-based photogrammetric techniques were selected for data acquisition rather than terrestrial lidar. For model 1, ground-based photogrammetry was chosen due to the outcrop being exposed in the canyon of a modern-day river with a pathway running parallel to the outcrop face. UAV-based photogrammetry could not be used due to restrictions on the flying of UAVs within the location. For model 2 (Comb Ridge), UAV-based photogrammetry was chosen due to poor outcrop accessibility. For model 3 (Squaw Trail), the outcrop was easily accessible, but to capture the full irregular nature of the outcrop face UAV-based photogrammetry was chosen as the most suitable method.

Data acquisition for both ground-based and UAV-based photogrammetry involved taking high-resolution photographs of the respective outcrops, with each outcrop feature captured in at least three images. The greater the overlap between adjacent photographs, the greater the precision and spatial accuracy of the resulting digital model using SfM photogrammetry (Bemis *et al.*, 2014; Chesley *et al.*, 2017).

In ground-based studies (model 1), a Nikon D800E digital single-lens reflex (DSLR) camera with a 36.3 megapixel 8.6 cm² sensor and a 60 mm fixed focal length lens (Nikon AF-S Micro Nikkor 60 mm F.2.8G ED) was used. This lens was used to capture the whole outcrop face quickly, to reduce any issues of reflection and intensity variations due to changing light conditions, which have the potential to cause problems during the subsequent digital image-matching process (Kehl *et al.*, 2017; Klawitter *et al.*, 2017). To capture as much of the outcrop as possible using ground-based terrestrial photogrammetry, photographs were taken from camera locations that were parallel to the outcrop face spaced 1 m apart. The distance between the camera locations and the outcrop face ranged between 30 and 50 m for model 1. Every tenth photograph was georeferenced using a 12-channel Garmin GPSmap64 handheld Global Navigation Satellite System (GNSS) operating in full Wide Area Augmentation System (WAAS) mode (using ground reference stations across the USA to correct for signal errors). In addition, several photographs were taken using a “fan” arrangement to cover as much of the rugged outcrop as possible and ensure sufficient overlap to capture the 3D nature of the outcrop face. This process was repeated across the entire length of each outcrop (Fig. 3.3).

In the UAV studies (models 2 and 3), a DJI Phantom 4 Pro drone with a 20-megapixel complementary metal oxide semiconductor (CMOS) sensor was used, controlled by the DJI GO 4 app on an iPhone 7 Plus smartphone. The Phantom 4 Pro drone was chosen for data acquisition due to the mechanical shutter on its camera, its relatively long flying time (30 minutes) between battery changes, its multiple direction obstacle sensing and its light weight. The UAV-based photographs were taken under manual control, with the drone flying parallel to the outcrop face; a photograph was taken every three seconds at a flying speed of approximately 0.3 m/s. For model 2 (Comb Ridge), the UAV was controlled from an operator position on the top of the outcrop, with the drone at a distance of 20 to 75m from the outcrop. The distance between the UAV and the outcrop faces for model 3 (Squaw Trail) ranged between 20 and 50 m.

Several flight paths were used on each outcrop to ensure the 3D nature of the outcrop was captured; one flight path with the camera horizontal, a second flight path with the camera tilted approximately 30° below the horizontal and a third with the camera tilted approximately 30° above the horizontal. This process was repeated several times due to the size of the outcrop and the irregular outcrop face (Fig. 3.3).

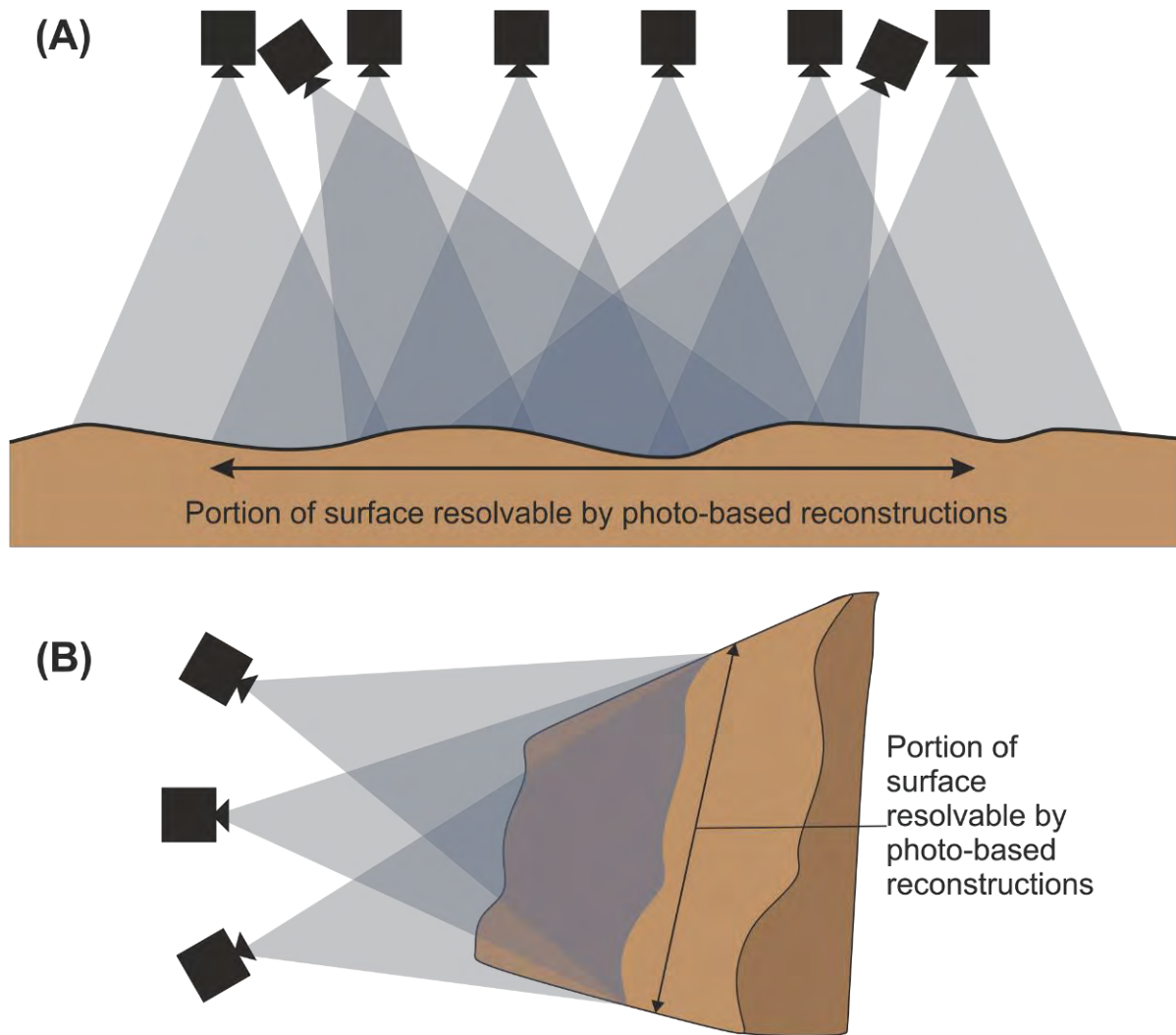


Figure 3.3. Simplified schematic representation of image acquisition for 3D photogrammetric modelling used in this study. The blue triangles represent the field of view of the camera from the positions shown, with the darkness of the triangles increasing with the amount of overlap. (A) Photo acquisition for ground-based photogrammetry in plan view, (B) Photo acquisition used for UAV-based photogrammetry in profile view, highlighting the angled camera locations to fully capture the 3D nature of the outcrop, looking obliquely to the outcrop face (modified after Bemis et al., 2014).

3.2.2. Data Processing

Agisoft PhotoScan (Version 1.4.3, July 2018) commercial software was used to build 3D digital models of the outcrops for both the ground-based and UAV-based photogrammetry. PhotoScan uses the structure-from-motion multiview stereo (SfM-MVS) method for reconstruction of an outcrop from multiple overlapping photographs without the need for manual input of orientation or camera locations (Eltner *et al.*, 2016). Before constructing the models, the photographs taken for each model were filtered to remove any blurred or unwanted images, and processed to remove any unnecessary sky or vegetation with the aim of reducing the processing time of each model. Sparse 3D point clouds were created using SfM to reconstruct the 3D virtual outcrop. Dense 3D point clouds were then generated using MVS with pixel grid-based matching (Fig. 3.4). The resulting 3D point clouds were generated in a relative (local) coordinate system with estimated camera location positions. GNSS positional readings of the camera locations, recorded in the field, were imported into PhotoScan to constrain the outcrop models into georeferenced real-world coordinates.

The final steps for completion of the 3D outcrop models, once the georeferenced dense 3D point clouds were created for each outcrop, included building a triangulated digital surface mesh and overlaying the combined outcrop photomosaic as a surface texture. These steps were important to undertake as they aided in the identification of geological features in the model, such as bedding planes, structural joints and sedimentary architectures at both small scale (such as cross-bedding) and large scale (for example, channels, sheets and erosive surfaces). Examples of the data processing outputs for each locality are shown in Figures 3.5, 3.6 and 3.7.

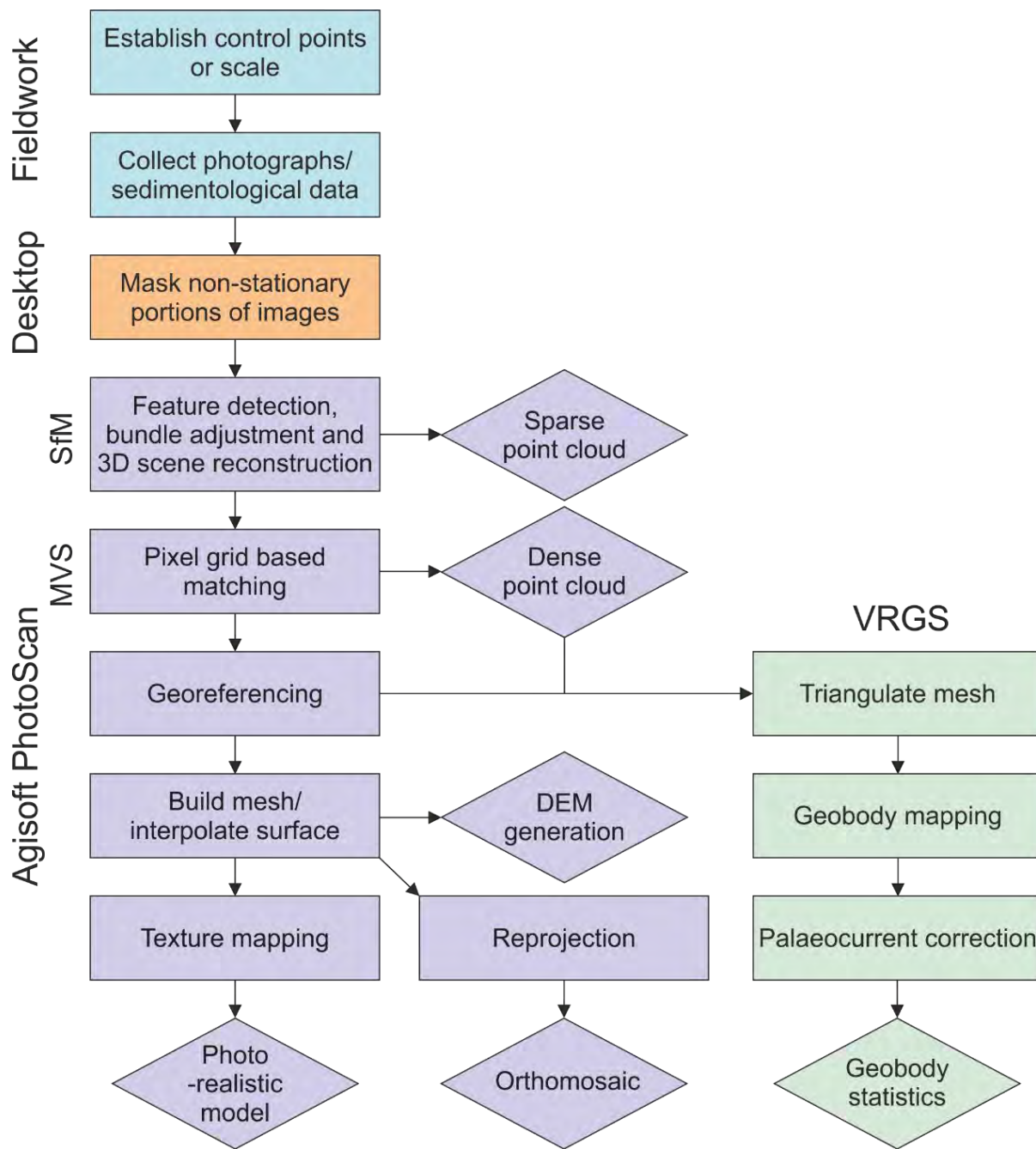


Figure 3.4. General workflow of the 3D photogrammetric model reconstruction process, data collection (blue), desktop processing (orange), the generation of 3D models using Agisoft PhotoScan™ (purple), including the points in which structure-from-motion (SfM) and multi-view stereo (MVS) were used, and post processing architectural element analysis within Virtual Reality Geological Studio (VRGS) software (green). Rectangle icons represent 3D photogrammetric model reconstruction steps, diamond icons represent outputs from each process (modified after Bemis et al. 2014; Schmitz et al. 2014; Kehl et al. 2017).

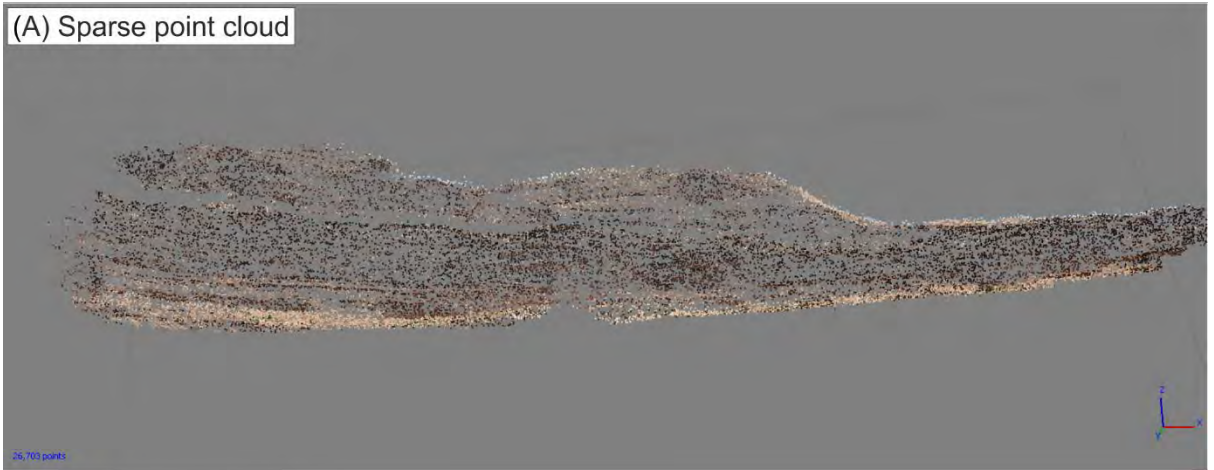
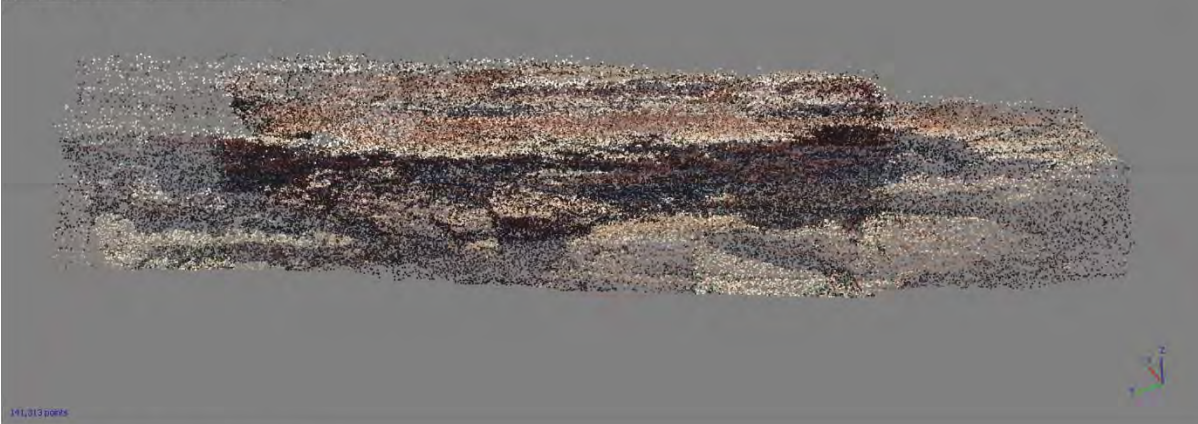
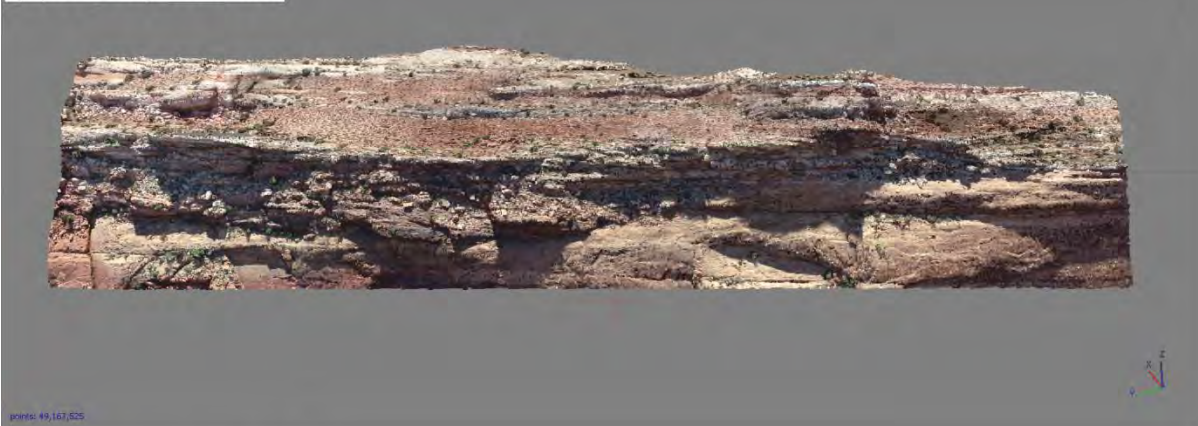


Figure 3.5. Construction of Model 1 (proximal – Lions Park) using Agisoft PhotoScan. (A) Sparse point cloud generated using SfM – 26,703 points. (B) Dense point cloud generated using MVS with pixel grid-based matching – 289,130,233 points. (C) Photo-realistic textured model.

(A) Sparse point cloud



(B) Dense point cloud



(C) Textured model

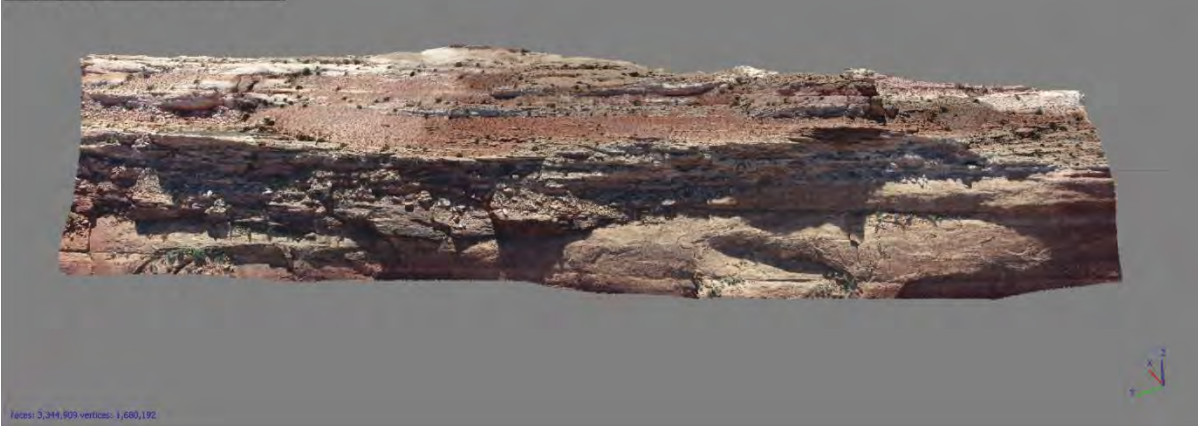


Figure 3.6. Construction of Model 2 (medial – Comb Ridge) using Agisoft PhotoScan. (A) Sparse point cloud generated using SfM – 141,313 points. (B) Dense point cloud generated using MVS with pixel grid-based matching – 49,167,525 points. (C) Photo-realistic textured model.

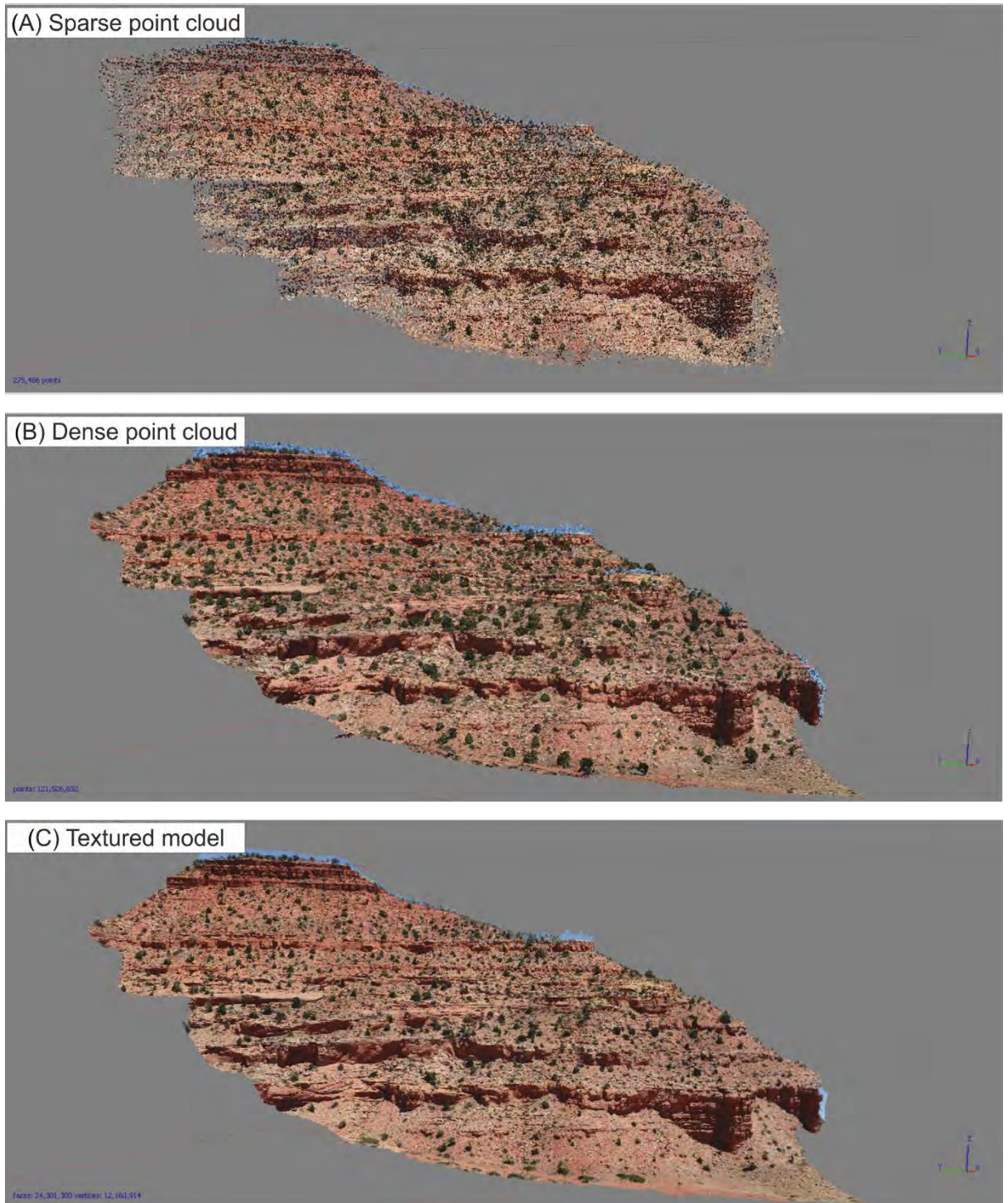


Figure 3.7. Construction of Model 3 (distal – Squaw Trail) using Agisoft PhotoScan. (A) Sparse point cloud generated using SfM – 275,486 points. (B) Dense point cloud generated using MVS with pixel grid-based matching – 121,506,632 points. (C) Photo-realistic textured model.

3.2.3. Post-processing

The 3D digital point cloud was then imported into VRGS (version 2.34; Hodgetts, 2017) – a 3D visualisation and interpretation software tool. By incorporating palaeocurrent measurements taken from cross-bedding in individual architectural elements at multiple locations across the outcrop, widths and heights of geobodies can be corrected automatically within the software for the attitude of the virtual model. These geobodies were subsequently digitised and extruded using palaeocurrent measurements to correct for their true facing orientation perpendicular to flow to avoid overestimation of the geobody width (Visser & Chessa, 2000a, Pringle *et al.*, 2010, Rarity *et al.*, 2013, Burnham & Hodgetts, 2018). This correction was based on the assumption that channel trajectory is reflected in the orientation of the internal cross-bedding within the fill of each channel (Pringle *et al.*, 2010). The geobody data has been divided into four categories dependant on geobody length/width: complete (bodies exposed in full by the outcrop), partial (bodies only partially exposed by the outcrop), unseen (bodies not exposed by the outcrop) and unlimited (bodies that are longer than the outcrop) (Fig. 3.8) (Geehan & Underwood, 1993; Visser & Chessa, 2000a). The dimensions of partial and unlimited elements within models have been approximated using the relationship between the relative lengths of the feature and outcrop and the expected proportion of the occurrences of partial measurements. This method uses the theory of conditional probability to calculate the additional dataset using partial lengths (Visser & Chessa, 2000b). The following equation was used:

$$\frac{\sum_{l \geq w} l N_c^l / (\lambda - l)}{\sum_{l \geq w} N_c^l / (\lambda - l)}$$

Where w is the partial length of the geobody, λ is the length of the outcrop and N_c^l is the number of complete lengths that belong to length class l .

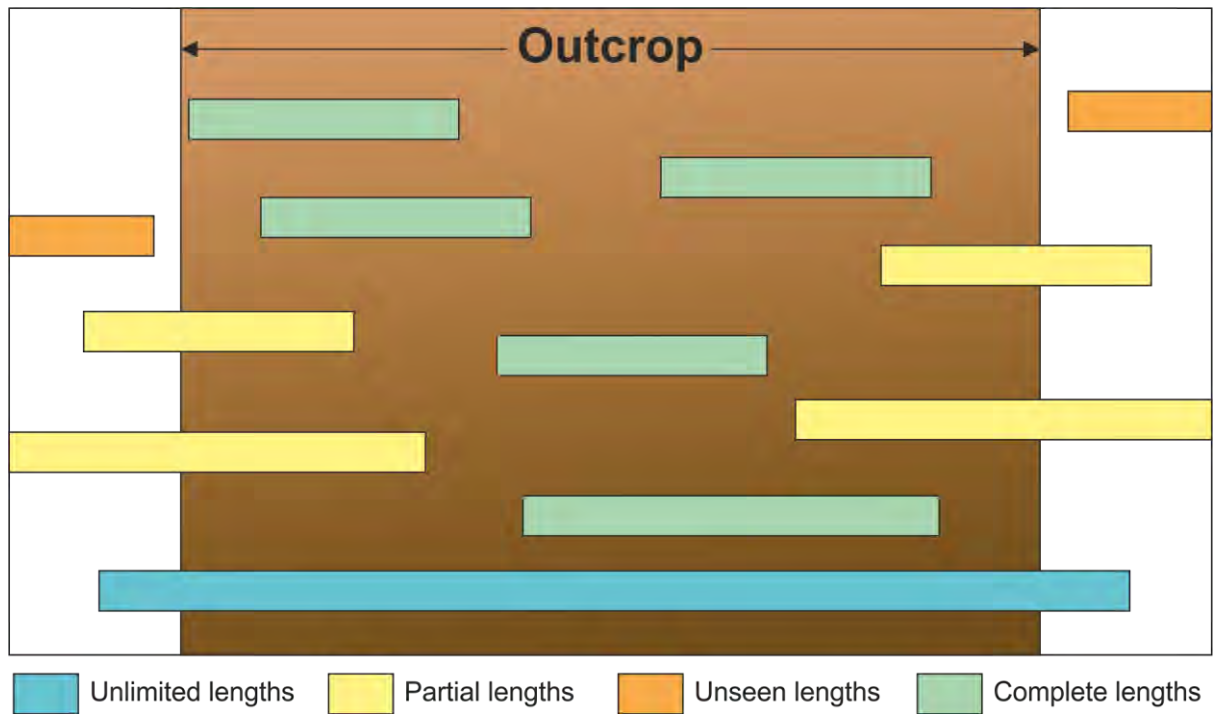


Figure 3.8. Categories of geobody lengths exposed at outcrop (modified after Geehan & Underwood, 1993; Visser & Chessa, 2000a).

3.3. Summary

To analyse and characterise the outcrop analogue of the Kayenta Formation, regional sedimentological fieldwork and three-dimensional photogrammetric techniques were conducted across the Colorado Plateau of south-western USA. A total of twenty-five detailed vertical sections were logged, with a combined measured length over 1700 m, 362 palaeocurrent measurements were collected and three photogrammetric models, totalling a combined outcrop length of 5 km, were generated.

To investigate the sedimentology of the Leman Sandstone of the Southern North Sea, a total of nineteen wells were logged, with a combined measured length of over 2000 m.

Facies analysis was conducted on both the Kayenta Formation and the Leman Sandstone to characterise their sedimentology. Further spatial analysis was performed on the data from the Kayenta Formation to investigate the change in fluvial characteristics and interactions with the aeolian system downstream.

This chapter details all data collection and analytical methods used throughout this body of work, and for the readers ease, Chapters Four to Eight include a summary of the relevant methods used in each section.

Chapter 4 – The Sedimentology of an Ephemeral Fluvial Outcrop

Analogue: The Kayenta Formation

This chapter describes the sedimentology of a dryland ephemeral fluvial system using the Lower Jurassic Kayenta Formation as an example. The chapter contains a summary literature review of the Kayenta Formation and its deposits before detailing the twenty-one facies observed. The facies are based principally on the lithological, sedimentary textures and structures present within them, and are grouped according to their depositional process as either sub-aqueous or sub-aerial processes. Chapter Five draws upon the observed facies described within this chapter and details interpreted architectural elements, depositional elements, and depositional environments.

4.1. Literature review summary

4.1.1. Kayenta Formation

The middle third of the Glen Canyon Group (Chapter 2) consists of the late Sinemurian to early Toarcian Kayenta Formation. A continental redbed assemblage of coarse to fine-grained sandstones, siltstones and occasional intraformational conglomerates (Harshbarger *et al.*, 1957; Peterson & Pippingos, 1979; Luttrell, 1993), deposited on a broad alluvial plain by south-westward to westward flowing rivers, sourced from the Ancestral Rocky Mountains (North & Taylor, 1996), and north-westward flowing rivers sourced from the Mogollon Highlands in the Cordilleran Magmatic Arc (Figure 4.1) (Luttrell, 1993). The thickness of the Kayenta ranges from 16.8 m at its eastern extent at Rock Point, Arizona to 206.7 m along Ward Terrace, Arizona (Harshbarger *et al.*, 1957).

Two distinct lithofacies can be recognised within the Kayenta Formation - the 'sandy' and 'silty' facies - resulting from the lateral variation of the fluvial system across the Colorado Plateau (Harshbarger *et al.*, 1957). In south-eastern Utah and western Colorado, the Kayenta is characterised by grey to reddish orange, fine to coarse-grained, well sorted, well to sub-rounded sandstones, with minor reddish-purple

siltstones and matrix-supported conglomerates (Wilson, 1958). In north-western Arizona, the Kayenta is characterised by reddish purple siltstones, mudstones and minor sandstones. The transition from predominately sandy in south-eastern Utah to predominately silty in north-western Arizona is a gradual progressive change across several miles in the Vermilion Cliffs (Wilson, 1958). The Kayenta is subdivided into three Members; the Springdale, main body and Tenny Canyon Tongue Members all of fluvial origin (Wilson, 1958).

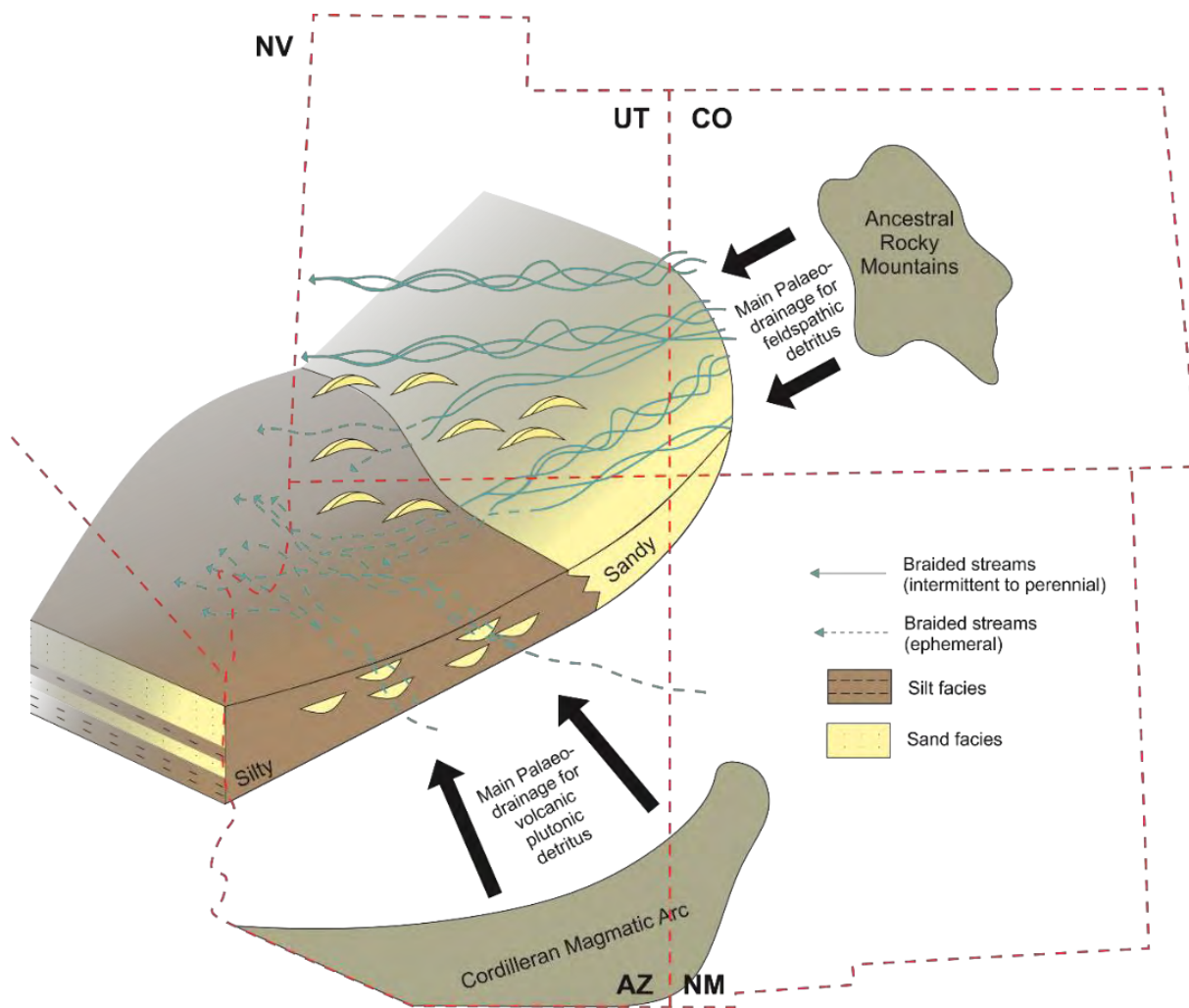


Figure 4.1. Generalised distribution of the 'sandy' and 'silty' facies of the Kayenta Formation across the Four Corners states and Nevada, with generalised fluvial palaeoflow direction and possible sources. (after Harshbarger et al., 1957; Middleton & Blakey, 1983; Luttrell, 1993).

4.1.2. Springdale Member

The Springdale Sandstone is the basal member of the Kayenta. However it was originally described as part of the Moenave Formation due to similar lithological characteristics (Wilson, 1967; Wilson &

Stewart, 1967; Pipiringos & O'Sullivan, 1978; Luttrell & Morales, 1993), but was reclassified due to its 'ledge-like' weathering and identification of a basal unconformity between the member and the underlying Moenave Formation and conformable, gradational upper contact with the Kayenta (Harshbarger *et al.*, 1957; Marzolf, 1994; Lucas *et al.*, 2005). The member comprises 32 m of medium to coarse-grained sandstones, with sporadic discontinuous conglomerates and subordinate mudstone lenses (Lucas & Tanner, 2007), deposited in a braided fluvial system, flowing northward, with small floodplains (Clemmensen & Blakey, 1989; Blakey, 1994).

4.1.3. Kayenta main body

The main body of the Kayenta conformably and gradational overlies the Springdale Sandstone and comprises approximately 28 to 460 m of reddish-brown fine to coarse-grained sandstones, siltstones and minor claystones (Luttrell, 1993). Occasional limestone and conglomeritic beds are also recognised and thought to have been derived from massive flooding events which ripped up the overbank and floodplain deposits (Doelling *et al.*, 1988; North & Taylor, 1996; Fillmore, 2011). Sandstone bodies dominate the eastern parts of the exposure, along with increased channel bodies, due to the proximity to the Ancestral Rocky Mountains, a potential sediment source for the Kayenta (Doelling *et al.*, 1988), whereas siltier deposits dominate towards the west of the exposed Kayenta Formation (Wilson, 1958). The main body was deposited by an ephemeral braided fluvial system and exhibits a gradational contact with the overlying Navajo Sandstone (Bromley, 1991; North and Taylor, 1996).

4.1.4. Tenny Canyon Tongue

The Tenny Canyon Tongue comprises up to 98 m of pale reddish-brown lenticular fine-grained sandstone, siltstone and mudstone deposits, with minor limestone and claystone beds. The tongue thins rapidly towards the east, with its maximum thickness exposed at Zion National Park and exhibits steep sloped and ledge-like cliffs before grading into the overlying Navajo Sandstone. The Tenny Canyon Tongue was deposited in a distal river and playa system (Luttrell, 1993).

4.1.5. Sedimentology of the Kayenta Formation

A variety of facies schemes have been described for the deposits of the Kayenta Formation across the Colorado Plateau, with the most widely used scheme proposed by Miall (1978). Table 4.1 and Table 4.2 include a short synopsis of published facies schemes up to the present day.

Thirteen fluvial facies have been identified in the Kayenta Formation (Table 4.1), along with four facies associations (Table 4.2) which have been recognised and compiled from several sources (Miall, 1977; 1978; Bromley, 1991; Luttrell, 1993; North & Taylor, 1996).

Table 4.1. Main facies identified in the Kayenta Formation in the eastern part of the Colorado Plateau (Modified after Miall, 1977; Miall, 1978; Bromley, 1991; Luttrell, 1993; North & Taylor, 1996).

Facies Code	Lithofacies	Sedimentary structures	Interpretation
Sm	Fine to coarse-grained sandstone with frequent intraclasts	Massive with occasional flame structures	Upper flow regime hyperconcentrated flows where rapid deposition inhibits bedform development. Flood events and debris flows
St	Medium to very coarse-grained sandstone, occasionally pebbly	Singular or grouped trough cross-bedding	Lower flow regime migration of sinuous crested dunes
Sp	Medium to very coarse-grained sandstone, occasionally pebbly	Singular or grouped planar cross-bedding	Lower flow regime migration of linguoid, transverse bars and sand waves
Sr	Very fine to coarse-grained sandstone	Ripple marks of all types	Lower flow regime migrating current ripples
Sh	Very fine to very coarse-grained sandstone, occasionally pebbly	Horizontal lamination parting or stream lineation	Upper and lower flow regime planar beds. Upper to transitional flow-regime plane-laminated beds occurring as channel fill or bar tops.
Sl	Fine-grained sandstone	Low angle cross-beds (< 10°) occasionally sigmoidal	Scour fills, crevasse splays, washed out dunes, antidunes. Migration of straight to slightly sinuous crested transitional dunes/bars

Sp	Fine to coarse-grained sandstone, occasionally muddy or pebbly	Overtuned parabolic cross-beds with minor massive intercalations	Bed shear due to sediment saturation
Sf	Mudstone, siltstone and fine-grained sandstone	Planar laminated	Lower flow regime suspension fallout
Cs	Medium-grained sandstone with pebble sized clasts	Chaotic beds with massive to parallel laminated internal structures	Erosive pulses during flood surges influenced by sediment supply
Cgu	Uncemented matrix supported conglomerate	Massive to very poorly laminated and bedded.	High energy flow resulting in bank erosion with clasts buried in place or transported over a short distance
Cgp	Uncemented mud pellet conglomerate	Massive to very poorly laminated and bedded.	High energy flow resulting in bank erosion with clasts transported over longer periods
Cgc	Uncemented clast supported conglomerate	Massive to very poorly laminated and bedded with imbrication of clasts	Mud clasts deposited by sand-starved flow
Cgc	Cemented conglomerate	Massive to very poorly laminated and bedded	High energy flow resulting in bank erosion with clasts buried in place or transported over a short distance also contains carbonate-rich flood plain material reworked into channel lag and yields cements after deposition

Table 4.2. Summary of the four main fluvial facies associations of the Kayenta Formation (Modified after Luttrell, 1993; Sanabria, 2001).

Facies Assoc.	Facies	Interpretation
1	St, Sh, Sp, Sl, Cgu	Sandy, low sinuosity fluvial systems with perennial discharge
2	Sr, Sf	Sandy, low sinuosity streams that experienced intermittent discharge and fluctuation flow conditions
3	Sh, Sf, Sm	Low- to moderately-sinuosity ephemeral streams enclosed in well-developed overbank areas
4	Cs, Cgp, Cgcl, Cgc, Cgu	High energy flows

4.1.6. Kayenta-Navajo Transition

An intertonguing relationship between the Kayenta and Navajo formations has been recognised. In the upper third of the Kayenta there are several sandy tongues of 'Navajo-type' lithology, including the Lamb Point and Shurtz Sandstone tongues, recognised in the Kanab and Cedar City regions (Wilson, 1958; Middleton & Blakey, 1983). The Lamb Point Tongue overlies the main body of the Kayenta and occurs up to 65 m below the base level of the Navajo. To the north-east of Kanab, the tongue thickens to over 160 m where it eventually joins with the Navajo Sandstone (Averitt *et al.*, 1955), however to the south-west of Kanab the tongue rapidly thins and merges with the silty facies of the Kayenta (Middleton & Blakey, 1983). The Shurtz Sandstone Tongue lies between 125–220 m below the base of the Navajo (Averitt *et al.*, 1955; Middleton & Blakey, 1983) and varies in thickness from 120 m near Cedar City to 10 m to the south of Cedar City where it thins rapidly (Wilson, 1958). This tongue is not traceable into the main body of the Navajo, however it is composed of lithologically identical sandstone (Averitt *et al.*, 1955; Middleton & Blakey, 1983).

Several tongues of 'Kayenta-type' lithology have also been recognised including the Cedar City and Tenny Canyon tongues. The Cedar City Tongue overlies the Navajo Shurtz Tongue and thickens towards the south as the Shurtz Tongue thins. The Tenny Canyon Tongue overlies the Lamb Point Tongue and reaches up to 35m thick in Kanab (Averitt *et al.*, 1955; Middleton & Blakey, 1983). Several smaller scale intertonguing relationships can also be recognised.

Several theories have been published about the processes behind the intertonguing interval including, climatic variations with an overall trend towards desertification (Middleton & Blakey, 1983), basin instability relating to salt tectonics (Bromley, 1991) and other tectonic effects causing the expansion and contraction of the erg system (Herries, 1993).

4.1.7. Dating the Kayenta Formation

The presence of several fossils have been reported including occasional fresh-water gastropods and bivalves (*Unio dumblei*, *Unio dockumensis* and *Unio iridoides*) as well as complete and partial skeletons

of dinosaurs belong to the superfamily *Trityloidontea*. The occurrence of these fossils allowed the Kayenta to be dated to Late Triassic to Late Jurassic age (Harshbarger *et al.*, 1957). Palynology of the Whitmore Point Member of the Moenave Formation allowed slightly more accurate dating and assigned an early Jurassic age to the Kayenta Formation due to the presence of palynomorphs *Corollina torosus*, *Corollina murphyi* and *Corollina meyeriana* (Peterson & Pippingos, 1979).

No palynomorphs or fossilised plants have been found in the Kayenta (Kietzke & Lucas, 1995; Lucas & Tanner, 2006), however numerous tetrapod footprints and body fossils have been identified (Sues *et al.*, 1994; Lockley & Hunt, 1994, 1995; Curtis & Padian, 1999). Footprints are mainly from *Eubrontes* and *Grallator* theropods, whereas body fossils range from frogs (*Prosalirus*) to theropod dinosaurs (*Megapnosaurus* and *Dilophosaurus*) (Sues *et al.*, 1994; Curtis & Padian, 1999). The presence of these footprints and body fossils has allowed the Kayenta Formation to be dated between Sinemurian to early Toarcian age (Lucas & Tanner, 2007).

4.2. Methods

This study uses extensive regional sedimentological fieldwork in conjunction with three-dimensional photogrammetry techniques (Chapter 3) to examine the sedimentary detail and interactions of fluvial and aeolian deposits of the Kayenta Formation across the Colorado Plateau, from proximal to distal settings. To investigate sedimentary interactions, twenty-five detailed vertical sections were logged (Chapter 3, Table 3.1), with a total measured length over 1700 m, distributed approximately in a grid-like pattern, each section approximately 25 km apart, over an area of approximately 200 km² (Figure 4.2). Sedimentary logs were combined with detailed photogrammetric panels through key sections within proximal, medial and distal fluvial settings to create digital outcrop models totalling a combined length of 5 km.

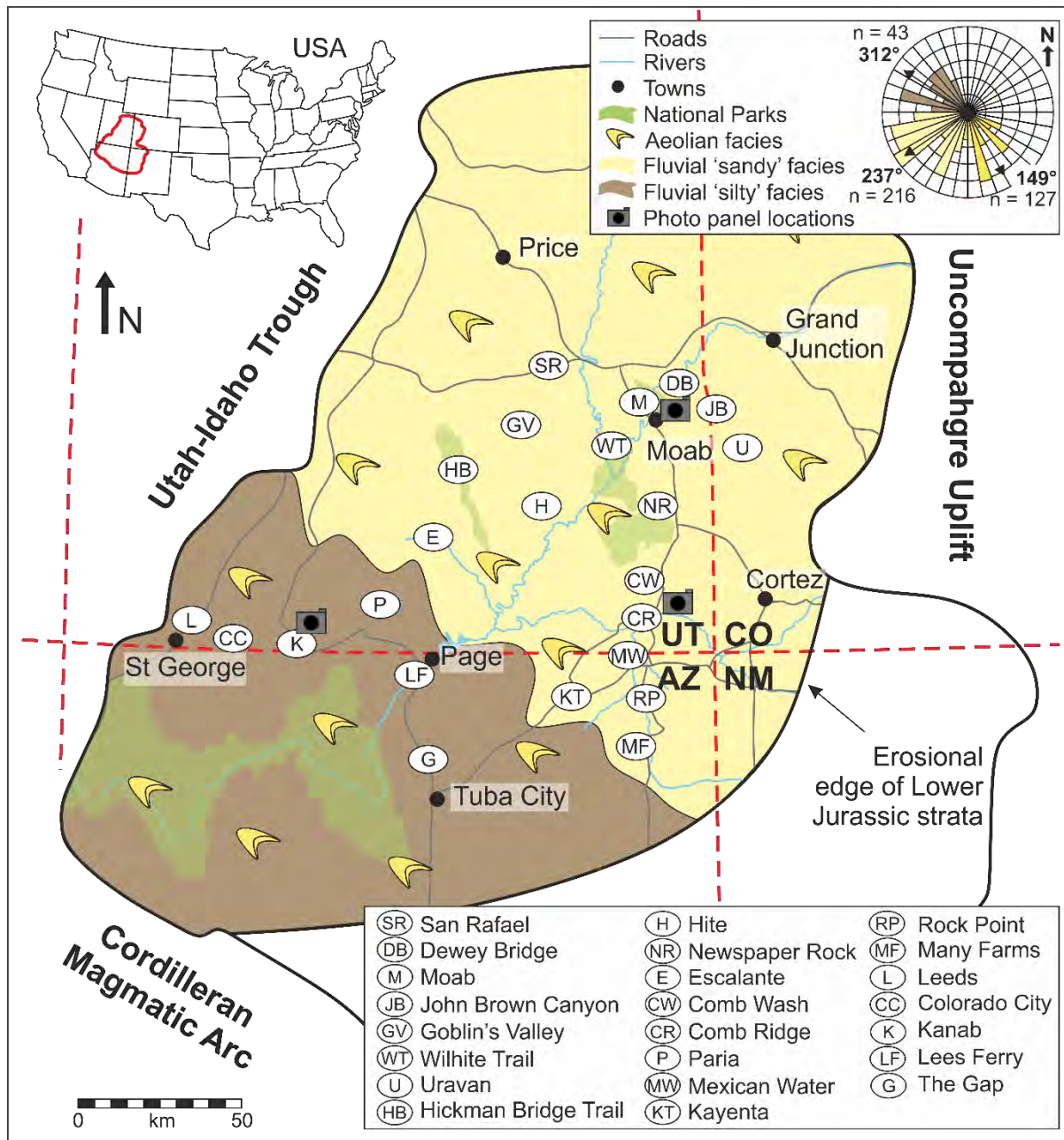


Figure 4.2. The Colorado Plateau, situated in the Four Corner states, USA, showing the extent of the Kayenta Formation deposition. The Kayenta fluvial systems deposited sediment across the Colorado Plateau sourced from the Ancestral Rocky Mountains (Uncompahgre Uplift) to the northeast and the Cordilleran Magmatic Arc to the southwest, locations of logged sections are indicated in white ellipses (see key) (modified after Harshbarger et al., 1957; Middleton & Blakey, 1983; Blakey 1994). The rose diagram depicts palaeocurrent measurements from the 'silty' (brown) and 'sandy' (light yellow) fluvial system and the aeolian system (yellow), along with their arithmetic averages (arrows); 'n' gives the number of measurements in each set.

4.3. Lithofacies of the Kayenta Formation

The facies scheme presented in this study builds upon the observations and interpretations of previously published work (e.g. Miall, 1977; 1978; Bromley, 1991; Luttrell, 1993; North & Taylor, 1996)

and provides further detail from a regional study. The descriptions and interpretations presented are all based upon primary field observations within this study. Twenty-one facies have been identified within the Kayenta Formation and they are summarised in Table 4.3 and depicted on representative sedimentary logs in Figure 4.3. Sixteen facies relate to sub-aqueous processes and the remainder relate to wind-blown processes. Analogous facies have been recognised previously by many workers to typify deposition in aeolian or fluvial settings (Hunter, 1977; Miall, 1988; Langford & Chan, 1989; Kocurek, 1991; North & Taylor, 1996; Hassan *et al.*, 2018), therefore these are described in Table 4.3. However, detailed descriptions of the more unique facies of the Kayenta Formation are described below (Figure 4.4).

Planar-bedded sandstone – Spb

The deposits of facies **Spb** (Figure 4.4A) are composed of brown medium-grained sub-arkosic arenite to quartz arenite, with moderate to well sorted, sub-rounded to well-rounded grains. The internal architecture comprises planar-bedding ranging in thickness between 1 cm and 5 cm within sets ranging from 20 cm to 1 m in thickness. Sporadic clasts near the base of **Spb** units and primary current lineations are common features. Facies **Spb** is common throughout the expanse of deposition but is most prevalent within the sheet-like elements.

Interpretation: Facies **Spb** is interpreted to be deposited under sub-aqueous upper flow regime flat bed conditions within a high velocity, rapidly shallowing flow (Arnott & Hand, 1989; Carling, 2013; Guan *et al.*, 2016).

Parallel-laminated sandstone – Spl

The deposits of facies **Spl** (Figure 4.4B) are composed of brown fine to medium-grained sub-arkosic arenite to quartz arenite, with moderate to well sorted and sub-rounded to well-rounded grains. The internal architecture comprises parallel-laminations ranging in thickness between 0.2 mm and 1 cm within sets ranging from 10 cm to 50 cm. Facies **Spl** is common throughout the expanse of deposition but is most prevalent within the sheet-like elements.

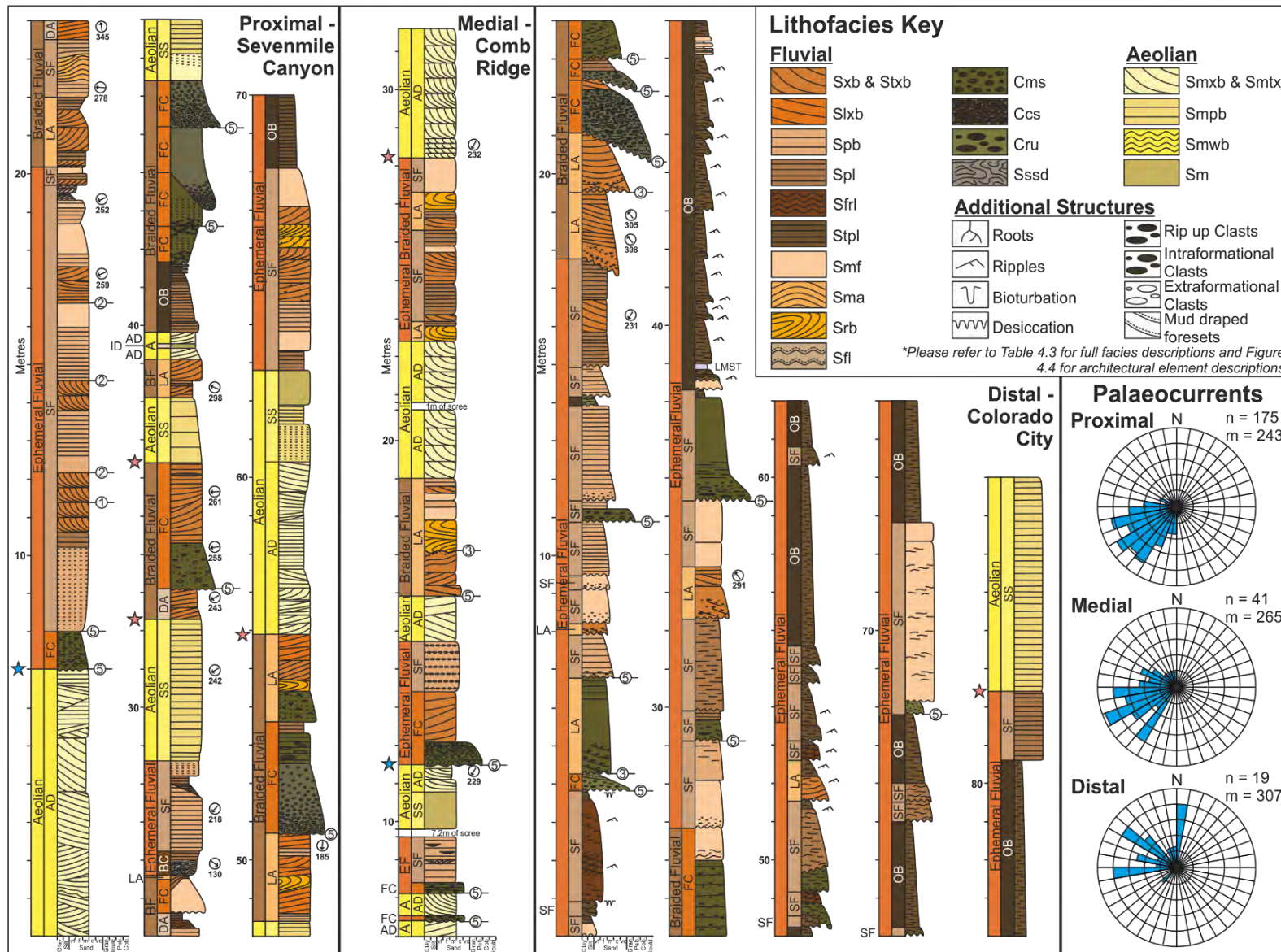

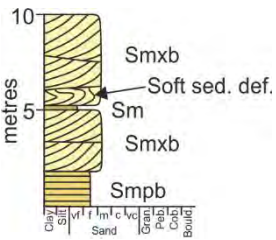

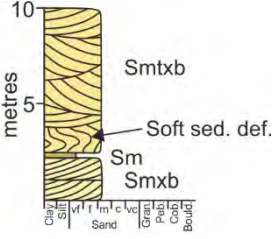

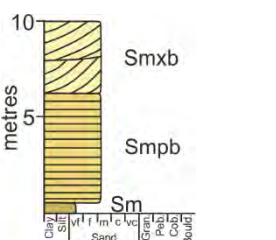

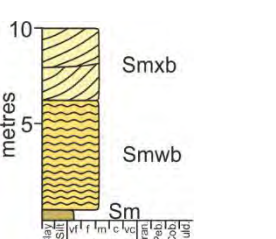

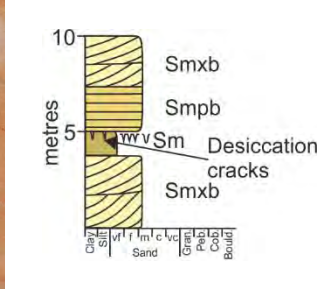

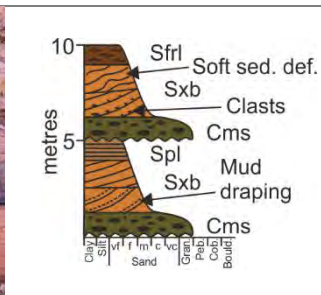

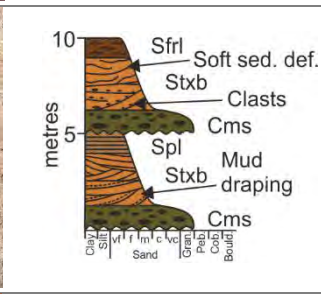

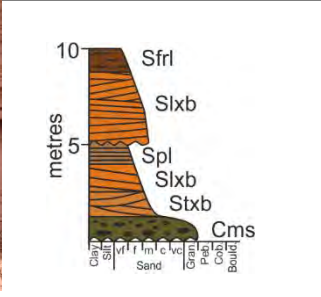
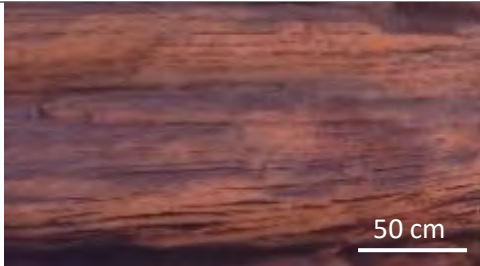
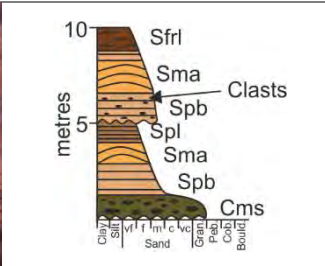

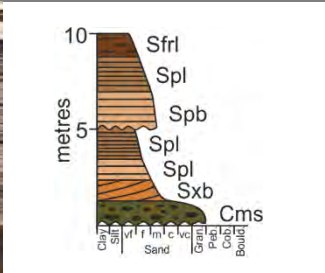

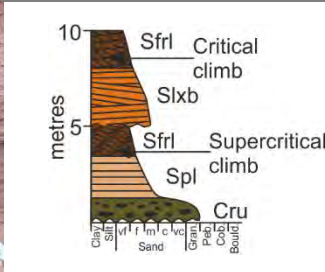

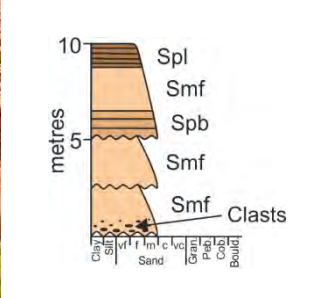

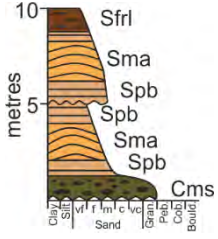

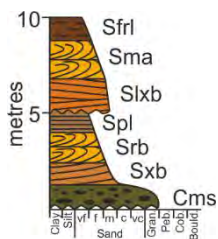

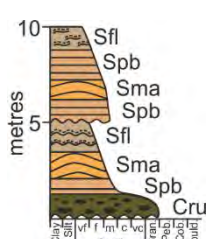
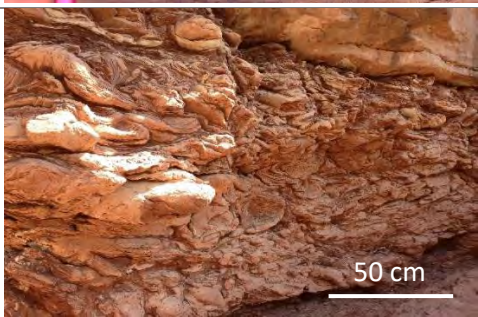
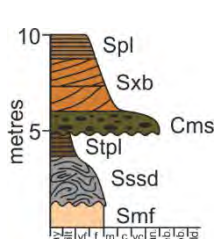



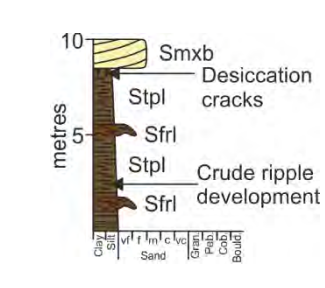

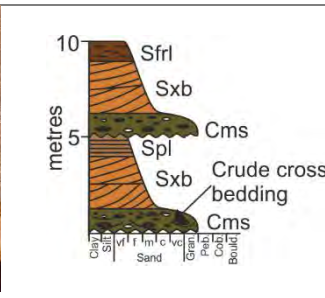

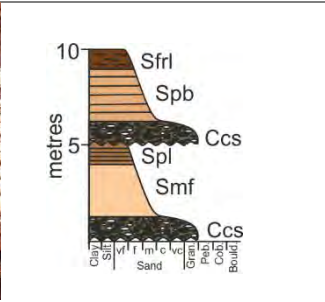
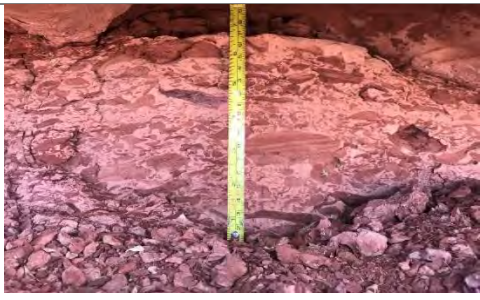
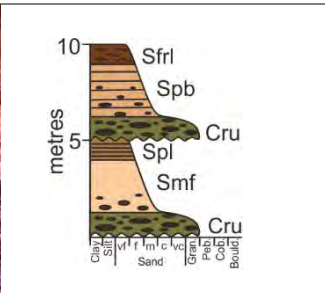
Figure 4.3. Representative sedimentary logs showing the downstream lithofacies and palaeocurrent variations observed in the Kayenta Formation. Sedimentary logs are coloured by lithofacies (see key) with architectural element codes and broad facies associations listed down the side. Examples of bounding surfaces are highlighted by hierarchical numbers. See Fig. 4.2 for locations.

Code	Lithofacies	Idealised Log	Lithology & Texture	Sedimentary Structures	Interpretation
Smxb			Grey to orange, fine to medium-grained sandstone well sorted & well rounded.	Planar cross-bedding with mm/cm scale alternations in grainsize in single or multiple sets, sporadic soft sediment deformation.	Migration of wind-blown straight-crested dune-scale bedforms and dune trains. Soft sediment deformation formed as a result of loading on a damp substrate.
Smtxb			Grey to orange, fine to medium-grained sandstone, well sorted & well rounded.	Trough cross-bedding with mm/cm scale alternations in grainsize in single or multiple sets, sporadic soft sediment deformation.	Migration of wind-blown sinuous-crested dune-scale bedforms and dune trains. Soft sediment deformation formed as a result of loading on a damp substrate.
Smpb			Grey to orange, fine to medium-grained sandstone, well sorted & well rounded.	Planar-bedding with millimetre scale alternations in grainsize.	Wind-blown deposits formed from the deflation of dune-scale bedforms.
Smwb			Grey to orange, fine to medium-grained sandstone, well sorted & well rounded.	Undulose-laminations with millimetre scale alternations in grainsize.	Migration of wind-blown ripple-scale bedforms, producing pinstripe laminae.

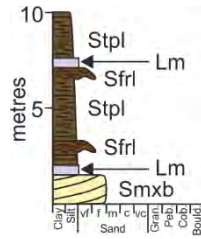
<p>Sm</p>			<p>Grey to orange, very fine to medium-grained sandstone, well sorted & well rounded.</p>	<p>Structureless, sporadic desiccation cracks and bioturbation.</p>	<p>Suspension settling of wind-blown sediment in areas affected by surface water, followed by drying.</p>
<p>Sxb</p>			<p>Brown medium-grained sandstone, moderate/well sorted & sub-rounded/well rounded.</p>	<p>Planar cross-bedding with normal grading, in single or multiple sets, sporadic clasts, mud draping and soft sediment deformation.</p>	<p>Migration of straight-crested dune-scale bedforms and dune trains sub-aqueously under lower flow regime conditions with high sediment load.</p>
<p>Stxb</p>			<p>Brown medium-grained sandstone, moderate/well sorted & sub-rounded/well rounded.</p>	<p>Trough cross-bedding with normal grading, in single or multiple sets, sporadic clasts and soft sediment deformation.</p>	<p>Migration of sinuous-crested dune-scale bedforms and dune trains sub-aqueously under lower flow regime conditions.</p>
<p>Slxb</p>			<p>Brown medium-grained sandstone, moderate/well sorted & sub-rounded/well rounded.</p>	<p>Low-angle cross-bedding in single or multiple lenticular sets and sporadic reactivation surfaces.</p>	<p>Lateral migration of macro-forms in lower flow regime conditions.</p>

<p>Spb</p>			<p>Brown medium-grained sandstone, moderate/well sorted & sub-rounded/well rounded.</p>	<p>Planar-bedding, sporadic clasts.</p>	<p>Sub-aqueous upper flow regime flat beds.</p>
<p>Spl</p>			<p>Brown fine to medium-grained sandstone, moderate/well sorted & sub-rounded/well rounded.</p>	<p>Parallel laminations.</p>	<p>Sub-aqueous upper flow regime flat beds.</p>
<p>Sfrl</p>			<p>Brown siltstone to medium-grained sandstone, moderate/well sorted & sub-rounded/well rounded.</p>	<p>Cross-laminations, with sub-critically to super-critically climbing multiple sets which form cosets.</p>	<p>Migration of ripple-scale bedforms in lower flow regime. Alternations in angle of climb suggests variations in sediment load.</p>
<p>Smf</p>			<p>Orange to brown medium-grained sandstone, moderate/well sorted & sub-rounded/well rounded.</p>	<p>Structureless, sporadic clasts concentrated in basal sections.</p>	<p>Rapid deposition in high sediment load suppressing bedform development.</p>

<p>Sma</p> 		<p>Orange to brown medium-grained sandstone, moderate/well sorted & sub-rounded/well rounded.</p>	<p>Sigmoidal-bedding with normally graded foresets in single or multiple sets.</p>	<p>Upper flow regime-antidune development and preservation.</p>
<p>Srb</p> 		<p>Orange to grey medium-grained sandstone, moderate/well sorted & sub-rounded/well rounded.</p>	<p>Recumbent cross-bedding, sporadic mud draping on foresets in single or multiple sets, with slightly concave set bounding surfaces.</p>	<p>Migration of sinuous-crested dune-scale bedforms in lower flow regime with high sediment load.</p>
<p>Sfl</p> 		<p>Brown siltstone to fine-grained sandstone.</p>	<p>Flaser laminations with silt lining foreset and set bounding surfaces.</p>	<p>Migration of ripple-scale bedforms in lower flow regime/waning flow conditions.</p>
<p>Sssd</p> 		<p>Purple to brown siltstone to fine-grained sandstone matrix, with locally derived sediment, forming moderate/poorly sorted & sub-rounded clasts.</p>	<p>Soft sediment deformed clasts with silt lining the contorted foresets and between the deformed clasts.</p>	<p>Sub-aqueous mass transport deposits: debris flow/slumping/sliding into a high sediment load flow.</p>

Stpl			Dark brown siltstone, sporadic mottling.	Parallel to faint undulose laminations, sporadic rhizoliths, desiccation cracks and bioturbation.	Suspension fall out from stationary waters. Stabilization for vegetation to develop.
Cms			Grey to brown medium-grained sand to pebble-grade, polyimictic conglomerate, poorly sorted, sub-rounded, matrix-supported.	Structureless to sporadic crude trough cross-bedding, with abundant clasts lining foresets.	Sub-aqueous lower flow regime conditions with high sediment load, intermittent development and migration of dune-forms.
Ccs			Grey to brown coarse-grained sand to pebble-grade, polyimictic conglomerate, poorly sorted, sub-rounded, clast-supported.	Structureless to very crude cross-bedding, abundant clasts throughout.	Sub-aqueous, high energy Newtonian flow under high sediment load conditions, with suppressed bedform development.
Cru			Grey to orange medium-grained, poorly sorted, sub-rounded/sub-angular, matrix-supported conglomerate. Rip up clasts ranging from granule to cobble grade.	Structureless to very sporadically crudely cross-bedded, rip up clasts at base.	Sub-aqueous high energy flow under high sediment load conditions and reworking of locally derived sediment.

Lm



Grey siliciclastic rich,
carbonate wackestone
with sporadic red chert.

Structureless to
undulose laminated.

Sub-aqueous
precipitation of
allochthomous
carbonate with
siliciclastic input.

Table 4.3. Summary of lithofacies observed in the Kayenta Formation. **Smbx**: Sub-aerial planar cross-bedded sandstone, **Smtxb**: Sub-aerial trough cross-bedded sandstone, **Smpb**: Sub-aerial planar bedded sandstone, **Smwb**: Sub-aerial undulose laminated sandstone, **Sm**: Sub-aerial structureless sandstone, **Sxb**: Sub-aqueous planar cross-bedded sandstone, **Stxb**: Sub-aqueous trough cross-bedded sandstone, **Slxb**: Sub-aqueous low-angle cross-bedded sandstone, **Spb**: Sub-aqueous planar bedded sandstone, **Spl**: Sub-aqueous parallel laminated sandstone, **Sfrl**: Sub-aqueous cross-laminated sandstone, **Smf**: Sub-aqueous structureless sandstone, **Sma**: Sub-aqueous sigmoidal bedded sandstone, **Srb**: Sub-aqueous recumbent cross-bedded sandstone, **Sfl**: Sub-aqueous flaser laminated sandstone, **Sssd**: Sub-aqueous soft sediment deformed sandstone, **Stpl**: Sub-aqueous parallel laminated siltstone, **Cms**: Sub-aqueous matrix-supported conglomerate, **Ccs**: Sub-aqueous clast-supported conglomerate, **Cru**: Sub-aqueous rip-up clast conglomerate, **Lm**: Sub-aqueous siliciclastic-rich limestone.

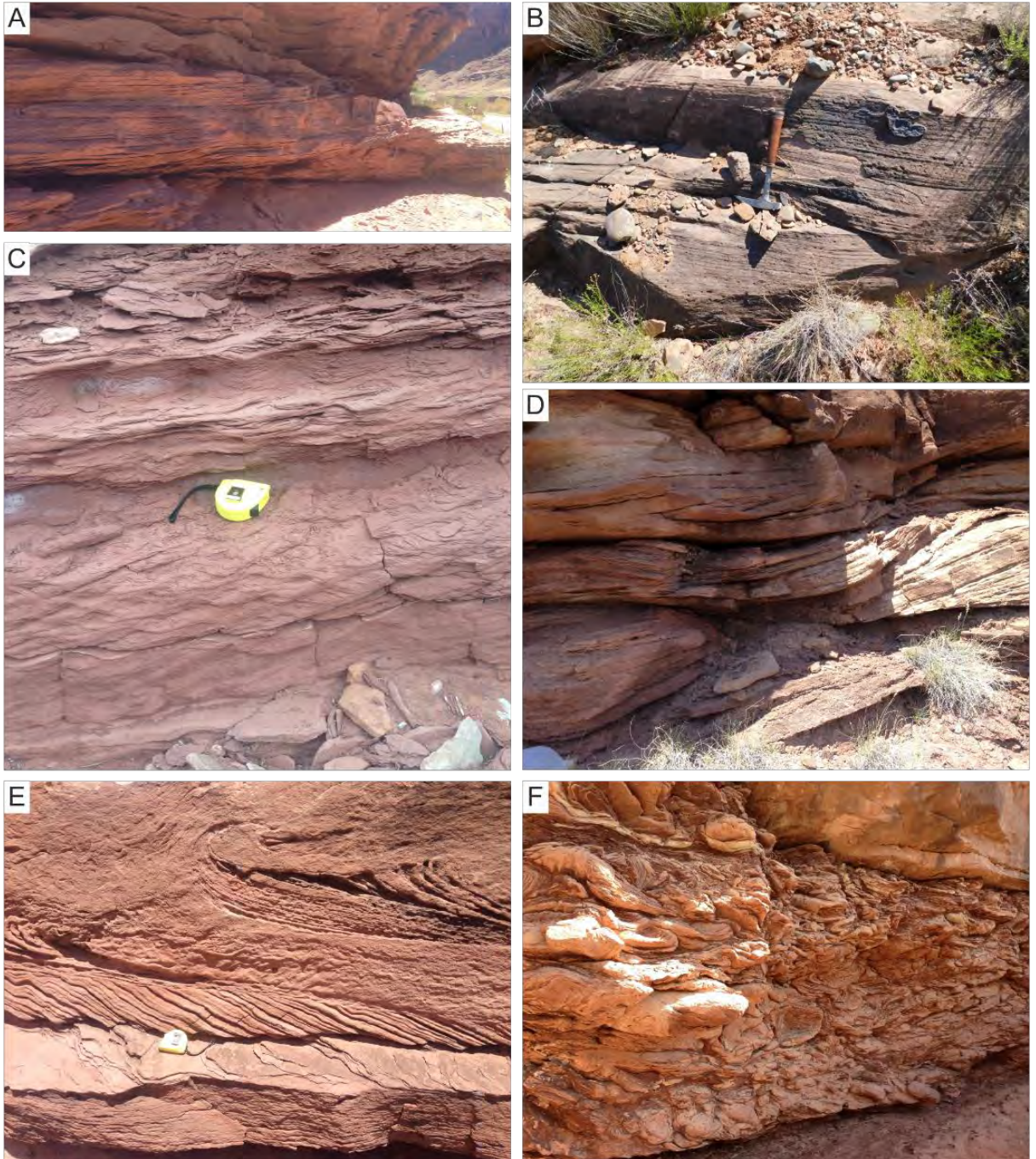


Figure 4.4. Photopanel of unique facies within the Kayenta Formation. A) Planar-bedded sandstone (*Spb*) formed under upper flow regime conditions, each bed is approximately 5-10 cm thick; B) Parallel-laminated sandstone (*Spl*) formed under upper flow regime conditions, 30 cm hammer for scale; C) Supercritical climbing ripples (*Sfri*) with preservation of both the stoss slope and less slope of the bedform and an angle of climb of 16° formed under lower flow regime conditions with significant sediment supply, yellow measuring tape for scale (6 cm); D) Sigmoidal bedded sandstone (*Sma*) - humpback cross-bedding of antidunes with a symmetrical geometry and preservation of the stoss and lee slope of the bedform, formed between conditions of lower flow regime dune formation to upper flow regime plane bed formation, gallon water jug for scale (30 cm); E) Recumbent cross-bedded sandstone (*Srb*) with 'ripped back' topsets of the foresets, formed under lower flow regime conditions with fluctuations within flow conditions and sediment load, yellow measuring tape for scale (6 cm); F) Soft sediment deformed sandstone (*Sssd*) (bank collapse) containing contorted intra-formational clasts with mud-draping along the folded foresets, interpreted as a mass-transport debris-flow deposit, clasts are approximately 20-30 cm wide.

Interpretation: Facies **Spl** is interpreted to be deposited under sub-aqueous upper flow regime flat bed conditions within a high velocity, rapidly shallowing flow (Arnott & Hand, 1989; Carling, 2013; Guan *et al.*, 2016).

Cross-laminated sandstone – Sfrl

The deposits of facies **Sfrl** (Figure 4.4C) are composed of brown siltstone to medium-grained sub-arkosic arenite, with moderate to well sorted and sub-rounded to well-rounded grains. The internal architecture comprises cross-laminations which climb sub-critically to super-critically in multiple sets forming cosets. Sets range in thickness from 2 cm to 6 cm within cosets up to 50 cm. Facies **Sfrl** is common throughout the expanse of deposition but is most prevalent within the upper units of the sheet-like and accretionary elements.

Interpretation: Facies **Sfrl** is interpreted to be deposited by the migration of sub-aqueous ripple-scale bedforms under lower flow regime conditions with sediment supply significant enough to promote supercritical climb (Hunter, 1977).

Sigmoidal bedded sandstone – Sma

The deposits of facies **Sma** (Figure 4.4D) are composed of orange to brown, medium-grained sub-arkosic arenite to quartz arenite, with moderate to well sorted and sub-rounded to well rounded grains. The internal architecture comprises sigmoidal bedding with a symmetrical convex upward geometry, mimicked by the internal structure of the bedding. Sets range in thickness from 20 cm to 70 cm. Facies **Sma** is common throughout the expanse of deposition but is most prevalent within the sheet-like elements.

Interpretation: Facies **Sma** is interpreted as humpback cross-bedding of antidunes with a symmetrical geometry and preservation of the stoss and lee slope of the bedform (Fielding, 2006; Lang & Winsemann, 2013). These structures represent the transition from conditions of lower flow regime dune formation to upper flow regime plane bed formation, and they were probably formed under high rates of sediment deposition (Fielding, 2006; Lang & Winsemann, 2013).

Recumbent cross-bedded sandstone – Srb

The deposits of facies **Srb** (Figure 4.4E) are composed of orange to grey, medium-grained sub-arkosic arenite to quartz arenite, with moderate to well sorted and sub-rounded to well-rounded grains. The internal architecture comprises recumbent cross-bedding with sporadic mud draping on foresets and ‘ripped back’ topsets of the foresets. Cross-bedding of this type occurs in single or multiple sets, with slightly concave set-bounding surfaces. Sets range in thickness from 15 cm to 1 m. Facies **Srb** is common throughout the expanse of deposition but is most prevalent within the accretionary elements.

Interpretation: Facies **Srb** is interpreted to have been deposited by the migration of sinuous-crested dune-scale bedforms in lower flow regime conditions with fluctuations within flow conditions and sediment load, causing the overriding flow to overturn the underlying saturated beds (Stikes, 2007). The sporadic mud-draping suggests a high sediment load within the flow with the finer sediment deposited after the flow reaches its full carrying capacity for fine material (Olsen, 1987).

Soft sediment deformed sandstone – Sssd

The deposits of facies **Sssd** (Figure 4.4F) are composed of a purple to brown, siltstone to fine-grained sub-arkosic arenite matrix with locally derived sediment forming moderate to poorly sorted and sub-rounded contorted clasts. The internal architecture comprises soft-sediment deformed, contorted intra-formational clasts with mud-draping along the folded foresets, which are held within a brown, parallel laminated siltstone matrix. Units of this type range in thickness from 1 m to 3 m. Facies **Sssd** is uncommon throughout the expanse of deposition but occurs sporadically near the base of the Kayenta Formation at several locations from the proximal to distal settings.

Interpretation: Facies **Sssd** is interpreted as a mass-transport debris-flow deposit formed by the collapse of the river’s banks into high sediment laden flow (Owen, 1996, 2017; Rana *et al.*, 2016; Van den Berg *et al.*, 2017; Carling & Leclair, 2019).

4.4. Summary

The Lower Jurassic Kayenta Formation comprises a continental redbed assemblage of fine to coarse-grained sandstones, siltstones and occasional intra-formational conglomerates deposited in a dominantly ephemeral-fluvial system, with minor perennial influxes and aeolian interactions.

The deposits of the Kayenta Formation have been studied across the expanse of the Colorado Plateau and twenty-one facies have been identified based upon lithology and sedimentary structures, summarised in Table 4.3. The facies have been grouped to relate to their dominant depositional process. Sixteen facies relate to sub-aqueous depositional processes (**Sxb, Stxb, Slxb, Spb, Spl, Sfrl, Smf, Sma, Srb, Sfl, Sssd, Stpl, Cms, Ccs, Cru** and **Lm**) and five relate to sub-aerial, wind-blown processes (**Smxb, Smtxb, Smpb, Smwb** and **Sm**). Six facies have been described in more detail due to their uniqueness, including **Spb, Spl**, and **Sma**, which are interpreted as the deposits of upper flow regime conditions, **Sfrl**, which is interpreted as supercritical climbing ripples, **Srb**, which is interpreted as the deposits of dune-scale bedforms, where fluctuations within flow conditions and sediment load, caused the overriding flow to overturn the underlying saturated beds and finally **Sssd**, which is interpreted as mass-transport debris-flow deposits.

Chapter Five will draw upon the observed facies described in this chapter and detail nine architectural elements, five depositional elements and three depositional environments.

Chapter 5: Interpretation of the Sedimentology of an Ephemeral Fluvial Outcrop Analogue: The Kayenta Formation

This chapter interprets the sedimentology of a dryland ephemeral fluvial system using the Lower Jurassic Kayenta Formation as an example. The chapter draws upon the observed facies described in Chapter Four and details nine architectural elements, five depositional elements and three depositional environments. The architectural elements contain multiple facies and are grouped by depositional environment, either: fluvial or aeolian. The depositional elements are grouped based upon the internal stacking patterns and composition of the architectural elements within them. Chapter Six will draw upon the observed facies within Chapter Four and depositional elements within this chapter to describe and quantify the spatial and temporal variations of these elements. The interactions between the fluvial and aeolian deposits will also be described and multiple scales.

5.1. Architectural Elements

The twenty-one facies; depicted on representative sedimentary logs in Chapter Four (Fig. 4.3), form nine architectural elements which are summarised in Figure 5.1. Each element is detailed below. Detailed photogrammetric panels through key sections within proximal (Fig. 5.2), medial (Fig. 5.3) and distal (Fig. 5.4) fluvial settings are also provided. The outcrop models depict: (i) the lateral and vertical relationships between fluvial and aeolian architectural elements; (ii) the geometry and dimensions of the elements; (iii) the nature of the interactions between the elements; (iv) the changes in architecture and sedimentology from proximal to distal settings; and (v) the vertical changes within the formation that represent the temporal evolution of the system.

5.1.1. Fluvial channel elements

In sections perpendicular to flow, elements of this type have a concave upward 'U'-shaped geometry. They can occur as isolated entities within overbank elements or stacked with repeated examples laterally and vertically amalgamated giving sheet-like or ribbon bodies at the larger scale (Fig. 5.5). Elements of this type have erosional fifth-order basal bounding surfaces (*sensu* Miall, 1996) and comprise eight facies: matrix-supported (**Cms**), clast-supported (**Ccs**) and rip-up clast dominated (**Cru**) conglomerates, which line the basal bounding surface with occasional very coarse to granule sized clasts lining crudely developed foresets and comprise 5% of the element. Planar cross-bedded sandstones (**Sxb**) that overlie the basal conglomerate and contain sets approximately 0.2 to 2.0 m thick with foresets occasionally lined with siltstone comprise most of the element (75%). Rarer trough cross-bedded (**Stxb**) and recumbent cross-bedded (**Srb**) sandstones comprise 5% of the element in more or less equal proportions and occur as sets in between sets of planar cross-bedded sandstones. Parallel-laminated (**Spl**), and structureless (**Smf**) sandstones form the upper units of the succession and comprise the remainder of the element. Preservation of the full element is rare (approximately 15% of examples) with most examples truncated and eroded by basal fifth-order surfaces from either other elements of this type or from sheet-like elements.

Interpretation

Elements with this geometry are interpreted as fluvial channels of a multi-storey, low-sinuosity, braided to ephemeral system (Miall, 1985; North & Taylor, 1996; Billi *et al.*, 2018). Conglomeratic basal units with clasts lining crude foreset development represent channel lag deposits formed with high flow velocities and dominantly bedload transport where the large sediment grain size prevents the mixed-load transport required for bedform formation. Structureless sands with crude foreset development suggest flows with a high sediment load which lead to rapid deposition and suppressed bedform development (Bridge & Best, 1988; Todd, 1996). Sets of planar cross-bedding and trough cross-bedding represent the migration of straight-crested and sinuous-crested dune-scale bedform trains along the bases of channels during times of lower sediment load.

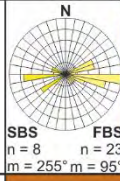
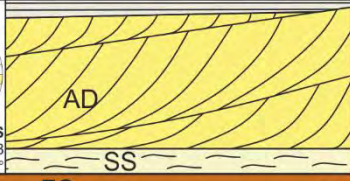
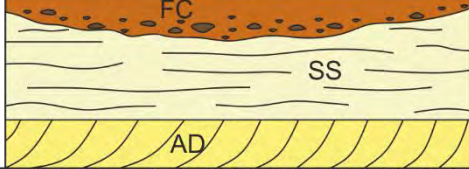
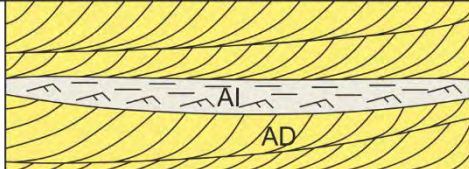


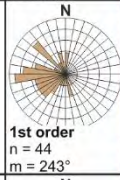

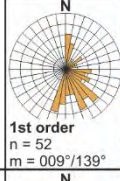

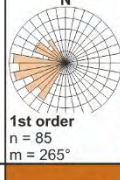


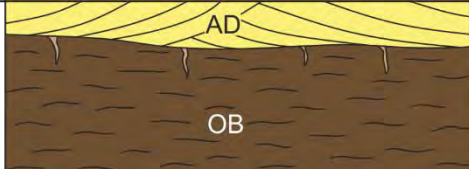
Element	Description	Facies	Bounding surfaces	
Aeolian Dune (AD)	Tabular bodies, lateral extents up to 300m, vertical extents up to 150m	Smxb, Smtxb, Smpl, Smwb	Basal: set or coset Top: set or coset Internal: foreset and set	 
Sandsheet (SS)	Tabular bodies, lateral extents over 100's m, vertical extent up to 3m	Smpl, Smwb, Sm	Basal: set or coset Top: set, coset or supersurface	
Interdune (AI)	Lensoidal or sheet-like bodies, lateral extents up to 20m, vertical extent up to 2m	Sm, Spl, Sfrl, Stpl	Basal: set, coset or supersurface Top: set, coset or supersurface	
Fluvial Channel (FC)	'U' shaped elements, lateral extents up to 115m, vertical extent up to 4m. Thickness to width ratio 1:50	Cms, Ccs, Cru, Sxb, Stxb, Spl, Srb, Smf	Basal: 5th order Top: 4th or 5th order Internal: 1st and 2nd order climbing bedforms	 
Sheetflood (SF)	Tabular bodies, lateral extents 250-400m, vertical extent up to 5m. Thickness to width ratio 1:100	Cru, Spb, Sma, Smf, Spl, Sfrl, Sfl	Basal: 5th order Top: 4th or 5th order Internal: 3rd order erosional surfaces and 1st and 2nd order climbing bedforms	 
Lateral Accretion (LA)	Lensoidal elements, lateral extents up to 50m, vertical extent up to 3m	Stxb, Slxb, Spl, Sfrl	Basal: 5th order Top: 4th or 5th order Internal: 3rd order reactivation surfaces and 1st and 2nd order climbing bedforms	 
Downstream Accretion (DA)	Lensoidal elements, lateral extents up to 100m, vertical extent up to 4m	Cms, Sxb, Slxb, Srb, Spl, Sfrl	Basal: 5th order Top: 4th or 5th order Internal: 3rd order reactivation surfaces and 1st and 2nd order climbing bedforms	 
Bank Collapse (BA)	Tabular bodies, lateral extent up to 20m, vertical extent up to 3m	Sssd, Stpl	Basal: 5th order Top: 4th or 5th order	
Overbank (OB)	Tabular bodies, rarely preserved, lateral extent up to 10m, vertical extent up to 4m	Stpl, Spl, Lm	Basal: 4th order Top: 5th order	

Figure 5.1. Summary table of architectural elements with brief description and geometry, their contained facies (see chapter 4, Table 4.3 for detailed facies descriptions), and bounding surface analysis. Two-dimensional illustrations of commonly occurring relationships with overlying and underlying elements are indicated along with their respective palaeocurrent measurements, n = number of measurements, m = mean palaeocurrent direction.

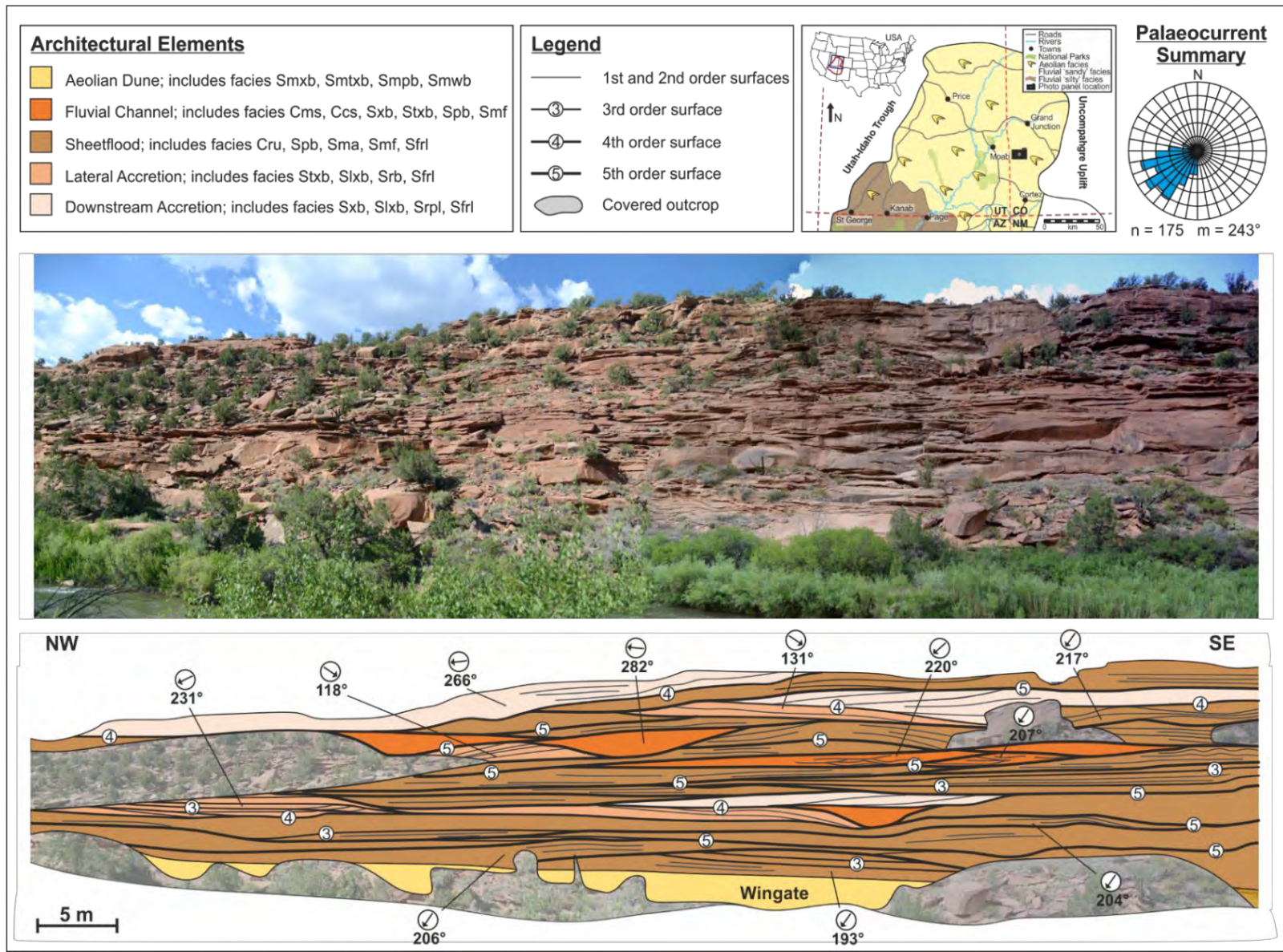


Figure 5.2. Architectural element outcrop panel for the proximal Kayenta Formation with hierarchical bounding surface analysis and palaeocurrent measurements. The proximal region is dominated by vertically and laterally amalgamated fluvial channel, sheets and accretionary elements with sporadic small isolated pockets of overbank.

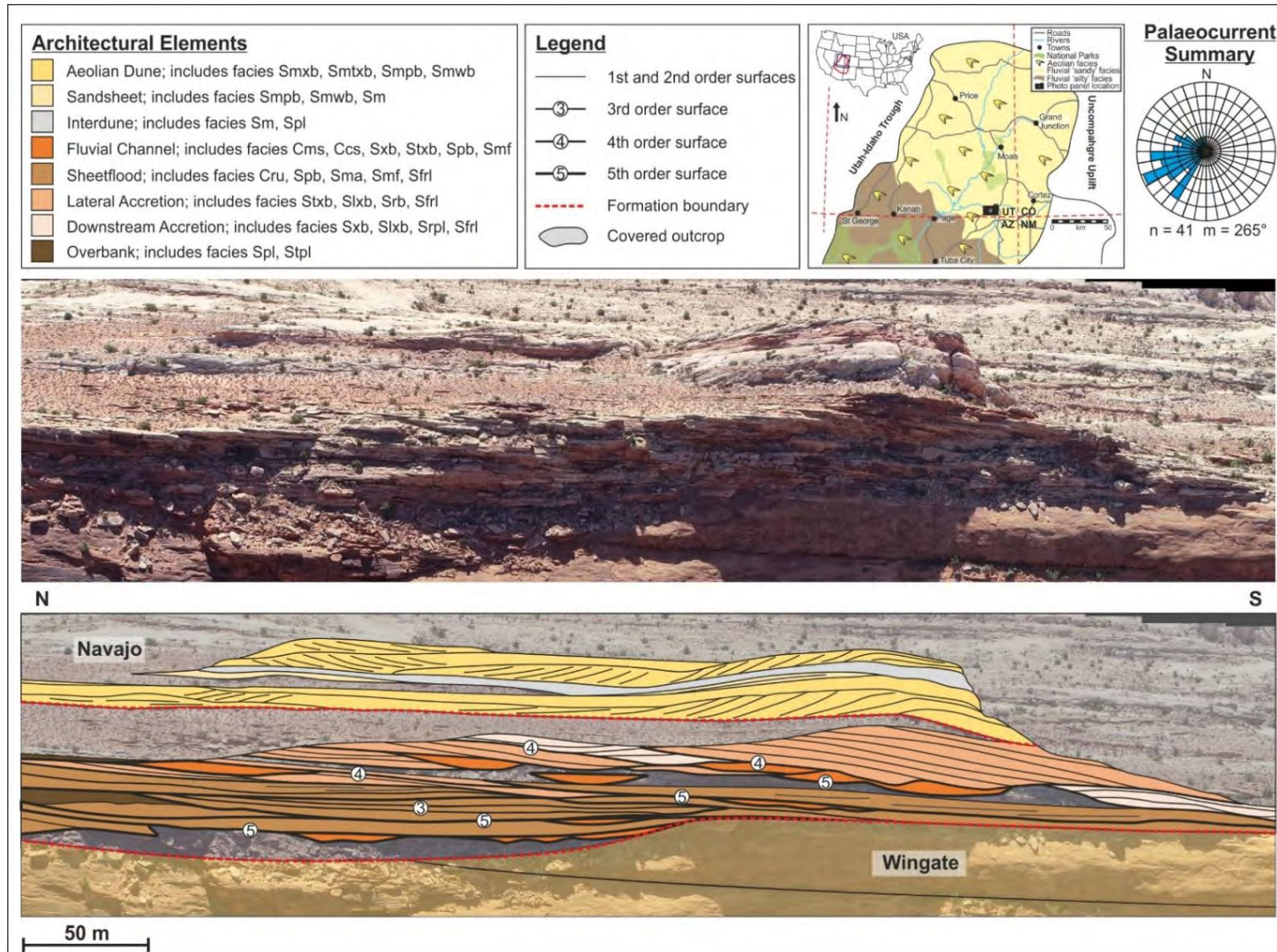


Figure 5.3. Architectural element outcrop panel for the medial Kayenta Formation with hierarchical bounding surface analysis and palaeocurrent measurements. The medial region is dominated by vertically and laterally amalgamated fluvial channel, sheets and accretionary elements, however, channels are more isolated and overbank elements are thicker and more laterally extensive.

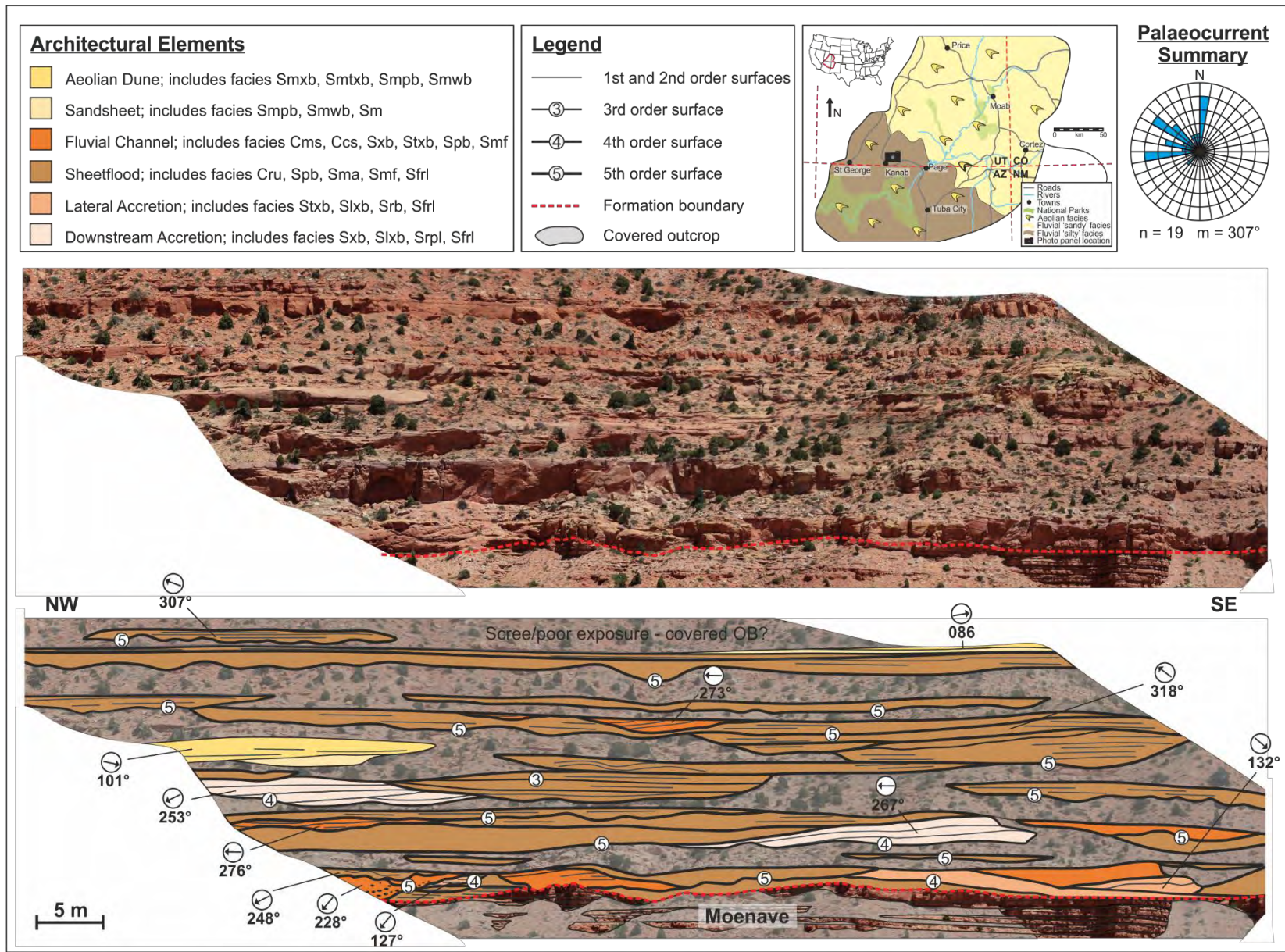


Figure 5.4. Architectural element outcrop panel for the distal Kayenta Formation with hierarchical bounding surface analysis and palaeocurrent measurements. In the distal region the degree of stacking between channel, sheets and accretionary elements is significantly reduced, with several channel and sheet-like elements being isolated within laterally extensive overbank deposits.

Fluvial Channel

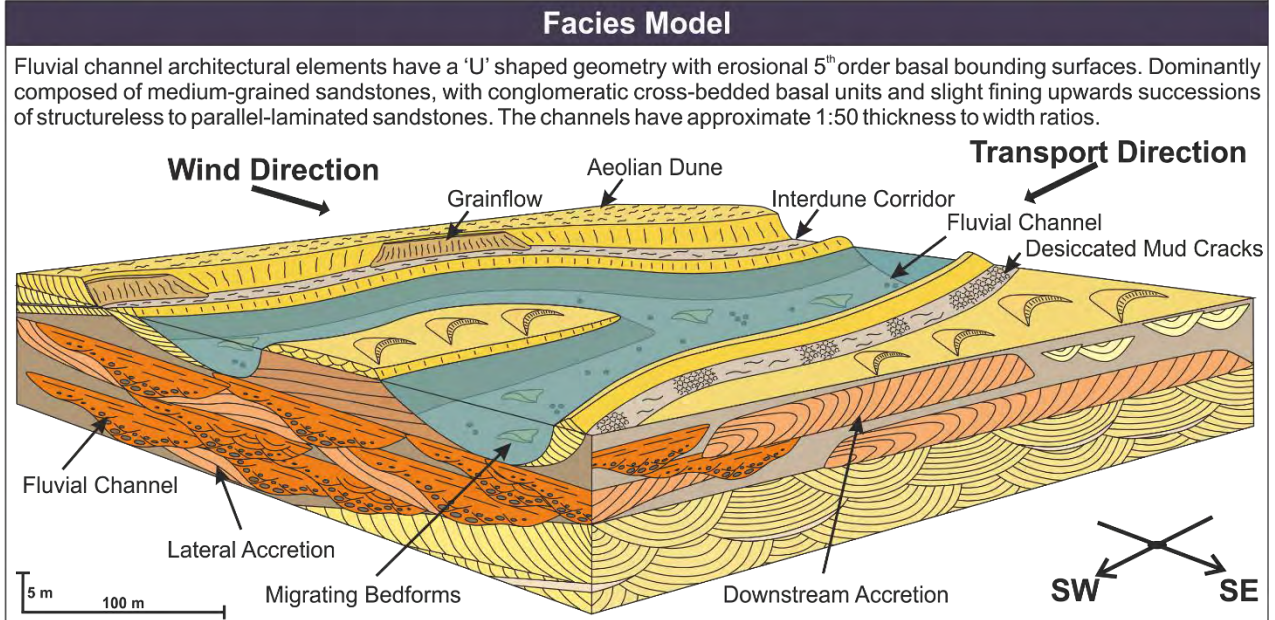
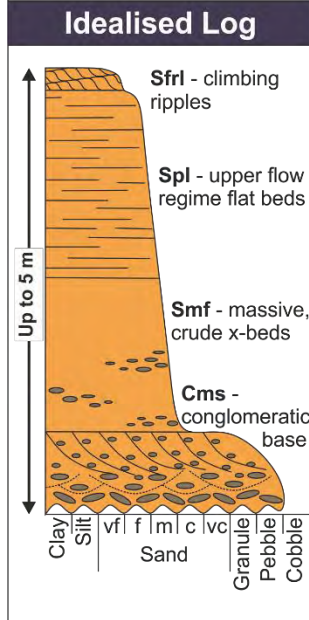
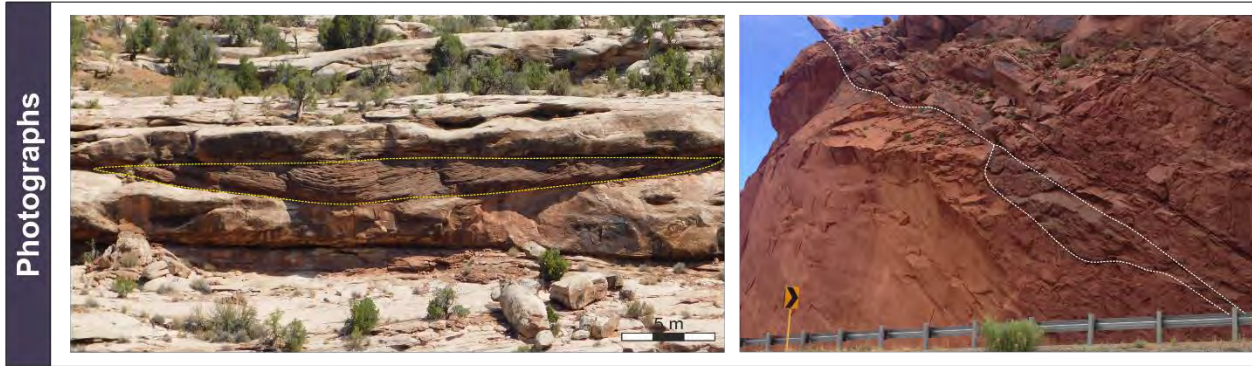
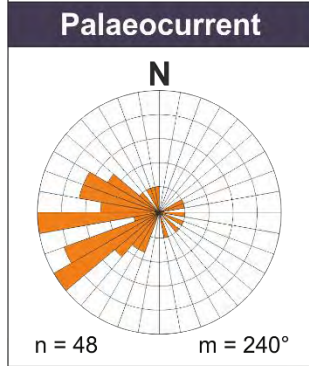


Figure 5.5. Summary panel of the fluvial channel architectural element with palaeocurrent, idealised log, photographs and facies model.

However, the evidence of mud-draping along foresets indicates either fluctuations in discharge (Miall, 1983) giving rise to alternations in coarse and fine clastic sediments (Puigdefabregas & Vliet, 1978), or deposition of silt derived from flow at maximum carrying capacity (Olsen, 1987; Nwajide, 1988). Sets of recumbent cross-bedding initially form in a similar manner; however, the tops of the foresets are ripped back in the direction of flow during periods of high sediment load (Allen & Banks, 1972). Palaeocurrent measurements indicate a strong west/south-westerly transport direction with a low degree of sinuosity to the channel plan-form. The arrangement of facies in a vertical section with no clear fining upward trend suggests deposition in a flow with fluctuating sediment load, with only minor evidence of waning flow preserved.

5.1.2. Fluvial sheet-like elements

Elements of this type consist of thin, tabular, laterally extensive bodies with flat to very slightly concave upward and erosional fifth-order basal bounding surfaces (Fig. 5.6). Rip-up clast conglomerates (**Cru**) comprise 5% of the element, and overlie the basal bounding surface with sporadic very coarse to granule-sized clasts (up to 30 cm along the long axis) forming crudely developed foresets. These sediments are overlain by planar bedded sandstones (**Spb**) with primary current lineation, that comprise the majority of the element (75%), and then by sigmoidal bedded (**Sma**), structureless (**Smf**) and parallel-laminated (**Spl**) sandstones, which comprise 15% of the total element in more or less equal proportions. Cross-laminated (**Sfrl**) sandstones, and flaser-laminated siltstones (**Sfl**) form the upper units of the succession and comprise the remaining 10% of the element. Units of sigmoidal-bedded sandstone have a symmetrical convex upward geometry, mimicked by the internal structure of the bedding. Preservation of the full, fining upward element is rare and examples are typically truncated and eroded by basal fourth-order surfaces from either other elements of this type, or from fluvial channel elements.

Interpretation

Elements of this type, with thin laterally extensive geometries and sedimentary fill from both upper and lower flow regime structures, are interpreted as unconfined sheet-like deposits (Miall, 1985; North & Davidson, 2012). Each individual fining upward succession with an erosive base represents an individual flood event (Miall, 2014). The basal conglomeratic unit suggests that the flood events had high enough energy to rip up underlying elements and transport up to boulder-sized clasts. The sigmoidal-bedded sandstones (**Sma**) are interpreted as humpback cross-bedding of antidunes with a symmetrical geometry and preservation of the stoss and lee slope of the bedform (Fielding, 2006; Lang & Winsemann, 2013). These structures represent the transition from conditions of lower flow regime dune formation to upper flow regime plane bed formation, and they were probably formed under high rates of sediment deposition (Fielding, 2006; Lang & Winsemann, 2013). The abundance of flat beds (**Spb**) with primary current lineation and sigmoidal-bedded sandstone (**Sma**) suggest that upper flow regime conditions dominated, with even the parallel-laminated sandstones most probably reflecting upper flow regime plane-bed conditions (Arnott & Hand, 1989; Carling, 2013; Guan *et al.*, 2016). Structureless sandstones indicate deposition from hyper-concentrated flows where rapid deposition suppressed bedform development (Olsen, 1987). Cross-laminated sandstones suggest that flow waned enough for bedform development and migration; however, sediment supply was significant enough to promote supercritical climb. Palaeocurrent measurements indicate a strong west/south-westerly transport direction with a low degree of sinuosity. The arrangement of facies in a vertical section with dominant upper flow regime structures and evident fining upward trend, suggests deposition within a high velocity flow that waned quickly in a dominantly aggradational setting.

Fluvial Sheet-like Element

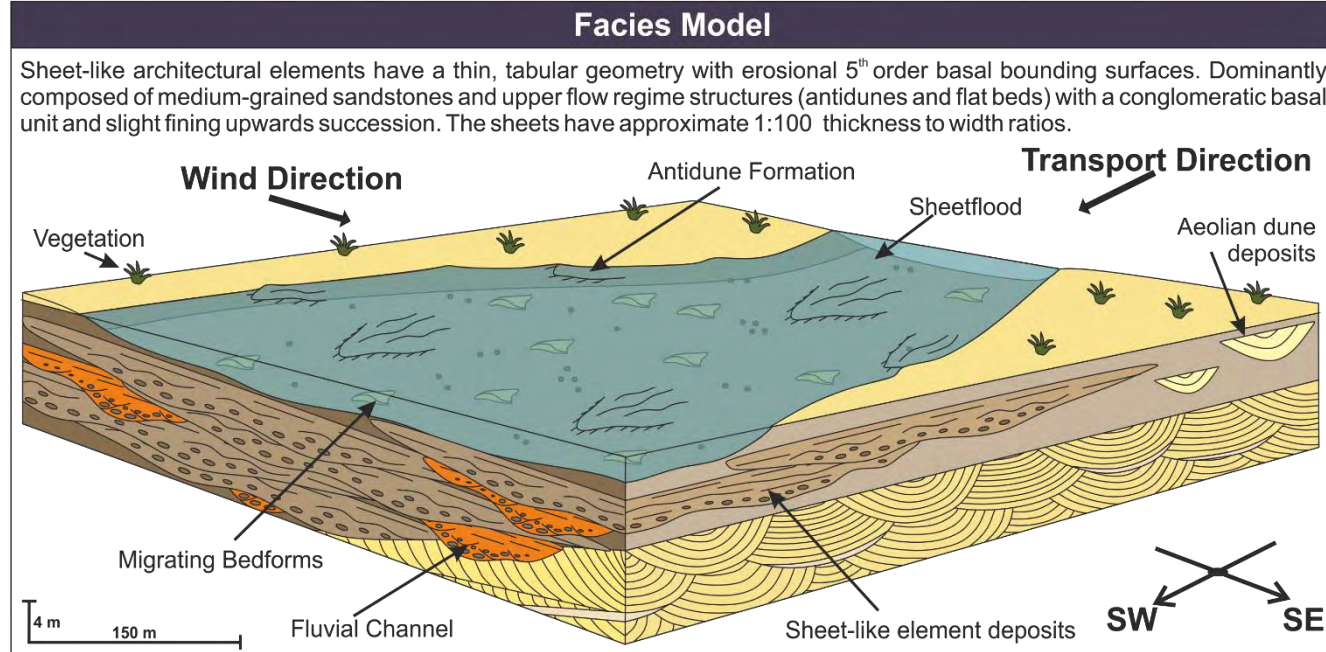
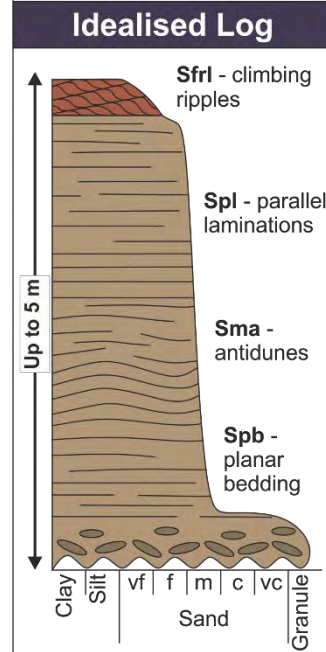
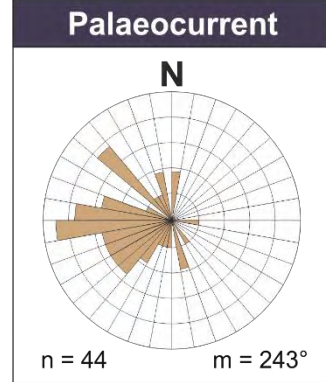


Figure 5.6. Summary panel of the fluvial sheet-like architectural element with palaeocurrent, idealised log, photographs and facies model.

5.1.3. Lateral accretion element

Elements of this type have a lensoidal to wedge-like geometry, internal second-order and third-order bounding surfaces and are bound typically by second-order surfaces or sporadically by basal fifth-order bounding surfaces that extend laterally and merge with the basal fifth-order bounding surfaces of examples of the fluvial channel element (Fig. 5.7) (Miall, 1996). Trough cross-bedded sandstones (**Stxb**), typically with clasts lining the foresets, form the basal 5% of this element and are overlain by low-angle cross-bedded sandstones (**Slxb**) with sporadic examples of mud draped foresets. Low-angle cross-bedded sandstones (**Slxb**), comprise approximately 85% of the element and are overlain by parallel-laminated (**Spl**) and cross-laminated (**Sfrl**) sandstones, which comprise the remaining upper units of the element in roughly equal proportions. Preserved examples of the full, fining upward element are rare, and most examples of the element are typically truncated and eroded by basal fourth-order or fifth-order surfaces from sheet-like or channel elements. Lateral extents of the element range from 2 m to 15 m, with thicknesses no greater than 3 m.

Interpretation

Elements with sets of low-angle cross-bedding dominating the sedimentary fill and lensoidal to wedge-like geometries with internal second-order and third-order bounding surfaces (sensu Miall, 1996) dipping approximately perpendicular to the average channel palaeoflow are interpreted as laterally accreting barforms (Miall, 1985; Simon & Gibling, 2017). Silt draped on foresets suggests a high sediment load within the flow with the finer sediment deposited after the flow reaches its full carrying capacity for fine material (Olsen, 1987; Thomas *et al.*, 1987; Russell *et al.*, 2019). Subcritically climbing trough cross-bedded sets of sandstone represent the migration of sinuous crested dune-scale bedforms in a flow with a normal sediment load. The presence of parallel laminated and cross-laminated sandstones towards the top of the element, as well as the presence of slight fining upward trend, indicate a reduction in flow depth as the barform builds towards the surface (Miall, 1985).

5.1.4. Downstream accretion element

Elements of this type have lensoidal geometries with internal convex-up, erosional third-order bounding surfaces (Fig. 5.7) (*sensu* Miall, 1996). A relatively flat fourth-order surface forms the upper bounding surface to the element, and a relatively flat to slightly concave fourth-order or fifth-order bounding surface forms the basal surface and extends sporadically to merge with a basal fifth-order bounding surface of the fluvial channel element. Matrix-supported conglomerates (**Cms**) comprise 5% of the element and immediately overlie the basal fourth-order or fifth-order bounding surface. These deposits are overlain by planar cross-bedded (**Sxb**), low-angle cross-bedded (**Slxb**) and recumbent cross-bedded (**Srb**) sandstones in sets ranging from 0.3 m to 1.2 m, that together comprise most of the element (approximately 80%), and parallel-laminated (**Spl**) and cross-laminated (**Sfri**) sandstones that comprise the remainder of the element in more or less equal proportions. Preserved examples of the full, fining upward element are rare, and the element is often truncated and eroded by basal fourth-order or fifth-order surfaces from sheet-like or channel elements.

Interpretation

Elements of this geometry and fill with internal erosional third-order bounding surfaces (*sensu* Miall, 1996) dipping approximately parallel to the average channel palaeoflow are interpreted as the incremental growth and downstream migration of simple or compound in-channel barforms (Miall, 1985; Ghinassi & Ielpi, 2018). Where the basal surfaces are fourth-order, barforms developed on top of existing barforms, without significant erosion, to form compound barforms (Jackson, 1975; Miall, 1977; Almeida *et al.*, 2016). Planar cross-bedding represents the downstream migration of straight crested dune-scale bedforms, and the occasional bi-directionality to some of the foresets may indicate a degree of lateral accretion on the outside margins of a downstream accreting bar (Rust, 1972; Miall, 1977). Recumbent cross-bedding represents possible fluctuations within flow conditions and sediment load, causing the overriding flow to overturn the underlying saturated beds (Stikes, 2007).

Lateral & Downstream Accretion

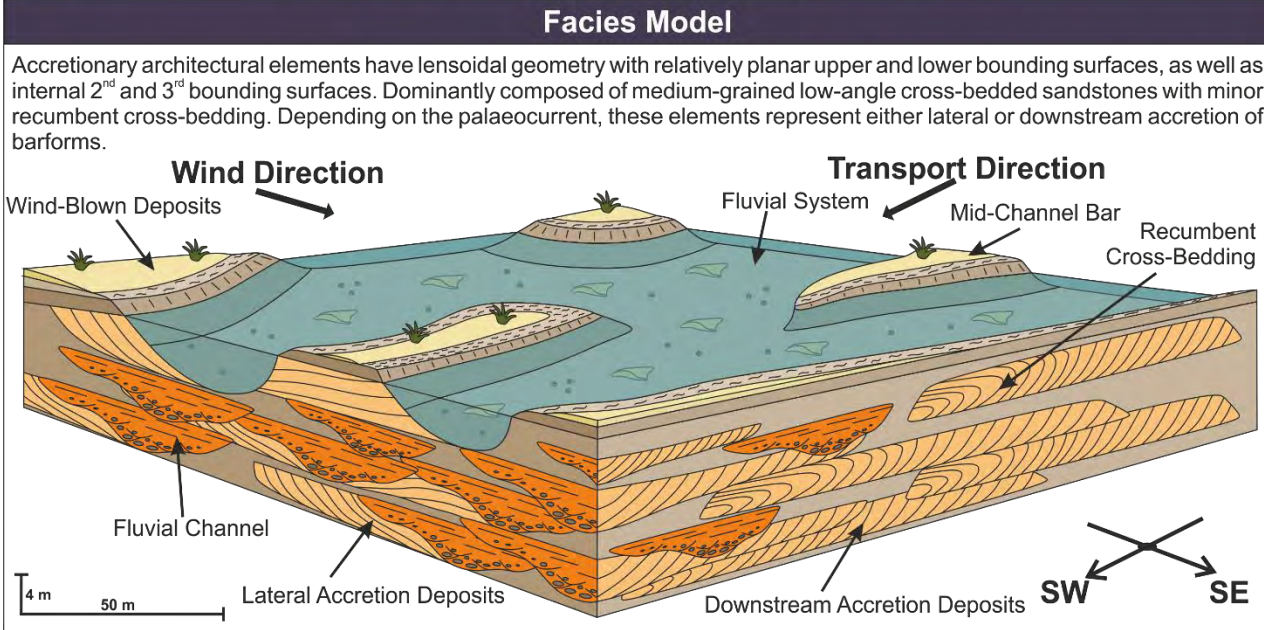
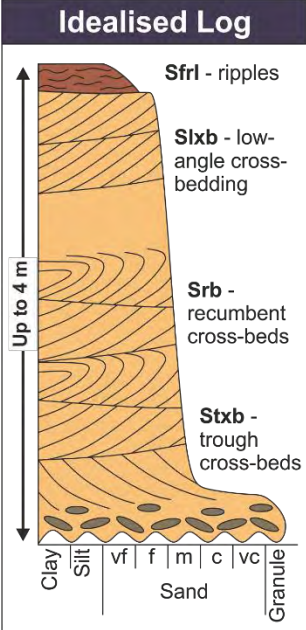
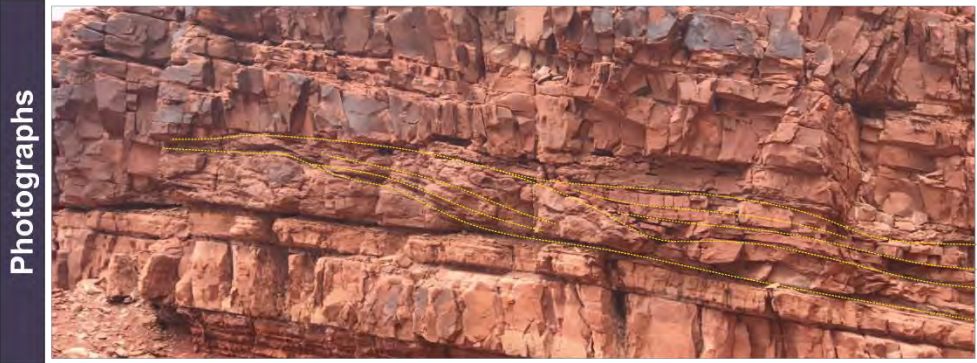
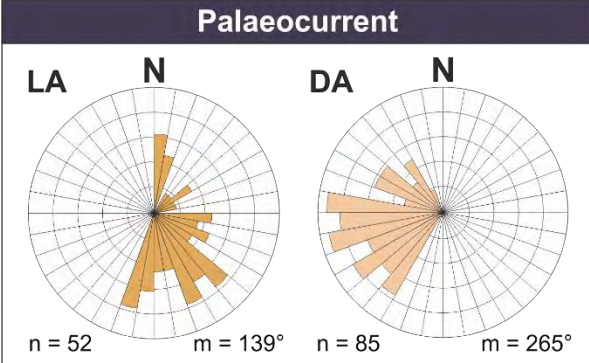


Figure 5.7. Summary panel of the lateral and downstream accretion architectural elements with palaeocurrent, idealised log, photograph and facies model.

The presence of parallel laminated and cross-laminated sandstones towards the top of the element and the presence of a slight fining upward trend indicates a reduction in flow depth as the barform builds towards the surface.

5.1.5. Bank collapse element

Elements of this type have flat erosive basal bounding surfaces that merge laterally with basal fifth-order bounding surfaces of the fluvial channel elements (Fig. 5.8). Examples of the element contain two facies: soft-sediment deformed sandstone (**Sssd**), which comprises the majority of the element (90%) and brown parallel-laminated siltstone (**Stpl**), which comprises the remainder. Units of soft-sediment deformed sandstone are present as contorted intra-formational clasts with mud-draping along the folded foresets, all held within a brown, parallel laminated siltstone matrix (**Stpl**). Elements of this type range from 1 to 3 m in thickness and have lateral extents up to 20 m.

Interpretation

Elements of this geometry and fill are interpreted as mass transport debris-flow deposits formed by the collapse of the river banks into high sediment load flow (Owen, 1996, 2017; Rana *et al.*, 2016; Van den Berg *et al.*, 2017; Carling & Leclair, 2019). The abundance of siltstone and silt/mud draping on foresets of the contorted clasts suggests a high sediment load within the flow with the finer sediment deposited after the flow reaches its maximum carrying capacity (Olsen, 1987).

5.1.6. Overbank/floodplain elements

Elements of this type have a laterally extensive tabular geometry and are bound by basal fourth-order surfaces (*sensu* Miall, 1996) and comprise three facies: parallel-laminated to faintly rippled siltstone (**Stpl**) and parallel-laminated sandstone (**Spl**), which together comprise most of the element (95%); and structureless to undulose laminated, siliclastic-rich, carbonate wackestones (**Lm**), which comprise the remainder (Fig. 5.9). Mottling, bioturbation, rhizoliths and desiccation cracks are common features within the siliclastic facies, whereas the carbonate wackestones occur as structureless to undulose laminated isolated lenses, with thicknesses of 5 to 20 cm and widths of 2 m,

or as very thin laterally extensive sheets. This element is very poorly preserved and regularly occurs as clasts within other fluvial elements.

Interpretation

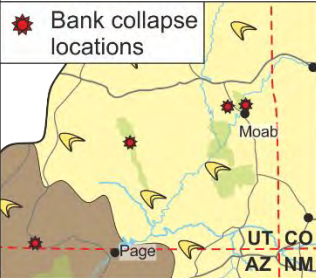
Elements of this type are interpreted as overbank or floodplain deposits (Miall, 1985). Laminated siltstones and sandstones represent deposition from suspension in standing water after flooding (Eberth & Miall, 1991). The sporadic mottling and bioturbation indicate pedogenesis and stabilisation of the floodplain (Eberth & Miall, 1991). Preserved examples of this element are extremely rare due to reworking and erosion by other elements. Atypically thick deposits occur near the top of the formation where they contain desiccation cracks and rhizoliths that indicate stabilization and drying of the floodplain (Miall, 1988), and within the distal region, where they represent waning of flow and channel abandonment. Isolated siliciclastic-rich carbonate wackestone lenses result from entrapment of water in small depressions for relatively long periods after the fluvial system wanes (Allen, 1974).

5.1.7. Compound aeolian dune element

Elements of this type comprise cross-stratified tabular bodies with sharp planar upper and lower bounding surfaces, and are composed of four facies: planar cross-bedded (**Smxb**) and trough cross-bedded (**Smtxb**) sandstones, which together comprise 85% of the element; planar bedded sandstones (**Smpb**), which comprise approximately 10%; and undulose to rippled (**Smwb**) sandstones, which comprise the remainder of the element (Fig. 5.10). The lateral extents of these elements range from 2 to 100 m, and elements often intertongue with overbank or sandsheet and interdunal elements. Individual sets of cross-strata range from 1 to 5 m in thickness and comprise couplets of alternating inversely graded medium-grained and finer grained sandstone exhibiting sweeping, sporadically deformed, asymptotic foresets with truncated tops and climbing cross-lamination (**Smwb**) at bases of toesets.

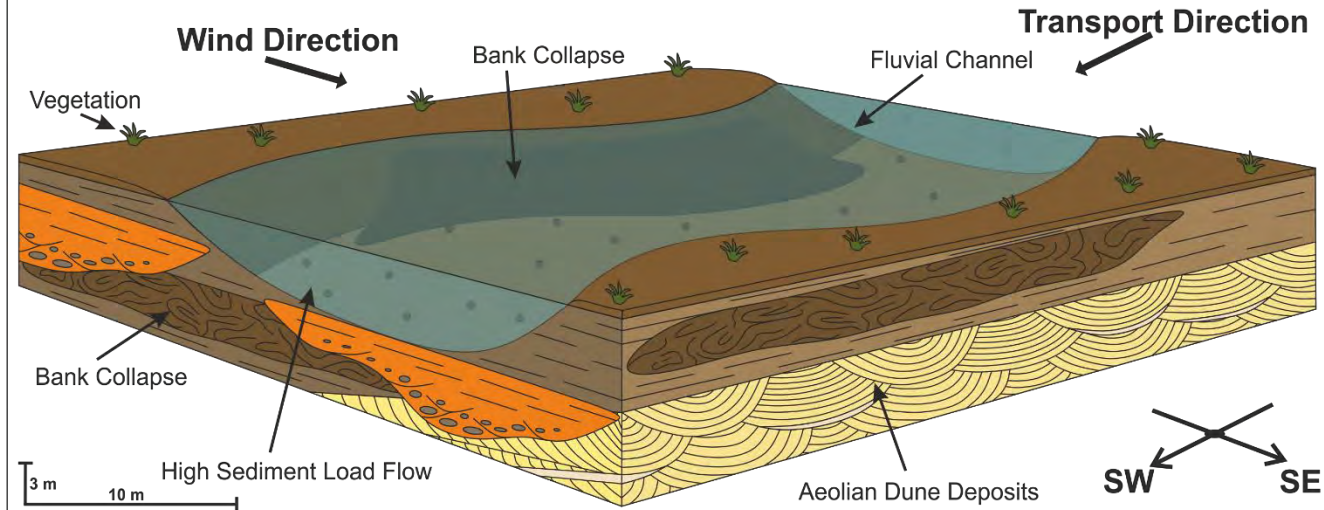
Bank Collapse

Photographs



Facies Model

Bank collapse architectural elements have a tabular geometry with a flat erosive basal bounding surface. Dominantly composed of soft sediment deformed, contorted intra-formational clasts with mud-draping along the folded foresets. These elements are interpreted as mass transport debris-flow deposits formed by the collapse of the river's banks into high sediment load flow.



Idealised Log

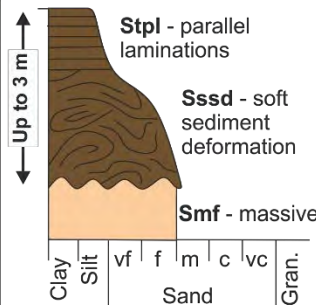


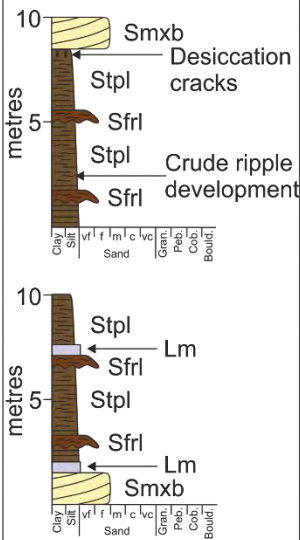
Figure 5.8. Summary panel of the bank collapse architectural element with locations map, idealised log, photographs and facies model.

Overbank/floodplain

Photographs



Idealised Log



Facies Model

Overbank/floodplain architectural elements have a laterally extensive tabular geometry and are bound by basal fourth-order surfaces. Dominantly composed of parallel-laminated to faintly rippled siltstone and parallel-laminated sandstone, with minor carbonate lenses. Mottling, bioturbation, rhizoliths and desiccation cracks are common features.

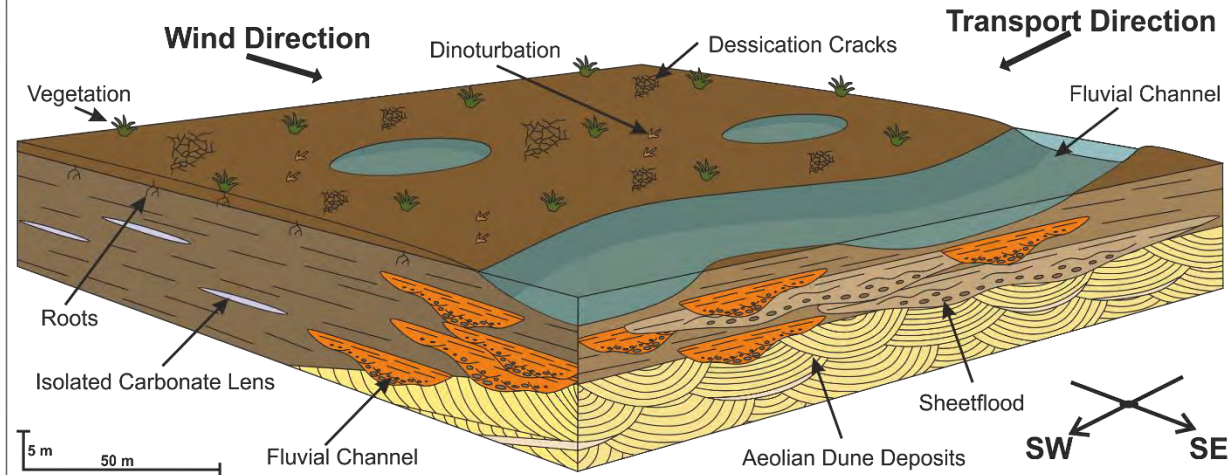


Figure 5.9. Summary panel of the overbank architectural element with idealised logs, photographs and facies model.

The average dip directions of the foresets are towards the east (095°) with a distribution between 57° and 150° (Fig. 5.10). The set-bounding surfaces range from planar where sets comprise dominantly planar cross-bedded sandstones (**Smb**), to slightly concave upward where sets comprise dominantly trough cross-bedded sandstones (**Smtxb**). Planar bedded sandstones (**Smpb**) are typically observed between sets of planar cross-bedded sandstone (**Smb**).

Interpretation

Large-scale cross-bedded sandstones with couplets of medium-grained and fine-grained sandstone, with sporadic inverse grading, represent dune-scale, wind-blown bedforms migrating by the combined processes of grainfall and grainflow (Hunter, 1977; Kocurek, 1981; 1991; 1996; Langford & Chan, 1989). Subcritically climbing planar cross-bedded sets (**Smb**) with planar bounding surfaces represent the migration of straight crested dunes, whereas trough cross-bedded sets (**Smtxb**) with slightly concave set bounding surfaces represent the migration of sinuous-crested dunes. The presence of both planar cross-bedded sets (**Smpb**) and trough cross-bedded sets (**Smtxb**) indicate compound dunes of sufficient size to affect sediment supply and wind direction locally. Palaeocurrent measurements indicate a dominantly eastward sediment transport direction and the dispersion of the measurements suggest either a degree of sinuosity to the migrating dunes or more localised changes of the wind direction. The undulose to cross-laminated facies (**Smb**) represent the superimposition of ripple-scale bedforms onto dune-scale bedforms (Sharp, 1963; Fryberger & Schenk, 1988). Soft-sediment deformation of the cross-bedding indicates fluctuation of the water table at or shortly after the time of deposition, before the cross-bedded sets were fully lithified (Mckee *et al.*, 1971; Doe & Dott, 1980; Bryant *et al.*, 2013; 2016).

Aeolian Dune

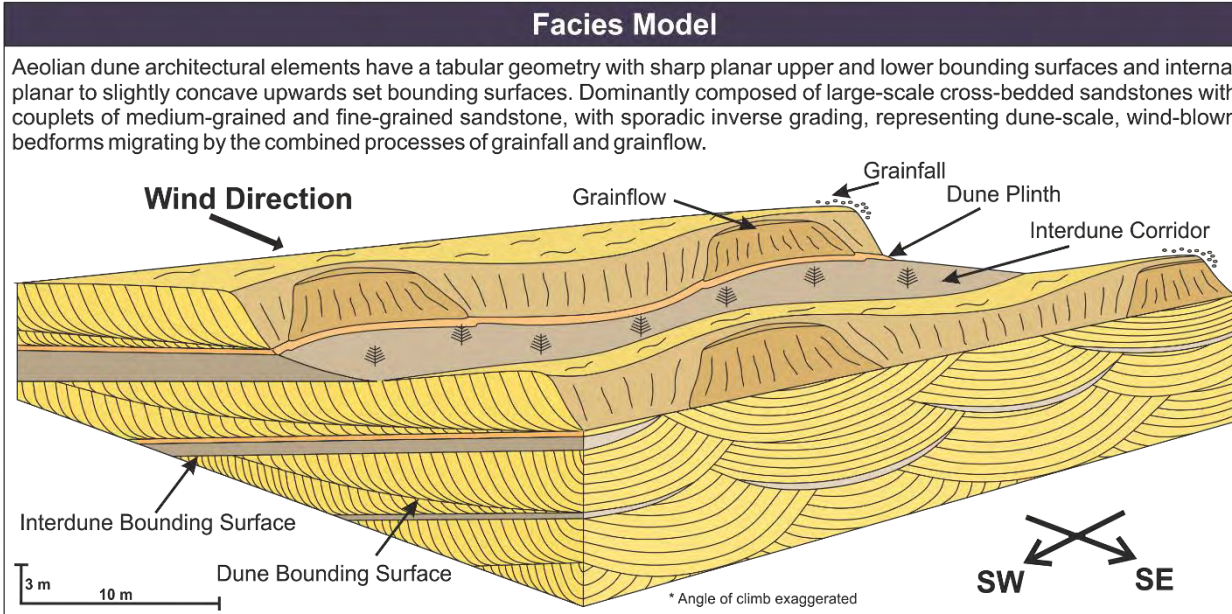
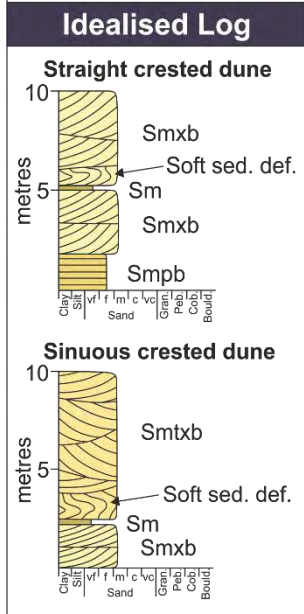
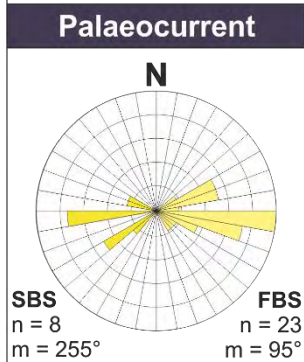


Figure 5.10. Summary panel of the aeolian dune architectural element with palaeocurrent, idealised logs, photographs and facies model.

5.1.8. Aeolian sandsheet element

Elements of this type comprise tabular bodies with large lateral extents over hundreds of metres and comprise three facies: planar bedded sandstone (**Smpb**) that comprises approximately 75% of the element; and undulose to cross-laminated (**Smwb**) sandstones and structureless (**Sm**) sandstones that comprise the remainder of the element in approximately equal proportions (Fig. 5.11). This element has an almost uniform grain size, making individual facies hard to distinguish. The upper and lower contacts have sharp planar bounding surfaces, with element thicknesses ranging from 0.1 to 3.0 m. Many examples of the element display gradual thinning and pinching out on a regional scale, with lateral extents of up to 100 m.

Interpretation

Planar bedded tabular bodies of well-sorted sandstone, with occasional undulose to cross-laminated beds are indicative of sandsheet depositional settings, where dune development is inhibited. Sediment supply available for dune development is limited because of either a high water table (Fryberger & Schenk, 1988; Mountney & Jagger, 2004) or episodic flooding (Kocurek & Nielson, 1986). Undulose to cross-laminated strata are interpreted as ballistic or translantent wind ripples formed by the migration of ripple-scale bedforms through the process of saltation of fine-grained sand, which accumulate along the saltation wavelength, then reptation of coarser grains over the accumulated grains (Sharp, 1963; Fryberger & Schenk, 1988).

5.1.9. Interdune elements

Elements of this type occur as either isolated lenses or continuous sheets that separate tabular aeolian deposits. They comprise four facies: massive (**Sm**) to parallel-laminated (**Spl**) sandstones, cross-laminated sandstones (**Sfri**) and parallel-laminated siltstones (**Stpl**) (Fig. 5.12). The upper and lower contacts can be either sharp or interfinger with aeolian dune and sandsheet elements. Two sub-types of elements are recognized: (i) lens-shaped to continuous sheets, approximately 0.2 to 0.5 m thick, comprising predominately structureless (**Sm**) and parallel-laminated (**Spl**) sandstones, that typically

occur gradational with aeolian dune elements, and have evidence of desiccation cracks and bioturbation; and (ii) lens-shaped to continuous sheets, approximately 0.5 to 1.0 m thick, comprising cross-laminated sandstones (**Sfri**) and parallel-laminated siltstones (**Stpl**) with evidence of rhizoliths, bioturbation and desiccation cracks.

Interpretation

Continuous sheets or lens-shaped elements composed predominately of massive (**Sm**) to parallel-laminated (**Spl**) well-sorted sandstone suggest deposition in a dry interdune environment where the water table has had very little to no influence on the depositional processes because it lies significantly below the depositional surface. The massive to parallel-laminated appearance is due to the lack of defined translent strata caused by a uniform grain-size (Kocurek, 1981). Continuous sheets to lens-shaped elements composed of cross-laminated sandstones (**Sfri**) and parallel-laminated siltstones (**Stpl**) suggest deposition in a damp interdune environment where the water table is within the capillary fringe of the surface (Mountney, 2006) resulting in the adhesion of grains, bioturbation and rhizolith development.

5.2. Depositional Elements

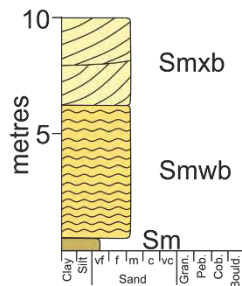
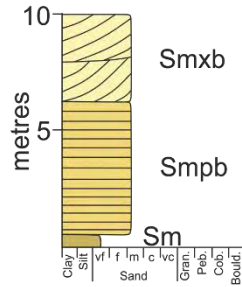
The fluvial architectural elements have been grouped into five depositional elements based upon their internal stacking patterns and composition: amalgamated sandstone-dominated channel-fill, isolated sandstone-dominated channel-fill, isolated gravel-dominated channel-fill, compound sandstone-dominated fluvial sheets and overbank (Fig. 5.13).

Aeolian Sandsheet

Photographs



Idealised Log



Facies Model

Aeolian sandsheet architectural elements have a tabular geometry with sharp planar upper and lower bounding surfaces and large lateral extents over hundreds of metres. Dominantly composed of well-sorted sandstone, with occasional undulose to ripple-laminated beds representing the suppression of dune development due to decreased sediment supply from either a high water table or episodic flooding.

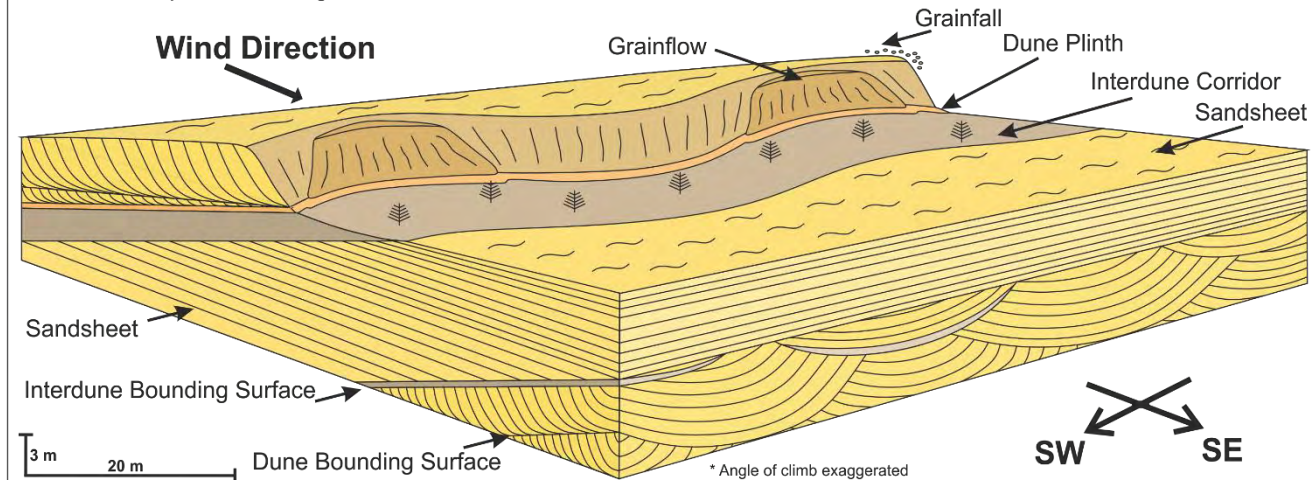


Figure 5.11. Summary panel of the aeolian sandsheet architectural element with idealised logs, photographs and facies model.

Aeolian Interdune

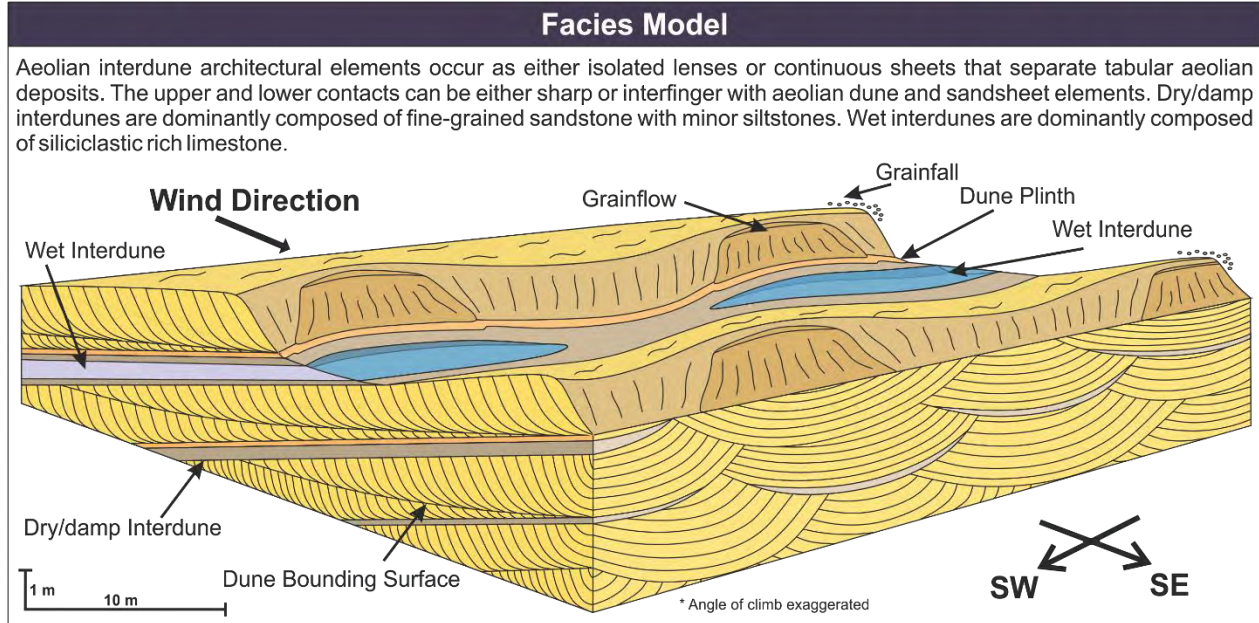
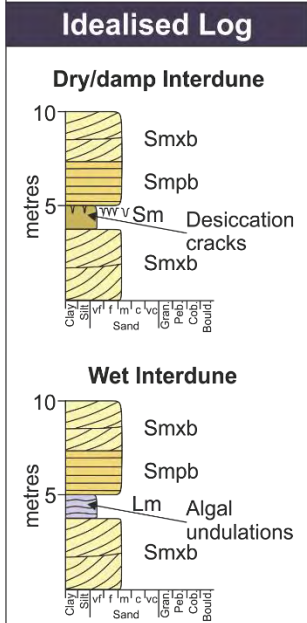
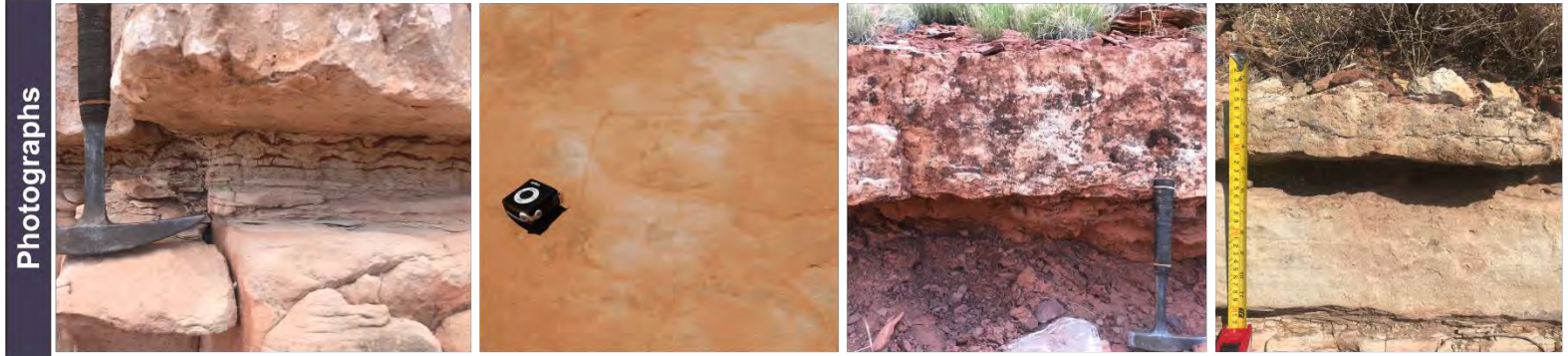
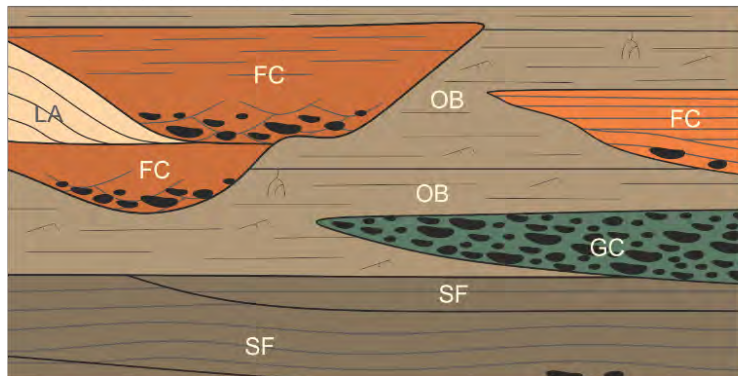


Figure 5.12. Summary panel of the aeolian interdune architectural elements with idealised logs, photographs and facies model.

Architectural Elements



Depositional Elements

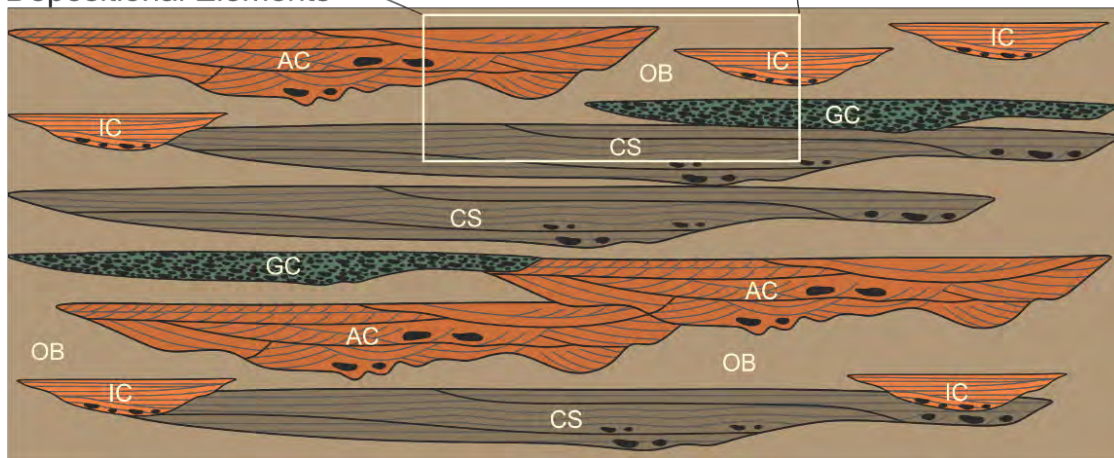


Figure 5.13. Representation of the internal composition, architecture, and geometries of the large-scale depositional elements. Architectural elements: FC = fluvial channel, LA = lateral accretion, GC = gravel-dominated channel, SF = fluvial sheet, OB = overbank. Depositional elements: AC = amalgamated sandstone-dominated channel-fill, IC = isolated sandstone-dominated channel-fill, GC = isolated gravel-dominated channel-fill, CS = compound sandstone-dominated fluvial sheet, OB = overbank.

5.2.1. Amalgamated Sandstone-Dominated Channel-Fill

Laterally and vertically amalgamated sandstone-dominated channel-fill depositional elements comprise predominantly channel and accretionary architectural elements (Fig. 5.13 & 5.14) and occur primarily within the proximal and medial regions of the Kayenta Formation, with the degree of element amalgamation decreasing downstream towards the south-west. Small, isolated lenses of overbank are sporadically observed between stacked channel architectural elements. Examples of the depositional element typically form large laterally extensive sheet-like complexes, which are up to 0.5 km wide in directions perpendicular to palaeoflow, and up to 25 m thick.

Internal channel architectural elements within this depositional element are dominated by successions of medium-grained planar to trough cross-bedded sandstones (**Sxb** & **Stxb**) with conglomeratic basal lags and sporadic very coarse to granule-grade clasts lining crudely developed foresets. The uppermost strata of the channel elements comprise structureless (**Smf**) to parallel laminated (**Spl**) sandstones. The accretionary elements within this depositional element are dominated by successions of medium-grained low-angle cross-bedded sandstones (**Slxb**) and sporadic planar (**Sxb**), trough (**Stxb**) and recumbent (**Srb**) cross-bedded sandstones, with the tops of the successions comprising ripple-cross-laminated sandstones (**Sfri**).

Interpretation

Amalgamated sandstone-dominated channel-fill depositional elements represent extensive erosive channel complexes (Gibling, 2006) that extended over the proximal and medial regions during periods of increased fluvial activity (*cf.* Cain & Mountney, 2009). The development of the sheet-like bodies of amalgamated channels most probably resulted from the repeated avulsion of channels across a common stratigraphical horizon, cannibalising any overbank that developed (Mackey & Bridge, 1995; Miall, 1996; Bridge, 2003; *cf.* Cain & Mountney, 2009). The individual channel-fills are dominated by sediments of bedload transport under conditions of high flow velocity and sediment load (Bridge, 2006). The vertical arrangement of facies, with no clear fining upward trend, suggests deposition in a flow with a strongly fluctuating sediment load, from which only minimal evidence of waning flow is preserved in the sedimentology (Section 5.1.1; Priddy & Clarke, 2020). This interpretation is supported by pebble and mud-lined foresets which, along with the abundance of upper flow regime plane beds, suggest deposition within a river with episodic discharge (Miall, 1977; Stear, 1985; Lorenz & Nadon, 2002; Owen *et al.*, 2015).

-



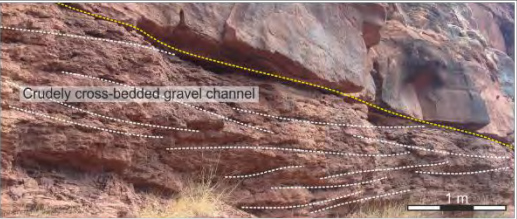

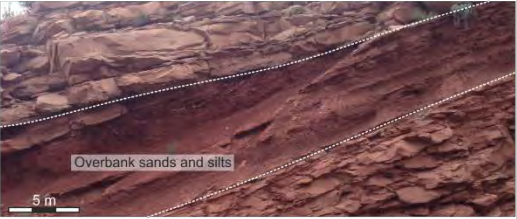
Depositional Element	Description	Elements contained	Dimensions	Occurance	
Amalgamated channel-fill	Large laterally extensive sheet-like complexes with erosional 5th order basal bounding surfaces	FC, LA, DA	Up to 25 m thick, with lateral extents up to 500 m	Predominantly within proximal and medial regions with decreased stacking towards the distal	
Isolated channel-fill	Lensoidal bodies with erosional 5th order basal bounding surfaces	FC	Between 0.5 m and 4 m thick, with lateral extents up to 115 m	Proximal, medial and distal regions	
Gravel-dominated channel-fill	Laterally extensive highly erosional elements with steep sides and basal 5th order bounding surfaces	FC	1 - 2 m thick, with lateral extents up to 50 m	Proximal, medial and distal regions	
Compound fluvial sheet	Lensoidal to sheet-like bodies with erosional 5th order basal bounding surfaces	SF	Up to 20 m thick, with lateral extents up to 750 m	Proximal, medial and distal regions, with decreased stacking towards the distal	
Overbank	Isolated lenses to laterally extensive tabular bodies	OB, SF	5 - 20 cm thick lenses with widths of 2 m, 2 - 15 m thick bodies with lateral extents over 100s metres	Predominantly within distal regions	

Figure 5.14. Summary table of fluvial depositional elements within the Kayenta Formation.

5.2.2. Isolated Sandstone-Dominated Channel-Fill

Isolated sandstone-dominated channel-fill depositional elements comprise predominantly channel architectural elements (Fig. 5.13 & 5.14) and occur within proximal, medial, and distal areas of the Kayenta Formation. In proximal and medial areas, the isolated depositional elements of this type are preserved sporadically between compound sandstone-dominated fluvial sheet deposits, but in the distal setting they are dominantly preserved within overbank deposits. The depositional elements have a lensoidal channel geometry, 0.5 m to 4 m thick in sections perpendicular to flow, with lateral extents up to 115 m, and a dominant palaeocurrent towards the south-west.

Individual channel architectural elements within this depositional element have erosional basal bounding surfaces and sedimentary fills similar to the channel elements within the amalgamated channel-fill depositional element. Within the proximal and medial regions, the individual channel elements are dominated by medium-grained low-angle cross-bedded (**Slxb**) and planar-bedded (**Spb**) to parallel-laminated (**Spl**) sandstones with a conglomeratic basal lag. Distal equivalents of these isolated channel elements are dominated by generally finer grained, structureless (**Smf**) to parallel-laminated (**Spl**) sandstones with rip-up-clast-dominated conglomeratic bases.

Interpretation

Isolated sandstone-dominated channel-fill depositional elements represent the deposits of largely fixed fluvial channels, typically termed ribbon channels (North & Taylor, 1996), which are generally stable and exhibit little lateral migration (*cf.* Friend *et al.*, 1979; Gibling, 2006; Cain & Mountney, 2009; Owen *et al.*, 2015). They occur along the same stratigraphical horizon, which may be due to the divergence of the active channel in a distributary network (Kelly & Olsen, 1993; Nichols & Fisher, 2007), the re-convergence and divergence of an anabranching channel pattern (Nanson & Knighton, 1996; Tooth & Nanson, 1999; Bridge, 2003), or a situation in which each isolated channel represents abandonment following avulsion (Bridge, 2006; North & Warwick, 2007). Planform channel patterns are difficult to determine within the Kayenta Formation. Consequently, any of these processes may be

responsible for depositing isolated channel depositional elements, but the ephemeral nature of the system suggests the latter process is more probable.

5.2.3. Isolated Gravel-Dominated Channel-Fill

Isolated gravel-dominated channel-fill depositional elements occur across the extent of Kayenta deposition, with the most prominent examples observed within the medial and distal regions. Each example of this depositional element is typically 1–2 m thick with lateral extents, in a direction perpendicular to flow, of tens of metres, or more. They are characterised by erosive basal bounding surfaces and lateral pinch-out displaying steep, near vertical profiles, and a representative succession dominantly composed of structureless to crudely cross-bedded clast-supported intraformational conglomerates (**Ccs**), fining upwards into structureless (**Smf**) to parallel-laminated (**Spl**) sandstones. The intraformational sediment in proximal and medial settings is dominantly composed of sub-lithic arenite and argillaceous material, with a minor calcareous content. The argillaceous and calcareous components increase towards the distal region.

Interpretation

Isolated gravel-dominated channel-fill depositional elements were deposited by high-energy fluvial channel discharge events that occasionally traversed into the distal alluvial plain (*cf.* Cain & Mountney, 2009). Within the proximal to medial regions, the presence of intraformational arenaceous clasts within individual channel elements suggests that the fluvial system eroded into adjacent non-cohesive sandy overbank/floodplain areas (Gómez-Gras & Alonso-Zarza, 2003). Within the distal region, abundant argillaceous and calcareous clasts suggest erosion of a 'silty' stabilised floodplain. The crude cross-bedding within the conglomeratic fill indicates periods of high flow velocities that were prolonged enough for some in-channel bedform development and migration (Williams, 1970), but generally the large sediment grain size prevented bedload transport and the formation of migrating bedforms. The structureless nature of overlying sandstones suggest rapid deposition from a system with a high sediment load that prevented the formation of bedforms (Bridge & Best, 1988; Todd, 1996).

5.2.4. Compound Sandstone-Dominated Fluvial Sheets

Compound sandstone-dominated fluvial sheet depositional elements occur across the expanse of the Kayenta, with high degrees of amalgamation in the proximal to medial regions, decreasing towards the distal setting. Examples of this depositional element are up to 1 km wide in directions perpendicular to a south-west palaeoflow, and up to 20 m thick.

The internal sheet-like architectural elements (Fig. 5.13 & 5.14) within the depositional element are dominated by medium-grained structureless sandstones (**Smf**) and planar-bedded (**Spb**) to sigmoidal-bedded (**Sma**) sandstones with basal rip-up clast conglomerates (**Cru**), with sporadic very coarse to granule (up to 30 cm along the long axis) sized rip-up clasts lining crudely developed foresets. The top of the element comprises parallel-laminated (**Spl**) to ripple-cross-laminated (**Sfrl**) sandstones.

Interpretation

Compound sandstone-dominated fluvial sheet depositional elements are attributed to the unconfined flow of flood waters across the alluvial plain (*cf.* Cain & Mountney, 2009). The un-channelised nature of the internal sheet-like elements probably initiated from breaches of the banks of active channels during times of high flow velocities (Tooth, 2000; 2005). Each individual fining upwards element with an erosive base represents an individual flood event (Miall, 1996; 2014) within which the arrangement of facies in a vertical succession dominated by the preservation of upper flow regime structures suggests deposition within a high velocity flow that waned quickly (Williams, 1971). Ripple-laminated sandstones suggest flow waned enough for ripple-scale bedform development and migration; however, sediment supply was still significant enough to promote supercritical climb.

5.2.5. Overbank

Overbank depositional elements are most prominent within the distal region and comprise overbank and sheet-like architectural elements (Fig. 5.13 & 5.14) as described in Section 5.1.2. The depositional element is dominated by parallel-laminated to faintly rippled siltstones (**Stpl**), parallel-laminated sandstones (**Spl**), and structureless to undulose laminated siliciclastic-rich carbonate wackestones

(**Lm**), with the proportion of each facies varying throughout the succession and depositional area. In the proximal region, preserved overbank depositional elements are very sporadic and do not exceed thicknesses of 1 m, but rip-up clasts of overbank material within fluvial channel and sheet architectural elements attest to probable greater overbank development than preservation may suggest. Similar observations hold true for the medial setting, but with a slight increase in abundance of the depositional element. Here, the depositional element attains thicknesses of up to 5 m and is dominated by parallel-laminated sandstone (**Spl**) and parallel-laminated to faintly rippled siltstone (**Stpl**). Overbank depositional elements comprise a significant proportion of the distal region with mottling, bioturbation, rhizoliths and desiccation cracks being typical features within the parallel-laminated to faintly rippled siltstone (**Stpl**). Occurrences of the depositional element generally range in thickness from 2–10 m, but sporadically reach in excess of 15 m. Isolated lenses of structureless to undulose laminated siliciclastic rich carbonate wackestone (**Lm**) are abundant within this depositional element in the distal setting, forming as thin and laterally extensive sheets, generally 5 – 20 cm thick and 2 m wide.

Interpretation

Overbank depositional elements resulted from unconfined flow when the discharge exceeded the bank-full capacity of the channel network (Bridge, 2003; *cf.* Cain & Mountney, 2009). Preservation of this depositional element is generally poor due to reworking and erosion by other depositional elements, except for thick deposits near top of formation, which contain desiccation cracks and rhizoliths indicating stabilisation and drying of the floodplain (Miall, 1988), and within the distal region, indicating waning of flow and channel abandonment. Isolated siliciclastic-rich carbonate wackestone lenses result from entrapment of water in small depressions for relatively long periods of time after the fluvial system wanes (Allen, 1974; Pettigrew *et al.*, 2020).

5.3. System-scale Associations

The nine architectural elements can be grouped into three broad system-scale associations related to aeolian, braided-fluvial and ephemeral-fluvial depositional settings. These associations are depicted on representative sedimentary logs in Chapter Four, Figure 4.3.

5.3.1. Dominantly aeolian deposition

The association comprises three architectural elements: aeolian dunes, sandsheets and interdunes. Most of the association (75%) is dominated by sets of grainfall and grainflow strata deposited by the migration of dune-scale bedforms. Most foresets within the aeolian sets exhibit soft sediment deformation. Sandsheet elements of planar to undulose laminated sandstone are typically preserved between aeolian dune and fluvial elements. Interdune sediments constitute a minor proportion of the association and are typically observed between sets of aeolian dunes.

This association represents the deposits of damp to wet aeolian environment that often interfingers with fluvial associations. The switch to aeolian dominated deposition is interpreted as a slight change in climatic regime, representing more arid conditions (Howell & Mountney, 1997).

5.3.2. Dominantly braided fluvial deposition

The association comprises five architectural elements: fluvial channels, lateral accretion, downstream accretion and minor sheet-like and overbank/floodplain elements. The association is dominated by channel and accretionary elements composed of fine to medium-grained sandstone. The channels are typically stacked and amalgamated. They display conglomeratic bases and progressively fining upward fill that is interpreted as the progressive abandonment of channels with fairly steady flow (Bromley, 1991). The lateral accretionary elements have a lensoidal to wedge-like geometry, with internal second-order and third-order bounding surfaces. The internal cross-bedding foresets dip approximately parallel to the strike of the higher order accretionary surfaces (Miall, 1988). This element is interpreted as a bank-attached macroforms/point-bars deposited on the inside bends of channels, indicating a moderate level of sinuosity (Miall, 1988). The downstream accretionary

elements have a lensoidal geometry with internal convex up erosional third-order bounding surfaces. The internal cross-bedding foresets dip approximately parallel to the dip of the higher order accretionary surfaces (Miall, 1988). This element is interpreted as the deposits of mid-channel bars within channels of indeterminate sinuosity (Miall, 1988). The occasional interfingering of the accretionary and channel elements is interpreted as mutually active deposition (i.e. the channel was active during the deposition of the accretionary elements) (Bromley, 1991). Sandy sheet-like elements constitute a minor proportion of the association and represent deposits of unconfined flow. Overbank/floodplain deposits also constitute a minor proportion, especially within the proximal region and become more prevalent and laterally extensive within the distal region.

Overall this association represents the build-up of a channel belt during the migration and deposition of low-amplitude compound braid bars. Discharge was relatively steady with minor more localized scours. Channel incision and abandonment as well as overbank/floodplain deposition followed periods of avulsion (Lowe & Arnott, 2016).

5.3.3. Dominantly ephemeral fluvial deposition

The association comprises three architectural elements: fluvial channels, sheet-like elements and overbank/floodplain. This association is dominated by laterally extensive sheet-like elements (80%) composed of dominantly upper flow regime structures such as antidunes and parallel-laminations (with parting lineations), often topped with climbing ripple cross-stratified structures. These elements are often stacked and amalgamated and are the result of unconfined, high-energy, waning flows. Within the distal setting, these sheet-like elements are isolated within overbank/floodplain deposits and are interpreted as terminal splays deposited by unconfined flows downstream of poorly/shallowly confined channels (Nichols & Fisher, 2007). Fluvial channels are less common features and are typically composed of scour and fill sedimentation. The channels either comprise laterally extensive, gravel-dominated, clast-supported, structureless to crudely cross-bedded conglomerates with clasts of intraformational sediment, or confined channels dominated by structureless sandstones within minor

basal rip-up clast, matrix-supported conglomerates. The laterally extensive gravel-dominated conglomerates are interpreted as highly erosive fluvial discharge events that occasionally traversed into the distal alluvial plain (Cain & Mountney, 2009). Whereas the structureless channels are interpreted as deposits from a heavy-laden flow with a rapid waning stage and the inclusion of rip-up clasts suggest that the flows were highly erosive and ripped up the previously deposited overbank/floodplain elements (Horn *et al.*, 2018).

Overall, this association represents the build-up of a distributive channel belt by deposition of high energy sheet-like terminal splays fed by distributary fluvial networks with episodic discharge (Lowe & Arnott, 2016).

5.4. Summary

The twenty-one facies described within chapter four have been grouped together to form nine architectural elements: fluvial channels, sheets, lateral accretion, downstream accretion, bank collapse, overbank, aeolian dunes, aeolian sandsheet and interdune elements. These architectural elements have been grouped further into five large-scale fluvial depositional elements based upon their internal stacking patterns and composition; amalgamated sandstone-dominated channel-fill, isolated sandstone-dominated channel-fill, isolated gravel-dominated channel-fill, compound sandstone-dominated fluvial sheets and overbank. Three broad-scale associations based upon fluvial and aeolian depositional process have also been described; dominantly aeolian deposition, dominantly braided fluvial deposition, and dominantly ephemeral fluvial deposition.

Chapter Six will draw upon the observed facies and depositional elements detailed in this and the previous chapter and describe and quantify the spatial and temporal variations of the depositional elements. The interactions between the fluvial and aeolian deposits will also be described and multiple scales.

Chapter 6: Spatial and Temporal Variations of the Ephemeral Fluvial Kayenta Formation and their Interactions with a Competing Aeolian Environment

This chapter analyses the spatial and temporal variations of the ephemeral fluvial system and in so doing, the work explores the controlling factors upon the sedimentology of such a system. The sedimentary interactions between the dryland ephemeral fluvial system and the competing coeval aeolian depositional system are also analysed from the facies-scale reworking of aeolian sediment into the fluvial system, to the system-scale inter-tonguing of the aeolian Navajo Sandstone within the top third of the Kayenta. Chapter Seven will draw upon the complex sedimentary architectural, spatial and temporal variations and interactions with the competing aeolian system, and combine them with quantified geobody data from photogrammetric models to build quantitative facies and depositional models at multiple scales.

6.1. Methods

This study is based upon extensive regional sedimentological outcrop logging, and construction of three-dimensional models using photogrammetry, to investigate the sedimentary characteristics and interactions between fluvial and aeolian deposits during deposition of the Kayenta Formation across the Colorado Plateau.

Twenty-five detailed vertical sections were logged, with a cumulative length of over 1700 m, each spaced approximately 25 km apart over an area of approximately 200 km², constrained to as close to a grid pattern as exposure allows (Chapter 3; Fig. 3.1; Table 3.1). The sedimentary logs record full successions of the Kayenta Formation, from the J-sub-K unconformity to the last main fluvial occurrence within the gradational contact with the overlying Navajo Sandstone. In southern Utah and

northern Arizona, this succession includes the basal Springdale Sandstone member of the Kayenta Formation. The deposits have been classified into proximal, medial, and distal sections from the Uncompahgre Uplift source, based upon regional changes in fluvial composition and stacking patterns. The proximal deposits are defined by greater than 70% amalgamated channels and less than 5% overbank, the medial deposits are defined by 30-70% amalgamated channels and less than 30% overbank, and the distal deposits are defined by less than 30% amalgamated channels and greater than 30% overbank.

Alongside the logs, an extensive palaeocurrent dataset was collected (Chapter 3; Section 3.1.3). This comprises 235 measurements from planar and trough cross-bedded foresets, ripple-cross-laminated foresets and primary current lineations within fluvial sediments and 127 measured from planar and trough cross-bedded foresets within aeolian sediments of the Kayenta Formation.

Three digital photogrammetric models of suitable outcrops from proximal, medial and distal fluvial settings, collected using both a DSLR camera (Nikon D800E) and a drone (DJI Phantom 4 Pro), were processed in Agisoft PhotoScan, and analysed using Virtual Reality Geological Studio (VRGS), courtesy of David Hodgetts (Chapter 3; Section 3.2). Each model comprises between 400 and 600 photographs, with each sedimentary feature pictured in at least five images (Chapter 3; Table 3.3; Fig. 3.3). Accompanying sedimentary logs along the outcrop face allow for 'ground-truthing' of the sedimentology displayed in the models. The models illustrate: (i) the lateral and vertical relationships between fluvial and aeolian architectural elements; (ii) the geometry and dimensions of the elements; (iii) the nature of contact between the elements; and (iv) differences in architecture and sedimentology between proximal, medial and distal settings.

Using VRGS, the dimensions of the depositional elements were mapped onto the digital outcrop models to determine apparent size of elements in the planes of the models (Chapter 3; Section 3.2.3). Palaeocurrent measurements were then used to correct for the orientation of the models and to calculate true element dimensions in a direction perpendicular to flow in each case (Visser & Chessa,

2000a; Pringle *et al.*, 2010; Rarity *et al.*, 2013). The dimensions of partial or incomplete elements within models have been approximated using methods outlined in Geehan & Underwood (1993) (Chapter 3; Section 3.2.3).

For the sediments of the Kayenta Formation, spatial variations in the compositional characteristics of the thicknesses of fluvial and aeolian strata, the percentage of sand, the percentage of conglomerate, and the grainsize distribution of the fluvial sediments, have been calculated and are illustrated as contour maps across the study area. The data used to analyse the spatial variations and downstream trends were determined as follows:

- Fluvial and aeolian sediment thicknesses are calculated as the total thicknesses of strata of each type observed within sediments of the Kayenta Formation at each locality.
- The percentages of fluvial sand and fluvial conglomerates at each locality were calculated by summing the thicknesses of individual beds of fluvial sediment with average grain sizes of each and comparing these values to the total thicknesses of fluvial sediment at each locality.
- The average grain size for each locality was calculated from the observed average grain size of each individual bed, with measurements determined per unit thickness of sediment in order to normalise by bed thickness.

Analysis of spatial variations in the five identified depositional elements of Chapter Five (Section 5.2) has also been conducted. The data used to analyse the spatial variations and downstream trends of the five depositional elements were determined as follows:

- The percentage of each depositional element per locality was determined from the total thicknesses of elements of each type displayed in the sedimentary logs and comparing these values to the total thicknesses of fluvial sediment at each locality.
- The average thickness of each depositional element per locality was determined from the sedimentary logs.

- The average grainsize of each type of depositional element per locality was calculated from the observed average grainsize of each individual bed, with measurements determined per unit thickness of sediment in order to normalise by bed thickness.

The results of these analyses are displayed as contour plots of data and each plot is supplemented with a line graph depicting the spatial variations in a general downstream direction that follows the dominant south-westward direction of flow indicated by palaeocurrent data, from the Uncompahgre Uplift. A line of best fit, and arithmetic averages for the proximal, medial, and distal regions are provided for the data. The localities affected by the secondary fluvial source from the Mogollon Highlands have been highlighted on each contour plot and each graph, and secondary lines of best fit demonstrate trends excluding these data. For the sake of ease, all four data points within the distal region have been excluded when calculating the best fit trend as it is difficult to determine the source of some depositional elements, particularly when no palaeocurrent data were available.

6.2. General Spatial Variations of the Kayenta Formation

Spatial variations in the architecture, cumulative thickness, composition and grainsize of the Kayenta Formation have been analysed across the expanse of the study area. The results focus on the data derived from the dominant south-westward flowing fluvial system sourced from the Uncompahgre Uplift. However, data from the second north-westward flowing axial system have been highlighted and the effects on the downstream trends are discussed.

6.2.1. Architecture of the Kayenta Formation

The proximal region of the fluvial Kayenta system around Moab, UT, comprises a series of laterally and vertically amalgamated sandstone-dominated channel-fill depositional elements with abundant compound sandstone-dominated fluvial sheet depositional elements, but very few overbank depositional elements (Fig. 6.1A). Lateral and vertical amalgamation of channel depositional elements decreases by the medial region of the system (around Comb Ridge, UT), but compound sandstone-dominated fluvial sheet depositional elements are still abundant and extend laterally for over 400 m

(Fig. 6.1B). Channel depositional elements are typically isolated within compound sandstone-dominated fluvial sheet depositional elements, and overbank depositional elements are prevalent between channels and compound fluvial sheets. The distal region around Kanab, UT, consists of isolated sandstone-dominated channel and compound sandstone-dominated fluvial sheet depositional elements preserved within overbank depositional elements (Fig. 6.1C). Compound sandstone-dominated fluvial sheet depositional elements form at distinct stratigraphic levels within the overbank to provide a relatively low degree of sandstone connectivity.

6.2.2. Thickness variations within the Kayenta Formation

The total thickness of the fluvial strata shows a gradual increase downstream, but with an abrupt thickening over a short distance within the distal region (62 m of fluvial sediment at Lees Ferry, compared to 154 m at Kanab, just 85 km away) (Fig. 6.2A & Fig. 6.2B). The thickness of the fluvial component of the succession also generally decreases towards the north-west and the south-east, perpendicular to palaeoflow. However, omitting the data within the distal region that is influenced by the secondary source, reveals an opposing trend, with cumulative fluvial sediment thickness decreasing downstream (Fig. 6.2A & Fig. 6.2B).

The coeval aeolian deposits also show a gradual increase in thickness with respect to downstream distance (of the fluvial system), again with an abrupt thickening over a short distance within the distal region (Fig. 6.2C & Fig. 6.2D). However, when comparing the data to the palaeowind direction, determined from the palaeocurrent measurements of the coeval aeolian deposits, the thickness of aeolian sediment generally decreases with the palaeowind direction towards the east/south-east, particularly within the medial region.

6.2.3. Composition of the Kayenta Formation

The percentage of sand within the fluvial system decreases downstream towards the south-west (Fig. 6.2E & Fig. 6.2F) from up to 100% in the proximal region (Dewey Bridge, UT, and John Brown Canyon, CO) to 58% distally (The Gap, UT). Slightly anomalous sandstone percentages are observed within

some medial sections (Kayenta, AZ - 95%; Mexican Water, UT - 96%), as well as Lees Ferry in the distal region (88%), but these values fit the general trend of a decrease in sandstone percentage towards the south-west. In the medial region, the percentage of sand is replaced with approximately 1-17% siltstone, increasing with distance downstream, however, within the distal region, the percentage of sand is replaced with approximately 9-24% siltstone and 3-8% conglomerates (Fig. 6.2G & Fig. 6.2H).

6.2.4. Overall Grainsize of the Kayenta Formation

The average grain size of all fluvial sediment, irrespective of the depositional element in which it is preserved, gradually decreases downstream from dominantly medium-grained sandstone within the proximal region to fine to very fine-grained sandstone within the distal region (Fig. 6.2I & Fig. 6.2J). The average grainsize also decreases radially from the dominant trend. A few anomalies are present, in particular, at Lees Ferry within the distal region where the largest average grainsize (1.26ϕ) of the whole system is observed. Despite local anomalies, a clear downstream fining is present.

6.3. Interpretation of the Spatial Variations in the Sedimentology of the Kayenta Formation

The high degree of channel and sheet amalgamation and connectivity within proximal region suggests the fluvial system was highly cannibalistic (North & Taylor, 1996; Hassan *et al.*, 2018; Chapter 5; Priddy & Clarke, 2020) with a high sediment supply (Weissman *et al.*, 2013; Owen *et al.*, 2015). The decrease in channel and sheet amalgamation, increase in the proportion of overbank, and overall grainsize reduction downstream can be attributed to a decrease in energy and a decrease in the river's carrying capacity downstream as a result of lateral expansion of the river system, channel bifurcation and high rates of evapotranspiration and infiltration into the dry substrate (Nichols & Fisher, 2007; Weissmann *et al.*, 2010; 2013; Sutfin *et al.*, 2014; Owen *et al.*, 2015).

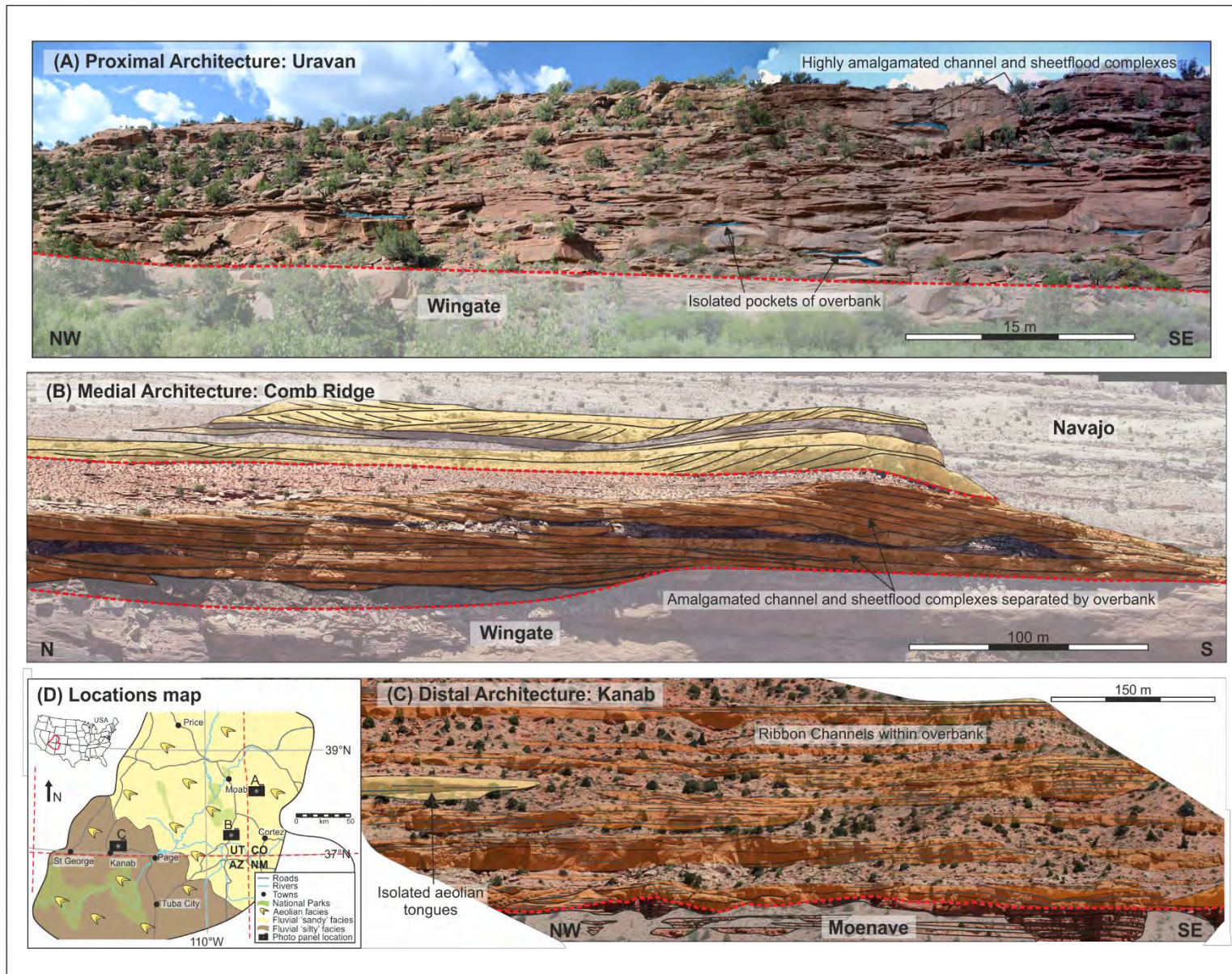


Figure 6.1. Architecture outcrop panels from three locations across the extent of the Kayenta Formation deposition depicting the change in architecture downstream, from highly amalgamated channels and sheets within the proximal to isolated channels and sheets within the distal. (A) Proximal architecture panel of Uravan, Colorado. (B) Medial architecture panel of Comb Ridge, southeast Utah. (C) Distal architecture panel of Kanab, southwest Utah. (D) Locations map illustrating the positions of panels A-C.

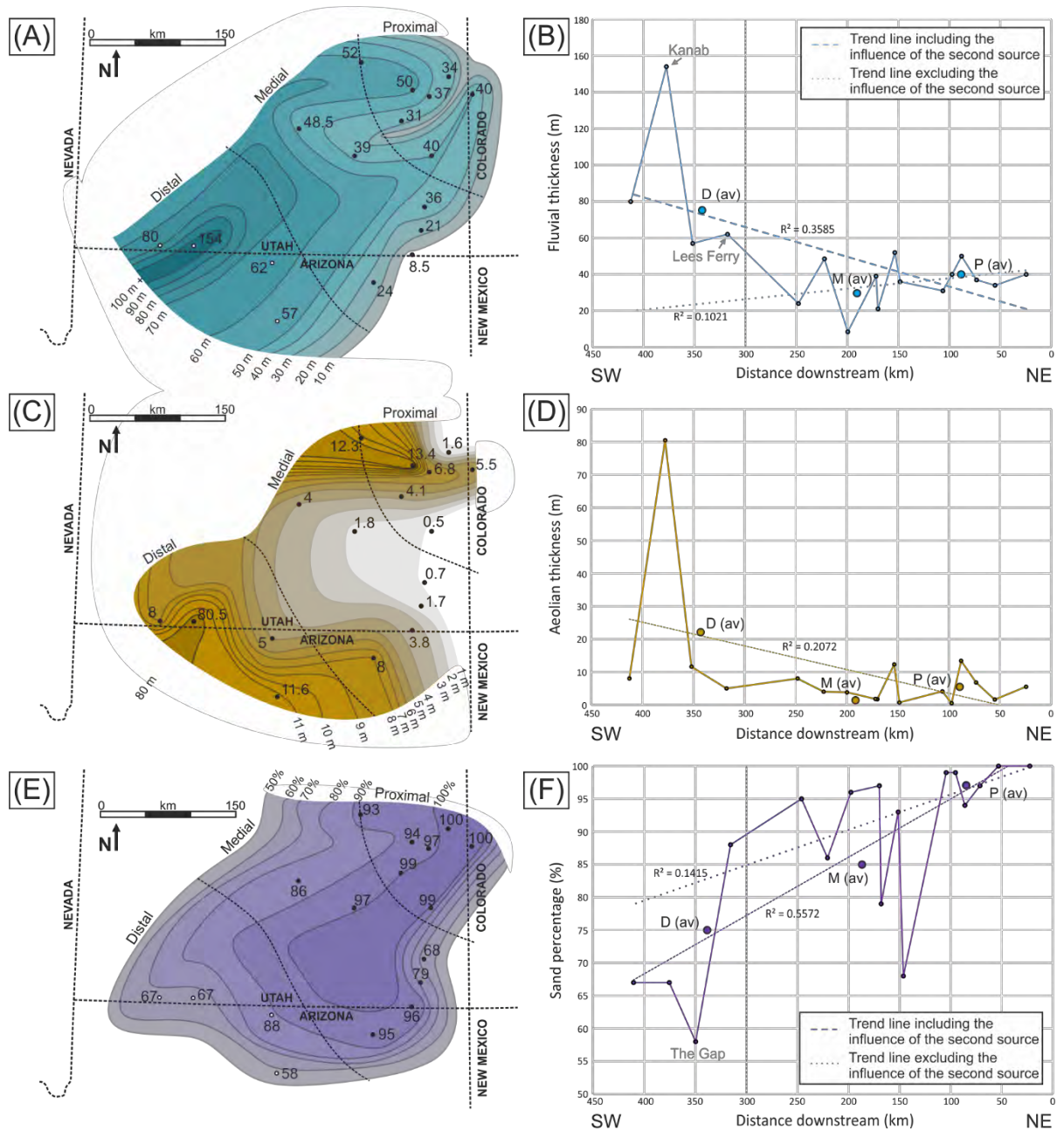


Figure 6.2. (A) Contour map of fluvial sediment thickness at each locality. (B) Graph of total fluvial sediment thickness against distance downstream. (C) Contour map of aeolian sediment thickness at each locality. (D) Graph of total aeolian sediment thickness against distance downstream. (E) Contour map of sand percentage at each locality. (F) Graph of sand percentage against distance downstream. (G) Contour map of conglomerate percentage at each locality. (H) Graph of conglomerate percentage against distance downstream. (I) Contour map of the average grainsize (Φ) at each locality. (J) Graph of average grainsize (Φ) against distance downstream. Average measurements of proximal, medial and distal portions are denoted as P (av), M (av), and D (av) on each graph. Dashed line in each case is a linear best fit to the total dataset and the dotted line is a linear best fit line excluding the data influenced by the secondary fluvial source.

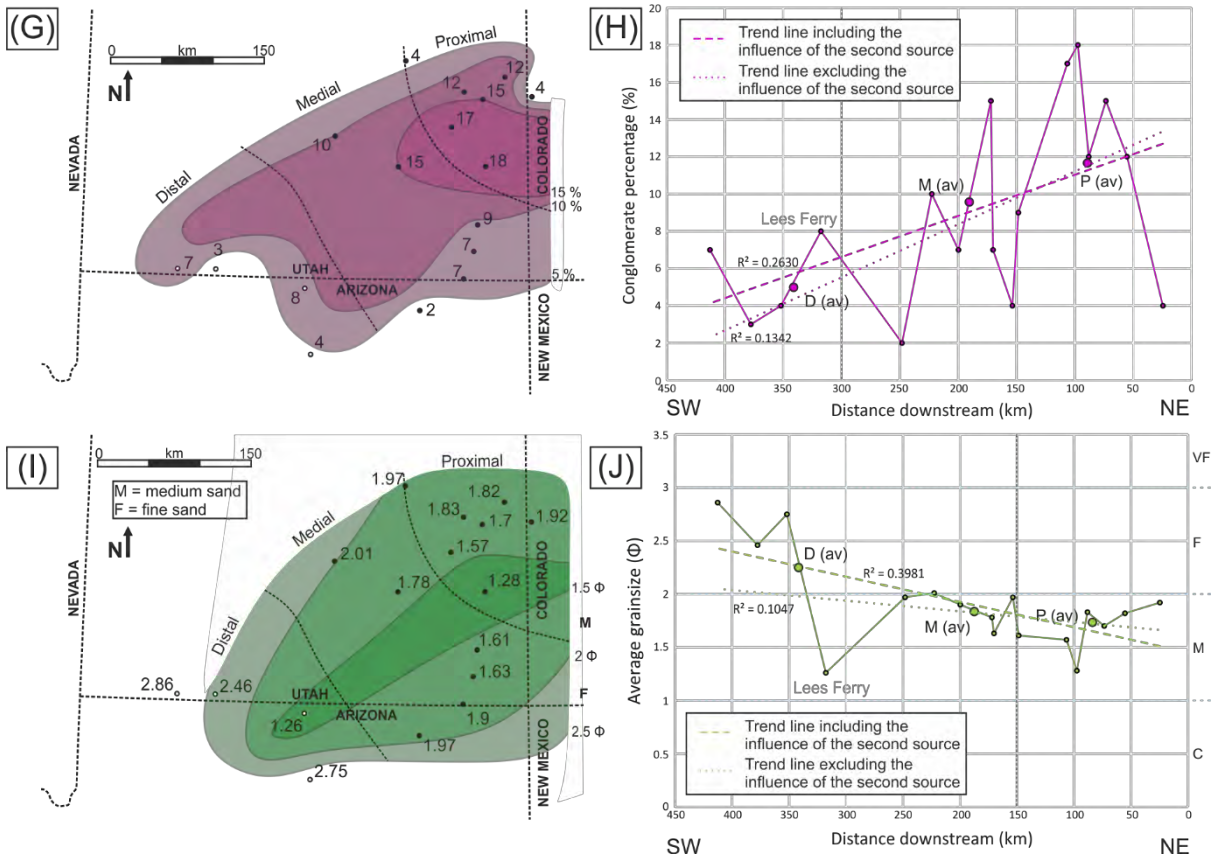


Figure 6.2. continued.

However, it must be noted that a decrease in amalgamation of channel and compound sheet elements, coupled with an overall increase in the total fluvial sediment thickness observed at each locality, could also be attributed to increased subsidence and the generation of additional accommodation space, coevally with deposition of the Kayenta sediments, as in the distal region where deposition of the Kayenta correlates with the location of the Zuni Sag (Chapter 2, Fig. 2.14) (Blakey, 1994). It is also possible that the increase in cumulative fluvial sediment thickness within the distal section may also be attributed to a secondary, axial fluvial system, sourced from the Mogollon Highlands in the Cordilleran Magmatic Arc (Luttrell, 1993; Hassan *et al.*, 2018) feeding additional sediment volume into the Zuni Sag, although ultimately the thickness of sediment preserved is probably controlled by developing accommodation space over any other factor.

6.4. Analysis of the Depositional Elements

Spatial variations in distribution, thickness and grainsize for each depositional element have been analysed across the expanse of the study area. The results focus on the data derived from the dominant south-westward flowing fluvial system sourced from the Uncompahgre Uplift. However, data from the second north-westward flowing axial system have been highlighted and the effects on the downstream trends are discussed.

6.4.1. Distribution of the Depositional Elements

The relative proportions of both amalgamated sandstone-dominated channel-fill (Fig. 6.3A & Fig. 6.3B) and overbank (Fig. 6.3I & Fig. 6.3J) depositional elements display strong downstream trends and radial patterns. Weaker trends are present for isolated sandstone-dominated channel-fill (Fig. 6.3C & Fig. 6.3D), isolated gravel-dominated channel-fill (Fig. 6.3E & Fig. 6.3F) and compound sandstone-dominated fluvial sheet depositional elements (Fig. 6.3G & Fig. 6.3H).

The proportions of overbank depositional elements increase with distance downstream (Fig. 6.3I & Fig. 6.3J), with the lowest proportions preserved within the central proximal region (John Brown Canyon, Dewey Bridge, Lions Park, Wilhite Trail and Hite). Downstream, in the medial region, overbank depositional elements become more prevalent to constitute between 1% of the fluvial sediments at Newspaper Rock and up 35% of the succession at Comb Ridge. Between 36% (Colorado City) to 44% (The Gap) of the fluvial sediments in the distal region are overbank depositional elements.

By contrast, the proportions of amalgamated sandstone-dominated channel-fill depositional elements decrease with distance downstream (Fig. 6.3A & Fig. 6.3B). The highest proportions are preserved in the fluvial sediments of the central proximal region, particularly those of Newspaper Rock (76%) and San Rafael Swell (71%). Downstream, the amalgamated sandstone-dominated channel-fill depositional elements decrease in abundance to constitute between 30% (Comb Ridge) and 69% (Hite) of the fluvial sediments by the medial region, and between 15% (The Gap) and 31% (Lees Ferry) by the distal regions.

By comparison to the amalgamated sandstone-dominated channel-fill and overbank depositional elements, there is a weak trend between the relative proportions of isolated sandstone-dominated channel-fill elements and the distance downstream, displaying a gradual increase in isolated channel elements downstream (Fig. 6.3C & Fig. 6.3D). Low proportions of isolated sandstone-dominated channel-fill are preserved within the fluvial sediments of the eastern proximal to medial regions (0% at Sevenmile Canyon and Kayenta, 1% at Newspaper Rock, and 3% at both Comb Ridge and Comb Wash) with slightly higher proportions preserved towards the west-southwest in the medial and distal regions (13% at The Gap, 12% at Hickman Bridge Trail and 11% at Kanab). Despite an apparent overall increase in abundance with distance downstream, the relative proportions of isolated sandstone-dominated channel elements in some proximal and medial areas are somewhat anomalous. For example, at Mexican Water, anomalously high proportions of isolated sandstone-dominated channel-fill elements (35%) may be a result of under-sampling due to the small outcrop. The relatively low gradient of the relationship between the proportions of isolated sandstone-dominated channel-fill elements and the distance downstream (Fig. 6.3C & Fig. 6.3D) may suggest this relationship is controlled primarily by the diminishing abundance of other channel-fill elements with distance downstream, and there is little downstream control on the presence of this depositional element.

Both isolated gravel-dominated channel-fill (Fig. 6.3E & Fig. 6.3F) and compound sandstone-dominated fluvial sheet (Fig. 6.3G & Fig. 6.3H) depositional elements display very weak decreasing trends in relative proportions with distance downstream.

6.4.2. Thickness of the Depositional Elements

Only very weak downstream trends in the average thicknesses of the depositional elements are observed (Fig. 6.4). The overbank depositional element has the strongest downstream trend (Fig. 6.4E), with an increase in thickness towards the distal region. The next strongest trend is observed within the isolated sandstone-dominated channel-fill element (Fig. 6.4B). A very weak increase in average channel thickness is observed with distance downstream.

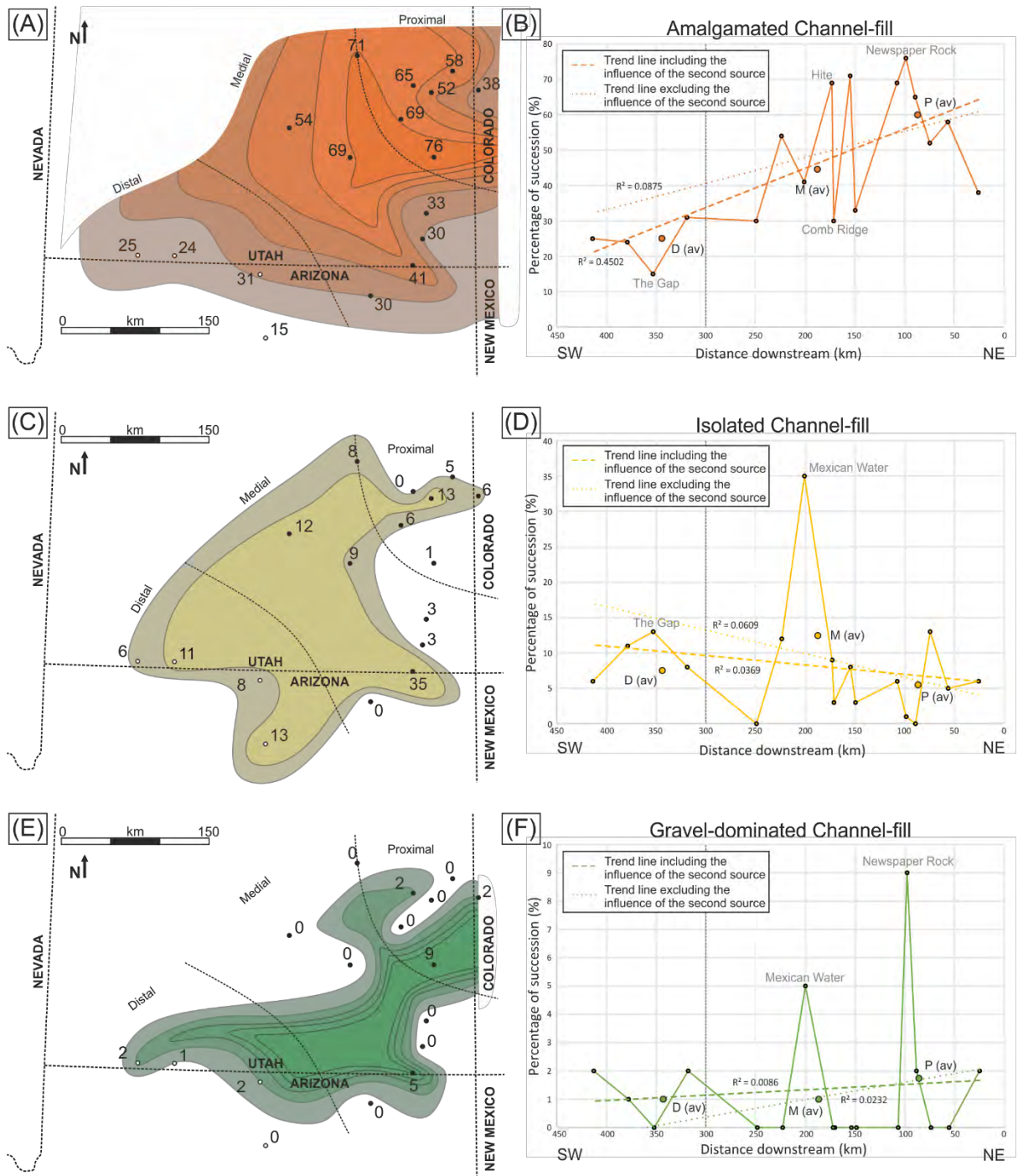


Figure 6.3. Contour maps and graphs illustrating the percentage that each depositional element constitutes of the whole fluvial succession at each locality. (A) Amalgamated channels contour map. (B) Graph of amalgamated channel percentage against distance downstream. (C) Isolated channels contour map. (D) Graph of isolated channel percentage against distance downstream. (E) Gravel-dominated channel contour map. (F) Graph of gravel-dominated channel percentage against distance downstream. (G) Compound fluvial sheet contour map. (H) Graph of compound fluvial sheet percentage against distance downstream. (I) Overbank contour map. (J) Graph of overbank percentage against distance downstream. Average measurements of proximal, medial and distal portions are denoted as P (av), M (av), and D (av) on each graph. Dashed line in each case is a linear best fit to the total dataset and the dotted line in each case is a linear best fit line excluding the data influenced by the secondary fluvial source.

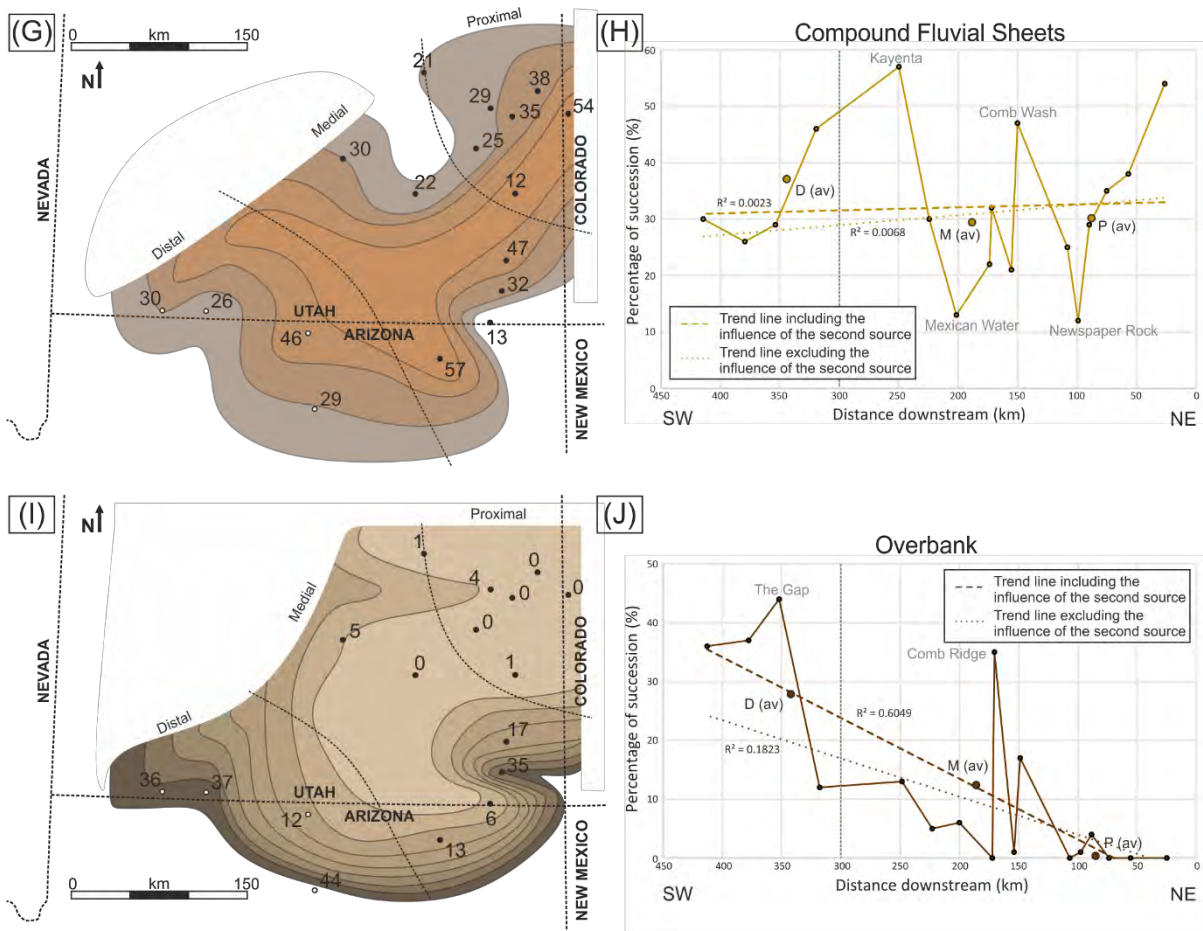


Figure 6.3 continued.

Amalgamated sandstone-dominated channel-fill (Fig. 6.4A), isolated gravel-dominated channel-fill (Fig. 6.4C) and compound sandstone-dominated fluvial sheet (Fig. 6.4D) depositional elements all show very little to no variation downstream. However, when the data from elements displaying sediment derived from the secondary fluvial source are removed, a strong downstream trend is observed, with the thickness of isolated gravel-dominated proximal channel-fill elements decreasing with distance downstream (Fig. 6.4C).

6.4.3. Grainsize Distribution of the Depositional Elements

Contrary to the first order trend that is typical of all fluvial systems, the amalgamated sandstone-dominated channel-fill depositional element shows no downstream decrease in grainsize (Fig. 6.5A & Fig. 6.5B).

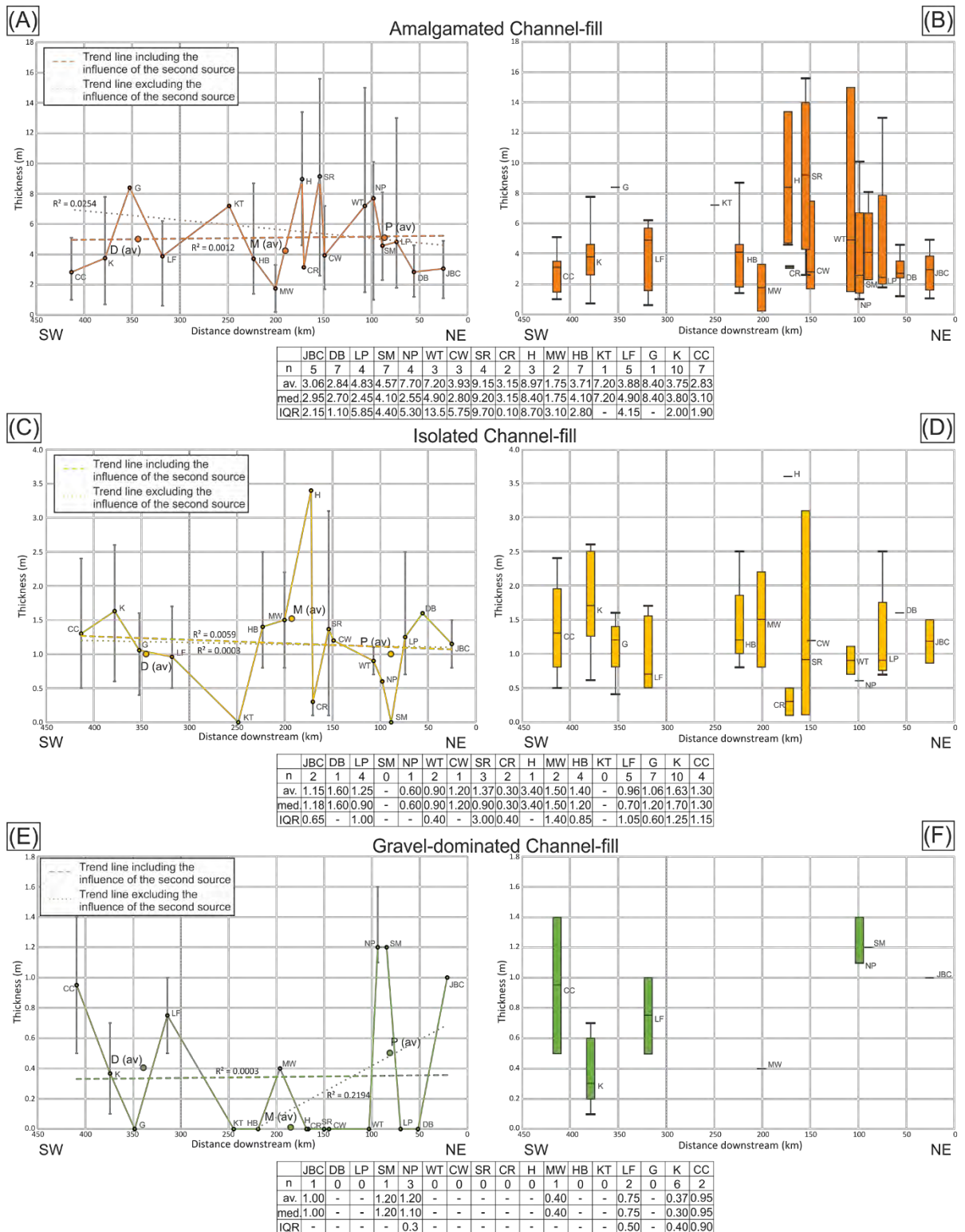


Figure 6.4. Graphs illustrating the average and range of sediment thickness at each locality for each depositional element plotted against distance downstream and box and whisker plots illustrating the median, interquartile range and outliers for each locality for each depositional element plotted against distance downstream. Average measurements of proximal, medial and distal portions are denoted as P (av), M (av), and D (av) on each graph. Dashed line in each case is a linear best fit to the total dataset and the dotted line in each case is a linear best fit line excluding the data influenced by the secondary fluvial source.

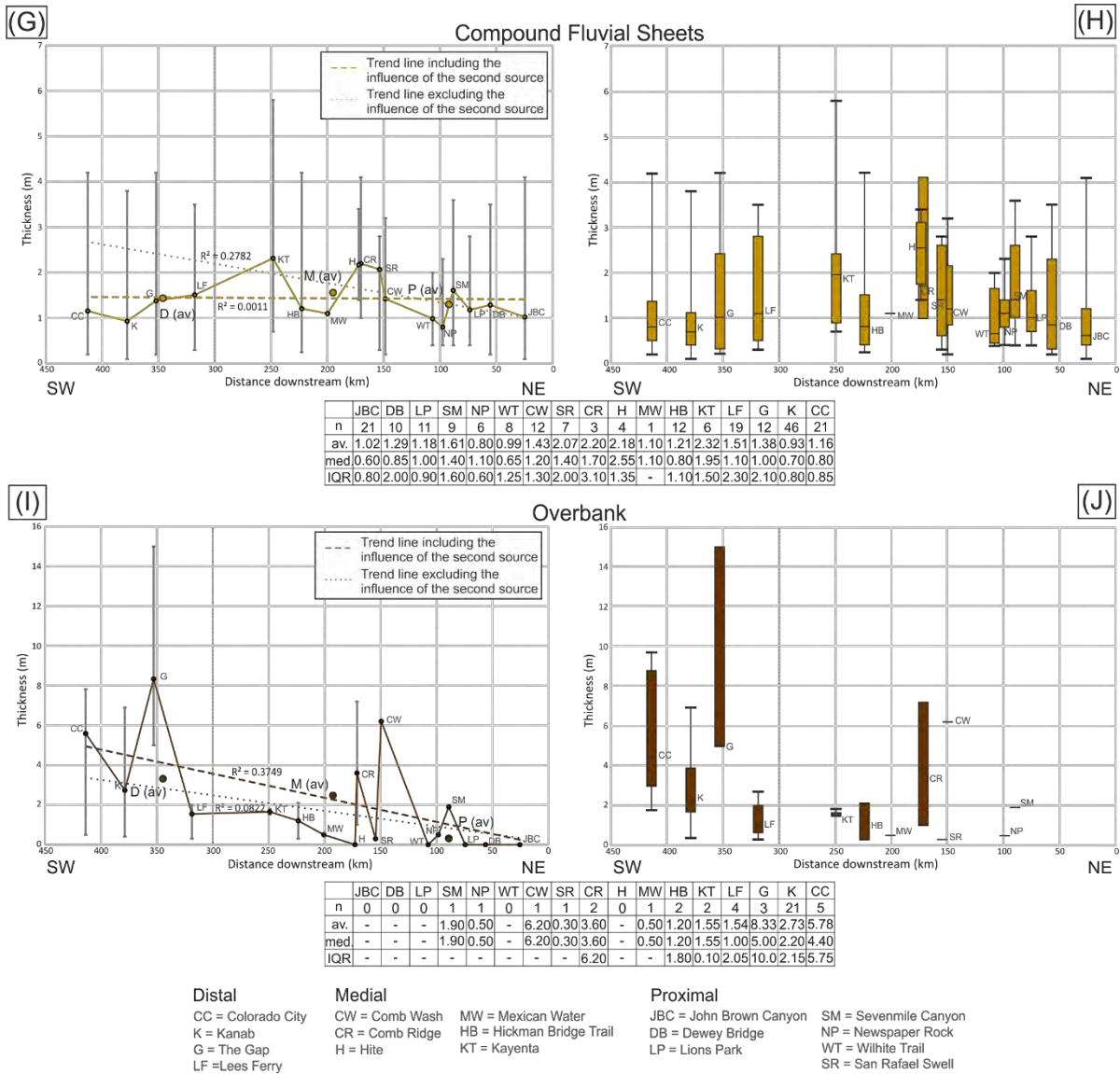


Figure 6.4. continued.

Sediment calibre is consistently medium-grained sandstone throughout most of the system, although a few locations in the proximal and medial regions preserve anomalously finer grained fluvial sediment (San Rafael Swell – 2.64ϕ and Hickman Bridge Trail – 2.48ϕ). However, once data from elements displaying sediment derived from the secondary fluvial source are removed, a weak trend is observed, with a decrease in grainsize with distance downstream (Fig. 6.5A & Fig. 6.5B). Isolated sandstone-dominated channel-fill elements have a very weak downstream trend, displaying a gradual decrease in grainsize, from medium-grained sandstone within the proximal to fine-grained sandstone within the distal (Fig. 6.75 & Fig. 6.5D).

The isolated gravel-dominated channel-fill depositional element has a strong downstream trend, but not in the manner that could be intuitively predicted (Fig. 6.5E & Fig. 6.5F). An increase in grain size with distance downstream is observed, from very coarse-grained sandstone within the proximal to medium to coarse-grained pebbles within the distal. However, once data from elements displaying sediment derived from the secondary fluvial source are removed, a strong decrease in grain size with distance downstream is observed, from a granule-grade conglomerate in the proximal to a coarse-grained sandstone in the distal. Compound sandstone-dominated fluvial sheet elements have a very weak downstream trend, displaying a gradual decrease in grain size, from medium-grained sandstone within the proximal region to fine-grained sandstone within the distal region (Fig. 6.5G & Fig. 6.5H). However, once the data from elements displaying sediment derived from the secondary fluvial source are removed, a strong downstream trend is observed, with a decrease in grain size from medium-grained sandstone within the proximal region to very fine-grained sandstone within the distal region (Fig. 6.5G & Fig. 6.5H). The overbank depositional element has the strongest trend, with an overall decrease in grain size with distance downstream, from fine to very fine-grained sandstone within the proximal to coarse siltstone within the distal (Fig. 6.5I & Fig. 6.5J).

6.5. Interpretation of the Spatial Variations in the Depositional Elements

Amalgamated sandstone-dominated channel-fill depositional elements display downstream fluvial trends typical of fluvial systems including a decrease in their abundance and decrease in their constituent grain size downstream. They can be attributed to a decrease in energy downstream as a result of high rates of evapotranspiration and infiltration into the dry substrate and channel bifurcation (Nichols & Fisher, 2007; Weissmann *et al.*, 2010; 2013; Sutfin *et al.*, 2014; Owen *et al.*, 2015).

A relatively flat linear trend line for the percentage of isolated sandstone-dominated channel-fill depositional elements suggests that there is no downstream control on the presence of this element.

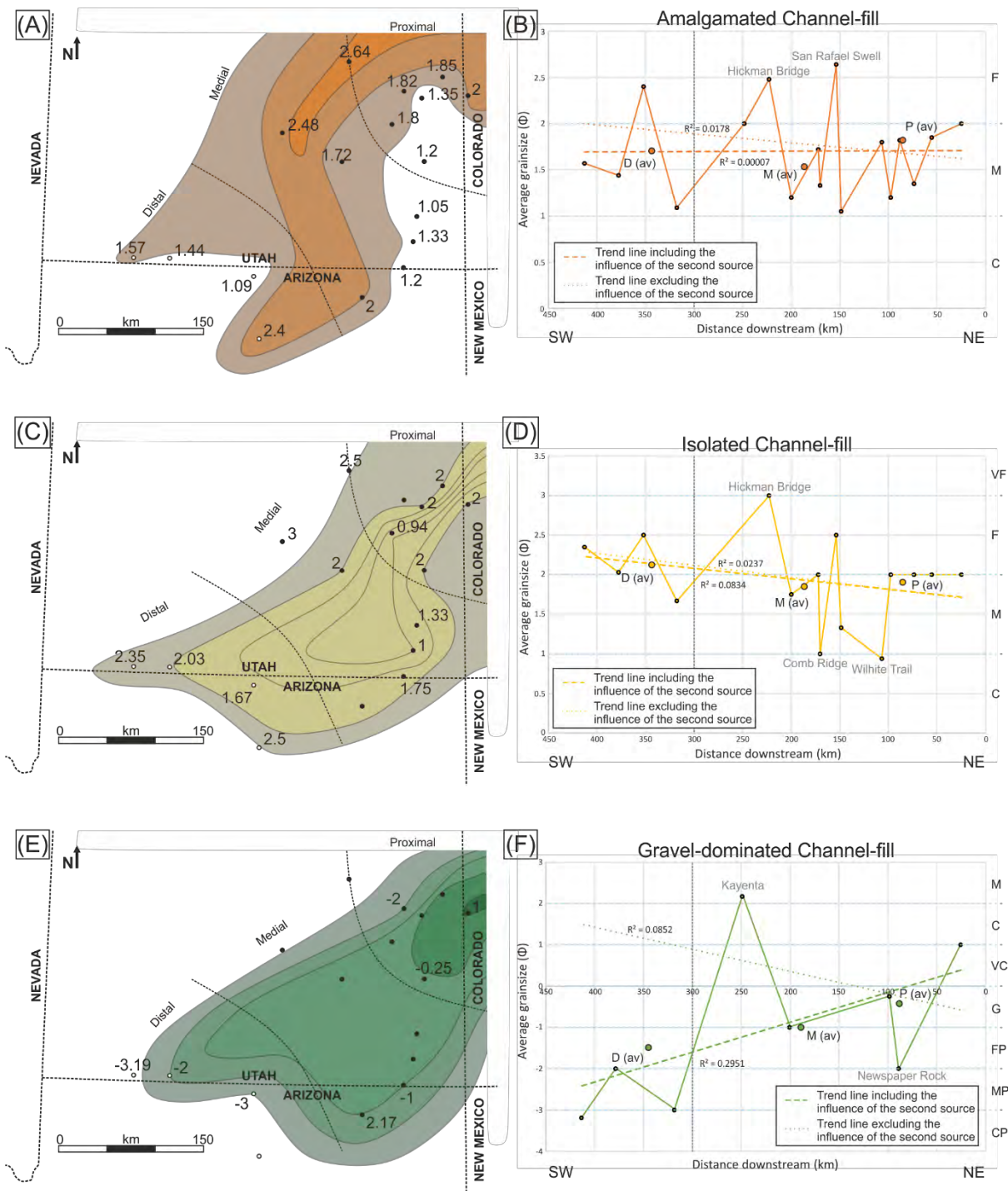


Figure 6.5. Contour maps and graphs illustrating the average grain size (Φ) that each depositional element constitutes of the fluvial succession at each locality. (A) Amalgamated channel contour map. (B) Graph of amalgamated channel average grain size against distance downstream. (C) Isolated channel contour map. (D) Graph of isolated channel average grain size against distance downstream. (E) Gravel-dominated channel contour map. (F) Graph of gravel-dominated channel average grain size against distance downstream. (G) Compound fluvial sheet contour map. (H) Graph of compound fluvial sheet average grain size against distance downstream. (I) Overbank contour map. (J) Graph of overbank average grain size against distance downstream. Average measurements of proximal, medial and distal portions are denoted as P (av), M (av), and D (av) on each graph. Dashed line in each case is a linear best fit to the total dataset and the dotted line in each case is a linear best fit line excluding the data influenced by the secondary fluvial source.

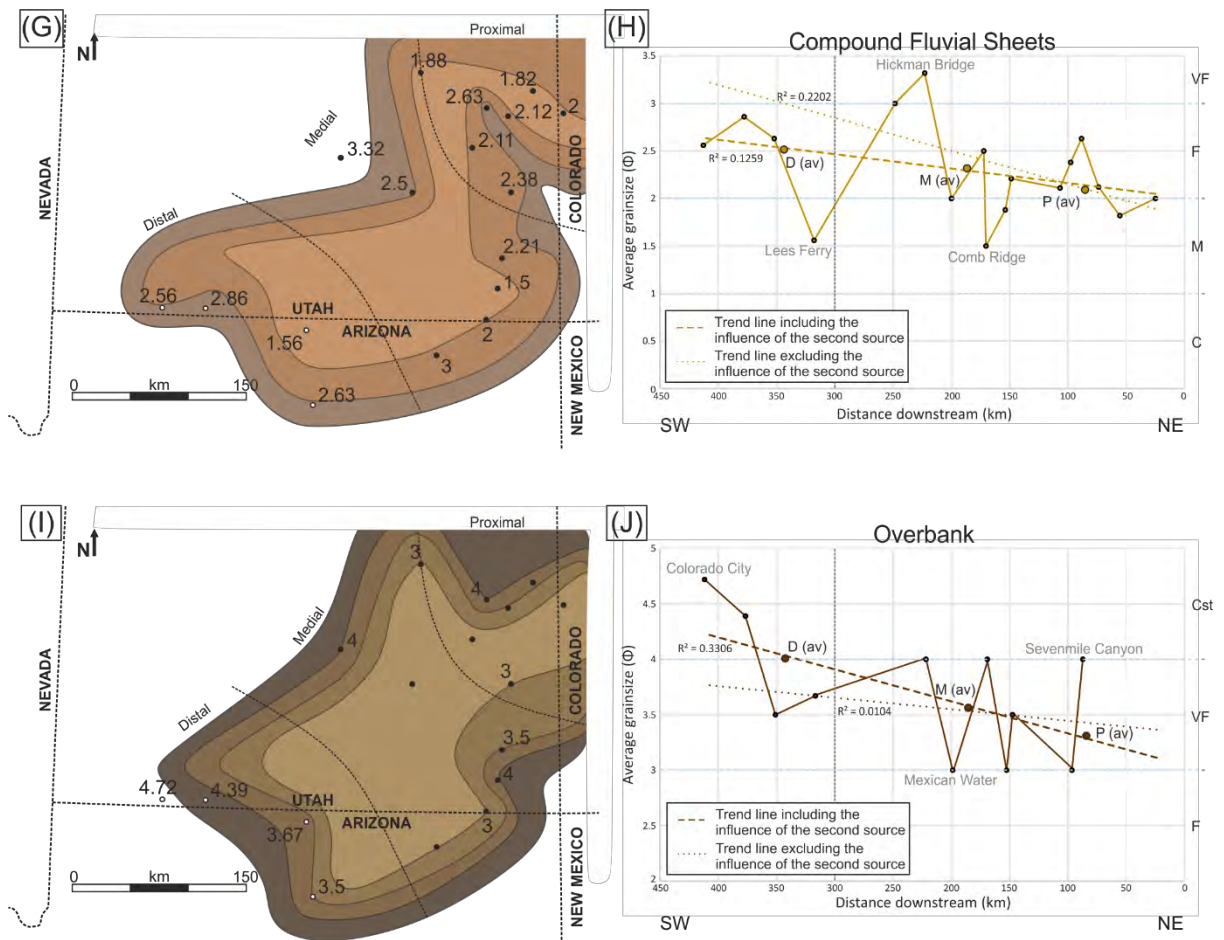


Figure 6.5. continued.

The very slightly higher prevalence in this element downstream that the data suggest is of little significance and may be due simply to the diminishing abundance of other channel-fill elements downstream. The increase in the average thicknesses of the isolated sandstone-dominated channel-fill depositional elements downstream is likely the result of increased preservation potential within the distal setting, where full thicknesses of the isolated channels are more likely to be preserved.

Isolated gravel-dominated channel-fill depositional elements comprise only a small proportion of the fluvial succession with distance downstream. However, the grain size of the isolated gravel-dominated channel-fill depositional elements increases downstream; a trend that is contrary to that intuitively expected for any waning fluvial system. This observation may be due directly to the secondary source

of coarse-grained Kayenta fluvial sediment in south-west Utah (Luttrell, 1993) and it is something that would require in-depth petrographical and provenance studies to examine further (Chapter 10).

Analysis of the compound sandstone-dominated fluvial sheet depositional elements reveal relatively constant percentage of elements and average thicknesses downstream. The flat linear trend lines for these characteristics suggests that there is no downstream control on the presence of this element, and the occasional more prevalent appearance downstream may be due to the interaction with the secondary fluvial system within the distal region.

The overbank depositional elements display the strongest trends within the data; an increase in the percentage and thickness of overbank downstream and a decrease in grainsize downstream, all of which are typical for waning fluvial system. These trends are a result of the decrease in energy and the river's carrying capacity downstream as a result of lateral expansion of the river system, channel bifurcation and high rates of evapotranspiration and infiltration into the dry substrate (Nichols & Fisher, 2007; Weissmann *et al.*, 2010; 2013; Sutfin *et al.*, 2014; Owen *et al.*, 2015).

The sand-dominated fluvial depositional elements (amalgamated channel, isolated channel and compound sheet elements) display no significant trends in grainsize distribution downstream. Each of these elements is dominated by fine to medium-grained sandstone of aeolian origin that has been blown off coeval dune fields, reworked and transported by the fluvial system (Chapter 5; Priddy & Clarke, 2020). Coeval aeolian systems are a typical feature of many modern arid ephemeral fluvial basins (Veiga *et al.*, 2002; Al-Masrahy & Mountney, 2015; Formolo Ferronato *et al.*, 2019; Reis *et al.*, 2019; Coronel *et al.*, 2020), and many preserved examples of arid fluvial strata contain significant proportions of aeolian sediment (Langford, 1989; Clarke & Rendell, 1998; Bullard & Livingstone, 2002; Field *et al.*, 2009). This relationship could be recognised as a characteristic of dryland ephemeral fluvial systems.

6.6. Temporal Variations

To analyse the temporal variations of the Kayenta Formation, channel body thicknesses of the amalgamated sandstone-dominated channel-fill, isolated sandstone-dominated channel-fill and isolated gravel-dominated channel-fill depositional elements were plotted against their height within the logged successions (Figs. 6.6, 6.7 & 6.8) in order to gain insight into the behaviour of the fluvial system through time.

The results show an overall decrease in channel body thickness with increasing height within the successions, particularly evident in the proximal successions of Sevenmile Canyon and Wilhite Trail (Fig. 6.6), the medial succession of Hickman Bridge Trail (Fig. 6.7) and the distal successions of Kanab and Colorado City (Fig. 6.8). However, some locations show very weak relationships with respect to channel body thickness and height within the succession, particularly within the medial successions (Fig. 6.7) but also including proximal sections of John Brown Canyon and San Rafael Swell (Fig. 6.6).

The results also show a general decrease in amalgamated channels and an increase in isolated channels up-succession across the proximal to distal regions. Concentrations of isolated gravel-dominated channels are also noted within the lower third of the distal successions (Fig. 6.8).

6.7. Interpretation of the Temporal Variations

The up-succession variations in channel body thickness have been interpreted to represent the transgression and regression of the fluvial system through time, but with an overall regressive trend (e.g. Kjemperud *et al.*, 2008; Cain & Mountney, 2009; Weissmann *et al.*, 2013; Rittersbacher *et al.*, 2014; Owen *et al.*, 2017; 2019; Martin *et al.*, 2021). Due to the coeval competing aeolian environment, the transgression and regression of the fluvial system may also relate to the contraction and expansion of the competing aeolian dune field (Cain & Mountney, 2009).

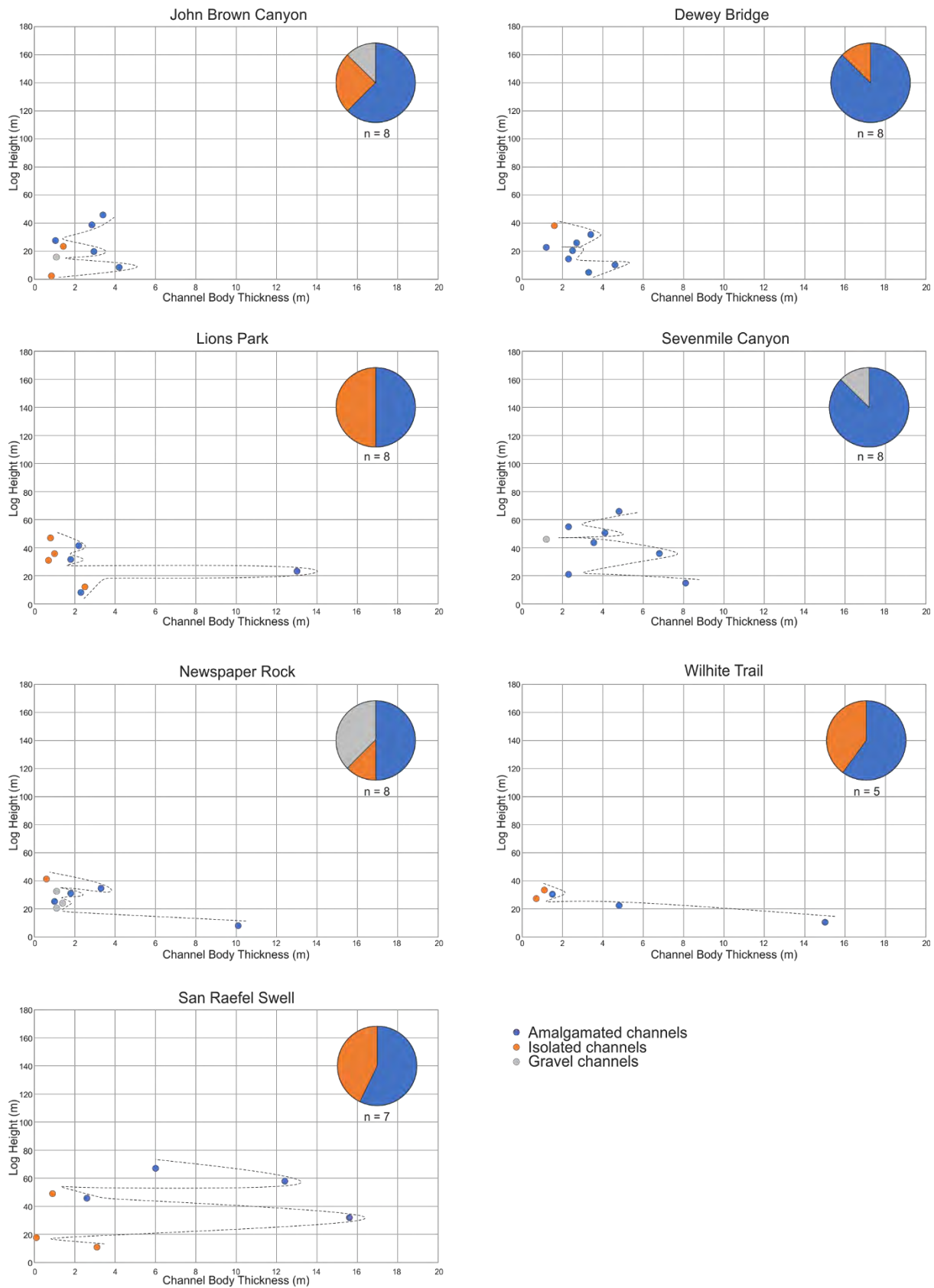


Figure 6.6. Log height of channel body against channel body thickness for each proximal succession studied. Coloured dots represent the interpreted channel depositional element present. The dashed line represents moving averages, and the pie chart breakdown shows the percentage of channel depositional element types for each locality.

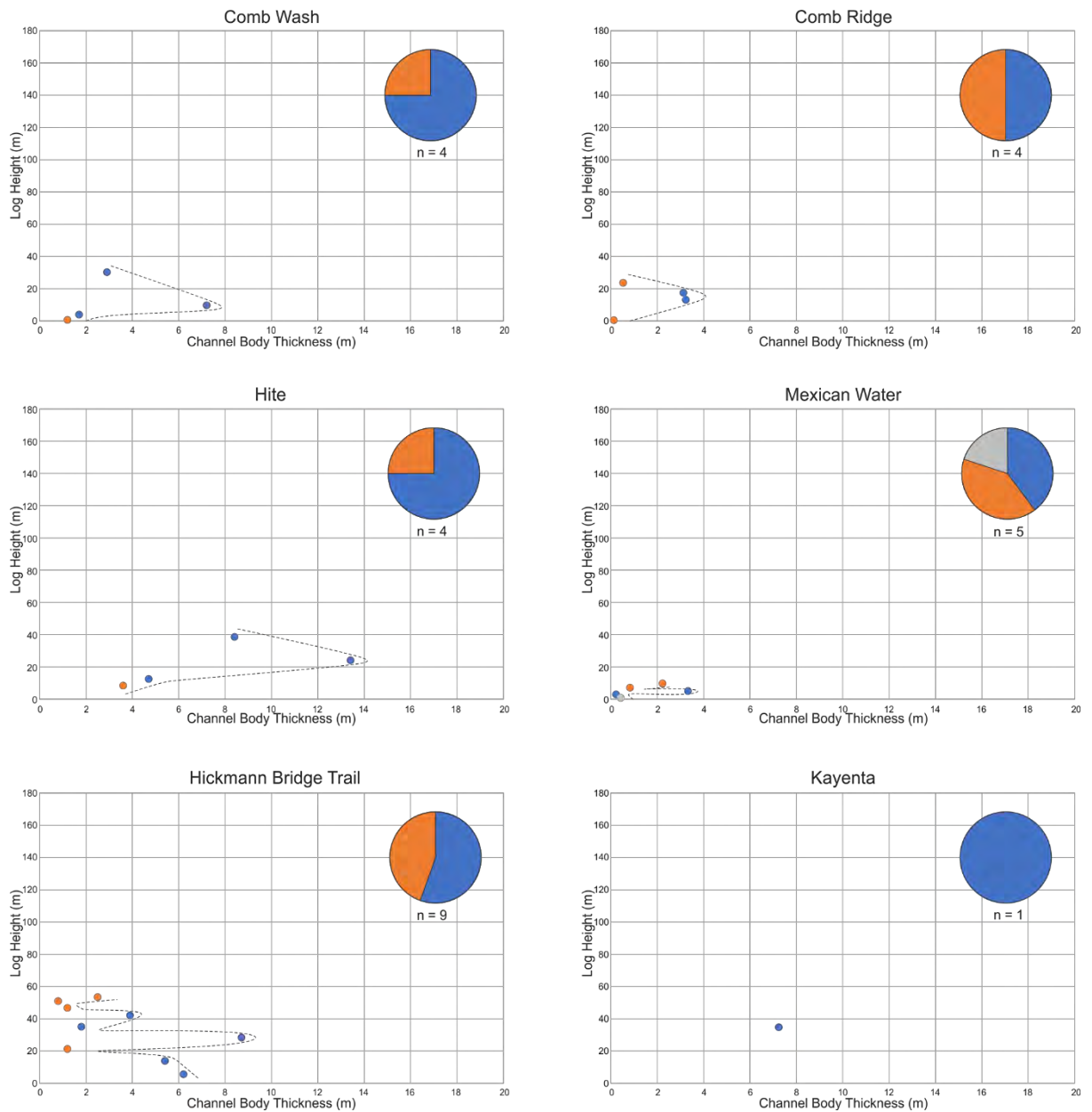


Figure 6.7. Log height of channel body against channel body thickness for each medial succession studied. Coloured dots represent the interpreted channel depositional element present. The dashed line represents moving averages, and the pie chart breakdown shows the percentage of channel depositional element types for each locality. See Fig. 6.6 for key to colours.

Climatic variations play a key role within arid continental settings, controlling the preserved architecture, facies distributions and stratigraphy of successions. The temporal interactions between the fluvial and aeolian systems occur as a result of climatic variations and depict the sedimentological change across the systems as the climate becomes wetter to establish a fluvial system or dries to promote expansion of the aeolian dune field. These trends also coincide with the overall change in dominant depositional environment through time. The lower Kayenta is a dominantly ephemeral

fluvial setting with most deposition the result of high-energy unconfined flows and minor large scour events from flash-flood discharge, resulting in thick amalgamated sandstone deposits within the lower sections of the succession. In the middle section of the Kayenta, a transition from dominantly ephemeral to dominantly braided fluvial deposits is observed, marked by the onset of large laterally extensive accretionary elements, before sedimentation switches back to dominantly ephemeral deposition. However, within the upper section of the Kayenta, sediments of the ephemeral system intertongue with the aeolian deposits of the transitional units of the Navajo Formation. This interaction alters the sedimentology observed within the ephemeral system as the ephemeral fluvial deposition now becomes confined to interdunal corridors within the aeolian dune field, resulting in the increase in isolated sandstone-dominated channel-fill depositional elements in the upper parts of the successions. Eventually, the aeolian system dominates and the fluvial system dries out.

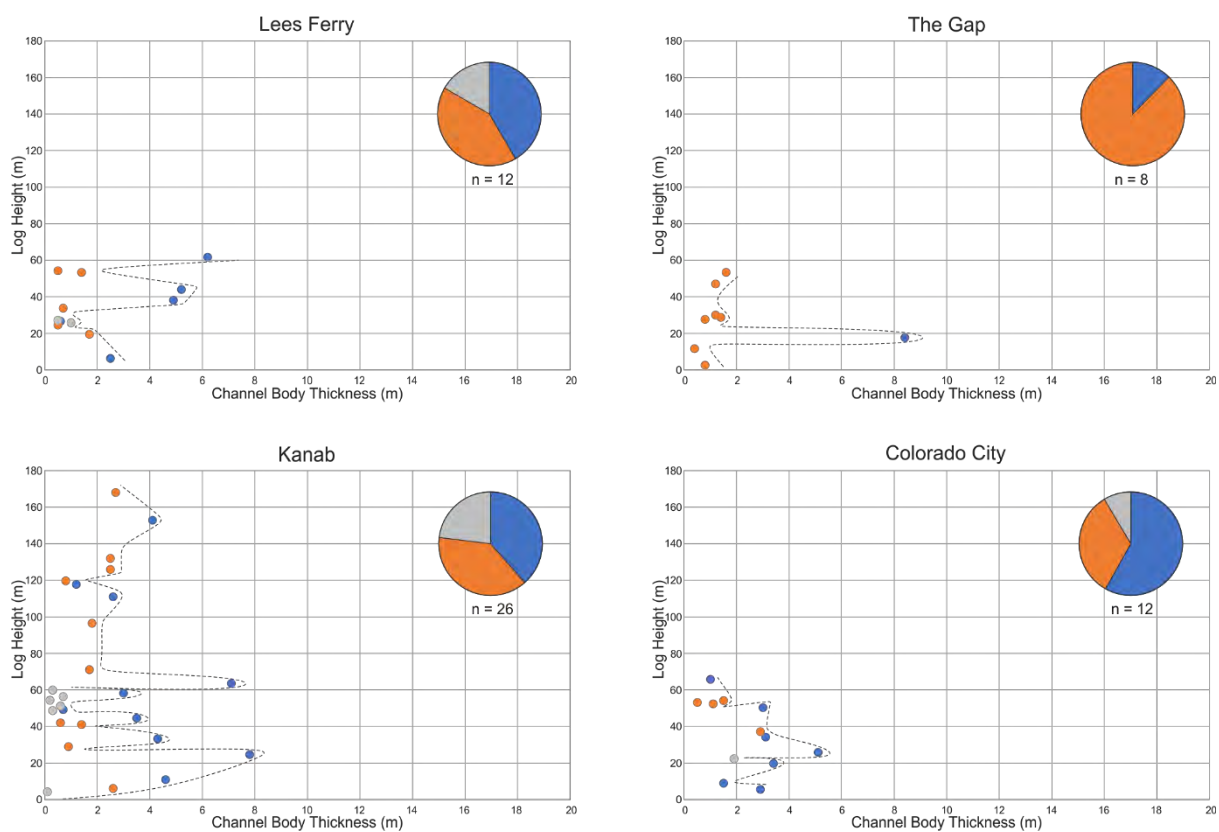


Figure 6.8. Log height of channel body against channel body thickness for each distal succession studied. Coloured dots represent the interpreted channel depositional element present. The dashed line represents moving averages, and the pie chart breakdown shows the percentage of channel depositional element types for each locality. See Fig. 6.6 for key to colours.

The presence of isolated gravel-dominated channel-fill depositional elements within the distal region has already been discussed within the spatial variations (Section 6.5) as being the result of a secondary fluvial source towards the south of the Colorado Plateau. However, the consistent location within the lower third of the logged sections suggests the possible timing of the influx of the secondary source. Gravel-dominated channels are observed between the lower third and upper two thirds of the distal successions (Fig. 6.8) before a sudden increase in amalgamated channel body thickness, particularly evident in the Lees Ferry, Kanab, and Colorado City sections, suggesting the sediments within the upper two thirds of the succession are more likely to be the result of the secondary system (Hassan *et al.*, 2018), however, in-depth petrographical and provenance studies are needed to examine this further (Chapter 10).

6.8. Interactions

Complex interactions between ephemeral fluvial and aeolian environments are present throughout the whole expanse of the Kayenta Formation and at a variety of scales, from small-scale reworking of aeolian sediment into the fluvial system, to large-scale intertonguing of the aeolian Navajo Sandstone within the top third of the Kayenta. These interactions can greatly influence reservoir characterisation at facies scale, element scale and system scale.

6.8.1. Facies-scale interactions

Facies-scale interactions include the reworking of aeolian sediment into the fluvial system. Ephemeral fluvial systems are usually dominated by mud or silt grade sediment (Olsen, 1989), however due to the interactions between aeolian environments in the Kayenta, little mud is available for sediment transport as the system is dominated by fine to medium grained sand. The majority of the 'sandy' fluvial facies are composed of aeolian-derived sediment which has been blown off deflating dune fields and transported by the fluvial system, therefore improving the reservoir quality potential, as the original grains are well sorted and well-rounded, increasing the porosity and permeability of the fluvial sediments originally derived from the Ancestral Rocky Mountains and Cordilleran Magmatic Arc. This

results in a very sandy ephemeral system with a much higher reservoir quality than the standard muddier ephemeral fluvial system. The fluvial sediment can also be seen being reworked into the aeolian system as the rivers dry out during more arid times. Evidence of this recycling and reworking can be seen in thin sections of sandy channels of the Kayenta (Fig. 6.9).

Soft-sediment deformation is a common feature within aeolian dunes in a mixed fluvial-aeolian system, which form due to the migration of the dune over a damp substrate left by the fluvial system, where the water table is within the capillary fringe. The deformation of the aeolian dune can affect fluid migration pathways within the subsurface, as the preferential pathways with aeolian foresets are through the slightly coarser, medium-grained grainflow units (Chandler *et al.*, 1989).

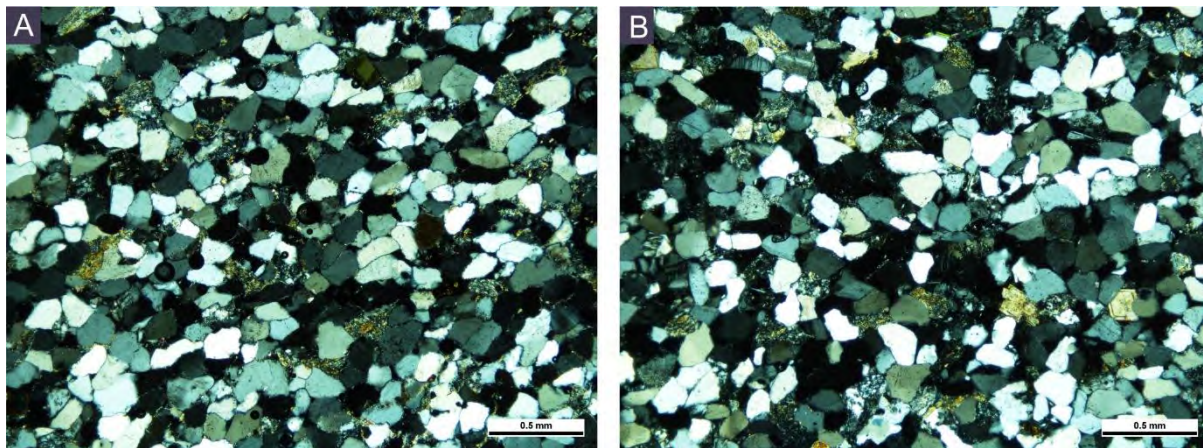


Figure 6.9. Thin sections in XPL of: (A) Aeolian sediments from Sevenmile Canyon, UT, and (B) Fluvial sediments from Comb Wash, UT, showing extensive recycling and reworking of sediments from both environments.

6.8.2. Element-scale interactions

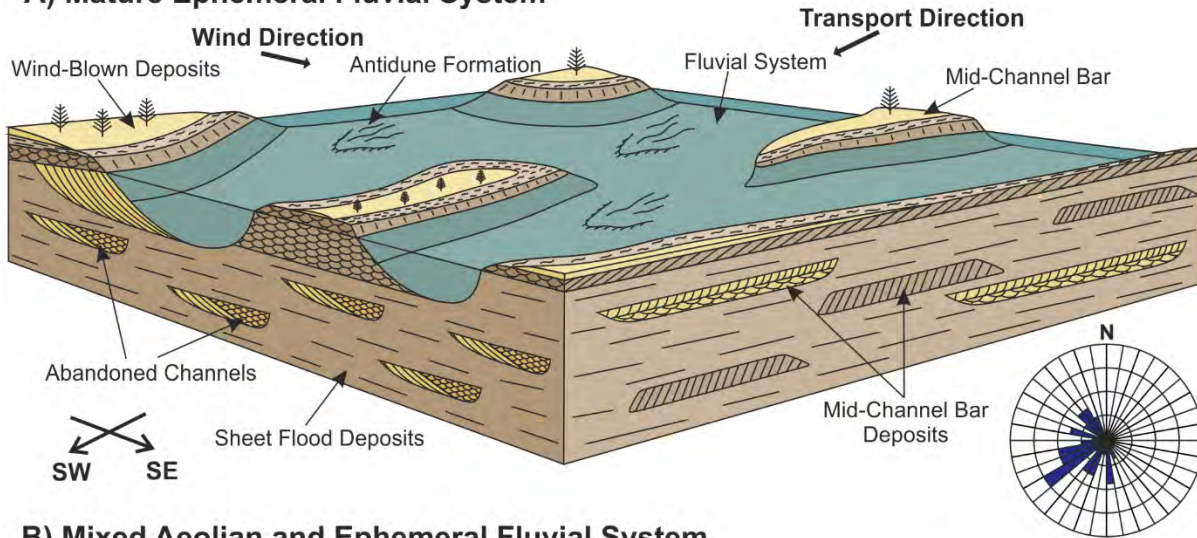
Element-scale interactions are limited in their vertical (temporal) extent due to rapid changes in the dominant environment. During more arid times, aeolian environments dominate, restricting the fluvial systems to interdunal corridors, controlling localised sediment supply, resulting in flash-flood and debris facies, comprising sediments of aeolian calibre and texture (Fig. 6.10). The confined channels are smaller in width with the palaeocurrent directions controlled by the shape of the aeolian dunes.

The aeolian system shuts down rapidly during slightly more humid times, allowing the fluvial system to dominate and preserve extensive ephemeral fluvial sediments, with fluvial textures dominated by intra-formational sediment. This results in small (2–5 m) and isolated aeolian dune elements, dominated by foresets; often exhibiting soft sediment deformation, and set bounding surfaces, with very sparse cosets (Fig. 6.10). Dispersion calculations (0.82) of the aeolian dunes suggest the likely style of dune was barchan to barchanoid. Sandsheet elements are also a common feature when fluvial systems dominate, as aeolian sediment becomes trapped by the damp fluvial substrate.

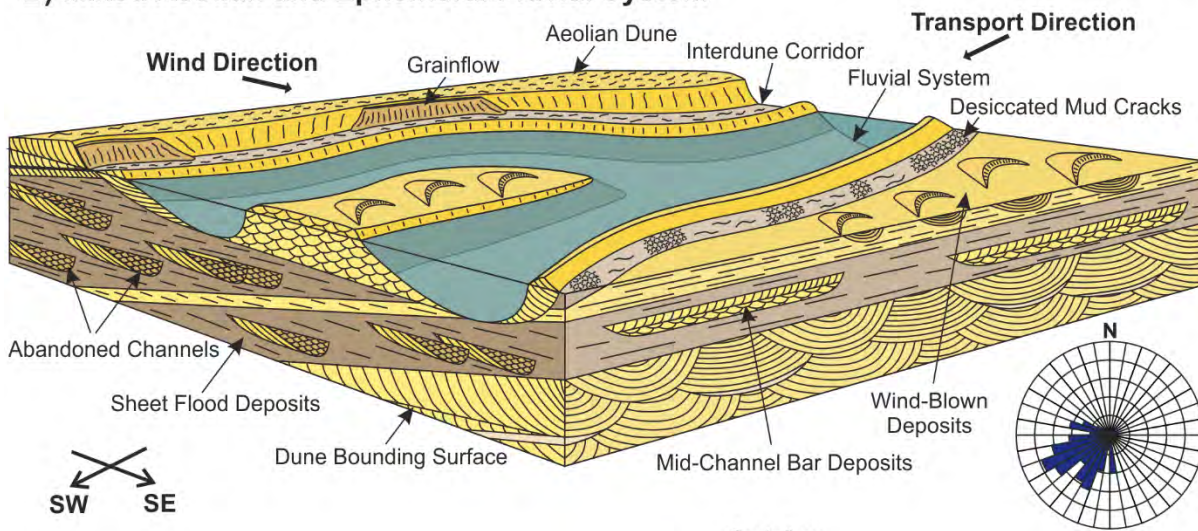
The contact between the underlying aeolian and overlying fluvial elements can be either gradual or, more typically, sharp erosive. For example, the most common transition between architectural elements occurs as aeolian dune fields are deflated into sandsheet elements before the encroachment of the fluvial system by erosive channel and sheet-like elements (Fig. 6.11). Moreover, during times of higher erosion in wetting upward trends, sandsheet elements are often not observed. Instead, a sharp erosive contact is typically observed between the aeolian dune and the overlying channel/sheet-like elements (Fig. 6.11). The local provenance of sediment from the aeolian system is evident within the sediments of fluvial channels and sheet-like elements.

Conversely, the contact between underlying fluvial and overlying aeolian architectural elements is characterised by a more gradual transition. This results from the stabilisation of the fluvial system before the encroachment of aeolian dune fields. For example, the most typical transition between architectural elements occurs as the overbank stabilises and dries – evidenced by desiccation cracks and rhizoliths – before the development of aeolian dunes that typically contain soft-sediment deformation features at the base (Fig. 6.11). Other elemental transitions occur as sandy channel, sheet-like, downstream and lateral accretion elements are reworked by aeolian processes to form dunes (Fig. 6.11).

A) Mature Ephemeral Fluvial System



B) Mixed Aeolian and Ephemeral Fluvial System



C) Mature Aeolian System

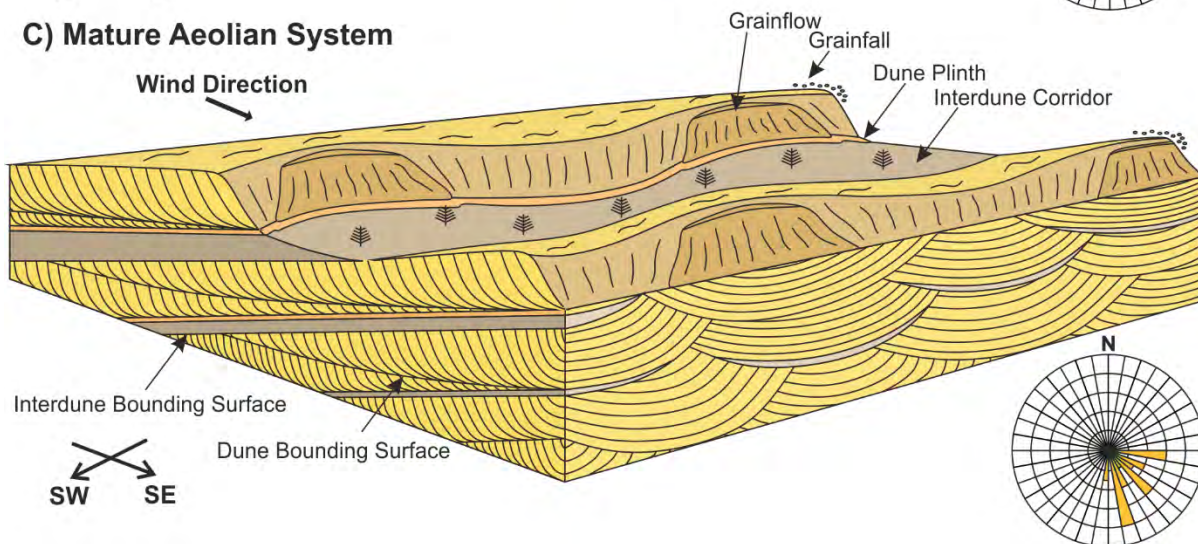


Figure 6.10. Element-scale interactions during differing dominant environments with rose diagrams depicting the variability in palaeocurrents dependant on the dominant depositional system.

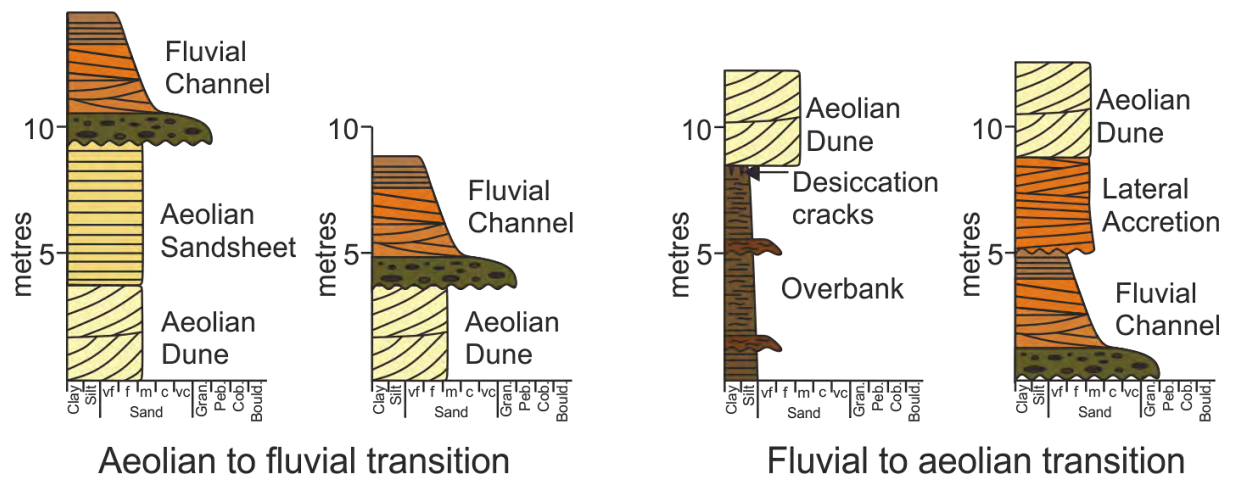


Figure 6.11. Element-scale transitions depicted on idealised log succession from dominantly aeolian to fluvial and dominantly fluvial to aeolian.

Understanding the element-scale interactions can help identify the three-dimensional geometry of baffles and barriers to flow, such as, isolated overbank and interdunal lenses and cemented channel lags (North & Taylor, 1996), as well as the internal heterogeneity of the reservoir.

6.8.3. System-scale interactions

System-scale interactions include the large-scale intertonguing between the aeolian and fluvial environments. The most prominent interactions are observed within the 'silty facies' of the Kayenta in the southwestern region of Utah from St George to Kanab, where tongues of the overlying aeolian Navajo Sandstone reach up to one-hundred metres thick, interfinger with Kayenta fluvial deposits, and can be individually mapped (Middleton & Blakey, 1983; Hassan *et al.*, 2018). Smaller scale intertonguing of the magnitude of tens of metres can also be identified across most of the formation, even within the more 'sandy facies' (Long, 2008; Hassan *et al.*, 2018). Large-scale intertonguing can add increased complexity to production, as the aeolian tongues can often act as thief zones within mixed continental reservoirs (Krystinik, 1990).

Palaeocurrent analysis across the fluvial-aeolian transition indicates a dominate fluvial palaeoflow direction towards the west-south-west and an aeolian palaeowind direction towards the south-east. However, analysis of the last fluvial and first aeolian influxes reveal a dominant aeolian palaeocurrent

direction very similar to that of the fluvial measurements, both towards the south-west (Fig. 6.12). The aeolian dunes which overlie fluvial deposits often show evidence of soft sediment deformation as previously mentioned in facies-scale interactions. The change in the dominant aeolian palaeoflow direction during the transition between fluvial and aeolian dominant processes, was caused by the restriction of aeolian sediment supply due to the encroachment of the fluvial system. This results in a deflationary setting, where minor proportions of wind-blown sediment adhere to the damp substrate left behind by ephemeral streams, due to the high capillary fringe. Localised topography caused by the incision of the fluvial system could have also restricted localised air currents, allowing the formation of small dunes within these depressions before the aeolian system dominated.

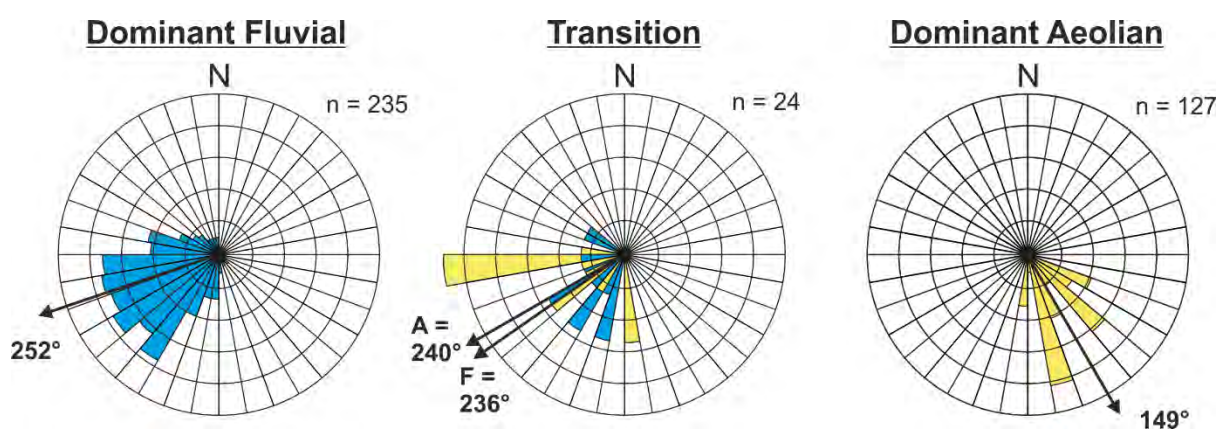


Figure 6.12. Palaeocurrent analysis across the fluvial-aeolian transition showing a dominant fluvial palaeoflow towards the southwest, a dominant aeolian palaeowind direction to the southeast and a transitional period with both fluvial and aeolian palaeoflow directions to the southwest. Arithmetic averages are given in bold, along with the number of measurements.

6.9. Summary

The spatial distribution and downstream trends of the fluvial system reveals a number of downstream trends in this ancient dryland ephemeral system. Some trends are similar to those observed in previously published DFS models, but there are also other relationships that do not match the DFS model. While some of these relationships may be explained by the influence of external factors inherent in this study, such as a secondary axial fluvial system and increased accommodation space within the distal setting, others are probably intrinsic to the dryland ephemeral nature of the system,

coupled with its interaction with the competing and coeval aeolian environment that is typically an inherent part of any dryland fluvial system.

The temporal variations and interactions with the competing aeolian environment reveal multiple scales of climatic cyclicity and reworking of sediment, from rapid switching of architectural elements, to large-scale fluvial and aeolian tongues within the distal setting.

Chapter Seven will draw upon the detailed sedimentological analysis within Chapters Four, Five and Six and combine the findings with analysis of photogrammetric models to compile quantified three-dimensional facies models of the depositional system at multiple scales.

Chapter 7: Digital Outcrop Models, Geobody Analysis and Reconstruction of Depositional Environments

This chapter analyses the geometry and dimensions of the architectural elements described in Chapter Five along with their variations in architecture between proximal, medial, and distal settings, using three-dimensional digital outcrop models. This chapter builds upon the sedimentological analysis within Chapters Four, Five and Six, and combines the analyses with quantified geobody data from photogrammetric models to build quantitative facies and depositional models.

7.1. Introduction

Terrestrial and unmanned aerial vehicle (UAV) photogrammetry surveys were used to study the geometry and geometrical relationships of preserved architectural elements within the mixed ephemeral fluvial and aeolian deposits of the Lower Jurassic Kayenta Formation across the expanse of the Colorado Plateau, south-western USA.

Three digital photogrammetric models of suitable outcrops from proximal, medial, and distal fluvial settings, collected using both a DSLR camera (Nikon D800E) and a drone (DJI Phantom 4 Pro), were processed in Agisoft PhotoScan, and analysed using Virtual Reality Geological Studio (VRGS). Model 1, from the proximal sediments of the Kayenta, was collected from beside the Colorado River in Moab, Utah. Model 2, from the medial sediments of the Kayenta, was collected from along the Comb Ridge monocline near Bluff, Utah. Model 3, from the distal sediments of the Kayenta, was collected from along Squaw Trail, Kanab, Utah. Each model comprises between 400 and 600 photographs, with each sedimentary feature pictured in at least five images.

The models illustrate: (i) the lateral and vertical relationships between fluvial and aeolian architectural elements; (ii) the geometry and dimensions of the elements; (iii) the nature of contact between the

elements; (iv) differences in architecture and sedimentology between proximal, medial, and distal settings and (v) the vertical changes within the formation that represent the temporal evolution of the system.

For more detailed methods on data acquisition, processing, and post-processing of the photogrammetric models the reader is referred to Chapter Three, Section 3.2.

7.2. Outcrop Photo Panels

Traditional two-dimensional sedimentary analysis of outcrops using photography, produced as an orthomosaic, by flattening the three-dimensional photogrammetric model onto a vertical plane, was undertaken in order to provide a direct comparison between methods. The photo panels were interpreted for architectural elements to provide a schematic panel (Figs. 7.1, 7.2 & 7.3). The analysis provides a representative interpretation of the outcrop as a whole, rather than a one-dimensional sedimentological log through the outcrop, which can often result in unrepresentative fluvial architectural element geometries, relative proportions and distributions of the elements (Table 7.1). The two-dimensional photo panels depict architectural element geometries, relative spatial distributions of sedimentary architectural elements and interpreted hierarchical bounding surfaces (Figs. 7.1, 7.2 & 7.3).

The two-dimensional photo panels demonstrate the highly varied sedimentology within the Kayenta depositional system along with palaeocurrent measurements and interpreted hierarchical bounding surfaces. The photo panels depict a general reduction in channel and sheet architectural element size and abundance with distance downstream (Figs. 7.1, 7.2 & 7.3).

In the proximal photo panel (Fig. 7.1), an average fluvial channel width to depth ratio of 20:1 and an average sheet width to depth ratio of 60:1 was observed (Table 7.1). In the medial photo panel (Fig. 7.2) an average channel width to depth ratio of 19:1 and an average sheet width to depth ratio of 55:1 was observed (Table 7.1), and in the distal photo panel (Fig. 7.3) an average channel width to depth ratio of 16:1 and an average sheet width to depth ratio of 42:1 was observed (Table 7.1).

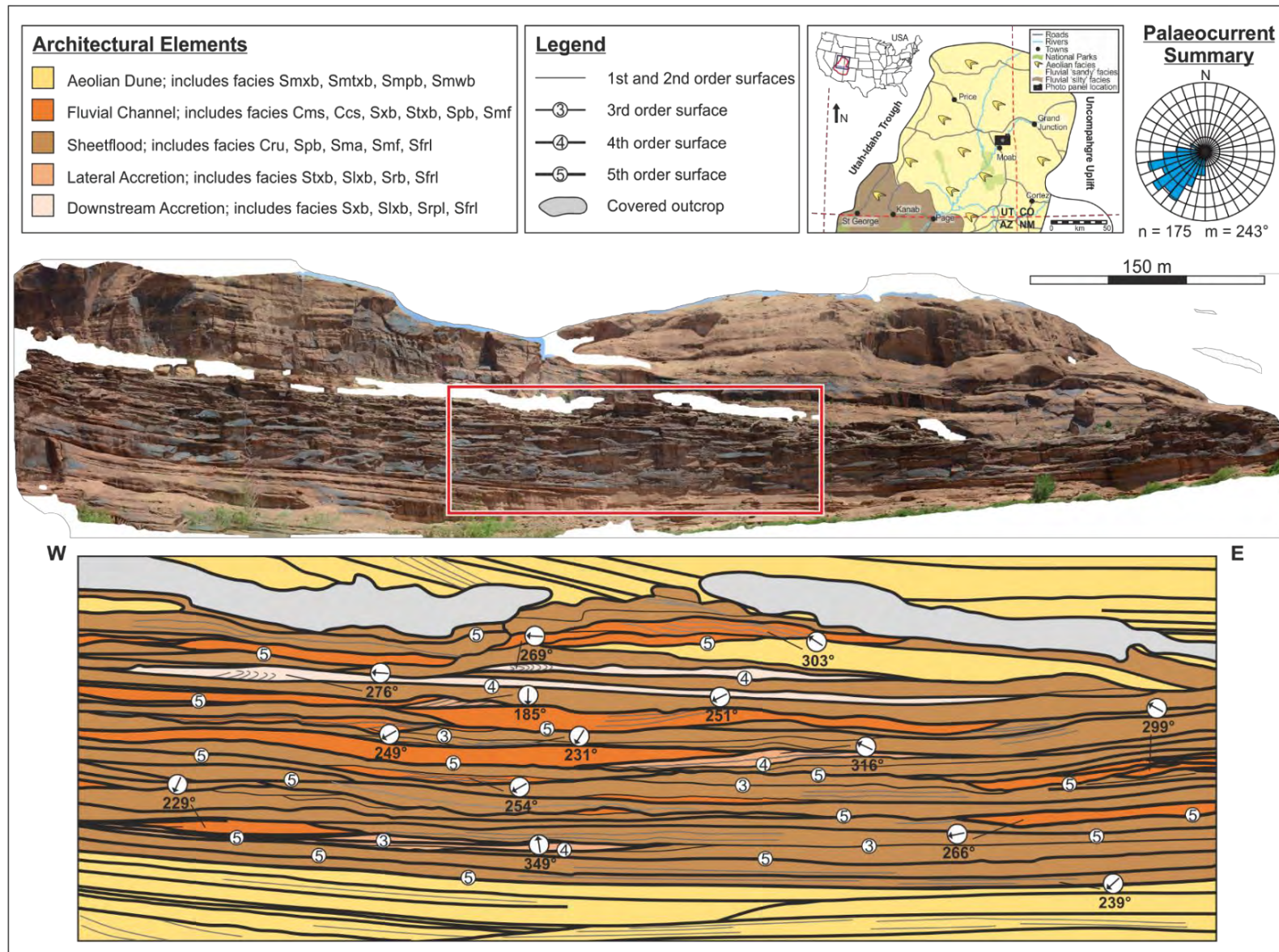


Figure 7.1. Architectural element outcrop panel for the proximal Kayenta Formation with hierarchical bounding surface analysis and palaeocurrent measurements. The proximal region is dominated by vertically and laterally amalgamated fluvial channel, sheets and accretionary elements with sporadic small isolated pockets of overbank.

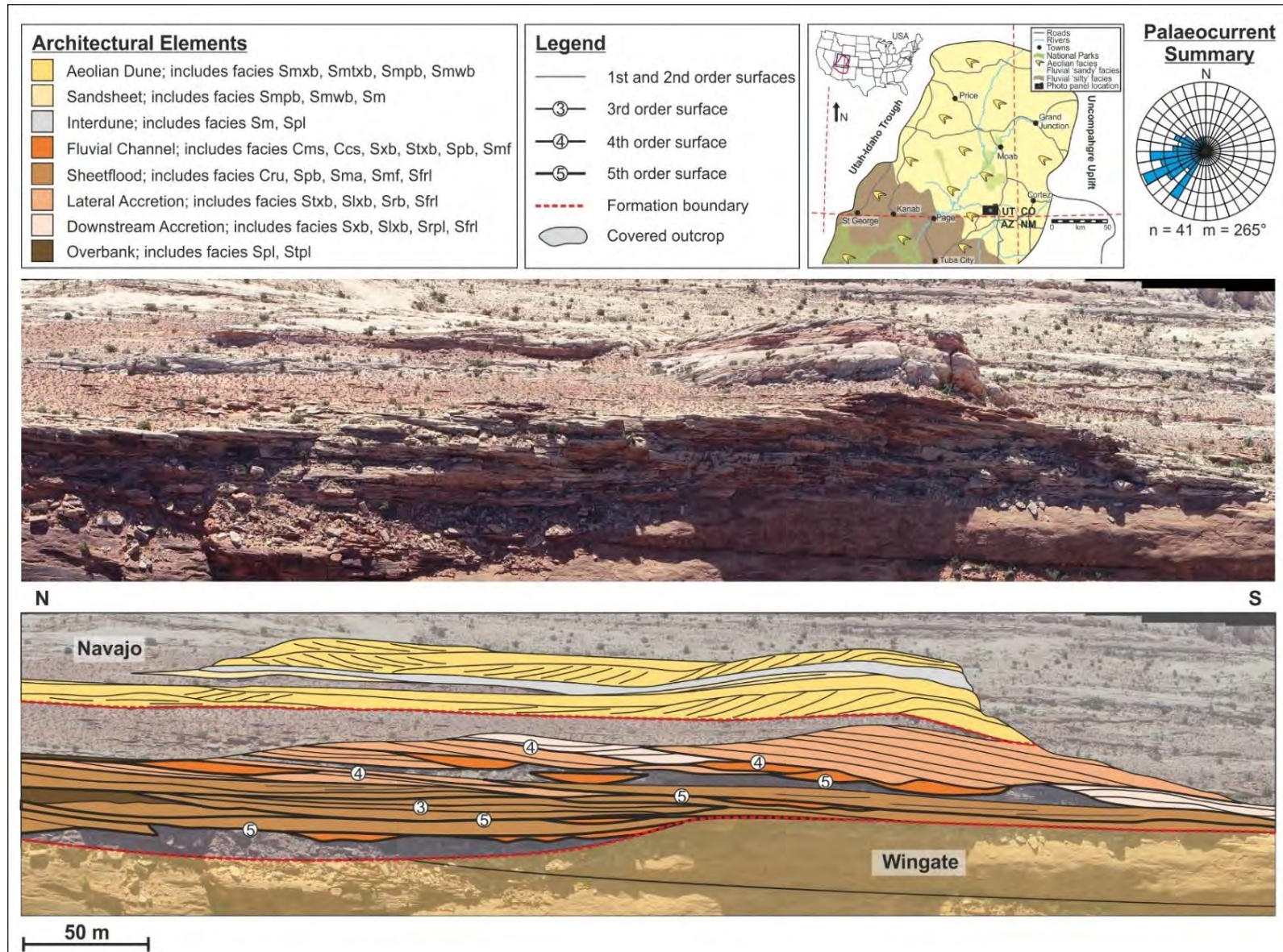


Figure 7.2. Architectural element outcrop panel for the medial Kayenta Formation with hierarchical bounding surface analysis and palaeocurrent measurements. The medial region is dominated by vertically and laterally amalgamated fluvial channel, sheets and accretionary elements, however, channels are more isolated and overbank elements are thicker and more laterally extensive.

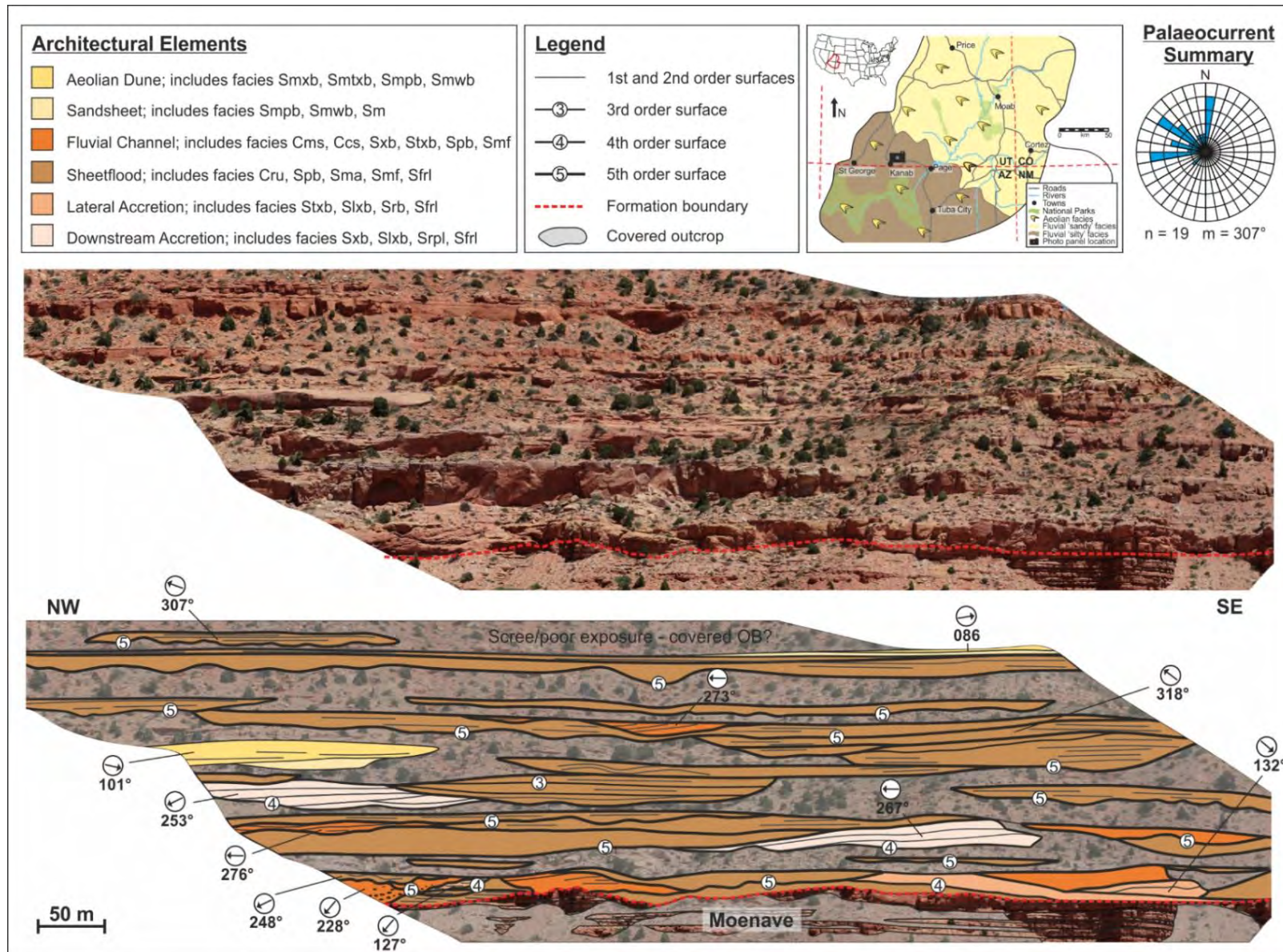


Figure 7.3. Architectural element outcrop panel for the distal Kayenta Formation with hierarchical bounding surface analysis and palaeocurrent measurements. In the distal region the degree of stacking between channel, sheets and accretionary elements is significantly reduced, with several channel and sheet-like elements being isolated within laterally extensive overbank deposits.

Table 7.1. Summary of average channel and sheetflood fluvial architectural element data including: 1D sedimentary log relative proportion and thickness data, 2D schematic panel thickness and width:depth data and 3D photogrammetric model relative proportion, width:depth ratios and thickness data. All based on 20 measurements each.

Architectural Element	Sedimentary Log 1D Data				Schematic 2D Photo Panel				Photogrammetry 3D Model			
	Relative Proportion (%)	Average Thickness (m)	1 SD	Relative Proportion (%)	Average Thickness (m)	Width: Depth	1 SD	Relative Proportion (%)	Average Thickness (m)	Width: Depth	1 SD	
Proximal: Model 1 (Moab)	Channel	25.3	1.1	0.25	39.2	3.9	20:1	1.36	37.6	2.6	50:1	1.51
	Sheet	33.2	1.3	0.34	56.4	3.9	60:1	1.47	44.7	3.6	100:1	1.63
Medial: Model 2 (Comb Ridge)	Channel	24.5	1.2	0.69	25.1	3.4	19:1	0.95	21.3	2.4	45:1	1.09
	Sheet	34.6	1.4	0.89	45.7	3.8	55:1	0.92	38.5	3.5	85:1	1.04
Distal: Model 3 (Squaw Trail)	Channel	19.4	1.0	0.74	20.3	3.2	16:1	1.14	15.7	1.9	40:1	1.32
	Sheet	23.3	0.9	0.32	39.6	3.4	42:1	0.89	32.1	2.8	70:1	0.98

7.3. Digital Outcrop Models

Using VRGS, the dimensions of the depositional elements were mapped onto the digital outcrop models to determine apparent size of elements in the planes of the models. By incorporating palaeocurrent measurements taken from cross-bedding in individual architectural elements at multiple locations across the outcrop, widths and heights of geobodies can be corrected automatically within the software for the attitude of the virtual model. These geobodies were subsequently digitised and extruded using palaeocurrent measurements to correct for their true facing orientation perpendicular to flow to avoid overestimation of the geobody width (Visser & Chessa, 2000a, Pringle *et al.*, 2010, Rarity *et al.*, 2013, Burnham & Hodgetts, 2018). The dimensions of partial or incomplete elements within models have been approximated using methods outlined in Geehan & Underwood (1993).

In Model 1 (proximal), an average fluvial channel width to depth ratio of 50:1 and an average sheet width to depth ratio of 100:1 was observed. In Model 2 (medial) an average channel width to depth ratio of 45:1 and an average sheet width to depth ratio of 85:1 was observed, and in Model 3 (distal) an average channel width to depth ratio of 40:1 and an average sheet width to depth ratio of 70:1 was observed (Table 7.1, Figs. 7.4 & 7.5).

This analysis demonstrates that thickness data derived from one-dimensional logs alone underestimate the average thickness of both sheet and channel architectural elements in the Kayenta Formation by more than half. Whereas the width and thickness measurements of sheet and channel architectural elements depicted on two-dimensional photo panels overestimate the element dimensions by up to a third in comparison to the data collected from the three-dimensional digital outcrop models, due to the fact the orientation of the outcrop face, with respect to palaeocurrent direction cannot be visualised in three-dimensions (Pringle *et al.*, 2010).

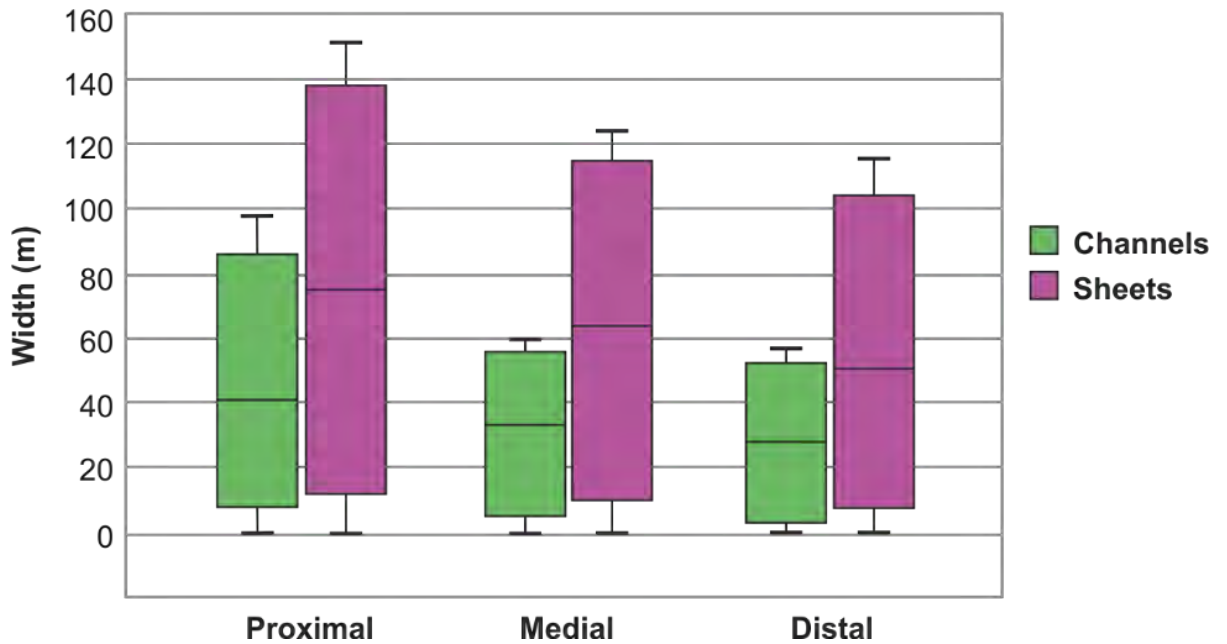


Figure 7.4. Summary sedimentary fluvial architectural element width to depth box and whisker plots of channels (green) and sheets (purple) extracted from models 1 (proximal), 2 (medial) and 3 (distal). Minimum, average and maximum width measurements are shown, along with 1 SD error bars.

7.4. Depositional Models

The geobody data collected from the three-dimensional outcrop models were combined with the detailed sedimentological analysis on the Kayenta Formation (Chapters 4, 5 & 6) to reconstruct the depositional environment and produce semi-quantified three-dimensional facies models (Fig. 7.6).

The depositional model depicts the preserved deposits of an ephemeral braided fluvial system with minor perennial and aeolian influxes. The most prominent preserved deposits of the system are sandy, bedload-dominated, multi-lateral sheet-like depositional elements with minor channelised scours and minimal floodplain/overbank elements (Fig. 7.6). The fluvial system was highly cannibalistic as very little overbank/floodplain is preserved, although clasts composed of overbank facies are common features within channel, sheet-like and lateral accretion elements (Fig. 7.6) and provide evidence of stabilised overbank being reworked (North & Taylor, 1996; Hassan *et al.*, 2018).

Channel architectures range from poorly defined sheet-like bodies, dominated by planar cross-bedding (Spxb) and parallel laminations (Spl) to channels with steeply dipping sides, dominated by features of debris-driven flow (matrix-support conglomerates (Cms) and structureless sandstones (Smf)).

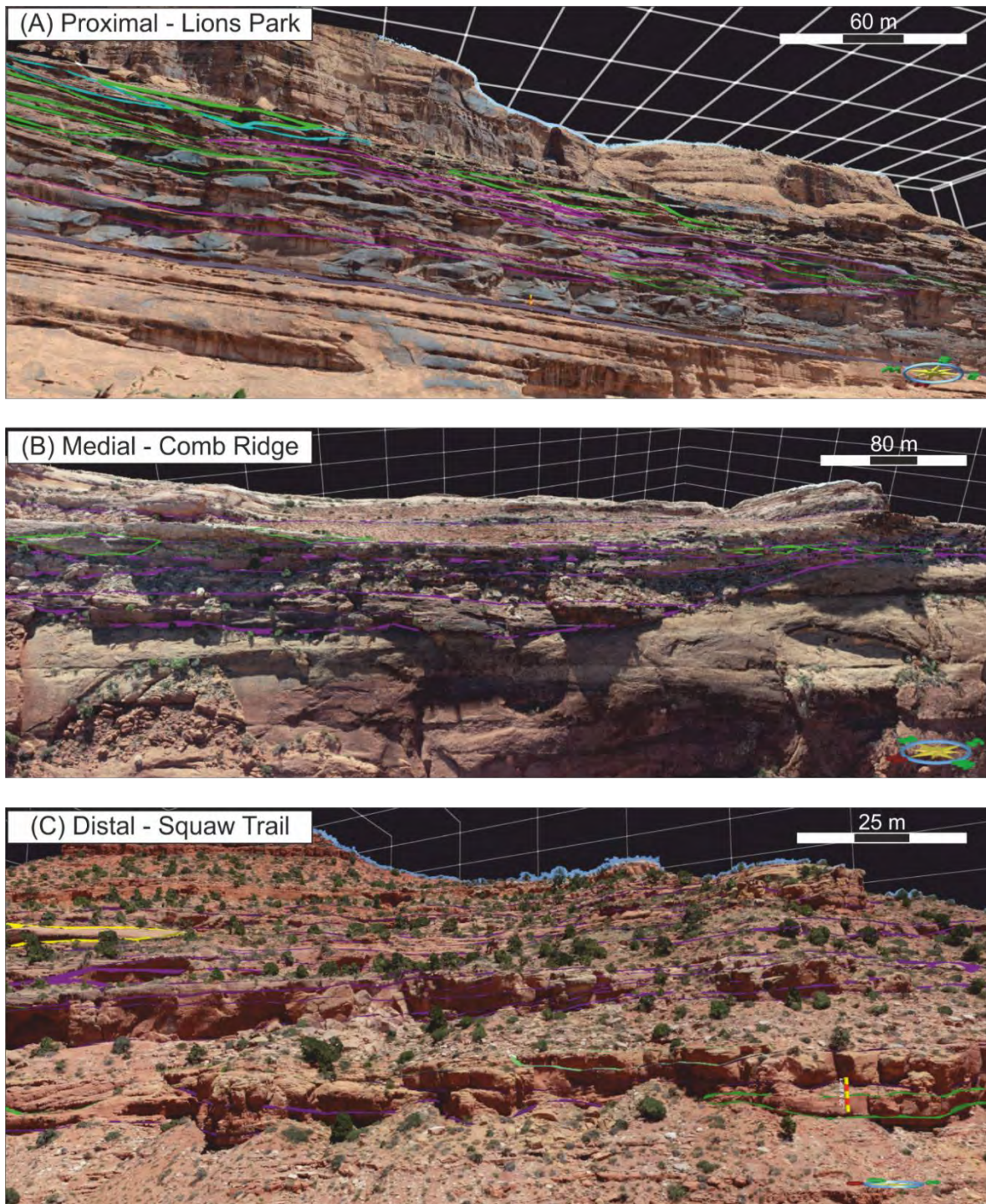


Figure 7.5. Mapped geobodies on (A) Model 1 - Lions Park, (B) Model 2 - Comb Ridge, and (C) Model 3 - Squaw Trail. Channel geobodies are depicted in green and sheet geobodies in purple.

Upper flow regime flat beds and high sediment load structures form the most dominant features, and typically occur between sediments representing periods of lower flow regime conditions. The fluctuation in flow regime, and the geometry and architecture of the fluvial system, indicate highly variable discharge, often with high velocity flows dominating (Fig. 7.6).

Architectural element analysis across the expanse of deposition shows a generally consistent percentage of fluvial channel and sheet-like elements within the system, but a decrease in amalgamation of these elements downstream (Fig. 7.7). The sediments of laterally and vertically amalgamated, poorly channelised sheets and fluvial channels dominate the preserved deposits (36% and 26% respectively) with corresponding element thickness-to-width ratios of 1:100 and 1:50 in the proximal region, 1:85 and 1:45 in the medial region, and 1:70 and 1:40 in the distal region.

An increase in the proportion of overbank sediments is also observed, from isolated pockets preserved within the proximal setting to laterally extensive sheets of overbank preserved within the distal setting. In proximal and medial settings, overbank sediments comprise less than 4% of the succession, but comprise up to 32% within the distal setting (Fig. 7.7).

The distributions of aeolian architectural elements remain fairly constant across the plateau (Fig. 7.7). Within the proximal region, smaller isolated dune elements (between 0.5–1 m thickness) occur in abundance. The aeolian dunes generally increase in size but decrease in abundance with proximity to the distal setting, eventually resulting in two large aeolian tongues reaching up to 100 m in thickness within the distal region around Kanab.

Analysis of the downstream trends of the ephemeral fluvial Kayenta Formation illustrates a number of characteristics that are similar to those displayed by typical terminal fluvial fans and some distributive fluvial systems described by Hampton & Horton (2007); Nichols & Fisher (2007); Fisher *et al.*, (2008); Cain & Mountney (2009); Hartley *et al.*, (2010); Weissmann *et al.*, (2010; 2013), and Owen *et al.*, (2015). A downstream decrease in amalgamation of channels and compound sheets, a small decrease in grain size downstream and an overall increase in the percentage of overbank depositional elements with distance downstream are observed, all of which are characteristics that are consistent with previously published models (Fig. 7.8) (Nichols & Fisher, 2007; Hartley *et al.*, 2010; Weissmann *et al.*, 2010; 2013; Owen *et al.*, 2015). An increase in the proportion of aeolian deposits with fluvial distance downstream is also observed (Fig. 7.8).

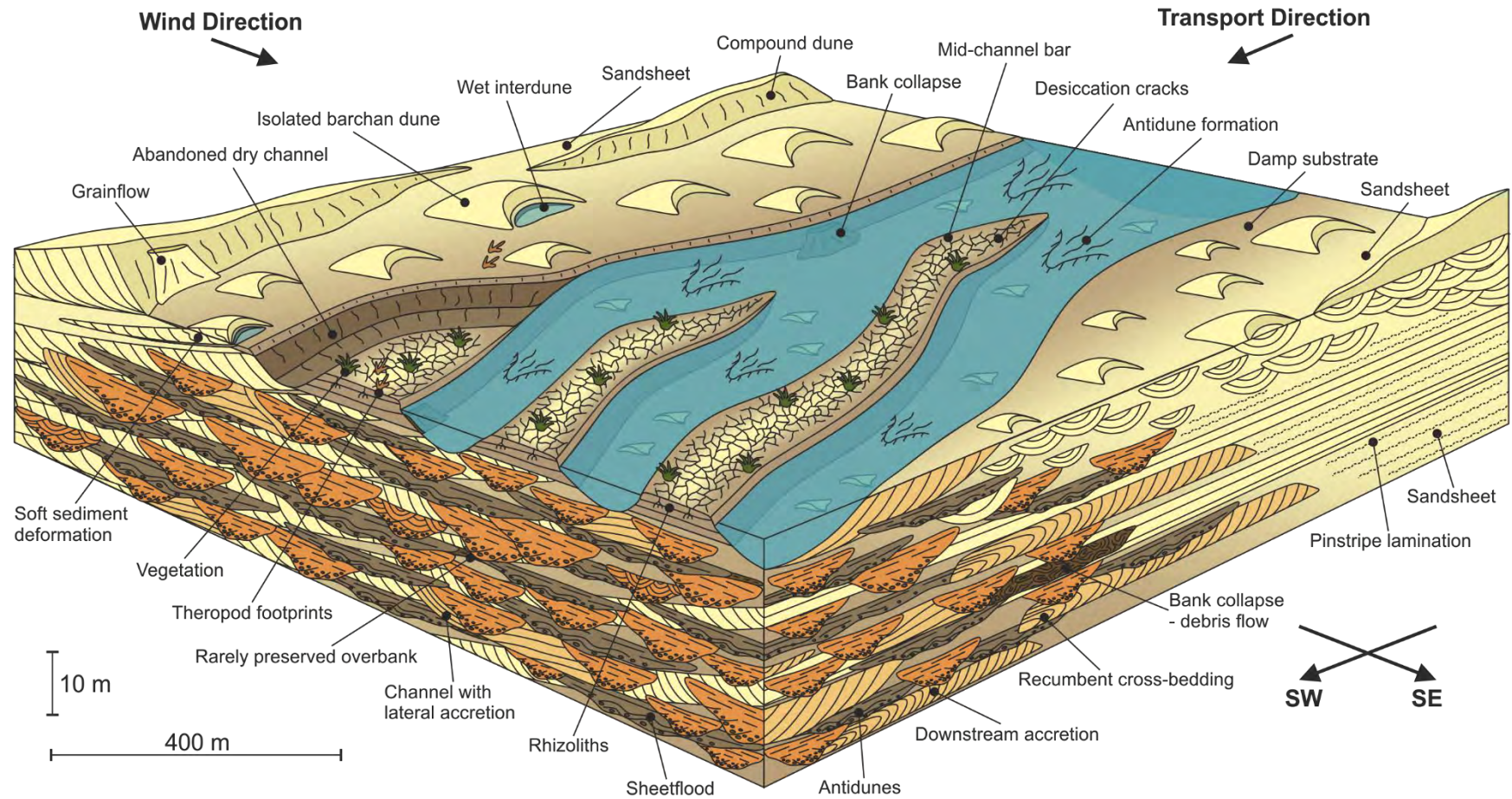


Figure 7.6. Depositional model of an ephemeral fluvial system based upon field data from the Kayenta Formation. The model highlights the interaction between the aeolian and fluvial environments, and the dominance of upper flow regime and high sediment load structures within the fluvial environment.

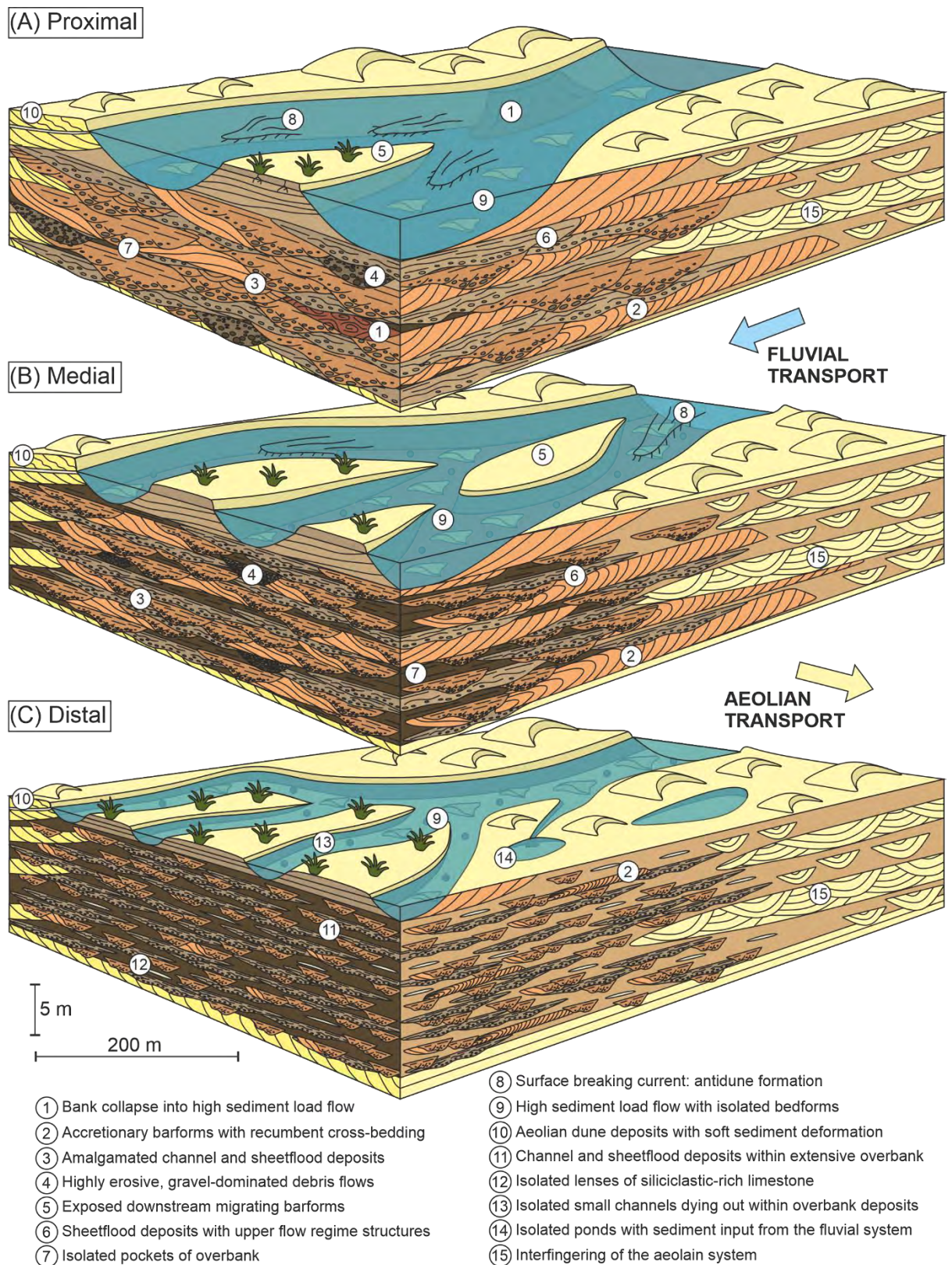


Figure 7.7. Depositional models of an arid ephemeral fluvial system from (A) proximal to (B) medial to (C) distal, based upon field data from the Kayenta Formation. The models show the detailed sedimentology and key characteristics observed, as along with the interaction between the aeolian and fluvial environment.

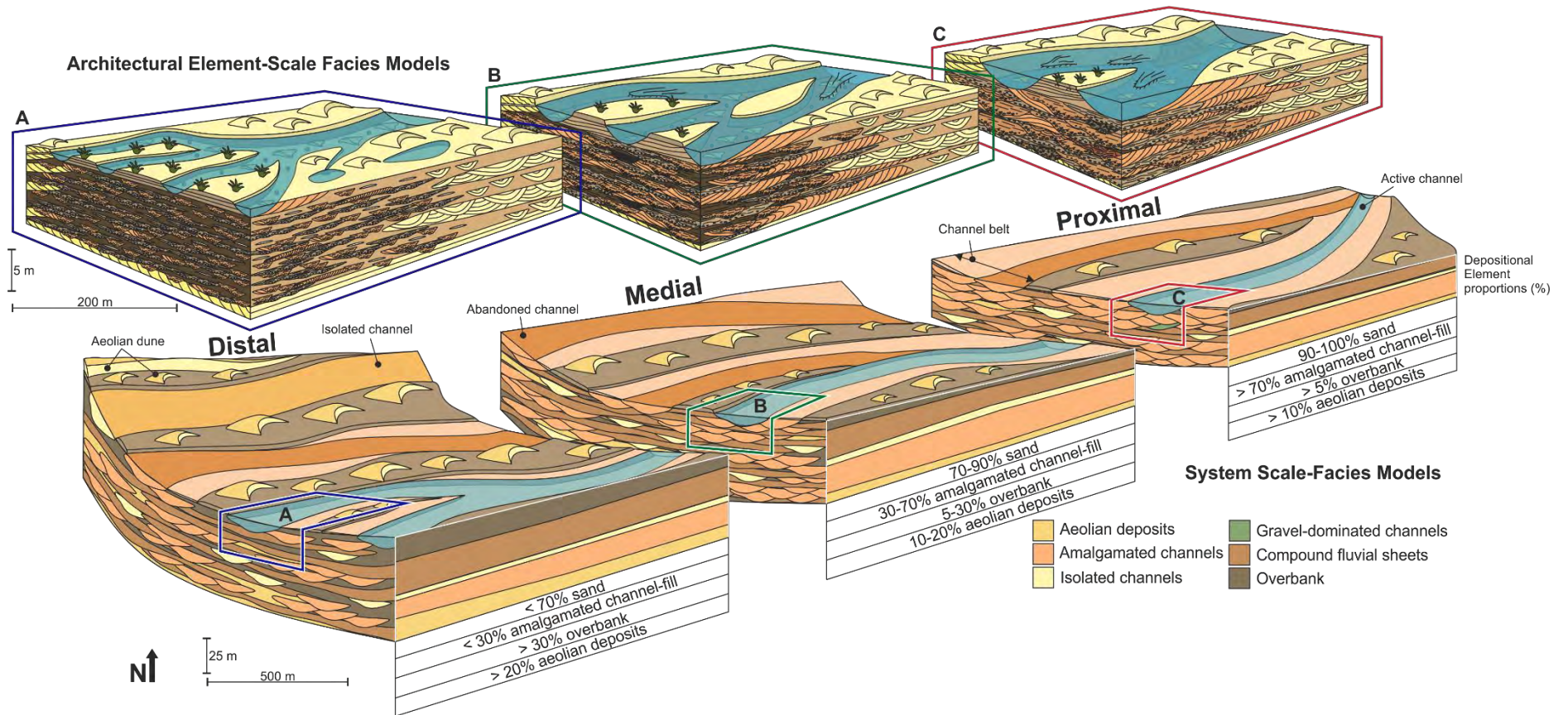


Figure 7.8. System-scale depositional model of the Kayenta Formation sub-divided into proximal, medial, and distal sections with a cross-section of the internal architecture and stacking patterns for each section. Depositional element proportions (%) are displayed along the side of each section of the system-scale model, along with their key characteristics. Architectural element-scale facies models (from Figure 7.7) of the proximal, medial, and distal settings highlight the detailed sedimentology observed within the depositional elements on the system-scale model.

7.5. Summary

In order to build semi-quantifiable facies and depositional models for the Kayenta Formation, the detailed sedimentology described in Chapters Four and Five, along with the spatial and temporal variations described in Chapter Six, were combined with reconstructed geobody data from three-dimensional digital outcrop models.

The results from geobody analysis reveal an average fluvial channel width to depth ratio of 50:1 and an average sheet width to depth ratio of 100:1 in the proximal region. An average channel width to depth ratio of 45:1 and an average sheet width to depth ratio of 85:1 in the medial region, and an average channel width to depth ratio of 40:1 and an average sheet width to depth ratio of 70:1 in the distal region.

Analysis of log data versus photo panels and digital outcrop data demonstrates that thickness data derived from one-dimensional logs alone underestimate the average thickness of both sheet and channel architectural elements in the Kayenta Formation by more than half. Whereas the width and thickness measurements of sheet and channel architectural elements depicted on two-dimensional photo panels overestimate the element dimensions by up to a third in comparison to the data collected from the three-dimensional digital outcrop models.

The semi-quantified depositional models produced depict the preserved deposits of an ephemeral braided fluvial system with minor perennial and aeolian influxes. The most prominent preserved deposits of the system are sandy, bedload-dominated, multi-lateral sheet-like depositional elements with minor channelised scours and minimal floodplain/overbank elements. Channel architectures range from poorly defined sheet-like bodies to channels with steeply dipping sides. Upper flow regime flat beds and high sediment load structures form the most dominant features, and typically occur between sediments representing periods of lower flow regime conditions. The fluctuation in flow regime, and the geometry and architecture of the fluvial system, indicate highly variable discharge, often with high velocity flows dominating.

Chapter Eight will use the results from the geobody analysis to aid in the reconstruction of the Leman Sandstone of the Southern North Sea, providing valuable three-dimensional data to an otherwise one-dimensional core study.

Chapter 8: Application of the Kayenta Formation to the Leman Sandstone of the Southern North Sea

This chapter details the sedimentology of the Leman Sandstone and Silverpit Formations of the UK sector of the Southern North Sea and applies the geometrical measurements of architectural elements identified within the Kayenta Formation - a similar depositional setting - to aid in reservoir characterisation and build semi-quantified depositional models.

8.1. Introduction

Field analogues are a well-used and useful technique in geology to help better understand subsurface geology. Subsurface data is usually in the form of seismic, core, or wireline well logs. While useful, these data are often limited in quantity and represent only a one-dimensional view of the rocks, apart from seismic data, which represents a two-dimensional/three-dimensional view. Field analogues can offer a more comprehensive study, in more detailed resolution, and help gain insights into the three-dimensional architecture, enabling more accurate interpretations of the limited downhole data.

8.2. Geological Setting

The early Permian Rotliegend Group of the Southern North Sea, UK, was deposited in a low-lying, land-locked desert basin, known as the Southern Permian Basin (Glennie, 1998). The deposits of the basin range from mixed evaporitic and clastic sediments deposited in sabkha and playa lake environments of the Silverpit Formation to coeval fluvial and aeolian environments of the Leman Sandstone Formation (Fig. 8.1) (Prosser, 1988). The Silverpit Formation was deposited in an extensive and intermittently expanding playa lake system with associated marginal sabkhas, fringed on its southerly and south-westerly margins by the predominantly aeolian dune fields of the Leman Sandstone (Bailey & Lloyd, 2001), resulting in extensive first-order bounding surfaces produced by lacustrine

transgression and regression of the Silverpit Lake towards the southerly aeolian dune fields (Howell & Mountney, 1997). The aeolian dune field is periodically punctuated by fluvial corridors with ephemeral rivers flowing northwards from the Variscan highland towards the Silverpit Lake (Marie, 1975). The Rotliegend Group unconformably overlies the Carboniferous Coal Measures and is topped by the Upper Permian Zechstein salt Supergroup (Fig. 8.2) (Howell & Mountney, 1997).

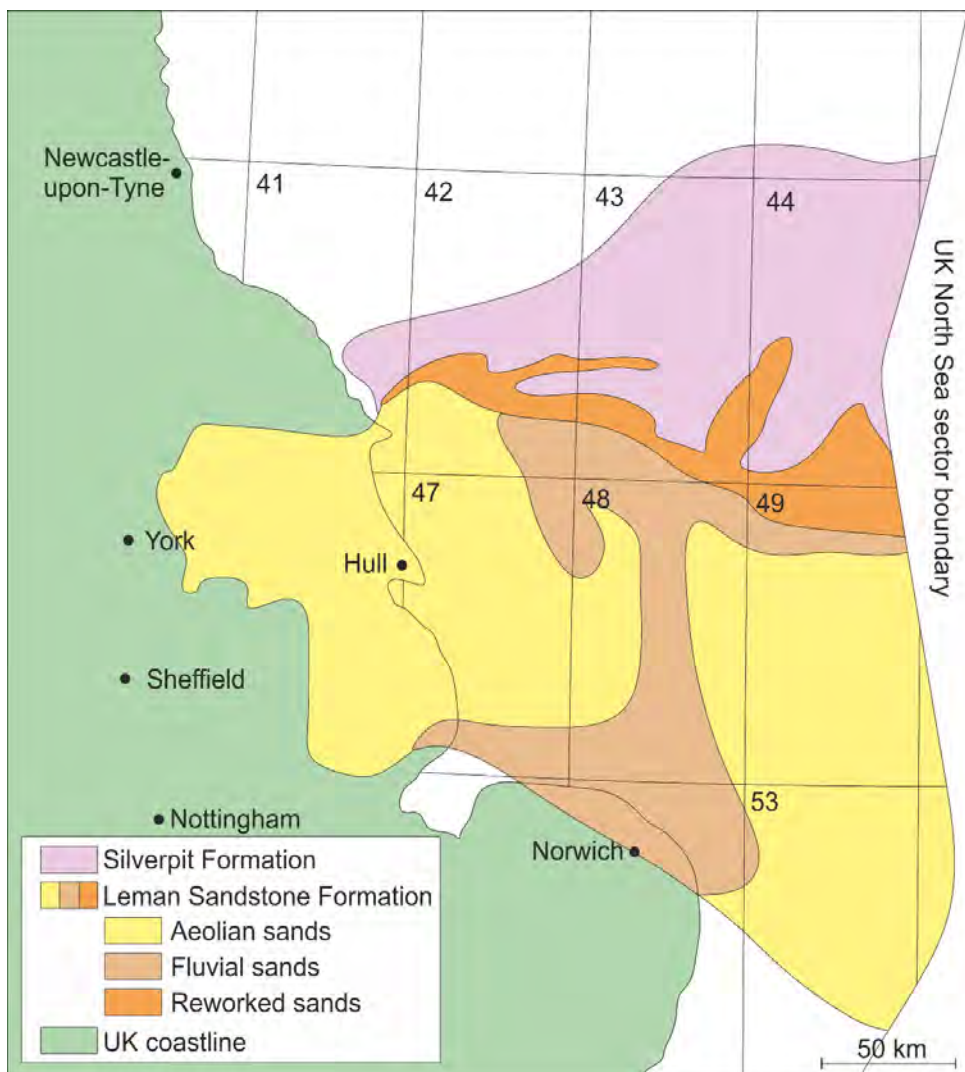


Figure 8.1. Distribution of the Lemman Sandstone and Silverpit Formation within the Southern North Sea, with detailed facies distribution within the Lemman Sandstone (modified after Cameron *et al.*, 1992).

8.2.1. Silverpit Formation

The Silverpit Formation was deposited within a desert lake, which extended east-west for 1000-1200 km from the North Sea to Poland, and north-south for 200 km (Glennie, 1983; Cameron *et al.*,

1992). Lake basin centre facies are characterised by monotonous successions of red-brown, anhydritic mudstones and grey siltstones (Cameron *et al.*, 1992), while lake margin facies comprise a complex interfingering of lacustrine, sabkha, aeolian and fluvial sediments. Lake margin facies are up to 50 m thick, consisting of interbedded claystones, siltstones and sandstones, often in upwards fining cycles (Butler, 1975). Sandstones are interpreted to have been deposited by distal sheetflood deposits entering the desert lake, with shoreline sabkha facies represented by adhesion-rippled sands and nodular anhydrite within clays and silts (Glennie, 1972). Rare interbedded aeolian and fluvial deposits indicate periods of lake retreat, however the sabkha and lacustrine deposits are gradational so the lateral limits of the sabkha facies is not easily determined (Cameron *et al.*, 1992). Long term expansion of the lake is seen within the south of the basin, as the lacustrine facies prograde over the lake margin aeolian/fluvial deposits of the Leman Sandstone Formation (Butler, 1975). Short term fluctuations are also seen within the lake margin facies, with complex interbedding of lacustrine, sabkha, aeolian and fluvial deposits (Cameron *et al.*, 1992).

8.2.2. Leman Sandstone

The Leman Sandstone is composed almost entirely of aeolian and fluvial strata, which form relatively distinct packages in core and wireline logs (Glennie, 1972; Cameron *et al.*, 1992).

The fluvial sediments of the Southern North Sea were deposited in alluvial plains and floodplains by rivers flowing northwards from the Variscan highland towards the Silverpit desert palaeolake in the centre of the North Sea basin (Marie, 1975). The thickest fluvial deposits occur in a north-east trending belt from the coast of East Anglia to the margin of the Silverpit desert palaeolake near Poland (Marie, 1975). Fluvial deposits comprise conglomeratic units which interfinger with red-brown sandstones and dark-red mudstones and claystones. Distinct deposits of fluvial strata are 100 m at their thickest, and intercalated with aeolian sandstones, elsewhere fluvial deposits average ~50 m in thickness (Glennie, 1986). The fluvial deposits are either structureless or have gently inclined laminae, with occasional rip-up clasts of red claystone and extra-formational pebbles, interpreted as having been scoured from

underlying deposits of ephemeral lakes within a wadi style system with occasional desiccation features suggesting sub-aerial exposure (Glennie, 1972; Cameron *et al.*, 1992). Conglomerates are interpreted to have formed around the basin margins (Goodchild & Bryant, 1986).

Age	Group	Formation	Lithology	Description
Upper Permian	Zechstein	Kupferschiefer		Carbonates and evaporites
	Upper Rotliegend	Upper Lemam Sst		Organic, black claystone Sandstone - only locally present
Silverpit			Claystone, siltstone, muddy sandstone and evaporites	
Lower Lemam Sandstone			Sandstone, occasionally conglomeratic, especially towards the base, with subordinate claystone	
Lower Permian				Micaceous sandstone and claystone
		Carboniferous		

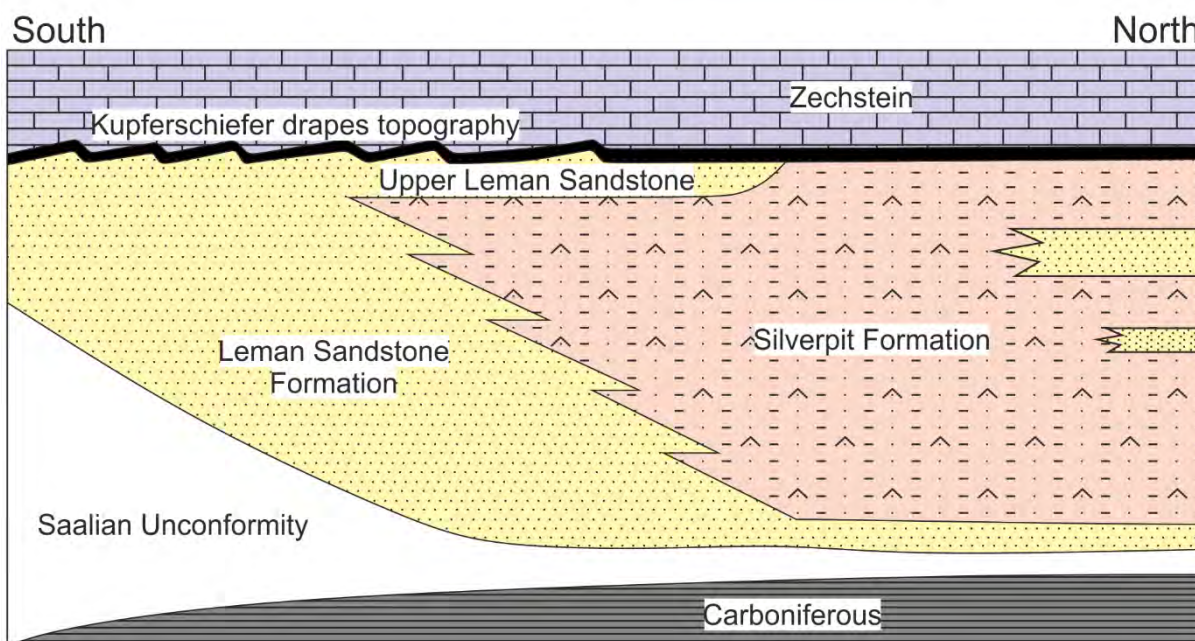


Figure 8.2. Lithostratigraphy of the Upper Rotliegend Group and relationships between the diachronous Lemam and Silverpit formations (modified after Glennie, 1986 and Howell & Mountney, 1997).

The sedimentary structures observed from core indicate an ephemeral fluvial system (Glennie, 1972). Rainfall was most likely seasonal, occurring in violent storms with floodwaters following interdune corridors between sand dunes eroding and reworking aeolian and previously deposited fluvial sands.

During dry periods, aeolian sediment encroached over these wadis but did not become well-established (Marie, 1975).

Aeolian sandstones dominate over fluvial facies towards the top of the Lemna Sandstone Formation, indicating a progressively drier environment (Cameron *et al.*, 1992). Aeolian facies occur in sequences up to 200 m thick, of dune sets and cosets. Dune sediments form almost the entire components of the Lemna Sandstone Formation in the east and south-east area of the basin (Marie, 1975; Van Veen, 1975). Towards the west of the basin these aeolian deposits interfinger with fluvial deposits described previously (Glennie, 1972). Within core data the aeolian sediments are represented by alternating planar and trough cross-laminations of fine and coarse-grained sandstone (Glennie, 1986). These laminations are inclined between 20-25° before being truncated by the following dune set and have been interpreted to represent both transverse and seif dunes (Glennie, 1972). Occasionally, thin packages of silty sands, with wavy laminations are encountered, and are interpreted to be the deposits of damp interdunes, where sediment has adhered to the damp surface caused by an elevated water table (Glennie, 1972; Conway, 1986).

8.3. Methods

The core data for this study was collected over three visits to the British Geological Survey's National Geological Repository, totalling over eight weeks of data collection. Nineteen detailed vertical sections were logged (Chapter 12, Appendices), with a cumulative length of over 2000 m, each spaced laterally approximately 20 km apart over an area of approximately 50 km², constrained to as close to a grid pattern as well localities allowed (Fig. 8.3). Where possible, the core logs record full successions of the Lemna Sandstone, from the unconformity with the underlying Carboniferous Coal Measures, through the Lower Lemna, Silverpit Formation and Upper Lemna intervals, to the overlying claystone of the Kupferschiefer Unit.

From the nineteen sedimentary logs, twenty-six facies were identified based principally on the lithological, sedimentary textures and structures present. The facies were grouped based upon depositional processes to form eleven facies associations (Fig. 8.4).

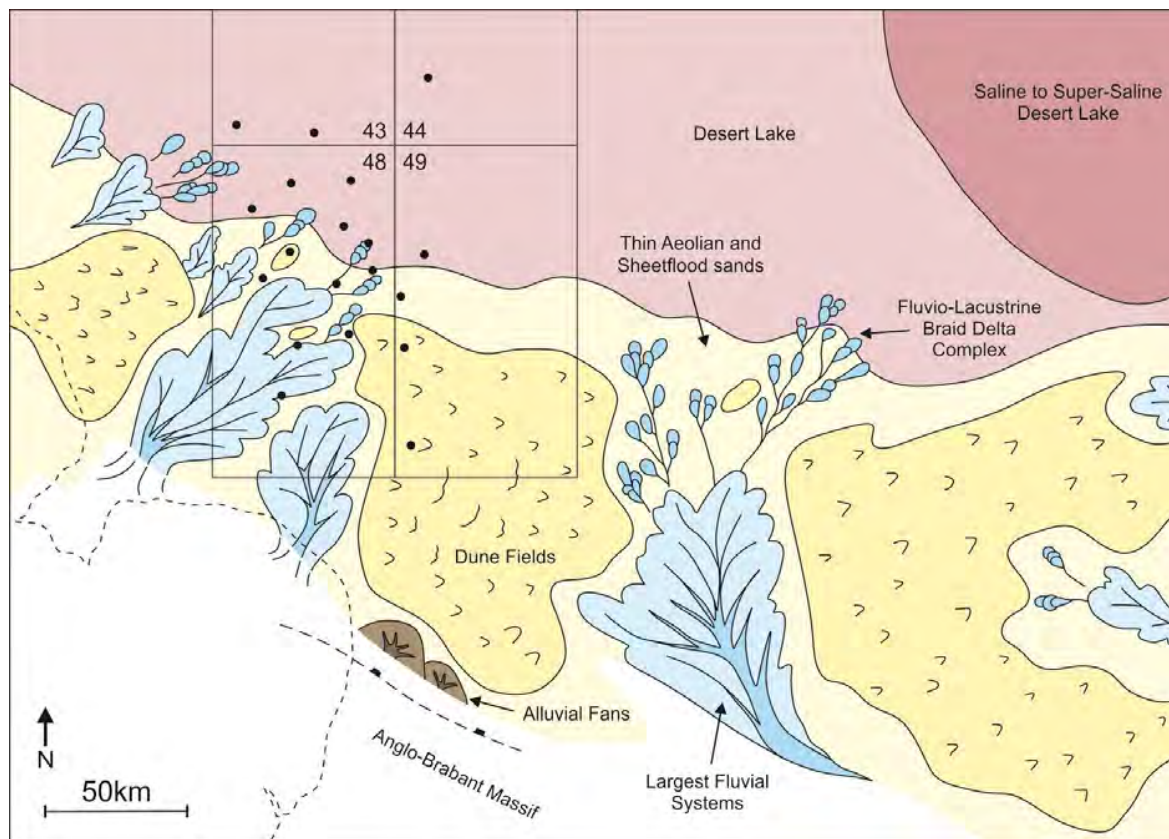


Figure 8.3. Palaeogeographical map of the Lemn Sandstone of the Southern North Sea with locations of studied wells within quadrants 43, 44, 48 and 49 (modified after George & Berry, 1997).

8.4. Lithofacies of the Lemn Sandstone and Silverpit Formations

The descriptions and interpretations presented are all based upon primary core observations within this study. Twenty-six facies have been identified within the Lemn Sandstone and Silverpit Formation interval and they are summarized in Table 8.1. Eighteen facies relate to sub-aqueous processes and the remainder relate to wind-blown processes.

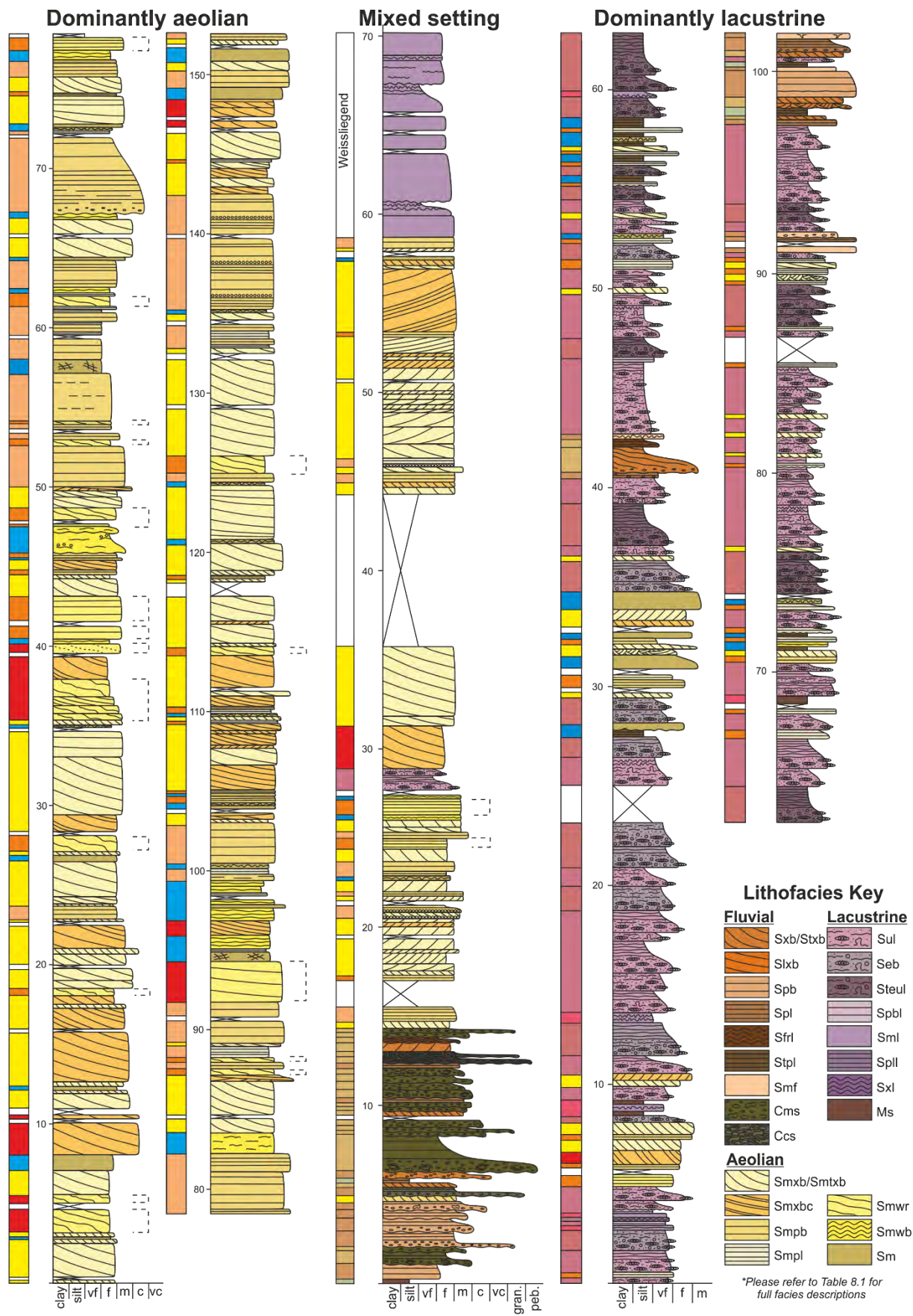






Figure 8.4. Selected logged sections depicting the varied sedimentology of the Lemna Sandstone/Silverpit transition.

Code	Name		Lithology & texture	Sedimentary structures	Interpretation
Smbx	Planar cross-bedded sandstone		Purple-yellow-grey, medium to coarse-grained sandstone, well sorted, well-rounded	Planar cross-bedding with mm/cm scale alternations in grainsize and reverse graded foresets	Migration of wind-blown straight-crested dune-scale bedforms formed by the avalanche of sediment down the lee slope of the dune
Smbc	Planar cross-bedded sandstone couplets		Purple-yellow-grey, fine to coarse-grained sandstone, well sorted, well-rounded	Couplets of fine-grained structureless sandstone and coarser grained, reverse graded sandstone	Migration of wind-blown straight-crested dune-scale bedforms formed by the avalanche and settlement of sediment down the lee slope of the dune
Smtxb	Trough cross-bedded sandstone		Brown-grey, fine to medium-grained sandstone, well sorted, well-rounded	Trough cross-bedding with mm/cm scale alternations in grainsize	Migration of wind-blown sinuous-crested dune-scale bedforms
Smpb	Planar-bedded sandstone		Purple-grey, fine to medium-grained sandstone, well sorted, well-rounded	Planar-bedding with millimetre scale alternations in grainsize and sporadic granule-rich surfaces	Wind-blown deposits formed by the deflation of dune-scale bedforms, with evidence of deflation lags

Smpl	Planar laminated sandstone		Purple-grey, very-fine to medium-grained sandstone, well sorted, well-rounded	Planar-laminated with millimetre scale alternations in grainsize	Wind-blown deposits formed by the fall out of sediment from suspension
Smwr	Ripple-cross-laminated sandstone		Purple-grey, very-fine to coarse-grained sandstone, bimodal sorted, well rounded	Undulose to ripple-cross-laminations with millimetre scale alternations in grainsize and sporadic coarse-grained lenses	Migration of wind-blown ripple-scale bedforms, producing pinstripe laminae
Smwb	Undulose-bedded sandstone		Purple-brown, very-fine to fine-grained sandstone, well sorted, well-rounded	Undulose to planar laminations with millimetre scale alternations in grainsize	Wind-blown deposits formed by the deflation of dune-scale bedforms over damp substrates
Sm	Structureless sandstone		Purple-grey, fine-grained sandstone, well sorted, well-rounded	Structureless with sporadic soft sediment deformation	Suspension settling of wind-blown sediment in areas affected by surface water, followed by drying

Sxb	Planar cross-bedded sandstone		Purple-brown, fine to medium-grained sandstone, moderate/well sorted, sub-rounded	Planar cross-bedding with normally graded foresets, in single or multiple sets with sporadic clasts, mud draping and soft sediment deformation	Migration of straight-crested dune-scale bedforms and dune trains sub-aqueously under lower flow regime conditions with high sediment load
Stxb	Trough cross-bedded sandstone		Purple-brown, very-fine to fine-grained sandstone, moderate/well sorted, sub-rounded	Trough cross-bedding with normal grading, in single or multiple sets	Migration of sinuous-crested dune-scale bedforms and dune trains sub-aqueously under lower flow regime conditions
Slxb	Low-angle cross-bedded sandstone		Purple-grey, fine-grained sandstone, moderate/well sorted, sub-rounded	Low-angle cross-bedding bedding in single or multiple lenticular sets with sporadic mud-draped foresets and soft sediment deformation	Lateral migration of macro-forms in lower flow regime conditions with high sediment load
Spb	Planar bedded sandstone		Purple-brown, fine to medium-grained sandstone, moderate/well sorted, sub-rounded	Planar bedding with sporadic rip-up clasts	Sub-aqueous upper flow regime flat beds

Spl	Planar laminated sandstone		Purple-brown, fine to medium-grained sandstone, moderate/well sorted, sub-rounded	Planar laminations with sporadic rip-up clasts and mottling	Sub-aqueous upper flow regime flat beds
Sfrl	Ripple-cross-laminated sandstone		Purple-brown, very-fine to fine-grained sandstone, moderate/well sorted, sub-rounded	Ripple-cross-laminations in singular or multiple sets	Migration of ripple-scale bedforms in lower flow regime
Smf	Structureless sandstone		Purple-brown-grey, fine to medium-grained sandstone, moderate/well sorted, sub-rounded	Structureless with sporadic rip-up clasts and soft sediment deformation	Rapid deposition in high sediment load suppressing bedform development
Stpl	Planar laminated mudstone to siltstone		Brown mudstone/siltstone	Planar laminations with sporadic rhizoliths and desiccation cracks	Suspension fall-out from stationary waters

Cms	Matrix-supported conglomerate		Brown-grey-purple, polymictic conglomerate with a fine to coarse-grained sandstone matrix and pebble to cobble-grade clasts, poorly sorted, sub-rounded, matrix supported	Structureless to planar bedded with sporadic rip-up clasts armoured with small extraformational granules and sporadic imbrication	Sub-aqueous lower flow regime conditions with high sediment load and suppressed bedform development
Ccs	Clast-supported conglomerate		Brown-grey, polymictic conglomerate with pebble-grade clasts, poorly sorted, sub-angular to sub-rounded, clast supported	Structureless to planar bedded	Sub-aqueous, high energy Newtonian flow under high sediment load conditions, with suppressed bedform development
Ms	Structureless mudstone		Brown mudstone	Structureless	Suspension fall-out in stationary waters
Sul	Undulose bedded sandstone		Brown, siltstone to fine-grained sandstone, moderate/poorly sorted, sub-rounded	Undulose laminations to bedding, sporadic coarser sandstone lenses, bioturbation, soft sediment deformation	Periodic sediment influx into stationary waters

Seb	Evaporitic bedded sandstone		Purple-grey, very-fine to fine-grained sandstone, moderate/well sorted, sub-rounded	Crude bedding, sporadic evaporitic clasts, soft sediment deformation and bioturbation	Periodic sediment influx into saline stationary waters and subsequent precipitation of evaporites
Steul	Evaporitic bedded siltstone		Purple-brown, mudstone to fine-grained sandstone, moderate sorting, sub-rounded	Undulose to planar-bedding, coarser sandstone lenses, sporadic evaporitic clasts, bioturbation and soft sediment deformation	Periodic sediment influx into saline stationary waters and subsequent precipitation of evaporites
Sml	Structureless sandstone		Grey, fine to medium-grained sandstone, well sorted, sub-rounded	Structureless, sporadic red diagenetic spots and soft sediment deformation	Rapid suspension fall-out from high density sediment influxes
Spbl	Planar-bedded sandstone		Grey, fine-grained sandstone, well sorted, sub-rounded	Planar bedding, sporadic soft sediment deformation and coarser sandstone lenses	Periodic sediment input and suspension fall-out in stationary waters

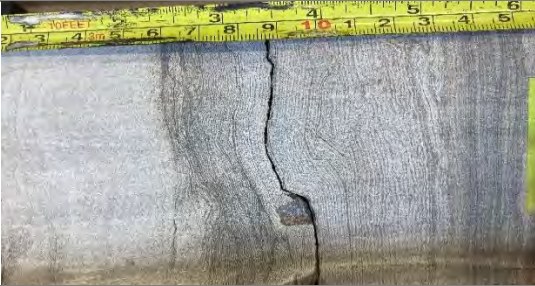

SpII	Planar-laminated siltstone		Brown-grey, siltstone to very-fine-grained sandstone, bimodal sorting, sub-rounded	Planar laminations with polygonal hummocks, sporadic bioturbation	Sediment binding by algal and microbial mats with laminations indicating shallow water to subaerial exposure
Sxl	Cross-laminated sandstone		Purple-brown-grey siltstone to fine-grained sandstone, moderate sorting, sub-rounded	Cross-laminations in singular to multiple sets	Sub-aqueous formation and migration of ripple-scale bedforms

Table 8.1. Summary of lithofacies observed in the Leman and Silverpit Formations. **Smbx**: Sub-aerial planar cross-bedded sandstone, **Smbxc**: Sub-aerial planar cross-bedded sandstone couplets, **Smtxb**: Sub-aerial trough cross-bedded sandstone, **Smpb**: Sub-aerial planar bedded sandstone, **Smpl**: Sub-aerial planar laminated sandstone, **Smwrr**: Sub-aerial ripple-cross-laminated sandstone, **Smwrb**: Sub-aerial undulose laminated sandstone, **Sm**: Sub-aerial structureless sandstone, **Sxb**: Sub-aqueous planar cross-bedded sandstone, **Stxb**: Sub-aqueous trough cross-bedded sandstone, **Sltxb**: Sub-aqueous low-angle cross-bedded sandstone, **Sspb**: Sub-aqueous planar bedded sandstone, **SpI**: Sub-aqueous parallel laminated sandstone, **Sfrl**: Sub-aqueous cross-laminated sandstone, **Smf**: Sub-aqueous structureless sandstone, **Stpl**: Sub-aqueous planar laminated mudstone/siltstone, **Cms**: Sub-aqueous matrix-supported conglomerate, **Ccs**: Sub-aqueous clast-supported conglomerate, **Ms**: Sub-aqueous structureless mudstone, **Sul**: Sub-aqueous undulose bedded sandstone, **Seb**: Sub-aqueous evaporitic bedded sandstone, **Steul**: Sub-aqueous evaporitic siltstone, **Sml**: Sub-aqueous structureless sandstone, **Spl**: Sub-aqueous planar bedded sandstone, **SpII**: Sub-aqueous planar laminated siltstone, **Sxl**: Sub-aqueous cross-laminated sandstone.

8.5. Facies Associations

8.5.1. Aeolian Dune

Facies associations of this type are characterised by centimetre-scale cross-bedded foresets of purple to grey, fine to coarse-grained sandstones that are composed of well-rounded and well to bimodally sorted grains (Fig. 8.5). The sandstones are arranged into sets of planar-cross-bedding (**Smx**b**) and more sporadically observed trough-cross-bedding (**Smt**xb**). The individual foresets (each up to 1-7 cm thick) are frequently reverse graded and in approximately 35-40% of occurrences the reverse graded foresets are separated by thin millimetre-scale finer grained laminae (**Smx**bc**). Sporadic occurrences of ripple-cross-laminated sandstones (**Sm**wr**) are present between sets of cross-bedded sandstones and range in thickness from 3-10 m and are also present along the foresets of the cross-bedded sandstones. The preserved occurrences of the association range in thickness from 20 cm to 13 m.********

Interpretation

Associations of this type represent the preserved deposits of aeolian dunes that accumulated through the migration and climb of duneforms that possessed a lee slope inclined at, or close to, the angle of repose (*cf.* Mountney, 2006). Couplets of fine-grained and coarse-grained sandstone, with reverse grading, represent dune-scale, wind-blown bedforms migrating by the combined processes of grainfall and grainflow (Hunter, 1977a; 1977b; Langford & Chan, 1989; Kocurek, 1991; 1996). The inverse grading within the inclined foresets is typical of aeolian dunes (Hunter, 1977a; 1977b; 1981) and represents the deposits of individual grainflow avalanches, whereas the finer grained fractions of the association represent the deposits of grainfall strata. The absence of the grainfall between individual grainflow avalanches may indicate deposition in the upper parts of the dune slipfaces (Besly *et al.*, 2018). Occurrences of facies **Smwr** along the foresets of the cross-bedded sandstone represent wind-ripple strata climbing up the dune toe from associated dune plinth associations, however thick units of the wind-ripple strata possibly indicate that some duneforms may have a linear geomorphology (Besly *et al.*, 2018).

8.5.2. Aeolian Dune Plinth

Facies associations of this type are characterised by millimetre to centimetre-scale cross-laminated foresets to planar-laminated beds of purple to grey, very-fine to coarse-grained sandstones that are composed of well-rounded and well to bimodally sorted grains (Fig. 8.6). The deposits comprise sets of 0.2-3 cm thick inclined couplets of fine-grained structureless sandstones and coarser grained, reverse graded sandstones (**Smxbc**), planar to slightly inclined laminations with strong bimodality in sets up to 3 m thick (**Smwr**), and fine-grained sandstones with planar laminations (**Smpl**) in units up to 0.5 m thick. The preserved occurrences of the association range in thickness from 20 cm to 7.5 m.

Interpretation

Associations of this type represent the preserved deposits of aeolian dune plinths. Units of planar to slightly inclined laminations with strong bimodality represent wind-ripple strata (Moscariello, 2011; Besly *et al.*, 2018), dominant features within dune plinth associations (Besly *et al.*, 2018), formed by the migration of ripple-scale bedforms through the process of saltation of fine-grained sand, which accumulate along the saltation wavelength, then reptation of coarser grains over the accumulated grains (Sharp, 1963; Fryberger & Schenk, 1988). The couplets of very-fine-grained and coarse-grained sandstones, with reverse grading, represent the processes of grainfall and grainflow (Hunter, 1977a; 1977b; Kocurek, 1981; 1988; 1991; 1996; Langford & Chan, 1989). Whereas planar-laminated, fine-grained sandstones represent the deposits of grainfall strata, where sand was entrained into suspension and later deposited upon dune plinth (Besly *et al.*, 2018). The limited couplet thicknesses combined with thick units of wind-ripple strata suggest deposition near the lowermost portions of the duneform.

8.5.3. Aeolian Sandsheet

Facies associations of this type are characterised by millimetre to centimetre-scale planar-laminated to bedded, purple to grey, very-fine to medium grained sandstones that are composed of well-rounded, moderate to well sorted grains (Fig. 8.7).

Aeolian Dune Association

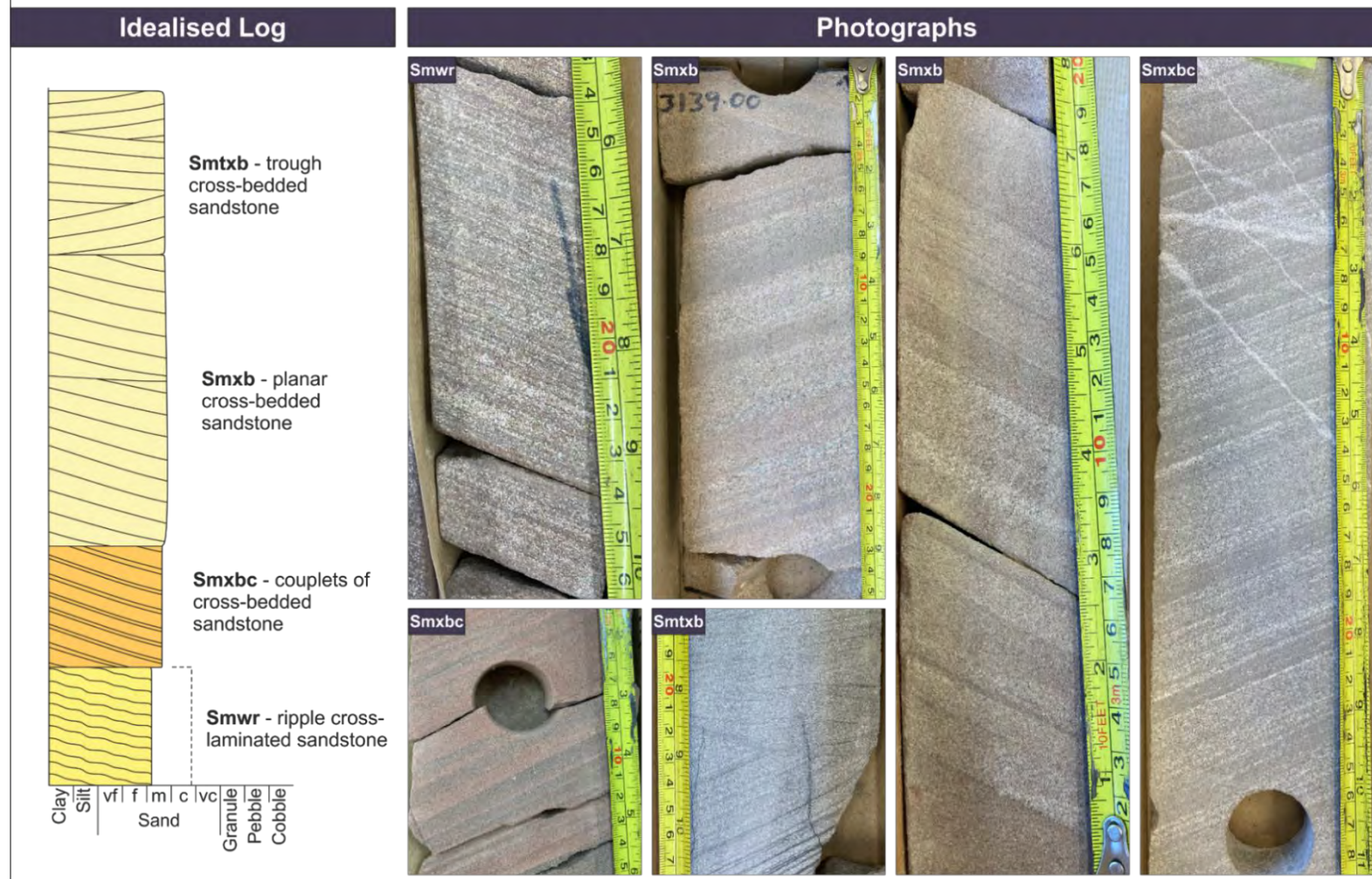


Figure 8.5. Summary panel of the aeolian dune association of the Lemna Sandstone with an idealised log and photographs of the internal facies.

aeolian dune plinth association



Figure 8.6. Summary panel of the aeolian dune plinth association of the Leman Sandstone with an idealised log and photographs of the internal facies.

The deposits comprise units of up to 5 m thick, of moderately sorted, planar-bedded sandstones (**Smpb**) with sporadic granule-rich bounding surfaces, and fine-grained planar-laminated sandstones (**Smpl**) in units up to 1.5 m thick. The preserved occurrences of the association range in thickness from 25 cm to 5 m.

Interpretation

Associations of this type represent the preserved deposits of aeolian sandsheet sub-environments, where dune development is inhibited (*cf.* Kocurek & Neilson, 1986). Several factors could have prevented dune development and promoted sandsheet development, including reduced sediment supply as a result of: (i) episodic flooding (Kocurek & Neilson, 1986; Neilson & Kocurek, 1986); (ii) sediment 'trapping' via vegetation (Bullard, 1997; Kocurek, 1999; Kocurek & Lancaster, 1999); (iii) a sediment grain population that is too coarse to become entrained effectively (Kocurek & Neilson, 1986); (iv) a high water table which is in contact with sediment surface (Fryberger *et al.*, 1988; Jagger, 2003; Mountney & Jagger, 2004). Planar-laminated, fine-grained sandstones represent the deposits of grainfall strata, where sand was entrained into suspension and later deposited as the duneforms deflate. Granule-rich bounding surfaces within planar-bedded sandstones represent deflationary surfaces, characteristic of sandsheet development (Langford & Chan, 1989).

8.5.4. Dry Interdune

Facies associations of this type are characterised by millimetre-scale cross to planar-laminated, purple to grey, very-fine to coarse-grained sandstones that are composed of well-rounded and well to bimodally sorted grains (Fig. 8.8). The deposits comprise planar to slightly inclined laminations with strong bimodality in sets up to 1 m thick (**Smwr**) and fine-grained sandstones with planar bedding and laminations (**Smpb** & **Smpl**) in sets up to 1.2 m thick. The preserved occurrences of the association range in thickness from 20 cm to 2 m.

Interpretation

Associations of this type represent the preserved deposits of a dry interdune setting where the water table is significantly beneath the level of the depositional surface such that sedimentation at the surface remained essentially uninfluenced by the effects of moisture (*cf.* Hunter, 1977a; 1977b; 1981; Ahlbrandt & Fryberger, 1981; Kocurek 1981; Mountney, 2006). The units of planar to slightly inclined laminations with strong bimodality represent wind-ripple strata (Moscariello, 2011; Besly *et al.*, 2018). Planar bedded to laminated, fine-grained sandstones represent the deposits of grainfall strata, where sand was entrained into suspension and later deposited within the interdune area (Besly *et al.*, 2018).

8.5.5. Damp to wet Interdune

Facies associations of this type are characterised by millimetre to centimetre-scale undulose laminated, purple to grey, very-fine to fine-grained sandstones that are composed of well-rounded and well sorted grains, along with structureless mudstones to fine-grained sandstones (Fig. 8.9). The undulose-laminated sandstones (**Smwb**) occur in units up to 1.5 m thick, whereas the structureless sandstones (**Sm**) and mudstones (**Ms**) range in thickness from 20 cm to 1.5 m. The preserved thickness of the association ranges from 15 cm to 2 m.

Interpretation

Associations of this type represent the preserved deposits of a damp to wet interdune setting where the water table is within the capillary fringe of the surface and occasionally above the depositional surface (*cf.* Hunter, 1977a; 1977b; 1981; Ahlbrandt & Fryberger, 1981; Kocurek 1981; Mountney, 2006). The undulose laminations are caused by the adhesion of wind-transported sediment to a predominantly damp to locally wet sediment surface (Moscariello, 2011). Structureless sandstones and mudstones were deposited by suspension settling when the water table was above the depositional surface.

Aeolian Sandsheet Association

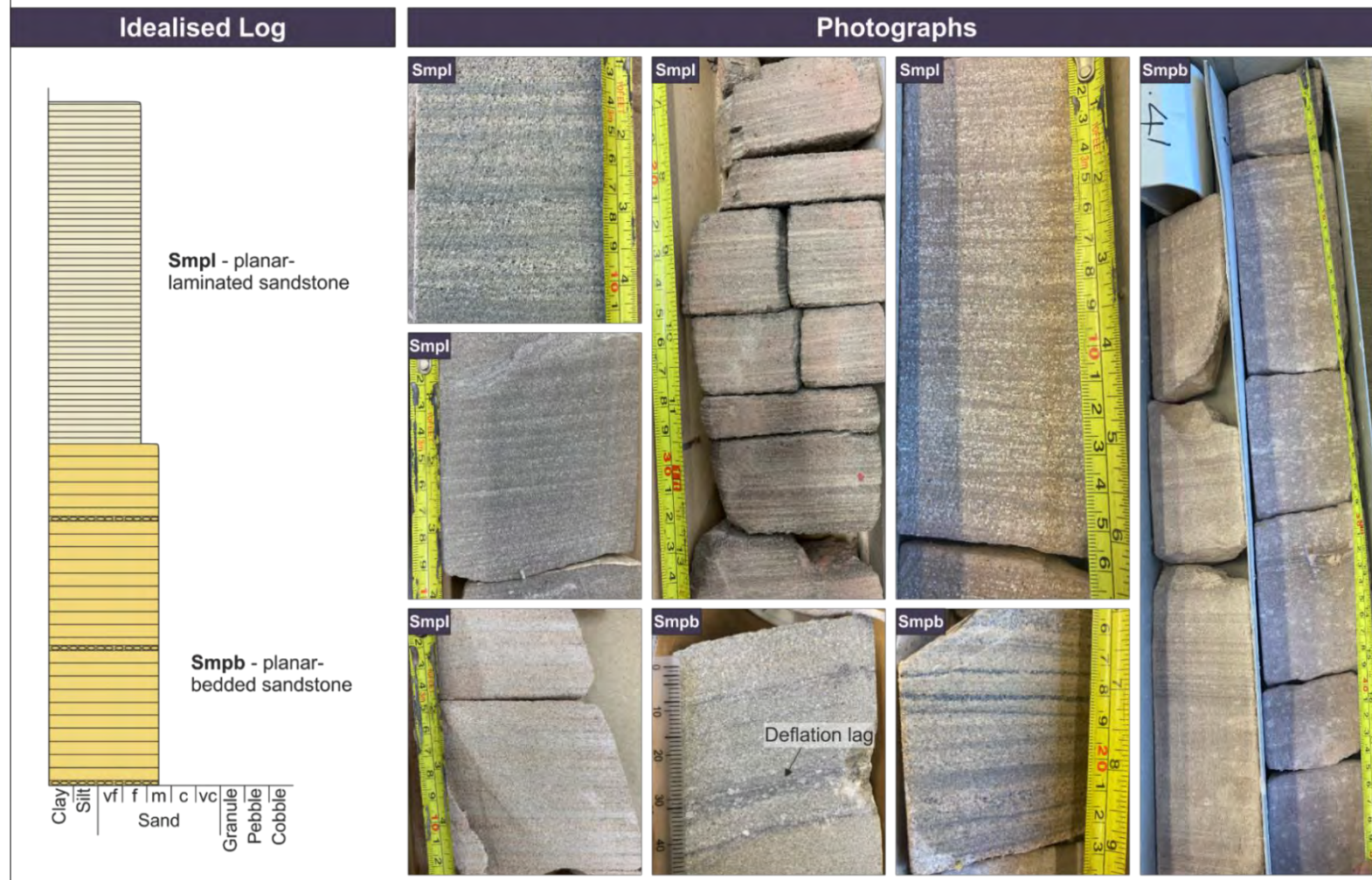


Figure 8.7. Summary panel of the aeolian sandsheet association of the Lemna Sandstone with an idealised log and photographs of the internal facies.

Aeolian Dry Interdune Association



Figure 8.8. Summary panel of the aeolian dry interdune association of the Lemna Sandstone with an idealised log and photographs of the internal facies.

Aeolian Damp/Wet Interdune Association

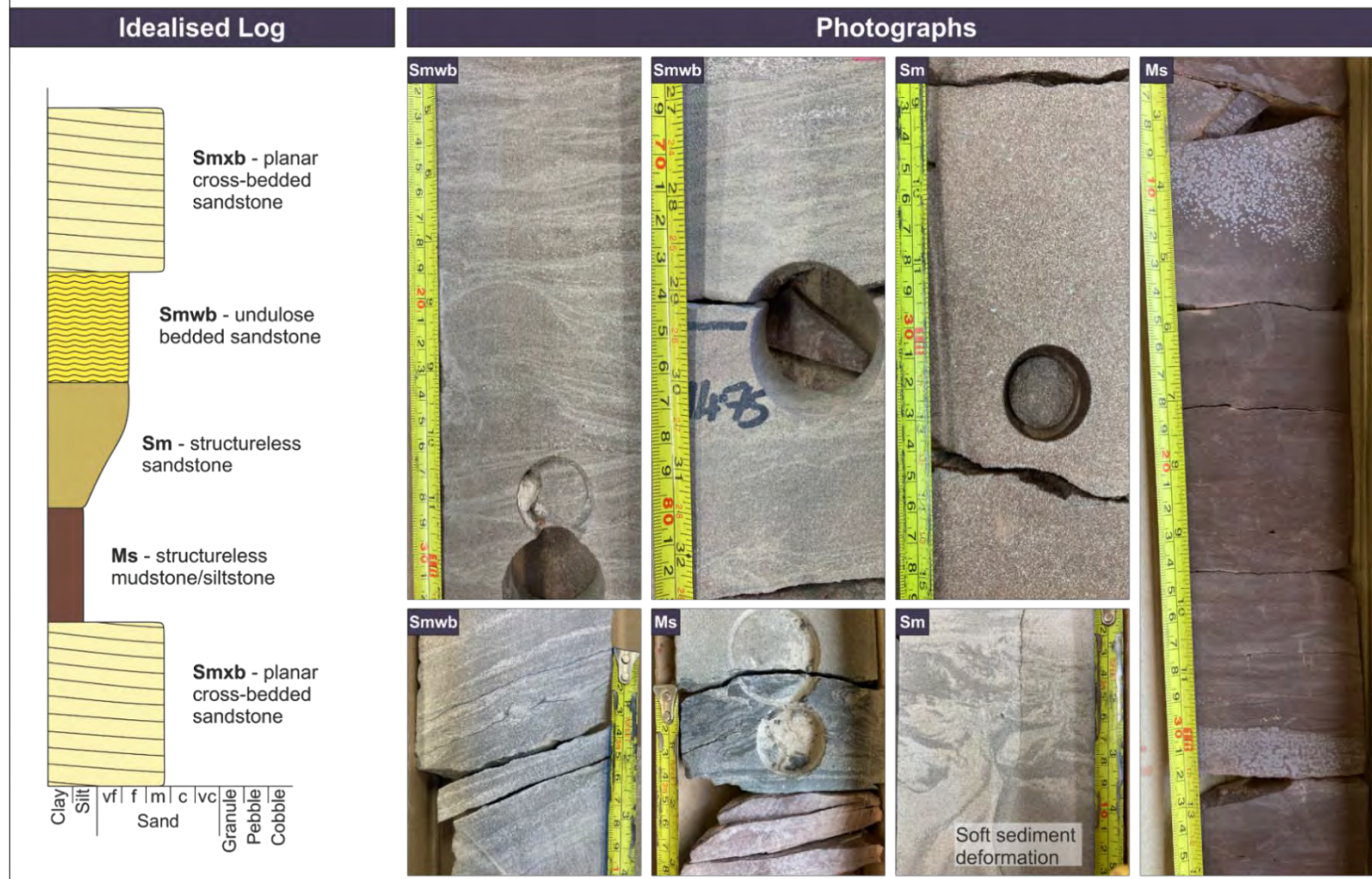


Figure 8.9. Summary panel of the aeolian damp/wet interdune association of the Lemna Sandstone with an idealised log and photographs of the internal facies.

8.5.6. Fluvial Channel

Facies associations of this type are characterised by fining upwards successions with erosional basal bounding surfaces (Fig. 8.10). The basal deposits of approximately 10 cm to 2.5 m thickness, comprise matrix (**Cms**) and clast-supported (**Ccs**) conglomerates composed of sub-angular to well-rounded, poorly sorted, polymictic pebble to cobble-grade clasts of both intraformational and extraformational origin. The mudstone clasts within the matrix-supported conglomerates (**Cms**) are often well-rounded and sporadically armoured with granule-grade extraformational clasts. The succession fines upwards into fine to medium-grained planar cross-bedded sandstones (**Sxb**) or more sporadically observed trough cross-bedded sandstones (**Stxb**) of sets between 20 cm to 2.2 m thick before grading into fine to medium-grained structureless sandstones (**Smf**) of no more than 2.75 m thickness. Fine to medium-grained planar-laminated (**Spl**) to planar-bedded (**Spb**) sandstones, between 10 cm to 2 m thick, overlie the units of structureless sandstone, and very-fine to fine-grained ripple-cross-laminated sandstones (**Sfri**) to form the upper unit of the fining upwards succession. The preserved thickness of the association ranges from 10 cm to 4.5 m.

Interpretation

Associations of this type represent the preserved deposits of fluvial channels (Bridge, 2003; 2006) associated with rapid deposition from high-energy currents in mostly likely an ephemeral fluvial system in a semi-arid desert environment (Moscariello, 2011). Conglomeratic basal units represent channel lag deposits formed with high flow velocities and dominantly bedload transport where the large sediment grainsize prevents the mixed-load transport required for bedform formation. The angularity of some of the intraclasts indicates erosion and deposition over relatively short distances (Moscariello, 2011). However, the presence of armoured mud balls suggests turbulent bedload transport, where the mudstone clasts has rolled along the basal substrate over comparatively longer distances (Bachmann & Wang, 2014). Both the armoured mud balls and structureless sandstones suggest deposition associated with hyperconcentrated flow which led to rapid deposition and suppressed bedform development (Bridge & Best, 1988; Todd, 1996). As the flow waned, sets of planar

cross-bedding and trough cross-bedding were deposited and represent the migration of straight-crested and sinuous-crested dune-scale bedform trains along the bases of channels during times of lower sediment load. Planar-laminated and planar-bedded sandstones near the top of the association represent upper flow regime deposits produced as a result of rapidly decreasing flow depth.

8.5.7. Fluvial Sheet

Facies associations of this type are characterised by fining upwards successions with little to no evidence of downcutting along the basal bounding surface (Fig. 8.11). The basal deposits of approximately 10 cm to 50 cm thickness, comprise matrix-supported conglomerates (**Cms**) composed of sub-angular to sub-rounded, poorly sorted, polymictic pebble-grade clasts of both intraformational and extraformational origin. The succession fines upwards into fine to medium-grained structureless sandstones (**Smf**) up to 2.5 m thick. Fine to medium-grained low-angle cross-bedded (**Slxb**), planar-bedded (**Spb**) and planar-laminated (**Spl**) sandstones, between 10 cm to 2.5 m thick, overlie the units of structureless sandstone, and very-fine to fine-grained ripple-cross-laminated sandstones (**Sfri**) form the upper unit of the fining upwards succession. The preserved thickness of the association ranges from 20 cm to 3.5 m.

Interpretation

Associations of this type represent the preserved deposits of unconfined flow during flash-flood events or possibly in relation to flooding from breaks in channel walls (*cf.* Abdullatif, 1989; Sadler & Kelly, 1993; Tooth, 1999; 2000; 2005; Billi, 2007; Sáez *et al.*, 2007; Moscariello, 2011). Each individual fining upward succession with an erosive base represents an individual flood event (Miall, 2014). The basal conglomeratic unit suggests that the flood events had high enough energy to rip up underlying elements. Structureless sandstones suggest deposition associated with hyperconcentrated flow which led to rapid deposition and suppressed bedform development (Bridge & Best, 1988; Todd, 1996). The presence of low-angle cross-bedding interspersed with planar-bedding represents the transition from conditions of lower flow regime dune formation to upper flow regime plane bed formation, probably

formed under high rates of sediment deposition (Fielding, 2006; Lang & Winsemann, 2013). The abundance of planar-bedded and planar-laminated sandstones suggest upper flow regime conditions dominated (Arnott & Hand, 1989; Carling, 2013; Guan *et al.*, 2016). Ripple-cross-laminated sandstones suggest flow waned enough for bedform development and migration.

8.5.8. Overbank

Facies associations of this type are characterised by brown, structureless mudstones (**Ms**) in units up to 4 m thick and parallel-laminated mudstones to siltstones (**Stpl**), which exhibit millimetre-scale laminations, sporadic rhizoliths and desiccation cracks, and occur in beds up to 1 m thick. The preserved thickness of the association ranges from 20 cm to 4 m (Fig. 8.12).

Interpretation

Associations of this type represent the preserved deposits of fluvial overbank environments where deposition resulted from suspension settling in standing water after flooding (Eberth & Miall, 1991), where discharge temporarily exceeded the bank-full capacity of the local channel network such that flood water could not be contained and spilled out over a floodplain (*cf.* Bridge, 1984; 2003; Bristow *et al.*, 1999). Planar-laminations within the siltstones and mudstones represent minor grain-size differences resulting from the alternation of episodic discharge of sediment (Moscariello, 2011). The presence of desiccation cracks and rhizoliths indicate stabilisation and drying of the floodplain (Miall, 1988).

Fluvial Channel Association

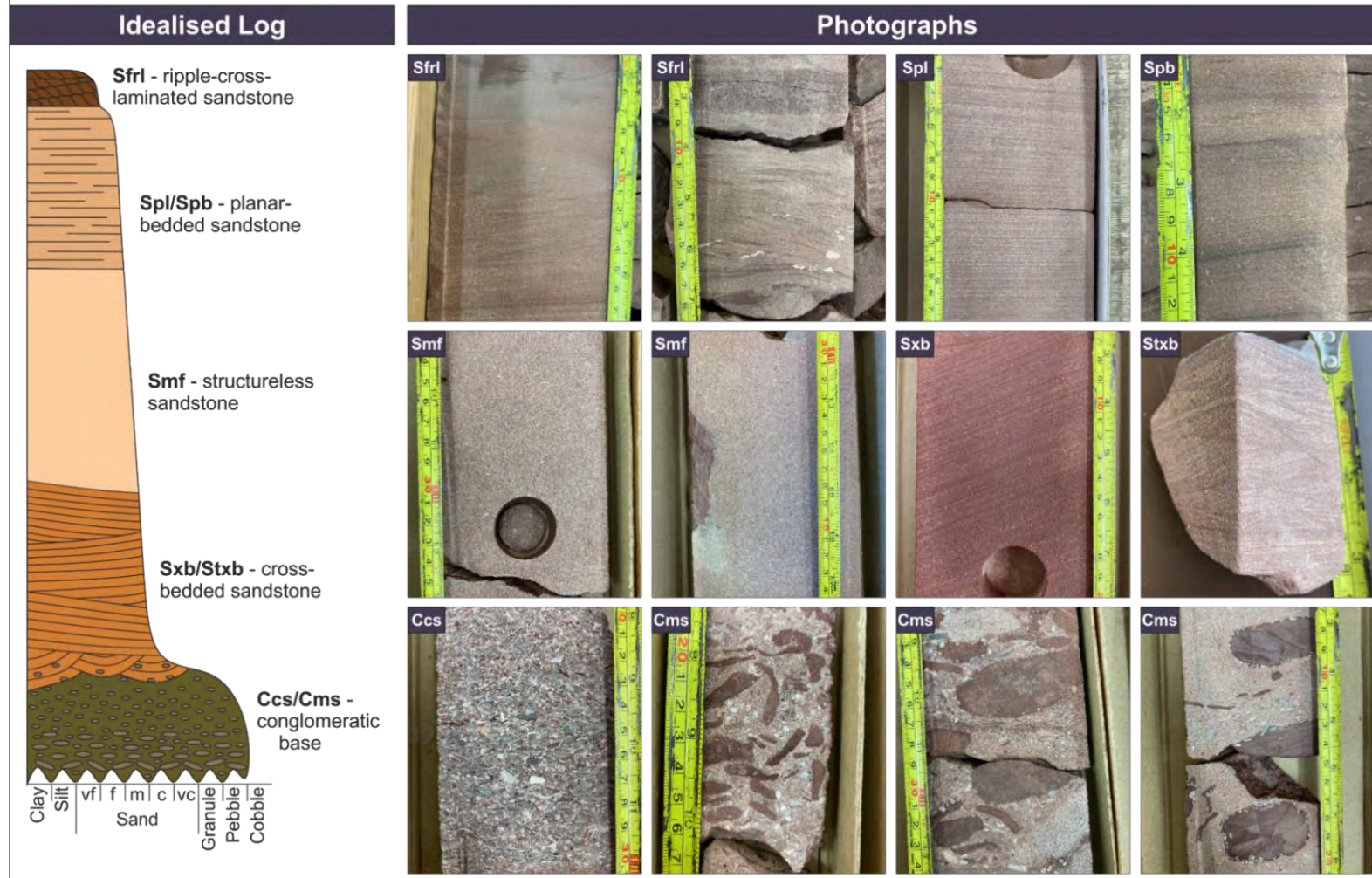


Figure 8.10. Summary panel of the fluvial channel association of the Lemna Sandstone with an idealised log and photographs of the internal facies.

Fluvial Sheet Association

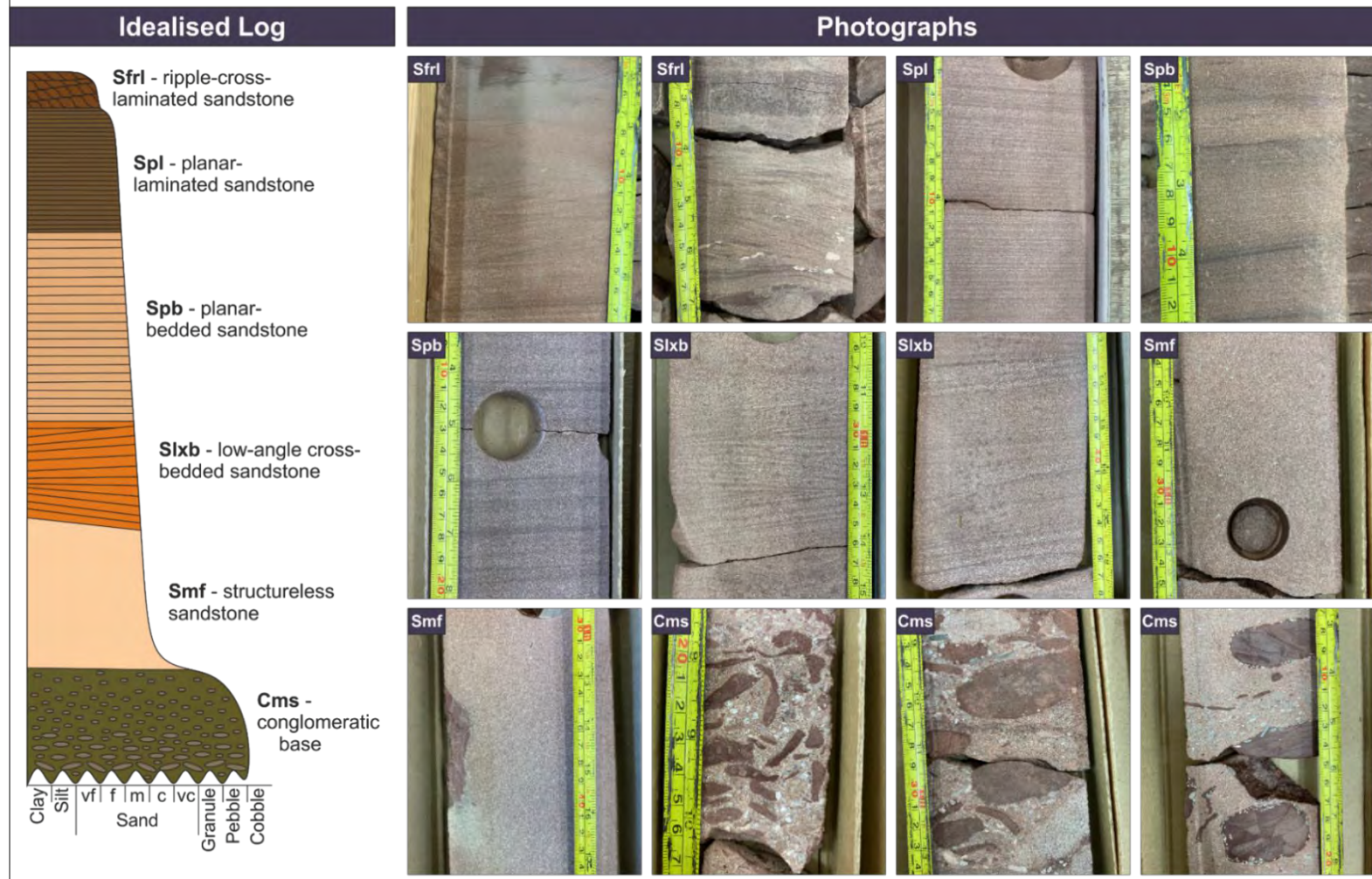


Figure 8.11. Summary panel of the fluvial sheet association of the Lemna Sandstone with an idealised log and photographs of the internal facies.

Overbank Association

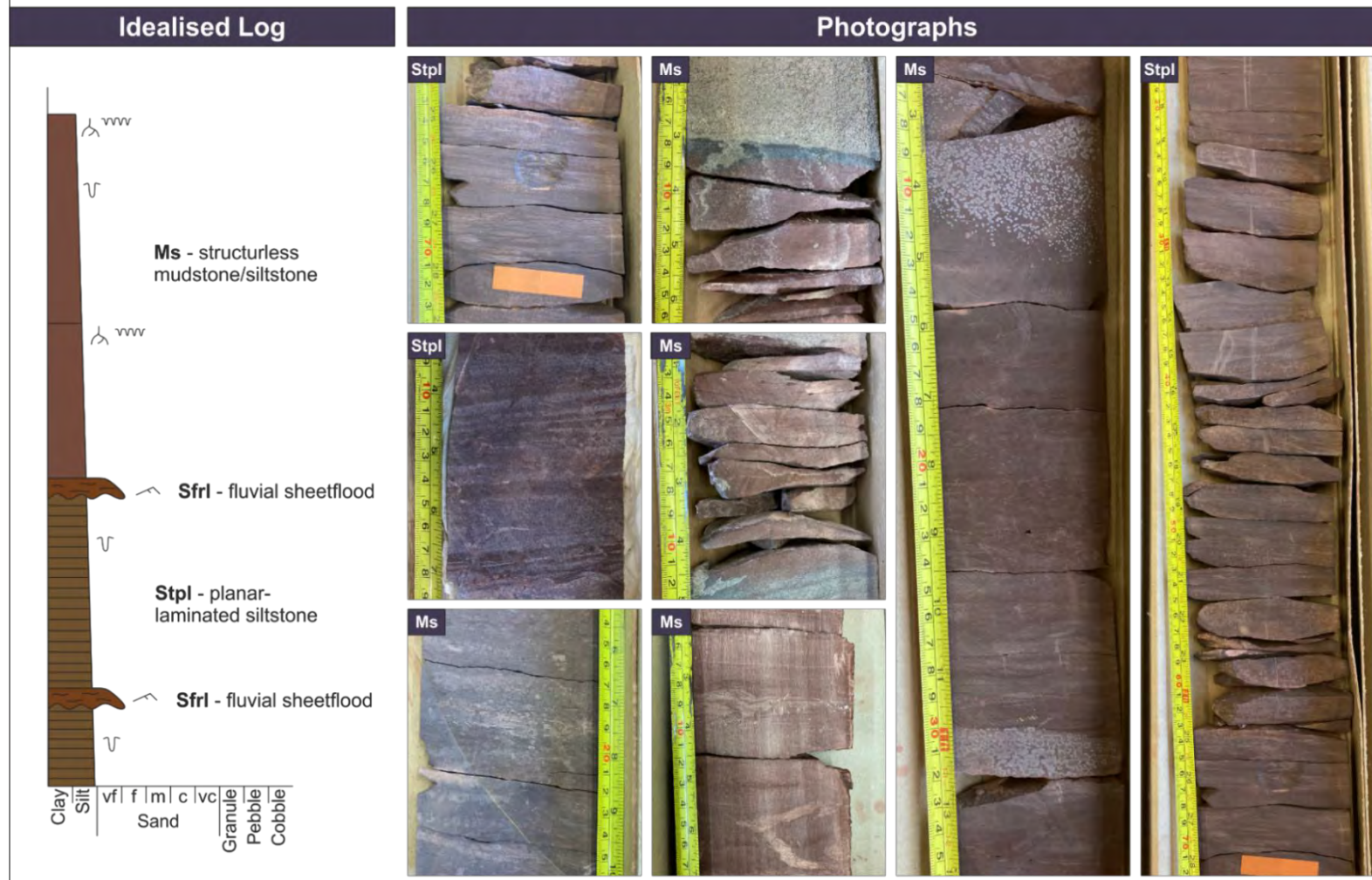


Figure 8.12. Summary panel of the overbank association of the Leman Sandstone with an idealised log and photographs of the internal facies.

8.5.9. Lake Margin

Facies associations of this type are characterised by centimetre-scale planar to undulose bedded, brown to grey, siltstones to fine-grained sandstones that are composed of sub-rounded, moderately to well sorted grains (Fig. 8.13). Along with millimetre-scale cross to planar-laminated, brown to grey, siltstones to fine-grained sandstones that are composed of sub-rounded, moderately to bimodally sorted grains. The undulose bedded sandstones (**Sul**) comprise 10 cm to 4 m beds with sporadic coarser grained lenses and silty undulations arranged in sets of up to 5 m. The planar-bedded sandstones (**Spbl**) exhibit normally graded beds no thicker than 75 cm, and the cross-laminated sandstones (**Sxl**) have sporadic mud-draping along foresets and are arranged in sets of approximately 10 to 70 cm thick. Soft sediment deformation, fluid escape structures and bioturbation are common features within the preserved association which ranges in thickness from 20 cm to 6.75 m.

Interpretation

Associations of this type represent the preserved deposits of a marginal lacustrine environment (Allen, 1981). The fine-grained nature of the facies suggests a predominantly low-energy environment, with deposition occurring within a standing body of water, while the undulose sandstone and siltstone laminae reflect periods of increased energy (Andrews & Hartley, 2015). Cross-laminated siltstones to sandstones result from sub-aqueous formation and migration of ripple-scale bedforms, possibly influenced by current circulation as a result of prevailing winds, indicating periods of high water table but shallow water depths (Allen, 1963; Nielsen, 1981). The presence of undulose and planar-bedded sandstones are the result of periodic sediment influxes into stationary bodies of water. Clastic sediment was likely supplied as wind-blown dust, or by river-generated inter- or overflows into the lake water (Rogers & Astin, 1991).

Lake Margin Association

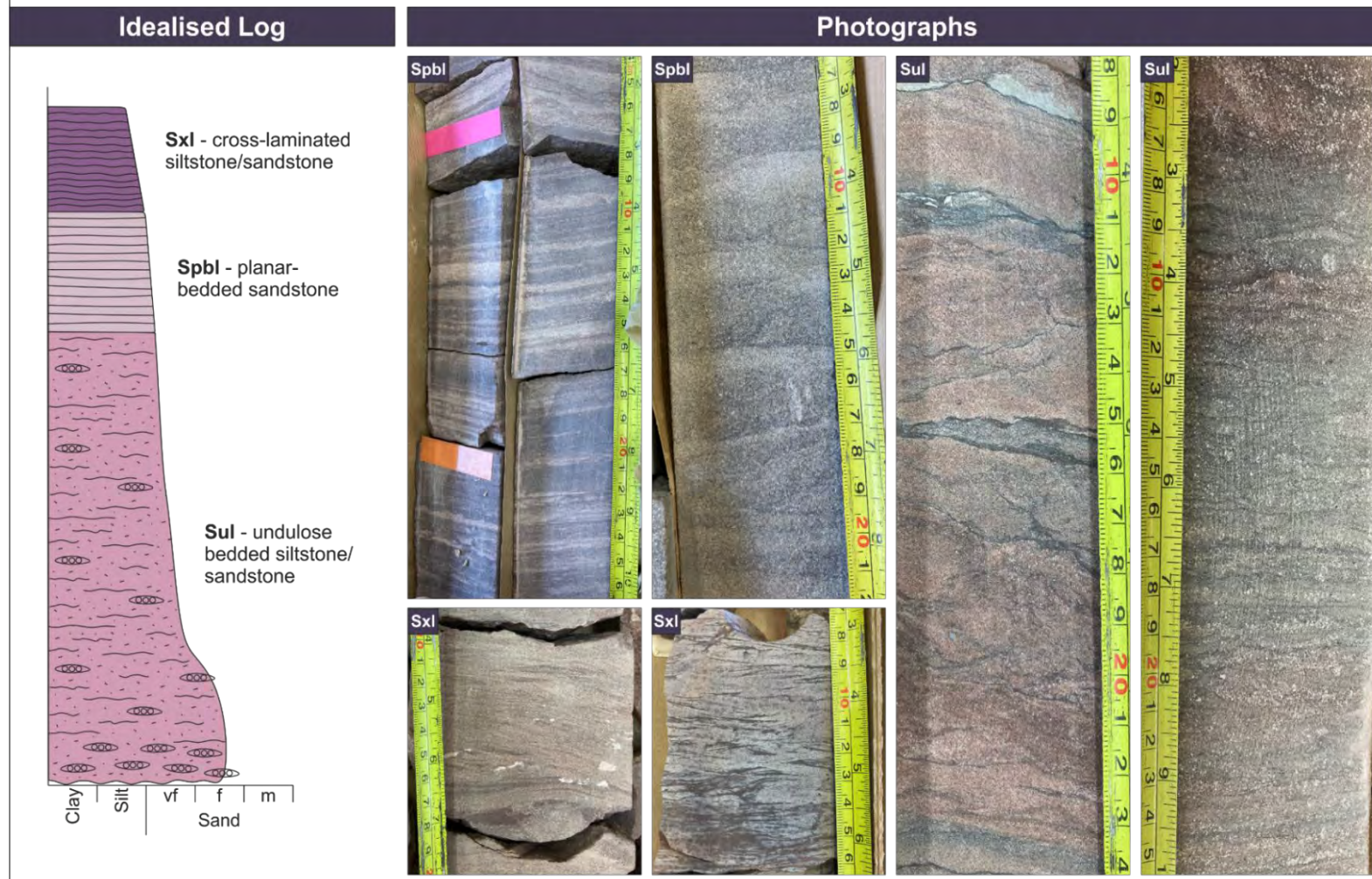


Figure 8.13. Summary panel of the lake margin association of the Lemna Sandstone with an idealised log and photographs of the internal facies.

8.5.10. Lake Centre

Facies associations of this type are characterised by structureless to crudely laminated to bedded, purple to brown, mudstones to fine-grained sandstones that are composed of sub-rounded, moderately sorted grains (Fig. 8.14). The structureless sandstones (**Sml**) and mudstones (**Ms**) range in thickness from 10 cm to 4.75 m and sporadically display convoluted laminations. The preserved thickness of the association ranges from 15 cm to 7.5 m.

Interpretation

Associations of this type represent the preserved deposits of a deeper lacustrine environment (George & Berry, 1993; Andrews & Hartley, 2015). The structureless mudstones indicate a dominantly low energy environment where sediment was deposited through suspension settling (Andrews & Hartley, 2015). The sporadic convoluted laminations represent minor grain-size changes resulting from the episodic discharge of sediment in a standing body of water (Moscariello, 2011).

8.5.11. Ephemeral Saline Lake/Mudflat

Facies associations of this type are characterised by millimetre to centimetre-scale crudely undulose laminated to bedded, purple to brown, mudstones to fine-grained sandstones that are composed of sub-rounded, moderately sorted grains (Fig. 8.15). Planar-laminations of alternating siltstones and very-fine-grained sandstones (**SpII**) with sporadic polygonal hummocks and bioturbation occur in up to 5 cm thick beds, whereas, the undulose laminated to bedded mudstones to fine-grained sandstones (**Steul**) and crudely bedded very-fine to fine-grained sandstones (**Seb**) occur in much larger units, up to 4 m thick and both contain sporadic coarser grained lenses with internal planar-laminations, evaporitic clasts up to 7 cm in diameter, soft sediment deformation and bioturbation. The preserved thickness of the association ranges from 50 cm to 19.5 m.

Lake Centre Association

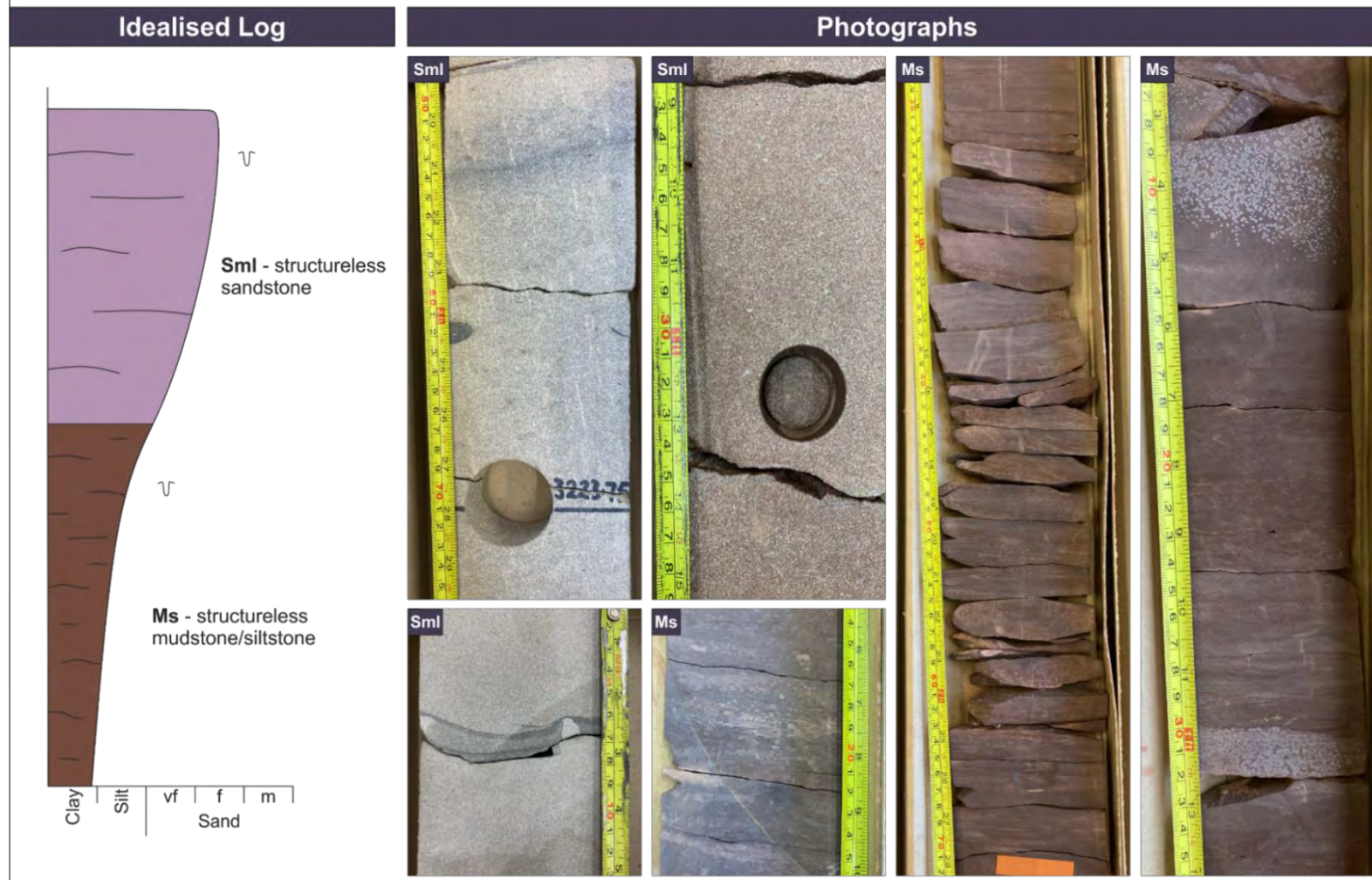


Figure 8.14. Summary panel of the lake centre association of the Leman Sandstone with an idealised log and photographs of the internal facies.

Ephemeral Saline Lake/Mudflat Association

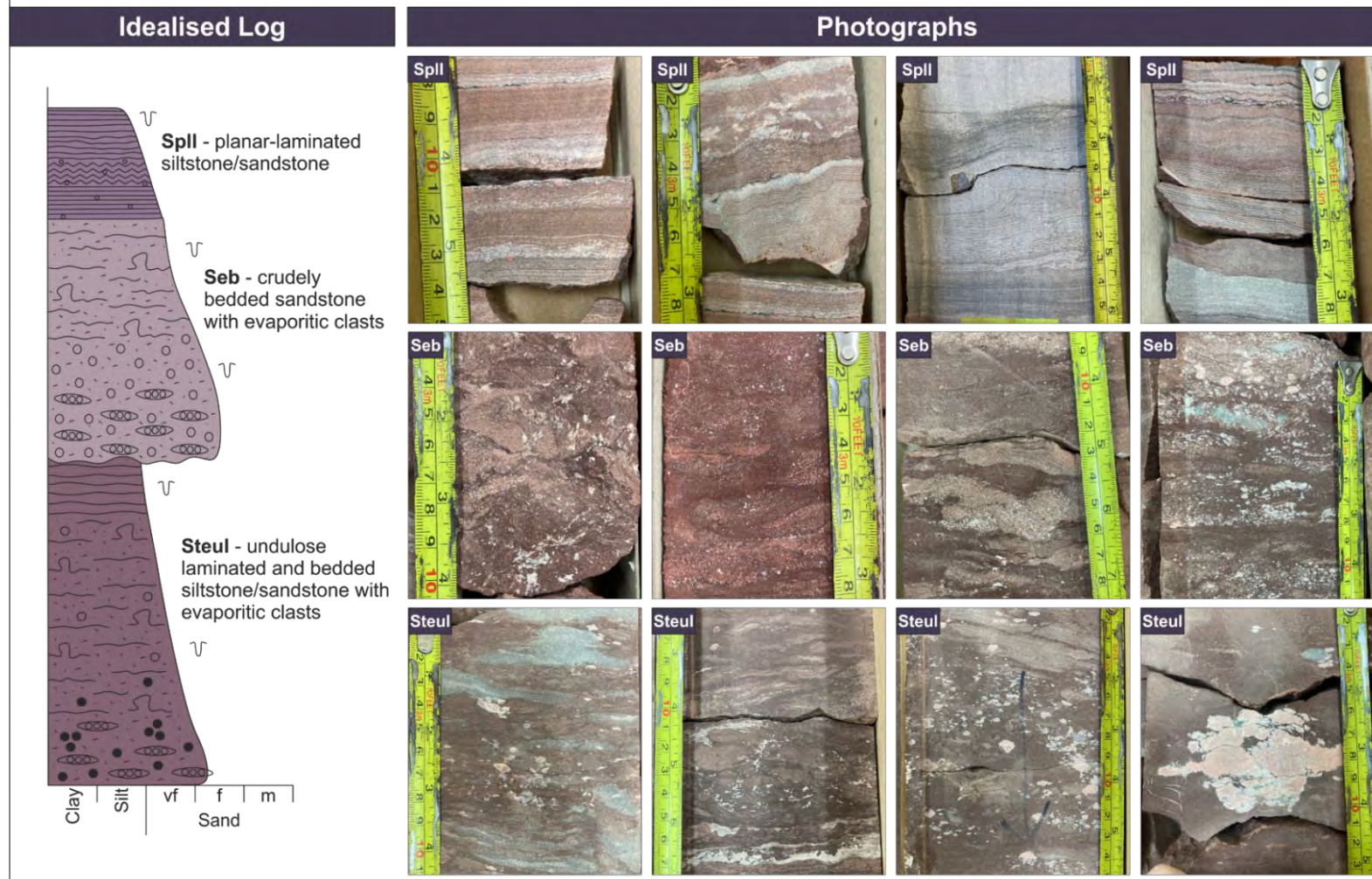


Figure 8.15. Summary panel of the ephemeral saline lake/mudflat association of the Lemna Sandstone with an idealised log and photographs of the internal facies.

Interpretation

Associations of this type represent the preserved deposits of saline mudflats and ephemeral saline lakes which formed from the evaporation and desiccation of previously more established lakes (*cf.* Pettigrew *et al.*, 2020; Pettigrew *et al.*, 2021). Parallel laminations of alternating siltstones and sandstones result from sediment binding by algal and microbial mats with laminations indicating shallow water to subaerial exposure and are commonly associated with saline mudflat environments in desert environments as the interaction between the salt flat and the groundwater provides sheltered habitats for microbial life (Van Dover, 2000; Reitner, 2011; McKay *et al.*, 2016; Pettigrew *et al.*, 2020; Pettigrew *et al.*, 2021). The undulose laminated to bedded mudstones to sandstones and crudely bedded sandstones with sporadic evaporitic clasts result from periodic sediment influx into saline stationary waters where there was subsequent precipitation of evaporites (Pettigrew *et al.*, 2020), with the mudstones and siltstones being deposited during calmer periods (Andrews & Hartley, 2015). Variations in ground water levels and circulation promote subsurface phreatic evaporite growth as random crystals or nodules (Smoot & Lowenstein, 1991; Boggs & Boggs, 2009; Warren, 2016; Pettigrew *et al.*, 2020; Pettigrew *et al.*, 2021).

8.6. Comparison to the Kayenta Formation

Outcrop analogues have long been used to further our understanding of the subsurface and provide valuable three-dimensional data for otherwise one-dimensional core datasets. Similarities between the Leman Sandstone and Kayenta Formations can be observed. To compare the two systems, channel, fluvial sheet and aeolian set thicknesses have been measured from both data sets (Fig. 8.16).

Channel, fluvial sheet and aeolian set thicknesses are much more varied within the Kayenta Formation (Fig. 8.16). Channel thicknesses range from 0.1 m to 6.4 m with an average thickness of 1.26 m, a median thickness of 1.0 m, and an interquartile range of 1.2 m (Fig. 8.16G). Fluvial sheet thicknesses range from 0.1 m to 5.8 m with an average thickness of 1.27 m, a median thickness of 1.0 m, and an

interquartile range of 1.1 m (Fig. 8.16G). Aeolian set thicknesses range from 0.2 m to 3.2 m with an average thickness of 0.97 m, a median thickness of 0.8 m, and an interquartile range of 1.0 m (Fig. 8.16G). Whereas the channel, fluvial sheet and aeolian set thicknesses of the Lemna Sandstone are all much lower than those of the Kayenta (Fig. 8.16). Channel thicknesses range from 0.05 m to 4.5 m with an average thickness of 0.39 m, a median thickness of 0.25 m, and an interquartile range of 0.34 m (Fig. 8.16G). Fluvial sheet thicknesses range from 0.05 m to 2.5 m with an average thickness of 0.38 m, a median thickness of 0.25 m, and an interquartile range of 0.35 m (Fig. 8.16G). Aeolian set thicknesses range from 0.05 m to 8.5 m with an average thickness of 0.58 m, a median thickness of 0.3 m, and an interquartile range of 0.45 m (Fig. 8.16G).

Key characteristic sedimentary structures of the Kayenta Formation (Chapter 4) can also be identified within core from the Lemna Sandstone, including mud-draping along foresets of fluvial elements, upper flow regime structures such as parallel laminated flat beds, debris-driven, matrix-supported conglomerates and armoured mudballs (Fig. 8.17). Equally, similarities between the aeolian-fluvial interactions can be observed, including the recycling of aeolian sediment within the fluvial system evidenced by the dominantly well-rounded and well sorted sand grains of fine to medium-grained distribution.

8.7. Depositional Model

The geobody data collected from the three-dimensional digital outcrop models of the Kayenta Formation were combined with the detailed sedimentological analysis on the Lemna Sandstone and Silverpit Formation to reconstruct the depositional environment and produce semi-quantified three-dimensional models (Fig. 8.18).

The depositional model for the Lemna Sandstone depicts a dominantly aeolian environment, with restricted fluvial corridors feeding a desert lake towards the north-northeast.

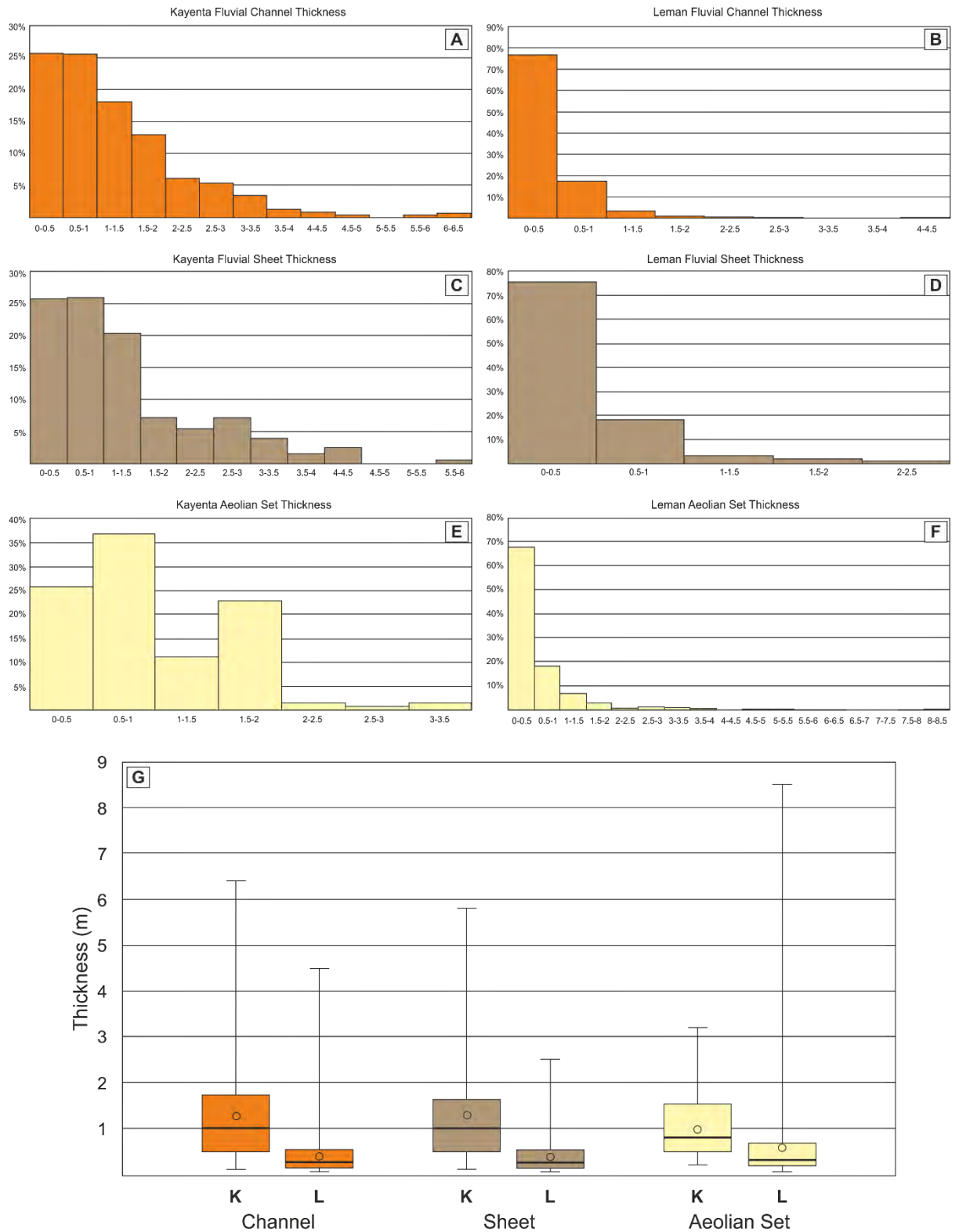


Figure 8.16. Comparison of channel, fluvial sheet and aeolian set thicknesses from the Kayenta Formation and Lemman Sandstone including (A-F) Histogram plots of thicknesses and (G) Box and whisker plots illustrating the median, average, interquartile range and outliers.

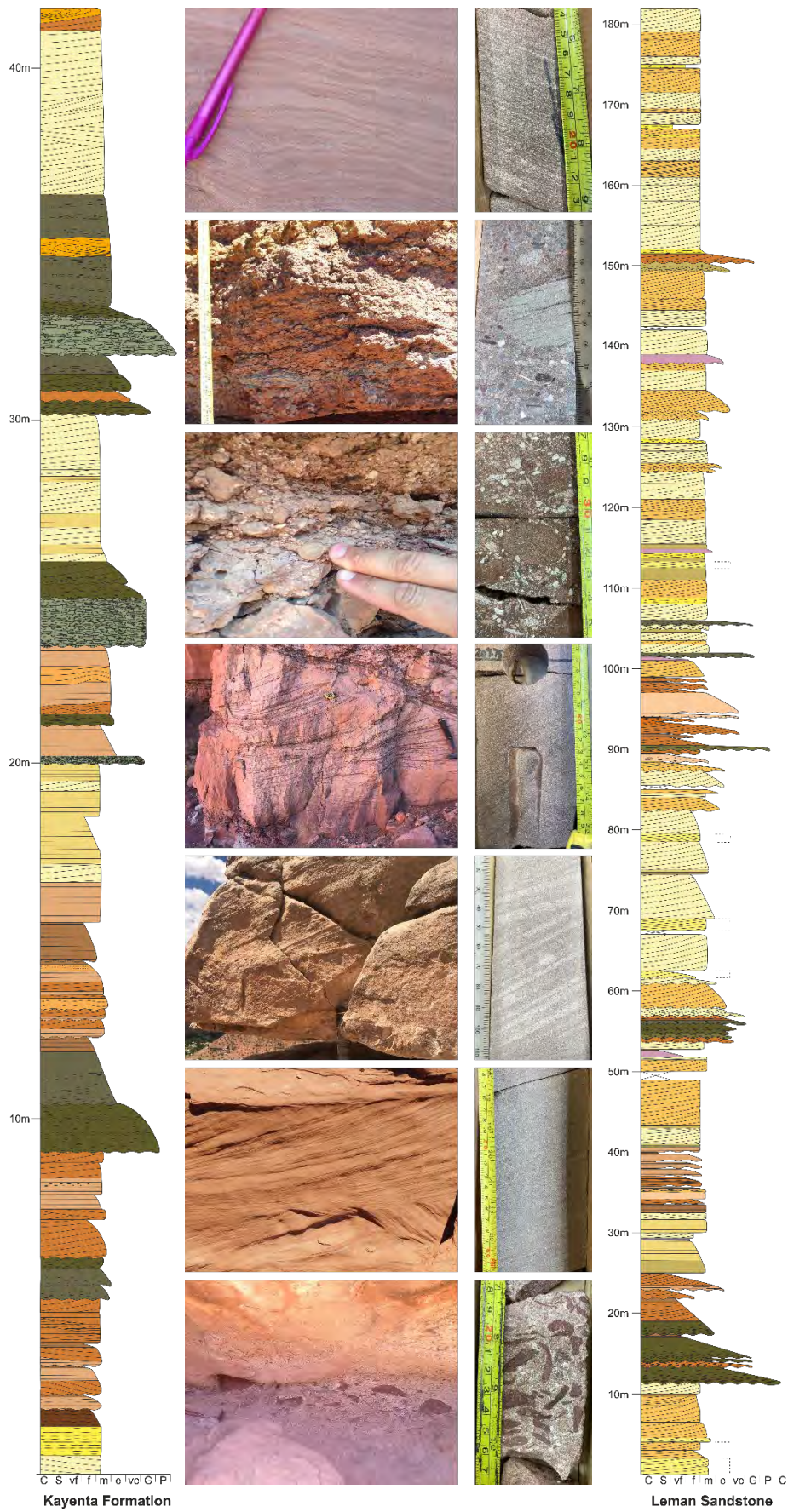


Figure 8.17. Comparison of sedimentary logs from the Kayenta Formation and Lemman Sandstone including photographs of key sedimentary structures.

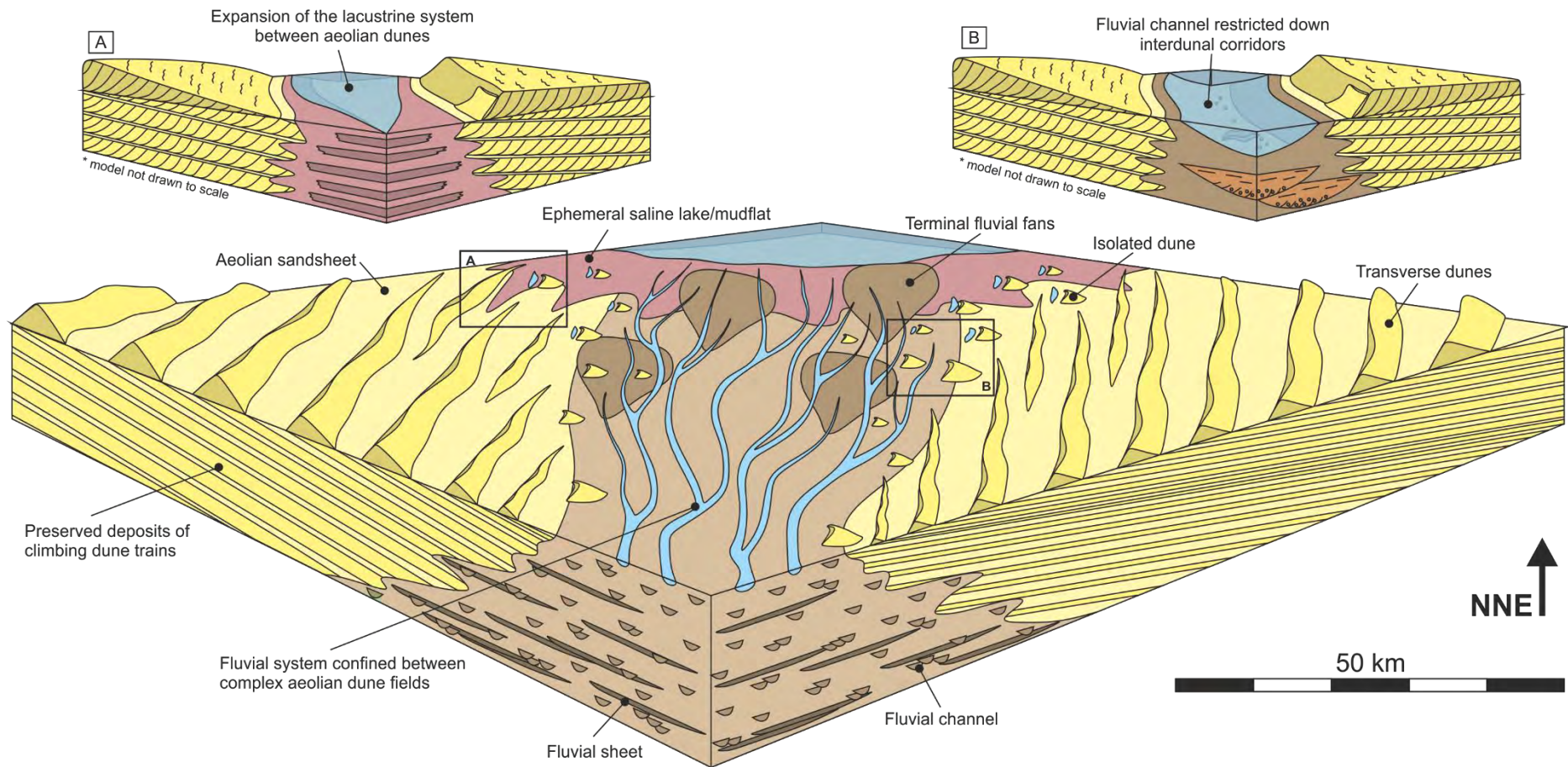


Figure 8.18. Large-scale depositional model of the Lemna Sandstone with two smaller-scale facies models depicting key sedimentary interactions. (A) Facies model depicting the sedimentary interactions between aeolian and lacustrine systems as the lake and saline mudflat expand into the dune field. (B) Facies model depicting the sedimentary interactions between aeolian and fluvial system as the rivers are confined down interdune corridors.

Fluvial deposition is much more prevalent within the lower portions of the Lemna compared to the upper portions, with fluvial architecture dominated by cross-bedded to structureless channels and sheets with conglomeratic erosional basal bounding surfaces. As the fluvial deposition diminishes, aeolian deposition takes over, where the aeolian deposits are initially dominated by sandsheet associations before the development of aeolian duneforms.

Within the lower half of the Lemna deposition, three to four cycles of fluvial deposition can be observed before the drying of the system and deposition of aeolian sediments. These rivers ultimately fed the lacustrine system towards the north and the repeated cycles of sediment input resulted in the expansion and contraction of the desert lake. The last major fluvial deposition occurs approximately halfway through the Lemna Sandstone due to the rejuvenation of the fluvial source terrain (George & Berry, 1993). From this point onwards aeolian deposition dominated within the proximal region, and lacustrine deposition dominated within distal region. Minor fluvial deposits are still observed between the deposits of aeolian dunes, as the fluvial system was funnelled through interdune corridors towards the desert lake (Fig. 8.18). Small scale cycles of lake expansion and contraction are also observed, with the fringes of the desert lake encroaching on the edge of the dune field (Fig. 8.18).

Aeolian deposition is concentrated in the eastern and western portions of the study area; either side of the fluvial corridor, with the preserved deposits of cross-bedded aeolian duneforms dominating the successions. The aeolian dune elements are composed of predominantly grainflow strata and couplets of grainfall/grainflow strata, suggesting the dune morphology was likely transverse. However, sporadic occurrences of thick units of the wind-ripple strata possibly indicate that some duneforms may have had a linear geomorphology.

Lacustrine deposition is concentrated to the north/north-eastern region of the study area, however the deposits extend relatively far south, particularly within the eastern portion of the study area, where extensive, thick lacustrine deposits are observed halfway down the border between quadrant 48/49. The lacustrine sediments are predominantly sandy in composition due to the interaction with

the aeolian system, preventing the carbonate development, however, during more arid conditions, the lake contracts and subsequent evaporites are precipitated within the lake margins.

In general, the deposition on the Leman and Silverpit formations indicate an overall progradation of the lacustrine system and retrogradation of the fluvial system through time. Leman deposition is first dominated by relatively short lived arid aeolian conditions before the expansion and development of an extensive fluvial corridor. Fluvial deposition gradually diminishes before aeolian deposition dominates within the proximal region and lacustrine dominates within the distal region.

8.8. Summary

The deposits of the Lower Permian Leman Sandstone and lateral equivalent Silverpit Formation have been studied across the expanse of quadrants 43, 44, 48 and 49 of the Southern North Sea. Twenty-six facies have been identified based upon lithology and sedimentary structures and are summarised in Table 8.1. The facies have then been grouped together to form eleven facies associations: aeolian dune, aeolian dune plinth, aeolian sandsheet, aeolian dry interdune, aeolian damp/wet interdune, fluvial channel, fluvial sheet, overbank, lake margin, lake centre and ephemeral saline lake/mudflat.

Comparisons with the outcrop analogue of the Kayenta Formation have been drawn, highlighting the similarities in sedimentology and interactions between the competing aeolian and fluvial environments. Geobody data from the Kayenta Formation coupled with the sedimentological analysis of the Leman and Silverpit formations have been used to build a semi-quantified depositional model for the Leman.

Chapter Nine discusses the applicability of outcrop analogues for subsurface models, along with the applicability of digital outcrop models and the data that can be collected from them. The results and interpretations of the sedimentology, spatial variations, and temporal variations of the Kayenta Formation are also discussed.

Chapter 9: Discussion

This chapter summarises and critically evaluates the results and interpretations within the preceding chapters. In particular, this chapter discusses: 1) the sedimentology of ephemeral fluvial systems and their published depositional models; 2) the spatial variations of the Kayenta Formation, possible depositional controls and probable larger scale depositional architecture; 3) the temporal variations of the Kayenta Formation and possible depositional controls; 4) the applicability of digital outcrop models and the subsequent data obtained; and finally, 5) the applicability to subsurface data sets like the Leman Sandstone of the Southern North Sea.

9.1. Sedimentology of the Kayenta Formation

Despite several detailed studies of ephemeral fluvial systems and their sedimentology, three-dimensional depositional facies models depicting their complex sedimentology, their lateral and vertical variations of architectural elements, and the nature of their interactions with competing depositional settings are less well documented compared to those for their meandering and braided fluvial counterparts. Typically, published models for ephemeral systems depict a braid plain in a distal setting with shallow, poorly defined, intercalated channels, laminated sandsheets and rare to no preservation of overbank sediments (e.g. Miall, 1985). Some models depict an abundance of downstream accretion (Colombera *et al.*, 2013; Batezelli *et al.*, 2019) in addition to those features outlined above, and recent advancements have focused more on quantification of models at multiple scales (Colombera *et al.*, 2013; Colombera & Mountney, 2019).

This study interprets the Kayenta Formation as the preserved deposits of an ephemeral braided fluvial system with minor perennial and aeolian influxes within an arid to semi-arid climate. The most prominent preserved deposits of the system are sandy, bedload-dominated, multi-lateral sheet-like

depositional elements with minor channelised scours (Chapter 7, Fig. 7.6). Minimal floodplain/overbank elements are preserved, suggesting the fluvial system was highly cannibalistic as clasts composed of overbank facies are typical features within channel, sheet-like and lateral accretion architectural elements (Chapter 7, Fig. 7.6) and provide evidence of stabilised overbank being reworked (North & Taylor, 1996; Hassan *et al.*, 2018).

The dominance of upper flow regime deposits implies high discharge events were most abundant but preservation of many of these features implies highly variable discharge; conditions attested to by frequent alternations in preserved strata between deposits of upper and lower flow regime conditions. Fluctuations in sediment supply and the interaction with the aeolian system plays an important role in the preserved sedimentology. Very coarse sand to granule size grains lining foresets and suppressing bedform development prove the only major grainsize change, with the majority of the fluvial sediment composed of fine to medium-grained, aeolian sourced sediment (Chapter 6, Fig. 6.9). Consequently, in some channel elements, bedforms are rare due to the high concentration of sediment within the flow. Other examples of high sediment load structures include recumbent cross-bedding (Chapter 7, Fig. 7.6) that are formed when the tops of bedforms are ripped over in the direction of flow in a concentrated solute that preserves the foresets in a relatively coherent state (Allen & Banks, 1972).

The model derived from the Kayenta Formation presented here represents an ephemeral sandy braided fluvial model for an arid to semi-arid, aeolian-influenced setting. It describes an ephemeral fluvial setting that lacks significant fines and in which typical fluvial facies, comprising well-rounded, well-sorted, reworked aeolian sediment, stack into vertically and horizontally amalgamated extensive sandstone bodies with high reservoir or aquifer potential. The proposed model shows differences in architecture and composition from previously published models, including a larger proportion of channel and accretionary elements with a lower proportion of sheets, as well as much smaller thickness-to-width ratios of both channel and sheet elements. On a facies-scale the published models also depict a much lower percentage of upper flow regime and high sediment load facies such as

parallel-laminated and structureless sandstones than observed within the Kayenta. However, when compared to quantitative studies of modern ephemeral fluvial systems (Colombera & Mountney, 2019), a dominance of upper flow regime flat beds and structureless sandstones is observed, similar to that of the preserved deposits of the Kayenta Formation.

Modern ephemeral fluvial systems also tend to display large proportions of mud or silt grade and/or gravel grade facies (e.g. Reid *et al.*, 1995; Billi, 2007; Tooth *et al.*, 2013), and studies of preserved ancient examples show a similar dominance (e.g. Olsen, 1989; Dreyer, 1993; Long, 2017). Whereas the Kayenta Formation is much sandier in composition due to the interaction with the competing coeval aeolian system.

Overall, the model derived from the study of the Kayenta Formation provides useful generic geometrical and compositional details for the characterisation of analogous settings.

9.2. Spatial variations of the Kayenta Formation

Regional analysis of the Kayenta Formation exposed across the Colorado Plateau identifies several spatial variations in sedimentary architecture and therefore provides grounding for analysis of the complex controls upon the depositional system.

The high degree of channel and sheet amalgamation and connectivity within proximal region suggests that the fluvial system was highly cannibalistic (North & Taylor, 1996; Hassan *et al.*, 2018; Priddy & Clarke, 2020) with a high sediment supply (Weissman *et al.*, 2013; Owen *et al.*, 2015). The decrease in channel and sheet amalgamation, increase in the proportion of overbank, and overall grain-size reduction downstream can be attributed to a downstream decrease in energy and a downstream decrease in the river's carrying capacity as a result of lateral expansion of the river system, channel bifurcation and high rates of evapotranspiration and infiltration into the dry substrate (Nichols & Fisher, 2007; Weissmann *et al.*, 2010; 2013; Sutfin *et al.*, 2014; Owen *et al.*, 2015) (Chapter 7, Fig. 7.8). The abundance of preserved channel depositional elements within the distal region may also be the result of preferential preservation and the function of channel belt avulsion, resulting in the

preservation of channel elements at the same stratigraphical level that are not time equivalent (North & Warwick, 2007).

However, it must be noted that a decrease in amalgamation of channel and compound sheet elements, coupled with an overall increase in the total fluvial sediment thickness observed at each locality, could also be attributed to increased subsidence and the generation of additional accommodation space, coevally with deposition of the Kayenta sediments, as in the distal region where deposition of the Kayenta correlates with the location of the Zuni Sag (Chapter 2, Fig. 2.14) (Blakey, 1994). It is also possible that the increase in cumulative fluvial sediment thickness within the distal section may also be attributed to a secondary, axial fluvial system, sourced from the Mogollon Highlands in the Cordilleran Magmatic Arc (Luttrell, 1993; Hassan *et al.*, 2018) feeding additional sediment volume into the Zuni Sag, although ultimately the thickness of sediment preserved is probably controlled by developing accommodation space over any other factor.

9.2.1. Spatial variations in architectural elements

Architectural element analysis across the expanse of Kayenta deposition shows a generally consistent percentage of fluvial channel and sheet-like elements, with an increase in the proportion of overbank sediments and decrease in accretionary elements towards the southwest (Fig. 9.1). The proximal region around Moab, UT, consists of a series of laterally and vertically amalgamated channel-fill complexes with abundant stacked sandy sheet-like deposits and very little overbank (Chapter 4, Fig. 4.6). The medial region around Comb Ridge, UT, illustrates a decrease in the lateral and vertical amalgamation of channels, but continues to display an abundance of stacked sheet-like deposits and minimal overbank fines (Chapter 4, Fig. 4.7). The decreasing trend in the amalgamation of channels continues into the distal region around Kanab, UT, where the amalgamation of sheet-like deposits also decreases, as they become more isolated within overbank fines (Chapter 4, Fig. 4.8). The regional sedimentology indicates a normal waning trend from proximal to distal settings with a decrease in flow

velocity and grainsize distribution that is similar to that of a distributive fluvial system (Blakey, 1994; North & Taylor, 1996).

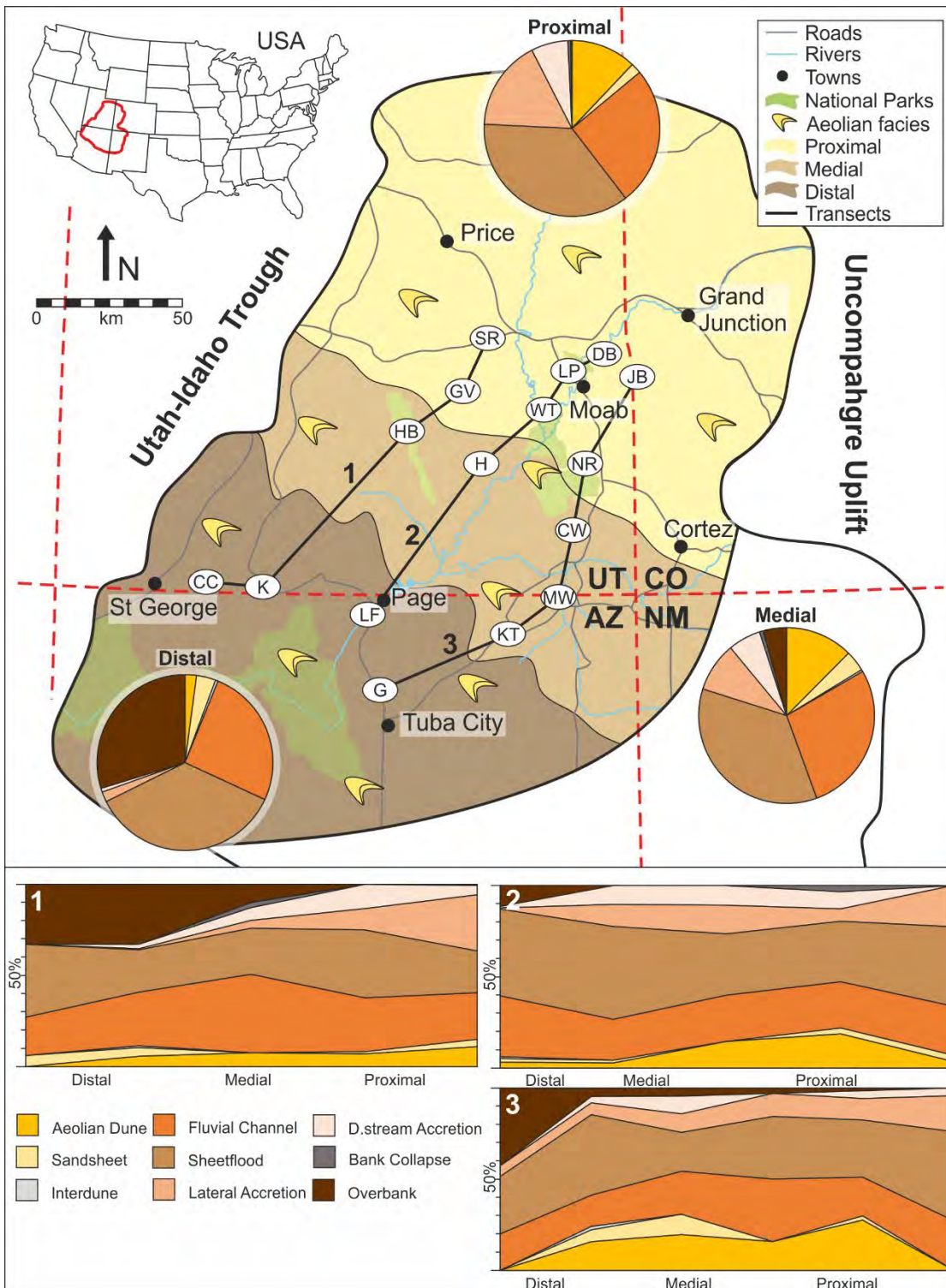


Figure 9.1. Spatial distribution of architectural elements across proximal, medial and distal settings within Kayenta Formation, with three transects through logged localities. Fluvial channel and sheet-like elements remain fairly constant across the system, accretionary elements are most prevalent within the proximal and medial regions, whereas overbank elements are most prevalent within the distal region.

Palaeocurrent analysis shows a general palaeoflow to the south-west/west and towards the Utah-Idaho Trough, where sediment accumulation also thickens to over 300 m. However, within the distal setting of this fluvial system large beds of polymictic conglomerates have been observed with palaeocurrents indicating flow towards the west and northwest, suggesting a second fluvial system was also present (Luttrell, 1993). Palaeocurrent measurements within this region are also comparatively more dispersed, with the average palaeoflow towards the northwest and a dispersion from west-southwest to north.

The distributions of aeolian architectural elements remain fairly constant across the plateau (Fig. 9.1). Within the proximal region, smaller isolated dune elements (between 0.5–1 m thickness) occur in abundance. The aeolian dunes generally increase in size but decrease in abundance with proximity to the distal setting, eventually resulting in two large aeolian tongues reaching up to 100 m in thickness within the distal region around Kanab. The fluctuations in aeolian dune sizes and abundances suggests possible expansion and contraction of a dune field located to the south-west of the Colorado Plateau, perhaps as a consequence of the developing fluvial system.

9.2.2. Spatial variations in depositional elements

Amalgamated sandstone-dominated channel-fill depositional elements display downstream fluvial trends typical of fluvial systems including a decrease in their abundance and decrease in their constituent grain size downstream. They can be attributed to a decrease in energy downstream as a result of high rates of evapotranspiration and infiltration into the dry substrate and channel bifurcation (Nichols & Fisher, 2007; Weissmann *et al.*, 2010; 2013; Sutfin *et al.*, 2014; Owen *et al.*, 2015) or avulsion of the channel belt (North & Warwick, 2007).

A relatively flat linear trend line for the percentage of isolated sandstone-dominated channel-fill depositional elements suggests that there is no downstream control on the presence of this element (Chapter 6, Fig. 6.3D). The very slightly higher prevalence in this element downstream is of little significance and may be due simply to the diminishing abundance of other channel-fill elements

downstream. The increase in the average thicknesses of the isolated sandstone-dominated channel-fill depositional elements (Chapter 6, Fig. 6.4C & D) downstream is probably the result of increased preservation potential within the distal setting, where full thicknesses of the isolated channels are more likely to be preserved.

Isolated gravel-dominated channel-fill depositional elements comprise only a small proportion of the fluvial succession with distance downstream (Chapter 6, Fig. 6.3E & F). However, the grain size of the isolated gravel-dominated channel-fill depositional elements increases downstream; a trend that is contrary to that intuitively expected for any waning fluvial system. This observation may be due directly to the secondary source of coarse-grained Kayenta fluvial sediment in south-west Utah (Luttrell, 1993) and it is something that would require in-depth petrographical and provenance studies to examine further.

Analysis of the compound sandstone-dominated fluvial sheet depositional elements reveal relatively constant percentages of elements (Chapter 6, Fig. 6.3G & H) and average thicknesses downstream (Chapter 6, Fig. 6.4G & H). The flat linear trend lines for these characteristics suggests that there is no downstream control on the presence of this element, and the occasional more prevalent appearance downstream may be due to the interaction with the secondary fluvial system within the distal region.

The overbank depositional elements display the strongest trends within the data; an increase in the percentage (Chapter 6, Fig. 6.3I & J) and thickness (Chapter 6, Fig. 6.4I & J) of overbank downstream and a decrease in grain size downstream (Chapter 6, Fig. 6.5I & J), all of which are typical for waning fluvial system. These trends are a result of the decrease in energy and the river's carrying capacity downstream as a result of lateral expansion of the river system, channel bifurcation and high rates of evapotranspiration and infiltration into the dry substrate (Nichols & Fisher, 2007; Weissmann *et al.*, 2010; 2013; Sutfin *et al.*, 2014; Owen *et al.*, 2015) or avulsion of the channel belt (North & Warwick, 2007).

The sand-dominated fluvial depositional elements (amalgamated channel, isolated channel and compound sheet elements) display no significant trends in grain-size distribution downstream. Each of these elements is dominated by fine to medium-grained sandstone of aeolian origin that has been blown off coeval dune fields, reworked and transported by the fluvial system (Chapter 6, Section 6.8). Coeval aeolian systems are a typical feature of many modern arid ephemeral fluvial basins (Veiga *et al.*, 2002; Al-Masrahy & Mountney, 2015; Formolo Ferronato *et al.*, 2019; Reis *et al.*, 2019; Coronel *et al.*, 2020) and many preserved examples of arid fluvial strata contain significant proportions of aeolian sediment (Langford, 1989; Clarke & Rendell, 1998; Bullard & Livingstone, 2002, Field *et al.*, 2009). This relationship could be recognised as a characteristic of dryland ephemeral fluvial systems.

9.2.3. Comparison of spatial trends to previously published models

Analysis of the downstream trends of the dryland ephemeral fluvial Kayenta Formation illustrates a number of characteristics that are similar to those displayed by typical terminal fluvial fans and some distributive fluvial systems described by Hampton & Horton (2007); Nichols & Fisher (2007); Fisher *et al.*, (2008); Cain & Mountney (2009); Hartley *et al.*, (2010); Weissmann *et al.*, (2010; 2013), and Owen *et al.*, (2015). The Kayenta fluvial sediments display a clear lack of confinement of the fluvial system sourced from the Uncompahgre Uplift, illustrating very little evidence of significant tributary inputs, until the intersection with the axial fluvial system sourced from the Cordilleran Magmatic Arc (Fig. 9.2). A downstream decrease in amalgamation of channels and compound sheets (Chapter 6, Fig. 6.1), a small decrease in grain size downstream (Chapter 6, Fig. 6.5I & J) and an overall increase in the percentage of overbank depositional elements with distance downstream (Chapter 6, Fig. 6.3I & J) are also observed, all of which are characteristics that are consistent with previously published models (Fig. 9.3) (Nichols & Fisher, 2007; Hartley *et al.*, 2010; Weissmann *et al.*, 2010; 2013; Owen *et al.*, 2015). Consequently, a downstream decrease in both energy and channel bifurcation, accompanied by high rates of evapotranspiration and infiltration of water into the substrate are considered the probable mechanisms that explain these trends in the Kayenta ephemeral fluvial sediments, just as they do in these models (Nichols & Fisher, 2007; Weissmann *et al.*, 2010; 2013; Sutfin *et al.*, 2014).

Conversely, there are several downstream relationships displayed by the Kayenta fluvial sediments that do not fit with published models. In the Kayenta, the total thicknesses of the fluvial sediment increases with distance downstream, the thicknesses of the channel-fill and sheet depositional elements display no significant relationships to distance downstream, and the channel-fill depositional elements downstream display no significant variation in average grain size with distance downstream (Fig. 9.3) (cf. Friend & Moody-Stuart, 1972; Friend, 1978; Nichols, 1987; Hirst, 1991; Stanistreet & McCarthy, 1993; Nichols & Fisher, 2007; Cain & Mountney, 2009; Hartley *et al.*, 2010; Weissmann *et al.*, 2010; 2013; Owen *et al.*, 2015).

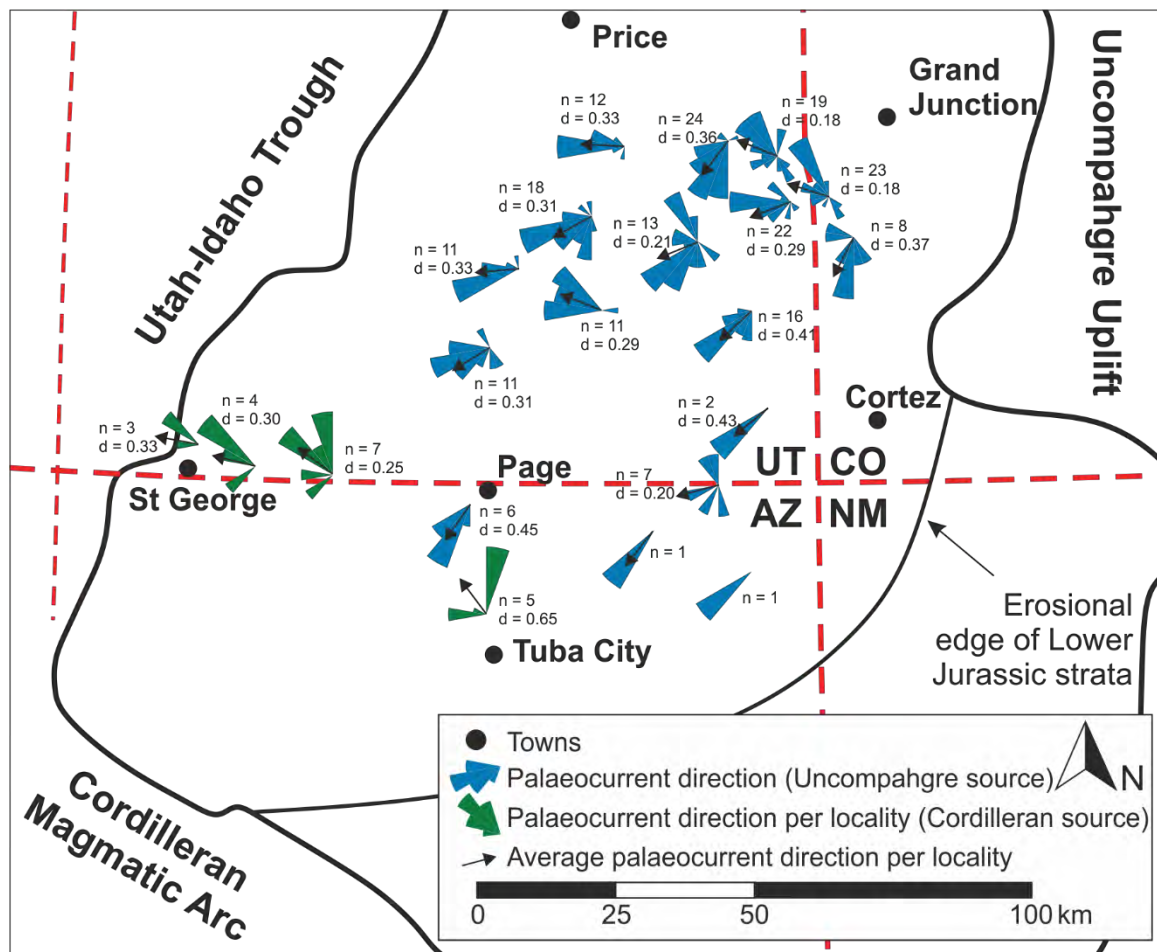


Figure 9.2. Palaeocurrent measurements of the fluvial sediment at each locality depicted by rose diagrams coloured by sediment source. The black arrows indicate the average palaeocurrent direction per locality along with the number of measurements and degree of dispersion per locality.

Some of these anomalous trends may be attributable to case-specific external factors – an increase in total thicknesses of fluvial sediment downstream may be attributed to the increase in accommodation

space provided by the Zuni Sag and Utah-Idaho trough (Blakey, 2008), and relatively constant thicknesses of channel-fill and sheet depositional elements with distance downstream may be attributed to the influence of the secondary fluvial source (Luttrell, 1993) – but, equally, external factors do not explain characteristics such as the channel-fill depositional elements that display no significant variation in average grain size with distance downstream. This relationship may be the consequence of the interaction between a fluvial system and an ever-present coeval aeolian system throughout the fluvial course. Significant volumes of sediment derived locally from the aeolian system and fluvially reworked, may limit the downstream grain-size distribution of the fluvial deposits. Given that dryland ephemeral fluvial systems are typified by their close spatial and temporal links to aeolian systems, it is possible that some of these trends are typical of drylands ephemeral fluvial systems in general.

9.3. Temporal variations of the Kayenta Formation

Climatic variations play a key role within arid continental settings, controlling the preserved architecture, facies distributions and stratigraphy of successions. The temporal interactions between the fluvial and aeolian systems occur as a result of climatic variations and depict the sedimentological change across the systems as the climate becomes wetter to establish a fluvial system or dries to promote expansion of the aeolian dune field.

Analysis of the regional logged sections revealed an overall decrease in channel body thickness with increasing height within the successions which is thought to represent an overall regression of the fluvial system through time (Chapter 6, Section 6.6). Variations within this overall trend are also observed. Peaks within the channel body thicknesses could represent cycles of transgression and regression within the fluvial system and due to the coeval competing aeolian environment, the transgression and regression of the fluvial system may also relate to the contraction and expansion of the competing aeolian dune field (*cf.* Cain & Mountney, 2009).

These trends also coincide with the overall change in dominant depositional environment through time. The lower Kayenta is a dominantly ephemeral fluvial setting with most deposition the result of high-energy unconfined flows and minor large scour events from flash-flood discharge, resulting in thick amalgamated sandstone deposits within the lower sections of the succession.

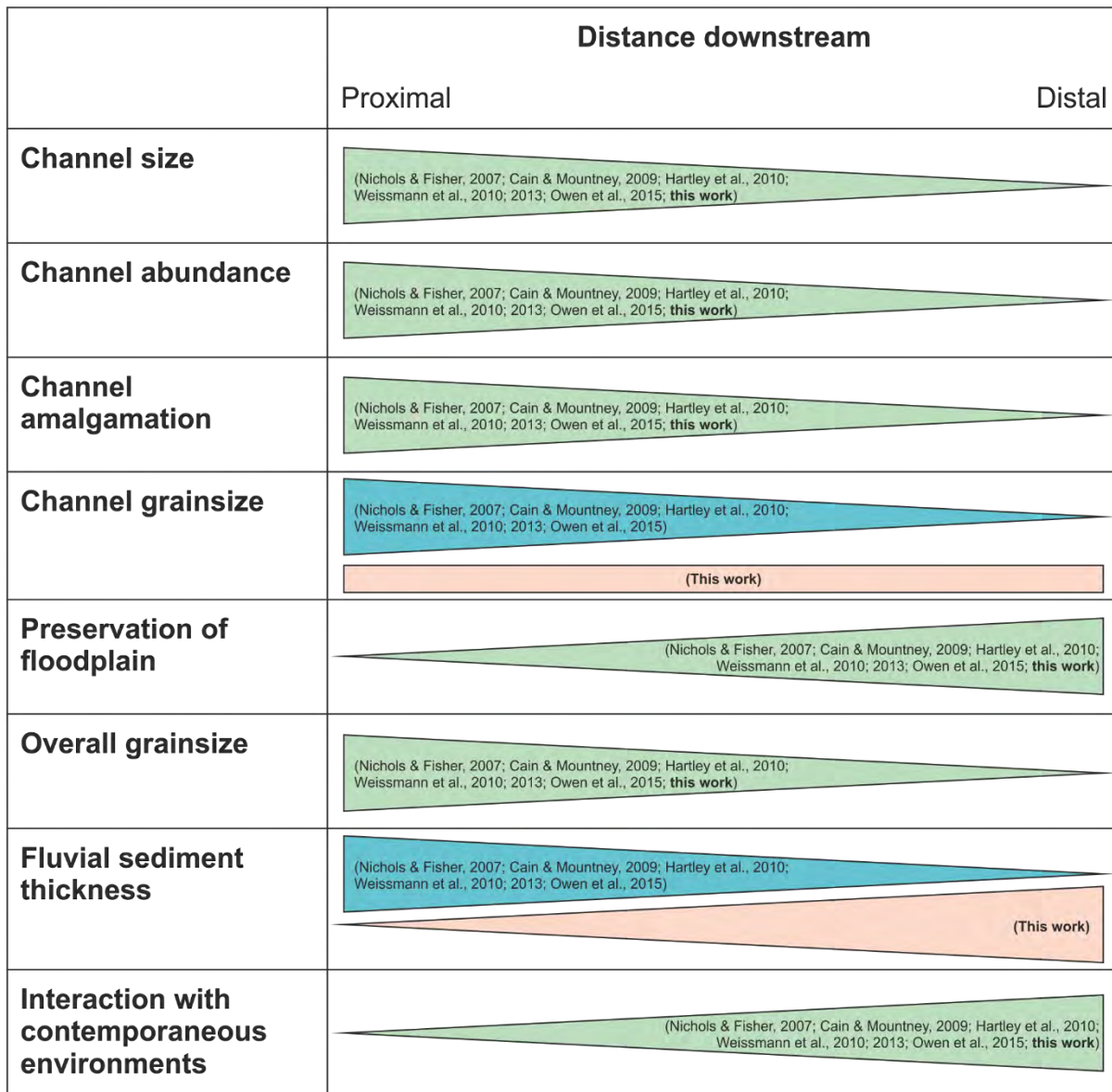


Figure 9.3. Comparison of key characteristics of a distributive fluvial system. Triangles represent whether a key characteristic increases or decreases downstream and are coloured by similarities and differences in findings from previously published literature.

In the middle section of the Kayenta, a transition from dominantly ephemeral to dominantly braided fluvial deposits is observed, marked by the onset of large laterally extensive accretionary elements,

before sedimentation switches back to dominantly ephemeral deposition. However, within the upper section of the Kayenta, sediments of the ephemeral system intertongue with the aeolian deposits of the transitional units of the Navajo Formation. This interaction alters the sedimentology observed within the ephemeral system as the ephemeral fluvial deposition now becomes confined to interdunal corridors within the aeolian dune field, resulting in the increase in isolated sandstone-dominated channel-fill depositional elements in the upper parts of the successions. These intertonguing events could be the reason behind the rapid changes in channel body thicknesses before the aeolian system dominates and the fluvial system dries out.

Variations within the overall regressive trend may also be the result of localised changes in sediment supply, discharge regime, avulsion, and subsidence differences (e.g. Shanley & McCabe, 1994; Posamentier & Allen, 1999; Holbrook *et al.*, 2006, Owen *et al.*, 2019; Martin *et al.*, 2021).

9.4. Digital outcrop models

Traditional data collection within outcrop analogues includes one-dimensional sedimentary logging and two-dimensional panel drawings, both of which can vastly under or overestimate the geometries and architectures of the system. One-dimensional sedimentological logs through the outcrop can often result in unrepresentative architectural element geometries, relative proportions and distributions of the elements and while the two-dimensional photo panels depict architectural and depositional element geometries and relative spatial distributions of these sedimentary elements, they are highly interpretative, time-consuming to produce and provide no real quantifiable three-dimensional measurements. The three-dimensional geometries of the outcrop are flattened to a two-dimensional plane and spatial distances are distorted. Consequently, measurements of architectural and depositional element geometries from these images are typically biased. In particular, width to depth ratios of fluvial elements are often overestimated because of the orientation of the outcrop face, with respect to palaeocurrent direction (see Pringle *et al.*, 2010). Fluvial geobodies can also be measured in

the field along the outcrop face, however, this is subject to accessibility and limits the number of measurements that can be collected.

With recent advancements in technology, digital outcrop models (DOMs) are now relatively simple to generate, and these limitations can be overcome using photogrammetric techniques and 3D geological visualisation/interpretation software (Enge *et al.*, 2007; Hodgetts, 2013; Schmitz *et al.*, 2014). Many geological features, including geobodies representing architectural and depositional elements, can be mapped using 3D polylines extruded through the DOMs or point clouds as surfaces. Orientation data (dip/azimuth) can be derived from these, and with the integration of palaeocurrent measurements, architectural element dimensions can be corrected for respective outcrop orientations. The digital outcrop models also allow for the interpretation of much larger datasets, thus making results statistically significant (Hodgetts, 2013).

The data presented in Chapter Seven demonstrate that thickness data derived from one-dimensional logs alone underestimate the average thickness of both sheetflood and channel architectural elements in the Kayenta Formation by more than half. The standard deviations, indicating the variability of architectural element thicknesses for both these elements, are also seriously underestimated by a one-dimensional log-based analysis. Whereas the width and thickness measurements of sheetflood and channel architectural elements depicted on two-dimensional photo panels overestimate the element dimensions by up to a third in comparison to the data collected from the three-dimensional digital outcrop models, due to the fact the orientation of the outcrop face, with respect to palaeocurrent direction cannot be visualised in three-dimensions (Pringle *et al.*, 2010).

Therefore, digital outcrop models of three-dimensional, spatially extensive outcrop provide a useful means of obtaining reliable statistical data on element dimensions, geometries, and distributions for incorporation into subsurface reservoir modelling workflows.

9.5. Application to the Leman Sandstone

Outcrop analogues are a well-used, valuable technique in geology that have played a vital role in improving understanding of subsurface reservoir geometries and architectures, as they provide geological input with which to condition static models (Pringle *et al.*, 2006; Howell *et al.*, 2014).

However, no two depositional systems are identical, and therefore there are no outcrop analogues that would be the perfect fit for the subsurface study (Howell *et al.*, 2014). Subsequently finding a suitable outcrop analogue should be based upon the aspects of the depositional system the user wishes to understand (Howell *et al.*, 2014). With the case of the outcrop analogue of the Kayenta Formation, the spatial variations of the fluvial system, along with the interaction of the competing, coeval aeolian environment were the focus of the study.

Several comparisons can be drawn between the Leman Sandstone and Kayenta Formation. Similar sedimentological features are observed between the fluvial-aeolian dominant sections of the Leman and the Kayenta, including mud-draping along foresets of fluvial elements, upper flow regime structures such as parallel laminated flat beds, debris-driven, matrix-supported conglomerates and armoured mudballs (Chapter 8, Fig. 8.17) (Priddy & Clarke, 2020). Equally, similarities between the aeolian-fluvial interactions can be observed, including the recycling of aeolian sediment within the fluvial system evidenced by the dominantly well-rounded and well sorted sand grains of fine to medium-grained distribution. Recycling of the fluvial sediment within the aeolian system is also observed and picked out by the gradual change in sediment colour, with dominantly red fluvial sandstones and grey aeolian sandstones.

The average channel and fluvial sheet thicknesses of the Leman Sandstone are roughly a third of the thicknesses of the same elements within the Kayenta and the median channel and fluvial sheet thicknesses are approximately a quarter of those within the Kayenta. The average aeolian set thickness of the Leman is roughly 28% smaller than the average measured within the Kayenta and the median

value approximately 60% smaller than the median measured within the Kayenta (Chapter 8, Section 8.6).

The differences between the thickness values for the Kayenta and Lemman could be due to several factors: general differences within the sedimentary environment; including tectonics, subsidence, avulsion and sediment supply, and differences in compaction and diagenesis. Both the Kayenta and Lemman were deposited in arid to semi-arid environments where ephemeral fluvial systems and aeolian deserts coevally interacted. However, the fluvial system within the Kayenta was much more prevalent and dominated most of the deposition, whereas the aeolian environment was more prevalent within the Lemman.

9.5.1. Fluid flow predictions

In outcrop, evidence of fluid flow through the aeolian system is present, either by discolouration of certain elements, differences in the weathering, and/or cementation. However, in the fluvial system of the Kayenta evidence of fluid flow is less obvious, despite the reworking of the aeolian system within the Kayenta Formation, producing similar calibre sediment. Therefore, understanding the interactions between the two depositional systems is vital for understanding fluid migration pathways at multiple scales for reservoir characterisation and enhanced recovery procedures.

Small-scale bounding surfaces and internal stratification can control the direction of migration, as can facies-scale interactions. Preferential migration pathways occur along the well sorted grainflow units of aeolian dunes, with least preferred pathways crossing through the foreset bounding surfaces due to the less permeable, fine-grained grainfall units (Fig. 9.4) (Chandler *et al.*, 1989). Similar observations can be made with cross-bedded units within ephemeral fluvial sediments, particularly when the foresets are draped with siltstone or mudstone (Fig. 9.4).

On an architectural element-scale, the fluvial elements are much more 'sandy' in composition because their interaction with the competing aeolian system and constant recycling and reworking of the

aeolian calibre sediment within the fluvial system. However, fine-grained or cemented fluvial deposits can act as baffles and barriers to flow (Fig. 9.4) (North & Taylor 1996).

On a system-scale, large-scale bounding surfaces, interdunes and super surfaces will also form significant flow barriers and compartmentalise the reservoir. Large-scale inter-tonguing between the competing aeolian and fluvial environments can also add increased complexity to production, as the aeolian tongues can often act as thief zones within mixed continental reservoirs.

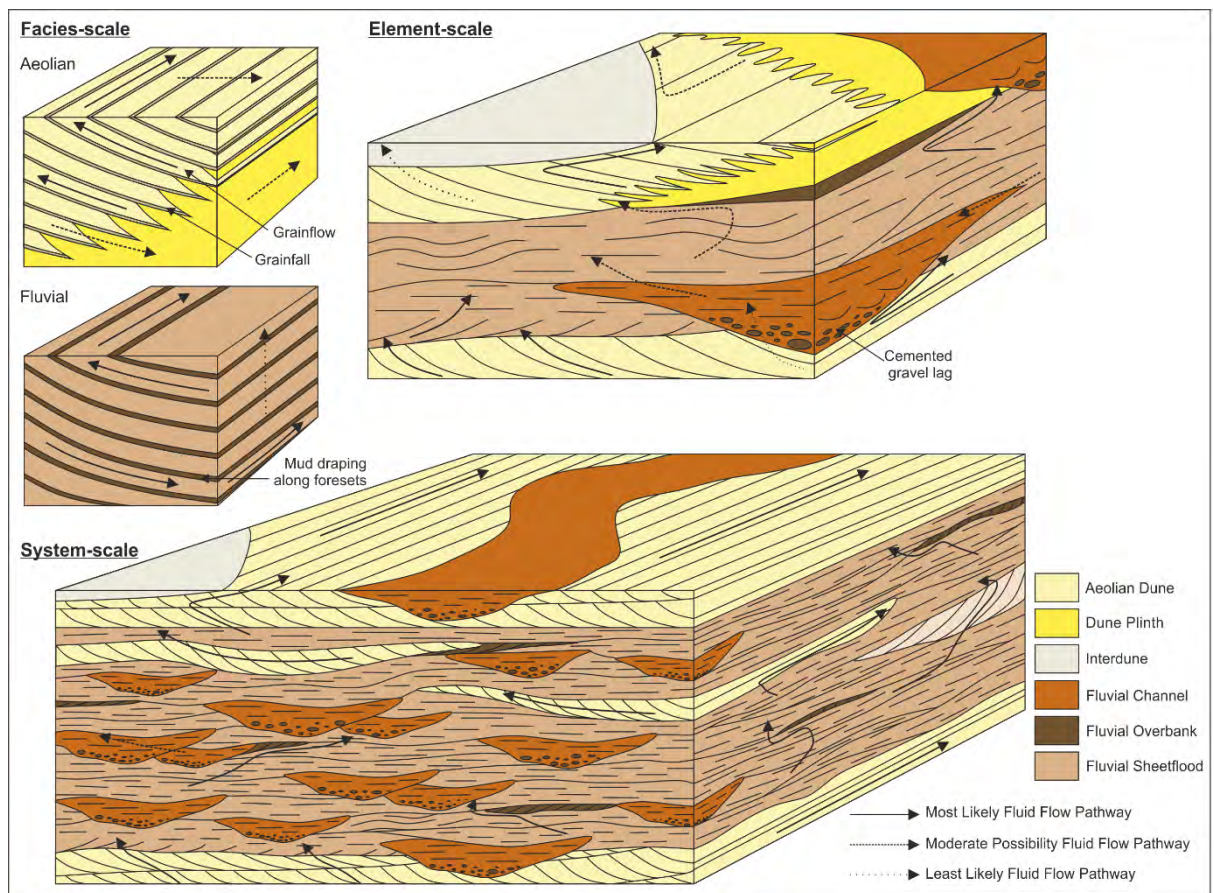


Figure 9.4. Block diagrams showing the most and least likely pathways through architectural elements and multiple scales, from facies-scale (top left) to element-scale (top right) and system-scale (bottom). Modified after Chandler et al., 1989.

9.6. Summary

The Kayenta Formation presented here represents an ephemeral sandy braided fluvial model for an arid to semi-arid, aeolian-influenced setting. The ephemeral fluvial setting lacks significant fines and the typical fluvial facies comprise well-rounded, well sorted, reworked aeolian sediment. The fluvial

channel and sheet elements often stack into vertically and horizontally amalgamated extensive sandstone bodies with high reservoir or aquifer potential.

Analysing the spatial variations of the Kayenta revealed several trends that are similar to terminal fluvial fans and some distributive fluvial systems, including a lack of confinement of the fluvial system, a downstream decrease in channel and sheet architectural element amalgamation, a downstream decrease in grain size; albeit very small, a downstream decrease in preserved channel and sheet width-to-thickness ratios and an increase in the percentage of overbank elements downstream. However, there are several downstream relationships displayed by the Kayenta fluvial sediments that do not fit with published models attributable to case-specific external factors including a secondary fluvial source and increased subsidence within the distal portion of the basin.

The up-succession variations in channel body thickness have been interpreted to represent the transgression and regression of the fluvial system through time, but with an overall regressive trend. Due to the coeval competing aeolian environment, the transgression and regression of the fluvial system have been related to the contraction and expansion of the competing aeolian dune field.

Outcrop analogues are a well-used, valuable technique in geology that have played a vital role in improving understanding of subsurface reservoir geometries and architectures, as they provide geological input with which to condition static models. However, no two depositional systems are identical, and therefore there are no outcrop analogues that would be the perfect fit for the subsurface study. Subsequently finding a suitable outcrop analogue should be based upon the aspects of the depositional system the user wishes to understand.

The Kayenta Formation was chosen as an outcrop analogue for the Lemn Sandstone of the Southern North Sea because of the similarities in depositional setting and interactions between the competing aeolian and fluvial systems. However, it is noted that there are some differences between the two formations, particularly in regard to the thickness of depositional elements. The average channel and fluvial sheet thicknesses of the Lemn Sandstone are roughly a third of the thicknesses of the same

elements within the Kayenta and the average aeolian set thickness of the Leman is roughly 28% smaller than the average measured within the Kayenta. These differences could be due to several factors including general differences within the sedimentary environment (e.g. tectonics, subsidence, avulsion and sediment supply) and differences in compaction and diagenesis.

However, the similarities between the two formations outweigh the differences and therefore, geobody analysis of three-dimensional, spatially extensive outcrops in key localities of the Kayenta Formation has been used to aid in the reconstruction of the Leman Sandstone of the Southern North Sea, providing valuable three-dimensional data to an otherwise one-dimensional core study. The detailed analysis of the sedimentary systems and interactions between the competing depositional environments has also been used to help predict fluid migration pathways between aeolian and fluvial systems.

Chapter 10: Conclusions and Further Work

Chapter Ten reviews the research aims proposed in Chapter One, summarises how these aims have been addressed through this study and considers the broader implications of the results of this research, in particular regarding the sedimentary architecture and spatial variations in dryland ephemeral fluvial systems and how these results can aid our understanding of similar depositional settings within the subsurface. This chapter also proposes a series of potential further research avenues arisen as an outcome of this body of work.

10.1. Introduction

This work focusses on an extensive outcrop analogue study of the Kayenta Formation of the Colorado Plateau, south-western USA. The Kayenta Formation comprises the deposits of a dominantly dryland ephemeral fluvial system with minor perennial influxes and aeolian interactions. Deposition occurred upon a broad alluvial plain by a dominantly south-westward to westward flowing ephemeral fluvial system sourced from the Uncompahgre Uplift in the Ancestral Rocky Mountains, supplemented by a north-westward flowing system sourced from the Mogollon Highlands in the Cordilleran Magmatic Arc.

This outcrop study provided exceptional exposure of a dryland ephemeral fluvial system in which the detailed sedimentology, architecture, geometries, and interactions of the competing fluvial and aeolian environments could be observed. Analysis of the spatial and temporal variations across the depositional system are also investigated to unravel the complex controls upon the sedimentology and provide insight into the trends in downstream spatial sedimentary architecture. The detailed sedimentological analysis combined with the spatial and temporal variations across the system are used to create semi-quantified depositional models of the proximal, medial and distal regions of the Kayenta, displaying the variations in sedimentary architecture downstream.

The resultant architectural element geometries and spatial variations within the sediments of the Kayenta Formation are applied to a subsurface study of the Lemna Sandstone of the Rotliegend Group of the Southern North Sea. The depositional models and architectural element geometries of the Kayenta Formation guide the interpretation and subsequent depositional models of the Lemna Sandstone, by adding the three-dimensional relationships that are often difficult to determine within one-dimensional subsurface studies of core.

10.2. Research aims

The overarching aim of this study is to develop a series of both small-scale and regional-scale models to better understand the sedimentary architecture and spatial variations of dryland fluvial systems and their competing coeval depositional environments. The models will be used to better understand the facies distributions, and geometry and interactions of associations within potential subsurface reservoir units. To achieve this overarching aim, this body of work sets out to address the following three key aims.

10.2.1. Aim 1: Identify and fully describe the sedimentology of a dryland ephemeral braided fluvial system and its competing coeval aeolian environment

Detailed sedimentary logging across the regional extent of the Kayenta Formation, utilising thorough sedimentological investigation of grain size, shape, sorting and mineralogy, was used to characterise the sedimentology of the deposits and was augmented by palaeocurrent measurements from both fluvial and aeolian structures.

Twenty-one facies have been identified across the expanse of the Kayenta Formation, sixteen facies relate to sub-aqueous processes and the remainder relate to wind-blown processes (Chapter 4; Section 4.3). The twenty-one facies have been grouped into nine architectural elements: fluvial channels, fluvial sheets, lateral accretion, downstream accretion, overbank, bank collapse, aeolian dunes, aeolian sandsheet and aeolian interdunes (Chapter 5; Section 5.1). The fluvial architectural elements

have also been grouped into five larger-scale depositional elements: amalgamated sandstone-dominated channels, isolated sandstone-dominated channels, isolated gravel-dominated channels, compound sandstone-dominated sheets and overbank (Chapter 5; Section 5.2).

The most prominent preserved deposits of the system are sandy, bedload-dominated, amalgamated channel and sheet depositional elements (Chapter 5; Section 5.2.1 & Section 5.2.4), composed of internal channel and sheet architectural elements. The internal channel architectural elements are dominated by successions of medium-grained planar to trough cross-bedded sandstones (**Sxb** & **Stxb**) with conglomeratic basal lags and sporadic very coarse to granule-grade clasts lining crudely developed foresets (Chapter 5; Section 5.1.1). Whereas the internal sheet architectural elements are dominated by medium-grained structureless sandstones (**Smf**) and planar-bedded (**Spb**) to sigmoidal-bedded (**Sma**) sandstones with basal rip-up clast conglomerates (**Cru**), with sporadic very coarse to granule (up to 30 cm along the long axis) sized rip-up clasts lining crudely developed foresets (Chapter 5; Section 5.1.2). Both of these elements have high thickness-to-width ratios, typical of an ephemeral fluvial system.

The detailed sedimentological analysis and geobody data were combined to create a semi-quantified depositional model for the Kayenta Formation (Chapter 7; Fig. 7.6). The model represents an ephemeral sandy braided fluvial system for an arid to semi-arid, aeolian-influenced setting. It describes an ephemeral fluvial setting that lacks significant fines and in which typical fluvial facies, comprising well-rounded, well sorted, reworked aeolian sediment, stack into vertically and horizontally amalgamated extensive sandstone bodies with high reservoir or aquifer potential (Chapter 7; Fig. 7.6).

10.2.2. Aim 2: Identify and quantify the regional spatial and temporal variations of the depositional system along with the interactions between the fluvial and aeolian environments

Analysis of the data derived from sedimentary logging and digital outcrop models across the Colorado Plateau was used to identify the spatial and temporal variations across the expanse of the Kayenta

Formation, unravel the complex controls upon the sedimentology and provide insight into the trends in downstream spatial sedimentary architecture.

Spatial variations in compositional characteristics including the thicknesses of fluvial and aeolian strata, the percentage of sand, the percentage of conglomerate, and the grain-size distribution of the fluvial sediments (Chapter 6; Section 6.2), along with spatial variations within the identified fluvial depositional elements (Chapter 6; Section 6.4), including the percentage of each depositional element per locality (Chapter 6; Section 6.4.1), and the average thickness (Chapter 6; Section 6.4.2) and average grain size (Chapter 6; Section 6.4.3) of each type of depositional element per locality, were analysed and revealed some downstream trends similar to those of a terminal fluvial fan and some distributive fluvial systems (Chapter 6; Section 6.5).

The Kayenta fluvial sediments display a clear lack of confinement of the fluvial system sourced from the Uncompahgre Uplift (Chapter 9; Fig. 9.2), illustrating very little evidence of significant tributary inputs, until the intersection with the axial fluvial system sourced from the Cordilleran Magmatic Arc. A downstream decrease in amalgamation of channels and compound sheets, a small decrease in grain size downstream and an overall increase in the percentage of overbank depositional elements with distance downstream are also observed (Chapter 6; Section 6.5), all of which are characteristics that are consistent with previously published models (Chapter 9; Section 9.2.3). Consequently, a downstream decrease in both energy and channel bifurcation, accompanied by high rates of evapotranspiration and infiltration of water into the substrate are considered the probable mechanisms that explain these trends (Chapter 9; Section 9.2.3).

Conversely, there are several downstream relationships displayed by the Kayenta fluvial sediments that do not fit with published models. An increase in total thicknesses of fluvial sediment downstream may be attributed to the increase in accommodation space provided by the Zuni Sag and Utah-Idaho trough (Blakey, 2008), and relatively constant thicknesses of channel-fill and sheet depositional elements with distance downstream may be attributed to the influence of the secondary fluvial source

(Chapter 9; Section 9.2.3). The channel-fill depositional elements downstream display no significant variation in average grain size with distance downstream which may be the consequence of the interaction between a fluvial system and an ever-present coeval aeolian system throughout the fluvial course (Chapter 9; Section 9.2.3).

The temporal variations in the system were analysed using the trends in the channel body thickness through time (Chapter 6; Section 6.6). An overall decrease in channel body thickness with increasing height within the successions was observed, representing an overall regression of the fluvial system and expansion of the aeolian system through time. Variations within this overall trend represent cycles between the transgression and regression of the fluvial system and the contraction and expansion of the competing aeolian dune field (Chapter 6; Section 6.7).

Several interactions between the fluvial and aeolian systems were analysed at different scales, including facies-scale reworking of aeolian sediment into the fluvial system and system-scale inter-tonguing between the fluvial sediments of the Kayenta Formation and the aeolian sediments of the overlying Navajo Sandstone (Chapter 6; Section 6.7).

The detailed sedimentological analysis combined with the spatial and temporal variations across the system were used to create semi-quantified depositional models of the proximal, medial and distal regions of the Kayenta, display the variations in sedimentary architecture downstream (Chapter 7; Figs. 7.7 & 7.8).

10.2.3. Aim 3: Apply findings to subsurface data of a similar depositional setting to better characterise architectural and geometrical relationships within potential reservoir units

Outcrop data was be complimented with study of core from the Lemn Sandstone of the Southern North Sea; a similar basinal setting. As with the Kayenta Formation, detailed core logging across the regional extent of the Lemn Sandstone, utilising thorough sedimentological investigation of grain size,

shape, sorting and mineralogy, was used to characterise the sedimentology of the deposits (Chapter 8; Sections 8.4 & 8.5).

Several comparisons were drawn between the Lemn Sandstone and Kayenta Formation, including similar sedimentological features, for example mud-draping along foresets of fluvial elements, upper flow regime structures such as parallel laminated flat beds, debris-driven, matrix-supported conglomerates and armoured mudballs. Equally, similarities between the aeolian-fluvial interactions can be observed, including the recycling of aeolian sediment within the fluvial system evidenced by the dominantly well-rounded and well sorted sand grains of fine to medium-grained distribution (Chapter 8; Section 8.6).

However, it is noted that there are some differences between the two formations, particularly with regards to the thickness of depositional elements. The average channel and fluvial sheet thicknesses of the Lemn Sandstone are roughly a third of the thicknesses of the same elements within the Kayenta and the average aeolian set thickness of the Lemn is roughly 28% smaller than the average measured within the Kayenta. These differences could be due to several factors including general differences within the sedimentary environment (e.g. tectonics, subsidence, avulsion and sediment supply) and differences in compaction and diagenesis (Chapter 9; Section 9.5).

However, the similarities between the two formations outweigh the differences and therefore, geobody analysis of three-dimensional, spatially extensive outcrops in key localities of the Kayenta Formation has been used to aid in the reconstruction of the Lemn Sandstone of the Southern North Sea, providing valuable three-dimensional data to an otherwise one-dimensional core study (Chapter 8; Fig. 8.18).

10.3. Further Work

This work presents a detailed sedimentological characterisation of dryland fluvial and aeolian sediments using a well-known succession of the Kayenta Formation and has applied detailed spatial

and temporal analysis which has previously not been done before on this succession. Application of these results to similar depositional settings has also been demonstrated. However, there are several limitations to this research that can form the basis of future work to better refine and enhance this study, including: (i) analysis of modern-day analogues, (ii) provenance studies, and (iii) numerical modelling.

10.3.1. Analysis of modern-day systems

This work is based upon the study of ancient sediments, where only parts of the depositional system are preserved. In order to better understand dryland fluvial systems along with their interaction with competing aeolian environments, it would be beneficial to conduct a modern-day analogue study on a similar, large-scale, dryland fluvial system.

One potential area for study would be the Luni River, which is the largest river in the Thar Desert of northwest India. The Luni River has a catchment area of approximately 37,363 km², with a 495 km long low-sinuosity course and frequent interactions with the aeolian deposits on the Thar Desert (Carling & LeClair, 2019).

Studying modern-day rivers like the Luni River would provide increased understanding of the depositional processes associated with dryland rivers and provide insight into the preferential preservation potential between the fluvial and aeolian deposits.

10.3.2. Provenance studies

Within fluvial environments both clast composition and palaeocurrent measurements can give an indication of source. This research has established that the dominant source region for the Kayenta Formation is the Uncompahgre Uplift, but a secondary axial fluvial system has been noted within the distal region, sourced from the Cordilleran Magmatic Arc. Evidence of this secondary fluvial system has been observed through increased gravel-dominated channels and differing palaeocurrent measurements within the distal region.

In order to ascertain the influence of the two fluvial systems, an extensive provenance study would be required. One of the most established methods for understanding provenance is through fission track dating, mainly through detrital zircon analysis, which would be ideal for a pilot provenance study, therefore methodical sampling of fluvial units and extensive collection of palaeocurrent data would be needed to infer the sediment source.

A recent provenance study using detrital zircons suggests the fluvial sandstones were derived from the East Mexico arc, which lay to the south-east of the Colorado Plateau (Dickinson & Gehrels, 2009). However, palaeocurrent analysis suggests some Lower Jurassic streams flowed south-westerly from the Ancestral Rocky Mountains, and others north-westerly from the Cordilleran Magmatic arc (Harshbarger *et al.*, 1957; Middleton & Blakey, 1983). It is also noted this study (Dickinson & Gehrels, 2009) only sampled four fluvial sandstones across the extent of the exposure of the Kayenta Formation and therefore would not be a representative study of the fluvial system as a whole and much more detailed, methodical sampling would be needed to infer the two possible sources.

Provenance analysis can not only indicate the source of the sediment, it can also highlight the transportation pathways prior to deposition, which in itself can provide strong correlative horizons throughout continental deposits (Haughton *et al.* 1991). This analysis can also aid in: (i) the interpretation of climate variations throughout deposition, which will give more quantitative values than the qualitative method presented in this work; (ii) can highlight individual tectonic events in tectonically active basins; and (iii) give an indication of the relief of the source area during deposition (e.g. Russell & Allison 1985; Hirst & Nichols 1986; Mack 1987; Johnsson *et al.* 1988; Haughton *et al.* 1991).

10.3.3. Numerical modelling

Outcrop analogue studies are a useful technique and have long been recognised as a valued guide for prediction of subsurface architectural elements and provide realistic geology to static models (Alexander, 1993; Bridge *et al.*, 2000; Al-Ajmi *et al.*, 2011). The outcrop analogue study of the Kayenta

Formation has provided valuable geobody data for the subsurface study of the Lemna Sandstone and a depositional model was created. However, to provide added value for reservoir characterisation a computerised reservoir model would be useful when accessing potential exploration prospects.

Reservoir models are used as three-dimensional representations of the sub-surface strata during exploration and production phases of hydrocarbon exploitation. The models are used to develop visualise reservoir strata, estimate resource volumes, develop risk profiles for specific plays, create frameworks for fluid flow simulations and to develop effective drilling plans.

Object-based models (OBMs) require manual inputs of geometric information to constrain geobodies within a stochastic framework (Holden *et al.*, 1998; Stephen *et al.*, 2001; Manzocchi *et al.*, 2007). Individual geobodies are constrained using input data derived directly from hard (well log or outcrop) or soft (seismic) conditioning data (Haldorsen & Damsleth 1990; Dubrule 1998). Predefined inputs given to the geobodies include: size, geometry, palaeocurrent and target fractions (the proportion of the total simulated volume the geobody should occupy).

All the data required to build object-based models have been collected in this study. Converting these data into an object-based model for the Lemna Sandstone and combining the model with additional petrophysical data including porosity and permeability, would allow for the more representative interpretation of fluid migration pathways through the depositional system.

10.4. Summary

The Kayenta Formation of the Colorado Plateau, south-western USA, provides unparalleled exposure to study dryland fluvial systems and their interaction with competing aeolian environments. The extensive nature of the Kayenta Formation makes it an ideal analogue for other, less exposed deposits or for comparison to borehole data, such as the Lemna Sandstone of the Southern North Sea. This study provides valuable sedimentological data for characterising dryland fluvial systems, particularly when analysing the spatial and temporal variations of the system. This data combined with the study

of the interactions between fluvial and aeolian deposits can be used in reservoir characterisation and help identify possible unexplored reservoir units within mature basins.

References

- Abdullatif, O.M.** (1989). Channel-fill and sheet-flood facies sequences in the ephemeral terminal River Gash, Kassala, Sudan. *Sedimentary Geology*, **63**, 171–184.
- Ahlbrandt, T.S., Andrews, S. and Gwynne, D.T.** (1978). Bioturbation in eolian deposits. *Journal of Sedimentary Research*, **48(3)**, 839–848.
- Ahlbrandt, T.S. and Fryberger, S.G.** (1981). Sedimentary features and significance of interdune deposits. In: *Recent and Ancient Nonmarine Depositional Environments: Models for Exploration*. (Eds. Ethridge, F.G. and Flores, R.M.) SEPM Special Publication, **31**, 293–314.
- Al-Ajmi, H. Hinderer, M. Keller, M. Rausch, R. Blum, P. and Bohnsack, D.** (2011). The Role of Outcrop Analogue Studies for the Characterization of Aquifer Properties. *International Journal of Water Resources and Arid Environments*, **1(1)**, 48–54.
- Alexander, J.** (1993). A discussion on the use of analogs for reservoir geology. In: *Advances in Reservoir Geology*. (Ed. Ashton, M.). Geological Society of London Special Publication, **69**, 175–194.
- Allen, J.R.L.** (1963). The classification of cross-stratified units, with notes on their origin. *Sedimentology*, **2**, 93–114.
- Allen, J.R.L.** (1965) A review of the origin and characteristics of recent alluvial sediments. *Sedimentology*, **5(2)**, 89–191.
- Allen, J.R.L.** (1974). Studies in fluvial sedimentation: Implications of pedogenic carbonate units. Lower Old Red Sandstone, Anglo-Welsh outcrop. *Geological Journal*, **9(2)**, 181–208.
- Allen, J.R.L.** (1982) *Sedimentary Structures. Their Character and Physical Basis*, Vol. 1. Elsevier, Amsterdam, 593.
- Allen, J.R.L.** (1983). Studies in fluvial sedimentation: Bars, bar-complexes and sandstone sheets (low sinuosity braided streams) in the Brownstones (L. Devonian), Welsh Borders. *Sedimentary Geology*, **33**, 237–293.
- Allen, J.R.L., and Banks, N.L.** (1972). An interpretation and analysis of recumbent-folded deformed cross-bedding. *Sedimentology*, **19(3-4)**, 257–283.
- Allen, P.A.** (1981) Wave-generated structures in the Devonian lacustrine sediments of south-east Shetland and ancient wave conditions. *Sedimentology*, **28(3)**, 369–379.
- Al-Masrahy, M.A., and Mounney, N.P.** (2015). A classification scheme for fluvial–aeolian system interaction in desert-margin settings. *Aeolian Research*, **17**, 67–88.
- Almeida, R.P., Freitas, B.T., Turra, B.B., Figueiredo, F.T., Marconato, A. and Janikian, L.** (2016). Reconstructing fluvial bar surfaces from compound cross-strata and the interpretation of bar accretion direction in large river deposits. *Sedimentology*, **63(3)**, 609–628.
- Andrews, S.D. and Hartley, A.J.** (2015) The response of lake margin sedimentary systems to climatically driven lake level fluctuations: Middle Devonian, Orcadian Basin, Scotland. *Sedimentology*, **62**, 1693–1716.
- Arnott, R.W.C. and Hand, B.M.** (1989). Bedforms, primary structures and grain fabric in the presence of suspended sediment rain. *Journal of Sedimentary Research*, **59(6)**, 1062–1069.

- Ashley, G.M.** (1990). Classification of large scale subaqueous bedforms: a new look at an old problem. *Journal of Sedimentary Petrology*, **60**, 160–172.
- Averitt, P., Detterman, J.S., Harshbarger, J.W., Repenning, C.A. and Wilson, R.F.** (1955), Revisions in correlation and nomenclature of Triassic and Jurassic formations in southwestern Utah and northern Arizona. *Bulletin of the American Association of Petroleum Geologists*, **39**, 2515–2524.
- Baars, D.L.** (2000) The Colorado Plateau: A geologic history. 1st Ed. Albuquerque. University of New Mexico Press, 1–272.
- Baars, D.L. and Doelling, H.H.** (1987). Moab salt-intruded anticline, east-central Utah. In: Rocky Mountain Section of the Geological Society of America: Geological Society of America Centennial Field Guide (Eds. Beus, S.S.), **2**, 275–280.
- Baars, D.L. and Stevenson, G.M.** (1981) Tectonic evolution of western Colorado and eastern Utah. *New Mexico Geological Society Guidebook*, 32nd Field Conference, Western Slope Colorado, 105-112.
- Baas, J.H.** (1993). Dimensional analysis of current ripples in recent and ancient depositional environments. *Geologica Ultraiectina*, 106.
- Baas, J.H.** (1994). A flume study on the development and equilibrium morphology of small-scale bedforms in very fine sand. *Sedimentology*, **41**, 185–209.
- Baas, J.H.** (1999). An empirical model for the development and equilibrium morphology of current ripples in fine sand. *Sedimentology*, **46**, 123–138.
- Babcock, H.M., and Cushing E.M.** (1941). Recharge to ground water from floods in a typical desert wash, Pinal County, Arizona, *Eos Trans. AGU*, **23**, 49–56.
- Bachmann, G.H. and Wang, Y.** (2014). Armoured mud balls as a result of ephemeral fluvial flood in a humid climate: Modern example from Guizhou Province, South China. *Journal of Palaeogeography*, **3(4)**, 410–418.
- Bagnold, R.** (1941). The Physics of Blown Sand and Desert Dunes. *The Geographical Journal*, **98(2)**, 109.
- Bailey, R.J. and Lloyd, D.A.** (2001) A log correlation of the Rotliegendes of the northern Cleaver Bank High: the search for controls on reservoir sand distribution. *Petroleum Geoscience*, **7(4)**, 351–358.
- Baker, A.A.** (1936). Geology of the Monument Valley-Navajo Mountain region: Washington D.C. *United States Geological Survey*, 106.
- Barbeau, D.L.** (2003) A flexural model for the Paradox Basin: implications for the tectonics of the Ancestral Rocky Mountains. *Basin Research*, **15**, 97–115.
- Bartz, M., Rixhon, G., Kehl, M., El Ouahabi, M., Klasen, N., Brill, D., Weniger, G.C., Mikdad, A. and Brückner, H.** (2017). Unravelling fluvial deposition and pedogenesis in ephemeral stream deposits in the vicinity of the prehistoric rock shelter of Ifri n'Ammar (NE Morocco) during the last 100 ka. *Catena*, **152**, 115–134.
- Baldi, P., Fabris, M., Marsella, M. and Monticelli, R.** (2005). Monitoring the morphological evolution of the Sciara del Fuoco during the 2002–2003 Stromboli eruption using multi-temporal photogrammetry. *ISPRS journal of photogrammetry and remote sensing*, **59(4)**, 199–211.

- Batezelli, A., Ladeira, F.S.B., Nascimento, D.L.D. and DA Silva, M.L.** (2019). Facies and palaeosol analysis in a progradational distributive fluvial system from the Campanian–Maastrichtian Bauru Group, Brazil. *Sedimentology*, **66** (2), 699–735.
- Beitler, B., Chan, M.A. and Parry, W.T.** (2003). Bleaching of Jurassic Navajo Sandstone on Colorado Plateau Laramide highs?: Evidence of exhumed hydrocarbon supergiants. *Geology*, **31**, 1041–1044.
- Bemis, S.P., Micklethwaite, S., Turner, D., James, M.R., Akciz, S., Thiele, S.T. and Bangash, H.A.** (2014). Ground-based and UAV-based photogrammetry: A multi-scale, high-resolution mapping tool for structural geology and paleoseismology. *Journal of Structural Geology*, **69**, 163–178.
- Besly, B., Romain, H.G. and Mountney, N.P.** (2018) Reconstruction of linear dunes from ancient aeolian successions using subsurface data: Permian Auk Formation, Central North Sea, UK. *Marine and Petroleum Geology*, **91**, 1–18.
- Best, J.L., Ashworth, P.J., Bristow, C.S. and Roden, J.** (2003) Three-dimensional sedimentary architecture of a large, mid-channel sand braid bar, Jamuna River, Bangladesh. *Journal of Sedimentary Research*, **73**(4), 516–530.
- Best, J.L.** (2005). The kinematics, topology and significance of dune related macroturbulence: Some observations from the laboratory and field. In: *Fluvial Sedimentology VII* (Eds. Blum, M.D. Marriott, S.B. and Leclair, S.) Special Publication of the International Association of Sedimentologists, **35**, 41–60.
- Billi, P.** (2007). Morphology and sediment dynamics of ephemeral stream terminal distributary systems in the Kobo Basin (northern Welo, Ethiopia). *Geomorphology*, **85**(1-2), 98–113.
- Billi, P.** (2011). Flash flood sediment transport in a steep sand-bed ephemeral stream. *International Journal of Sediment Research*, **26**(2), 193–209.
- Billi, P., Demissie, B., Nyssen, J., Moges, G., Fazzini, M.** (2018). Meander hydromorphology of ephemeral streams: similarities and differences with perennial rivers. *Geomorphology*, **319**, 35–46.
- Birdseye, C.H.** (1940). Stereoscopic phototopographic mapping. *Annals of the Association of American Geographers*, **30**(1), 1–24.
- Bjerrum, C.J. and Dorsey, R.J.** (1995). Tectonic Controls on deposition of Middle Jurassic strata in a retroarc foreland basin, Utah-Idaho trough, western interior, United States. *Tectonics*, **(14)**4, 962–978.
- Blakey, R.C.** (1994). Paleogeographic and tectonic controls on some Lower and Middle Jurassic erg deposits, Colorado Plateau. In: *Mesozoic Systems of the Rocky Mountain Region, USA*, (Eds. M.V. Caputo, J.A. Peterson and K.J. Franczyk), Rocky Mountain Section (SEPM), Denver, 273–298.
- Blakey, R.C.** (2008). Pennsylvanian–Jurassic sedimentary basins of the Colorado Plateau and southern Rocky Mountains. In: *Sedimentary Basins of the World* (Ed. A.D. Miall), **5**, 245–296.
- Blakey, R.C., Peterson, F. and Kocurek, G.** (1988). Synthesis of late Paleozoic and Mesozoic eolian deposits of the Western Interior of the United States. *Sedimentary Geology*, **56**, 3–125.
- Blakey, R. and Ranney, W.** (2008) *Ancient Landscapes of the Colorado Plateau*. Grand Canyon Association, Arizona. 1st Ed.
- Boggs Jr, S. and Boggs, S.** (2009). *Petrology of sedimentary rocks*. (Ed. Boggs, Jr, S.). 2nd Ed. Cambridge university press, Edinburgh Building, Cambridge.

- Bridge, J.S.** (1984). Large-scale facies sequences in alluvial overbank environments. *Journal of Sedimentary Research*, **54**, 85–170.
- Bridge, J.S.** (2001). Characterization of fluvial hydrocarbon reservoirs and aquifers: problems and solutions. *Revista de la Asociación Argentina de Sedimentología*, **8(2)**, 87–114.
- Bridge, J.S.** (2003). *Rivers and floodplains: forms, processes, and sedimentary record*. Blackwell Scientific Publishing, 491.
- Bridge, J.S.** (2006). Fluvial facies models: recent developments, In: *Facies Models Revisited* (Eds. H.W. Posamentier and R.G. Walker), SEPM Special Publication, **84**, 85–170.
- Bridge, J.S.** and **Best, J.L.** (1988). Flow, sediment transport and bedform dynamics over the transition from dunes to upper-stage plane beds: implications for the formation of planar laminae. *Sedimentology*, **35(5)**, 753–763.
- Bridge, J.S., Jafin, G.A.** and **Georgieff, S.M.** (2000), Geometry, lithofacies, and spatial distribution of Cretaceous fluvial sandstone bodies, San Jorge basin, Argentina: Outcrop analog for the hydrocarbon-bearing Chubut Group. *Journal of Sedimentary Research*, **70(2)**, 341 – 359.
- Bristow, C.S.** (1993). Sedimentary structures exposed in bar tops in the Brahmaputra River, Bangladesh. In: *Braided Rivers*. (Eds. Best, J. L. and Bristow, C.S.). Geological Society of London Special Publication, **75**, 277–289.
- Bristow, C.S.** (1995). Internal geometry of ancient tidal bedforms revealed using ground penetrating radar. In: *Tidal signatures in modern and ancient sediments*. (Eds. Flemming, B.W. and Bartoloma, A.), International Association of Sedimentologists, **24**, 313–328.
- Bristow, C., Skelly, R.** and **Ethridge, F.** (1999). Crevasse splays from the rapidly aggrading, sand-bed, braided Niobrara River, Nebraska: effect of base-level rise. *Sedimentology*, **46**, 1029–1048.
- Bromley, M.H.** (1991). Architectural features of the Kayenta Formation (Lower Jurassic), Colorado Plateau, USA: relationship to salt tectonics in the Paradox Basin. *Sedimentary Geology*, **73(1-2)**, 77–99.
- Brookfield, M.E.** (1977). The origin of bounding surfaces in ancient aeolian sandstones. *Sedimentology*, **24(3)**, 303–332.
- Brookfield, M.E.** (1992) Eolian systems. In: *Facies Models. Response to Sea Level Change* (Eds. Walker, R.G. and James, N.P.) Geological Association of Canada, 143–156.
- Bryant, G., Cushman, R., Nick, K.** and **Miall, A.** (2016). Paleohydrologic controls on soft-sediment deformation in the Navajo Sandstone. *Sedimentary Geology*, **344**, 205–221.
- Bryant, G., Monegato, G.** and **Miall, A.** (2013). An example of liquefaction-induced interdune sedimentation from the early Jurassic Navajo Sandstone, USA. *Sedimentary Geology*, **297**, 50–62.
- Bullard, J.E.** (1997). Vegetation and dryland geomorphology. *Arid Zone Geomorphology*, 109–131.
- Bullard, J.E.** and **Livingstone, I.** (2002). Interactions between aeolian and fluvial systems in dryland environments. *Area*, **34(1)**, 8–16.
- Burnham, B.S.** and **Hodgetts, D.** (2018). Quantifying spatial and architectural relationships from fluvial outcrops. *Geosphere*, **15**, 236–253.

- Butler, J.B.** (1975). The West Sole Gas-Field. In: *Petroleum and the Continental Shelf of North-West Europe*. (Ed. Woodland, A.W) Institute of Petroleum Geology, London, 213–223.
- Cain, S.A.** (2009) Sedimentology and stratigraphy of a terminal fluvial fan system: the Permian Organ Rock Formation, South East Utah. Unpublished Keele University, 341.
- Cain, S.A. and Mountney, N.P.** (2009). Spatial and temporal evolution of a terminal fluvial fan system: the Permian Organ Rock Formation, South-east Utah, USA. *Sedimentology*, **56(6)**, 1774–1800.
- Cain, S.A. and Mountney, N.P.** (2011). Downstream changes and associated fluvial-aeolian interactions in an ancient terminal fluvial fan system: the Permian Organ Rock Formation, SE Utah. In: *From River to Rock Record* (Eds. S. Davidson, S. Leleu and C. North), SEPM Special Publication, **97**, 165–187.
- Cameron, T.D.J., Crosby, A., Balson, P.S., Jeffery, D.H., Lott, G.K., Bulat, J. and Harrison, D.J.** (1992). *United Kingdom offshore regional report: the geology of the southern North Sea*. (London: HMSO for the British Geological Survey).
- Cant, D.J. and Walker, R.G.** (1978). Fluvial processes and facies sequences in the sandy braided South Saskatchewan River, Canada. *Sedimentology*, **25**, 625–648.
- Carling, P.A.** (2013). Freshwater megaflood sedimentation: what can we learn about generic processes? *Earth-Science Reviews*, **125**, 87–113.
- Carling, P.A. and Leclair, S.F.** (2019). Alluvial stratification styles in a large, flash-flood influenced dryland river: The Luni River, Thar Desert, north-west India. *Sedimentology*, **66(1)**, 102–128.
- Carrivick, J.L., Smith, M.W. and Quincey, D.J.** (2016). *Structure from Motion in the Geosciences*. First Edition. Wiley, Chichester, UK. 208 pages.
- Chandler, J.** (1999). Effective application of automated digital photogrammetry for geomorphological research. *Earth Surface Processes and Landforms*, **24(1)**, 51–63.
- Chandler, M.A. Kocurek, G. Goggin, D.J. and Lake, L.W.** (1989) Effects of stratigraphic heterogeneity on permeability in eolian sandstone sequences, Page Sandstone, Northern Arizona. *American Association of Petroleum Geologists Bulletin*, **73**, 658–668.
- Chesley, J.T., Leier, A.L., White, S. and Torres, R.** (2017). Using unmanned aerial vehicles and structure-from-motion photogrammetry to characterize sedimentary outcrops: An example from the Morrison Formation, Utah, USA. *Sedimentary Geology*, **354**, 1–8.
- Clarke, M.L. and Rendell, H.M.** (1998). Climate change impacts on sand supply and the formation of desert sand dunes in the south-west USA. *Journal of Arid Environments*, **39(3)**, 517–531.
- Clemmensen, L.B. and Blakey, R.C.** (1989). Erg deposits in the Lower Jurassic Wingate Sandstone, northeastern Arizona: oblique dune sedimentation. *Sedimentology*, **36**, 449–470.
- Collinson, J.** (1994). Chapter 4: Sedimentary deformational structures. In: *The geological deformation of sediments*. (Eds. Maltman, A). Springer, 95–125.
- Collinson, J. and Mountney, N.** (2019) Chapter 3: Basic properties of fluids, flows and sediment. In: *Sedimentary Structures*. (Eds. Collinson, J. and Mountney, N.) 4th Ed., Dunedin Academic Press, 21–43.

- Collinson, J., Mountney, N. and Thompson, D.** (2006). Chapter 6: Depositional Structures of Sands and Sandstones. In: *Sedimentary Structures*. 3rd Ed., Terra Publishing, Hertfordshire, 111–128.
- Colombera, L. and Mountney, N.P.** (2019). The lithofacies organization of fluvial channel deposits: A metaanalysis of modern rivers. *Sedimentary Geology*, **383**, 16–40.
- Colombera, L., Mountney, N.P. and McCaffrey, W.D.** (2013). A quantitative approach to fluvial facies models: methods and example results. *Sedimentology*, **60**, 1526–1558.
- Colombera, L., Mountney, N.P. Howell, J.A. Rittersbacher, A. Felletti, F. and McCaffrey, W.D.** (2016). A test of analog-based tools for quantitative prediction of largescale fluvial architecture. *AAPG Bulletin*, **100**, 237–267
- Conway, A. M.** (1986). Geology and petrophysics of the Victor field. In: *Habitat of Palaeozoic gas in northwest Europe*. (Eds. Brooks, J., Goff, J. and van Hoorn, B.). Geological Society of London Special Publication, **23**, 237–249.
- Cornish, J. H.** (1961). Flow losses in dry sandy channels. *Journal of Geophysical Research*, **66(6)**, 1845–1853.
- Coronel, M.D., Isla, M.F., Veiga, G.D., Mountney, N.P. and Colombera, L.** (2020). Anatomy and facies distribution of terminal lobes in ephemeral fluvial successions: Jurassic Tordillo Formation, Neuquén Basin, Argentina. *Sedimentology*, **67(5)**, 2596–2624.
- Costello, W.R.** (1974). *Development of Bed Configuration in Coarse Sands*. PhD Thesis. Massachusetts Institute of Technology, Cambridge, Massachusetts.
- Curtis, K. and Padian, K.** (1999). An Early Jurassic microvertebrate fauna from the Kayenta of northeastern Arizona: Microfaunal change across the Triassic-Jurassic boundary. *PaleoBios*, **19**, 19–37.
- Dalziel, I.W.D.** (1997). Overview. Neoproterozoic-Palaeozoic geography and tectonics: review, hypothesis, environmental speculation. Geological Society of America Bulletin, **109**, 16–42.
- Davidson, S., Hartley, A.J., Weissmann, G.S., Nichols, G.J. and Scuderi, L.A.** (2013). Geomorphic elements on modern distributive fluvial systems. *Geomorphology*, **180–181**, 82–95.
- Dickinson, W.R.** (2018). Tectonosedimentary relations of Pennsylvanian to Jurassic Strata on the Colorado Plateau. *Geological Society of America Special Papers*, **533**, 1–184.
- Diskin, M.H. and Lane, L.J.** (1972). A basinwide stochastic model of ephemeral stream runoff on southeastern Arizona. *International Association Scientific Hydrologists Bulletin*, **17**, 61–76.
- Doe, T.W. and Dott JR, R.H.** (1980). Genetic significance of deformed cross bedding - with examples from the Navajo and Weber Sandstones of Utah. *Journal of Sedimentary Research*, **50(3)**.
- Doelling, H.H., Oviatt, C.G. and Huntoon, P.W.** (1988). Salt deformation in the Paradox region. Bulletin of the Utah Geological Mineral Survey, **122**, 93.
- Donohoo-Hurley, L.L. Geissman, J.W. and Lucas, S.G.** (2010). Magnetostratigraphy of the uppermost Triassic and lowermost Jurassic Moenave Formation, western United States: correction with strata in the United Kingdom, Morocco, Turkey, Italy, and eastern United States. *Geological Society of America Bulletin*, **122**, 2005–2019.
- Dreyer, T.** (1993). Quantified fluvial architecture in ephemeral stream deposits of the Esplugafreda Formation (Palaeocene), Tremp-Graus Basin, northern Spain. *Alluvial sedimentation*, 337–362.

Driese, S.G. (1985). Interdune pond carbonates, Weber Sandstone (Pennsylvanian-Permian), northern Utah and Colorado. *Journal of Sedimentary Research*, **55(2)**, 187–195.

Dubrule, O. (1998). *Geostatistics in petroleum geology*. AAPG Course Notes 38, 52.

Durán, O., Claudin, P. and Andreotti, B. (2011) On aeolian transport: Grain-scale interactions, dynamical mechanisms and scaling laws. *Aeolian Research*, **3(3)**, 243–270.

Eberth, D.A. and Miall, A.D. (1991). Stratigraphy, sedimentology and evolution of a vertebrate-bearing, braided to anastomosed fluvial system, Cutler Formation (Permian-Pennsylvanian), north-central New Mexico. *Sedimentary Geology*, **72(3-4)**, 225–252.

Eltner, A., Kaiser, A., Castillo, C., Rock, G., Neugirg, F. and Abellan, A. (2016). Image-based surface reconstruction in geomorphometry—merits, limits and developments. *Earth Surf. Dynam.*, **4**, 1445–1508.

Enge, H.D., Buckley, S.J., Rotevatn, A. and Howell, J.A. (2007). From outcrop to reservoir simulation model: Workflow and procedures. *Geosphere*, **3(6)**, 469–490.

Field, J.P., Breshears, D.D. and Whicker, J.J. (2009). Toward a more holistic perspective of soil erosion: why aeolian research needs to explicitly consider fluvial processes and interactions. *Aeolian Research*, **1(1-2)**, 9–17.

Fielding, C.R. (2006). Upper flow regime sheets, lenses and scour fills: extending the range of architectural elements for fluvial sediment bodies. *Sedimentary Geology*, **190(1-4)**, 227–240.

Fielding, C.R., Alexander, J. and Allen, J.P. (2018). The role of discharge variability in the formation and preservation of alluvial sediment bodies. *Sedimentary Geology*, **365**, 1–20.

Fillmore, R. (2011). Geological evolution of the Colorado Plateau of Eastern Utah and Western Colorado, including the San Juan River, Natural Bridges, Canyonlands, Arches, and the Book Cliffs. University of Utah Press, Salt Lake City.

Fisher, J.A., Krapf, C.B., Lang, S.C., Nichols, G.J. and Payenberg, T.H. (2008). Sedimentology and architecture of the Douglas Creek terminal splay, Lake Eyre, central Australia. *Sedimentology*, **55(6)**, 1915–1930.

Fisher, J.A., Nichols, G.J. and Waltham, D.A. (2007). Unconfined flow deposits in distal sectors of fluvial distributary systems: examples from the Miocene Luna and Huesca Systems, northern Spain. *Sedimentary Geology*, **195(1-2)**, 55–73.

Foley, M.G. (1978). Scour and fill in steep, sand-bed ephemeral streams. *Geological Society of America Bulletin*, **89(4)**, 559–570.

Fonstad, M.A., Dietrich, J.T., Courville, B.C., Jensen, J.L. and Carbonneau, P.E. (2013). Topographic structure from motion: a new development in photogrammetric measurement. *Earth Surface Processes and Landforms*, **38(4)**, 421–430.

Foos, A. (1999) Geology of the Colorado Plateau. Geology Field Trip Guides by Anabelle Foos. University of Akron. Available online at <http://www2.nature.nps.gov/geology/education>.

Formolo Ferronato, J.P., dos Santos Scherer, C.M., de Souza, E.G., dos Reis, A.D. and de Mello, R.G. (2019). Genetic units and facies architecture of a Lower Cretaceous fluvial-aeolian succession, São Sebastião Formation, Jatobá Basin, Brazil. *Journal of South American Earth Sciences*, **89**, 158–172.

- Friend, P.F.** (1978). Distinctive features of some ancient river systems. In: *Fluvial Sedimentology* (Ed. A.D. Miall), Canadian Society of Petroleum Geologists Memoir, **5**, 531–542.
- Friend, P.F. and Moody-Stuart, M.** (1972). Sedimentation of the Wood Bay Formation (Devonian) of Spitsbergen: regional analysis of a late orogenic basin. *Norsk Polarinstitutt Skrifter*, **157**, 1–77.
- Friend, P.F., Slater, M.J. and Williams, R.C.** (1979). Vertical and lateral building of river sandstone bodies, Ebro Basin, Spain. *Journal of the Geological Society*, **136(1)**, 39–46.
- Fryberger, S.** (1990). Chapter 5: Role of water in eolian deposition. In: *Modern and Ancient Eolian Deposits: Petroleum Exploration and Production*. (Eds. Fryberger, S. Krystinik, L.F. and Schenk, C.J.) Rocky Mountain Section (SEPM), Denver, Colorado. 41–52.
- Fryberger, S.G. and Schenk, C.J.** (1988). Pin stripe lamination: a distinctive feature of modern and ancient eolian sediments. *Sedimentary Geology*, **55(1-2)**, 1–15.
- Fryberger, S.G. Schnek, C.J. and Krystinik, L.F.** (1988) Stokes Surfaces and the effects of Near-Surfaces Groundwater-Table on Aeolian Deposition. *Sedimentology*, **35**, 21–41.
- Geehan, G. and Underwood, J.** (1993). The use of length distributions in geological modeling. In: *The Geologic Modelling of Hydrocarbon Reservoirs and Outcrop Analogs* (Eds. S.S. Flint and I.D. Bryant), International Association of Sedimentologists Special Publication, **15**, 205–212.
- George, G.T. and Berry, J.K.** (1993) A new lithostratigraphy and depositional model for the Upper Rotliegend of the UK Sector of the Southern North Sea. In: *Characterisation of Fluvial and Aeolian Reservoirs*. (Eds. North, C.P. and Prosser, D.J.) *Geological Society Special Publication*, **73**, 291–319.
- George, G.T. and Berry, J.K.** (1997). Permian Upper Rotliegend synsedimentary tectonics, basin development and palaeogeography of the southern North Sea. In: *Petroleum geology of the southern North Sea*. (Eds. Ziegler, P., Turner, P., and Daines, S.R.). *Geological Society of London Special Publication*, **123**, 31-61.
- Ghazi, S. and Mountney, N.P.** (2009) Facies and architectural element analysis of a meandering fluvial succession: The Permian Warchha Sandstone, Salt Range, Pakistan. *Sedimentary Geology*, **221**, 99–112.
- Ghinassi, M. and Ielpi, A.** (2018). Precambrian snapshots: Morphodynamics of Torridonian fluvial braid bars revealed by three-dimensional photogrammetry and outcrop sedimentology. *Sedimentology*, **65(2)**, 492–516.
- Gibling, M.R.** (2006). Width and thickness of fluvial channel bodies and valley fills in the geological record: a literature compilation and classification. *Journal of sedimentary Research*, **76(5)**, 731–770.
- Gilfillan, S.M.V., Ballentine, C.J., Holland, G., Dave Blagburn, D., Lollar, B.S., Stevens, S., Schoell, M. and Cassidy, M.** (2008). The noble gas geochemistry of natural CO₂ gas reservoirs from the Colorado Plateau and Rocky Mountain provinces, USA. *Geochimica et Cosmochimica Acta*, **72(4)**, 1174–1198.
- Glennie, K.W.** (1972). Permian Rotliegendes of north-west Europe interpreted in light of modern desert sedimentation studies. *American Association of Petroleum Geologists Bulletin*, **56**, 1048–1071.
- Glennie, K.W.** (1983). Early Permian (Rotliegendes) palaeowinds of the North Sea. *Sedimentary Geology*, **34**, 245–265.

- Glennie, K.W.** (1986). Development of NW Europe's Southern Permian gas basin. In: *Habitat of Palaeozoic gas in northwest Europe*. (Eds. Brooks, J., Goff, J. and van Hoorn, B.). Geological Society of London Special Publication, **23**, 3–22.
- Glennie, K.W.** (1998). Lower Permian-Rotliegend. In: *Petroleum geology of the North Sea—Basic concepts and recent advances* (Ed. Glennie, K.W.) London, Blackwell Scientific Publishers, 137–173.
- Gómez-Gras, D.** and **Alonso-Zarza, A.M.** (2003). Reworked calcretes: their significance in the reconstruction of alluvial sequences (Permian and Triassic, Minorca, Balearic Islands, Spain). *Sedimentary Geology*, **158(3-4)**, 299–319.
- Goodchild, M.W.** and **Bryant, P.** (1986). The Geology of the Rough Gas Field. In: *Habitat of Palaeozoic gas in northwest Europe*. (Eds. Brooks, J., Goff, J. and van Hoorn, B.). Geological Society of London Special Publication, **23**, 223–235.
- Goudie, A.,** and **Viles, H.** (2015). The Ephemeral Rivers and Dunes of the Skeleton Coast. *World Geomorphological Landscapes*, 69–71.
- Guan, Q., Wang, L., Wang, F., Pan, B., Song, N., Li, F. and Lu, M.** (2016). Phosphorus in the catchment of high sediment load river: A case of the Yellow River, China. *Science of The Total Environment*, **572**, 660–670.
- Gulliford, A.R., Flint, S.S. and Hodgson, D.M.** (2014). Testing applicability of models of distributive fluvial systems or trunk rivers in ephemeral systems: reconstructing 3-D fluvial architecture in the Beaufort Group, South Africa. *Journal of Sedimentary Research*, **84(12)**, 1147–1169.
- Guy, H.P., Simons, D.B. and Richardson, E.V.** (1966). Summary of alluvial channel data from flume experiments 1956–1961. *US Geological Survey Professional Papers*, **461-I**, 1–96.
- Haldorsen, H.H. and Damsleth, E.** (1993). Challenges in reservoir characterization: GEOHORIZONS. *AAPG bulletin*, **77(4)**, 541–551.
- Hampton, B.A. and Horton, B.K.** (2007). Sheetflow fluvial processes in a rapidly subsiding basin, Altiplano plateau, Bolivia. *Sedimentology*, **54(5)**, 1121–1148.
- Harshbarger, J.W., Repenning, C.A. and Irwin, J.H.** (1957). Stratigraphy of the uppermost Triassic and the Jurassic rocks of the Navajo Country (Colorado Plateau). *Professional Paper. US Geological Survey*, **291**, 74.
- Hartley, A.J., Weissmann, G.S., Nichols, G.J. and Warwick, G.L.** (2010). Large distributive fluvial systems: characteristics, distribution, and controls on development. *Journal of Sedimentary Research*, **80(2)**, 167–183.
- Hasiotis, S.** (2002). Continental Trace Fossils: SEPM (Society for Sedimentary Geology) Short Course Notes no. 51. *Society for Sedimentary Geology, Tulsa, Oklahoma*. 134.
- Hasiotis, S.** (2007). Continental ichnology: fundamental processes and controls on trace fossil distribution. In: *Trace Fossils: Concepts, Problems, Prospects* (Ed. Miller, W.) Elsevier, 268–284.
- Hassan, M.S., Venetikidis, A., Bryant, G. and Miall, A.D.** (2018). The Sedimentology of an ERG Margin: The Kayenta–Navajo Transition (Lower Jurassic), Kanab, Utah, USA. *Journal of Sedimentary Research*, **88(5)**, 613–640.

- Haughton, P.D.W., Todd, S.P. and Morton, A.C.** (1991). Sedimentary provenance studies. In: *Developments in Sedimentary Provenance Studies*. (Eds. Morton, A.C., Todd, S.P. and Haughton, P.D.W.) Geological Society of London, Special Publications, **57**, 1–11.
- Herries, R.D.** (1993). Contrasting styles of fluvial-eolian interaction at a downwind erg margin: Jurassic Kayenta-Navajo transition, northeastern Arizona, USA. In: *Characterization of Fluvial and Aeolian Reservoirs* (Eds. C.P. North and D.J. Prosser), Geological Society Special Publication, **73**, 199–21.
- Hirst, J.P.P.** (1991). Variations in alluvial architecture across the Oligo-Miocene Huesca fluvial system, Ebro Basin, Spain, In: *The three dimensional facies architecture of terrigenous clastic sediments and its implications for hydrocarbon discovery and recovery* (Eds. A.D. Miall and N. Tyler). SEPM Concepts in Sedimentology and Paleontology, **3**, 111–121.
- Hirst, J.P.P. and Nichols, G.** (1986). Thrust tectonic controls on Miocene alluvial distribution patterns, southern Pyrenees. In: *Foreland Basins*. (Eds. Allen, P.A. and Homewood, P.) Blackwell Publishing, Oxford, 247–258.
- Hodgetts, D.** (2013). Laser scanning and digital outcrop geology in the petroleum industry: a review. *Marine and Petroleum Geology*, **46**, 335–354.
- Holbrook, J., Scott, R.W. and Oboh-Ikuenobe, F.E.** (2006). Base-Level buffers and buttresses: A model for upstream versus downstream control on fluvial geometry and architecture within sequences. *Journal of Sedimentary Research*, **76**, 162–174.
- Holden, L. Hague, R. Skare, Ø. and Skorstad, A.** (1998). Modelling of fluvial reservoirs with object models. *Maths Geology*, **30(5)**, 473–496.
- Hooke, J.M.** (2016). Morphological impacts of flow events of varying magnitude on ephemeral channels in a semiarid region. *Geomorphology*, **252**, 128–143.
- Horn, B.L.D., Goldberg, K. and Schultz, C.L.** (2018). Interpretation of massive sandstones in ephemeral fluvial settings: A case study from the Upper Candelária Sequence (Upper Triassic, Paraná Basin, Brazil). *Journal of South American Earth Sciences*, **81**, 108–121.
- Hornung, J. and Aigner, T.** (1999). Reservoir and aquifer characterization of fluvial architectural elements: Stubensandstein, Upper Triassic, southwest Germany. *Sedimentary Geology*, **129**, 215–280.
- Horowitz, D.H.** (1982). Geometry and origin of large-scale deformation structures in some ancient wind-blown sand deposits. *Sedimentology*, **29(2)**, 155–180.
- Horton, B.K. and DeCelles, P.G.** (2001). Modern and ancient fluvial megafans in the foreland basin system of the central Andes, southern Bolivia: implications for drainage network evolution in foldthrust belts. *Basin Research*, **13(1)**, 43–63.
- Howell, J. and Mountney, N.** (1997). Climatic cyclicity and accommodation space in arid to semi-arid depositional systems: an example from the Rotliegend Group of the UK southern North Sea. In: *Petroleum Geology of the Southern North Sea: Future Potential* (Ed. A.J. Fleet) Geological Society, London, Special Publications, **123(1)**, 63–86.
- Howell, J. and Mountney, N.** (2001). Aeolian grain flow architecture: hard data for reservoir models and implications for red bed sequence stratigraphy. *Petroleum Geoscience*, **7(1)**, 51–56.

- Howell, J.A., Martinius, A.W. and Good, T.R.** (2014). The application of outcrop analogues in geological modelling: A review, present status and future outlook. In: *Sediment-Body Geometry and Heterogeneity: Analogue Studies for Modelling the Subsurface* (Eds. A.R. Martinius, J.A. Howell & T.R. Good). Geological Society, London, Special Publications, **387**, 1–25.
- Hsu, T.-J., Jenkins, J.T. and Liu, P.L.-F.** (2004) On two-phase sediment transport: sheet flow of massive particles. *Proceedings of the Royal Society*, **460(2048)**, 1–14.
- Hsu, T.-J. and Hanes, D.M.** (2004). Effects of wave shape on sheet flow sediment transport. *Journal of Geophysical Research: Oceans*, **109(C5)**, 1–15.
- Hunter, R.E.** (1977a). Basic types of stratification in small eolian dunes. *Sedimentology*, **24(3)**, 361–387.
- Hunter, R.E.** (1977b) Terminology of cross-stratified sedimentary layers and climbing ripple structures. *Journal of Sedimentary Petrology*, **47**, 697–706.
- Hunter, R.E.** (1981). Stratification styles in eolian sandstones: some Pennsylvanian to Jurassic examples from the Western Interior, U.S.A. *SEPM Special Publication*, **31**, 315–329.
- Ielpi, A. and Rainbird, R.H.** (2015). Architecture and morphodynamics of a 1·6 Ga fluvial sandstone: Ellice Formation of Elu Basin, Arctic Canada. *Sedimentology*, **62(7)**, 1950–1977.
- Ilg, B.R., Karlstrom, K.E., Hawkins, D.P. and Williams, M.L.** (1996). Tectonic evolution of Paleoproterozoic rocks in the Grand Canyon: insights into middle-crustal processes. *Geological Society of America Bulletin*, **108**, 1149–1166.
- Jackson, R.G.** (1975). Hierarchical attributes and a unifying model of bedforms composed of cohesionless material and produced by shearing flow. *Bulletin of the Geological Society of America*, **86**, 1523–1533.
- Jaeger, K.L., Sutfin, N.A., Tooth, S., Michaelides, K. and Singer, M.** (2017). Geomorphology and sediment regimes of intermittent rivers and ephemeral streams. In: *Intermittent Rivers and Ephemeral Streams Ecology and Management* (Eds. T. Datry, N. Bonada and A. Boulton). Academic Press. 21–49.
- Jagger, A.** (2003) Sedimentology and Stratigraphic Evolution of the Permian Cedar Mesa Sandstone, SE Utah. Unpublished PhD Thesis, University of Keele, Keele, 391.
- Johnsson, M.J., Stallard, R.F. and Meade, R.H.** (1988). First-Cycle Quartz Arenites in the Orinoco River Basin, Venezuela and Colombia. *Journal of Geology*, **96**, 263–277.
- Karcz, I.** (1972). Sedimentary structures formed by flash floods in southern Israel. *Sedimentary Geology*, **7(3)**, 161–182.
- Kehl, C., Buckley, S.J., Viseur, S., Gawthorpe, R.L. and Howell, J.A.** (2017). Automatic illumination-invariant image-to-geometry registration in outdoor environments. *The Photogrammetric Record*, **32(158)**, 93–118.
- Kelly, S.B. and Olsen, H.** (1993). Terminal fans—a review with reference to Devonian examples. *Sedimentary Geology*, **85(1-4)**, 339–374.
- Kennedy, J.F.** (1969). The formation of sediment ripples, dunes and antidunes. In: *Annual Review of Fluid Mechanics* (Eds. Sears, W.R.) Annual Reviews Inc, Palo Alto, California, **1**, 147–168.

- Kietzke, K.K. and Lucas, S.G.** (1995). Ostracoda and Gastropoda from the Kayenta Formation (Lower Jurassic) of Arizona, U.S.A. *Journal of the Arizona-Nevada Academy of Science*, **28**, 23–32
- Kjemperud, A.V. Schomacker, E.R. and Cross, T.A.** (2008). Architecture and stratigraphy of alluvial deposits, Morrison Formation (Upper Jurassic), Utah. *Bulletin of the American Association of Petroleum Geologists*, **92(8)**, 1055–1076.
- Klawitter, M., Pistellato, D., Webster, A. and Esterle, J.** (2017). Application of photogrammetry for mapping of solution collapse breccia pipes on the Colorado Plateau, USA. *The Photogrammetric Record*, **32(160)**, 443–458.
- Kocurek, G.** (1981). Significance of interdune deposits and bounding surfaces in aeolian dune sands. *Sedimentology*, **28(6)**, 753–780.
- Kocurek, G.** (1988). First-order and super bounding surfaces in eolian sequences—Bounding surfaces revisited. *Sedimentary Geology*, **56(1-4)**, 193–206.
- Kocurek, G.** (1991). Interpretation of ancient eolian sand dunes. *Annual Review of Earth and Planetary Sciences*, **19(1)**, 43–75.
- Kocurek, G.** (1996). Desert aeolian systems, In: *Sedimentary environments: Processes, facies and stratigraphy* (Ed. H.G. Reading) 3rd Ed., Blackwell Science Ltd, Cambridge, 125–153.
- Kocurek, G.** (1999) The aeolian rock record (Yes, Virginia, it exists, but it really is rather special to create one). In: *Aeolian Environments Sediments and Landforms* (Eds. Goudie, A.S., Livingstone, I. and Stokes, S.). John Wiley and Sons, Chichester, 239–259.
- Kocurek, G., Havholm, K.G., Deynoux, M., and Blakey, R.C.** (1991). Amalgamated accumulations resulting from climatic and eustatic changes. *Sedimentology*, **38**, 751–772.
- Kocurek, G. and Lancaster, N.** (1999) Aeolian system sediment state: theory and Mohave Desert Kelso dune field example. *Sedimentology*, **46**, 505–515.
- Kocurek, G. and Nielson, J.** (1986). Conditions favorable for the formation of warm-climate aeolian sand sheets. *Sedimentology*, **33(6)**, 795–816.
- Kok, J.F., Parteli, E.J.R., Michaels, T.I. and Bou Karam, D.** (2012) The physics of windblown sand and dust. *Reports on Progress in Physics*, **75**, 106901.
- Krigstrom, A.** (1962). Geomorphological studies of sandur plains and their braided rivers in Iceland. *Geografiska Annaler*, **44**, 328–346.
- Krystinik, L.F.** (1990) Characteristics of cores from a wave-dominated barrier/tidal inlet deposit: Cretaceous Almond Formation, south-central Wyoming. In: *Tidal Inlet and Related Sand Bodies Modern and Ancient*. (Eds. Davis, R.A. Nummendal, D. and Tillman, R.). SEPM Research Conference San Juan Basin, New Mexico.
- Lancaster, N.** (1989) The dynamics of star dunes: an example from the Gran Desierto, Mexico. *Sedimentology*, **36(2)**, 273–289.
- Lancaster, N.** (2005) Draa (Megadune). In: *Encyclopaedia of geomorphology*. (Eds. Goudie, A.S.) Routledge, London, 272.

- Lancaster, N.** and **Nickling, W.G.** (1994). Chapter 17: Aeolian sediment transport. In: *Geomorphology of Desert Environments*. (Eds. Abrahams, A.D. and Parsons, A.J.) Chapman and Hall, Springer, Netherlands, 447–473.
- Lane, L.J., Diskin, M.H.** and **Renard, K.G.** (1971). Input-output relationships for an ephemeral stream channel system. *Journal of Hydrology*, **13**, 22–40.
- Lang, J.** and **Winsemann, J.** (2013). Lateral and vertical facies relationships of bedforms deposited by aggrading supercritical flows: from cyclic steps to humpback dunes. *Sedimentary Geology*, **296**, 36–54.
- Langford, R.P.** (1989). Fluvial-aeolian interactions: Part I, modern systems. *Sedimentology*, **36(6)**, 1023–1035.
- Langford, R.P.** and **Chan, M.A.** (1989). Fluvial-aeolian interactions: Part II, ancient systems. *Sedimentology*, **36(6)**, 1037–1051.
- Lawton, T.F.** (1994) Tectonic setting of Mesozoic sedimentary basins, Rocky Mountain region, United States. In: *Mesozoic systems of the Rocky Mountain region, USA*. (Eds. Caputo, M. V., Peterson, J. A., and Franczyk, K. J.) Denver, Colorado, Rocky Mountain Section SEPM, 1–26.
- Lebeau, L.E.** and **Ielipi, A.** (2017). Fluvial channel-belts, floodbasins, and aeolian ergs in the Precambrian Meall Dearg Formation (Torridonian of Scotland): Inferring climate regimes from pre-vegetation clastic rock records. *Sedimentary Geology*, **357**, 53–71.
- Leeder, M.R.** (1980). On the stability of lower stage plane beds and the absence of ripples in coarse sands. *Journal of the Geological Society London*, **137**, 423–430.
- Leeder, M.R.** (1982) Chapter 4: Grain Properties. In: *Sedimentology: Process and Product*. (Eds. Leeder, M.R.) Chapman and Hall, 35–43.
- Leeder, M.R.** (1983). On the interactions between turbulent flow, sediment transport and bedform mechanics in channelized flows. In: *Modern and Ancient Fluvial Systems*. (Eds. Collinson, J.D. & Lewin, J.) International Association of Sedimentologists Special Publications, **6**, 5–18.
- Leeder, M.** (2011) Chapter 6: Sediment in fluid and fluid flow. In: *Sedimentology and Sedimentary Basins: From Turbulence to Tectonics*. 2nd Ed. Wiley-Blackwell. Chichester, West Sussex. UK, 233–270.
- Lima, K.C.** and **Lupinacci, C.M.** (2019). Fluvial morphologies in semiarid environment: Theoretical issues applied to a case study. *Revista Brasileira de Geomorfologia*, **20(3)**, 475–490.
- Li, H.Y., Gao, Y., Wang, Y.J.** et al. (2015) Intercalation pattern and its impact on development of braided river reservoirs: A case of Fengcheng oilfield, Junggar basin, NW China. *Petroleum Exploration and Development*, **42(3)**, 397–373.
- Lockley, M.** and **Hunt, A.P.** (1994). A review of Mesozoic vertebrate ichnofaunas of the Western Interior United States: Evidence and implications of a superior track record. In: *Mesozoic systems of the Rocky Mountain region, USA*. (Eds. Caputo, M.V., Peterson, J.A., and Franczyk, K.J.). Denver, RMS-SEPM, 95–108.
- Lockley, M.** and **Hunt, A.P.** (1995). *Dinosaur tracks and other fossil footprints of the western United States*. New York, Columbia University Press, 338.

- Lockley, M.G., Lucas, S.G., Hunt, A.P. and Gaston, R.** (2004) Ichnofaunas from the Triassic-Jurassic boundary sequences of the Gateway area, western Colorado: implications for faunal composition and correlations with other areas. *Ichnos*, **11**, 89–102.
- Lockley, M.G., Tedrow, A.R., Chamberlain, K.C., Minter, N.J. and Lim, J.D.** (2011), Footprints and invertebrate traces from a new site in the Nugget Sandstone (Lower Jurassic) of Idaho: Implications for life in the northern reaches of the great Navajo-Nugget erg system in the western USA. In: Fossil Record 3, (Eds. Lucas, S.G. and Spielmann, J.A.). New Mexico Museum of Natural History and Science, Bulletin, **53**.
- Long, D.F.G.** (2006) Architecture of pre-vegetation sandybraided perennial and ephemeral river deposits in Paleoproterozoic Athabasca Group, northern Saskatchewan, Canada as indicators of Precambrian fluvial style. *Sedimentary Geology*, **190**, 71–95.
- Long, D.F.G.** (2011). Architecture and depositional style of fluvial systems before land plants: a comparison of Precambrian, early Paleozoic and modern river deposits. In: *From river to rock record: The preservation of fluvial sediments and their subsequent interpretation* (Eds. SK Davidson, S. Leleu, & CP North), SEPM (Society for Sedimentary Geology), **97**, 37–61.
- Long, D.G.F.** (2017). Evidence of flash floods in Precambrian gravel dominated ephemeral river deposits. *Sedimentary Geology*, **347**, 53-66.
- Long, J.H.** (2008), Architectural and Stratigraphic Analysis of the Lower Jurassic Kayenta Formation, Northeastern Arizona, USA. *Unpublished M.Sc. Thesis*. Northern Arizona University.
- Loope, D.B.** (1988). Rhizoliths in ancient eolianites. *Sedimentary Geology*, **56(1-4)**, 301–314.
- Lorenz, J.C. and Nadon, G.C.** (2002). Braided-river deposits in a muddy depositional setting: the Molina Member of the Wasatch Formation (Paleogene), west-central Colorado, USA. *Journal of Sedimentary Research*, **72(3)**, 376–385.
- Lowe, D.G. and Arnott, R.W.C.** (2016). Composition and architecture of braided and sheetfloodingdominated ephemeral fluvial strata in the Cambrian–Ordovician Potsdam Group: a case example of the morphodynamics of Early Phanerozoic fluvial systems and climate change. *Journal of Sedimentary Research*, **86(6)**, 587–612.
- Lucas, S.G., Heckert, A.B. and Tanner, L.H.** (2005) Arizona’s Jurassic Fossil Vertebrates and the age of the Glen Canyon Group: Vertebrate Paleontology in Arizona. *New Mexico Museum of Natural History and Science Bulletin*, **29**, 95–104.
- Lucas, S.G., Lockley, M.G., Hunt, A.P. and Tanner, L.H.** (2006). Biostratigraphic significance of tetrapod footprints from the Triassic-Jurassic Wingate Sandstone on the Colorado Plateau. New Mexico Museum of Natural History and Science Bulletin, **37**, 109–117.
- Lucas, S.G., Tanner, L.H., Donohoo-Hurley, L.L., Geissman, J.W., Kozur, H.W. and Weems, R.E.** (2011). Position of the Triassic-Jurassic boundary and timing of the end-Triassic extinctions on land: Data from the Moenave Formation on the southern Colorado Plateau, USA. *Palaeogeography, Palaeoclimatology, Palaeoecology*, **302**, 194–205.
- Lucas, S.G. and Tanner, L.H.** (2006). The Springdale Member of the Kayenta Formation, Lower Jurassic of Utah-Arizona, *New Mexico Museum of Natural History and Science Bulletin*, **37**, 71–76.

Lucas, S.G. and Tanner, L.H. (2007). Tetrapod biostratigraphy and biochronology of the Triassic-Jurassic transition on the southern Colorado Plateau, USA. *Palaeogeography, Palaeoclimatology, Palaeoecology*, **244**, 242–256.

Lucas, S.G. and Tanner, L.H. (2014). Unconformable contact of the lower Jurassic Wingate and Kayenta Formations, southeastern Utah. In: *Geology of Utah's Far South* (Eds. J.S. MacLean, R.F. Biek and J.E. Huntoon), *Utah Geological Association Publication*, **43**, 311–320.

Luttrell, P.R. (1993). Basinwide sedimentation and the continuum of paleoflow in an ancient river system: Kayenta Formation (Lower Jurassic), central portion Colorado Plateau. *Sedimentary Geology*, **85(1-4)**, 411–434.

Luttrell, P.R. and Morales, M. (1993) Bridging the gap across Moenkopi Wash: a lithostratigraphic correlation. *Museum of Northern Arizona Bulletin*, **59**, 111–127.

Mabutt, J.A. (1977). *Desert Landforms: An introduction to systematic geomorphology*. Vol. 2, MIT Press, Cambridge, Massachusetts, 340 pp.

Mack, G.H. (1987). Mid-Cretaceous (late Albian) change from rift to retroarc foreland basin in southwestern New Mexico. *Geological Society of America Bulletin*, **98(5)**, 507–514.

Mackey, S.D. and Bridge, J.S. (1995). Three-dimensional model of alluvial stratigraphy; theory and applications. *Journal of Sedimentary Research*, **65(1b)**, 7–31.

Mantz, P.A. (1980). Laboratory flume experiments on the transport of cohesionless silica silts by water streams. *Proc. Instn. Civ. Engrs*, **2(69)**, 977–994.

Manzocchi, T., Walsh, J.J., Tomasso, M., Strand, J., Childs, C. and Haughton, P.D. (2007). Static and dynamic connectivity in bed-scale models of faulted and unfaulted turbidites. Geological Society, London, Special Publications, **292(1)**, 309–336.

Marie, J.P.P. (1975). Rotliegendes stratigraphy and diagenesis. In: *Petroleum and the Continental Shelf of North-west Europe*. (Ed. Woodland, A.W.). Applied Science Publishers, Barking, 205–210.

Martin, A. (2000). Flaser and wavy bedding in ephemeral streams: a modern and an ancient example. *Sedimentary Geology*, **136(1-2)**, 1–5.

Martin, B. Owen, A. Nichols, G.J. Hartley, A.J. and Williams, R.D. (2021) Quantifying Downstream, Vertical and Lateral Variation in Fluvial Deposits: Implications From the Huesca Distributive Fluvial System. *Frontiers in Earth Science*, **8**, 1-19.

Marzolf, J.E. (1994) Reconstruction of the early Mesozoic Cordilleran cratonic margin adjacent to the Colorado Plateau. In: *Mesozoic Systems of the Rocky Mountain Region, USA*. (Eds. Caputo, M.V., Peterson, J.A. and Franczyk, K.J.) Rocky Mountain Section SEPM, Denver, 181–215.

Mather, A. (2007). Arid Environments. In: Perry, C. & Taylor, K. (Eds.) *Environmental Sedimentology*. Blackwell Publishing, Oxford. 144–189.

Mather, A., Stokes, M., Pirrie, D. and Hartley, R. (2008). Generation, transport and preservation of armoured mudballs in an ephemeral gully system. *Geomorphology*, **100**, 104–119.

Mazumder, R. (2003). Sediment transport, aqueous bedform stability and morphodynamics under unidirectional current: A brief overview. *Journal of African Earth Science*, **36**, 1–14.

- McKay, C.P., Rask, J.C., Detweiler, A.M., Bebout, B.M., Everroad, R.C., Lee, J.Z. and Al-Awar, M.** (2016). An unusual inverted saline microbial mat community in an interdune sabkha in the Rub'al Khali (the Empty Quarter), United Arab Emirates. *PloS one*, **11(3)**, e0150342.
- McKee, E.D.** (1979). Introduction to A Study of Global- Sand Seas. In: *A study of global sand seas*. (Eds. McKee, E.D.) *U.S.G.S., Professional Paper*, **1052**, 8–13.
- McKee, E.D., Douglass, J.R. and Rittenhouse, S.** (1971). Deformation of lee-side laminae in eolian dunes. *Geological Society of America Bulletin*, **82(2)**, 359–378.
- McLaurin, B.T. and Steel, R.J.** (2007) Architecture and origin of an amalgamated fluvial sheet sand, lower Castlegate Formation, Book Cliffs, Utah. *Sedimentary Geology*, **197**, 291–311.
- Meyers, M.J.** (2010) Flow Regime Prediction via Froude Number Calculation in a Rock-Bedded Stream. Unpublished MSc Thesis. Brock University, St Catherines, Ontario.
- Miall, A.D.** (1977). A review of the braided-river depositional environment. *Earth-Science Reviews*, **13(1)**, 1–62.
- Miall, A.D.** (1978). Lithofacies types and vertical profile models in braided river deposits: a summery. In: *Fluvial Sedimentology*. (Eds. Miall, A.D.) Canadian Society of Petroleum Geologists, Canada, 597–604.
- Miall, A.D.** (1983). Basin analysis of fluvial sediments. In: *Modern and Ancient Fluvial Systems* (Eds. J.D. Collinson and J. Lewin) *IAS Special Publication*, **6**, 279–286.
- Miall, A.D.** (1984) Variations in fluvial style in the lower Cenozoic synorogenic sediments of the Canadian Arctic Islands. *Sedimentary Geology*, **38(1-4)**, 499–523.
- Miall, A.D.** (1985). A new method of facies analysis applied to fluvial deposits. *Earth-Science Review*, **22**, 261–308.
- Miall, A.D.** (1988). Architectural elements and bounding surfaces in fluvial deposits: anatomy of the Kayenta Formation (Lower Jurassic), southwest Colorado. *Sedimentary Geology*, **55(3-4)**, 233–262.
- Miall, A.D.** (1991) Sedimentology of a Sequence Boundary within the Nonmarine Torrivio Member, Gallup Sandstone (Cretaceous), San Juan Basin, New Mexico. In: *Concepts in Sedimentology and Paleontology: The Three-Dimensional Facies Architecture of Terrigenous Clastic Sediments and its Implications for Hydrocarbon Discovery and Recovery*. (Eds. Miall, A.D. and Tyler, N.) SEP Society for Sedimentary Geology, **3**.
- Miall, A.D.** (1993) The architecture of fluvial-deltaic sequences in the Upper Mesaverde Group (Upper Cretaceous), Book Cliffs, Utah. In: *Braided Rivers* (Eds. J.L. Best and C.S. Bristow), Geological Society of London Special Publication, **75**, 305–332.
- Miall, A.D.** (1994). Reconstructing fluvial macroform architecture from two-dimensional outcrops; examples from the Castlegate Sandstone, Book Cliffs, Utah. *Journal of Sedimentary Research*, **64(2b)**, 146–158.
- Miall, A.D.** (1996). *The Geology of Fluvial Deposits, Sedimentary Facies, Basin Analysis and Petroleum Geology*. 1st Ed. Springer-Verlag, Berlin. 582pp.
- Miall, A.D.** (2010). Alluvial deposits. In: *Facies Models 4* (Eds. James, N.P. and Dalrymple, R.W.) St. John's, Geological Association of Canada, 105–138.

Miall, A.D. (2013). *The Geology of Fluvial Deposits, Sedimentary Facies, Basin Analysis and Petroleum Geology*. 4th Ed., Springer-Verlag, Berlin. 575 pp.

Miall, A.D. (2014). Chapter 2: The facies and architecture of fluvial systems. In: *Fluvial Depositional Systems* (Ed. A.D. Miall) 1st Ed., Springer, Cham. 9–68.

Miall, A.D. (2016) The valuation of unconformities. *Earth-Science Reviews*, **163**, 22–71.

Middleton, L.T. and **Blakey, R.C.** (1983). Processes and controls on the intertonguing of the Kayenta and Navajo Formations, northern Arizona: eolian-fluvial interactions. In: *Eolian Sediments and Processes* (Ed. M. E. Brookfield and T. S. Ahlbrandt). *Dev. Sediment.*, **38**, 613–634. Elsevier, Amsterdam.

Miller, D.M., Nilsen, T.H. and **Bilodeau, W.L.** (1992) Late Cretaceous to early Eocene geologic evolution of the U.S. Cordillera. In: *The Geology of North America - The Cordilleran Orogen: Coterminous U.S.* (Eds. Burchfield, B.C. Lipman, P.W. and Zoback, M.L.) Geological Society of America, Boulder, Colorado, **G-3**, 205-260.

Morgan, P. (2003). Colorado Plateau and southern Rocky Mountains uplift and erosion. In: *Cenozoic systems of the Rocky Mountain region: Denver, Colorado*. (Eds. Reynolds, R.G., and Flores, R.M.) Rocky Mountain Section SEPM (Society for Sedimentary Geology), 1–31.

Moscariello, A. (2011) Sedimentary facies, correlation, and architecture of Rotliegend reservoirs at the Southern Permian basin margin: The P01-FA case study and the challenged myth of layer-cake stratigraphy. SEPM Special Publication, **98**, 177–190.

Mountney, N.P. (2006). Periodic accumulation and destruction of aeolian erg sequences in the Permian Cedar Mesa Sandstone, White Canyon, southern Utah, USA. *Sedimentology*, **53(4)**, 789–823.

Mountney, N.P. and **Jagger, A.** (2004). Stratigraphic evolution of an aeolian erg margin system: the Permian Cedar Mesa Sandstone, SE Utah, USA. *Sedimentology*, **51(4)**, 713–743.

Nanson, G.C. and **Knighton, A.D.** (1996). Anabranching rivers: their cause, character and classification. *Earth Surface Processes and Landforms*, **21(3)**, 217–239.

Nichols, G.J. (1987). Structural controls on fluvial distributary systems—the Luna System, Northern Spain. In: *Recent Developments in Fluvial Sedimentology* (Eds. F.G. Ethridge, R.M. Florez and M.D. Harvey), SEPM Special Publication, **39**, 269–277.

Nichols, G.J. (1989). Structural and sedimentological evolution of part of the west central Spanish Pyrenees in the Late Tertiary. *Journal of the Geological Society (London)*, **146**, 851–857.

Nichols, G.J. (2009) *Sedimentology and Stratigraphy*. 2nd Ed. Wiley-Blackwell. Chichester, West Sussex. UK. 418 pp.

Nichols, G.J. and **Fisher, J.A.** (2007). Processes, facies and architecture of fluvial distributary system deposits. *Sedimentary Geology*, **195(1-2)**, 75–90.

Nickling, W.G. and **McKenna Neuman, C.** (2009). Chapter 17: Aeolian sediment transport. In: *Geomorphology of desert environments* (Eds. Parsons, J. and Abrahams, A.D.) 2nd Ed. Chapman and Hall, Springer, Netherlands, 517-555.

Nielsen, P. (1981) Dynamics and Geometry of Wave-Generated Ripples. *Journal of Geophysical Research*, **86(C7)**, 6467–6472.

- Nielson, J. and Kocurek, G.** (1986). Climbing zibars of the Algodones. *Sedimentary Geology*, **48(1)**, 1–15.
- Niethammer, U., James, M.R., Rothmund, S., Travelletti, J. and Joswig, M.,** (2012). UAV-based remote sensing of the Super-Sauze landslide: Evaluation and results. *Engineering Geology*, **128**, 2–11.
- North, C.P. and Davidson, S.K.** (2012). Unconfined alluvial flow processes: recognition and interpretation of their deposits, and the significance for palaeogeographic reconstruction. *Earth Science Reviews*, **111(1- 2)**, 199–223.
- North, C.P. and Taylor, K.S.** (1996). Ephemeral-fluvial deposits: integrated outcrop and simulation studies reveal complexity. *AAPG Bulletin*, **80(6)**, 811–830.
- North, C.P. and Warwick, G.L.** (2007). Fluvial fans: myths, misconceptions, and the end of the terminal-fan model. *Journal of Sedimentary Research*, **77(9)**, 693–701.
- Nwajide, C.S.** (1988). Convergent mud drapes on some planar cross-beds in the fluvial Turonian sandstones of the Makurdi formation, Benue Trough, Nigeria. *Journal of African Earth Sciences (and the Middle East)*, **7**, 113–120.
- Olsen, H.** (1987). Ancient ephemeral stream deposits: a local terminal fan model from the Bunter Sandstone Formation (L. Triassic) in the Tønder-3,-4 and-5 wells, Denmark. In: *Desert Sediments: Ancient and Modern* (Eds. L. Frostick and I. Reid), Geological Society Special Publications, London, **35**, 69–86.
- Olsen, H.** (1989). Sandstone-body structures and ephemeral stream processes in the Dinosaur Canyon Member, Moenave Formation (Lower Jurassic), Utah, USA. *Sedimentary Geology*, **61(3-4)**, 207-221.
- Owen, G.** (1996) Experimental soft-sediment deformation: structures formed by liquefaction of unconsolidated sands and some ancient examples. *Sedimentology*, **43**, 279–293.
- Owen, G.** (2017) Origin and significance of soft-sediment deformation in the Old Red Sandstone of central South Wales, UK. *Proceedings of the Geologists' Association*, **128**, 422–430.
- Owen, A., Hartley, A.J., Ebinghaus, A., Weissmann, G.S. and Santos, M.G.M.** (2019) Basin-scale predictive models of alluvial architecture: constraints from the Palaeocene-Eocene, Bighorn Basin, Wyoming, USA. *Sedimentology*, **66**, 736–763
- Owen, A., Nichols, G.J., Hartley, A.J. and Weissmann, G.S.** (2017). Vertical trends within the prograding Salt Wash distributive fluvial system, SW United States. *Basin Research*, **29**, 64– 80.
- Owen, A., Nichols, G. J., Hartley, A. J., Weissmann, G. S. and Scuderi, L. A.** (2015). Quantification of a distributive fluvial system: the Salt Wash DFS of the Morrison Formation, SW USA. *Journal of Sedimentary Research*, **85(5)**, 544–561.
- Paola, C. and Borgman, L.** (1991) Reconstructing random topography from preserved stratification. *Sedimentology*, **38**, 553–565.
- Perry, C. and Taylor, K.** (2007). Environmental Sedimentology: introduction. In: *Environmental Sedimentology* (Eds. Perry, C. & Taylor, K.). Blackwell Publishing, Oxford. 1–31.
- Peterson, F. and Pipiringos, G.N.** (1979). Stratigraphic relations of the Navajo Sandstone to Middle Jurassic formations, southern Utah and northern Arizona. *Professional Paper. US Geological Survey*, **1035-B**, 1–43.

- Pettigrew, R.P., Priddy, C., Clarke, S.M. Warke, M.R., Stüeken, E.E. and Claire, M.W.** (2021) Sedimentology and isotope geochemistry of transitional evaporitic environments within arid continental settings: From erg to saline lakes. *Sedimentology*, **68(3)**, 907–942.
- Pettigrew, R.P., Rogers, S.L. and Clarke, S.M.** (2020). A microfacies analysis of arid continental carbonates from the Cedar Mesa Sandstone Formation, Utah, USA. *The Depositional Record*, **6(1)**, 41–61.
- Picard, M.D. and High, L.R.** (1973). Sedimentary Structures of Ephemeral Streams. *Developments in Sedimentology*, **17**, 223.
- Pipiringos, G.N., and O'Sullivan, R.B.** (1978). *Principal unconformities in Triassic and Jurassic rocks, western interior United States; a preliminary survey* (No. 1035-A). United States Government Printing Office.
- Posamentier, H.W. and Allen, G.P.** (1999). Siliciclastic Sequence Stratigraphy: Concepts and Applications. *SEPM (Society for Sedimentary Geology)*, Tulsa, Vol. 7.
- Priddy, C. L. and Clarke, S.M.** (2020). The sedimentology of an ephemeral fluvial-aeolian succession. *Sedimentology*, **67(5)**, 2392–2425.
- Priddy, C.L., Pringle, J.K., Clarke, S.M. and Pettigrew, R.P.** (2019). Application of photogrammetry to generate quantitative geobody data in ephemeral fluvial systems. *The Photogrammetric Record*, **34(168)**, 428–444.
- Pringle, J.K., Howell, J.A., Hodgetts, D., Westerman, A.R. and Hodgson, D.M.** (2006). Virtual outcrop models of petroleum reservoir analogues: a review of the current state-of-the-art. *First Break*, **24(3)**, 33–42.
- Pringle, J.K., Brunt, R.L., Hodgson, D.M., and Flint, S.S.** (2010). Capturing stratigraphic and sedimentological complexity in 3D digital outcrop models of submarine channel complexes, Karoo Basin, South Africa. *Petroleum Geoscience*, **16(4)**, 307–330.
- Prosser, D.J.** (1988) The sedimentology and diagenesis of Lower Permian (Rotliegend) sediments: (onshore UK and southern North Sea). Unpublished PhD Thesis. The University of Aston in Birmingham, 1, 39–279.
- Puigdefabregas, C. and Vliet, A. Van** (1978). Meandering stream deposits from the Tertiary of the Southern Pyrenees. In: Fluvial Sedimentology (Ed. Miall, A.D.). *Memoir of the Canadian Society of Petroleum Geologists*, **5**, 469–486.
- Rana, N., Sati, S.P., Sundriyal, Y. and Juyal, N.** (2016) Genesis and implication of soft-sediment deformation structures in high-energy fluvial deposits of the Alaknanda Valley, Garhwal Himalaya, India. *Sed. Geol.*, **344**, 263–276.
- Rarity, F., Van Lanen, X.M.T., Hodgetts, D., Gawthorpe, R.L., Wilson, P., Fabuel-Perez, I. and Redfern, J.** (2013). LiDAR-based digital outcrops for sedimentological analysis: workflows and techniques. Geological Society, London, Special Publications, **387(1)**, 153–183.
- Ravi, S., D'Odorico, P., Over, T. and Zobeck, T.** (2004). On the effect of air humidity on soil susceptibility to wind erosion: The case of air-dry soils. *Geophysical Research Letters*, **31(9)**, 1–4.
- Reading, H.G.** (1978). Sedimentary environments and facies. Blackwell Scientific Publications, London. 557 pp.

- Reid, I. and Laronne, J.B.** (1995). Bed load sediment transport in an ephemeral stream and a comparison with seasonal and perennial counterparts. *Water Resources Research*, **31(3)**, 773–781.
- Reid, I., Laronne, J.B. and Powell, D.M.** (1995). The Nahal Yatir bedload database: Sediment dynamics in a gravel-bed ephemeral stream. *Earth Surface Processes and Landforms*, **20(9)**, 845–857.
- Reis, A.D.D., Scherer, C.M.D.S., Amarante, F.B.D., Rossetti, M.D.M.M., Kifumbi, C., Souza, E.G.D., Ferronato, J.P.F. and Owen, A.** (2019). Sedimentology of the proximal portion of a large-scale, Upper Jurassic fluvial-aeolian system in Paraná Basin, southwestern Gondwana. *Journal of South American Earth Sciences*, **95**, 102248.
- Reitner, J.** (2011). Microbial mats. In: Encyclopedia geobiology. Part of the series of encyclopedia of earth sciences. (Eds. Reitner, J. and Thiel, V.). Heidelberg, Springer, 606–608.
- Rittersbacher, A., Buckley, S.J., Howell, J.A., Hampson, G.J. and Vallet, J.** (2014) Helicopter-based laser scanning: a method for quantitative analysis of large-scale sedimentary architecture. *Geological Society of London Special Publication*, **387**, 185–202.
- Rogers, D.A. and Astin, T.R.** (1991) Ephemeral lakes, mud pellet dunes and wind-blown sand and silt: reinterpretations of Devonian lacustrine cycles in north Scotland. In: *Lacustrine Facies Analysis* (Eds. Anadon, P., Cabrera, L. and Kelts, K.). Special Publication of the International Association of Sedimentologists, **13**, 199–221.
- Russell, K.L. Vietz, G.J. and Fletcher, T.D.** (2019). Urban sediment supply to streams from hillslope sources. *Science of the Total Environment*, **653**, 684–697.
- Russell, M.J. and Allison, I.** (1985). Agalmatolite and the maturity of sandstones of the Appin and Argyll groups and Eriboll Sandstone. *Scottish Journal of Geology*, **21(2)**, 113–122.
- Rust, B.R.** (1972). Pebble orientation in fluvial sediments. *Journal of Sedimentary Research*, **42(2)**, 348–388.
- Rust, B.R.** (1978) Depositional models for braided alluvium. In: *Fluvial sedimentology* (Eds. Miall, A.D.) Canadian Society of Petroleum Geologist Memoirs, **5**, 605–626.
- Sáez, A., Anadón, P., Herrero, M.J. and Moscariello, A.** (2007) Variable style of transition between Palaeogene fluvial fan and lacustrine systems, southern Pyrenean foreland, NE Spain. *Sedimentology*, **54(2)**, 367–390.
- Sadler, S.P. and Kelly, S.B.** (1993). Fluvial processes and cyclicity in terminal fan deposits: an example from the Late Devonian of southwest Ireland. In: *Current Research in Fluvial Sedimentology*. (Ed. Fielding, C.R.). *Sedimentary Geology*, **85**, 375–386.
- Sambrook Smith, G.H., Ashworth, P.J., Best, J.L., Woodward, J. and Simpson, C.J.** (2006). The sedimentology and alluvial architecture of the sandy braided South Saskatchewan River, Canada. *Sedimentology*, **53**, 413–434.
- Sanabria, D.I.** (2001) Sedimentology and Sequence Stratigraphy of the Lower Jurassic Kayenta Formation, Colorado Plateau, USA. Unpublished PhD Thesis, Rice University, Houston.
- Schmitz, J., Deschamps, R., Joseph, P., Lerat, O., Doligez, B. and Jardin, A.** (2014). From 3D photogrammetric outcrop models to reservoir models: an integrated modelling workflow. In *Vertical Geology Conference, University of Lausanne, Switzerland* 143–147.

Shanley, K.W. and McCabe, P.J. (1994) Perspective on the sequence stratigraphy of continental strata. *American Association of Petroleum Geologists Bulletin*, **78(4)**, 544–568.

Sharp, R.P. (1963). Wind ripples. *The Journal of Geology*, **71(5)**, 617–636.

Simon, S.S. and Gibling, M.R. (2017). Fine-grained meandering systems of the Lower Permian Clear Fork Formation of north-central Texas, USA: Lateral and oblique accretion on an arid plain. *Sedimentology*, **64(3)**, 714–746.

Simons, D.B., Richardson, E.V., and Albertson, M.L. (1961) Flume studies using medium sand (0.45 mm). United States geological survey water supply paper number **1498-A**, United States Government Printing Office, Washington, DC.

Simons, D.B., Richardson, E.V. and Nordin Jr, C.F. (1965). Bedload equation for ripples and dunes. U.S. Geological Survey Professional Paper, **462-H**, 1–9.

Smoot, J.P. and Lowenstein, T.K. (1991) Depositional environments of non-marine evaporites. In: *Evaporites, Petroleum and Mineral Resources* (Ed. Melvin, J.L.). *Developments in sedimentology*, **50**, 189–347.

Sneh, A. (1983) Desert stream sequences in the Sinai Peninsula. *Journal of Sedimentary Petrology*, **53**, 1271–1280.

Soares, M.V.T., Basilici, G., Dal’Bó, P.F., da Silva Marinho, T., Mountney, N.P., Colombera, L., de Oliveira, E.F. and da Silva, K.E.B. (2018). Climatic and geomorphologic cycles in a semiarid distributive fluvial system, Upper Cretaceous, Bauru Group, SE Brazil. *Sedimentary Geology*, **372**, 75–95.

Soreghan, G.S. (1994). The impact of glacioclimatic change on Pennsylvanian cyclostratigraphy. In: *Pangea — Global Environments and Resources*. (Eds. Embry, A.F., Beauchamp, B. and Glass, D.J.). Canadian Society of Petroleum Geologists Memoirs, **17**, 523–543.

Southard, J.B. (1971) Representation of bed configurations in depth-velocity-size diagrams. *Journal of Sedimentary Petrology*, **41**, 903–915.

Southard, J.B. and Boguchwal, L.A. (1990) Bed configurations in steady unidirectional flows: Part 2. Synthesis of flume data. *Journal of Sedimentary Petrology*, **60**, 658–679.

Stanistreet, I.G. and McCarthy, T.S. (1993). The Okavango Fan and the classification of subaerial fan systems. *Sedimentary Geology*, **85(1-4)**, 115–133.

Stear, W.M. (1985). Comparison of the bedform distribution and dynamics of modern and ancient sandy ephemeral flood deposits in the southwestern Karoo region, South Africa. *Sedimentary Geology*, **45(3-4)**, 209–230.

Stephen, K.D., Clark, J.D. and Gardiner, A.R. (2001). Outcrop-based stochastic modelling of turbidite amalgamation and its effects on hydrocarbon recovery. *Petroleum Geoscience*, **7(2)**, 163–172.

Stikes, M.W. (2007). Fluvial Facies and Architecture of the Poison Strip Sandstone Lower Cretaceous Cedar Mountain Formation, Grand County, Utah. *Utah Geological Survey*, **6(2)**, 1–60.

Sturzenegger, M. and Stead, D. (2012). The Palliser Rockslide, Canadian Rocky Mountains: characterization and modeling of a stepped failure surface. *Geomorphology*, **138(1)**, 145–161.

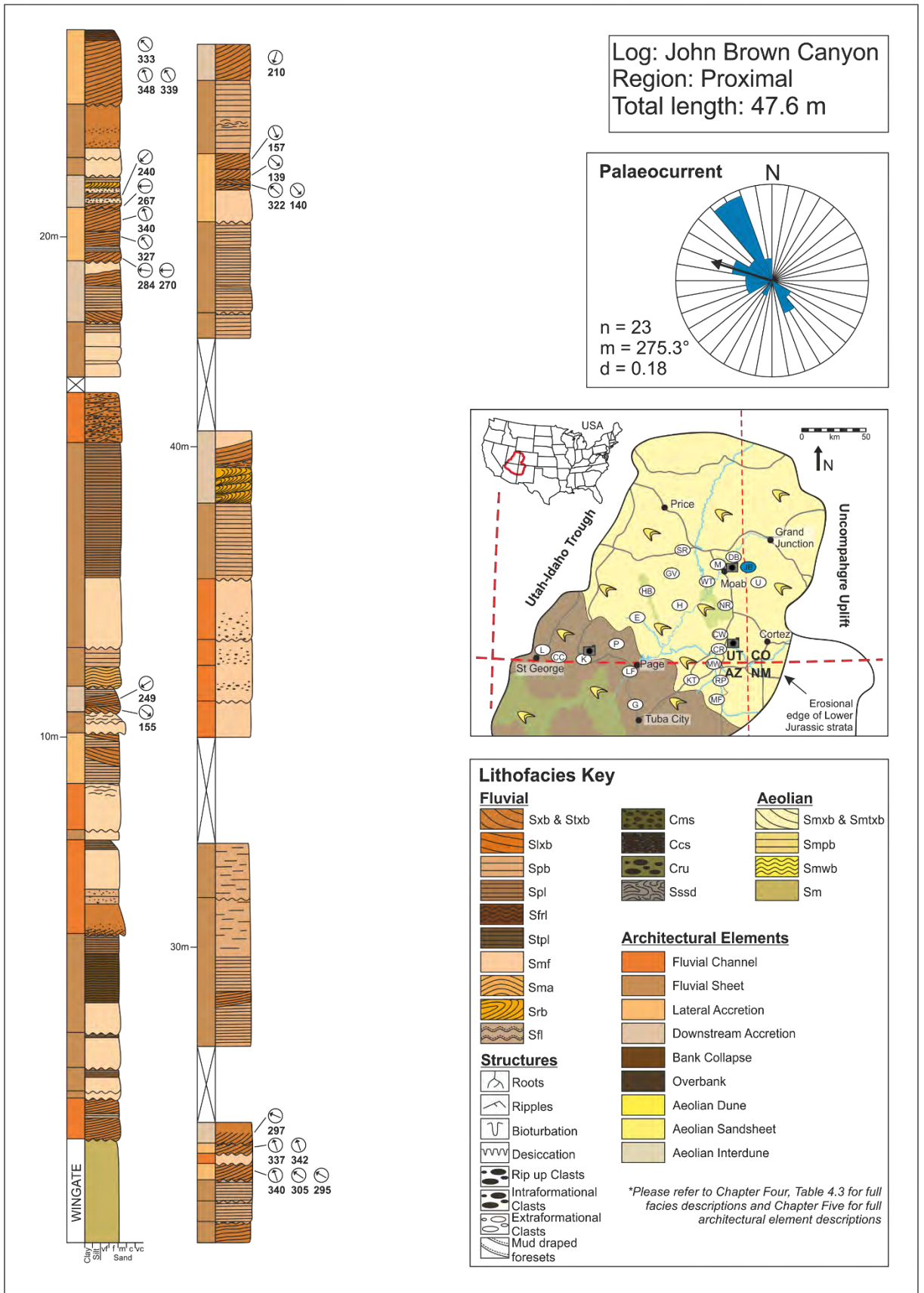
- Sues, H.D., Clark, J.M. and Jenkins, F.A., Jr.** (1994). A review of the Early Jurassic tetrapods from the Glen Canyon Group of the American Southwest. In: *In the shadow of dinosaurs: Early Mesozoic tetrapods*. (Eds. Fraser, N.C. and Sues, H.D.). Cambridge, Cambridge University Press, 285–294.
- Sutfin, N.A., Shaw, J.R., Wohl, E.E. and Cooper, D.J.** (2014). A geomorphic classification of ephemeral channels in a mountainous, arid region, southwestern Arizona, USA. *Geomorphology*, **221**, 164–175.
- Tanner, L.H. and Lucas, S.G.** (2007). The Moenave Formation: Sedimentologic and stratigraphic context of the Triassic-Jurassic boundary in the Four Corners area, southwestern USA. *Palaeogeography, Palaeoclimatology, Palaeoecology*, **244**, 111–125.
- Terwisscha van Scheltinga, R.C., McMahon, W.J., van Dijk, W.M., Eggenhuisen, J.T. and Kleinhans, M.G.** (2020). Experimental distributive fluvial systems: Bridging the gap between river and rock record. *The Depositional Record*, **6(3)**, 670–684.
- Thomas, D.S.G., Stokes, S. and Shaw, P.A.** (1997). Holocene aeolian activity in the southwestern Kalahari Desert, southern Africa: significance and relationships to late-Pleistocene dune-building events. *The Holocene*, **7(3)**, 273–281.
- Tjerry, S. and Fredsøe, J.** (2005) Calculation of dune morphology. *Journal of Geophysical Research: Earth Surface*, **110(F4)**, 1–13.
- Todd, S.P.** (1996). Process deduction from fluvial sedimentary structures. In: *Advances in Fluvial Dynamics and Stratigraphy* (Eds. P.A. Carling, M.R. Dawson), Wiley, West Sussex, England, 299–350.
- Tooth, S.** (1999). Downstream changes in floodplain character on the Northern Plains of arid central Australia. In: *Fluvial sedimentology VI*. (Eds. Smith, N.D. and Rogers, J.). Oxford: Blackwell. International Association of Sedimentologists, Special Publication, **28**, 93–112.
- Tooth, S.** (2000). Process, form and change in dryland rivers: a review of recent research. *Earth-Science Reviews*, **51(1-4)**, 67–107.
- Tooth, S.** (2005). Splay formation along the lower reaches of ephemeral rivers on the Northern Plains of arid central Australia. *Journal of Sedimentary Research*, **75(4)**, 636–649.
- Tooth, S.** (2013). Dryland fluvial environments: assessing distinctiveness and diversity from a global perspective. In: *Fluvial Geomorphology*. (Eds. Shroder, J. and Wohl, E.E.). Treatise on Geomorphology, Academic Press, San Diego, **9**, 612–644.
- Tooth, S. and Nanson, G.C.** (1999). Anabranching rivers on the Northern Plains of arid central Australia. *Geomorphology*, **29(3-4)**, 211–233.
- Tunbridge, I.P.** (1981). Sandy high-energy flood sedimentation—some criteria for recognition, with an example from the Devonian of SW England. *Sedimentary Geology*, **28(2)**, 79–95.
- Tunbridge, I.P.** (1984). Facies model for a sandy ephemeral stream and clay playa complex; the Middle Devonian Trentishoe Formation of North Devon, UK. *Sedimentology*, **31(5)**, 697–715.
- Tucker M.E.** (2001). *Sedimentary Petrology*. 3rd Ed. Blackwell Science. 262 pp.
- Ungar, J.E. and Haff, P.K.** (1987). Steady state saltation in air. *Sedimentology*, **34(2)**, 289–299.

- Van den Berg, J.H., Martinus, A.W. and Houthuys, R.** (2017) Breaching-related turbidites in fluvial and estuarine channels: Examples from outcrop and core and implications to reservoir models. *Marine and Petroleum Geology*, **82**, 178–205.
- Van Dover, C.L.** (2000). *The Ecology of Deep-Sea Hydrothermal Vents*. Princeton University Press, Princeton, 424.
- Van Veen, F.R.** (1975). Geology of Lemna Gas-Field. *Geology*, **1**, 223–231.
- Veiga, G.D., Spalletti, L.A. and Flint, S.** (2002). Aeolian/fluvial interactions and high-resolution sequence stratigraphy of a non-marine lowstand wedge: the Avilé Member of the Agrío Formation (Lower Cretaceous), central Neuquén Basin, Argentina. *Sedimentology*, **49**, 1001–1019.
- Ventra, D. and Clarke, L.E.** (2018). Geology and geomorphology of alluvial and fluvial fans: current progress and research perspectives. *Geological Society, London, Special Publications*, **440(1)**, 1–21.
- Visser, C.A. and Chessa, A. G.** (2000a). A new method for estimating lengths for partially exposed features. *Mathematical Geology*, **32(1)**, 109–126.
- Visser, C.A. and Chessa, A.G.** (2000b). Estimation of length distributions from outcrop datasets – application to the Upper Permian Cutler Formation, Utah. *Petroleum Geoscience*, **6**, 29–36.
- Walker, I.J. and Nickling, W.G.** (2002). Dynamics of secondary airflow and sediment transport over and in the lee of transverse dunes. *Progress in Physical Geography*, **26(1)**, 47–75.
- Walker, R.G.** (1979). *Facies models*. 1st Ed. Geological Association of Canada. 211 pp.
- Walker, R.G.** (1984). *Facies models*. 2nd Ed. Geological Association of Canada. 317 pp.
- Walker, R.G.** (2006). *Facies models revisited*. SEPM Special Publication, **84**, 1–17.
- Warren, J.K.** (2016) *Evaporites: A geological compendium*. 2nd Ed. Springer, Switzerland, 1783.
- Weissmann, G.S., Hartley, A.J., Nichols, G.J., Scuderi, L.A., Olson, M., Buehler, H. and Banteah, R.** (2010). Fluvial form in modern continental sedimentary basins: distributive fluvial systems. *Geology*, **38(1)**, 39–42.
- Weissmann, G.S., Hartley, A.J., Scuderi, L.A., Nichols, G.J., Davidson, S.K., Owen, A., Atchley, S.C., Bhattacharyya, P., Chakraborty, T., Ghosh, P. and Nordt, L.C.** (2013). Prograding distributive fluvial systems: geomorphic models and ancient examples. In: *New Frontiers in Paleopedology and Terrestrial Paleoclimatology* (Eds. S.G. Driese, L.C. Nordt), SEPM, Special Publication, **104**, 131–147.
- Westoby, M.J., Brasington, J., Glasser, N.F., Hambrey, M.J. and Reynolds, J.M.,** (2012). ‘Structure-from-Motion’ photogrammetry: A low-cost, effective tool for geoscience applications. *Geomorphology*, **179**, 300–314.
- Williams, G.E.** (1971). Flood deposits of the sand-bed ephemeral streams of central Australia. *Sedimentology*, **17(1-2)**, 1–40.
- Williams, G.P.** (1970). Flume width and water depth effects in some sediment-transport experiments: *U.S. Geological Survey Professional Paper*, **562-H**, 37.
- Wilson, I.** (1972). Aeolian Bedforms: Their development and origins. *Sedimentology*, **19(3-4)**, 173–210.

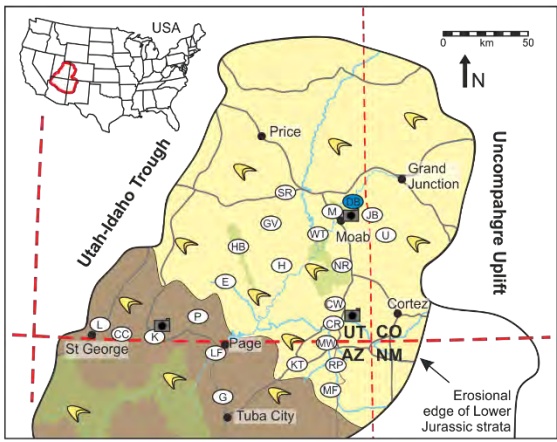
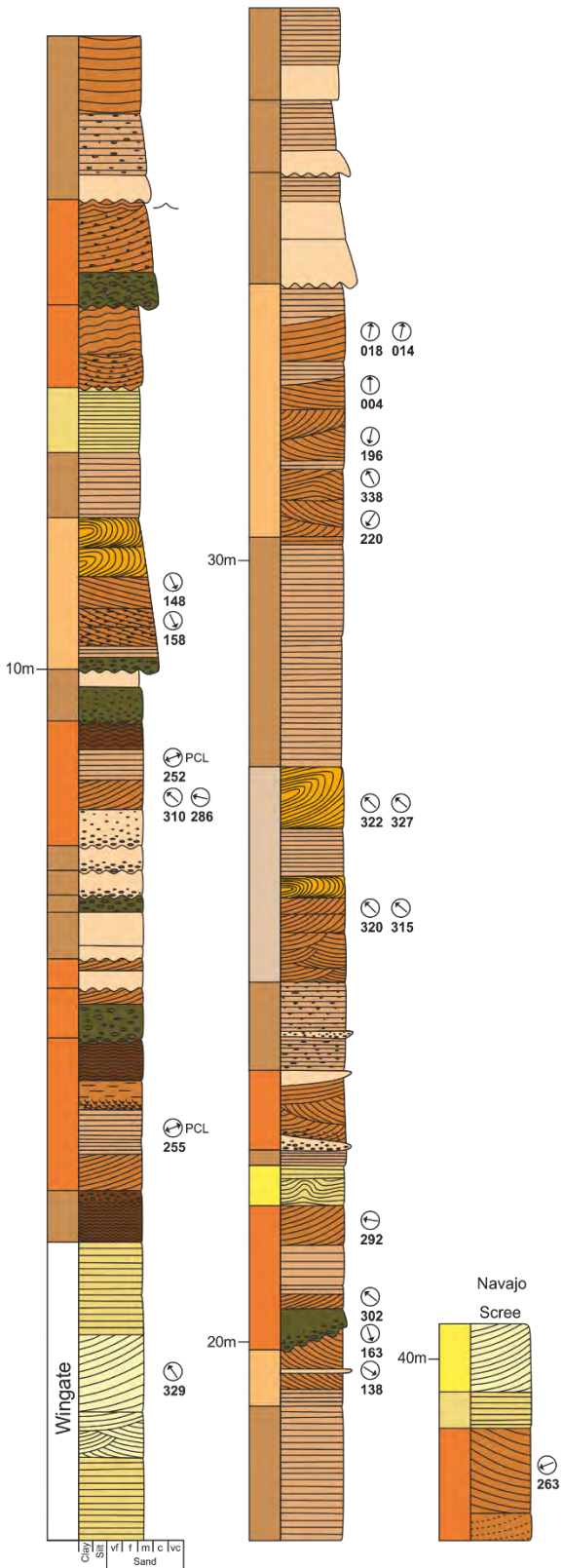
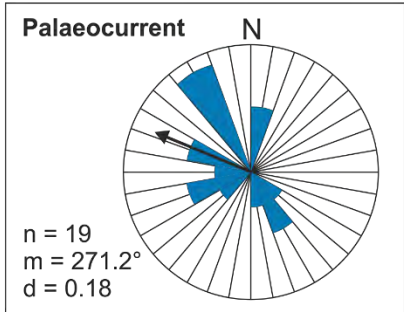
- Wilson, R.F.** (1958). The stratigraphy and sedimentology of the (Jurassic) Kayenta and (?Triassic) Moenave Formations, Vermilion Cliffs region, Utah and Arizona. Unpublished PhD Thesis, Stanford University.
- Wilson, R.F.** (1967) Whitmore Point, a new member of the Moenave Formation in Utah and Arizona. *Plateau*, **40**, 29–40.
- Wilson, R.F.** and **Stewart, J.H.** (1967) Correlation of Upper Triassic and Triassic (?) Formations Between Southwestern Utah and Southern Nevada. *US Geological Survey Bulletin*. No. 1244-D.
- Wolman, M.G.** and **Gerson, R.** (1978). Relative scales of time and effectiveness of climate in watershed geomorphology. *Earth Surface Processes*, **3**, 189–208.
- Xu, H., Liu, Y., Kuang, H.** and **Peng, N.** (2019). Late Jurassic fluvial–eolian deposits from the Tianchihe Formation, Ningwu–Jingle Basin, Shanxi Province, China. *Journal of Asian Earth Sciences*, **174**, 245–262.
- Yaalon, D.** (1990). Desert sediments: Ancient and modern, In: *Earth Surface Processes and Landforms* (Eds. Frostick, L.E., and Reid, I.), Geological society special publication, no. 35, Blackwell scientific publishers, Oxford, 385–386.

Appendices

Appendix 1 - Kayenta logs



Log: Dewey Bridge
 Region: Proximal
 Total length: 40.5 m

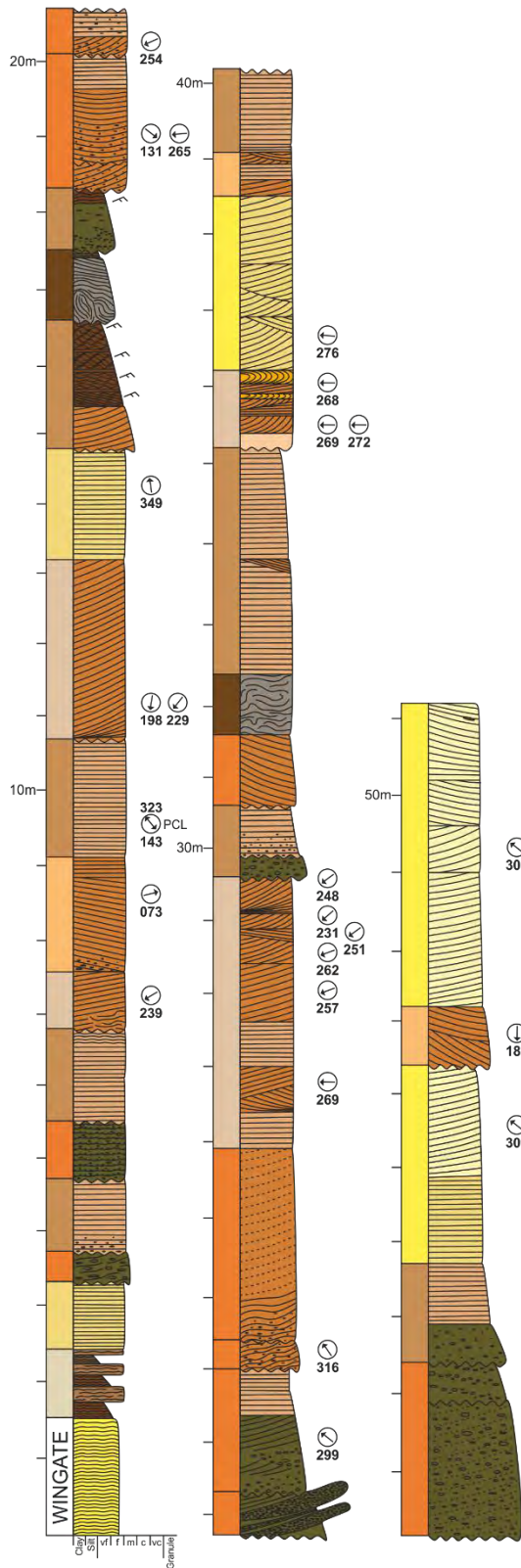
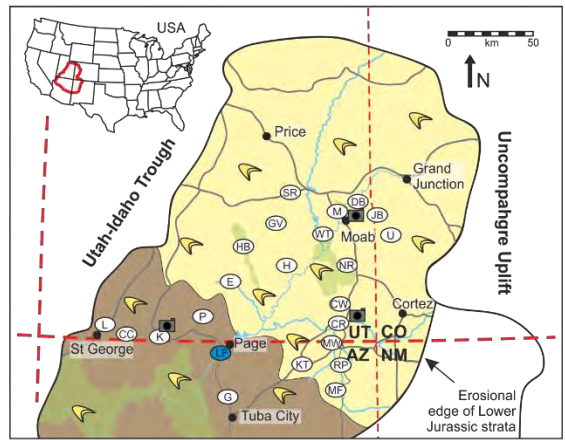
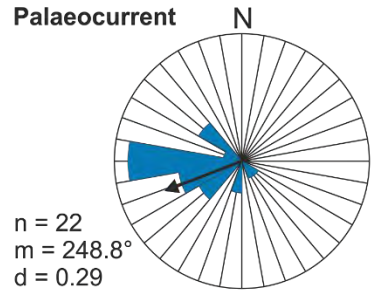


Lithofacies Key

Fluvial	Aeolian	
Sxb & Stxb	Cms	Smxb & Smtxb
Slxb	Ccs	Smpb
Spb	Cru	Smwb
Spl	Sssd	Sm
Sfrl		
Stpl		
Smf		
Sma		
Srb		
Sfi		
Structures	Architectural Elements	
Roots	Fluvial Channel	
Ripples	Fluvial Sheet	
Bioturbation	Lateral Accretion	
Desiccation	Downstream Accretion	
Rip up Clasts	Bank Collapse	
Intraformational Clasts	Overbank	
Extraformational Clasts	Aeolian Dune	
Mud draped foresets	Aeolian Sandsheet	
	Aeolian Interdune	

**Please refer to Chapter Four, Table 4.3 for full facies descriptions and Chapter Five for full architectural element descriptions*

Log: Lions Park
 Region: Proximal
 Total length: 51.2 m

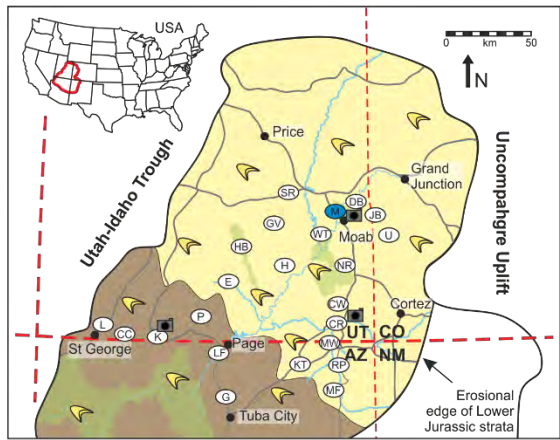
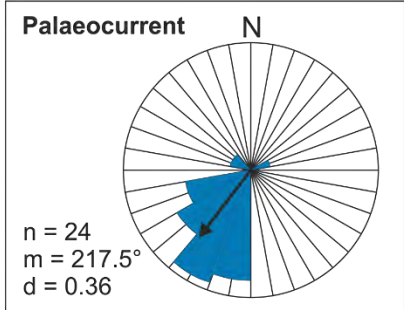
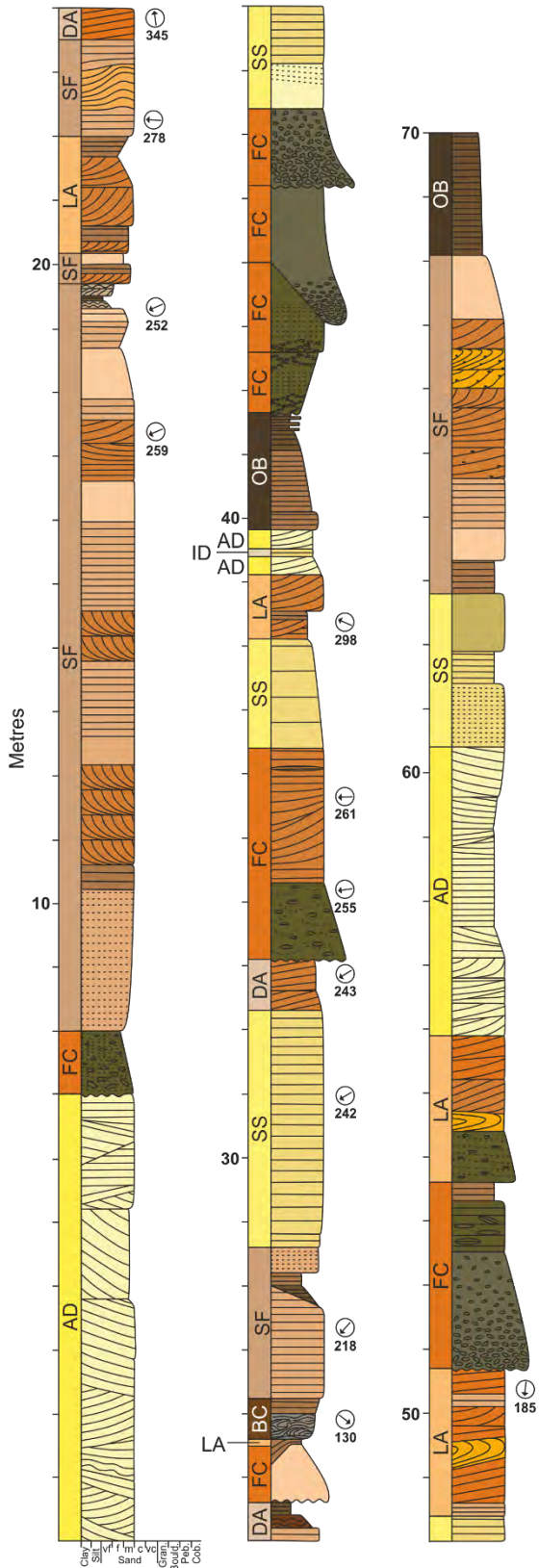


Lithofacies Key

Fluvial		Aeolian	
	Sxb & Slxb		Cms
	Slxb		Ccs
	Spb		Cru
	Spl		Sssd
	Sfri		Smxb & Smtxb
	Stpl		Smpb
	Smf		Smwb
	Sma		Sm
	Srb		
	Sfl		
Architectural Elements			
	Fluvial Channel		Bank Collapse
	Fluvial Sheet		Overbank
	Lateral Accretion		Aeolian Dune
	Downstream Accretion		Aeolian Sandsheet
	Rip up Clasts		Aeolian Interdune
	Ripples		
	Bioturbation		
	Desiccation		
	Intraformational Clasts		
	Extraformational Clasts		
	Mud draped foresets		

*Please refer to Chapter Four, Table 4.3 for full facies descriptions and Chapter Five for full architectural element descriptions

Log: Sevenmile Canyon
 Region: Proximal
 Total length: 70.0 m

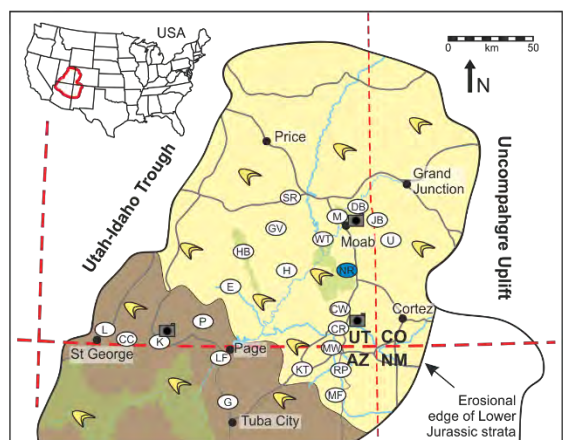
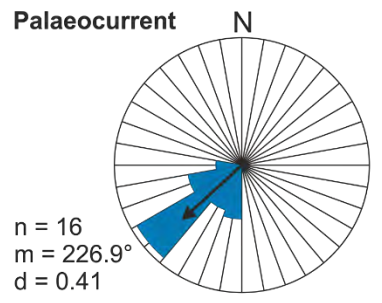
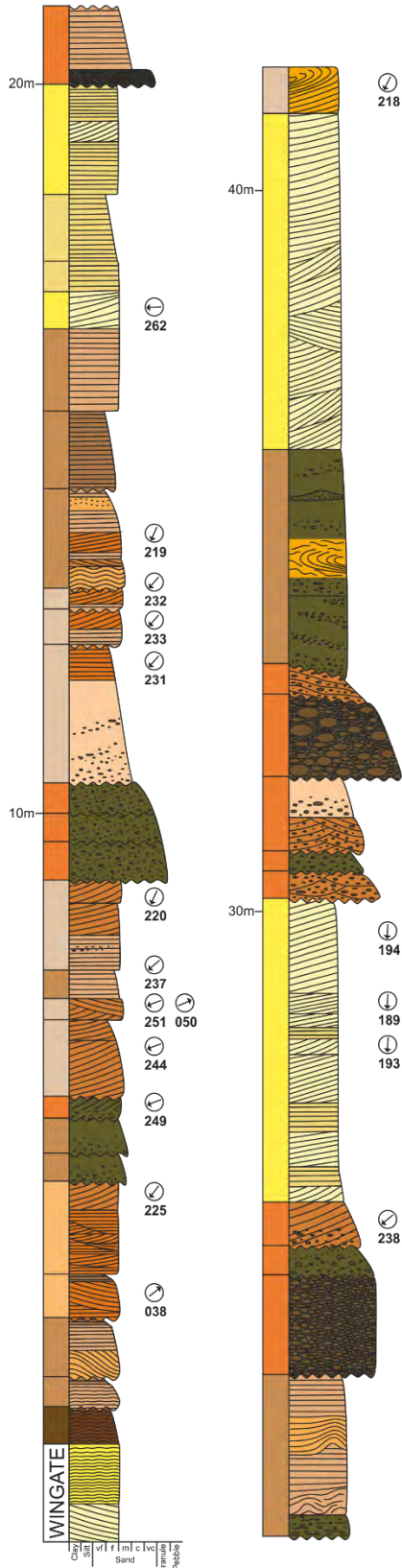


Lithofacies Key

Fluvial	Aeolian
Sxb & Stxb	Smbx & Smtxb
Slxb	Smpb
Spb	Smw
Spl	Sm
Sfri	
Stpl	
Smf	
Sma	
Srb	
Sfi	
Structures	Architectural Elements
Roots	Fluvial Channel
Ripples	Fluvial Sheet
Bioturbation	Lateral Accretion
Desiccation	Downstream Accretion
Rip up Clasts	Bank Collapse
Intraformational Clasts	Overbank
Extraformational Clasts	Aeolian Dune
Mud draped foresets	Aeolian Sandsheet
	Aeolian Interdune

**Please refer to Chapter Four, Table 4.3 for full facies descriptions and Chapter Five for full architectural element descriptions*

Log: Newspaper Rock
 Region: Proximal
 Total length: 41.6 m

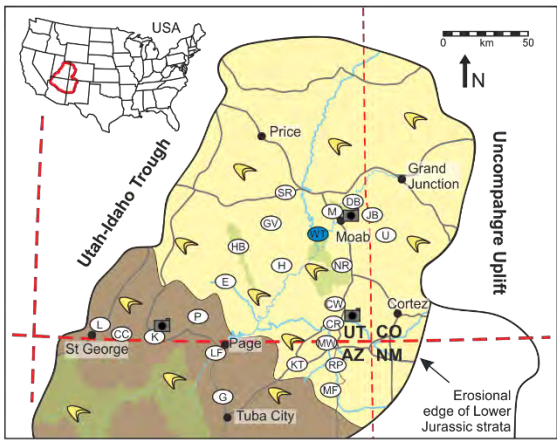
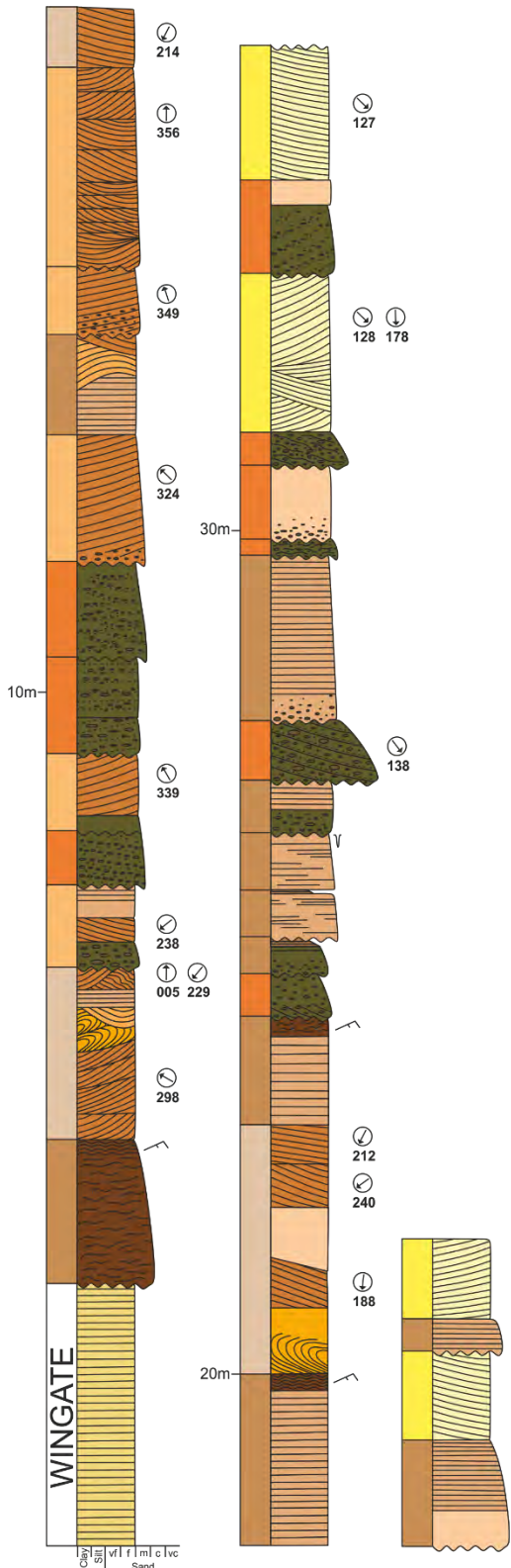
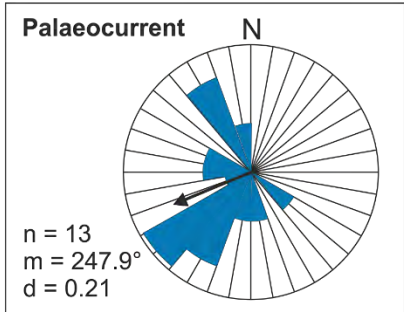


Lithofacies Key

Fluvial	Aeolian
Sxb & Slxb	Smxb & Smtxb
Slxb	Smpb
Spb	Smwb
Spl	Sm
Sfri	
Stpl	
Smf	
Sma	
Srb	
Sfl	
Structures	Architectural Elements
Roots	Fluvial Channel
Ripples	Fluvial Sheet
Bioturbation	Lateral Accretion
Desiccation	Downstream Accretion
Rip up Clasts	Bank Collapse
Intraformational Clasts	Overbank
Extraformational Clasts	Aeolian Dune
Mud draped foresets	Aeolian Sandsheet
	Aeolian Interdune

**Please refer to Chapter Four, Table 4.3 for full facies descriptions and Chapter Five for full architectural element descriptions*

Log: Wilhite Trail
 Region: Proximal
 Total length: 39.4 m

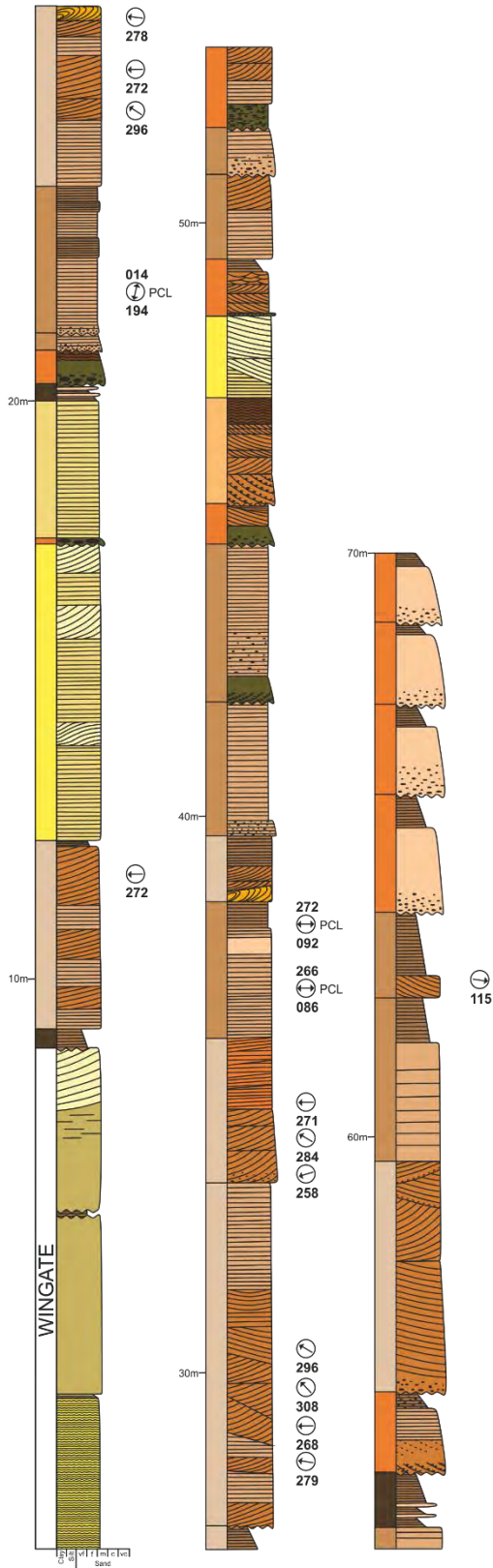
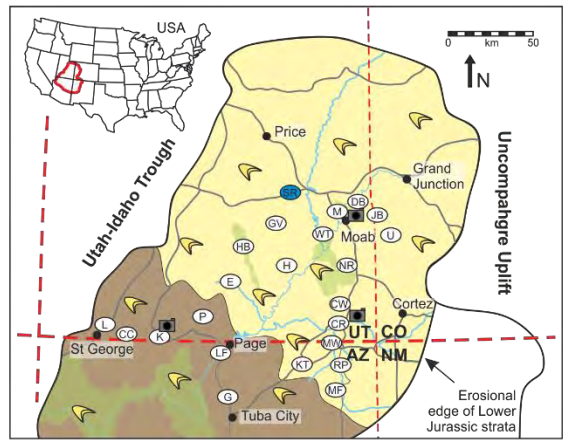
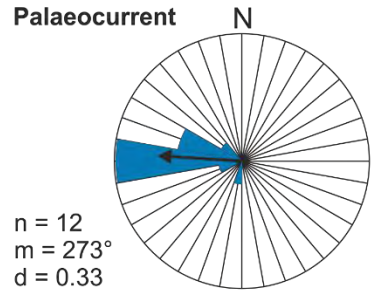


Lithofacies Key

Fluvial	Aeolian	
Sxb & Stxb	Cms	Smxb & Smtxb
Slxb	Ccs	Smpb
Spb	Cru	Smwb
Spl	Sssd	Sm
Sfri		
Stpl		
Smf		
Sma		
Srb		
Sfi		
Structures	Architectural Elements	
Roots	Fluvial Channel	
Ripples	Fluvial Sheet	
Bioturbation	Lateral Accretion	
Desiccation	Downstream Accretion	
Rip up Clasts	Bank Collapse	
Intraformational Clasts	Overbank	
Extraformational Clasts	Aeolian Dune	
Mud draped foresets	Aeolian Sandsheet	
	Aeolian Interdune	

**Please refer to Chapter Four, Table 4.3 for full facies descriptions and Chapter Five for full architectural element descriptions*

Log: San Rafael Swell
 Region: Proximal
 Total length: 70 m



Lithofacies Key

Fluvial		Aeolian	
Sxb & Slxb	Cms	Smxb & Smtxb	
Slxb	Ccs	Smpb	
Spb	Cru	Smwb	
Spl	Sssd	Sm	
Sfrl			
Stpl			
Smf			
Sma			
Srb			
Sfl			

Architectural Elements

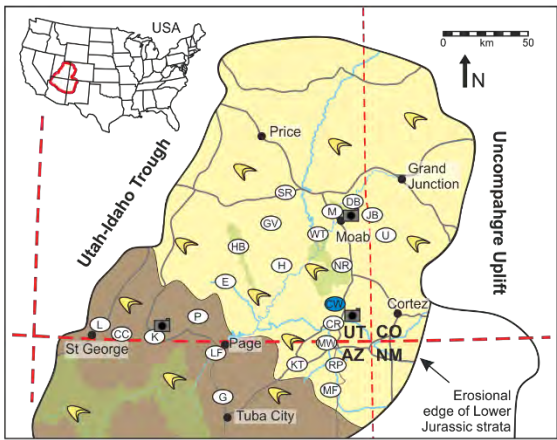
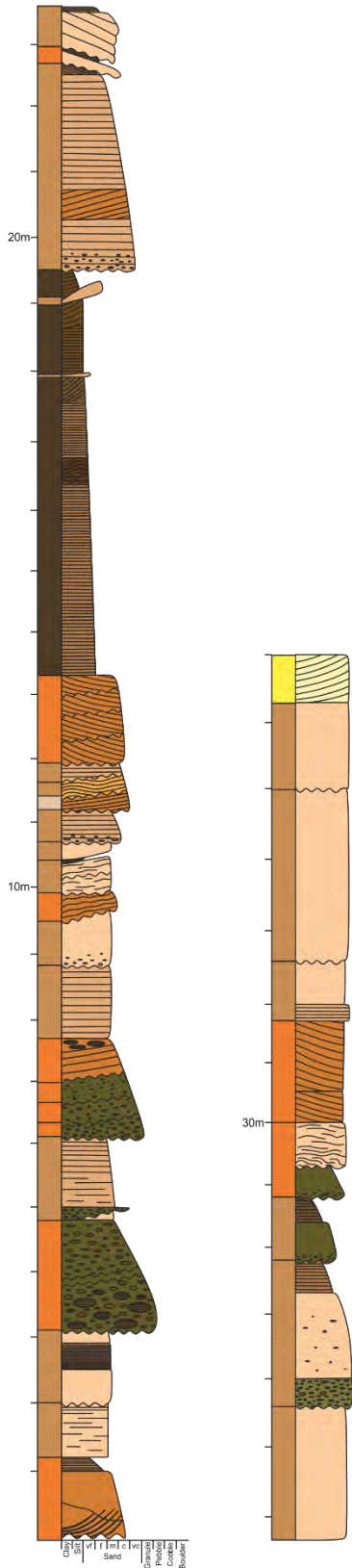
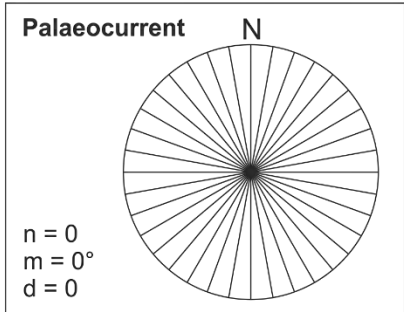
	Fluvial Channel
	Fluvial Sheet
	Lateral Accretion
	Downstream Accretion
	Bank Collapse
	Overbank
	Aeolian Dune
	Aeolian Sandsheet
	Aeolian Interdune

Structures

	Roots
	Ripples
	Bioturbation
	Desiccation
	Rip up Clasts
	Intraformational Clasts
	Extraformational Clasts
	Mud draped foresets

**Please refer to Chapter Four, Table 4.3 for full facies descriptions and Chapter Five for full architectural element descriptions*

Log: Comb Wash
 Region: Medial
 Total length: 37 m



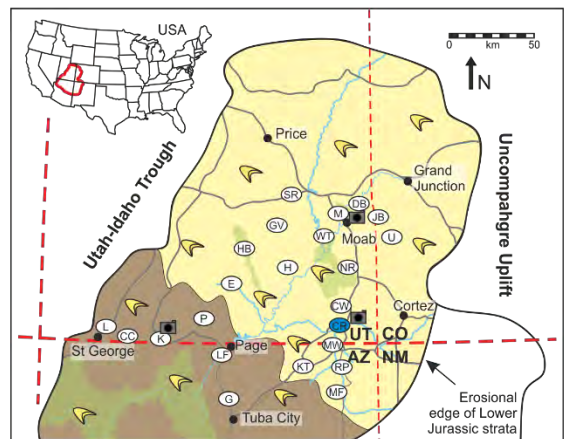
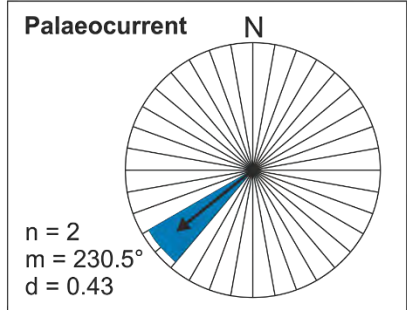
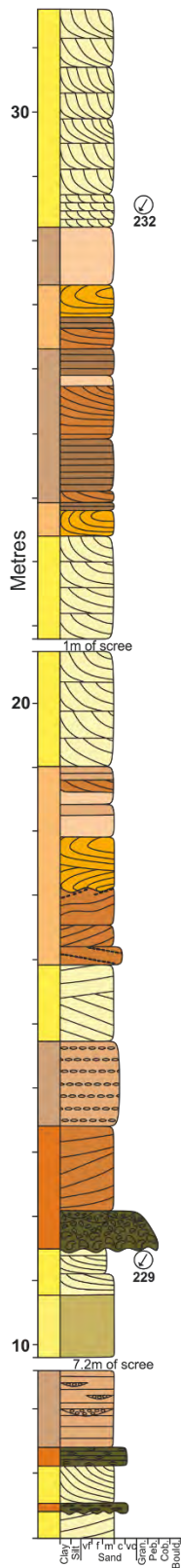
Lithofacies Key

Fluvial	Sxb & Stxb	Cms	Smxb & Smtxb
	Slxb	Ccs	Smpb
	Spb	Cru	Smwb
	Spl	Sssd	Sm
	Sfrl		
	Stpl		
	Smf		
	Sma		
	Srb		
	Sfi		
Structures	Roots		
	Ripples		
	Bioturbation		
	Desiccation		
	Rip up Clasts		
	Intraformational Clasts		
	Extraformational Clasts		
	Mud draped foresets		
	Fluvial Channel		
	Fluvial Sheet		
	Lateral Accretion		
	Downstream Accretion		
	Bank Collapse		
	Overbank		
	Aeolian Dune		
	Aeolian Sandsheet		
	Aeolian Interdune		

Architectural Elements

**Please refer to Chapter Four, Table 4.3 for full facies descriptions and Chapter Five for full architectural element descriptions*

Log: Comb Ridge
 Region: Medial
 Total length: 37.6 m



Lithofacies Key

Fluvial		Aeolian	
	Sxb & Stxb		Cms
	Slxb		Ccs
	Spb		Cru
	Spl		Sssd
	Sfri		Smxb & Smtxb
	Stpl		Smpb
	Smf		Smwb
	Sma		Sm
	Srb		
	Sfl		

Architectural Elements

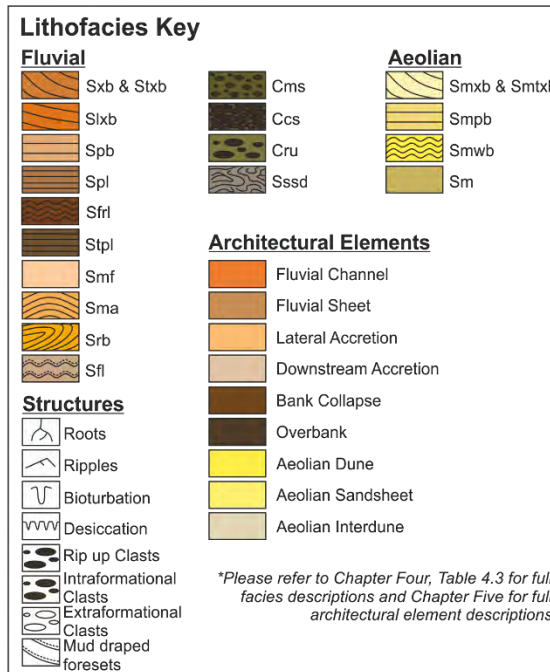
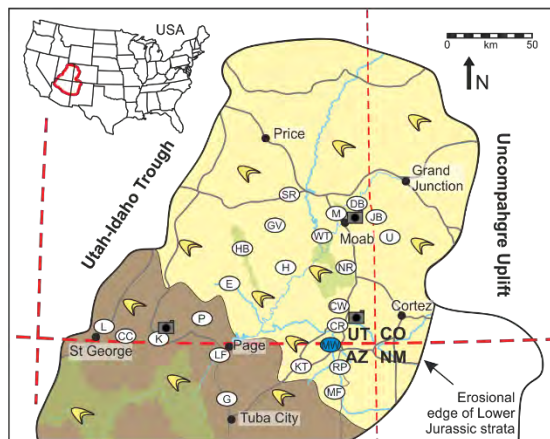
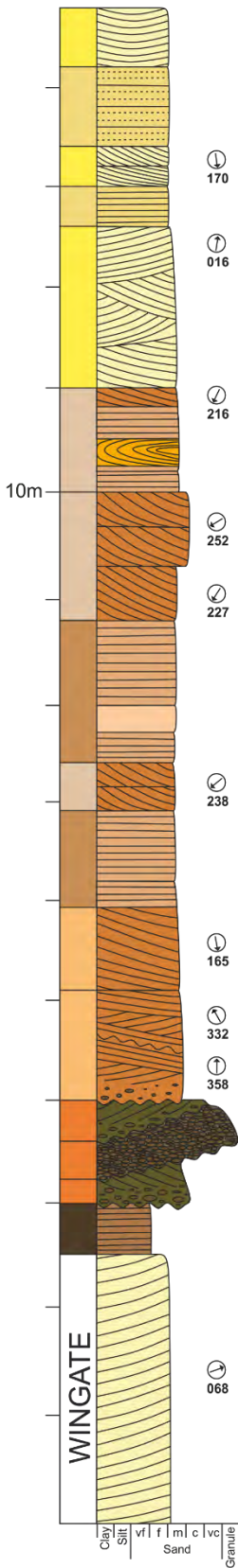
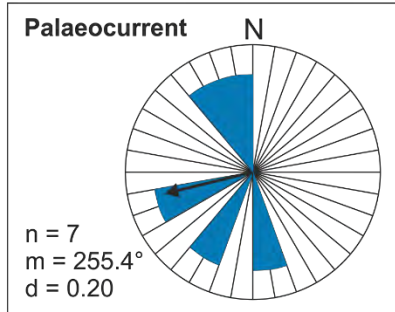
	Fluvial Channel
	Fluvial Sheet
	Lateral Accretion
	Downstream Accretion
	Bank Collapse
	Overbank
	Aeolian Dune
	Aeolian Sandsheet
	Aeolian Interdune

Structures

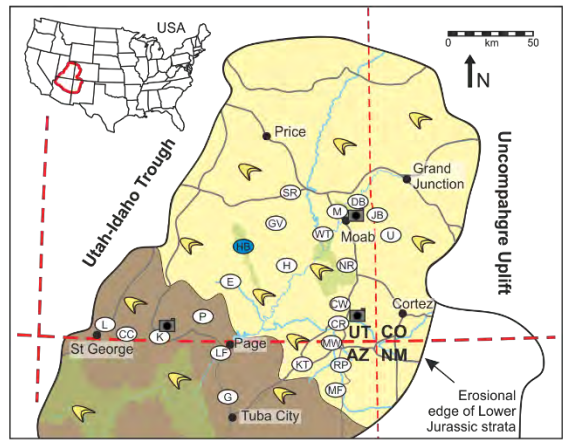
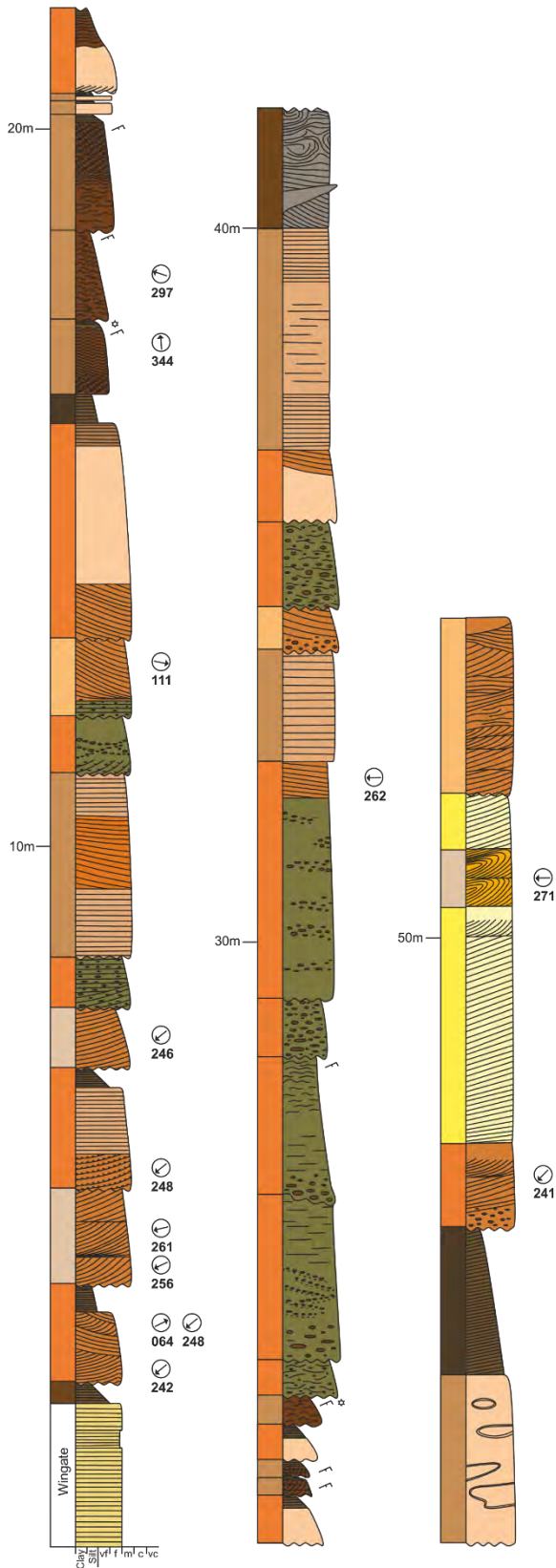
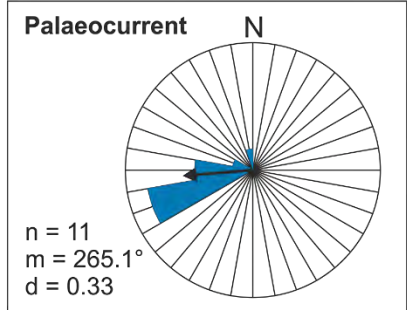
	Roots
	Ripples
	Bioturbation
	Desiccation
	Rip up Clasts
	Intraformational Clasts
	Extraformational Clasts
	Mud draped foresets

**Please refer to Chapter Four, Table 4.3 for full facies descriptions and Chapter Five for full architectural element descriptions*

Log: Mexican Water
 Region: Medial
 Total length: 14.8 m



Log: Hickman Bridge Trail
 Region: Medial
 Total length: 54.5 m



Lithofacies Key

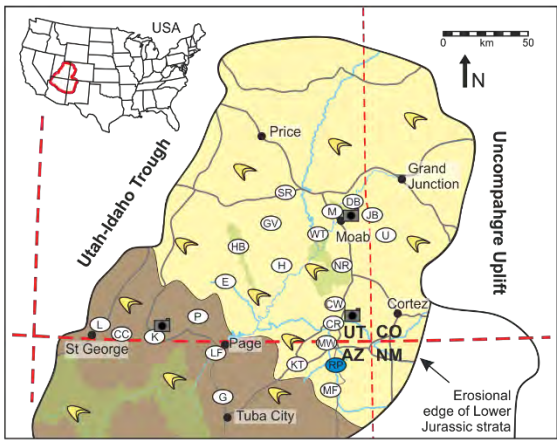
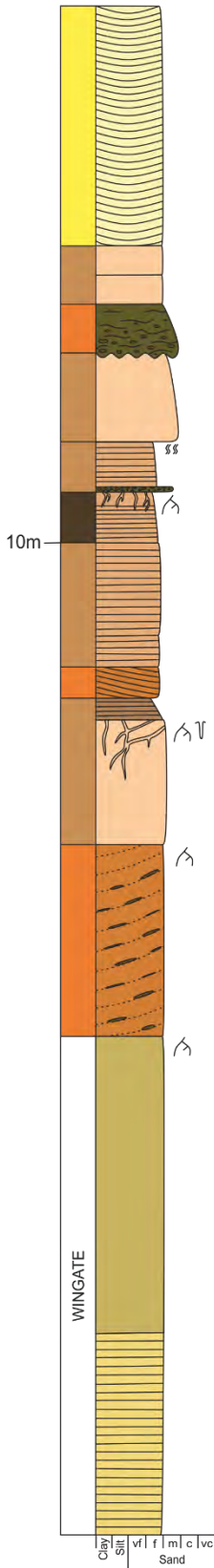
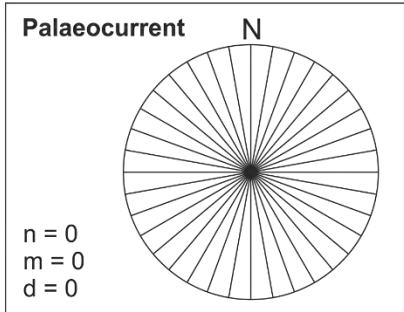
Fluvial	Aeolian
Sxb & Slxb	Smbx & Smtxb
Slxb	Smpb
Spb	Smbw
Spl	Sm
Sfri	
Stpl	
Smf	
Sma	
Srb	
Sfl	
Structures	
Roots	
Ripples	
Bioturbation	
Desiccation	
Rip up Clasts	
Intraformational Clasts	
Extraformational Clasts	
Mud draped foresets	

Architectural Elements

Fluvial Channel
Fluvial Sheet
Lateral Accretion
Downstream Accretion
Bank Collapse
Overbank
Aeolian Dune
Aeolian Sandsheet
Aeolian Interdune

**Please refer to Chapter Four, Table 4.3 for full facies descriptions and Chapter Five for full architectural element descriptions*

Log: Rock Point
 Region: Medial
 Total length: 15.5 m

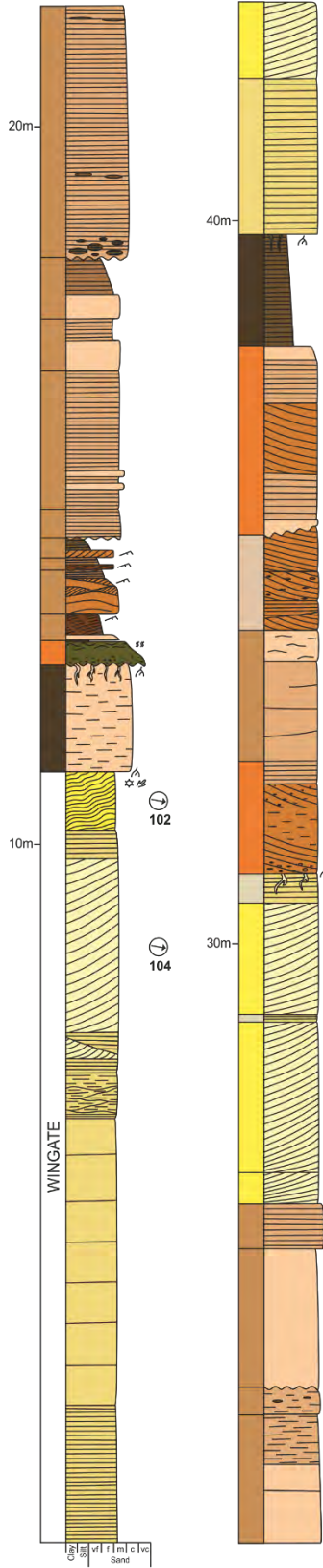


Lithofacies Key

Fluvial		Aeolian
Sxb & Stxb	Cms	Smxb & Smtxb
Slxb	Ccs	Smpb
Spb	Cru	Smwb
Spl	Sssd	Sm
Sfri		
Stpl		
Smf		
Sma		
Srb		
Sfi		
Structures		
Roots		
Ripples		
Bioturbation		
Desiccation		
Rip up Clasts		
Intraformational Clasts		
Extraformational Clasts		
Mud draped foresets		
	Architectural Elements	
	Fluvial Channel	
	Fluvial Sheet	
	Lateral Accretion	
	Downstream Accretion	
	Bank Collapse	
	Overbank	
	Aeolian Dune	
	Aeolian Sandsheet	
	Aeolian Interdune	

**Please refer to Chapter Four, Table 4.3 for full facies descriptions and Chapter Five for full architectural element descriptions*

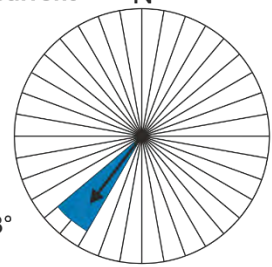
Log: Kayenta
 Region: Medial
 Total length: 64 m



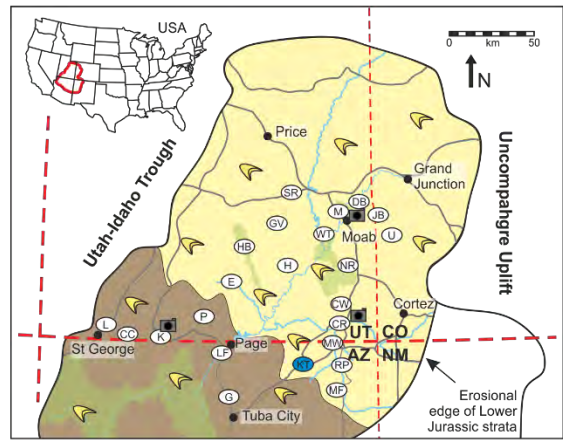
218

104

Palaeocurrent



n = 1
 m = 218°
 d = 0



Lithofacies Key

Fluvial		Aeolian	
	Sxb & Slxb		Cms
	Slxb		Ccs
	Spb		Cru
	Spl		Sssd
	Sfri		Smxb & Smtxb
	Stpl		Smpb
	Smf		Smwb
	Sma		Sm
	Srb		
	Sfl		

Architectural Elements

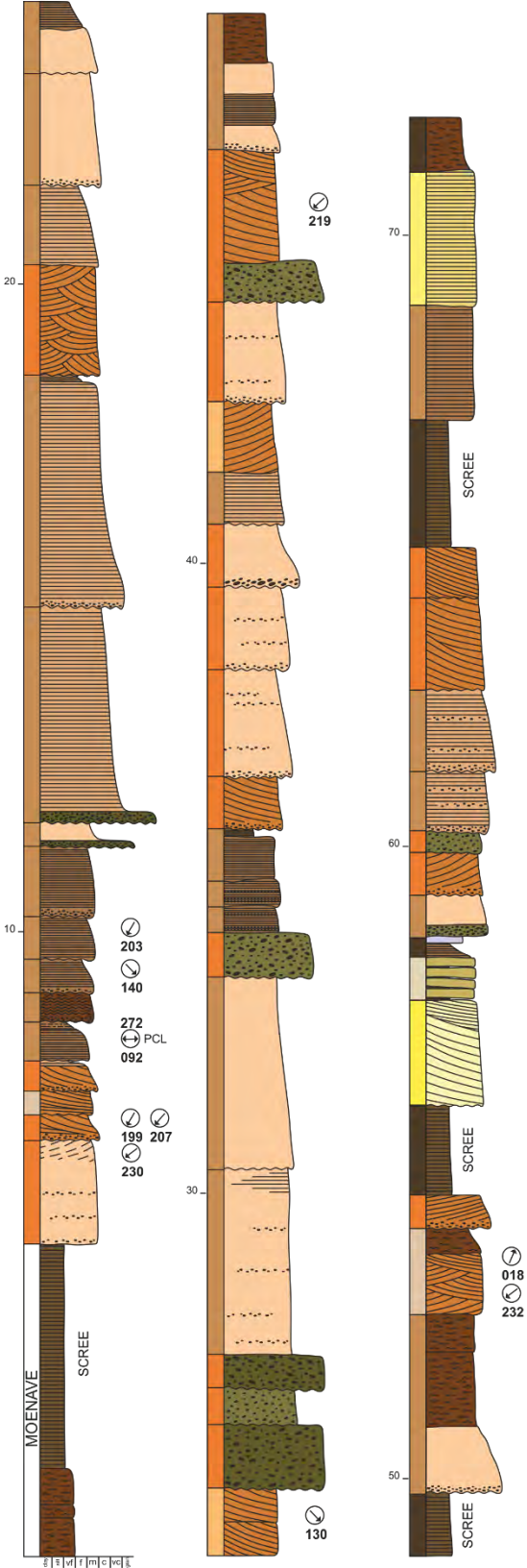
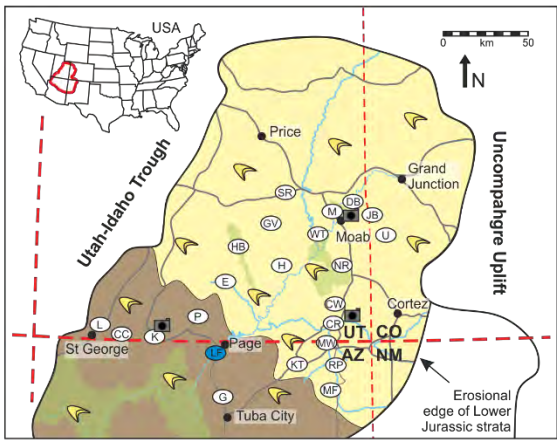
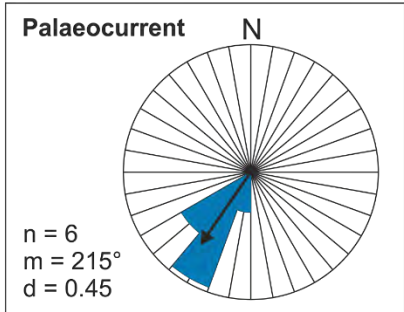
	Fluvial Channel
	Fluvial Sheet
	Lateral Accretion
	Downstream Accretion
	Bank Collapse
	Overbank
	Aeolian Dune
	Aeolian Sandsheet
	Aeolian Interdune

Structures

	Roots
	Ripples
	Bioturbation
	Desiccation
	Rip up Clasts
	Intraformational Clasts
	Extraformational Clasts
	Mud draped foresets

**Please refer to Chapter Four, Table 4.3 for full facies descriptions and Chapter Five for full architectural element descriptions*

Log: Lee's Ferry
 Region: Distal
 Total length: 72 m



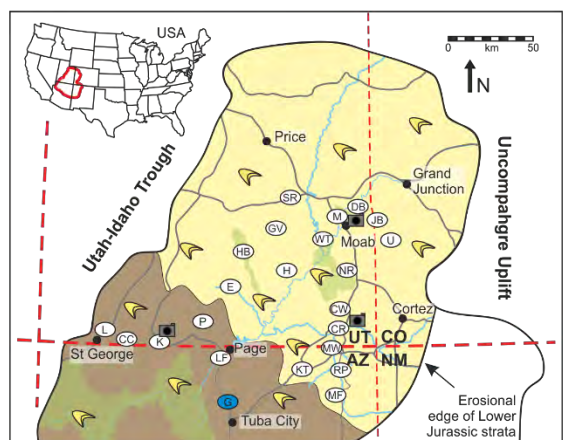
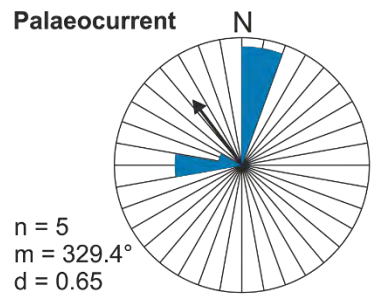
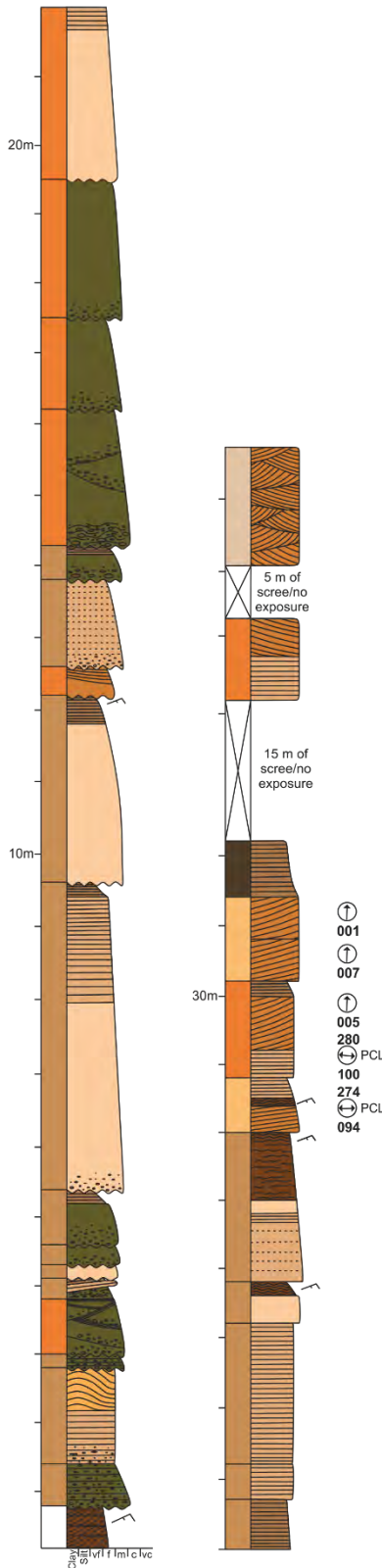
Lithofacies Key

Fluvial		Aeolian	
	Sxb & Stxb		Cms
	Slxb		Ccs
	Spb		Cru
	Spl		Sssd
	Sfrl		Smxb & Smtxb
	Stpl		Smpb
	Smf		Smwb
	Sma		Sm
	Srb		
	Sfi		
Structures			
	Roots		Fluvial Channel
	Ripples		Fluvial Sheet
	Bioturbation		Lateral Accretion
	Desiccation		Downstream Accretion
	Rip up Clasts		Bank Collapse
	Intraformational Clasts		Overbank
	Extraformational Clasts		Aeolian Dune
	Mud draped foresets		Aeolian Sandsheet
			Aeolian Interdune

Architectural Elements

**Please refer to Chapter Four, Table 4.3 for full facies descriptions and Chapter Five for full architectural element descriptions*

Log: The Gap
 Region: Distal
 Total length: 94 m



Lithofacies Key

Fluvial	Aeolian
Sxb & Slxb	Smxb & Smtxb
Slxb	Smpb
Spb	Smwb
Spl	Sm
Sfri	
Stpl	
Smf	
Sma	
Srb	
Sfl	

Structures

- Roots
- Ripples
- Bioturbation
- Desiccation
- Rip up Clasts
- Intraformational Clasts
- Extraformational Clasts
- Mud draped foresets

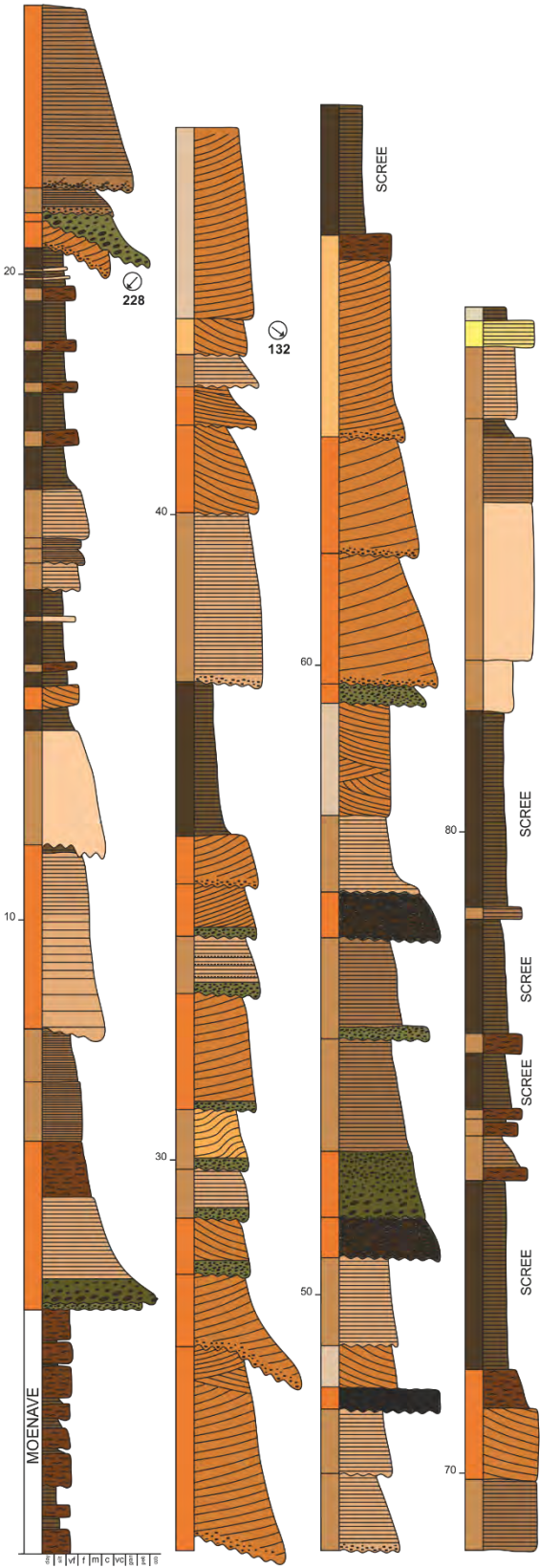
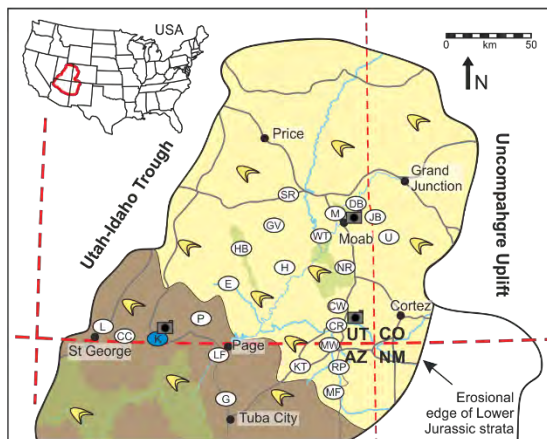
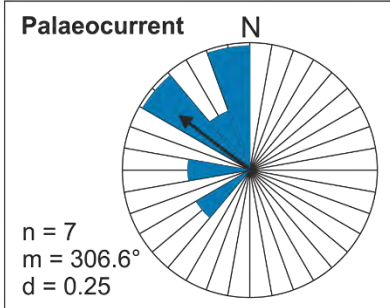
Architectural Elements

- Fluvial Channel
- Fluvial Sheet
- Lateral Accretion
- Downstream Accretion
- Bank Collapse
- Overbank
- Aeolian Dune
- Aeolian Sandsheet
- Aeolian Interdune

**Please refer to Chapter Four, Table 4.3 for full facies descriptions and Chapter Five for full architectural element descriptions*

34 m of Moenave Fm. below

Log: Kanab - Squaw Trail
 Region: Distal
 Total length: 90.0 m

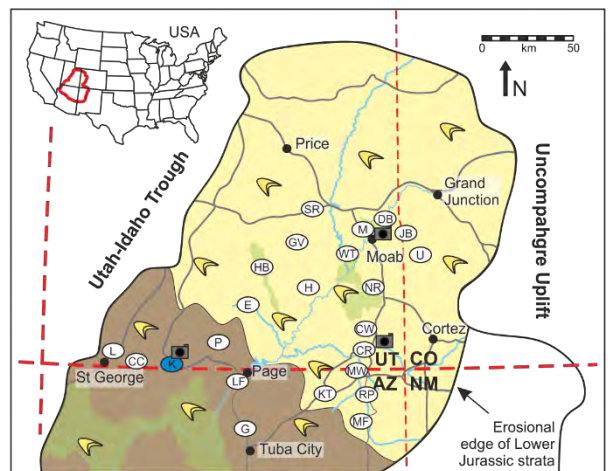
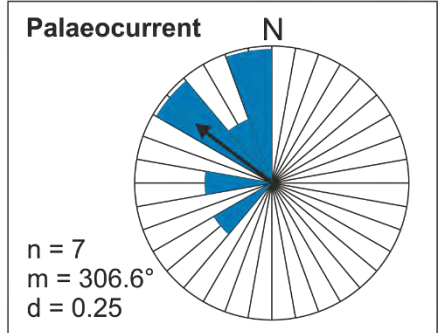
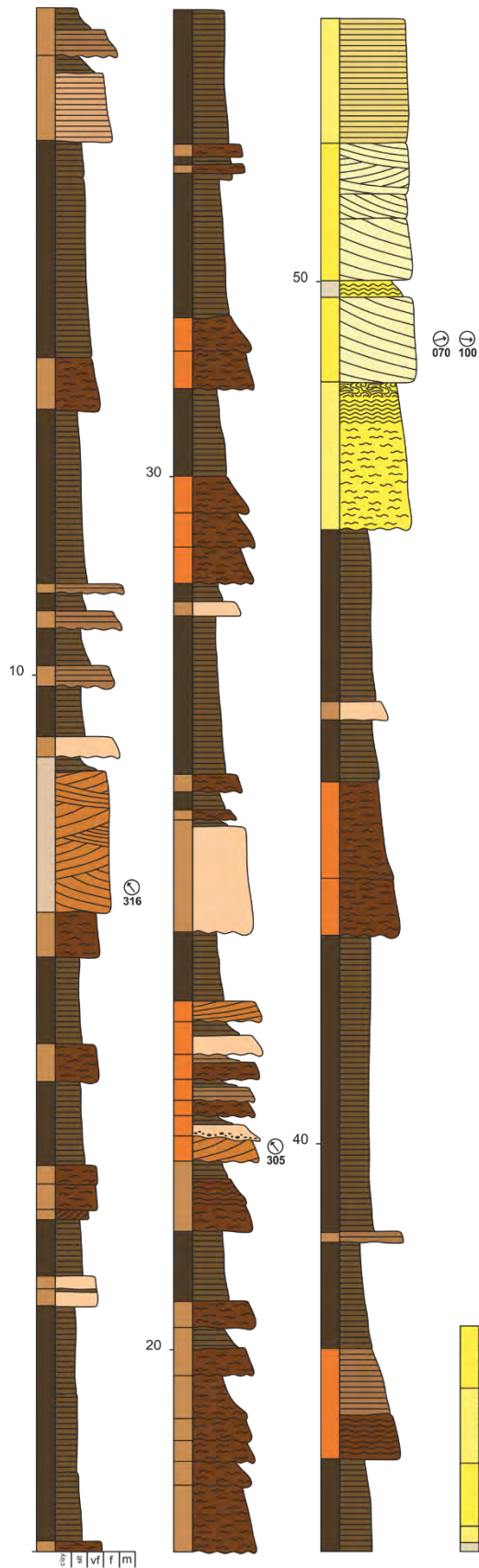


Lithofacies Key

Fluvial		Aeolian	
	Sxb & Stxb		Cms
	Slxb		Ccs
	Spb		Cru
	Spl		Sssd
	Sfri		Smxb & Smtxb
	Stpl		Smpb
	Smf		Smwb
	Sma		Sm
	Srb		
	Sfi		
Structures			
	Roots		Fluvial Channel
	Ripples		Fluvial Sheet
	Bioturbation		Lateral Accretion
	Desiccation		Downstream Accretion
	Rip up Clasts		Bank Collapse
	Intraformational Clasts		Overbank
	Extraformational Clasts		Aeolian Dune
	Mud draped foresets		Aeolian Sandsheet
			Aeolian Interdune

**Please refer to Chapter Four, Table 4.3 for full facies descriptions and Chapter Five for full architectural element descriptions*

Log: Kanab - White Rim
 Region: Distal
 Total length: 55.7 m



Lithofacies Key

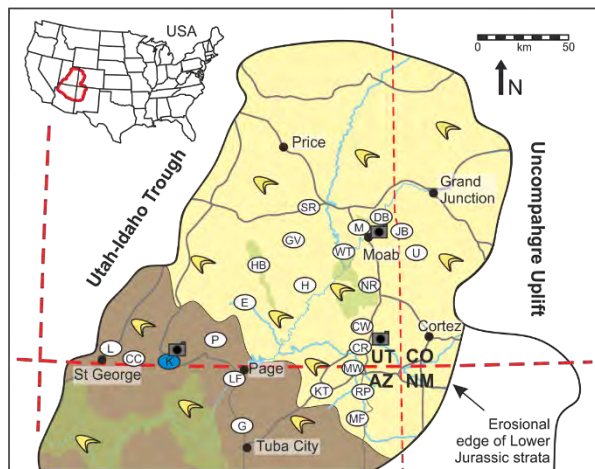
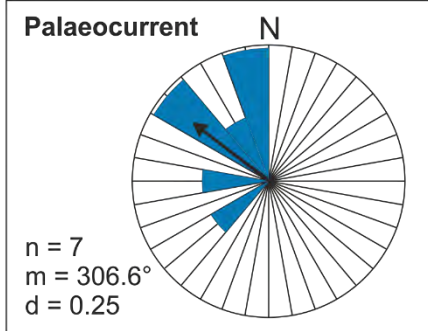
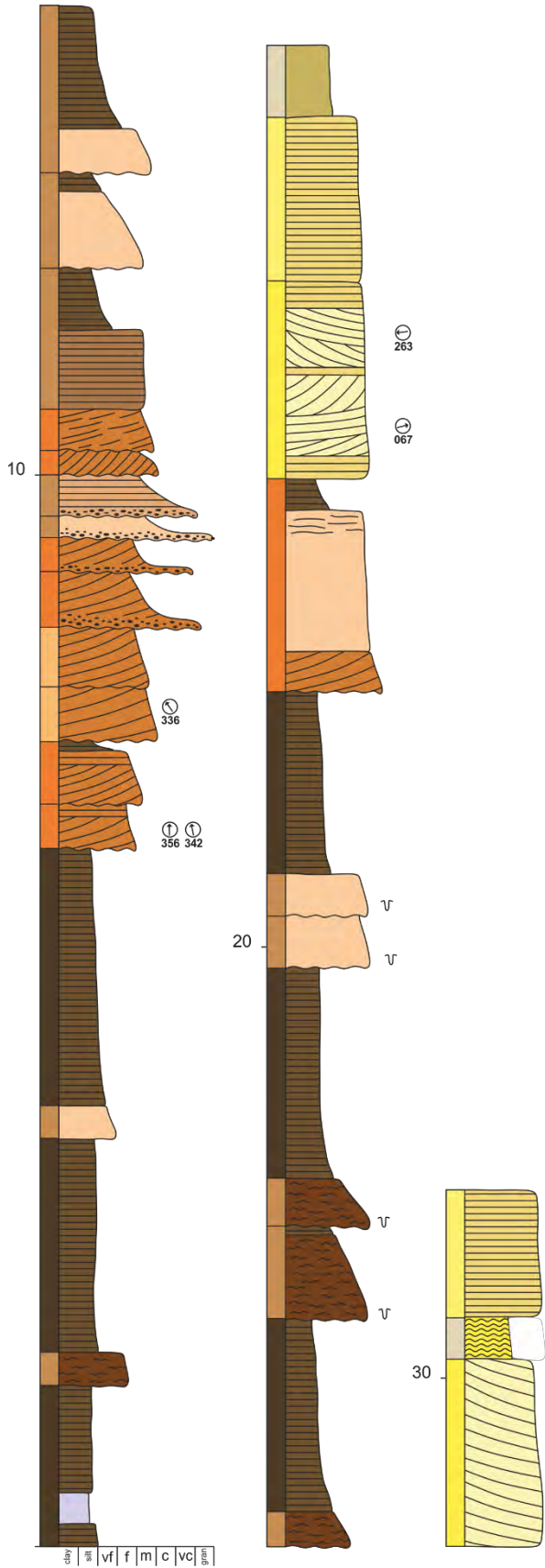
Fluvial		Aeolian	
	Sxb & Stxb		Cms
	Slxb		Ccs
	Sspb		Cru
	Spl		Sssd
	Sfrl		Smxb & Smtxb
	Stpl		Smpb
	Smf		Smwb
	Sma		Sm
	Srb		
	Sfl		

Architectural Elements	
	Fluvial Channel
	Fluvial Sheet
	Lateral Accretion
	Downstream Accretion
	Bank Collapse
	Overbank
	Aeolian Dune
	Aeolian Sandsheet
	Aeolian Interdune

Structures	
	Roots
	Ripples
	Bioturbation
	Desiccation
	Rip up Clasts
	Intraformational Clasts
	Extraformational Clasts
	Mud draped foresets

**Please refer to Chapter Four, Table 4.3 for full facies descriptions and Chapter Five for full architectural element descriptions*

Log: Kanab - Moqui Cave
 Region: Distal
 Total length: 33.6 m



Lithofacies Key

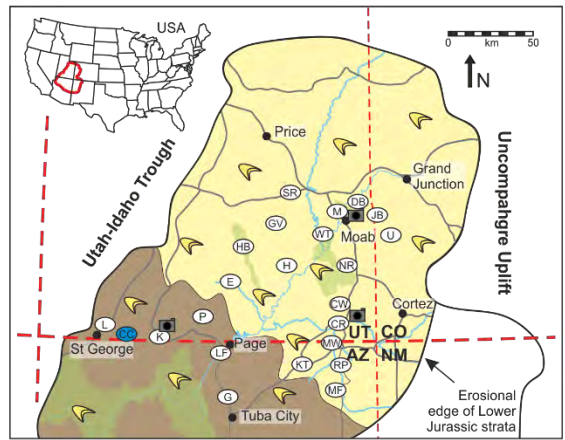
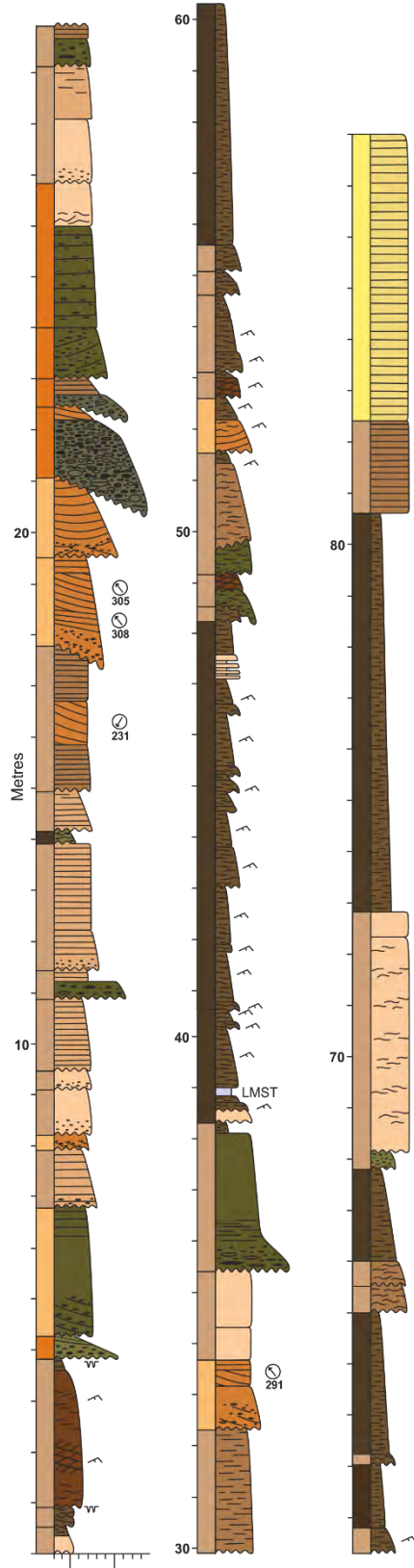
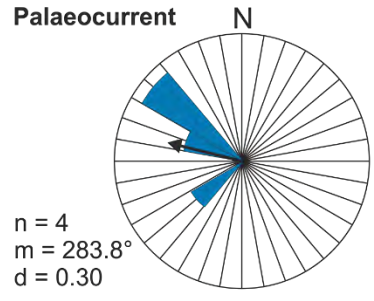
Fluvial		Aeolian	
	Sxb & Stxb		Cms
	Slxb		Ccs
	Spb		Cru
	Spl		Sssd
	Sfrl		Smxb & Smtxb
	Stpl		Smpb
	Smf		Smwb
	Sma		Sm
	Srb		
	Sfl		

Architectural Elements	
	Fluvial Channel
	Fluvial Sheet
	Lateral Accretion
	Downstream Accretion
	Bank Collapse
	Overbank
	Aeolian Dune
	Aeolian Sandsheet
	Aeolian Interdune

Structures	
	Roots
	Ripples
	Bioturbation
	Desiccation
	Rip up Clasts
	Intraformational Clasts
	Extraformational Clasts
	Mud draped foresets

**Please refer to Chapter Four, Table 4.3 for full facies descriptions and Chapter Five for full architectural element descriptions*

Log: Colorado City
 Region: Distal
 Total length: 87.8 m



Lithofacies Key

Fluvial		Aeolian	
	Sxb & Stxb		Cms
	Slxb		Ccs
	Spb		Cru
	Spl		Sssd
	Sfri		Smxb & Smtxb
	Stpl		Smpb
	Smf		Smwb
	Sma		Sm
	Srb		
	Sfl		

Architectural Elements

	Fluvial Channel
	Fluvial Sheet
	Lateral Accretion
	Downstream Accretion
	Bank Collapse
	Overbank
	Aeolian Dune
	Aeolian Sandsheet
	Aeolian Interdune

Structures

	Roots
	Ripples
	Bioturbation
	Desiccation
	Rip up Clasts
	Intraformational Clasts
	Extraformational Clasts
	Mud draped foresets

**Please refer to Chapter Four, Table 4.3 for full facies descriptions and Chapter Five for full architectural element descriptions*

Appendix 2 - Kayenta statistics

Depositional Element thickness, percentage and grainsize

Proximal	JBC			NPR			DB			LP		
	m	%	Grainsize	m	%	Grainsize	m	%	Grainsize	m	%	Grainsize
SFC	15.3	38.2	2	30.8	76.4	1.2	19.9	57.8	1.85	19.3	51.7	1.35
IFC	2.3	5.7	2	0.6	1.5	2	1.6	4.7	2	5	13.4	2
GC	1	2.5	1	3.6	8.9	-0.25	0	0.0		0	0.0	
SF	21.5	53.6	2	4.8	11.9	2.38	12.9	37.5	1.82	13	34.9	2.12
OB	0	0		0.5	1.2	3	0	0.0		0	0.0	
Total F	40.1			40.3			34.4			37.3		
Total A	5.5			0.5			1.6			6.8		
Total Log	45.6			40.8			36			44.1		

Medial	CW			MW			KT			H		
	m	%	Grainsize	m	%	Grainsize	m	%	Grainsize	m	%	Grainsize
SFC	11.8	32.5	1.05	3.5	41.2	1.2	7.2	29.8	2	26.9	69.0	1.72
IFC	1.2	3.3	1.33	3	35.3	1.75	0	0.0		3.4	8.7	2
GC	0	0.0		0.4	4.7	-1	0	0.0		0	0.0	
SF	17.1	47.1	2.21	1.1	12.9	2	13.9	57.4	2.17	8.7	22.3	2.5
OB	6.2	17.1	3.5	0.5	5.9	3	3.1	12.8	3	0	0.0	
Total F	36.3			8.5			24.2			39		
Total A	0.7			3.8			8			1.8		
Total Log	37			12.3			32.2			40.8		

Distal	G			LF			K			CC		
	m	%	Grainsize	m	%	Grainsize	m	%	Grainsize	m	%	Grainsize
SFC	8.4	14.6	2.4	19.4	31.2	1.09	37.5	24.4	1.44	19.8	24.7	1.57
IFC	7.4	12.9	2.5	4.8	7.7	1.67	16.3	10.6	2.03	5.2	6.5	2.35
GC	0	0.0		1.5	2.4	-3	2.2	1.4	-2	1.9	2.4	-3.19
SF	16.6	28.9	2.63	28.7	46.2	1.56	40.1	26.1	2.86	24.3	30.3	2.56
OB	25	43.6	3.5	7.7	12.4	3.67	57.4	37.4	4.39	28.9	36.1	4.72
Total F	57.4			62.1			153.5			80.1		
Total A	11.6			4.9			80.5			7.9		
Total Log	69			67			234			88		

Proximal	WT			SRS			TMC		
	m	%	Grainsize	m	%	Grainsize	m	%	Grainsize
SFC	21.6	69.0	1.8	36.6	70.8	2.64	32	64.5	1.82
IFC	1.8	5.8	0.94	4.1	7.9	2.5	0	0.0	
GC	0	0.0		0	0.0		1.2	2.4	-2
SF	7.9	25.2	2.11	10.7	20.7	1.88	14.5	29.2	2.63
OB	0	0.0		0.3	0.6	3	1.9	3.8	4
Total F	31.3			51.7			49.6		
Total A	4.1			12.3			13.4		
Total Log	35.4			64			63		

Medial	HB			CR		
	m	%	Grainsize	m	%	Grainsize
SFC	26	53.6	2.48	6.3	30.4	1.33
IFC	5.6	11.5	3	0.6	2.9	1
GC	0	0.0		0	0.0	
SF	14.5	29.9	3.32	6.6	31.9	1.5
OB	2.4	4.9	4	7.2	34.8	4
Total F	48.5			20.7		
Total A	4			1.7		
Total Log	52.5			22.4		

Downstream trends

Distance from apex	Log	km	Sand %	Cong. %	Thickness (F)	Fluvial %	Thickness (A)	Aeolian %	Grainsize	SFC %	IFC %	GC %	SF %	OB %
JBC	25.8	100	4	40	87.9	5.5	12.1	1.92	38	6	2	54	0	
DB	56.4	100	12	34	95.5	1.6	4.5	1.82	58	5	0	38	0	
LP	74.6	97	15	37	84.5	6.8	15.5	1.7	52	13	0	35	0	
7MC	89.3	94	12	50	78.9	13.4	21.1	1.83	65	0	2	29	4	
NPR	98.6	99	18	40	98.8	0.5	1.2	1.28	76	1	9	12	1	
WT	107.7	99	17	31	88.3	4.1	11.7	1.57	69	6	0	25	0	
CW	149.6	68	9	36	98.1	0.7	1.9	1.61	33	3	0	47	17	
SRS	154.7	93	4	52	80.9	12.3	19.1	1.97	71	8	0	21	1	
CR	171.3	79	7	21	92.5	1.7	7.5	1.63	30	3	0	32	35	
H	173.1	97	15	39	95.6	1.8	4.4	1.78	69	9	0	22	0	
MW	200.9	96	7	8.5	69.1	3.8	30.9	1.9	41	35	5	13	6	
HB	223.8	86	10	48.5	92.4	4	7.6	2.01	54	12	0	30	5	
KT	249.3	95	2	24	75.0	8	25.0	1.97	30	0	0	57	13	
LF	318.8	88	8	62	92.5	5	7.5	1.26	31	8	2	46	12	
G	353	58	4	57	83.1	11.6	16.9	2.75	15	13	0	29	44	
K	378.8	67	3	154	65.7	80.5	34.3	2.46	24	11	1	26	37	
CC	413.8	67	7	80	90.9	8	9.1	2.86	25	6	2	30	36	
P (av)	86.73	97.43	11.71	40.57	87.82	6.31	12.18	1.73	61.29	5.57	1.86	30.57	0.86	
M (av)	183.74	85.20	9.60	30.60	89.54	2.40	10.46	1.79	45.40	12.40	1.00	28.80	12.60	
D (av)	342.74	75.00	4.80	75.40	81.44	22.62	18.56	2.26	25.00	7.60	1.00	37.60	28.40	

Downstream trends in depositional element thicknesses

Log	Distance from apex km	Av. SFC	Amalgamated Channels						Isolated Channels					
			Median SFC	Q1 SFC	Q3 SFC	Min SFC	Max SFC	Av. IFC	Median IFC	Q1 IFC	Q3 IFC	Min IFC	Max IFC	
JBC	25.8	3.06	2.95	1.65	3.80	1.10	4.90	1.15	1.18	0.85	1.50	0.80	1.50	
DB	56.4	2.84	2.70	2.40	3.50	1.20	4.60	1.60	1.60	0.00	0.00	1.60	1.60	
LP	74.6	4.83	2.45	2.00	7.85	1.80	13.00	1.25	0.90	0.75	1.75	0.70	2.50	
ZMC	89.3	4.57	4.10	2.30	6.70	2.30	8.10	0.00	0.00	0.00	0.00	0.00	0.00	
NPR	98.6	7.70	2.55	1.40	6.70	1.00	10.10	0.60	0.60	0.00	0.00	0.60	0.60	
WT	107.7	7.20	4.90	1.50	15.00	1.50	15.00	0.90	0.90	0.70	1.10	0.70	1.10	
CW	149.6	3.93	2.80	1.70	7.45	1.70	7.20	1.20	1.20	0.00	0.00	1.20	1.20	
SRS	154.7	9.15	9.20	4.30	14.00	2.60	15.60	1.37	0.90	0.10	3.10	0.10	3.10	
CR	171.3	3.15	3.15	3.10	3.20	3.10	3.20	0.30	0.30	0.10	0.50	0.10	0.50	
H	173.1	8.97	8.40	4.70	13.40	4.60	13.40	3.40	3.60	0.00	0.00	3.40	3.40	
MW	200.9	1.75	1.75	0.20	3.30	0.20	3.30	1.50	1.50	0.80	2.20	0.80	2.20	
HB	223.8	3.71	4.10	1.80	4.60	1.40	8.70	1.40	1.20	1.00	1.85	0.80	2.50	
KT	249.3	7.20	7.20	0.00	0.00	7.20	7.20	0.00	0.00	0.00	0.00	0.00	0.00	
LF	318.8	3.88	4.90	1.55	5.70	0.60	6.20	0.96	0.70	0.50	1.55	0.50	1.70	
G	353	8.40	8.40	0.00	0.00	8.40	8.40	1.06	1.20	0.80	1.40	0.40	1.60	
K	378.8	3.75	3.80	2.60	4.60	0.70	7.80	1.63	1.70	1.25	2.50	0.60	2.60	
CC	413.8	2.83	3.10	1.50	3.50	1.00	5.10	1.30	1.30	0.80	1.95	0.50	2.40	
P (av)		5.62						1.14						
M (av)		4.30						1.56						
D (av)		5.21						1.24						

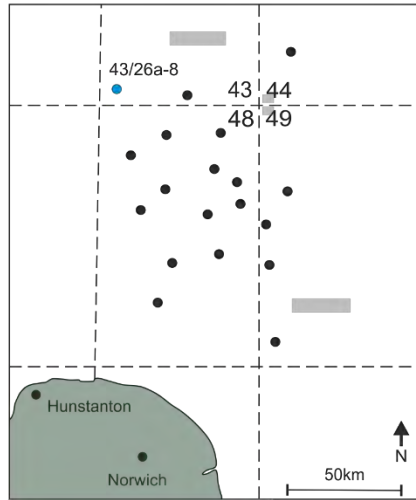
Distance from apex	km	Gravel Channels						Sheets					
		Av. GC	Median GC	Q1 GC	Q3 GC	Min GC	Max GC	Av. SF	Median SF	Q1 SF	Q3 SF	Min SF	Max SF
JBC	25.8	1.00	1.00	0.00	0.00	1.00	1.00	1.02	0.60	0.40	1.20	0.10	4.10
DB	56.4	0.00	0.00	0.00	0.00	0.00	0.00	1.29	0.85	0.30	2.30	0.20	3.50
LP	74.6	0.00	0.00	0.00	0.00	0.00	0.00	1.18	1.00	0.70	1.60	0.40	2.80
ZMC	89.3	1.20	1.20	0.00	0.00	1.20	1.20	1.61	1.40	1.00	2.60	0.40	3.60
NPR	98.6	1.20	1.10	1.10	1.40	1.10	1.60	0.80	1.10	0.80	1.40	0.40	2.30
WT	107.7	0.00	0.00	0.00	0.00	0.00	0.00	0.99	0.65	0.45	1.65	0.40	2.00
CW	149.6	0.00	0.00	0.00	0.00	0.00	0.00	1.43	1.20	0.85	2.15	0.20	3.20
SRS	154.7	0.00	0.00	0.00	0.00	0.00	0.00	2.07	1.40	0.60	2.60	0.30	2.80
CR	171.3	0.00	0.00	0.00	0.00	0.00	0.00	2.20	1.70	1.00	4.10	1.00	4.10
H	173.1	0.00	0.00	0.00	0.00	0.00	0.00	2.18	2.55	1.75	3.10	1.40	3.40
MW	200.9	0.40	0.40	0.00	0.00	0.40	0.40	1.10	1.10	0.00	0.00	1.10	1.10
HB	223.8	0.00	0.00	0.00	0.00	0.00	0.00	1.21	0.80	0.40	1.50	0.25	4.20
KT	249.3	0.00	0.00	0.00	0.00	0.00	0.00	2.32	1.95	0.90	2.40	0.70	5.80
LF	318.8	0.75	0.75	0.50	1.00	0.50	1.00	1.51	1.10	0.50	2.80	0.30	3.50
G	353	0.00	0.00	0.00	0.00	0.00	0.00	1.38	1.00	0.30	2.40	0.20	4.20
K	378.8	0.37	0.30	0.20	0.60	0.10	0.70	0.93	0.70	0.40	1.10	0.10	3.80
CC	413.8	0.95	0.95	0.50	1.40	0.50	1.40	1.16	0.80	0.50	1.35	0.20	4.20
P (av)		0.49						1.28					
M (av)		0.08						1.62					
D (av)		0.41						1.46					

Distance from apex	Overbank							
	Log	km	Av. OB	Median OB	Q1 OB	Q3 OB	Min OB	Max OB
JBC		25.8	0.00	0.00	0.00	0.00	0.00	0.00
DB		56.4	0.00	0.00	0.00	0.00	0.00	0.00
LP		74.6	0.00	0.00	0.00	0.00	0.00	0.00
7MC		89.3	1.90	1.90	0.00	0.00	1.90	1.90
NPR		98.6	0.50	0.50	0.00	0.00	0.50	0.50
WT		107.7	0.00	0.00	0.00	0.00	0.00	0.00
CW		149.6	6.20	6.20	0.00	0.00	6.20	6.20
SRS		154.7	0.30	0.30	0.00	0.00	0.30	0.30
CR		171.3	3.60	3.60	1.00	7.20	1.00	7.20
H		173.1	0.00	0.00	0.00	0.00	0.00	0.00
MW		200.9	0.50	0.50	0.00	0.00	0.50	0.50
HB		223.8	1.20	1.20	0.30	2.10	0.30	2.10
KT		249.3	1.65	1.55	1.50	1.60	1.50	1.80
LF		318.8	1.54	1.00	0.65	2.70	0.30	2.00
G		353	8.33	5.00	5.00	15.00	5.00	15.00
K		378.8	2.73	2.20	1.70	3.85	0.40	6.90
CC		413.8	5.78	4.40	3.00	8.75	1.80	9.70
P (av)			0.39					
M (av)			2.30					
D (av)			4.01					

Appendix 3 - Leman logs



Well Number: 43/26a-8
 Total length: 39.85 m
 Core Recovery: 88.4%



Lithofacies Key

Fluvial

- Sxb & Stxb
- Slxb
- Spb
- Spl
- Sfri
- Stpl
- Smf
- Cms
- Ccs

Lacustrine

- Sul
- Seb
- Steul
- Spbl
- Sml
- Spil
- Sxl
- Ms

**Please refer to Table 8.1 for full facies descriptions*

Aeolian

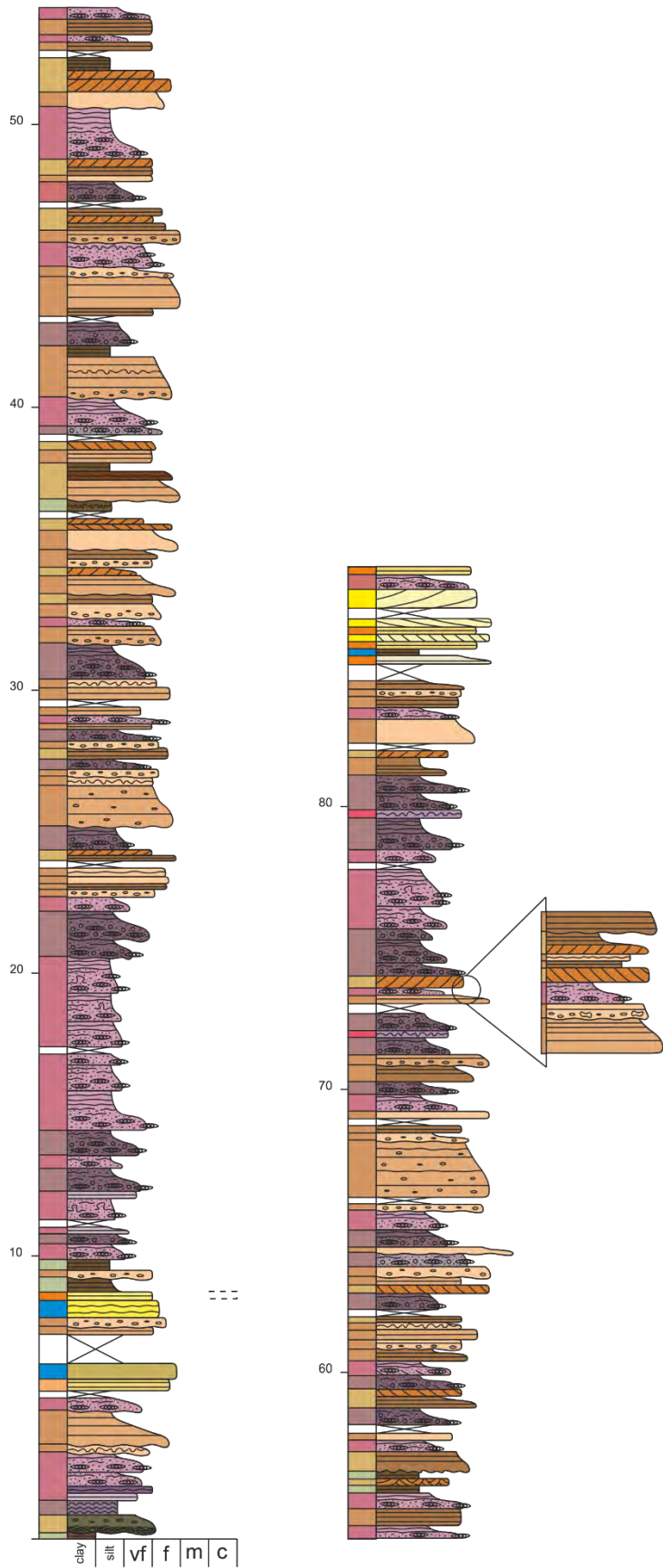
- Smxb & Smtxb
- Smxbc
- Smpb
- Smpl
- Smwr
- Smwb
- Sm

Additional Structures

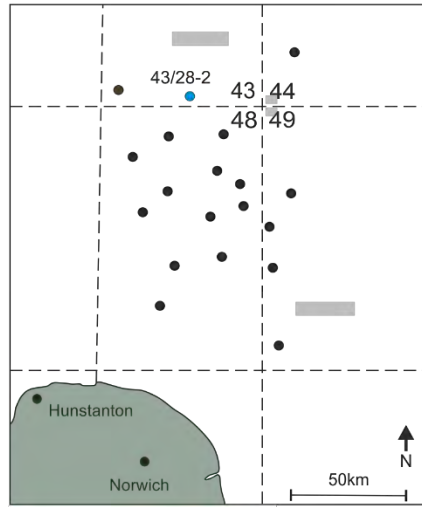
- Roots
- Ripples
- Bioturbation
- Desiccation
- Soft sediment deformation
- Coarser grained lenses
- Intraformational Clasts
- Extraformational Clasts
- Evaporitic grains
- Evaporitic clasts

Facies Associations

- Aeolian Dune
- Aeolian Dune Plinth
- Aeolian Sandsheet
- Dry Interdune
- Lake Margin
- Ephemeral Saline Lake/Mudflat
- Damp to wet Interdune
- Fluvial Channel
- Fluvial Sheet
- Overbank
- Lake Centre



Well Number: 43/28-2
 Total length: 88.35 m
 Core Recovery: 99.2%



Lithofacies Key

Fluvial		Lacustrine	
	Sxb & Stxb		Sul
	Slxb		Seb
	Spb		Steul
	Spl		Spbl
	Sfrl		Sml
	Stpl		Spil
	Smf		Sxl
	Cms		Ms
	Ccs		

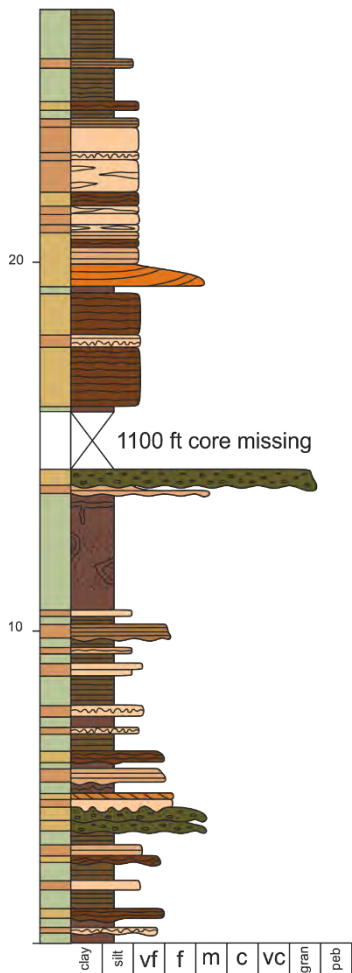
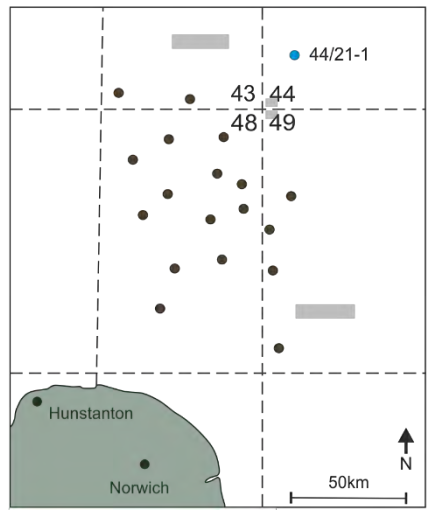
**Please refer to Table 8.1 for full facies descriptions*

Aeolian	
	Smxb & Smtxb
	Smxbc
	Smpb
	Smpl
	Smwr
	Smwb
	Sm

Additional Structures			
	Roots		Coarser grained lenses
	Ripples		Intraformational Clasts
	Bioturbation		Extraformational Clasts
	Desiccation		Evaporitic grains
	Soft sediment deformation		Evaporitic clasts

Facies Associations			
	Aeolian Dune		Damp to wet Interdune
	Aeolian Dune Plinth		Fluvial Channel
	Aeolian Sandsheet		Fluvial Sheet
	Dry Interdune		Overbank
	Lake Margin		Lake Centre
	Ephemeral Saline Lake/Mudflat		

Well Number: 44/21-1
 Total length: 28.75 m
 Core Recovery: 7.8%



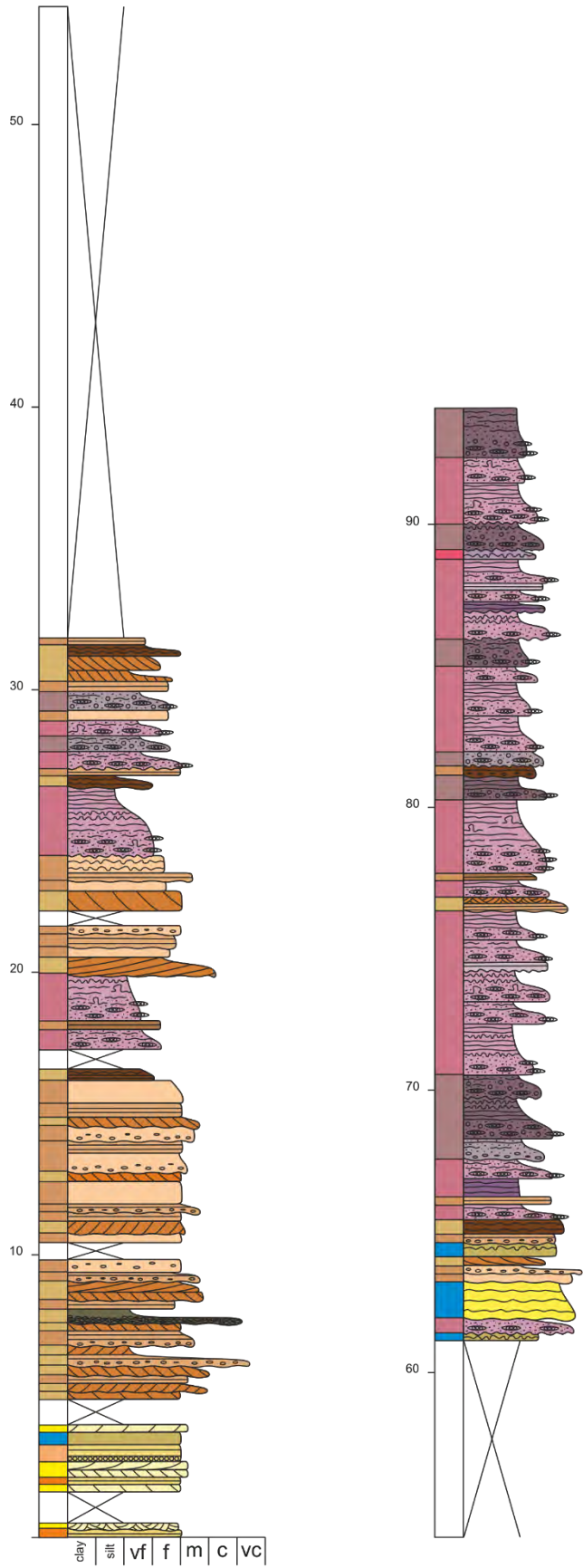
Lithofacies Key

Fluvial		Lacustrine	
	Sxb & Stxb		Sul
	Slxb		Seb
	Spb		Steul
	Spl		Spbl
	Sfri		Sml
	Stpl		Sppl
	Smf		Sxl
	Cms		Ms
	CCS	<i>*Please refer to Table 8.1 for full facies descriptions</i>	

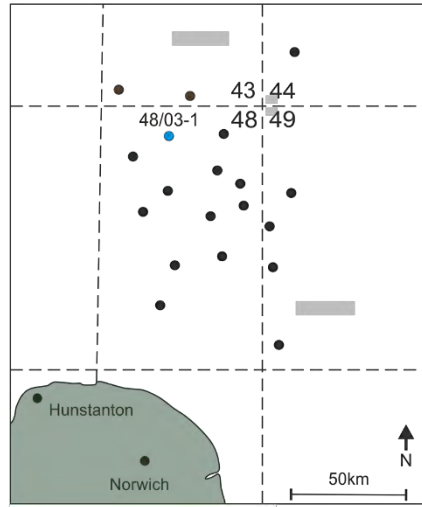
Aeolian	
	Smxb & Smtxb
	Smxbc
	Smpb
	Smpl
	Smwr
	Smwb
	Sm

Additional Structures			
	Roots		Coarser grained lenses
	Ripples		Intraformational Clasts
	Bioturbation		Extraformational Clasts
	Desiccation		Evaporitic grains
	Soft sediment deformation		Evaporitic clasts

Facies Associations			
	Aeolian Dune		Damp to wet Interdune
	Aeolian Dune Plinth		Fluvial Channel
	Aeolian Sandsheet		Fluvial Sheet
	Dry Interdune		Overbank
	Lake Margin		Lake Centre
	Ephemeral Saline Lake/Mudflat		



Well Number: 48/03-1
 Total length: 65.8 m
 Core Recovery: 64.3%



Lithofacies Key

Fluvial		Lacustrine	
	Sxb & Stxb		Sul
	Slxb		Seb
	Spb		Steul
	Spl		Spbl
	Sfrl		Sml
	Stpl		Sppl
	Smf		Sxl
	Cms		Ms
	Ccs		

**Please refer to Table 8.1 for full facies descriptions*

Aeolian	
	Smxb & Smtxb
	Smxbc
	Smpb
	Smpl
	Smwr
	Smwb
	Sm

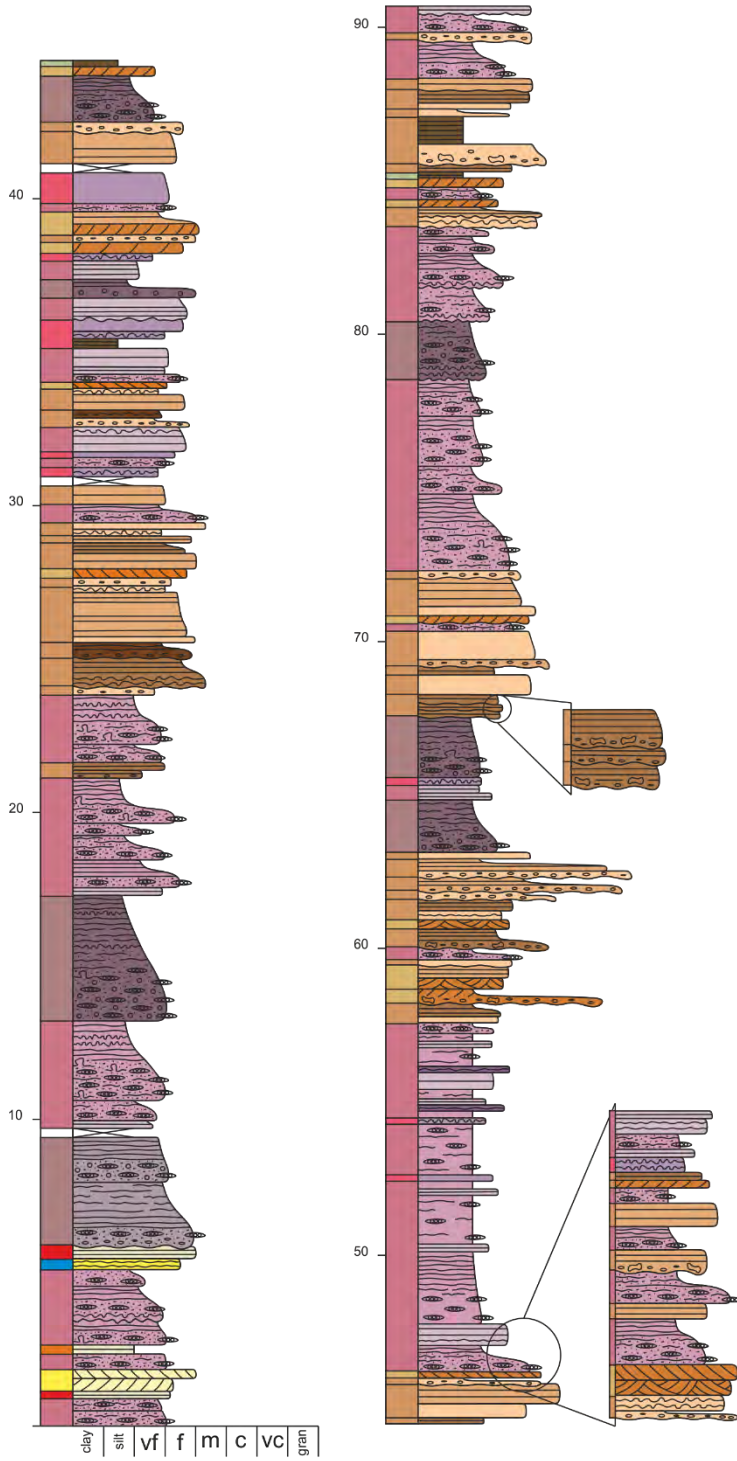
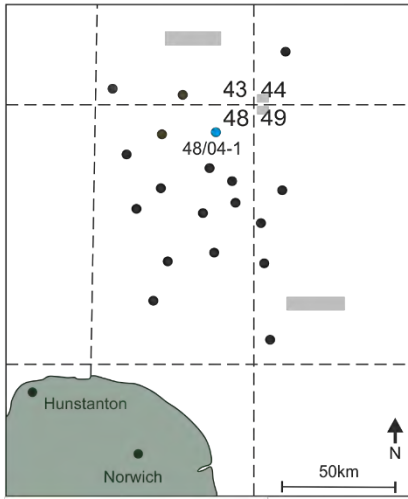
Additional Structures

	Roots		Coarser grained lenses
	Ripples		Intraformational Clasts
	Bioturbation		Extraformational Clasts
	Desiccation		Evaporitic grains
	Soft sediment deformation		Evaporitic clasts

Facies Associations

	Aeolian Dune		Damp to wet Interdune
	Aeolian Dune Plinth		Fluvial Channel
	Aeolian Sandsheet		Fluvial Sheet
	Dry Interdune		Overbank
	Lake Margin		Lake Centre
	Ephemeral Saline Lake/Mudflat		

Well Number: 48/04-1 (1 of 2)
 Total length: 120.85 m
 Core Recovery: 99.9%



Lithofacies Key

Fluvial

- Sxb & Stxb
- Slxb
- Spb
- Spl
- Sfrl
- Stpl
- Smf
- Cms
- Ccs

Lacustrine

- Sul
- Seb
- Steul
- Spbl
- Sml
- Spll
- Sxl
- Ms

**Please refer to Table 8.1 for full facies descriptions*

Aeolian

- Smxb & Smtxb
- Smxbc
- Smpb
- Smpl
- Smwr
- Smwb
- Sm

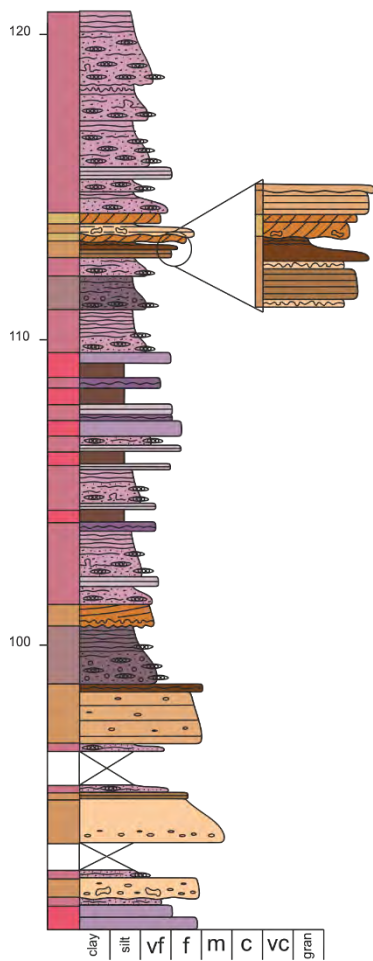
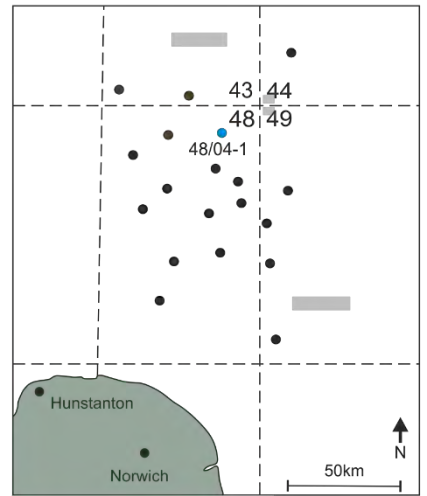
Additional Structures

- Roots
- Ripples
- Bioturbation
- Desiccation
- Soft sediment deformation
- Coarser grained lenses
- Intraformational Clasts
- Extraformational Clasts
- Evaporitic grains
- Evaporitic clasts

Facies Associations

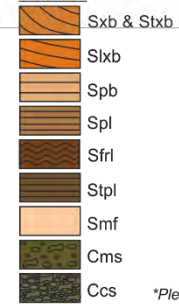
- Aeolian Dune
- Aeolian Dune Plinth
- Aeolian Sandsheet
- Dry Interdune
- Lake Margin
- Ephemeral Saline Lake/Mudflat
- Damp to wet Interdune
- Fluvial Channel
- Fluvial Sheet
- Overbank
- Lake Centre

Well Number: 48/04-1 (2 of 2)
 Total length: 120.85 m
 Core Recovery: 99.9%

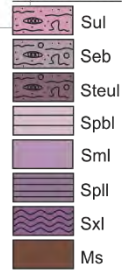


Lithofacies Key

Fluvial

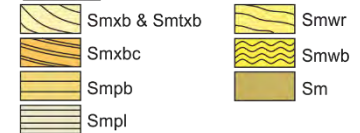


Lacustrine

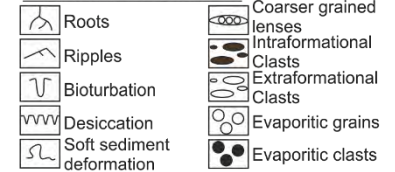


*Please refer to Table 8.1 for full facies descriptions

Aeolian



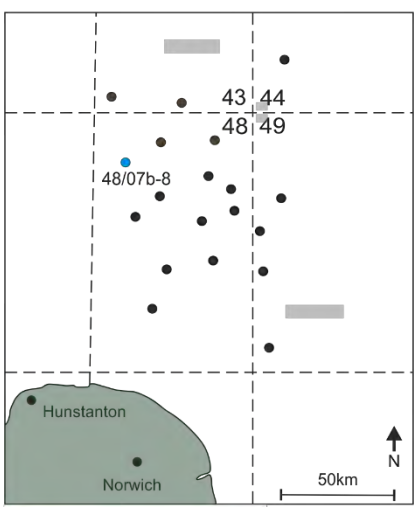
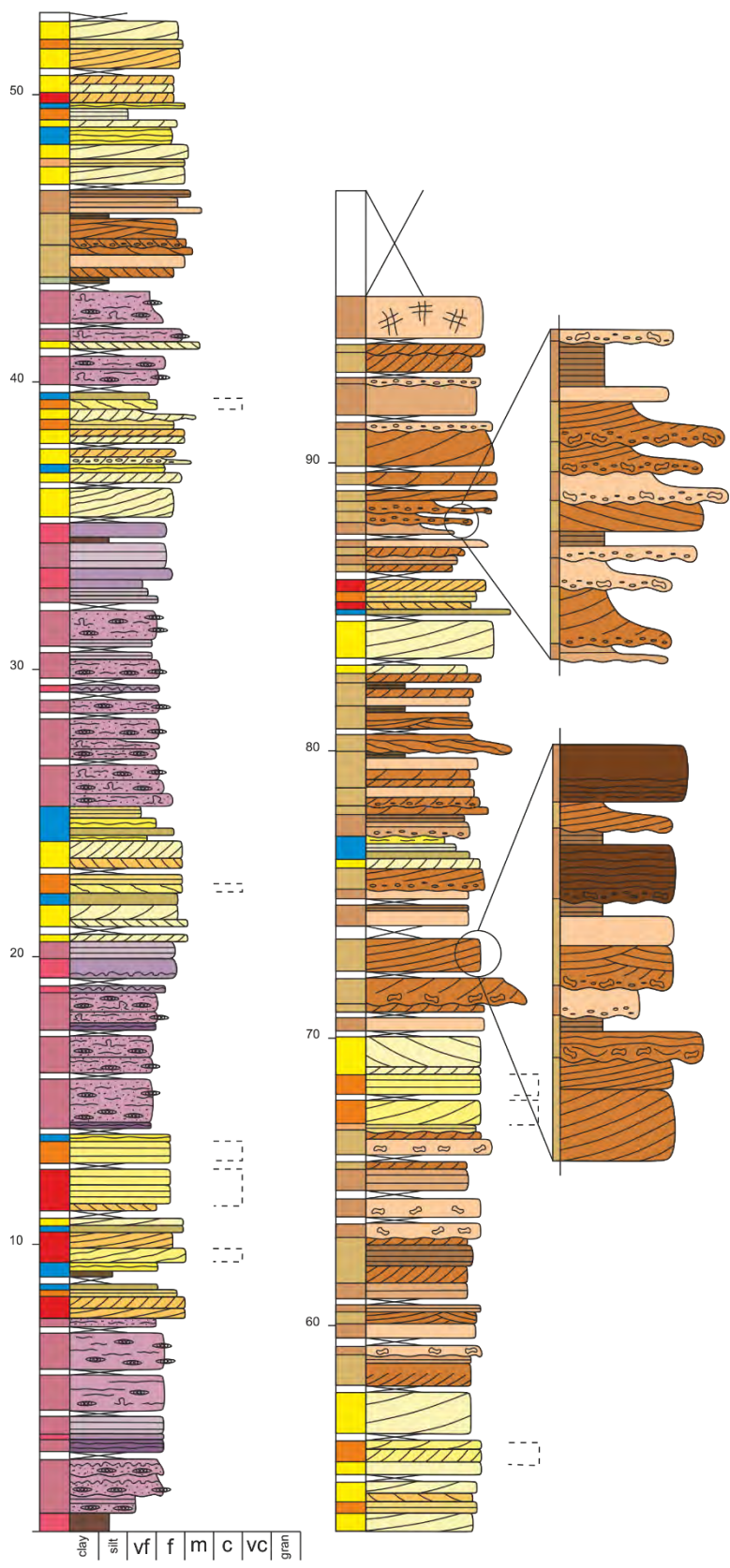
Additional Structures



Facies Associations



Well Number: 48/07b-8 (1 of 2)
 Total length: 187 m
 Core Recovery: 93.4%



Lithofacies Key

Fluvial		Lacustrine	
	Sxb & Stxb		Sul
	Slxb		Seb
	Spb		Steul
	Spl		Spbl
	Sfri		Sml
	Stpl		Sppl
	Smf		Sxl
	Cms		Ms
	CCS		

**Please refer to Table 8.1 for full facies descriptions*

Aeolian

	Smxb & Smtxb		Smwr
	Smxbc		Smwb
	Smpb		Sm
	Smpl		

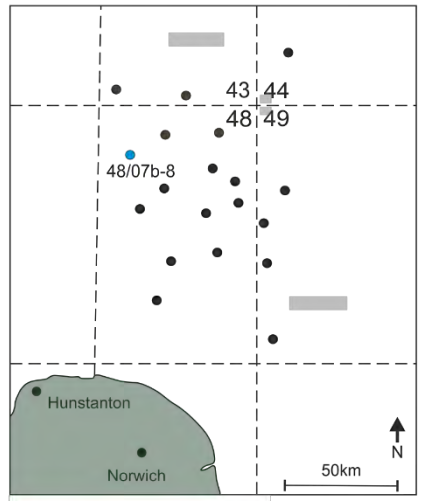
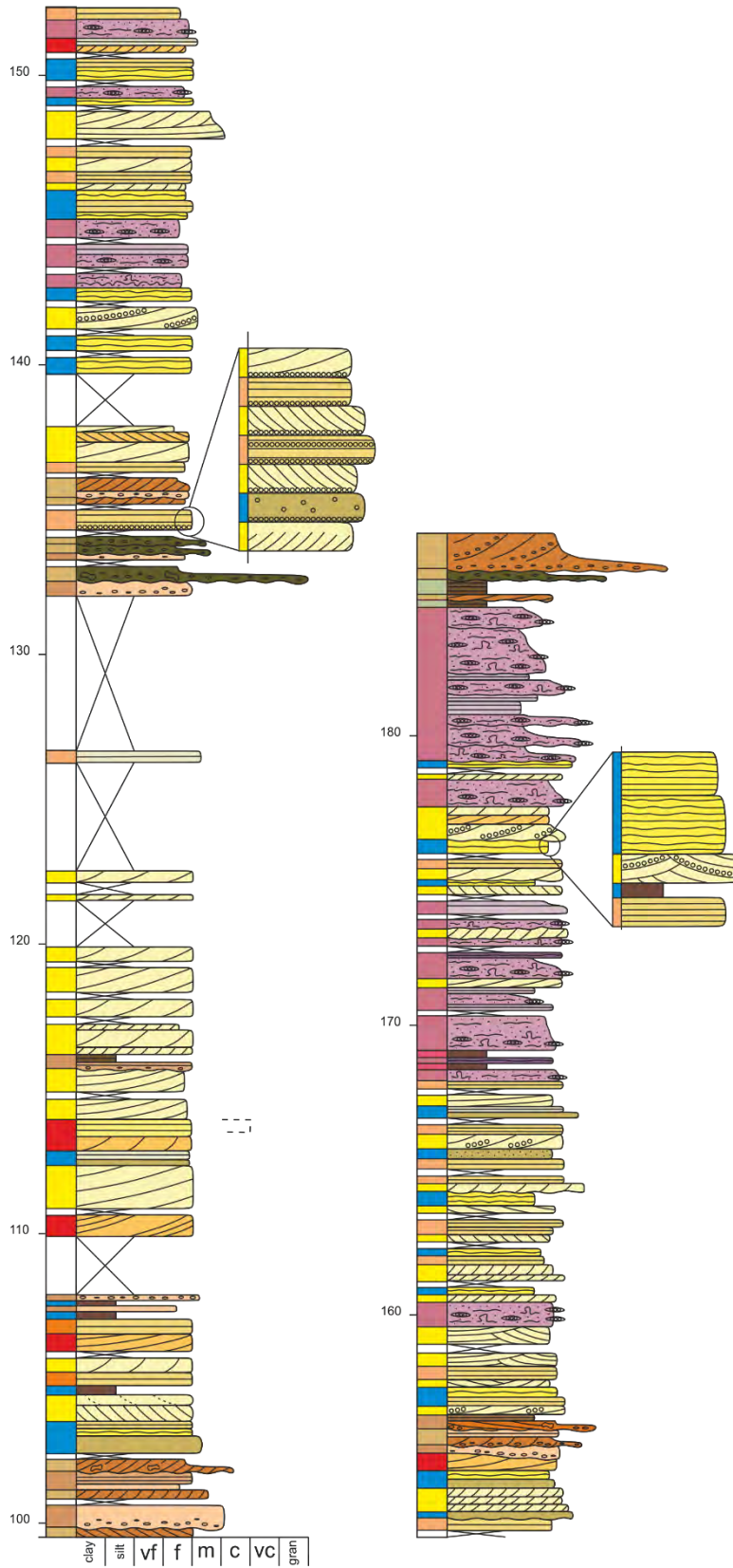
Additional Structures

	Roots		Coarser grained lenses
	Ripples		Intraformational Clasts
	Bioturbation		Extraformational Clasts
	Desiccation		Evaporitic grains
	Soft sediment deformation		Evaporitic clasts

Facies Associations

	Aeolian Dune		Damp to wet Interdune
	Aeolian Dune Plinth		Fluvial Channel
	Aeolian Sandsheet		Fluvial Sheet
	Dry Interdune		Overbank
	Lake Margin		Lake Centre
	Ephemeral Saline Lake/Mudflat		

Well Number: 48/07b-8 (2 of 2)
 Total length: 187 m
 Core Recovery: 93.4%



Lithofacies Key

Fluvial	Lacustrine
Sxb & Stxb	Sul
Slxb	Seb
Spb	Steul
Spl	Spbl
Sfri	Sml
Stpl	Sppl
Smf	Sxl
Cms	Ms
Ccs	

**Please refer to Table 8.1 for full facies descriptions*

Aeolian

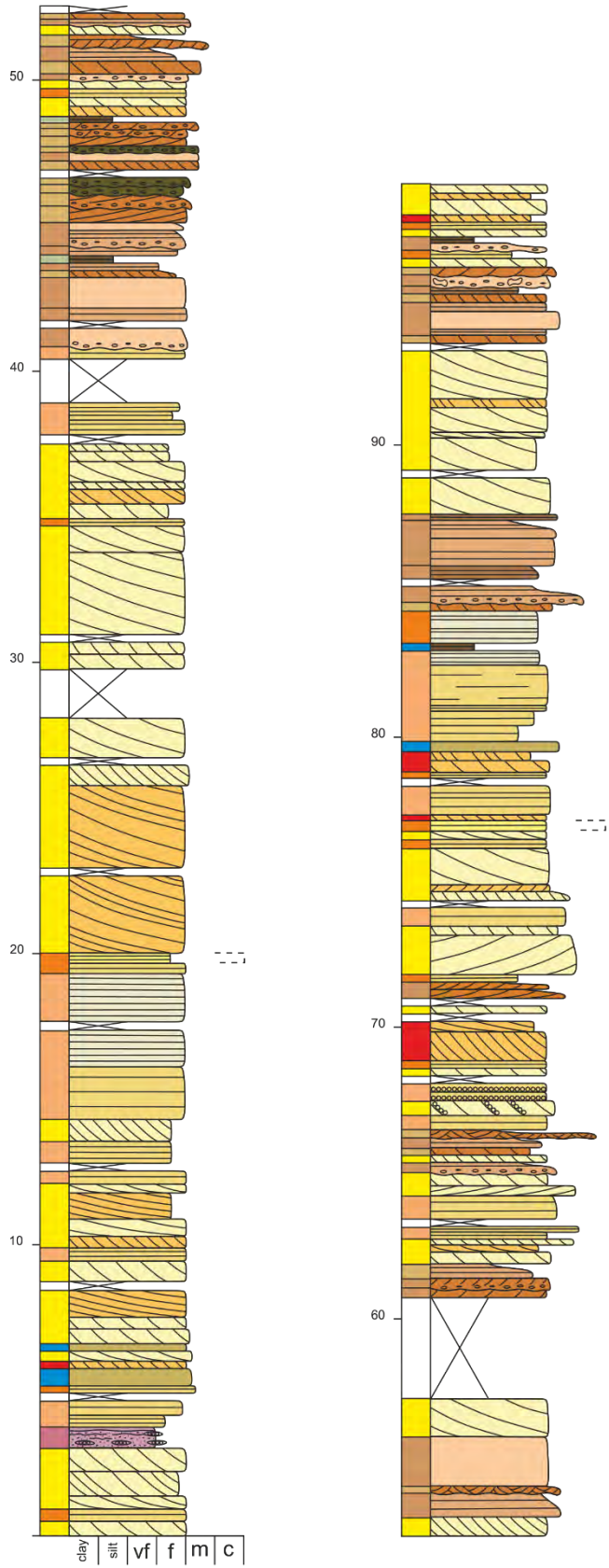
Smbx & Smtxb	Smwr
Smbc	Smwb
Smpb	Sm
Smpl	

Additional Structures

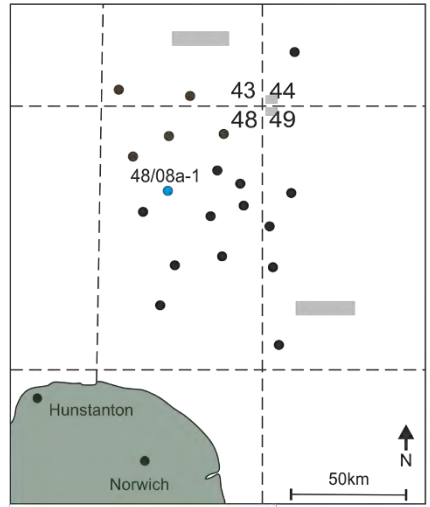
Roots	Coarser grained lenses
Ripples	Intraformational Clasts
Bioturbation	Extraformational Clasts
Desiccation	Evaporitic grains
Soft sediment deformation	Evaporitic clasts

Facies Associations

Aeolian Dune	Damp to wet Interdune
Aeolian Dune Plinth	Fluvial Channel
Aeolian Sandsheet	Fluvial Sheet
Dry Interdune	Overbank
Lake Margin	Lake Centre
Ephemeral Saline Lake/Mudflat	



Well Number: 48/08a-1
 Total length: 99 m
 Core Recovery: 94.8%



Lithofacies Key

Fluvial		Lacustrine	
	Sxb & Stxb		Sul
	Slxb		Seb
	Spb		Steul
	Spl		Spbl
	Sfri		Sml
	Stpl		Sppl
	Smf		Sxl
	Cms		Ms
	Ccs		

**Please refer to Table 8.1 for full facies descriptions*

Aeolian

	Smxb & Smtxb		Smwr
	Smxbc		Smwb
	Smpb		Sm
	Smpl		

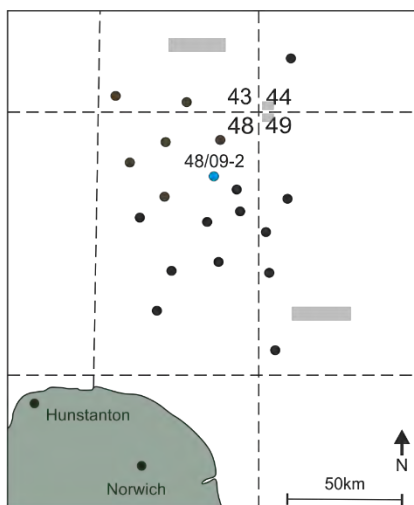
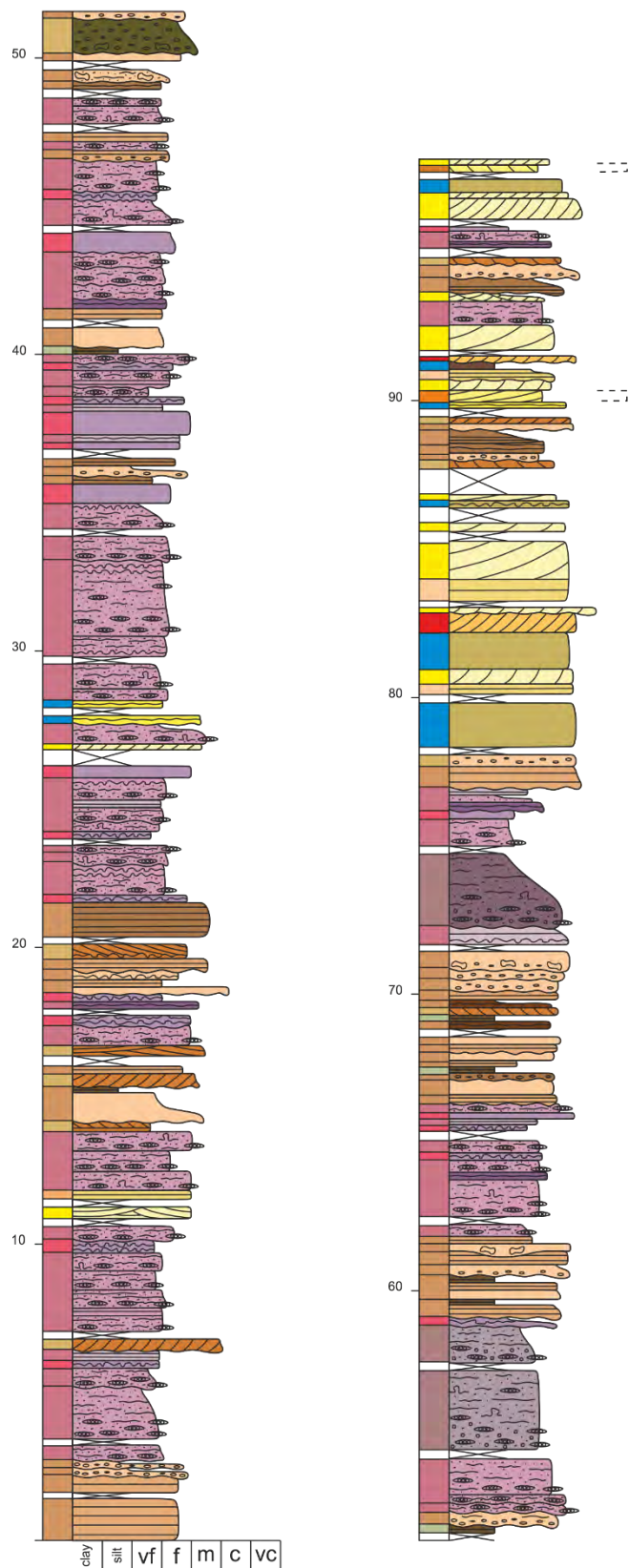
Additional Structures

	Roots		Coarser grained lenses
	Ripples		Intraformational Clasts
	Bioturbation		Extraformational Clasts
	Desiccation		Evaporitic grains
	Soft sediment deformation		Evaporitic clasts

Facies Associations

	Aeolian Dune		Damp to wet Interdune
	Aeolian Dune Plinth		Fluvial Channel
	Aeolian Sandsheet		Fluvial Sheet
	Dry Interdune		Overbank
	Lake Margin		Lake Centre
	Ephemeral Saline Lake/Mudflat		

Well Number: 48/09-2 (1 of 2)
 Total length: 137.35 m
 Core Recovery: 99.1%



Lithofacies Key

Fluvial

- Sxb & Stxb
- Slxb
- Spb
- Spl
- Sfrl
- Stpl
- Smf
- Cms
- Ccs

Lacustrine

- Sul
- Seb
- Steul
- Spbl
- Sml
- Spil
- Sxl
- Ms

**Please refer to Table 8.1 for full facies descriptions*

Aeolian

- Smxb & Smtxb
- Smxbc
- Smpb
- Smpl
- Smwr
- Smwb
- Sm

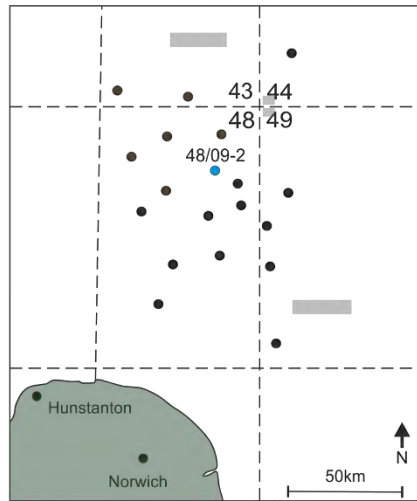
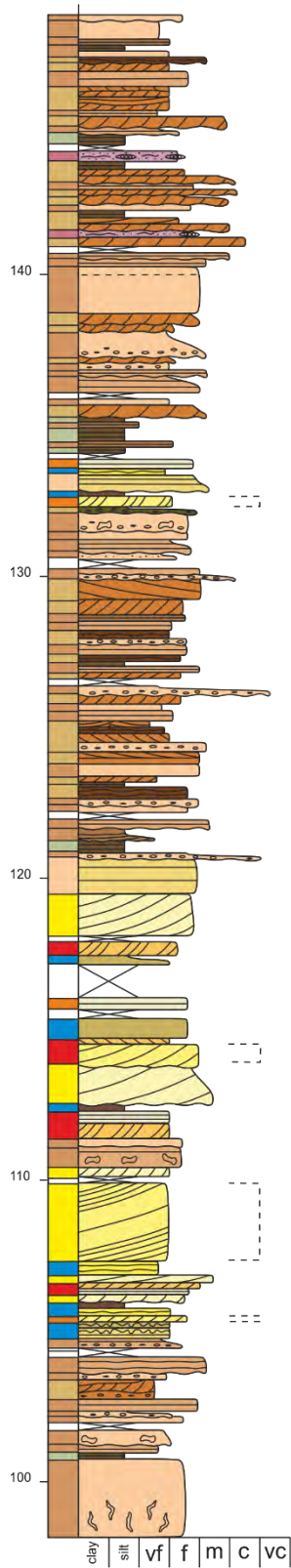
Additional Structures

- Roots
- Ripples
- Bioturbation
- Desiccation
- Soft sediment deformation
- Coarser grained lenses
- Intraformational Clasts
- Extraformational Clasts
- Evaporitic grains
- Evaporitic clasts

Facies Associations

- Aeolian Dune
- Aeolian Dune Plinth
- Aeolian Sandsheet
- Dry Interdune
- Lake Margin
- Ephemeral Saline Lake/Mudflat
- Damp to wet Interdune
- Fluvial Channel
- Fluvial Sheet
- Overbank
- Lake Centre

Well Number: 48/09-2 (2 of 2)
 Total length: 137.35 m
 Core Recovery: 99.1%



Lithofacies Key

Fluvial

- Sxb & Stxb
- Slxb
- Spb
- Spl
- Sfrl
- Stpl
- Smf
- Cms
- Ccs

Lacustrine

- Sul
- Seb
- Steul
- Spbl
- Sml
- Sppl
- Sxl
- Ms

**Please refer to Table 8.1 for full facies descriptions*

Aeolian

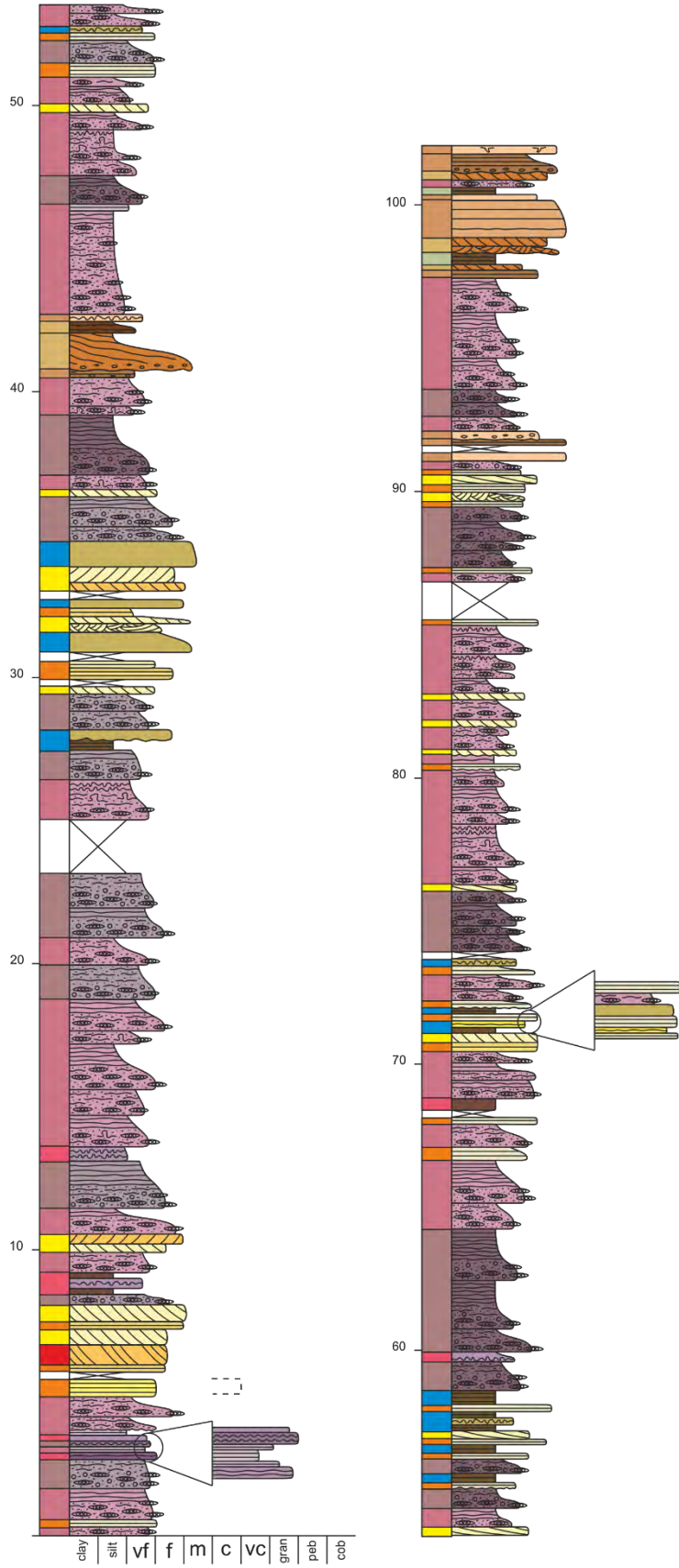
- Smxb & Smtxb
- Smxbc
- Smpb
- Smpl
- Smwr
- Smwb
- Sm

Additional Structures

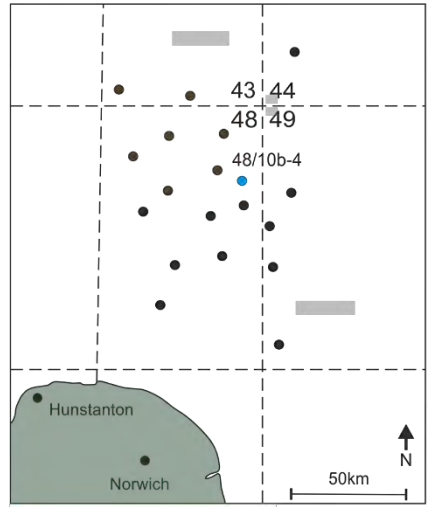
- Roots
- Ripples
- Bioturbation
- Desiccation
- Soft sediment deformation
- Coarser grained lenses
- Intraformational Clasts
- Extraformational Clasts
- Evaporitic grains
- Evaporitic clasts

Facies Associations

- Aeolian Dune
- Aeolian Dune Plinth
- Aeolian Sandsheet
- Dry Interdune
- Lake Margin
- Ephemeral Saline Lake/Mudflat
- Damp to wet Interdune
- Fluvial Channel
- Fluvial Sheet
- Overbank
- Lake Centre



Well Number: 48/10b-4
 Total length: 102.1 m
 Core Recovery: 96.1%



Lithofacies Key

Fluvial		Lacustrine	
	Sxb & Stxb		Sul
	Slxb		Seb
	Spb		Steul
	Spl		Spbl
	Sfrl		Sml
	Stpl		Sppl
	Smf		Sxl
	Cms		Ms
	Ccs		

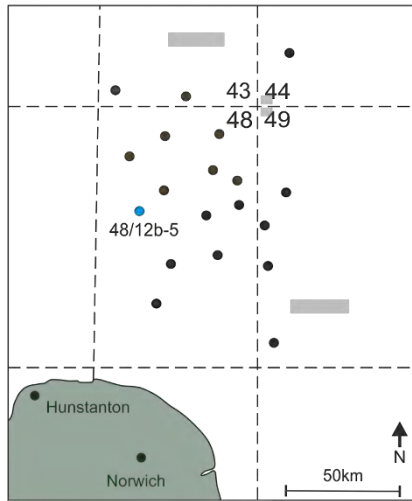
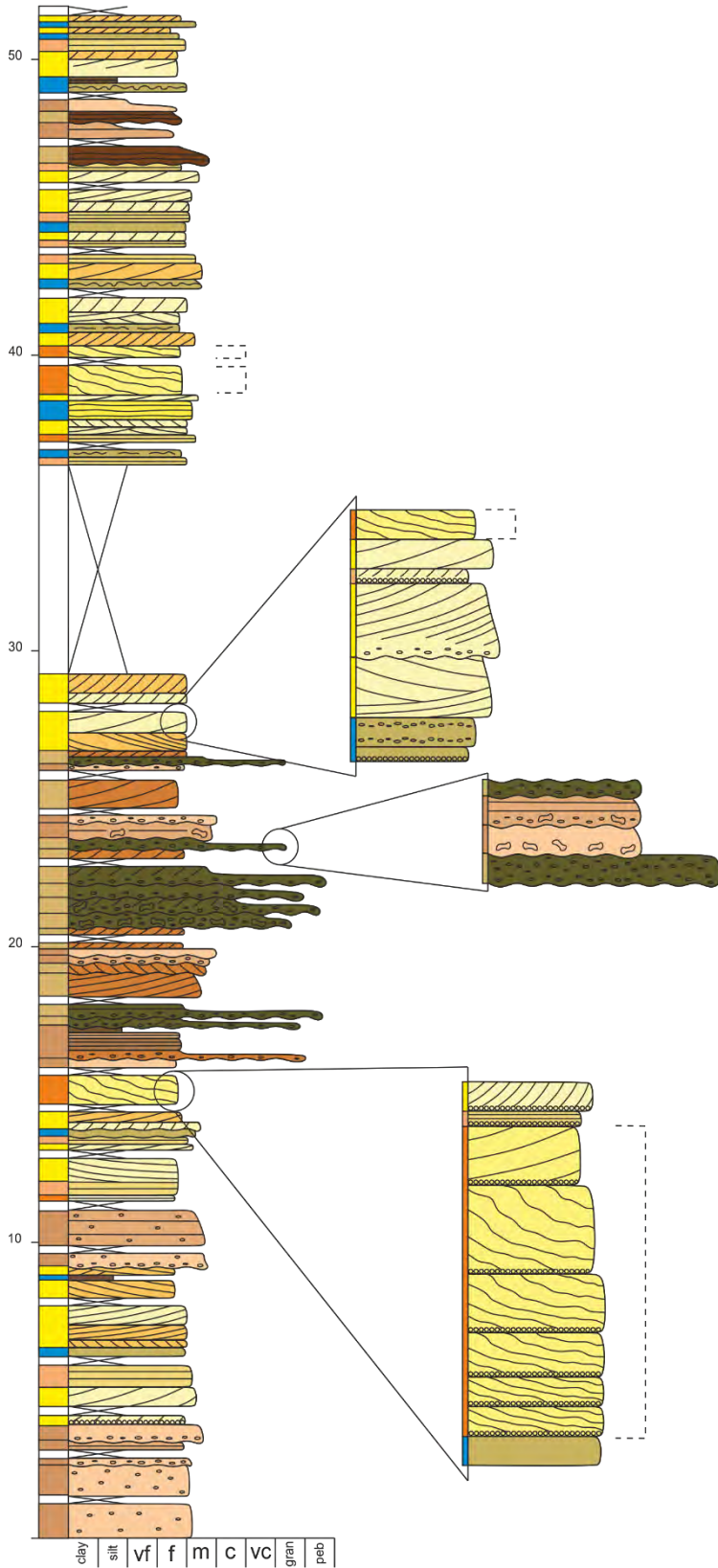
**Please refer to Table 8.1 for full facies descriptions*

Aeolian	
	Smxb & Smtxb
	Smxbc
	Smpb
	Smpl
	Smwr
	Smwb
	Sm

Additional Structures			
	Roots		Coarser grained lenses
	Ripples		Intraformational Clasts
	Bioturbation		Extraformational Clasts
	Desiccation		Evaporitic grains
	Soft sediment deformation		Evaporitic clasts

Facies Associations			
	Aeolian Dune		Damp to wet Interdune
	Aeolian Dune Plinth		Fluvial Channel
	Aeolian Sandsheet		Fluvial Sheet
	Dry Interdune		Overbank
	Lake Margin		Lake Centre
	Ephemeral Saline Lake/Mudflat		

Well Number: 48/12b-5 (1 of 2)
 Total length: 115.85 m
 Core Recovery: 99.9%



Lithofacies Key

Fluvial		Lacustrine	
	Sxb & Stxb		Sul
	Slxb		Seb
	Spb		Steul
	Spl		Spbl
	Sfrl		Sml
	Stpl		Spl
	Smf		Sxl
	Cms		Ms
	Ccs		

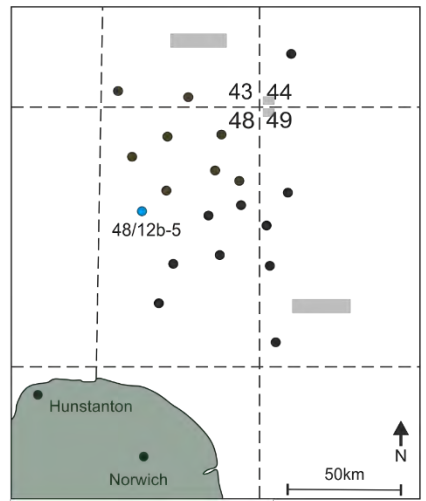
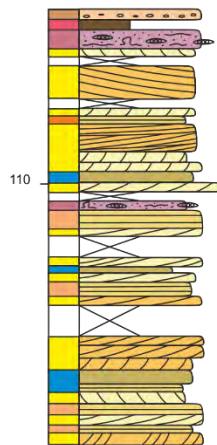
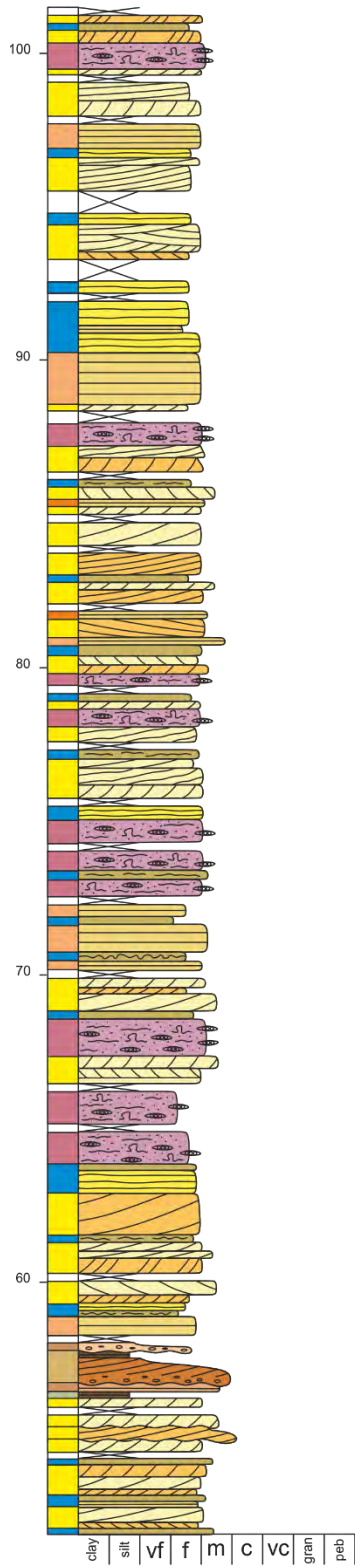
**Please refer to Table 8.1 for full facies descriptions*

Aeolian	
	Smxb & Smtxb
	Smxbc
	Smpb
	Smpl
	Smwr
	Smwb
	Sm

Additional Structures	
	Roots
	Ripples
	Bioturbation
	Desiccation
	Soft sediment deformation
	Coarser grained lenses
	Intraformational Clasts
	Extraformational Clasts
	Evaporitic grains
	Evaporitic clasts

Facies Associations			
	Aeolian Dune		Damp to wet Interdune
	Aeolian Dune Plinth		Fluvial Channel
	Aeolian Sandsheet		Fluvial Sheet
	Dry Interdune		Overbank
	Lake Margin		Lake Centre
	Ephemeral Saline Lake/Mudflat		

Well Number: 48/12b-5 (2 of 2)
 Total length: 115.85 m
 Core Recovery: 99.9%



Lithofacies Key

Fluvial

- Sxb & Stxb
- Slxb
- Spb
- SpI
- Sfrl
- Stpl
- Smf
- Cms
- CCS

Lacustrine

- Sul
- Seb
- Steul
- Spbl
- Sml
- SpII
- Sxl
- Ms

*Please refer to Table 8.1 for full facies descriptions

Aeolian

- Smxb & Smtxb
- Smxhc
- Smpb
- Smpl
- Smwr
- Smwb
- Sm

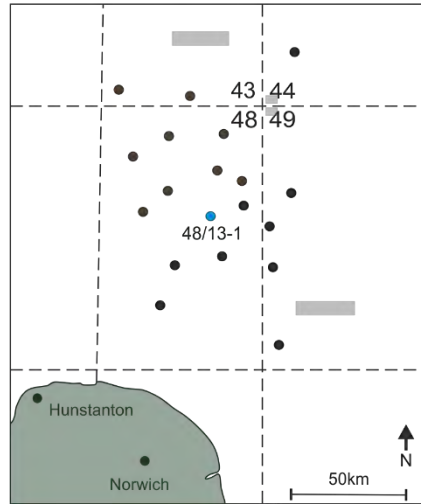
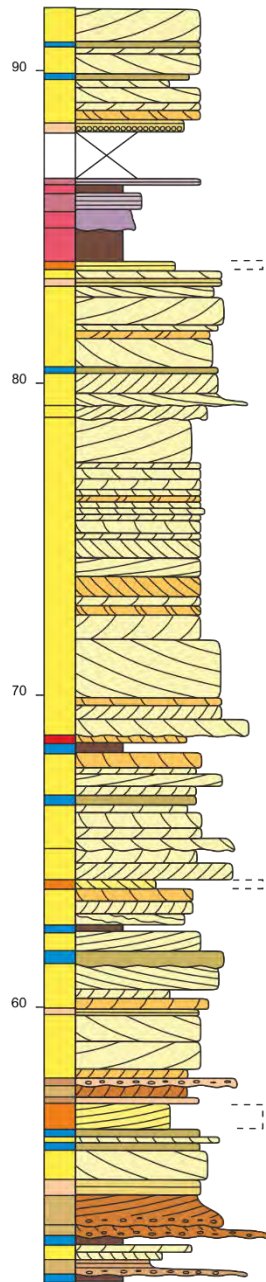
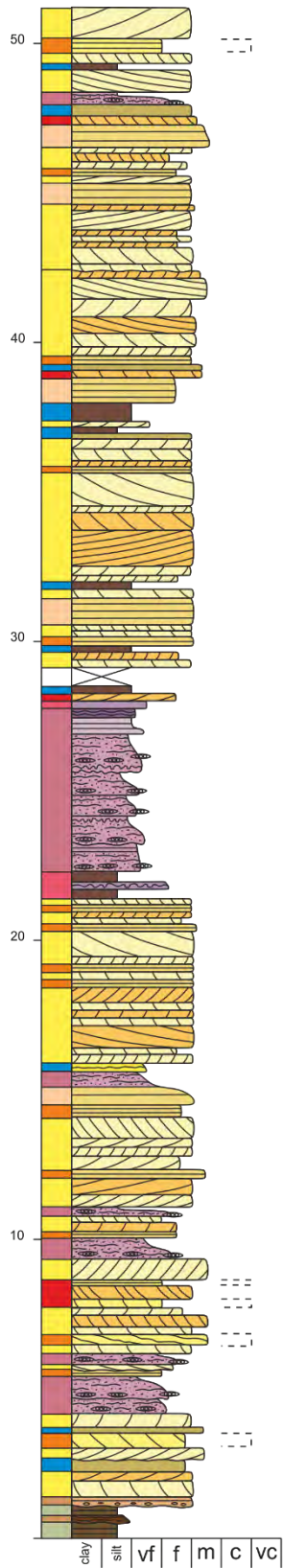
Additional Structures

- Roots
- Ripples
- Bioturbation
- Desiccation
- Soft sediment deformation
- Coarser grained lenses
- Intraformational Clasts
- Extraformational Clasts
- Evaporitic grains
- Evaporitic clasts

Facies Associations

- Aeolian Dune
- Aeolian Dune Plinth
- Aeolian Sandsheet
- Dry Interdune
- Lake Margin
- Ephemeral Saline Lake/Mudflat
- Damp to wet Interdune
- Fluvial Channel
- Fluvial Sheet
- Overbank
- Lake Centre

Well Number: 48/13-1 (1 of 2)
 Total length: 192.8 m
 Core Recovery: 82.9%



Lithofacies Key

Fluvial

- Sxb & Stxb
- Slxb
- Spb
- Spl
- Sfri
- Stpl
- Smf
- Cms
- CCS

Lacustrine

- Sul
- Seb
- Steul
- Spbl
- Sml
- Sppl
- Sxl
- Ms

*Please refer to Table 8.1 for full facies descriptions

Aeolian

- Smxb & Smtxb
- Smxbc
- Smpb
- Smpl
- Smwr
- Smwb
- Sm

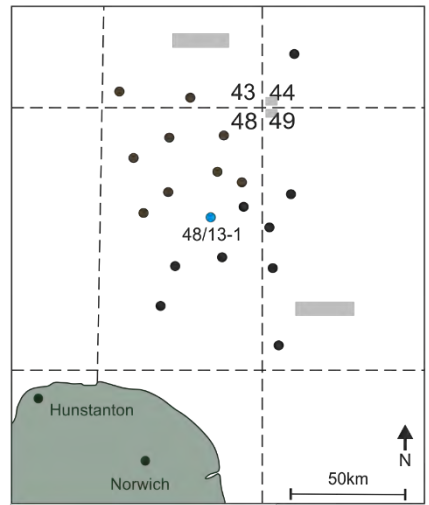
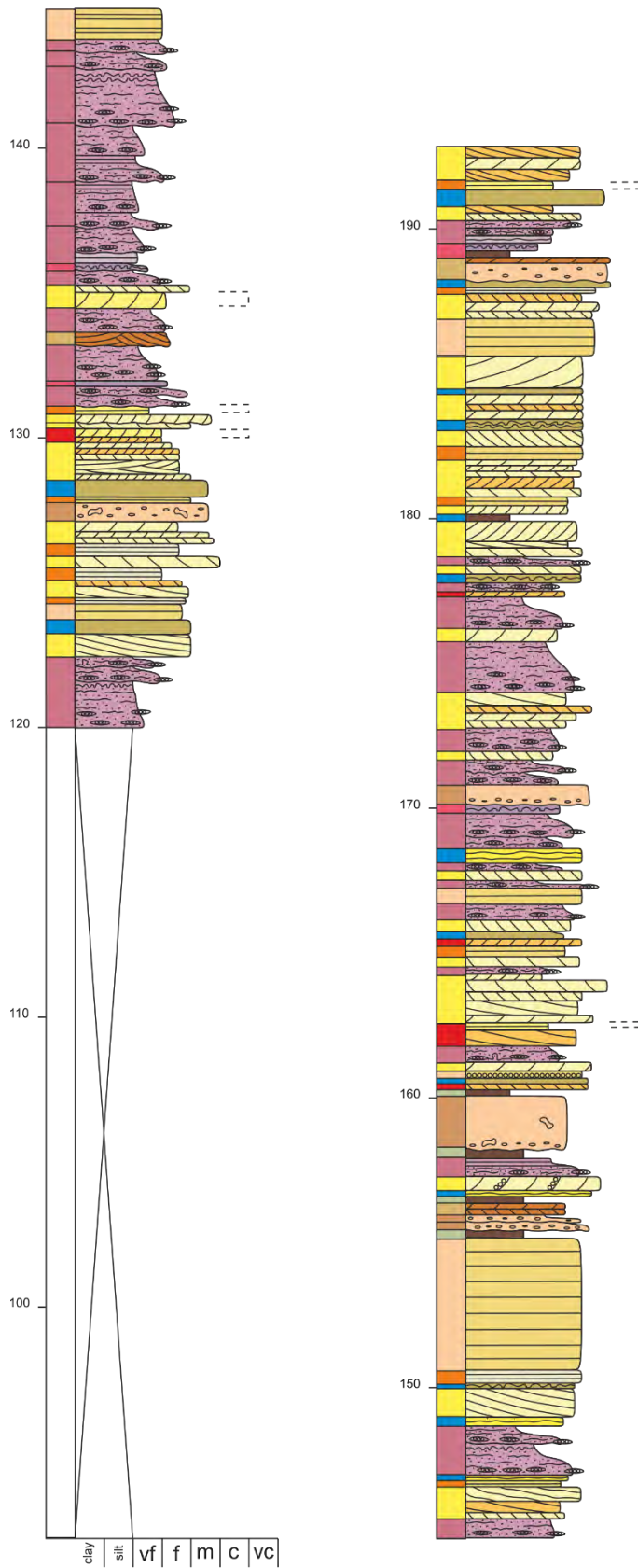
Additional Structures

- Roots
- Ripples
- Bioturbation
- Desiccation
- Soft sediment deformation
- Coarser grained lenses
- Intraformational Clasts
- Extraformational Clasts
- Evaporitic grains
- Evaporitic clasts

Facies Associations

- Aeolian Dune
- Aeolian Dune Plinth
- Aeolian Sandsheet
- Dry Interdune
- Lake Margin
- Ephemeral Saline Lake/Mudflat
- Damp to wet Interdune
- Fluvial Channel
- Fluvial Sheet
- Overbank
- Lake Centre

Well Number: 48/13-1 (2 of 2)
 Total length: 192.8 m
 Core Recovery: 82.9%



Lithofacies Key

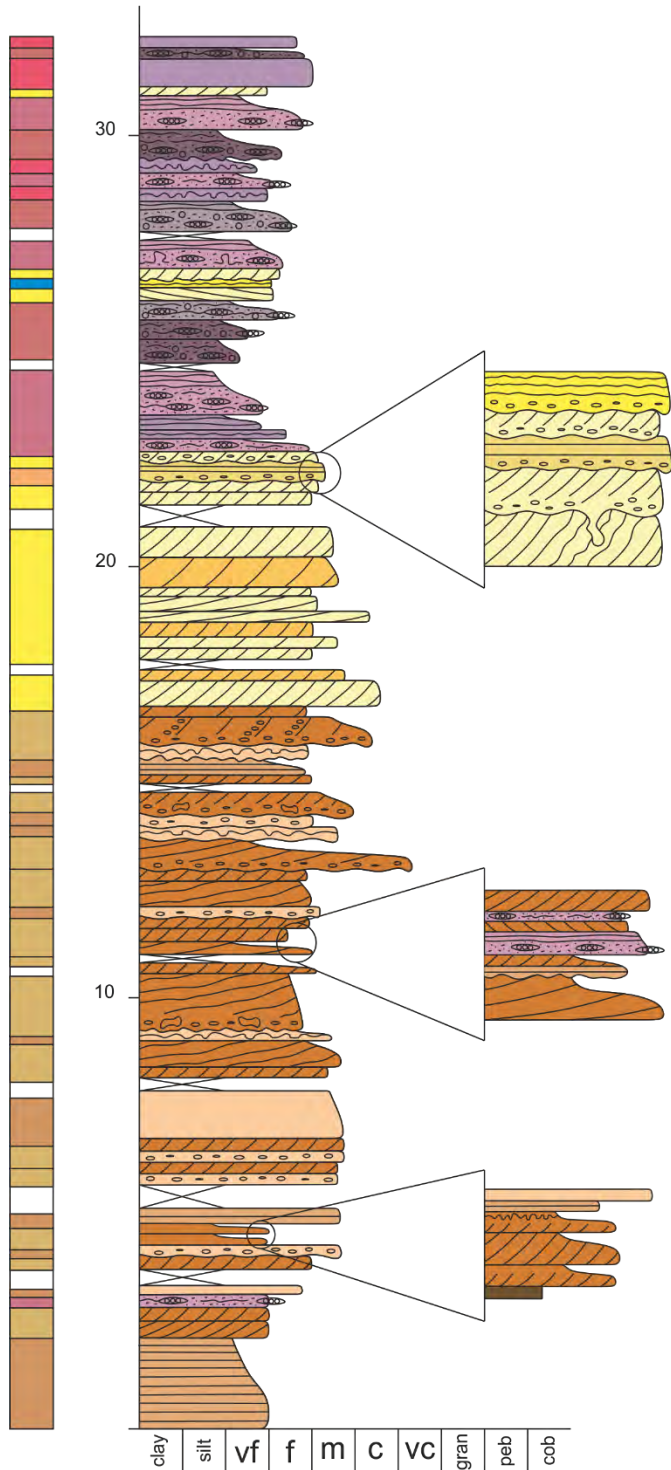
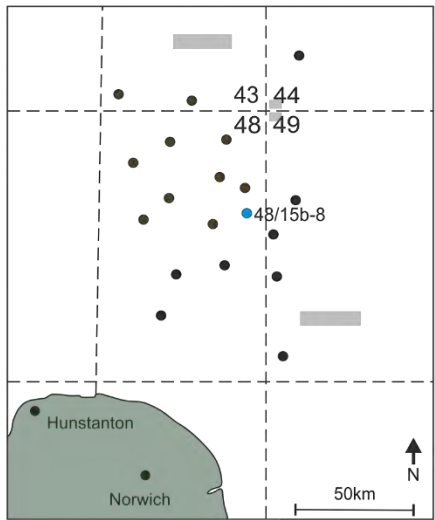
Fluvial		Lacustrine	
	Sxb & Stxb		Sul
	Slxb		Seb
	Spb		Steul
	Spl		Spbl
	Sfrl		Sml
	Stpl		Sppl
	Smf		Sxl
	Cms		Ms
	Ccs	<i>*Please refer to Table 8.1 for full facies descriptions</i>	

Aeolian	
	Smxb & Smtxb
	Smxbc
	Smpb
	Smpl
	Smwr
	Smwb
	Sm

Additional Structures			
	Roots		Coarser grained lenses
	Ripples		Intraformational Clasts
	Bioturbation		Extraformational Clasts
	Desiccation		Evaporitic grains
	Soft sediment deformation		Evaporitic clasts

Facies Associations			
	Aeolian Dune		Damp to wet Interdune
	Aeolian Dune Plinth		Fluvial Channel
	Aeolian Sandsheet		Fluvial Sheet
	Dry Interdune		Overbank
	Lake Margin		Lake Centre
	Ephemeral Saline Lake/Mudflat		

Well Number: 48/15b-8
 Total length: 30.25 m
 Core Recovery: 92.8%



Lithofacies Key

Fluvial		Lacustrine	
	Sxb & Stxb		Sul
	Sixb		Seb
	Spb		Steul
	Spl		Spbl
	Sfrl		Sml
	Stpl		Sppl
	Smf		Sxl
	Cms		Ms
	Ccs		

**Please refer to Table 8.1 for full facies descriptions*

Aeolian

	Smxb & Smtxb		Smwr
	Smxbc		Smwb
	Smpb		Sm
	Smpl		

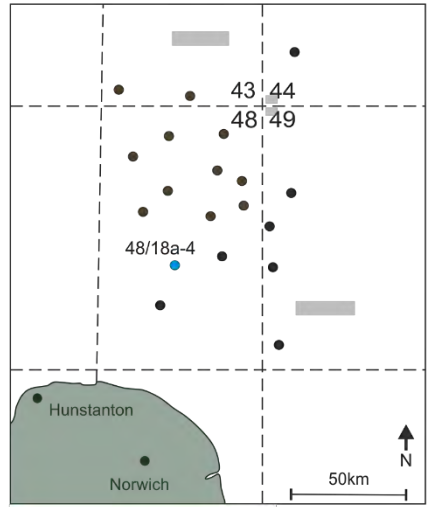
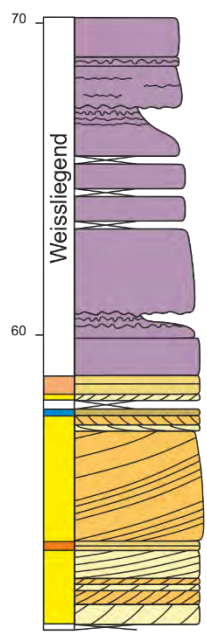
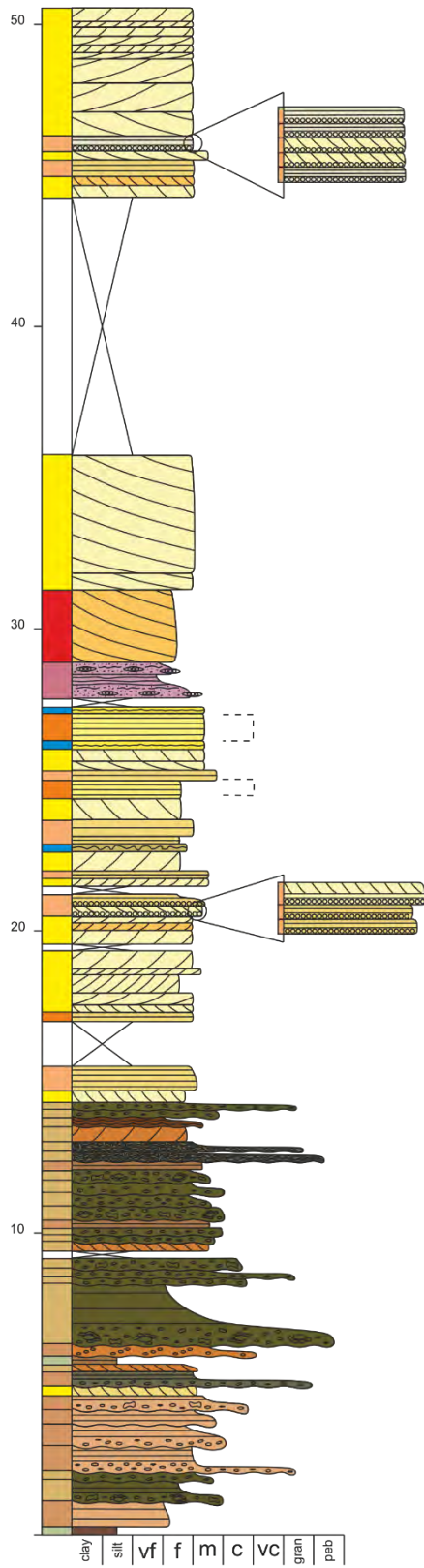
Additional Structures

	Roots		Coarser grained lenses
	Ripples		Intraformational Clasts
	Bioturbation		Extraformational Clasts
	Desiccation		Evaporitic grains
	Soft sediment deformation		Evaporitic clasts

Facies Associations

	Aeolian Dune		Damp to wet Interdune
	Aeolian Dune Plinth		Fluvial Channel
	Aeolian Sandsheet		Fluvial Sheet
	Dry Interdune		Overbank
	Lake Margin		Lake Centre
	Ephemeral Saline Lake/Mudflat		

Well Number: 48/18a-4
 Total length: 70.15 m
 Core Recovery: 89.6%



Lithofacies Key

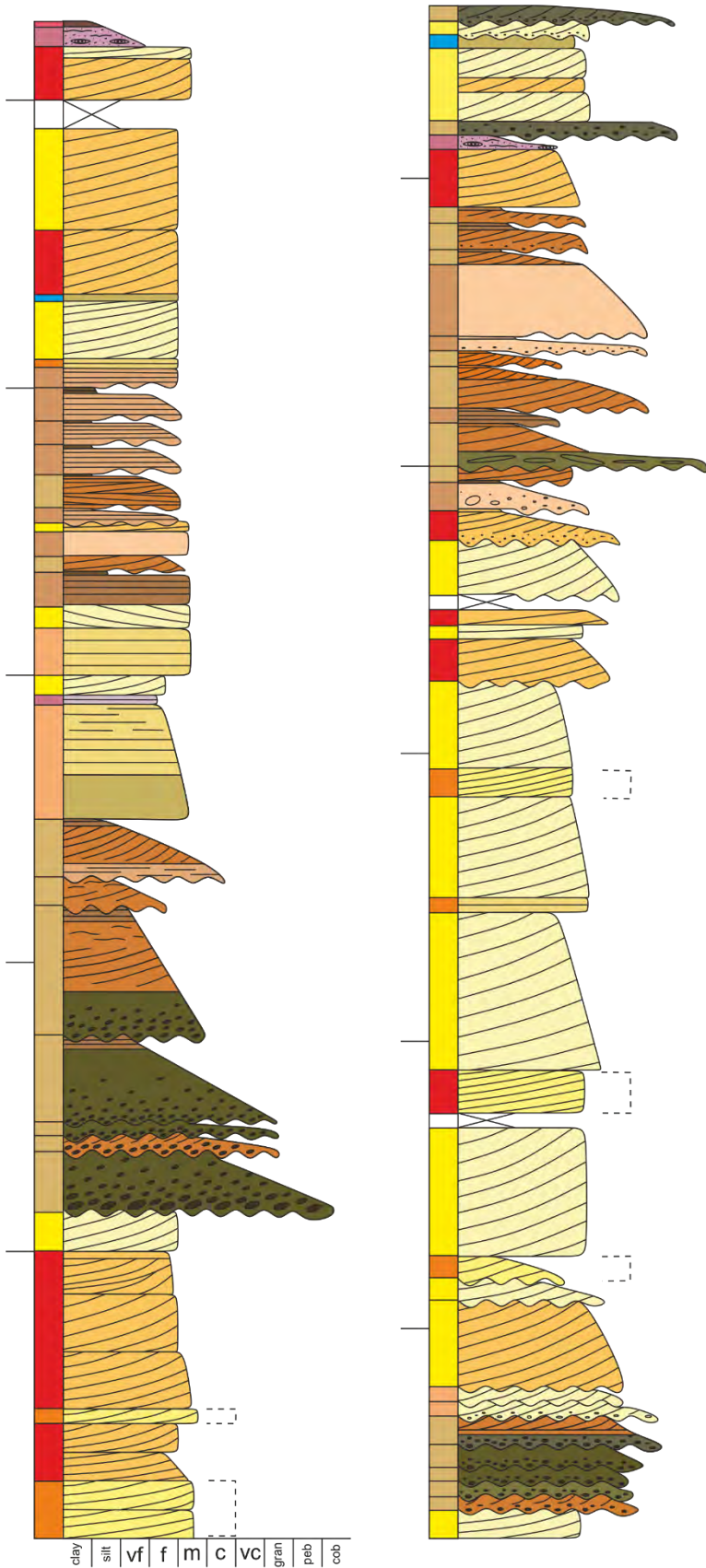
Fluvial		Lacustrine	
	Sxb & Stxb		Sul
	Slxb		Seb
	Spb		Steul
	Spl		Spbl
	Sfrl		Sml
	Stpl		Sppl
	Smf		Sxl
	Cms		Ms
	Ccs		

**Please refer to Table 8.1 for full facies descriptions*

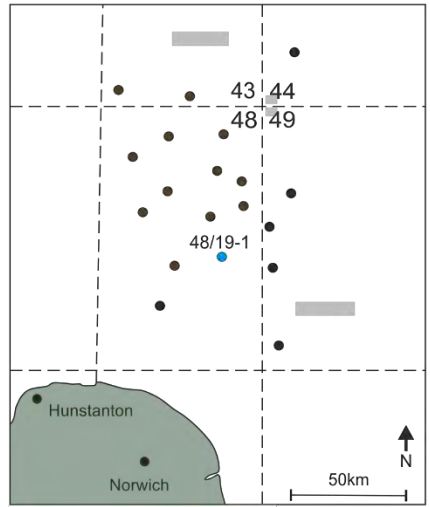
Aeolian	
	Smxb & Smtxb
	Smxbc
	Smpb
	Smpl
	Smwr
	Smwb
	Sm

Additional Structures	
	Roots
	Ripples
	Bioturbation
	Desiccation
	Soft sediment deformation
	Coarser grained lenses
	Intraformational Clasts
	Extraformational Clasts
	Evaporitic grains
	Evaporitic clasts

Facies Associations			
	Aeolian Dune		Damp to wet Interdune
	Aeolian Dune Plinth		Fluvial Channel
	Aeolian Sandsheet		Fluvial Sheet
	Dry Interdune		Overbank
	Lake Margin		Lake Centre
	Ephemeral Saline Lake/Mudflat		



Well Number: 48/19-1 (2 of 2)
 Total length: 142.4 m
 Core Recovery: 71.5%



Lithofacies Key

Fluvial		Lacustrine	
	Sxb & Stxb		Sul
	Slxb		Seb
	Spb		Steul
	Spl		Spbl
	Sfrl		Sml
	Stpl		Sppl
	Smf		Sxl
	Cms		Ms
	Ccs		

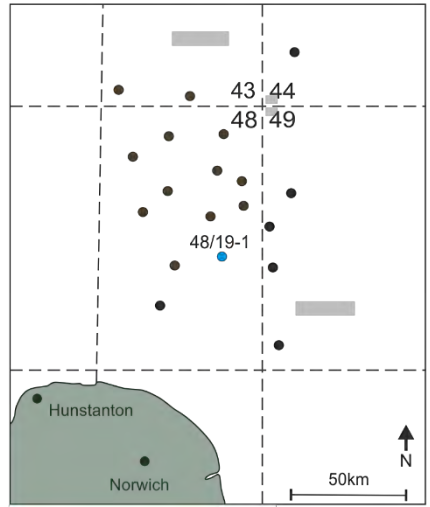
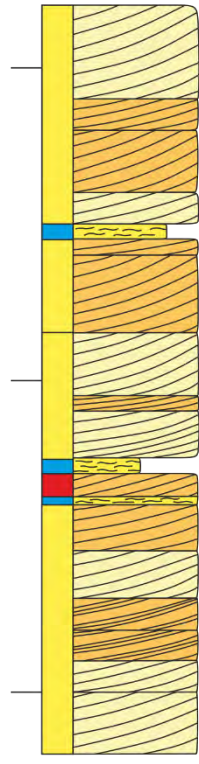
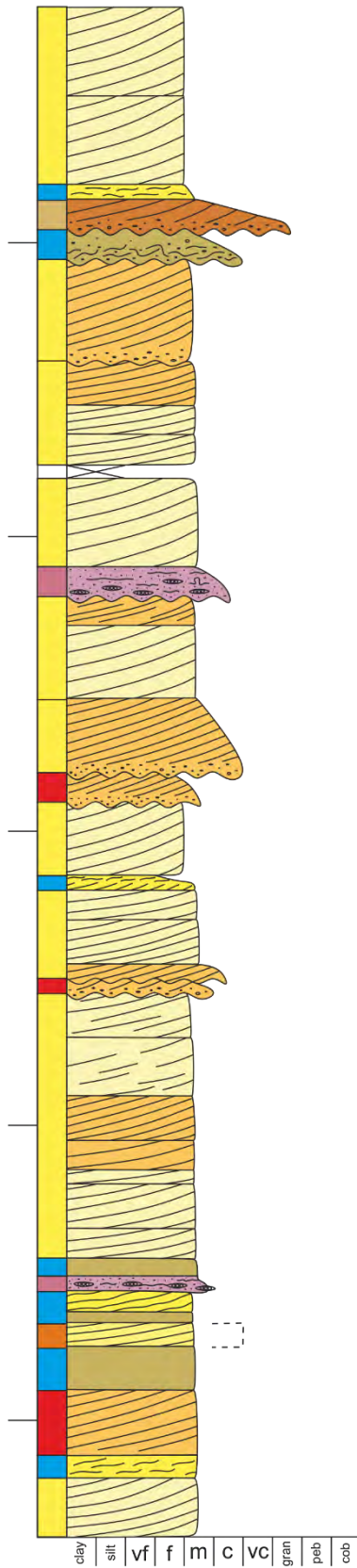
**Please refer to Table 8.1 for full facies descriptions*

Aeolian	
	Smxb & Smtxb
	Smxbc
	Smpb
	Smpl
	Smwr
	Smwb
	Sm

Additional Structures			
	Roots		Coarser grained lenses
	Ripples		Intraformational Clasts
	Bioturbation		Extraformational Clasts
	Desiccation		Evaporitic grains
	Soft sediment deformation		Evaporitic clasts

Facies Associations			
	Aeolian Dune		Damp to wet Interdune
	Aeolian Dune Plinth		Fluvial Channel
	Aeolian Sandsheet		Fluvial Sheet
	Dry Interdune		Overbank
	Lake Margin		Lake Centre
	Ephemeral Saline Lake/Mudflat		

Well Number: 48/19-1 (2 of 2)
 Total length: 142.4 m
 Core Recovery: 71.5%



Lithofacies Key

Fluvial		Lacustrine	
	Sxb & Stxb		Sul
	Slxb		Seb
	Spb		Steul
	Spl		Spbl
	Sfrl		Sml
	Stpl		Sppl
	Smf		Sxl
	Cms		Ms
	Ccs		

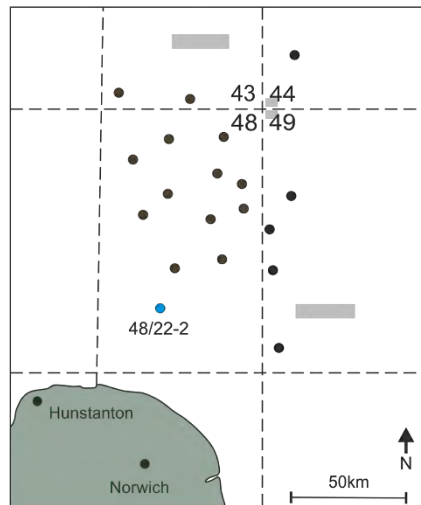
**Please refer to Table 8.1 for full facies descriptions*

Aeolian	
	Smxb & Smtxb
	Smxbc
	Smpb
	Smpl
	Smwr
	Smwb
	Sm

Additional Structures			
	Roots		Coarser grained lenses
	Ripples		Intraformational Clasts
	Bioturbation		Extraformational Clasts
	Desiccation		Evaporitic grains
	Soft sediment deformation		Evaporitic clasts

Facies Associations			
	Aeolian Dune		Damp to wet Interdune
	Aeolian Dune Plinth		Fluvial Channel
	Aeolian Sandsheet		Fluvial Sheet
	Dry Interdune		Overbank
	Lake Margin		Lake Centre
	Ephemeral Saline Lake/Mudflat		

Well Number: 48/22-2
 Total length: 13.15 m
 Core Recovery: 87.7%



Lithofacies Key

Fluvial

- Sxb & Stxb
- Slxb
- Spb
- Spl
- Sfri
- Stpl
- Smf
- Cms
- CCS

Lacustrine

- Sul
- Seb
- Steul
- Spbl
- Sml
- Sppl
- Sxl
- Ms

**Please refer to Table 8.1 for full facies descriptions*

Aeolian

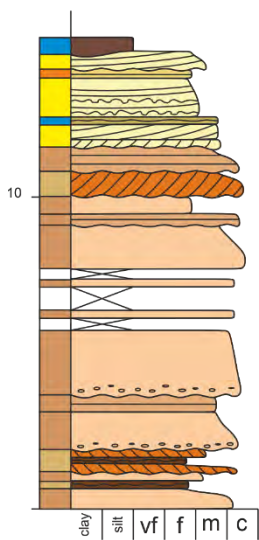
- Smxb & Smtxb
- Smxbc
- Smpb
- Smpl
- Smwr
- Smwb
- Sm

Additional Structures

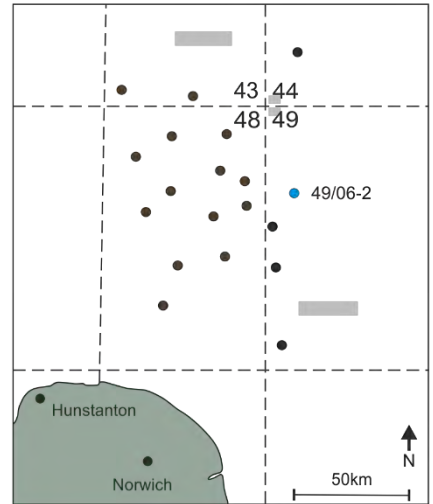
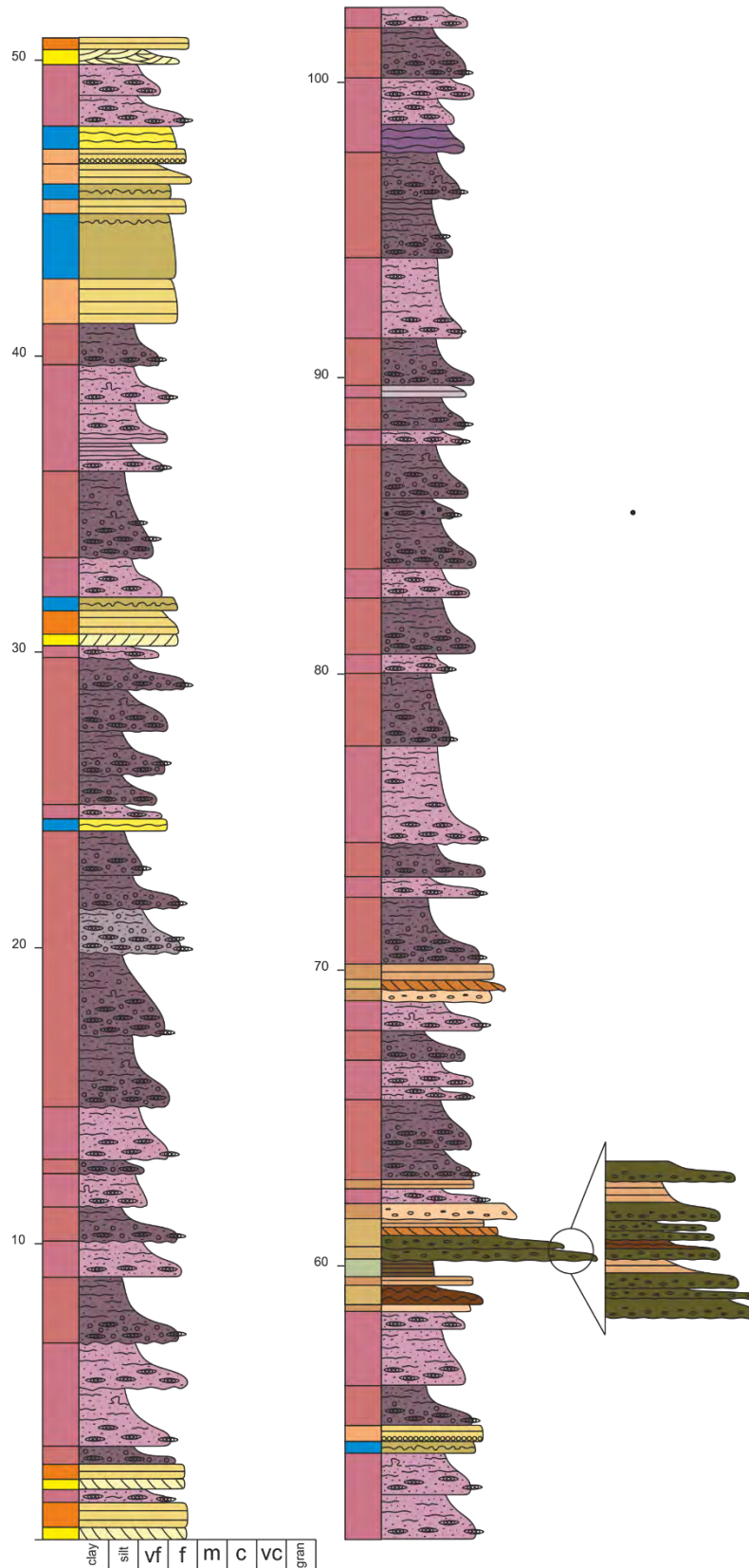
- Roots
- Ripples
- Bioturbation
- Desiccation
- Soft sediment deformation
- Coarser grained lenses
- Intraformational Clasts
- Extraformational Clasts
- Evaporitic grains
- Evaporitic clasts

Facies Associations

- Aeolian Dune
- Aeolian Dune Plinth
- Aeolian Sandsheet
- Dry Interdune
- Lake Margin
- Ephemeral Saline Lake/Mudflat
- Damp to wet Interdune
- Fluvial Channel
- Fluvial Sheet
- Overbank
- Lake Centre



Well Number: 49/06-2 (1 of 2)
 Total length: 169.7 m
 Core Recovery: 97.2%



Lithofacies Key

Fluvial

- Sxb & Stxb
- Slxb
- Spb
- Spl
- Sfrl
- Stpl
- Smf
- Cms
- Ccs

Lacustrine

- Sul
- Seb
- Steul
- Spbl
- Sml
- Spil
- Sxl
- Ms

**Please refer to Table 8.1 for full facies descriptions*

Aeolian

- Smxb & Smtxb
- Smxbc
- Smpb
- Smpl
- Smwr
- Smwb
- Sm

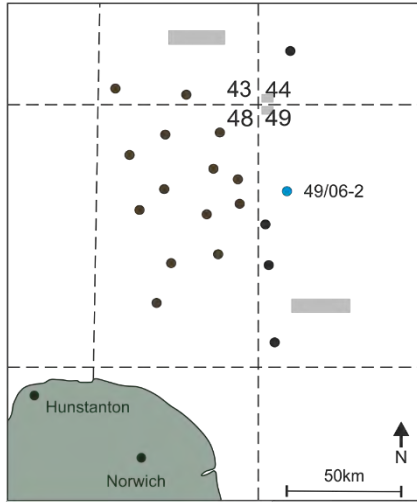
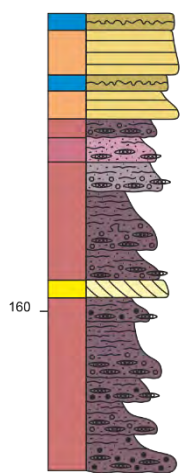
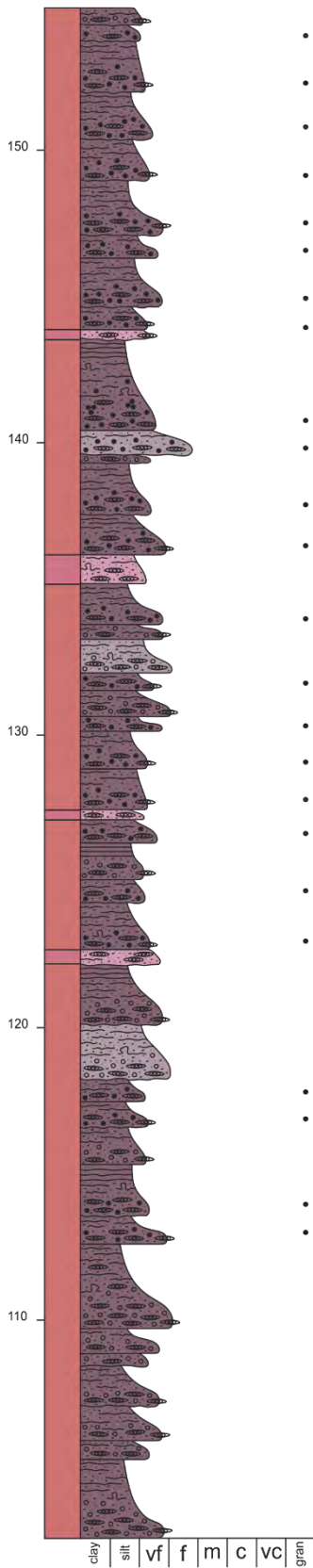
Additional Structures

- Roots
- Ripples
- Bioturbation
- Desiccation
- Soft sediment deformation
- Coarser grained lenses
- Intraformational Clasts
- Extraformational Clasts
- Evaporitic grains
- Evaporitic clasts

Facies Associations

- Aeolian Dune
- Aeolian Dune Plinth
- Aeolian Sandsheet
- Dry Interdune
- Lake Margin
- Ephemeral Saline Lake/Mudflat
- Damp to wet Interdune
- Fluvial Channel
- Fluvial Sheet
- Overbank
- Lake Centre

Well Number: 49/06-2 (2 of 2)
 Total length: 169.7 m
 Core Recovery: 97.2%



Lithofacies Key

Fluvial		Lacustrine	
	Sxb & Stxb		Sul
	Slxb		Seb
	Spb		Steul
	Spl		Spbl
	Sfri		Sml
	Stpl		Spil
	Smf		Sxl
	Cms		Ms
	Ccs		

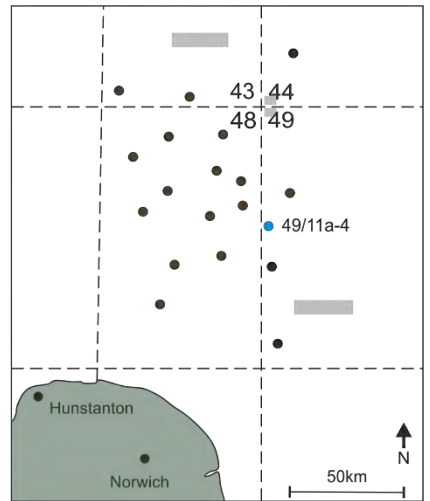
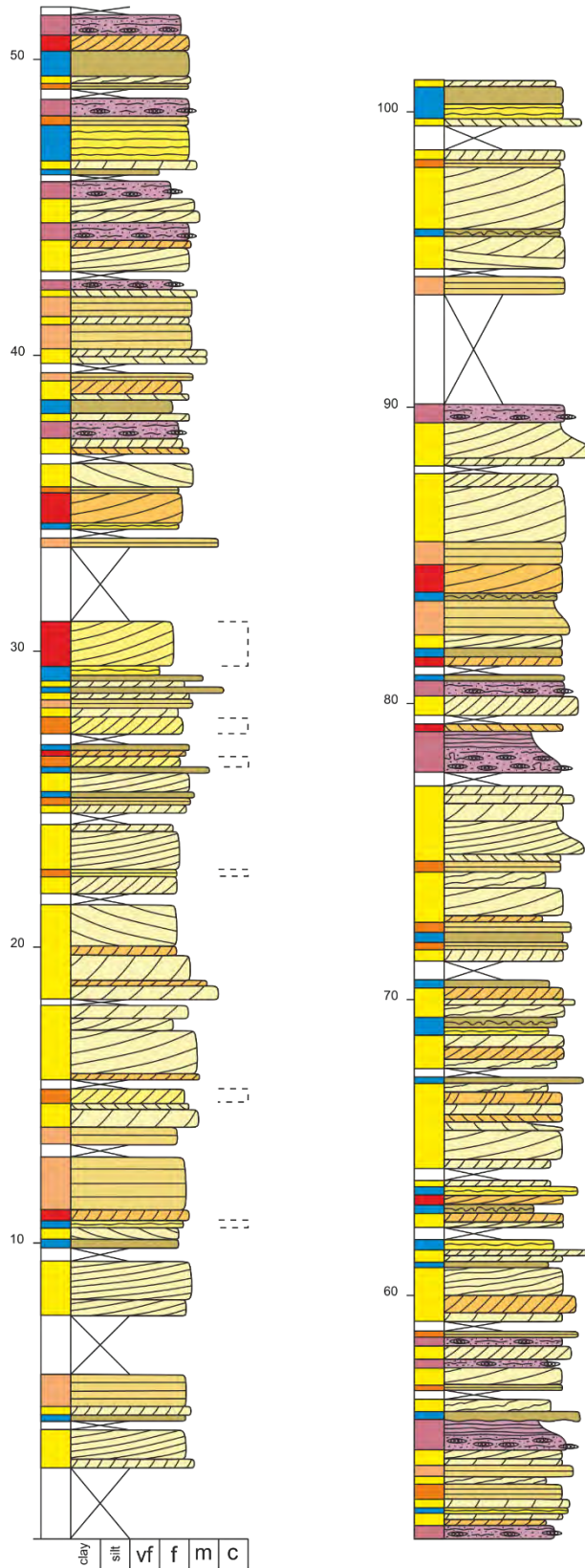
**Please refer to Table 8.1 for full facies descriptions*

Aeolian			
	Smxb & Smtxb		Smwr
	Smxbc		Smwb
	Smpb		Sm
	Smpl		

Additional Structures			
	Roots		Coarser grained lenses
	Ripples		Intraformational Clasts
	Bioturbation		Extraformational Clasts
	Desiccation		Evaporitic grains
	Soft sediment deformation		Evaporitic clasts

Facies Associations			
	Aeolian Dune		Damp to wet Interdune
	Aeolian Dune Plinth		Fluvial Channel
	Aeolian Sandsheet		Fluvial Sheet
	Dry Interdune		Overbank
	Lake Margin		Lake Centre
	Ephemeral Saline Lake/Mudflat		

Well Number: 49/11a-4 (1 of 2)
 Total length: 162.6 m
 Core Recovery: 98.8%



Lithofacies Key

Fluvial

- Sxb & Stxb
- Slxb
- Spb
- Spl
- Sfri
- Stpl
- Smf
- Cms
- Ccs

Lacustrine

- Sul
- Seb
- Steul
- Spbl
- Sml
- Spll
- Sxl
- Ms

*Please refer to Table 8.1 for full facies descriptions

Aeolian

- Smxb & Smtxb
- Smxbc
- Smpb
- Smpl
- Smwr
- Smwb
- Sm

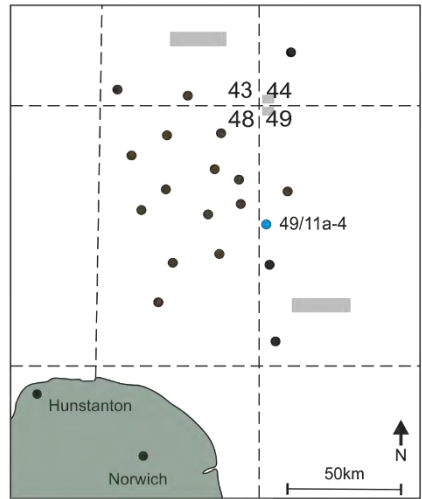
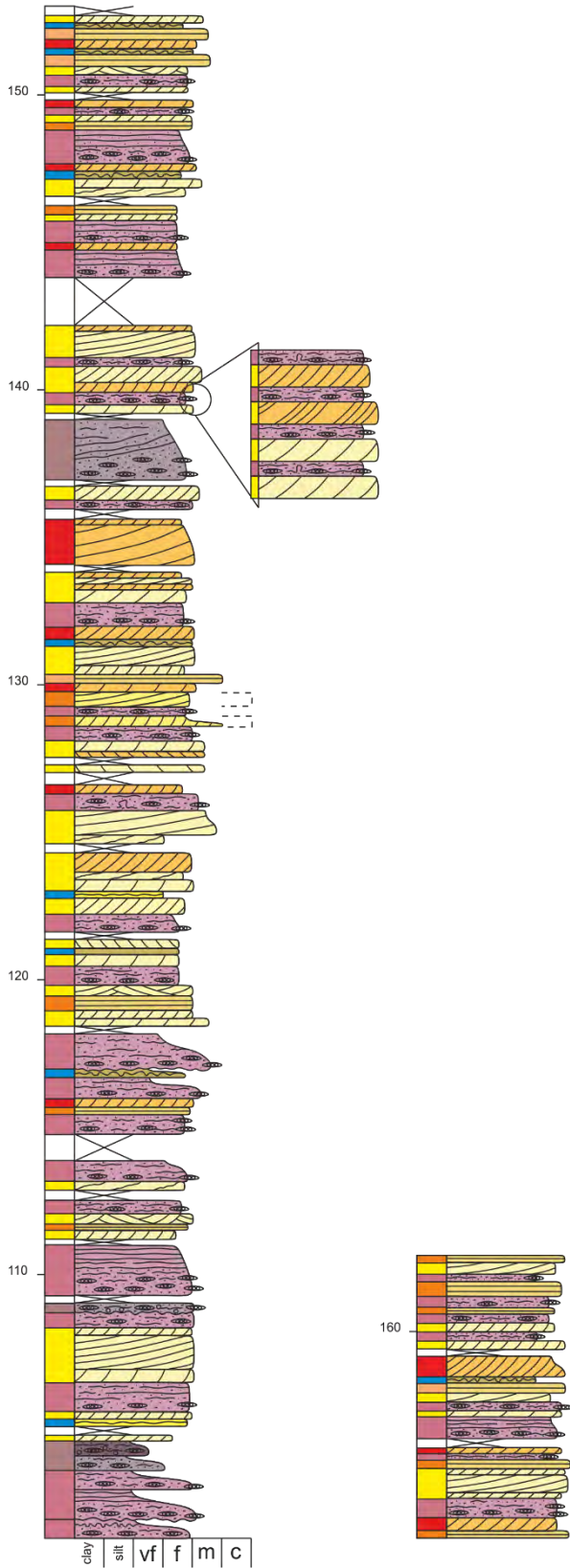
Additional Structures

- Roots
- Ripples
- Bioturbation
- Desiccation
- Soft sediment deformation
- Coarser grained lenses
- Intraformational Clasts
- Extraformational Clasts
- Evaporitic grains
- Evaporitic clasts

Facies Associations

- Aeolian Dune
- Aeolian Dune Plinth
- Aeolian Sandsheet
- Dry Interdune
- Lake Margin
- Ephemeral Saline Lake/Mudflat
- Damp to wet Interdune
- Fluvial Channel
- Fluvial Sheet
- Overbank
- Lake Centre

Well Number: 49/11a-4 (1 of 2)
 Total length: 162.6 m
 Core Recovery: 98.8%



Lithofacies Key

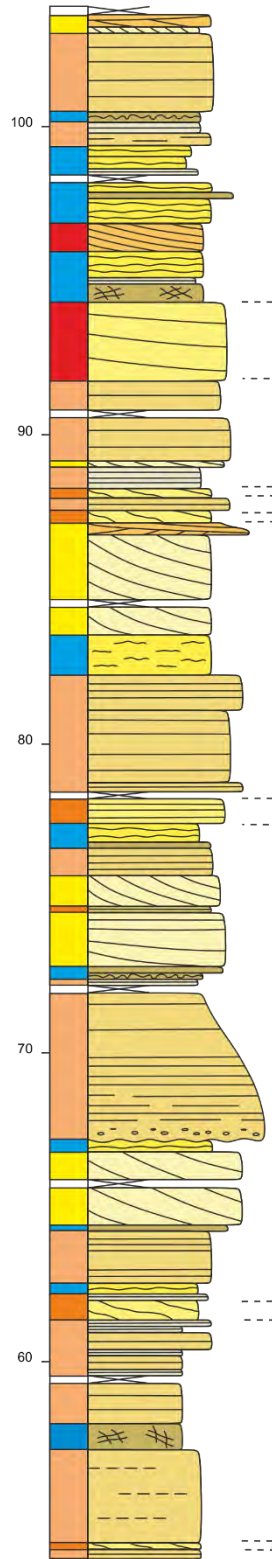
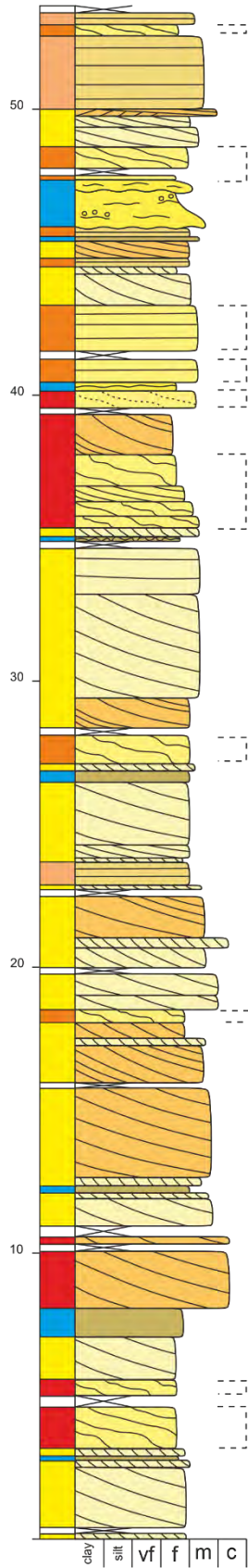
Fluvial		Lacustrine	
	Sxb & Stxb		Sul
	Slxb		Seb
	Spb		Steul
	Spl		Spbl
	Sfrl		Sml
	Stpl		Spil
	Smf		Sxl
	Cms		Ms
	Ccs		

**Please refer to Table 8.1 for full facies descriptions*

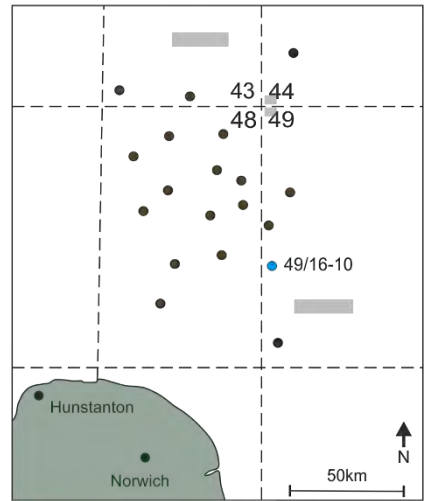
Aeolian	
	Smxb & Smtxb
	Smxbc
	Smpb
	Smpl
	Smwr
	Smwb
	Sm

Additional Structures	
	Roots
	Ripples
	Bioturbation
	Desiccation
	Soft sediment deformation
	Coarser grained lenses
	Intraformational Clasts
	Extraformational Clasts
	Evaporitic grains
	Evaporitic clasts

Facies Associations			
	Aeolian Dune		Damp to wet Interdune
	Aeolian Dune Plinth		Fluvial Channel
	Aeolian Sandsheet		Fluvial Sheet
	Dry Interdune		Overbank
	Lake Margin		Lake Centre
	Ephemeral Saline Lake/Mudflat		



Well Number: 49/16-10 (1 of 2)
 Total length: 152.4 m
 Core Recovery: 98.6%



Lithofacies Key

Fluvial

- Sxb & Stxb
- Slxb
- Spb
- SpI
- Sfrl
- Stpl
- Smf
- Cms
- CCS

Lacustrine

- Sul
- Seb
- Steul
- Spbl
- Sml
- SpIl
- Sxl
- Ms

*Please refer to Table 8.1 for full facies descriptions

Aeolian

- Smxb & Smtxb
- Smxbc
- Smpb
- Smpl

- Smwr
- Smwb
- Sm

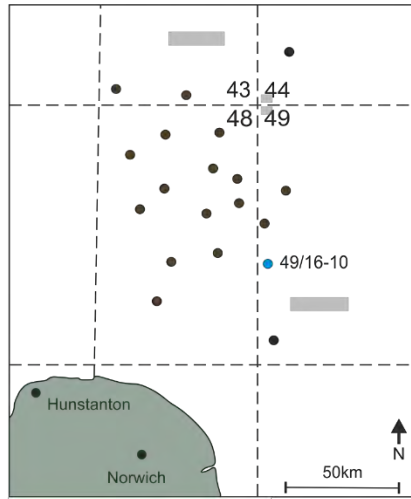
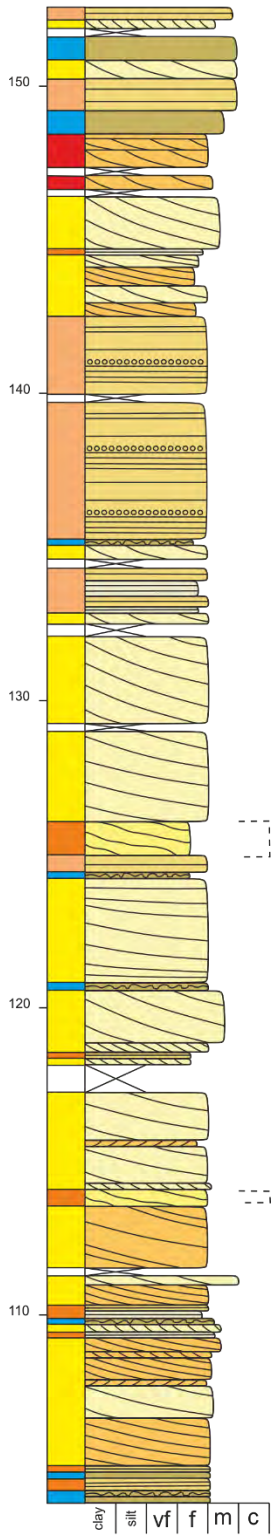
Additional Structures

- Roots
- Ripples
- Bioturbation
- Desiccation
- Soft sediment deformation
- Coarser grained lenses
- Intraformational Clasts
- Extraformational Clasts
- Evaporitic grains
- Evaporitic clasts

Facies Associations

- Aeolian Dune
- Aeolian Dune Plinth
- Aeolian Sandsheet
- Dry Interdune
- Lake Margin
- Ephemeral Saline Lake/Mudflat
- Damp to wet Interdune
- Fluvial Channel
- Fluvial Sheet
- Overbank
- Lake Centre

Well Number: 49/16-10 (2 of 2)
 Total length: 152.4 m
 Core Recovery: 98.6%



Lithofacies Key

Fluvial

- Sxb & Stxb
- Sixb
- Spb
- Spl
- Sfri
- Stpl
- Smf
- Cms
- Ccs

Lacustrine

- Sul
- Seb
- Steul
- Spbl
- Sml
- Spl
- Sxl
- Ms

**Please refer to Table 8.1 for full facies descriptions*

Aeolian

- Smxb & Smtxb
- Smxbc
- Smpb
- Smpl
- Smwr
- Smwb
- Sm

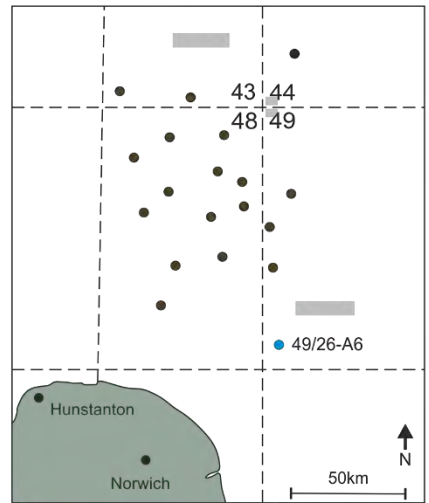
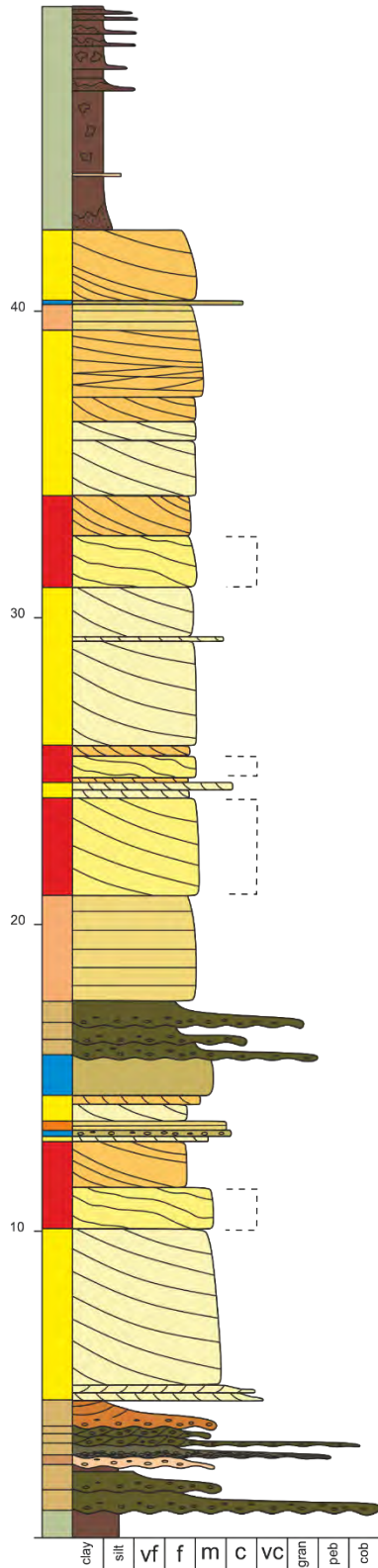
Additional Structures

- Roots
- Ripples
- Bioturbation
- Desiccation
- Soft sediment deformation
- Coarser grained lenses
- Intraformational Clasts
- Extraformational Clasts
- Evaporitic grains
- Evaporitic clasts

Facies Associations

- Aeolian Dune
- Aeolian Dune Plinth
- Aeolian Sandsheet
- Dry Interdune
- Lake Margin
- Ephemeral Saline Lake/Mudflat
- Damp to wet Interdune
- Fluvial Channel
- Fluvial Sheet
- Overbank
- Lake Centre

Well Number: 49/26-A6 (1 of 4)
 Total length: 271.6 m
 Core Recovery: 85.1%



Lithofacies Key

Fluvial

- Sxb & Stxb
- Slxb
- Spb
- Spl
- Sfri
- Stpl
- Smf
- Cms
- Ccs

Lacustrine

- Sul
- Seb
- Steul
- Spbl
- Sml
- Sppl
- Sxl
- Ms

**Please refer to Table 8.1 for full facies descriptions*

Aeolian

- Smxb & Smtxb
- Smxbc
- Smpb
- Smpl
- Smwr
- Smwb
- Sm

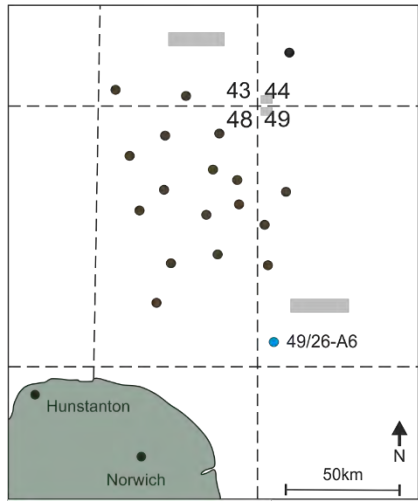
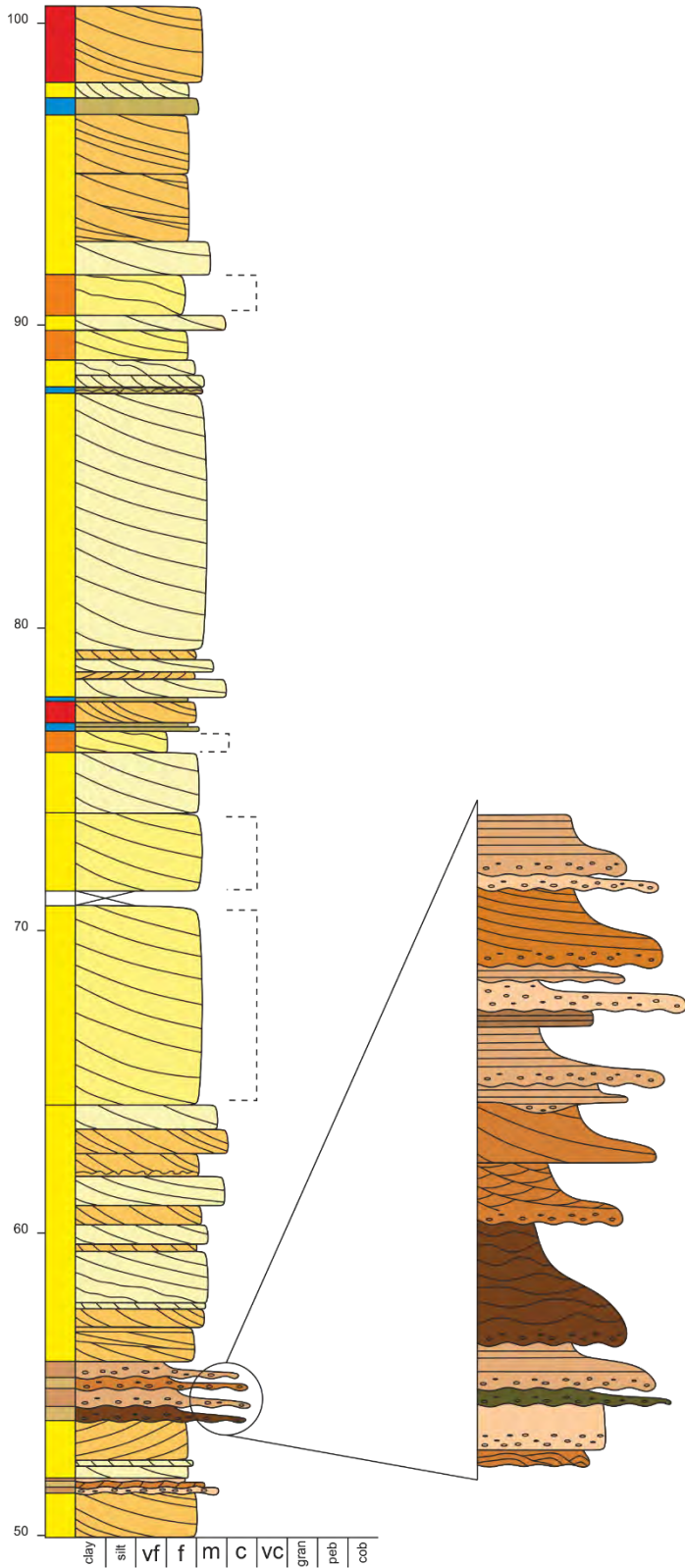
Additional Structures

- Roots
- Ripples
- Bioturbation
- Desiccation
- Soft sediment deformation
- Coarser grained lenses
- Intraformational Clasts
- Extraformational Clasts
- Evaporitic grains
- Evaporitic clasts

Facies Associations

- Aeolian Dune
- Aeolian Dune Plinth
- Aeolian Sandsheet
- Dry Interdune
- Lake Margin
- Ephemeral Saline Lake/Mudflat
- Damp to wet Interdune
- Fluvial Channel
- Fluvial Sheet
- Overbank
- Lake Centre

Well Number: 49/26-A6 (2 of 4)
 Total length: 271.6 m
 Core Recovery: 85.1%



Lithofacies Key

Fluvial		Lacustrine	
	Sxb & Stxb		Sul
	Slxb		Seb
	Spb		Steul
	Spl		Spbl
	Sfri		Sml
	Stpl		Sppl
	Smf		Sxl
	Cms		Ms
	Ccs		

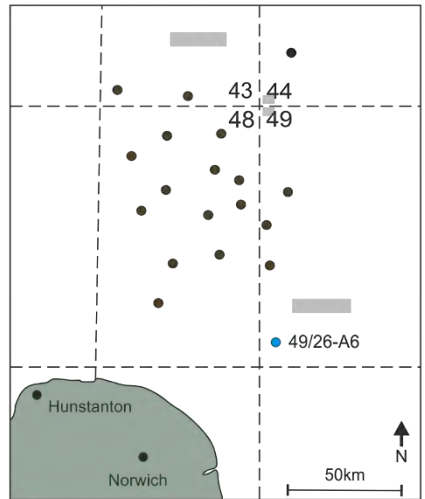
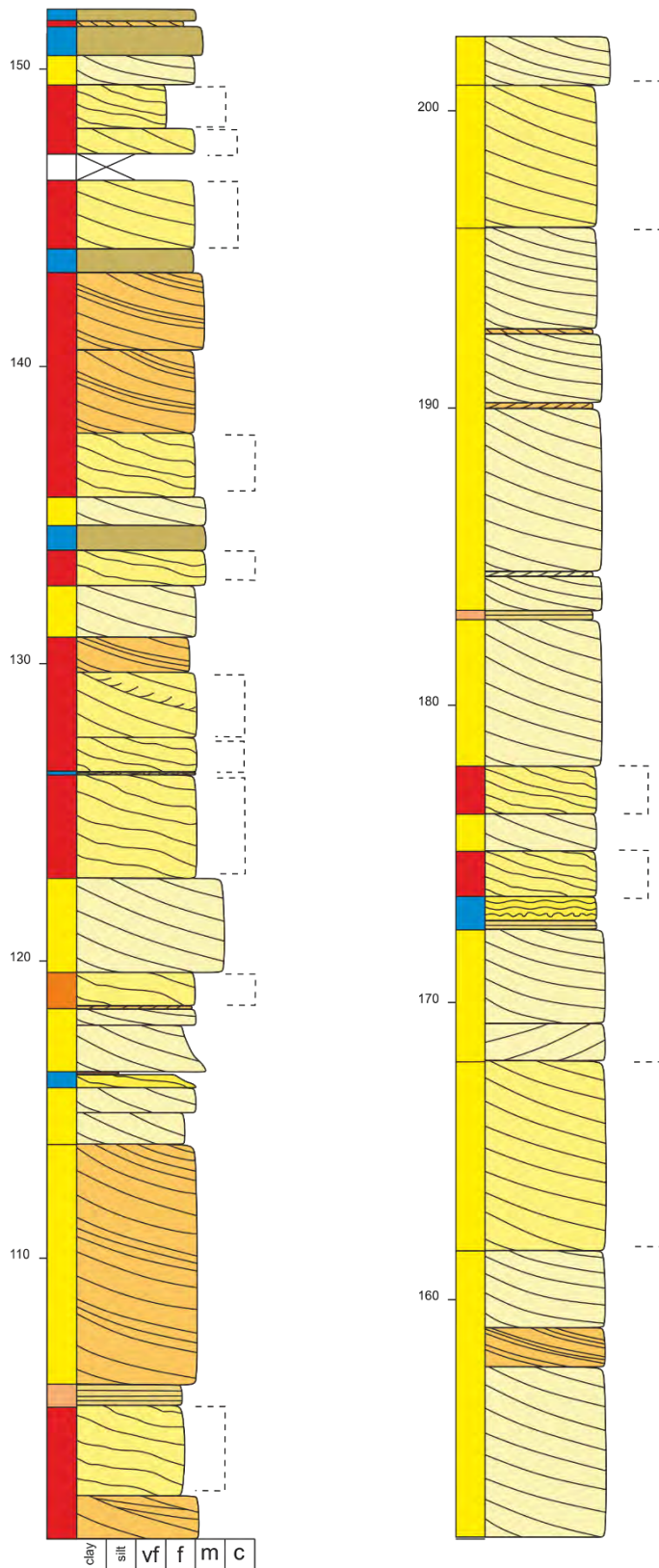
**Please refer to Table 8.1 for full facies descriptions*

Aeolian	
	Smxb & Smtxb
	Smxbc
	Smpb
	Smpl
	Smwr
	Smwb
	Sm

Additional Structures	
	Roots
	Ripples
	Bioturbation
	Desiccation
	Soft sediment deformation
	Coarser grained lenses
	Intraformational Clasts
	Extraformational Clasts
	Evaporitic grains
	Evaporitic clasts

Facies Associations			
	Aeolian Dune		Damp to wet Interdune
	Aeolian Dune Plinth		Fluvial Channel
	Aeolian Sandsheet		Fluvial Sheet
	Dry Interdune		Overbank
	Lake Margin		Lake Centre
	Ephemeral Saline Lake/Mudflat		

Well Number: 49/26-A6 (3 of 4)
 Total length: 271.6 m
 Core Recovery: 85.1%



Lithofacies Key

Fluvial		Lacustrine	
	Sxb & Stxb		Sul
	Slxb		Seb
	Spb		Steul
	Spl		Spbl
	Sfri		Sml
	Stpl		Spil
	Smf		Sxl
	Cms		Ms
	Ccs	<i>*Please refer to Table 8.1 for full facies descriptions</i>	

Aeolian

	Smxb & Smtxb		Smwr
	Smxbc		Smwb
	Smpb		Sm
	Smpl		

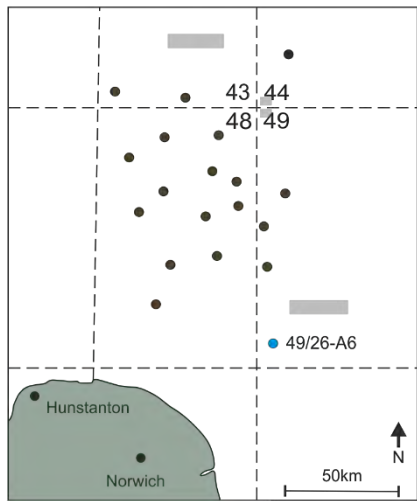
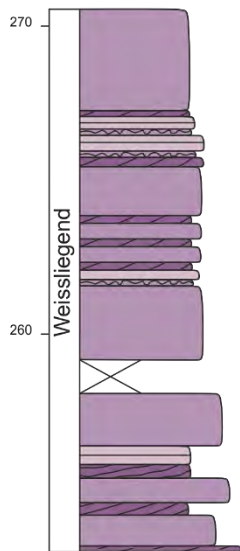
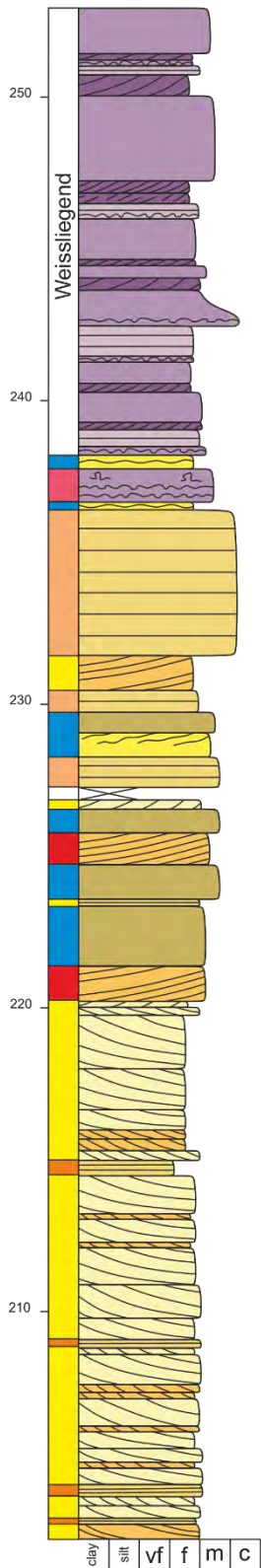
Additional Structures

	Roots		Coarser grained lenses
	Ripples		Intraformational Clasts
	Bioturbation		Extraformational Clasts
	Desiccation		Evaporitic grains
	Soft sediment deformation		Evaporitic clasts

Facies Associations

	Aeolian Dune		Damp to wet Interdune
	Aeolian Dune Plinth		Fluvial Channel
	Aeolian Sandsheet		Fluvial Sheet
	Dry Interdune		Overbank
	Lake Margin		Lake Centre
	Ephemeral Saline Lake/Mudflat		

Well Number: 49/26-A6 (4 of 4)
 Total length: 271.6 m
 Core Recovery: 85.1%



Lithofacies Key

Fluvial		Lacustrine	
	Sxb & Stxb		Sul
	Slxb		Seb
	Spb		Steul
	Spl		Spbl
	Sfrl		Sml
	Stpl		Spil
	Smf		Sxl
	Cms		Ms
	Ccs		

**Please refer to Table 8.1 for full facies descriptions*

Aeolian	
	Smxb & Smtxb
	Smxbc
	Smpb
	Smpl
	Smwr
	Smwb
	Sm

Additional Structures			
	Roots		Coarser grained lenses
	Ripples		Intraformational Clasts
	Bioturbation		Extraformational Clasts
	Desiccation		Evaporitic grains
	Soft sediment deformation		Evaporitic clasts

Facies Associations			
	Aeolian Dune		Damp to wet Interdune
	Aeolian Dune Plinth		Fluvial Channel
	Aeolian Sandsheet		Fluvial Sheet
	Dry Interdune		Overbank
	Lake Margin		Lake Centre
	Ephemeral Saline Lake/Mudflat		